PALEOCLIMATE CHANGE IN SOUTHERN INDIANA DETERMINED FROM SPELEOTHEM CLIMATE PROXIES AND ANALYSIS OF MODERN PRECIPITATION OXYGEN ISOTOPE VARIATIONS

by

PETE DOUGLAS AKERS

(Under the Direction of George A. Brook)

ABSTRACT

A narrative of southern Indiana climate and environmental changes for portions of the past 90,000 years has been created by integrating data from field-sampled stalagmites with a modern precipitation stable isotope database. Proper paleoenvironmental research in the American Midwest requires understanding the modern relationships between climate and precipitation stable oxygen isotope ratios ($\delta^{18}O$) at multiple temporal scales. While a novel weekly precipitation-day climate dataset did not produce results significantly different from previous studies, it did identify considerable isotope-climate relationship variability between individual months and seasons. Atmospheric flow patterns are the dominant control on multi-annual precipitation $\delta^{18}O$ variability, with precipitation seasonality playing a lesser, yet related, role. This new understanding of Midwestern precipitation $\delta^{18}O$ variability was applied to proxy climate data from fifteen stalagmites collected from four southern Indiana caves. A high-resolution analysis of two stalagmites from Upper Porter Cave provides a record of hydroclimate changes for much of the Holocene from multiple paleoenvironmental proxies. The timing of stalagmite growth and hiatus, with support from petrography, luminescence, and stable oxygen and carbon isotope values, suggests a drier-than-modern Indiana during the periods 2.3-2.7, 2.9-3.1, 3.6-4.2, 4.7-4.9, and

7.3-8.5 thousand years before present (ka BP). In contrast, the past 2300 years and the period of maximum Holocene warmth in the Midwest (5-7 ka BP) were relatively wet. Dry periods in southern Indiana during the Holocene may be driven partly by eastward shifts in the position of the Bermuda High in response to abrupt global climate changes. At millennial timescales, analysis of all sampled stalagmites suggests that high northern hemisphere summer insolation and relative global warmth favor stalagmite growth in the four sampled caves. The environment of southern Indiana during periods of stalagmite growth in the Pleistocene (57-59 and 80-85 ka BP) may have been roughly similar to early Holocene conditions, but the uncertainty involved with quantitative comparison between caves makes definitive conclusions difficult. The results from this research help fill a spatial void in the understanding of North American paleoenvironmental change and suggest that the transition to a future warmer climate may include significant dry episodes in southern Indiana.

INDEX WORDS: paleoclimatology, stalagmite, speleothem, Indiana, American Midwest, precipitation isotopes, Holocene, Pleistocene, insolation, stable isotopes

PALEOCLIMATE CHANGE IN SOUTHERN INDIANA DETERMINED FROM SPELEOTHEM CLIMATE PROXIES AND ANALYSIS OF MODERN PRECIPITATION OXYGEN ISOTOPE VARIATIONS

by

PETE DOUGLAS AKERS

B.S., Purdue University, 2009

M.S., The University of Georgia, 2011

A Dissertation Submitted to the Graduate Faculty of The University of Georgia in Partial Fulfillment of the Requirements of the Degree

DOCTOR OF PHILOSOPHY

ATHENS, GEORGIA

2016

PALEOCLIMATE CHANGE IN SOUTHERN INDIANA DETERMINED FROM SPELEOTHEM CLIMATE PROXIES AND ANALYSIS OF MODERN PRECIPITATION OXYGEN ISOTOPE VARIATIONS

by

PETE DOUGLAS AKERS

Major Professor: George A. Brook

Committee: L. Bruce Railsback
David S. Leigh
David F. Porinchu

Electronic Version Approved:

Suzanne Barbour
Dean of the Graduate School
The University of Georgia
May 2016

DEDICATION

For my dear Leslie, who has supported and loved me unconditionally throughout my studies, my research, and our life experiences.

ACKNOWLEDGEMENTS

This research could not have been completed without the help of many people over the past five years. Primary thanks must be given to Dave Everton, Keith Johnson, Gary Roberson, Carol Groves, Rob Houchens, Linda Hobbs, and the staff at Indiana Caverns for cave access and sampling permission. Jeff Welker granted access to the USNIP database, which has been critical to all parts of this dissertation. I would also like to thank my parents, Doug and Marilyn Akers, and sister, Suzanne Akers, for housing and cave sampling assistance during field work. David Leigh, Genevieve Holdridge, and Robert Sorrells offered excellent conference presentation advice, Steve Holland gave initial teaching and help with the R programming language, and George Brook, Bruce Railsback, and Voari Ny provided much advice on my stalagmite analysis. Jordan McLeod, Tom Mote, Victor Gensini, Craig Ramseyer, and Kyle Mattingly supplied critical climatological advice and data for this research. Special thanks are given to Jake McDonald for manuscript editing, listening to and evaluating my various research theories and complaints, and generally offering scientific and moral support whenever called upon. Finally, I must thank the National Science Foundation (grant #1433904), the Paleoenvironmental Change group of the American Association of Geographers, and the University of Georgia Graduate School for funding this research and thank my committee members George Brook, Bruce Railsback, Dave Porinchu, and David Leigh for their guidance and advice.

TABLE OF CONTENTS

LIST OF TABLES

LIST OF FIGURES

CHAPTER ONE:

INTRODUCTION

1.1 Introduction

A solid understanding of past climate forcings and variability is critical to comprehending modern and future global climates. This knowledge is particularly crucial as anthropogenic climate change threatens to alter modern climates to a global degree unseen since the last deglaciation (Pachauri and Reisinger, 2008; PCCRC, 2008). Paleoenvironmental research has increased rapidly in scope and significance over the past few decades and offers valuable insight into past climate changes and environmental responses. New technologies and paleoenvironmental proxy sources such as deep ocean cores that emerged in the latter half of the 20th century overturned or refined previous assumptions about the variability of Earth's climate and ecosystems (Broecker and van Donk, 1970; Emiliani, 1955; Hays et al., 1976; Imbrie, 1984; Shackleton et al., 1990; Shackleton and Opdyke, 1973). In particular, this research ushered in a new understanding of the glacial-interglacial cycles that have dominated Earth's history in the current Quaternary Period that began 2.58 million years ago.

Speleothems (secondary calcium carbonate cave formations) and specifically stalagmites were recognized as a potential source of paleoenvironmental data as early as the 1960s and 1970s (Hendy, 1971; Hendy and Wilson, 1968), but difficulties in accurate dating and an incomplete understanding of speleothem paleoenvironmental proxies restricted the usefulness of speleothem records. A better understanding of the multiple climate controls on global and regional precipitation stable oxygen isotope ($\delta^{18}O$) variations (Dansgaard, 1964; Lachniet, 2009; LeGrande and Schmidt, 2006; Rozanski et al., 1993) and the emergence of uranium-thorium disequilibrium (U-Th) dating (Drysdale et al., 2012; Shen

et al., 2002) have made speleothem records a valued component of high-quality paleoenvironmental studies.

This dissertation details the production and findings of a series of paleoenvironmental records from fifteen stalagmites collected in four southern Indiana caves. First, the modern relationships between climate and precipitation $\delta^{18}O$ variations are examined across the eastern and central United States using the United States Network for Isotopes in Precipitation (USNIP), the most complete precipitation isotope database currently available for the region. An emphasis is placed on quantifying changes to climate and precipitation $\delta^{18}O$ relationships that occur with temporal aggregation as well as on monthly and seasonal cycles. The potential effects of changing moisture source and precipitation seasonality on precipitation $\delta^{18}O$ values are explored, culminating in a chapter that identifies the climate controls on multi-annual precipitation $\delta^{18}O$ values for southern Indiana. These findings are applied first to two high-resolution Holocene stalagmite records from Upper Porter Cave, Indiana, and later to stalagmite $\delta^{18}O$ data from all four cave sites. Combined with other paleoenvironmental proxy data, the result is a narrative of southern Indiana environmental change that covers portions of the past 90,000 years. As a whole, this research both significantly expands the knowledge of Midwestern paleoenvironmental change and integrates southern Indiana climate changes into a broader regional and global narrative.

1.2 Research impetus

Past millennial-scale global climate change in the Quaternary Period is largely attributed to predicable orbital fluctuations and associated feedbacks (Clark et al., 1999; Kawamura et al., 2007). Climate and environmental changes are typically smaller in magnitude in the Holocene, the epoch stretching from present day to 11,700 calendar years before present (cal yr BP, where 'present' in this dissertation is defined as 1950 CE), but significant regional climate variations still existed (Mayewski et

al., 2004; Wanner et al., 2008; Wanner et al., 2011). Multiple paleoclimate records with a broad spatial and temporal coverage are thus needed to understand the full climate variability present in a given region. Accurate climate and ecological forecasts are needed to help mitigate economic damage from future climate change (Clark et al., 2001; Hansen et al., 2001), and these forecasts require a firm comprehension of both regional climate drivers and environmental responses. Modern observations alone cannot provide all analogs and data for these forecasts as climate change may result in climate and ecological conditions unlike anything seen in modern times (Grimm and Jacobson Jr., 2003; Williams and Jackson, 2007). Paleoenvironmental studies allow us to extend the period of record far beyond modern observations as well as glimpse a wider variety of environmental setups and responses.

The Midwestern United States has much potential as a location to study past environments, due to previous climate changes of considerable magnitude, the existence of a diverse climatically-sensitive flora and fauna, and a large base of accessible paleoenvironmental data (NOAA, 2015d; Wahl et al., 2012). Additionally, the changeable weather in the American Midwest responds to global forcings that allow discoveries about past Midwestern climate change to potentially have global implications. Southern Indiana was located at the boundary of many climate zones throughout the Quaternary. During the Pleistocene, maximum glacial extent of the Laurentide Ice Sheet (LIS) was just north of the caves sampled for this research. Climate gradients along this southernmost margin of the LIS were particularly exaggerated (Bromwich et al., 2005; Dorale et al., 2010), and these sharp gradients would emphasize even small climate changes in a paleoenvironmental record. While the modern prairie-forest boundary is currently located in northwestern Indiana and Illinois, prairie taxa were pushed east toward the studied cave region during drier-than-modern periods (Baker et al., 2002; Denniston et al., 2007; Denniston et al., 1999c; Wang et al., 2012). Despite the potential for important new findings, southern Indiana has not seen the level of paleoenvironmental research found elsewhere in the United States and Great Plains. However, southern Indiana has numerous caves with the potential to provide proxy

climate data through a significant portion of the Pleistocene, allowing for analysis of both glacial and interglacial conditions. To date, there have been only two unpublished speleothem studies in the region between the Appalachian Mountains and the Mississippi River valley (Chirienco, 2010; Zhang et al., 2007), but both studies are spatially limited, isolated, and generally unavailable. This dearth of cave-based information has led to calls in the scientific literature for Midwestern speleothem records (Wang et al., 2012). Certainly, multiple site records extending across climate gradients are needed for a true understanding of the past climate and environment of the Midwest.

Despite decades of work, many research questions concerning Quaternary climate changes in eastern and central North America remain unresolved, but the paucity of Indiana paleoenvironmental records limits our ability to answer some of these outstanding questions. The nature of Midwestern climate during the last glacial period is not well-understood, particularly during the deglaciation (Semken et al., 2010) and for periods prior to the Last Glacial Maximum (LGM) that experienced rapid global warming and cooling events (Litwin et al., 2013; Wood et al., 2010a). Some models suggest torrential precipitation from air masses clashing over the southern margin of the LIS during the LGM and deglaciation (Bromwich et al., 2005), but no field data have been obtained to support or reject these models in southern Indiana. For the Holocene, very few paleoenvironmental records are available for Indiana despite the state being ideally situated between areas to the west that show intense middle Holocene drought and areas to the east with limited drought signal (Denniston et al., 2007; Hardt et al., 2010). While the research detailed in this dissertation cannot address all of these unanswered questions, it provides a solid foundation for future regional studies.

1.3 Dissertation objectives

- Better constrain and quantify the climate controls on modern precipitation $\delta^{18}O$ variability in the eastern and central United States with a focus on southern Indiana.

- Determine how to best apply the findings from modern precipitation $\delta^{18}O$ studies to stalagmite-based paleoenvironmental data.
- Identify and describe changes in the climate and environment of southern Indiana during the Holocene and Pleistocene based upon stalagmite paleoenvironmental data.
- Examine what the new stalagmite paleoenvironmental data suggest about the climate connections beyond the American Midwest and future climate change in southern Indiana.

1.4 Dissertation outline

- Chapter 2 begins the dissertation research with an initial analysis of the relationships between modern precipitation isotope variability and climate. This chapter identifies the basic statistics for and influences on modern precipitation $\delta^{18}O$ values for the study region, and the database constructed in this chapter is used for later analyses in Chapters 3-6.
- Chapter 3 examines how the relationships calculated in Chapter 2 change when data are temporally aggregated and grouped. Quantifying these changes allows better comparison between studies of different temporal settings and resolutions as well as bridging to paleoenvironmental climate proxy data.
- Chapter 4 examines the influence of moisture source on precipitation $\delta^{18}O$ values in the study region through air mass back trajectory modeling. Changes in moisture source composition are often cited as a driver of long-term $\delta^{18}O$ changes, but little research has been performed on this topic in the American Midwest.
- Chapter 5 covers the creation and validation of a new metric to quantify precipitation seasonality: the Summer Signal Anomaly, or SSA. This metric is an attempt to link changes in annual precipitation $\delta^{18}O$ values to shifts in seasonal precipitation balances.

- Chapter 6 combines the results and data from Chapters 2-5 to determine what controls the multi-annual changes in precipitation $\delta^{18}O$ values. The results from this chapter are directly applicable to interpreting stalagmite $\delta^{18}O$ values in Chapters 7 and 8.
- Chapter 7 covers the paleoenvironmental analysis of two Holocene stalagmites from Upper Porter Cave, Indiana. The paleoenvironmental record is largely based upon the growth and hiatuses of the stalagmites, with supporting evidence from stable isotopes, visual data, and petrographic analysis.
- Chapter 8 is an overview of the periods of growth observed in all stalagmites collected from southern Indiana as part of this research. These stalagmites grow during discrete periods over the past 90,000 years, and both the timing of stalagmite growth and stable isotope data give insight into millennial-scale climate changes in the American Midwest.
- Chapter 9 summarizes the findings of this dissertation research and relates it back to the dissertation objectives identified in this chapter. The potential impact of this research for both science and policy is highlighted and a focus for future research is proposed.

1.5 Study region

The four caves examined in this research are found on the Mitchell Plateau of southern Indiana, a karst landscape with a high concentration of sinkholes and caves extending 170 km along a north-northwest (NNW) to south-southeast (SSE) transect (a 1.5° latitudinal gradient from 38.0 to 39.5°N) from the southern limit of the LIS during the LGM to the Ohio River and spanning 10-25 km east to west. The plateau is dissected by a number of larger rivers, but small surface streams are scarce. Dated cave formations on the plateau show speleothem growth over the past 350 thousand years before present (ka BP), with the bulk of formations dating from present to the penultimate glaciation (0-150 ka BP) (Chirienco, 2010). Stalagmites in four cave systems were sampled in this study: Porter Cave on the north

of the plateau (~10 km south of the LGM glacial limit), Roadcut Cave and Johnson Cave in the central plateau portion, and Indiana Caverns (part of the Binkley Cave system) 20 km from the Ohio River in the southern limits (Figure 1). Porter Cave is 60 km NNW of Roadcut Cave, which is itself 15 km NNW of Johnson Cave. Johnson Cave is 65 km NNW of Indiana Caverns. None of these caves was covered by ice during the LGM, but Porter Cave was within 10 km of the ice sheet margin. Modern natural vegetation is temperate deciduous hardwood forest dominated by oak, hickory, maple, and beech, but a significant portion of the Mitchell Plateau has been deforested and is used for agricultural purposes today.

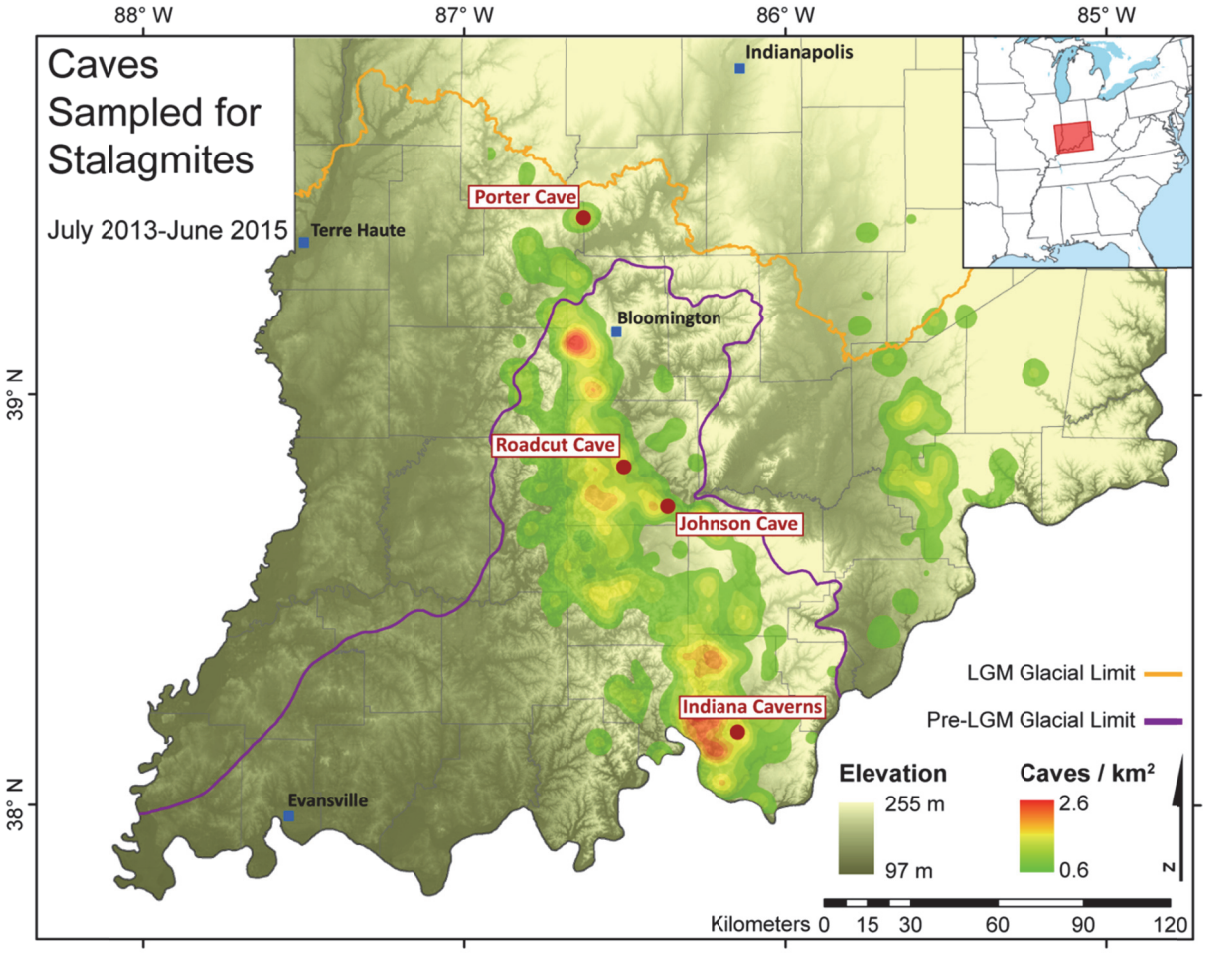

Figure 1. Map of southern Indiana showing the location of caves sampled for stalagmites, elevation, density of caves, and glacial limits.

Mean annual surface air temperature in southern Indiana ranges between 11.6°C and 14.0°C, and mean annual precipitation is 110 cm (NOAA, 2015c). The Midwest today experiences strong seasonal changes in air mass source with Pacific and Arctic air masses dominating during winter months and increased dominance of air masses from the Gulf of Mexico during the summer (Bryson and Hare, 1974). Climate oscillations such as the El Niño-Southern Oscillation (ENSO), the North Atlantic (NAO) and Arctic Oscillations (AO), and the Pacific-North American Pattern (PNA) can influence the regional climate on daily to monthly scales (Hurrell, 1995; Leathers et al., 1991; Thompson and Wallace, 1998; Trenberth, 1997). Predictive climate models suggest a generally warmer and wetter future in southern Indiana due to anthropogenic climate change, possibly with an increased risk of summer drought stress (PCCRC, 2008).

1.6 Regional climate history

Southern Indiana has experienced pronounced changes in climate over the Pleistocene and Holocene. Glacial ice reached maximum dimensions during the penultimate glaciation and the initial melting of this ice sheet created several pro-glacial lakes in the region (Wood et al., 2010b). Relatively little has been discovered about the environment from the last interglacial through the LGM, although there may have been a significant ice advance into central Indiana around 60-70 ka BP (Wood et al., 2010a). Approximately 24 rapid warming events known as interstadials or Dansgaard-Oeschger events have been identified in Greenland ice cores (Dansgaard et al., 1993; Johnsen et al., 1992). These interstadials provoked vegetation shifts in eastern North America during the last glacial period (Litwin et al., 2013), but possible effects in southern Indiana have not yet been identified. Greatest LGM ice extent in Indiana appears to have been reached by 23.3 ka BP, and the greater region was deglaciated entirely by 12 ka BP (Glover et al., 2011). Although some permafrost may have existed south of the glacial limit during the LGM (French and Millar, 2013), speleothem ages from southern Indiana indicate growth

throughout the recent glacial period (Chirienco, 2010) suggesting only sporadic permafrost, if any, that allowed liquid drip water and speleothem deposition in caves. Vegetation along the southern margin of the LIS during the LGM was herbaceous and similar to modern sedge-dominated muskegs of northern Canada, while spruce reappeared in southern Indiana around 21 ka BP (Heusser et al., 2002). However, some conifers may have survived quite close to the glacial ice margin (Jackson et al., 2000).

The deglaciation transition from LGM to the Holocene included several global climate fluctuations (Johnson et al., 1997) expressed as dramatic environmental changes in the American Midwest. Extreme regional aridity may have produced a massive aeolian event from 18 to 16.3 ka BP across the Midwest (Wang et al., 2012). Winds in central and northern Indiana switched from an easterly direction in the warm Bølling-Allerød period (12.9-14.7 ka BP) to the more modern westerly dominance in the colder Younger Dryas period (11.7-12.9 ka BP) (Kilibarda and Blockland, 2011). The nature of Midwestern hydroclimate during the last deglaciation is not currently settled. While the Bølling-Allerød is generally agreed to have been wet in the Midwest, some evidence points to a cool and wet Younger Dryas (Curry and Filippelli, 2010; Curry et al., 2013; Voelker et al., 2015) while others argue for a dry Younger Dryas (Dorale et al., 2010; Wang et al., 2013; Wang et al., 2012). Vegetation shifted rapidly from boreal forest into near-modern hardwood forest in Indiana after glacial retreat (Delcourt and Delcourt, 1984; Whitehead et al., 1982), but vegetation compositions unlike any modern plant community existed during the transitional period (Grimm and Jacobson Jr., 2003; Williams and Jackson, 2007).

Although the Holocene has a more stable climate in the American Midwest than the dramatic changes of the Pleistocene, there were deviations from modern climate norms across the region. These deviations include changes in mean storm track and oscillation phase dominance over the Holocene that have been detected and tracked through a variety of proxies (Lachniet et al., 2004; Liu et al., 2014a; Steinman et al., 2012; Trouet and Taylor, 2010). The Great Plains region was more arid than present

between 4.5 and 8.5 ka BP (Denniston et al., 1999c), and prairie expanded eastward during the generally warmer middle Holocene from 6000 to 3000 cal yr BP (Baker et al., 2002; King and Allen Jr, 1977; Nelson et al., 2006). The eastward expansion of drier conditions has typically been linked to increased Pacific air mass dominance, but this explanation may be too simple and require more complex climate changes (Shinker et al., 2006). Peaks in aridity in Missouri are noted during 2.6-3.4 and 1.0-1.2 ka BP (Denniston et al., 2007), and dune fields across the Great Plains became active at 3.0-4.0 and 0.7-1.0 ka BP (Forman et al., 2001; Hanson et al., 2010; Seifert et al., 2009). Cyclical dry events in North America related to ice-rafted debris peaks and Bond events have been proposed for the Holocene, but are not accepted by all (Springer et al., 2008; Viau et al., 2002; Viau et al., 2006). Pollen-based temperature reconstructions suggest warmer conditions in central North America from 750 to 450 cal yr BP and cooler conditions from 450 until 50 cal yr BP (Wahl et al., 2012). Modern records of climate and environment began with European-American settlement around 150 cal yr BP (1800 CE).

1.7 Research significance

Two-thirds of Indiana is farmland, and agriculture contributed an estimated $31.2 billion in direct sales value in 2012 with an additional $12.9 billion in related sales. Combined, all agriculture-related sales accounted for 5% of Indiana's gross domestic product and supported over 180,000 jobs. Rain-dependent grain and oilseed farming is the largest fraction of the agricultural economy, while forestry is also an important economic contributor, particularly in parts of southern Indiana ill-suited for commercial agriculture (IBRC, 2015). The increased risk of heat waves and summer drought in a future warmer climate (Pachauri and Reisinger, 2008; PCCRC, 2008) is a major concern for both agriculture and forestry in Indiana and the greater Midwest. The drought of 2012 affected nearly all of the American corn belt with all Midwestern states marking a top three warmest year and most marking a top-fifteen driest year (Fuchs et al., 2013). June through August were particularly warm and dry, with extreme and

exceptional drought developing over a large portion of the Midwest (Mallya et al., 2013). Indiana corn yields were 38% below pre-drought expectations, and crop insurance payouts were greater than $1 billion (Fuchs et al., 2013). A return to relatively-normal precipitation in the autumn and winter helped limit long-term effects of the drought, but a general increase in summer dryness and heat risk in future years will significantly stress the current agricultural systems and economy of Indiana. Substantial mature forest dieback is expected in the future as existing tree species become maladapted to a changing climate combined with a shift from forest to open savanna along the current prairie-forest border (Frelich and Reich, 2010). Economic and ecological services provided by forests will likely be reduced during the transitional period as the forest community realigns with a new climate.

Identifying and comprehending how the climate and environment of Indiana reacted to past climate changes can assist mitigation strategies developed for future climate change. Previously published paleoenvironmental data in Indiana are limited to a few tree ring records, fire histories, and pollen studies (Cole and Taylor, 1995; Guyette et al., 2003; Singer et al., 1996; Wang, 2013), but these records are generally short in timespan, relatively coarsely-resolved, and/or somewhat dated. Additionally, all formally-published records from Indiana are restricted to the Holocene. Published stalagmite-based records are rare in the eastern United States, and the only United States stalagmite data east of 90°W in the NOAA Paleoclimatology database is from Buckeye Creek Cave in West Virginia (Hardt et al., 2010; NOAA, 2015d; Springer et al., 2014; Springer et al., 2008). The caves involved in this dissertation research fill a void in the spatial coverage of stalagmite paleoclimate data, and the nearest other published stalagmite data come from caves 500 km away to both the west and east (Figure 2). Thus, the data from southern Indiana can aid in tracking past east-west precipitation and climate shifts that have occurred at continent-wide spatial scales

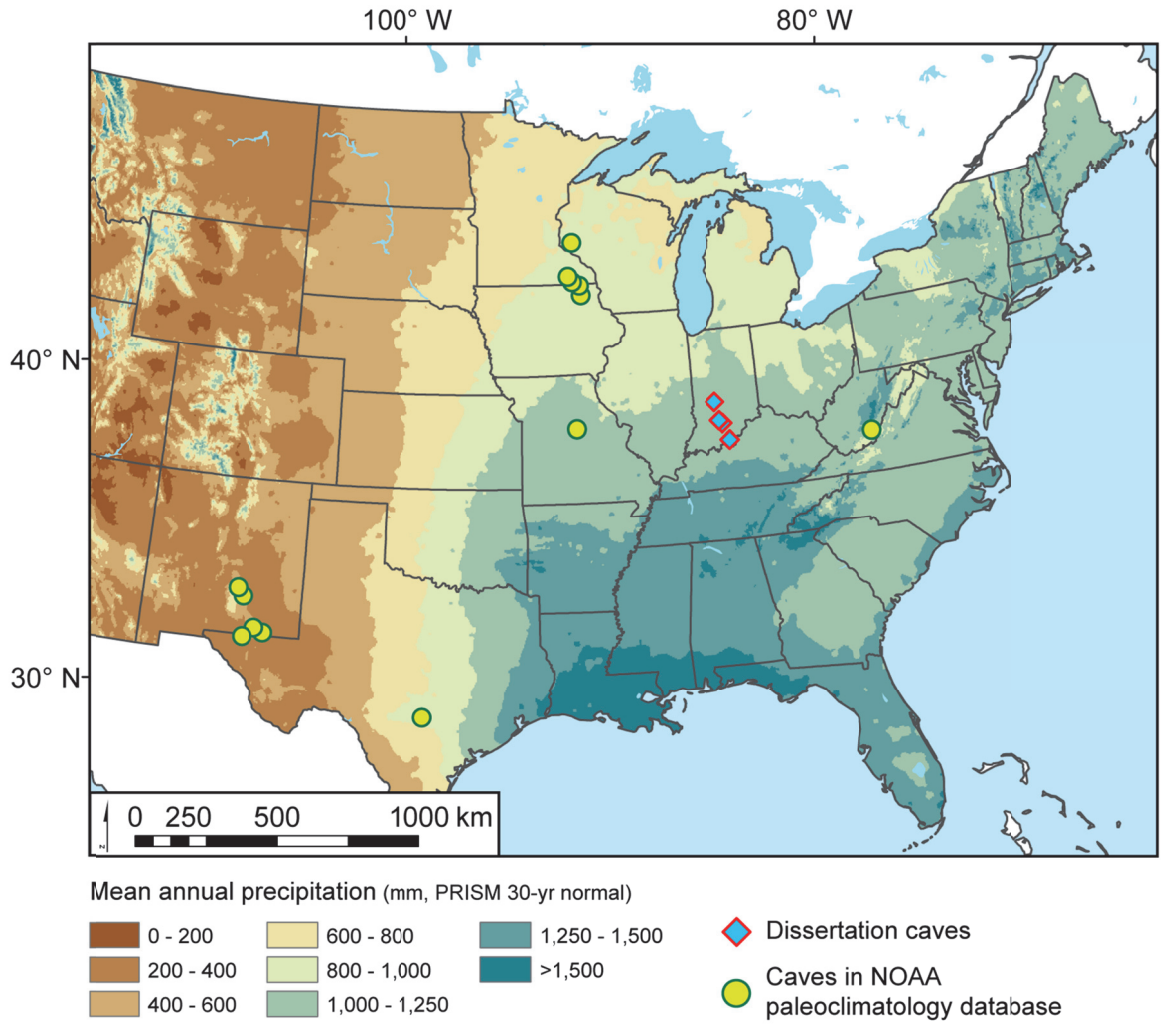

Figure 2. Caves sampled for this dissertation research (diamonds) relative to published cave data available online (circles; NOAA, 2013). Background shading reflects mean annual precipitation over the United States (PRISM, 2004).

The lack of paleoenvironmental data for Indiana requires predictions of future environmental changes to be based largely on modeling. This modeling is extremely important and useful, particularly for estimating climate changes for which there are no past analogs. However, such models may struggle to identify rapid climate change or short, intense climate events that are imbedded with an overall warmer climate. Thus, physical records of past environmental responses are important for both verifying model predictions and providing more nuanced detail. A better understanding of the atmospheric

drivers behind Midwestern climate change in the Pleistocene transition and Holocene will prove valuable in correctly modeling future climate change. While simply identifying past environmental changes is useful, applying the findings of paleoenvironmental research to modern day concerns requires a deeper understanding of the past climate-environment system. Joining modern day precipitation $\delta^{18}O$ climatology with the stalagmite paleoenvironmental records in this dissertation research allows our understanding of modern climate to be transferred back to periods well-beyond the instrumental record. Lessons learned about environmental responses to past climate changes in southern Indiana can be useful when preparing for future climate change mitigation.

This multi-faceted research transforms southern Indiana from a void in our current paleoclimate understanding to a source of robust information, and the conclusions produce a greater understanding of climate variability and processes in a region with industries and economies sensitive to climate fluctuations. Future climate predictions and mitigation require a firm grasp on regional climate forcers, with past climate changes offering the best insight into relevant processes and trends. The research detailed in this dissertation is not limited in importance to the study region, as the environmental changes identified are linked to regional and global climate. The computer code used for data management, statistical analysis, and figure creation (Appendix 6) is easily adaptable to both updated data supplemental to this research and to new datasets at other locations. As a whole, this research offers not only a glimpse at the history of Earth, but also a preview into its possible future.

CHAPTER TWO:

RELATIONSHIPS BETWEEN CLIMATE AND PRECIPITATION OXYGEN ISOTOPE VARIABILITY IN THE EASTERN AND CENTRAL UNITED STATES USING A WEEKLY CLIMATE AND ISOTOPE DATABASE

2.1 Introduction

The understanding of spatial variations in precipitation stable isotope values has advanced considerably since the foundational papers published on the subject in the 1960s (Craig, 1961a; Dansgaard, 1964). New precipitation isotope data have improved spatial coverage beyond the original Global Network for Isotopes in Precipitation (GNIP) dataset (IAEA/WMO, 2016; Rozanski et al., 1993), and this higher spatial density of records improves documentation of small-scale isotopic variations. The United States Network for Isotopes in Precipitation (USNIP) consists of 75 stations across the United States with weekly-resolved precipitation stable oxygen and hydrogen isotope ratios ($\delta^{18}O$ and δD, respectively) (Welker, 2000). This database has been used repeatedly for North American precipitation isotope studies where GNIP lacks resolution and coverage (for example, Liu et al., 2010; Vachon et al., 2010; Welker, 2012; this study). In this dissertation, references to 'weekly data' refer to data that is either sampled at weekly resolution (e.g., isotope data) or aggregated to a weekly resolution (e.g., climate data) and references to 'weekly relationships' refer to relationships calculated from weekly-resolved data.

To better understand the relationship between $\delta^{18}O$ and climate, a precipitation stable isotope and climate database was created for the eastern and central United States from weekly USNIP isotope data and daily climate data from the Global Historical Climatology Network (GHCN). The focus of precipitation stable isotope analysis in this chapter is on $\delta^{18}O$ because δD is not preserved as a paleoclimate proxy in stalagmite calcium carbonate; additionally, the relationship between $\delta^{18}O$ and δD

data are strongly linear, and thus most conclusions about $\delta^{18}O$ variability can be applied to δD as well. The use of daily climate data weighted by precipitation amount approximates precipitation event climatology in an attempt to more accurately quantify the relationships between precipitation $\delta^{18}O$ values and climate variables. The potential effect of using precipitation day climatology rather than standard time-averaged climatology has been previously described (Kohn and Welker, 2005), but not yet examined at the broad spatial scale detailed here. Results from this new database and analysis can be compared with previous studies to determine if precipitation day climatology is better than time-averaged climatology for quantifying the relationships between $\delta^{18}O$ and climate variables.

2.2 Objectives

- Calculate and examine linear regressions for the relationships between precipitation $\delta^{18}O$ and both precipitation day temperature (PDt) and amount (PDa) using the new weekly dataset for 25 sites in the eastern and central United States.
- Describe the spatial trends in the relationship and regression values between precipitation $\delta^{18}O$ and both PDt and PDa.
- Determine how the documented relationships based on PDt data differ from previous research findings that use time-averaged temperature data.

2.3 Background

2.3.1 History of precipitation stable isotope studies

Initial studies into the spatial distribution of $\delta^{18}O$ and δD in precipitation began in the mid-20th century with the development of mass spectrometry, and the potential impact for paleoclimate research was quickly recognized (Craig, 1961a; Dansgaard, 1964). The $\delta^{18}O$ term refers to the ratio of

^{18}O to ^{16}O, defined as: $\delta^{18}O = (^{18}O / ^{16}O)_{sample} / (^{18}O / ^{16}O)_{standard} \times 1000$. Stable oxygen isotope ratio values are reported relative to a standard (Craig, 1961b; Gonfiantini, 1978), and all water stable isotopes in this dissertation are reported versus Vienna Standard Mean Ocean Water (V-SMOW) while all calcium carbonate stable isotopes are reported versus Vienna Pee Dee Belemnite (V-PDB). Globally-applicable relationships between precipitation $\delta^{18}O$ and environmental variables such as air temperature, latitude, and altitude were later interpreted through the Rayleigh condensation conceptual model, where isotopic equilibrium and kinetic fractionation alter the mean $\delta^{18}O$ value of a water vapor air parcel depending upon the temperature and humidity at phase change (Clark and Fritz, 1997; Dansgaard, 1964; Gat, 1996; Gonfiantini, 1986; Rozanski et al., 1993). As water vapor moves away from its moisture source, cooling promotes vapor condensation and precipitation that preferentially removes ^{18}O over ^{16}O; as a result, the $\delta^{18}O$ of a water vapor parcel will steadily decrease as it cools and loses moisture to precipitation (Alley and Cuffey, 2001; Dansgaard, 1964; Lachniet, 2009). This drop in $\delta^{18}O$ values as water vapor cools, known as Rayleigh distillation, is the foundation of the numerous spatial effects described for precipitation $\delta^{18}O$ variations.

Precipitation oxygen isoscapes in the eastern United States are largely a function of latitude and continentality (i.e., distance from the major water vapor sources of the Atlantic and Gulf of Mexico) (Rozanski et al., 1993; Vachon et al., 2010a; Welker, 2000). The continental effect is most pronounced in winter due to sharper temperature contrasts and is greatly subdued in summer due to more homogenous temperatures and greater evapotranspiration (Aemisegger et al., 2014; Gat and Matsui, 1991; Peixóto and Oort, 1983; Vachon et al., 2010a; Winnick et al., 2014). Monthly-resolved precipitation $\delta^{18}O$ values are primarily controlled by air temperature for the eastern United States, with the highest correlations and slopes observed inland and northward. However, this relationship between precipitation $\delta^{18}O$ and air temperature is very weak or non-existent in southeastern states and along the coasts, perhaps due to greater local sensitivity to changing conditions in the nearby oceanic moisture

source (Vachon et al., 2010a). Although the Rayleigh model states that precipitation $\delta^{18}O$ is correlated to the condensation temperature in the clouds producing precipitation, surface air temperature has typically been used as a substitute (Rozanski et al., 1993). This is due to the difficulty of accurately measuring or estimating actual condensation temperatures and the fact that regressions with surface air temperature are much more useful for practical application of precipitation $\delta^{18}O$ research. Additionally, as rain falls it tends to isotopically equilibrate with moisture along its path and approaches the $\delta^{18}O$ value expected from the surface air temperature (Rozanski et al., 1993). Frozen precipitation, however, does not equilibrate and will produce lower than expected $\delta^{18}O$ values relative to surface air temperature (Jouzel and Merlivat, 1984). Additionally, the temperature effect can differ if air temperatures are measured only during precipitation events rather than averaged across all days (Kohn and Welker, 2005). Although the amount effect (where greater precipitation amounts are correlated with lower $\delta^{18}O$ values) is dominant in many tropical locations (Dansgaard, 1964), it is not a significant force on monthly $\delta^{18}O$ variations in the eastern United States with the exception of south Florida (Vachon et al., 2010a).

Despite the strong relationship between precipitation $\delta^{18}O$ and air temperature across the eastern United States, air temperature rarely explains more than 60% of the variability in $\delta^{18}O$ (Welker, 2012). Changes in moisture source, mean storm track, and global climate teleconnections and oscillations have all been found to significantly alter precipitation $\delta^{18}O$ values away from the values predicted by temperature alone (e.g., Berkelhammer and Stott, 2008; Birks and Edwards, 2009; Burnett et al., 2004; Liu et al., 2010; Welker, 2012). Before examining the potential role on precipitation $\delta^{18}O$ values of these other climate variables, the temperature and amount effects must be quantified.

2.3.2 Modern climatology

The eastern United States has a humid continental or subtropical climate grading toward semiarid in the west. Precipitation is typically 500-1500 mm per year with lower amounts found to the

west and greatest amounts at high elevations in the southeast. Precipitation seasonality varies from summer-skewed in the north and west to winter-skewed in the south, although no portion of the region has a pronounced dry season with the exception of south Florida. Mean annual temperatures decrease northward from 20 to 5˚C (NOAA, 2015b). The Gulf of Mexico is the predominant moisture source for most of the region, with the Atlantic an important moisture contributor east of the Appalachian Mountains. Pacific and Arctic moisture is increasingly influential toward the northern and western boundaries (Sjostrom and Welker, 2009), but Pacific- and Arctic-sourced air masses hold comparatively little precipitable water upon reaching the study region. Thus, Gulf of Mexico moisture remains the chief source for precipitation even in the semiarid Great Plains (Harvey and Welker, 2000).

The commonly-utilized GNIP database contains monthly-resolved $\delta^{18}O$ and surface air temperature data. GNIP temperature data is simply an un-weighted average of all daily temperatures in the month regardless of precipitation amount or occurrence. Quality GNIP data for the United States is limited to less than ten sites with large spatial gaps in coverage (Rozanski et al., 1993). Although the weekly USNIP database has much better spatial coverage, previous studies using USNIP data to examine large spatial trends typically aggregated data into monthly- or seasonally-weighted averages to compare with monthly or seasonal climate data (e.g., Liu et al., 2014). Examining data at the original weekly resolution may result in more accurate and/or precise relationship estimates.

2.3.3 Database improvements

The database created in this study is an improvement over the GNIP database for determining specific climate controls on $\delta^{18}O$ variability. Weather in the central and eastern United States can change dramatically week to week in response to changing air masses and the passage of extratropical cyclones (ETCs), and the weekly USNIP dataset can capture shorter-term weather fluctuations that are muted in a monthly aggregation. In addition, short-term climate teleconnections such as the North Atlantic Oscillation and Pacific-North American teleconnection are better captured at weekly rather than

monthly resolution (NOAA, 2016). This study does not approach the temporal resolution needed for the study of daily precipitation events or for studies where the exact time of precipitation is known (e.g., Wu et al., 2015). However, daily precipitation $\delta^{18}O$ records rarely extend longer than a year and are faced with serious logistical and financial challenges to expand beyond single site studies. The weekly database detailed here can serve as a link between studies using daily or precipitation event-level data and studies using monthly, seasonal, or annual data.

The dataset only uses meteorological data from days when precipitation was recorded, unlike the majority of other studies on spatial trends of precipitation $\delta^{18}O$, which use climatic means calculated from all days in the temporal unit chosen. Although the daily meteorological data used here have been aggregated to weekly resolution, only days with measurable precipitation are included in the aggregation. Additionally, the aggregated meteorological data are weighted by the fraction of the total precipitation within the aggregate; thus, days with heavy precipitation that dominate an aggregated $\delta^{18}O$ signal have equally-dominant meteorological data. Even when this new dataset is further aggregated to a monthly resolution comparable to GNIP, the aggregated monthly meteorological data in this project's dataset are much more reflective of conditions that occur during the actual precipitation events than the typical monthly meteorological data. As such, it is proposed that this database will produce more accurate relationships and stronger correlations between $\delta^{18}O$ and meteorological variables because the non-precipitation day climate 'noise' has been removed.

2.4 Methods

2.4.1 USNIP data

Precipitation stable oxygen isotope data for 25 sites were retrieved from the USNIP database. These sites (Table 1, Figure 3) are located in the eastern and central United States and provide weekly precipitation stable isotope data for the period 1989 to 2006. The sites were chosen to provide a broad

spatial context for the southern Indiana cave study region. A defined study region containing the USNIP sampling sites used in this analysis was created for isotopic and climate data interpolation. This region is bounded by the extremes in USNIP site location and extends from North Dakota and Vermont south to central Georgia and southwestern New Mexico. Coastal sites were avoided due to the previously noted greater sensitivity of such sites to local moisture source conditions that might interfere with the more continental relationships being examined in this study (Vachon et al., 2010a). The sites in the study region are only a subset of the entire USNIP database; however, the chosen sites broadly share a similar climatology focused on southern Indiana.

The USNIP precipitation samples were originally collected for the National Atmospheric Deposition Program (NADP), frozen, and later analyzed for stable isotopes (Welker, 2000). The data are not continuous inclusive of all precipitation events from 1989 to 2006, although precipitation data for some years (e.g., 1992, 1993, and 2004) are largely complete for most sites. Although discontinuous, the available data are well-distributed throughout the year and capture the natural trends in precipitation seasonality and variability. Despite the missing data, the dataset in this study still contains data from over 6200 precipitation samples (~250 samples per site) and is a substantial improvement over GNIP data based upon the spatial coverage and total number of isotope samples.

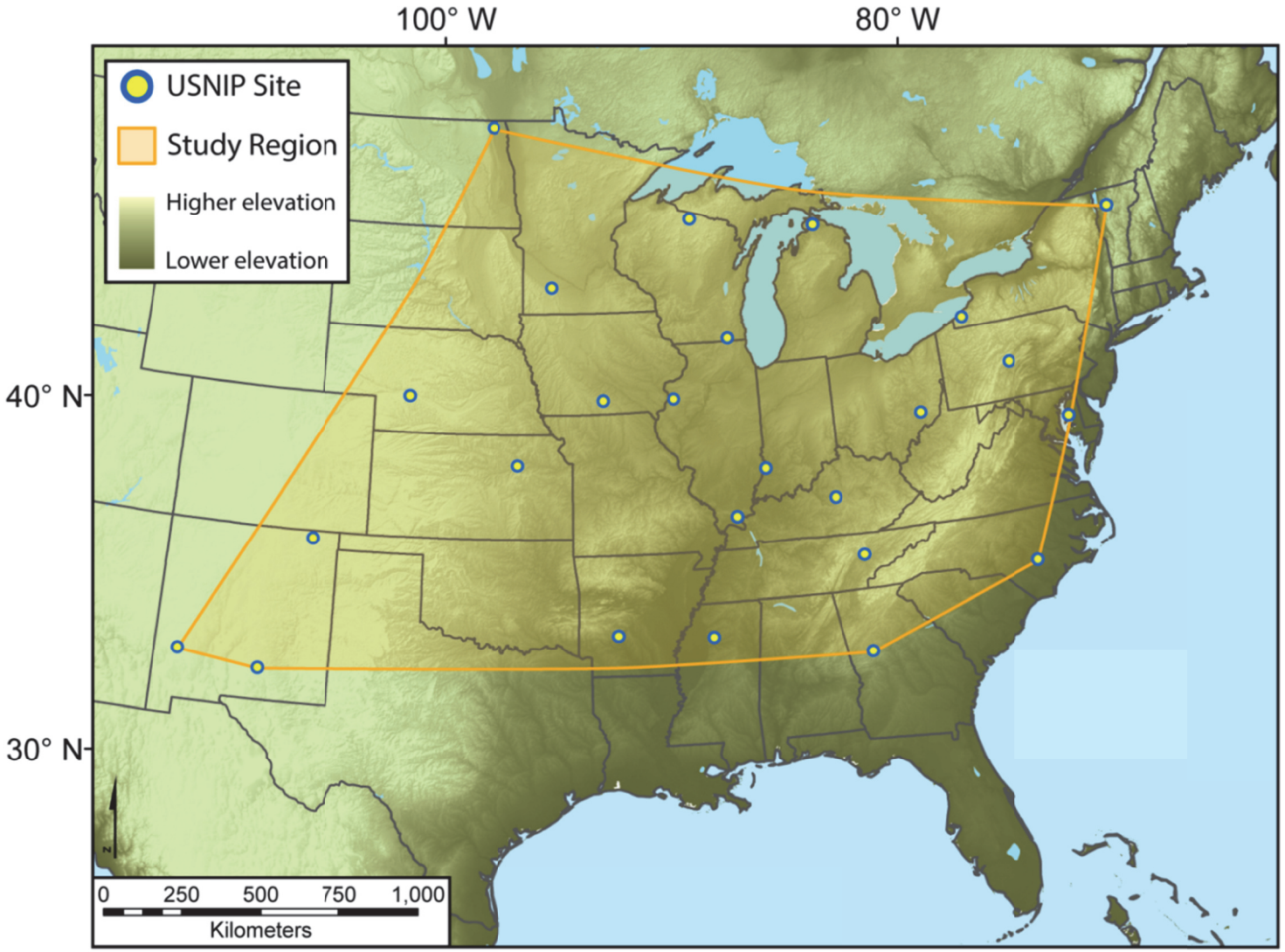

Figure 3. Locations of USNIP sites used in this analysis and the study region bounds for interpolated statistics (shaded orange) with elevation indicated by background shading.

Table 1. USNIP sites and GHCN stations used in the study of modern precipitation $\delta^{18}O$ values. USNIP precipitation samples were taken at NADP stations listed. USNIP sites were matched to the nearest GHCN station with quality data; these GHCN station IDs and names are listed with their corresponding NADP station.

USNIP ID	*NADP Station Name*	*Latitude (°)*	*Longitude (°)*	*Elevation (m)*	*GHCN Station ID*	*GHCN Station Name*
AR03	Caddo Valley	34.1795	-93.0992	71	USC00030220	Arkadelphia
GA41	Georgia Station	33.1805	-84.4103	267	USC00096335	Newnan
IA23	McNay Research Center	40.9631	-93.3925	320	USC00136316	Osceola
IL63	Dixon Springs Agricultural Center	37.4356	-88.6719	161	USC00112353	Dixon Springs
IL78	Monmouth	40.9333	-90.7231	229	USC00115768	Monmouth
IN22	Southwest Purdue Agricultural Center	38.7408	-87.4855	134	USC00129113	Vincennes 5 NE
KS31	Konza Prairie	39.1022	-96.6092	350	USC00144972	Manhattan
KY03	Mackville	37.7047	-85.0489	293	USC00152040	Danville
MD13	Wye	38.9131	-76.1525	6	USC00187806	Royal Oak 2 SSW
MI09	Douglas Lake	45.5608	-84.6783	238	USW00014841	Pellston Regional Airport
MN27	Lamberton	44.2370	-95.3011	367	USC00214546	Lamberton SW
MS30	Coffeeville	34.0025	-89.7993	134	USC00223645	Grenada
NC35	Clinton Crops Research Station	35.0258	-78.2783	41	USC00311881	Clinton 2 NE
ND08	Icelandic State Park	48.7820	-97.7546	306	USC00321435	Cavalier 7 NW
NE99	North Platte Experiment Station	41.0592	-100.7464	919	USC00256075	North Platte Experimental
NM01	Gila Cliff Dwellings National Monument	33.2203	-108.2347	1772	USC00293530	Gila Hot Springs National Monument
NM08	Mayhill	32.9096	-105.4710	2022	USC00292865	Elk National Monument
NM12	Capulin Volcano National Monument	36.7790	-103.9810	2190	USC00293706	Grenville National Monument
NY10	Chautauqua	42.2994	-79.3964	488	USC00304207	Jamestown
OH49	Caldwell	39.7928	-81.5311	276	USC00331197	Cambridge
PA15	Penn State	40.7883	-77.9458	393	USC00368449	State College
TN00	Walker Branch Watershed	35.9614	-84.2872	341	USC00405158	Lenoir City
VT99	Underhill	44.5283	-72.8684	399	USC00432769	Enosburg Falls
WI36	Trout Lake	46.0512	-89.6541	509	USC00475516	Minocqua
WI99	Lake Geneva	42.5792	-88.5006	288	USC00471205	Burlington

2.4.2 Climate data retrieval and creation of an isotope-climate database

Daily surface temperature (maximum and minimum) and precipitation data were downloaded from GHCN stations located within 10 km of each USNIP site (Table 1) (NOAA, 2015c). Selected GHCN stations had reliable data and a similar elevation to corresponding USNIP sites. Mean daily surface temperatures were calculated from reported maximum and minimum daily temperatures. When necessary, missing climate data from the GHCN stations were filled using data from the second-closest quality GHCN station. Meteorological data from each GHCN station dataset were joined with isotope data from the associated USNIP site (Figure 4). For each week with USNIP data, the corresponding week of daily climate data were aggregated into a single weekly value.

Weekly temperature values were produced by weighting the mean of daily temperatures by the fraction of weekly precipitation that fell each day, as expressed by:

$T_{week} = \sum_{i=1\ n=7} (T_i * P_i / P_{week})$ where T=daily temperature and P= daily precipitation amount

Thus, temperatures for days with no precipitation were excluded in the weekly temperature aggregation, and days with heavier precipitation contributed more to the weekly temperature aggregation. This weighting produces a surface temperature reflective of the temperature during precipitation events rather than mean air temperature; thus the weighted temperature data is referred to 'precipitation day temperature' in this study. Precipitation amount is independently measured at both the USNIP and GHCN sites, allowing comparison of the same variable in the two datasets. Correlation between USNIP and GHCN weekly precipitation amounts was very high ($r > +0.84$) for most sites, and most deviations appear attributable to localized coverage by summer convective precipitation. Weeks with large differences in precipitation amount (where ln[USNIP precipitation amount / GHCN precipitation amount] > 1) were excluded from further analysis. The USNIP isotope data and aggregated climate data were combined into a single database with weekly resolution.

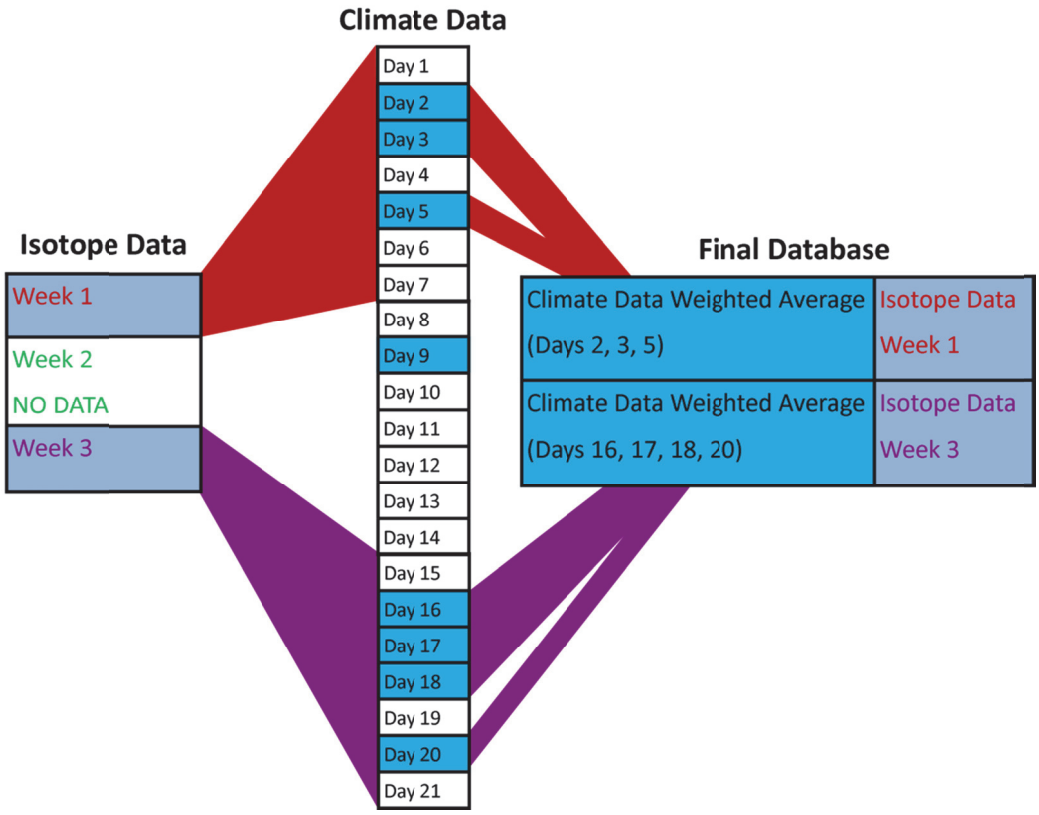

Figure 4. Graphic showing how isotopic data is combined with climate data to make the joint isotope-climate database. Blue boxes in the climate data indicate days with precipitation. For weeks with isotope data, the daily climate data on precipitation days are weight-averaged into weekly climate data. Climate data on non-precipitation days (e.g., day 1, day 4, etc.) or during weeks with no corresponding isotope data (days 8-14 here) are not included in the final database.

2.4.3 Statistical calculations

Correlations between $\delta^{18}O$ and maximum, minimum, and mean PDt were calculated for each site, but correlations were not significantly different. Thus, mean PDt was chosen as the representative temperature variable. Correlations between $\delta^{18}O$ and PDa (subjected to a logarithmic nonlinear transformation for all statistical work) were also calculated for each site. Standard deviations of $\delta^{18}O$ were calculated for intervals of 10°C from -20°C to 30°C at each site to examine the relationship between temperature and $\delta^{18}O$ variability.

Linear regression was performed for $\delta^{18}O$ versus both PDt and PDa. Plots of the relationships and regressions were examined for deviations away from a linear relationship and for evidence of climate influences beyond PDt and PDa. Values for slope, y-intercept, and fit (r^2) were interpolated across the study region by ordinary kriging using a spherical semivariogram model with an output cell size of 0.01 decimal degrees. Interpolated values were mapped for visual analysis of spatial trends and distributions.

2.5 Results

2.5.1 Relationships between $\delta^{18}O$ and climate variables

Correlations between $\delta^{18}O$ and PDt vary in strength across the 25 study sites while correlations between $\delta^{18}O$ and PDa are consistently low (Table 2). Data and figures for individual sites can be found in Appendix 5. Similarly, linear regression produced $\delta^{18}O$ vs. PDt relationships with a wide range in strength ($0.08 < r^2 < 0.65$), while the $\delta^{18}O$ vs. PDa regression produced very weak ($r^2 < 0.06$) relationships for all sites (Table 3). P-values are not a robust indicator of actual scientific significance in this analysis because the large sample sizes produce p-values < 0.05 even for near-zero correlations and very weak relationships. Thus, scientific importance of results was largely determined by the coefficient of determination (r^2).

Table 2. Correlations between precipitation $\delta^{18}O$ and PDt and between $\delta^{18}O$ and PDa for sites in this study.

		Correlation	
USNIP Site	***Number of Weeks***	***$\delta^{18}O$ & PDt***	***$\delta^{18}O$ & PDa***
AR03	274	0.46	-0.04
GA41	234	0.28	-0.26
IA23	211	0.72	0.18
IL63	190	0.51	0.02
IL78	240	0.68	0.18
IN22	260	0.58	0.08
KS31	265	0.71	0.15
KY03	201	0.53	-0.09
MD13	280	0.61	0.01
MI09	280	0.80	0.11
MN27	286	0.78	0.22
MS30	279	0.51	-0.21
NC35	222	0.43	-0.20
ND08	233	0.77	0.22
NE99	213	0.72	0.00
NM01	175	0.65	-0.16
NM08	173	0.70	0.08
NM12	170	0.78	0.06
NY10	296	0.74	0.04
OH49	249	0.67	-0.03
PA15	50	0.61	0.10
TN00	213	0.58	-0.13
VT99	399	0.67	0.14
WI36	411	0.75	0.21
WI99	373	0.72	0.14
Mean		0.64	0.03
Maximum		0.80	0.22
Minimum		0.28	-0.26

Table 3. Regression mean, maximum, and minimum values for the 25 study sites.

	Slope			*y-Intercept*			r^2		
Regression	***Mean***	***Max***	***Min***	***Mean***	***Max***	***Min***	***Mean***	***Max***	***Min***
$\delta^{18}O$ vs. PDt	0.32	0.51	0.12	-11.72	-6.50	-15.99	0.42	0.65	0.08
$\delta^{18}O$ vs. PDa	0.17	1.57	-1.06	-8.55	-2.15	-15.88	0.02	0.07	0.02

2.5.2 Nonlinear $\delta^{18}O$ vs. PDt trends

The relationship between $\delta^{18}O$ and PDt at the 25 study sites is best described as linear. However, precipitation events when the PDt is below freezing typically plot along a steeper slope while the relationship also tends to flatten with higher temperature, generally greater than 10°C (Figure 5). These deviations from linearity are known from previous studies (e.g., Jouzel and Merlivat, 1984 and Rozanski et al., 1993), and their existence in this dataset (where only precipitation-day climate data are included) suggests that the deviations are not an artifact of climate data aggregation. Attempts to describe the relationship differently (e.g., with a quadratic or logarithmic fit) do not significantly improve the correlation or offer a better fit. Thus, a linear relationship was adopted as it best describes the relationship at moderate air temperatures. Only two sites (MI09 and NY10) have a statistically significant difference in slope when comparing frozen and liquid precipitation events. These two sites are in the Great Lakes snow belt, and the observed larger slope difference may be due to “lake effect” snowfall, which has markedly low $\delta^{18}O$ values (Burnett et al., 2004).

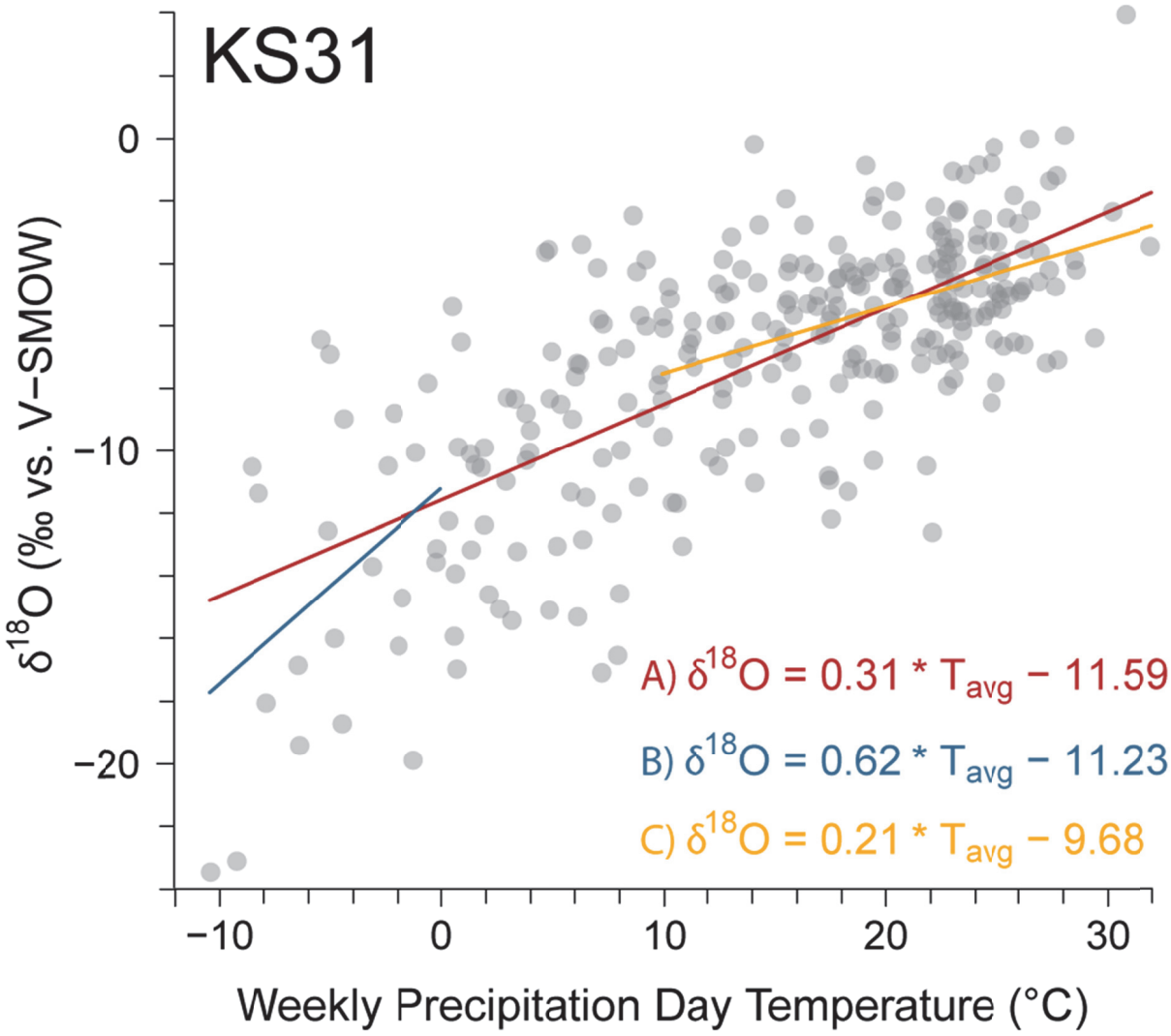

Figure 5. An example from site KS31 of the changes to the $\delta^{18}O$ vs. PDt relationship toward temperature extremes. Three regression trends and equations are shown: A) all data (red), B) PDt <0°C (blue), and C) PDt >10°C (yellow).

2.5.3 Variability in $\delta^{18}O$ values related to PDt

At each site, the variability of $\delta^{18}O$ values decreases as PDt increases (Table 4). The mean standard deviation of $\delta^{18}O$ values for precipitation events on days with a mean temperature between 20 and 30˚C is 2.30‰, and at temperatures from 10 to 20˚C it is 2.73‰. However, the standard deviation

of $\delta^{18}O$ values is significantly higher at temperatures from 0 to 10°C and -10 to 0°C, being 3.79‰ and 4.42‰, respectively. Only four sites have enough samples (n >= 10) to chart in the -20 to -10°C interval. Three sites continue the trend of increasing variability with decreasing temperature, but site MI09 has a standard deviation of only 2.08‰ for the -20 to -10°C range. This standard deviation is the lowest seen in any MI09 temperature interval and violates the clear trend of increasing variability with decreasing temperature otherwise present at MI09. Excluding the MI09 anomaly, the three remaining sites have an average standard deviation of 4.99‰ for the -20 to -10°C interval. Thus, with an occasional exception, the trend of increasing variability in $\delta^{18}O$ values with decreasing surface temperature is observed across the entire study region.

Spatial variations in temperature across sites are also accompanied by changes in $\delta^{18}O$ variability. Sites that have colder mean temperatures have greater overall $\delta^{18}O$ variability (Figure 6); however, this relationship is expected since sites with colder mean temperatures have greater seasonal temperature ranges and thus greater annual variability in $\delta^{18}O$ values. The effect of greater seasonality can be removed by examining the standard deviation of the residuals from the $\delta^{18}O$ vs. PDt regression. When this is done, colder sites still have a greater $\delta^{18}O$ variability than warmer sites for a given temperature (Figure 7), suggesting the potential range of precipitation $\delta^{18}O$ truly is larger at a given temperature for colder areas of the study region than for warmer areas.

Table 4. Site and mean values of the standard deviation of $\delta^{18}O$ for different temperatures.*

USNIP Site	-20°C to -10°C	-10°C to 0°C	0°C to 10°C	10°C to 20°C	20°C to 30°C
AR03	--	--	3.21	2.12	1.94
GA41	--	--	2.67	2.74	2.61
IA23	--	4.09	3.19	2.76	2.12
IL63	--	--	4.11	2.38	2.90
IL78	--	5.07	3.58	2.82	2.13
IN22	--	5.05	3.57	2.57	2.10
KS31	--	4.59	3.68	2.69	1.96
KY03	--	--	3.96	3.07	2.30
MD13	--	5.00	3.48	1.95	1.81
MI09	*2.08*	4.24	3.93	2.81	2.09
MN27	--	3.76	3.94	2.40	2.40
MS30	--	--	3.50	2.01	2.15
NC35	--	--	3.66	2.45	1.85
ND08	5.16	3.86	4.82	3.23	2.41
NE99	--	3.24	4.05	2.78	2.22
NM01	--	--	5.07	3.60	3.33
NM08	--	4.30	3.94	3.12	2.61
NM12	--	3.51	4.25	3.29	3.03
NY10	--	3.66	3.45	2.92	1.94
OH49	--	6.18	3.64	3.00	2.26
PA15	--	--	3.23	3.02	2.40
TN00	--	--	3.61	2.31	2.21
VT99	5.01	4.49	4.15	3.19	2.46
WI36	4.81	4.86	4.23	2.48	2.29
WI99	--	4.76	3.75	2.54	2.03
Mean	***4.99***	***4.42***	***3.79***	***2.73***	***2.30***

* Values are only presented for sites with 10 or more samples that fall in the temperature range. Italicized values are considered anomalous.

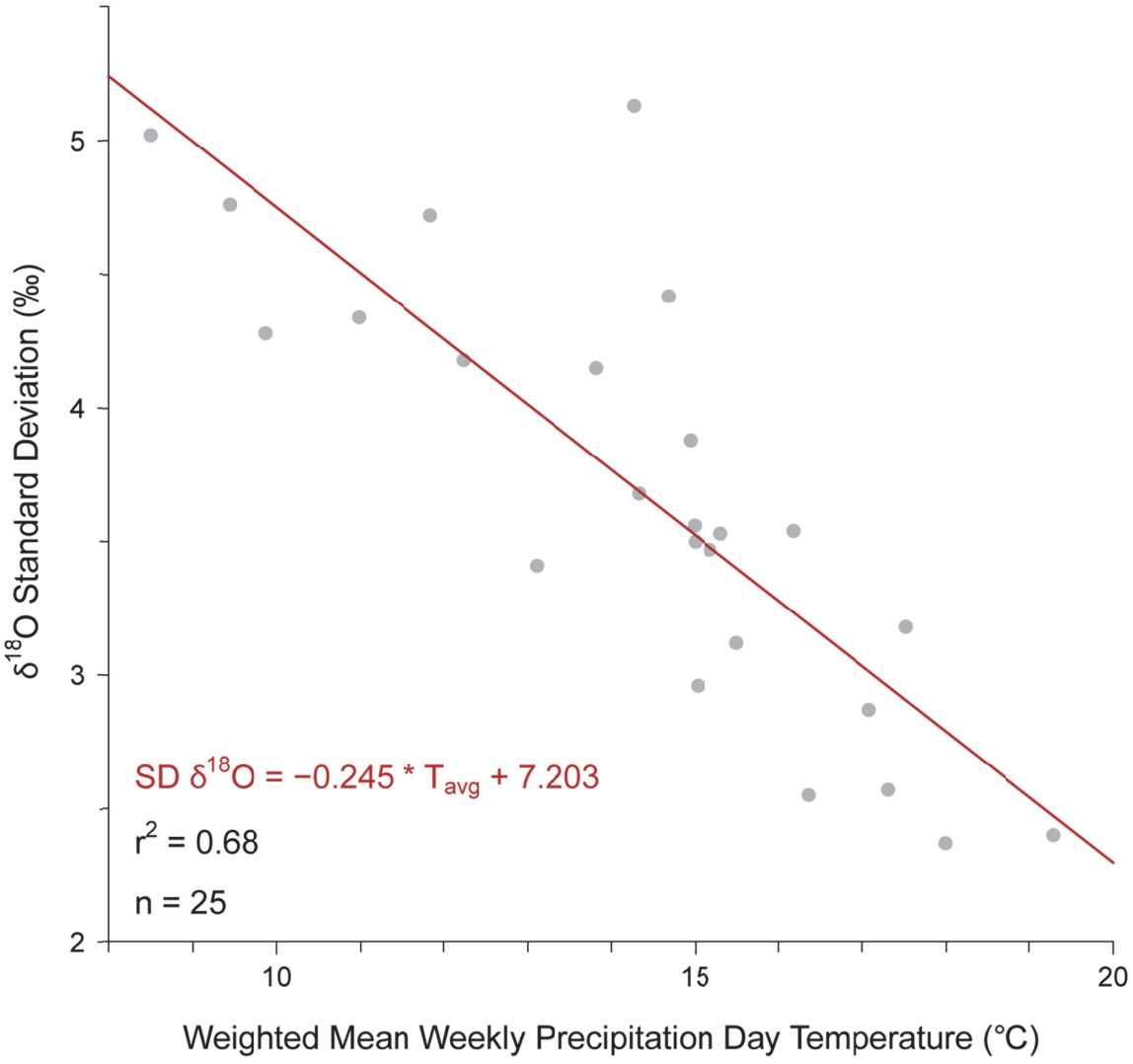

Figure 6. Standard deviation of precipitation $\delta^{18}O$ plotted against the weighted mean PDt for USNIP sites.

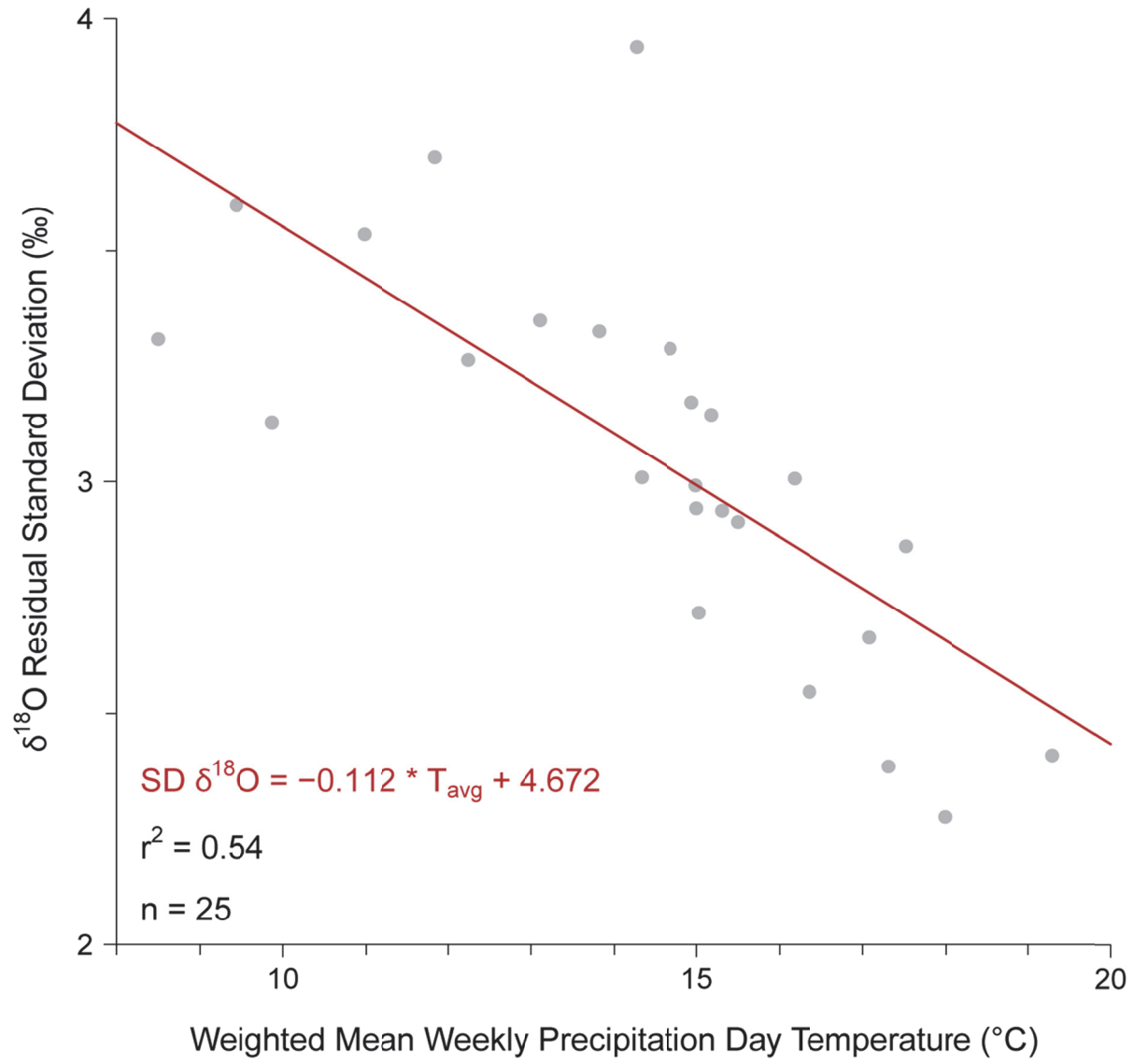

Figure 7. Standard deviation of precipitation $\delta^{18}O$ vs. PDt residuals plotted against the weighted mean PDt for USNIP sites.

2.5.5 Spatial trends between $\delta^{18}O$ and meteorological variables

The slope, y-intercept, and r^2 from the $\delta^{18}O$ vs. PDt regression vary along a northwest-southeast axis in a similar pattern to that described in Vachon et al. (2010a). The slope and y-intercept of the relationship between $\delta^{18}O$ and PDt varies spatially (Figure 8b, 9c). All sites have a positive slope (mean

slope = 0.32‰/°C), but this increases to the north and west. This slope spatial pattern is very similar to the pattern seen with r^2, but the absolute maximum slope value is located in New Mexico rather than the upper Midwest. The y-intercepts show an inverse relationship with slope values, with highest values in the southeast and lowest values in the north and west. Areas north of the Ohio River and in the Great Plains have higher r^2 values with maximum r^2 values in Minnesota and Michigan, while regions to the southeast have much lower r^2 values (Figure 8c). This spatial distribution corresponds to the regional climate and $\delta^{18}O$ seasonality: regions with moderate to strong relationships between $\delta^{18}O$ and PDt also have greater annual variation in air temperature and $\delta^{18}O$ values. In general, sites with higher slopes and lower y-intercepts have higher r^2.

All sites have a very weak or no relationship (all $r^2 < 0.07$) between precipitation $\delta^{18}O$ values and PDa (Figure 8f). As expected with such low correlations, regression line slopes vary greatly between sites and have a mean slope value near zero (Table 2). However, a spatial trend is evident in the $\delta^{18}O$ vs. PDa slopes and y-intercepts despite the weak relationship. Positive slopes are present in the Upper Midwest while slopes grade to negative in the southeast. The y-intercept values are lowest in the north and highest in the southeast. The spatial pattern of y-intercept values roughly parallels mean precipitation $\delta^{18}O$ value and is probably due to the lack of a strong relationship fit.

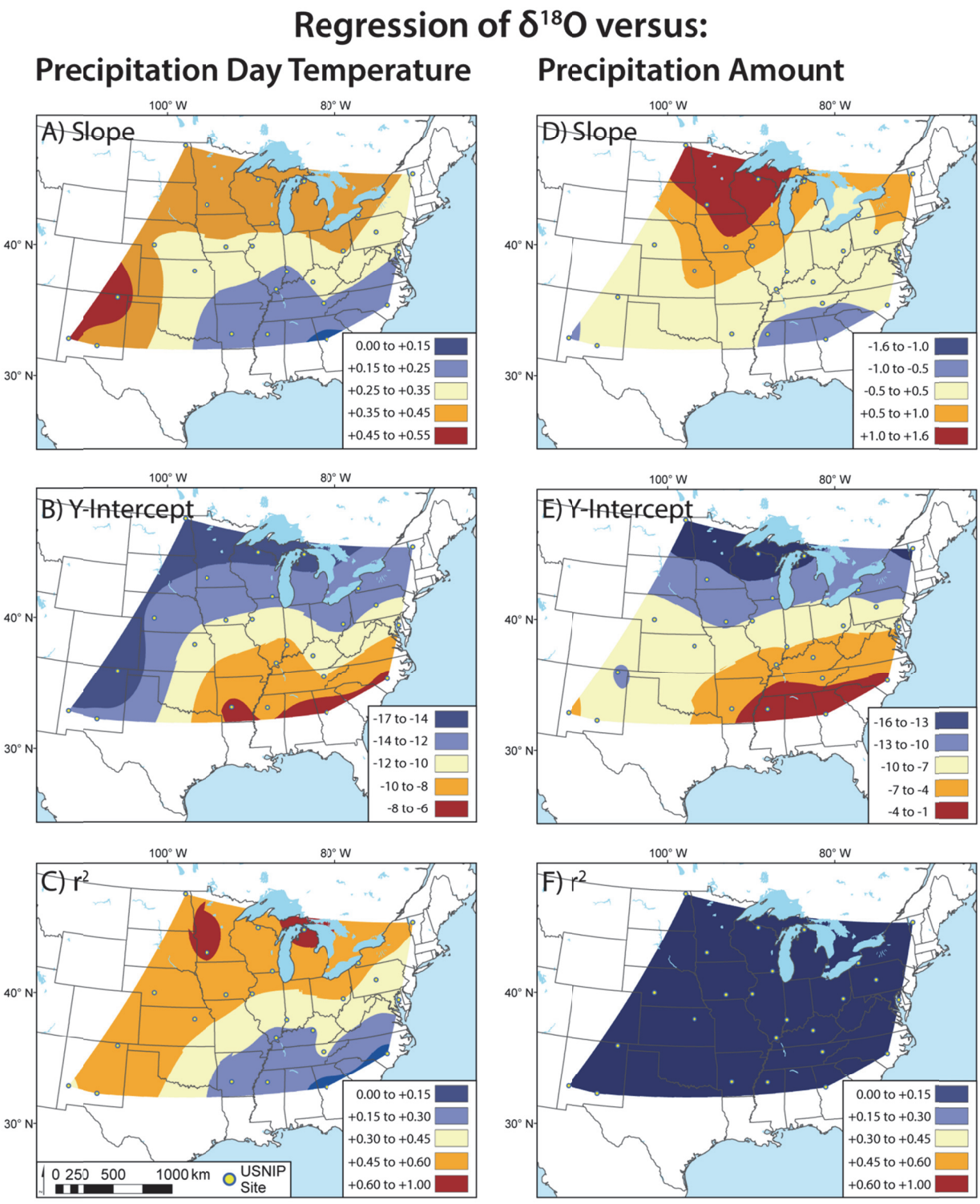

Figure 8. Spatial interpretations of regression slope, y-intercept, and r^2 values for $\delta^{18}O$ vs. PDt (A, B, C) and $\delta^{18}O$ vs. PDa (D, E, F). The exact values of each color are different between maps, except the color values for both r^2 maps are the same (C, F) to aid comparison of regression strength.

2.6 Discussion

2.6.1 Individual site relationships

The decrease in the slope of the precipitation $\delta^{18}O$ vs. PDt relationship at higher temperatures found at nearly all study sites may be the result of increased moisture recycling during warmer conditions. Moisture recycling decreases the rain -out effect by re-supplying water vapor with relatively high $\delta^{18}O$ values from evapotranspiration (ET) (Gat and Matsui, 1991; Peixóto and Oort, 1983; Worden et al., 2007). Since ET increases at higher temperature, moisture recycling is more effective during warmer conditions (Aemisegger et al., 2014). A site with no moisture recycling effect would have a maximum $\delta^{18}O$ value when the site temperature equaled the temperature at the moisture source and $\delta^{18}O$ values would decrease linearly with decreasing temperature due to Rayleigh distillation. However, moisture recycling dampens the effect of Rayleigh distillation at high temperatures; thus, $\delta^{18}O$ values at a site with moisture recycling would initially decrease more slowly than expected as temperatures lowered. At cooler temperatures, moisture recycling is less effective and the slope would steepen to eventually coincide with the expected rain-out trend (Figure 9).

Another possible explanation for the lessened decrease in $\delta^{18}O$ values at higher temperatures is a rise in condensation height during warmer months due to convective precipitation. As previously mentioned, although precipitation $\delta^{18}O$ values theoretically reflect the temperature at condensation, accurate condensation temperatures are difficult to determine and so surface air temperatures are used as an approximation. This implicitly assumes that the altitude of condensation is consistent for a location and that the difference in temperature between the surface and the height of condensation is a constant value due to lapse rates (Vachon et al., 2010b). In reality, convection can drive condensation heights higher and thus produce precipitation with lower than expected $\delta^{18}O$ values due to colder temperatures at higher altitude (Scholl et al., 2009). This effect is mitigated somewhat by equilibration

with lower moisture as the precipitation falls, but may partially explain the decrease in slope seen at warmer surface temperatures when convective precipitation is more likely (Figure 9).

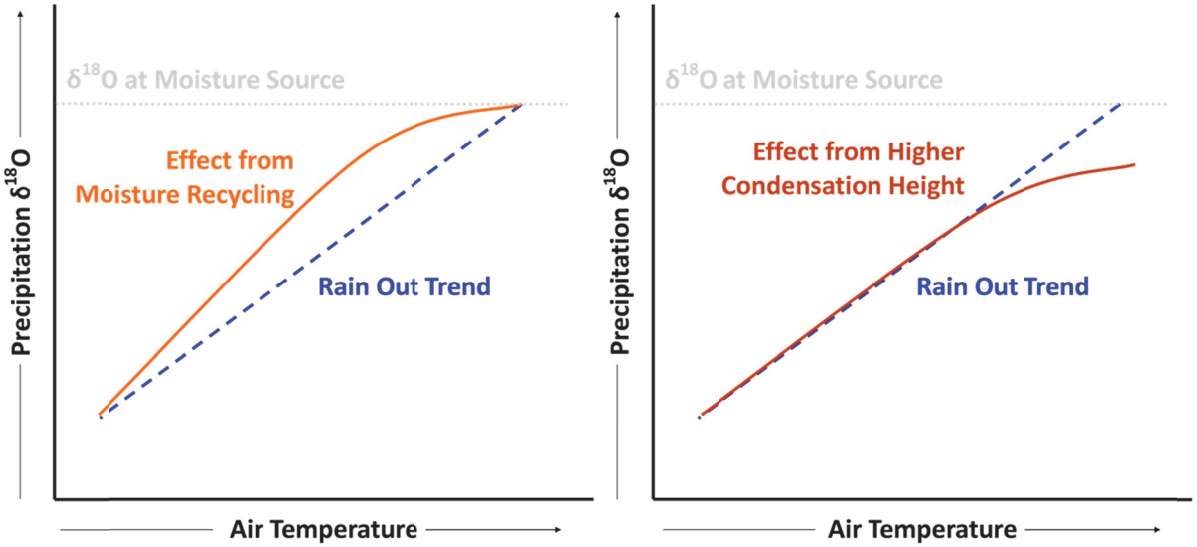

Figure 9. Possible impacts of moisture recycling and condensation height on precipitation $\delta^{18}O$ values at higher temperatures, as observed at many USNIP sites.

The increase in $\delta^{18}O$ variability at lower temperatures (Table 4) is likely a product of climatological differences between cold-weather events and warm-weather events. Cold-season weather in the central and eastern United States is dominated by extratropical cyclones. These large synoptic-scale systems can take various tracks as they move across the continent, and this leads to variable moisture travel paths and associated degree of rain-out. Thus, even though a site may have the same temperature for two different precipitation events, the different travel paths followed by the moistures may have led to different rates of rain-out and thus different precipitation $\delta^{18}O$ values. In Figure 10, Gulf of Mexico moisture is advected much farther west in cyclone A than the moisture advected by cyclone B. Even if the surface temperature at the starred site is the same in both scenarios, the different moisture travel paths may produce different precipitation $\delta^{18}O$ values. The degree of wrap-

around precipitation (precipitation occurring behind the core of the cyclone, often from spill-over warm sector moisture) may also produce variable $\delta^{18}O$ values depending on the travel path of the moisture. Transport of moisture from the Arctic and Pacific is believed to increase during the cold season, and different moisture sources would skew the expected $\delta^{18}O$ value at a given temperature. This potential effect of changing moisture sources is examined in more detail in Chapter 4.

Additionally, temperatures in colder months are generally more variable across the study region than during warmer months. Although daily temperature measurements are better than the monthly temperatures used in other studies, a daily mean temperature may be quite different than the temperature at the time of precipitation. This is a larger risk in the cold season when strong cold fronts trigger rain along the edge of the warm sector of an extratropical cyclone, but bring a major drop in temperature after passing. During the warm season, the overall synoptic pattern of the study region is more predictable with weaker cyclogenesis and heightened dominance of Gulf of Mexico air masses, and temperature changes behind cold fronts occurring in summer months are not usually as severe as typical of fronts in colder months.

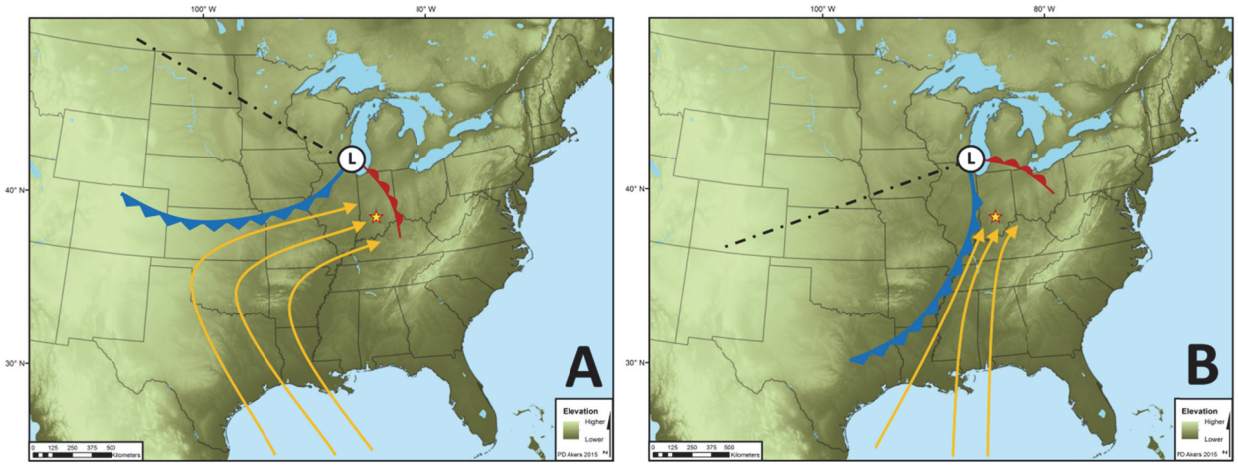

Figure 10. Two hypothetical extratropical cyclone tracks (black dashed line) and structures with different moisture travel paths (orange arrows) to the starred site in southern Indiana.

2.6.2 Spatial trends in the relationship between $\delta^{18}O$ and PDt

The decline in the strength of the $\delta^{18}O$ vs. PDt relationship from northwest to southeast is clear (Figure 8c), but competition from the amount effect in the southeast does not appear to cause this decline. Although a small amount effect was detected at some southeastern sites during some months, the overall data do not show a strong amount effect that could significantly affect precipitation $\delta^{18}O$ values. The steeper regression slopes for northern and western sites is not solely due to a higher percentage of frozen precipitation (which plots along a steeper slope than liquid precipitation). These sites still have steeper slopes than southeastern sites when the data include only samples with temperatures above freezing. The shallower slopes in warmer areas may be due to a greater concentration of precipitation near the warm extreme where moisture recycling or convection flattens the linear trend (Figure 9). Additionally, the growing season and associated transpiration is shorter at northern sites, and less transpiration would reduce the potential influence of moisture recycling. The strength of the temperature effect at northern and western sites appears to be a direct result of higher temperature variability at these sites, and the lower temperature range in the southeast likely explains the weaker temperature effect.

While the temperature effect is a major control on precipitation $\delta^{18}O$ values for the study region, deviations from the temperature-predicted $\delta^{18}O$ value are likely due to other climate effects (e.g., moisture track, moisture source, condensation height, evaporation, and moisture recycling). The noise produced by these non-temperature-driven effects on $\delta^{18}O$ values weakens the calculated relationship between $\delta^{18}O$ and PDt. The magnitude of this inherent non-temperature-driven variability is similar across sites; however, a site that has a wider range of temperatures will have a stronger $\delta^{18}O$ and PDt relationship than a site with a lower temperature range. Because the noise is lower proportion of the overall $\delta^{18}O$ variability, the greater $\delta^{18}O$ range associated with greater temperature variability reduces the relative impact of the $\delta^{18}O$ noise. In contrast, sites with only modest temperature variations

may see the temperature signal overwhelmed by the $\delta^{18}O$ noise because the temperature effect is relatively small. Although the standard deviation of $\delta^{18}O$ values for a given temperature also increases at sites with greater overall temperature range, the rate of $\delta^{18}O$ standard deviation increase is less than the rate of mean PDt decrease which results in a stronger $\delta^{18}O$ vs. PDt relationship at colder sites.

This proposed relationship between overall temperature variability and $\delta^{18}O$ vs. PDt regression strength is borne out in the data used here: the correlation between precipitation day temperature standard deviation and the r^2 of the $\delta^{18}O$ vs. PDt regression for the 25 sites is +0.74 (n=25, p-value << 0.001). This effect is also seen at sites in the sub-annual variability, as lower $\delta^{18}O$ vs. PDt r^2 values are found in the summer months and season (periods with relatively stable temperatures) and the highest r^2 values are found in the thermally-diverse spring and autumn seasons (Figure 19).

2.6.2 Spatial trends in the relationship between $\delta^{18}O$ and PDa

A clear spatial trend exists in the slope values of the $\delta^{18}O$ vs. PDa relationship with positive slopes in the north and negative slopes in the south. The positive northern slopes are likely reflecting the higher moisture capacity of warmer air, which is not as significant in warmer regions where the more typical amount effect with negative slope manifests. An intermediate region that has slopes near zero is likely due to competing effects of cool temperature moisture capacity and the standard convective amount effect.

2.6.4 Comparison of the $\delta^{18}O$ and PDt relationship with previous studies

Regression slope values of the $\delta^{18}O$ vs. PDt relationship for all sites examined in this study are lower than the global 0.69‰/°C slope originally proposed by Dansgaard (1964). This is not surprising as Dansgaard had many more high latitude sites that have steeper $\delta^{18}O$ vs. PDt regression slope values. Seasonally-resolved data from mid-latitude global GNIP stations produce a slope of 0.31‰/°C (Rozanski et al., 1993), and this value matches well with the mean slope of 0.32‰/°C found in this study.

However, the range in slope values, even in the relatively small area studied here, is large (0.12 to 0.51) and suggests that any attempt to generalize or apply a mean $\delta^{18}O$ vs. temperature relationship to large regions is fraught with large potential error.

Ideally, to explore the difference between climate data used in this study (daily data on precipitation days aggregated to weekly data) and the typical monthly climate data used in other studies, one should construct non-weighted monthly climate data from all daily GHCN data in each month. This was not attempted due to incomplete and missing GHCN climate data. This study used data from nearby GHCN climate stations to increase meteorological accuracy, but these small stations are prone to frequent missing data. Filling this missing data was very time consuming just for the precipitation days that corresponded to USNIP isotope data, and filling in all missing climate data would be a major undertaking. The nearest larger climate stations with limited missing data are often very distant from the USNIP sites, and meteorological accuracy would be forfeited. Additionally, the incomplete nature of the USNIP database would require significant analysis on the problems of comparing incomplete USNIP isotope data to complete climate data, such as covered in Vachon et al. (2010a) (referred to in the remainder of this chapter as V2010a). However, the results of this study can be compared with of the findings of V2010a to determine how the methodology used here changed the calculated relationship between $\delta^{18}O$ and temperature relative to a more typical approach.

V2010a also used data from the USNIP database to study the relationship between $\delta^{18}O$ and temperature for the United States. However, Vachon et al. aggregated the original weekly USNIP isotopic data into weighted monthly values to be analyzed with monthly temperature averages. In contrast, this research analyzed weekly isotopic and temperature data (Table 5). Additionally, the research presented here only included temperature measurements from days with precipitation, whereas V2010a derived monthly temperatures by averaging data for every data in the month. Finally,

when V2010a conducted their study, data were only available from 1989 to 1994, while the research presented here examined data spanning the years from 1989 to 2006.

Table 5. Summary of major database differences between this study and that conducted by Vachon et al. (2010a).

	This Study	**Vachon et al., 2010a**
$\delta^{18}O$ Resolution	Weekly	Weekly aggregated to monthly
Temperature Resolution	Daily aggregated to weekly	Monthly
Years Included in Database	1989-2006	1989-1994

The spatial characteristics of the slope of the $\delta^{18}O$ vs. PDt regression for weekly data in this study are similar to those obtained by V2010a (Figure 11). Both studies have maximum slope values in the northern Great Lakes and far western Great Plains and lower slopes in the southeast. However, in this study there is no embayment of lower slope values extending up the Mississippi and Ohio River Valleys. The difference in slope between the two sets of results in this region is between 0.05 and 0.10 ‰/°C.

Greater differences exist in the spatial distribution of r^2 values between the two studies (Figure 11). While the patterns are similar in the southeast and Mississippi Valley, more significant differences are found along the northern and western boundaries of the study area. Vachon et al. (2010a) has a large area of r^2 values greater than 0.6 extending from New York to Nebraska with some regions peaking in the 0.7-0.8 range. The research presented here found r^2 values greater than 0.6 in only two small regions in Minnesota and northern Michigan and no values were greater than 0.7. In this study, r^2 values were 0.1-0.2 lower in the Mid-Atlantic region, while higher r^2 values extend farther south along the western boundary of the study area. This latter difference may be an artifact of the lack in this study of Oklahoma and Texas data used in V2010a

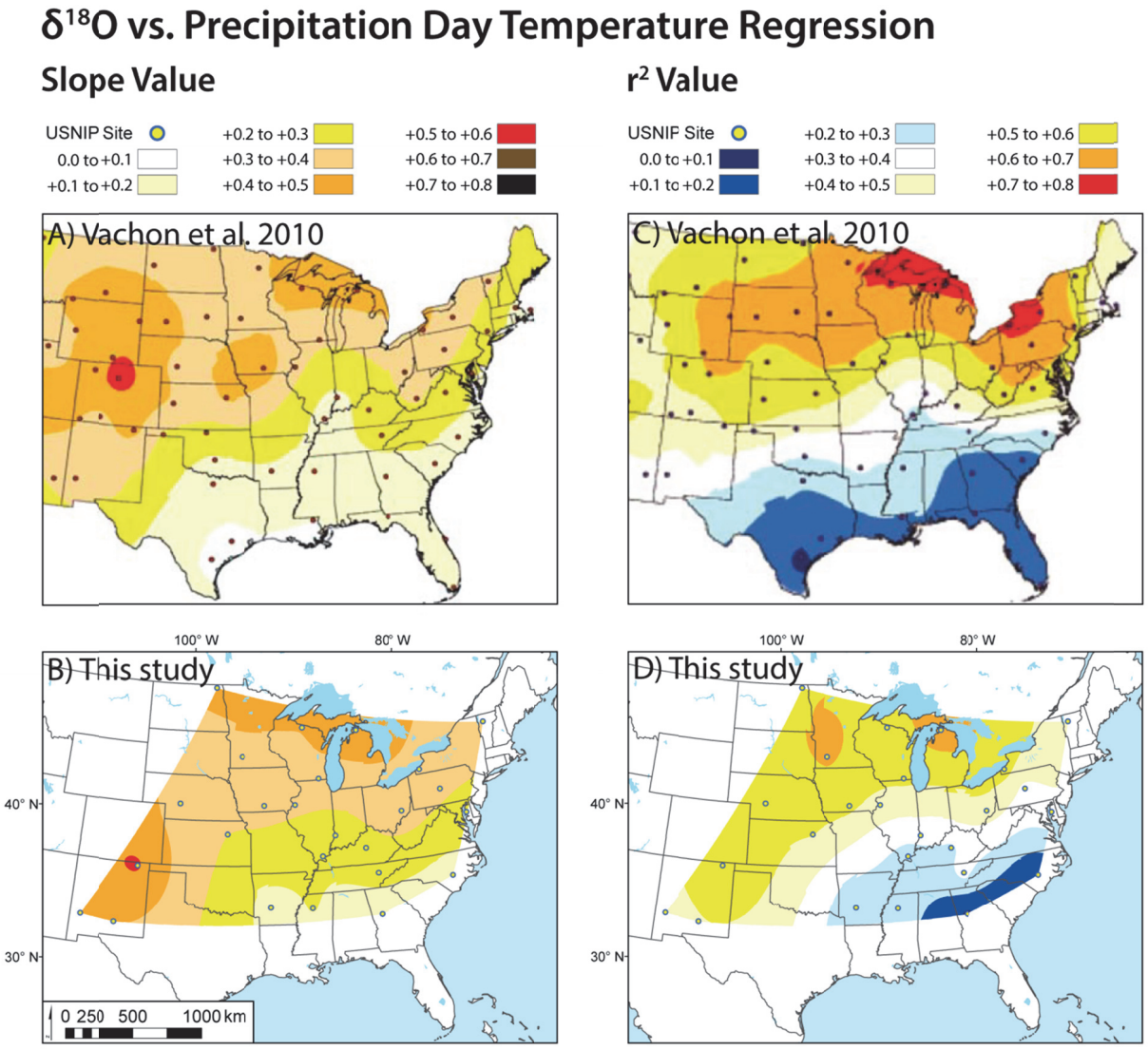

Figure 11. A comparison of the interpolated $\delta^{18}O$ vs. surface temperature relationship from Vachon et al. 2010 (A, C) with the interpolations of this study (B, D). Vachon et al. used monthly aggregated data, while this study has interpolations from weekly data. The color shading is matched between studies to represent the same values.

It is unclear which factors may be responsible for the differences between the results of Vachon et al. (2010a) and those obtained in this study. Difference in the resolution of the temperature data (aggregated daily data used here compared to the monthly data of Vachon et al.) could be a contributing factor, although it is unclear why V2010a obtained a better fit. If temperature is the dominant control on

$\delta^{18}O$ values, then temperature data coming only from the days of precipitation should be better correlated than a mean monthly temperature of all days. It is possible that correlations in this study are more representative of the true correlative value between $\delta^{18}O$ and temperature, and the higher r^2 values in V2010a are a result of a less variable aggregated temperature database that still gives evidence of seasonal trends. The overall differences are not large, though, and this study supports the general conclusions made in V2010a.

The weekly data in this study, using meteorological data only from precipitation days, did not result in stronger relationships calculated between $\delta^{18}O$ and PDt compared to the monthly climate data used in V2010a. Relationships are, in fact, weaker with the new database for much of the northern tier of the study region. This suggests that the temperature effect may be best expressed with aggregated data that blurs the inherent short-term (less than monthly) variability. Since the inclusion of short-term $\delta^{18}O$ variability weakens the $\delta^{18}O$-temperature relationship, this suggests that the bulk of this short-term variability is driven by non-temperature controlled factors. The emergence of a small amount effect in individual monthly data (Chapter 3) is a possible example of a short-term control on $\delta^{18}O$ that reduces the strength of the $\delta^{18}O$ vs. PDt relationship, but whose impact greatly lessens with aggregation. Moisture source or track changes (Figure 10) may also have a stronger effect on $\delta^{18}O$ at shorter-time scales, but lessen in magnitude with aggregation. Although the climate database in this study produces weaker relationships than seen in Vachon et al. (2010a), this does not necessarily indicate that it is an inferior methodology. Rather, the more precise meteorological data used to create the weekly database suggests that research using aggregated climate data may overestimate the strength of the relationship between $\delta^{18}O$ and temperature as well as underestimate the actual variability.

2.7 Conclusions

2.7.1 Remarks

Analysis of over 6200 weekly isotopic samples and associated climate data from 25 sites across the east-central United States confirmed previous findings on spatial distributions of $\delta^{18}O$ values and their relationship with climate variables. Precipitation day temperature has the clearest relationship with $\delta^{18}O$ values, with the highest r^2 values in the northern and western portions of the study region where temperature ranges are greatest. Precipitation amount does not have a significant relationship with precipitation $\delta^{18}O$ at any of the 25 sites. The novel method of using weighted climate data only from days with precipitation does not significantly improve correlations or change isotopic relationships compared to previous studies. However, this database is still believed to provide more precise and accurate estimates of the true relationships between $\delta^{18}O$ and meteorological variables than using aggregated monthly climate data.

Although the new weekly database did not improve the strength of relationships between precipitation $\delta^{18}O$ and climate variables in the eastern and central United States, this does not mean that analysis of $\delta^{18}O$ records cannot be significantly improved. Chapter 3 examines the changes to these relationships that occur due to data aggregation and grouping to better understand what factors affect the uncertainty and strength of these relationships. Changes in $\delta^{18}O$ values due to differences in moisture source may play an important role in precipitation $\delta^{18}O$ variability in the eastern and central United States, and this topic will be covered in Chapter 4. Seasonality of precipitation changes is important to our understanding of longer-term synoptic and global climate patterns, and the strong seasonal difference in $\delta^{18}O$ values seen at many of the sites examined offers potential to view $\delta^{18}O$ as a proxy for changes in precipitation seasonality. This idea will be explored further in Chapter 5. Finally, controls on interannual $\delta^{18}O$ variability can sometimes be very different from the controls observed in

an analysis using data with sub-annual resolution as shown in this chapter, and Chapter 6 will attempt to determine if other climate relationships emerge at the interannual scale.

2.7.2 Most important findings

- The linear relationship between precipitation $\delta^{18}O$ values and precipitation day temperature (temperature effect) is strongest ($r^2 > 0.4$) in the northern and western areas of the study region.
- The relationship between precipitation $\delta^{18}O$ values and precipitation amount (amount effect) is very weak ($r^2 < 0.06$) across the entire study region.
- The weekly isotope data resolution and use of climate data weighted by precipitation did not improve correlation or relationship strength between precipitation $\delta^{18}O$ and climate variables compared with previous studies using monthly aggregated data.

CHAPTER THREE:

CHANGES IN THE RELATIONSHIPS BETWEEN CLIMATE AND PRECIPITATION OXYGEN ISOTOPE VARIABILITY FROM TEMPORAL AGGREGATION AND ON SUB-ANNUAL SCALES IN THE EASTERN AND CENTRAL UNITED STATES

3.1 Introduction

Temporal variations in precipitation stable isotopes have generally not received the level of research dedicated to spatial variations. This is partly because the original spatially-diverse precipitation stable isotope datasets were only offered at a monthly resolution, while databases of daily or event-level records are spatially limited by cost and logistics. However, new precipitation stable isotope records offer the chance to investigate isotopic variability at different temporal resolutions. The weekly database created in Chapter 2 from United States Network for Isotopes in Precipitation (USNIP) isotope data and weighted precipitation day climate data presents an ideal opportunity to examine how temporal aggregation and temporal grouping of stable oxygen isotope ratios ($\delta^{18}O$) and climate data affects the relationships between these variables. Temporal aggregation combines data from shorter temporal resolutions into new data with longer resolutions (e.g., averaging weekly data into monthly data). Quantifying how aggregation changes relationship values and strength can help bridge the gap between monthly isotope records with wide spatial coverage and daily- or event-level isotope records typically restricted to a single location. Temporal grouping of data permits analysis of sub-annual trends in isotope-climate relationships (e.g., changes observed month-to-month and season-to-season). Since most applied uses of these relationships use parameters calculated from data coming from throughout the entire year, substantial sub-annual relationship variability will significantly affect these applications.

Understanding changes to the relationships between precipitation $\delta^{18}O$ and climate variables at different temporal scales is the initial step in understanding the drivers of long-term $\delta^{18}O$ variations recorded in stalagmites and other paleoenvironmental archives. Through this work, a better understanding of how temporal aggregation level and temporal grouping affects the relationships between precipitation $\delta^{18}O$ and climate variables is gained. In addition, this new understanding will help minimize the potential errors involved when applying a relationship derived from one aggregation level or temporal grouping to data from a different aggregation or grouping.

3.2 Objectives

- Quantify how aggregating from weekly to monthly- and seasonally-resolved data affects the relationships between precipitation $\delta^{18}O$ and both precipitation day temperature (PDt) and precipitation day amount (PDa) in the study region.
- Quantify sub-annual changes in the relationships between precipitation $\delta^{18}O$ and both PDt and PDa by grouping the data by month and by season.
- Determine the impact of changes from temporal aggregation and grouping on paleoclimate and environmental applications of the relationships.

3.3 Methods

3.3.1 Temporal aggregation of the isotope-climate database

The weekly database created in Chapter 2 was further aggregated per site by month and season to perform statistical analysis of relationships at different temporal resolutions, as expressed by:

$X_{month} = \sum_{i=1\ n=N} (X_i * P_i / P_{month})$ where X is any variable being aggregated ($\delta^{18}O$, temperature, etc.), P is the precipitation amount, and N equals the number of data points per month.

$X_{season} = \sum_{i=1\ n=N} (X_i * P_i / P_{season})$ where X is any variable being aggregated ($\delta^{18}O$, temperature, etc.), P is the precipitation amount, and N equals the number of data points per season.

References to aggregated data are indicated by the adjectives 'monthly' and 'seasonal' (e.g., monthly relationships, seasonal r^2). Data were not aggregated by year due to wide differences in the number of weekly values from year-to-year in the USNIP database, unlike the more even distribution of monthly and seasonal values. In fact, many years have only a few weeks of data, and although rare years have almost complete records (e.g., 1992, 1993, 2004). The incompleteness of the database has less impact on the monthly and seasonal aggregates because variations in $\delta^{18}O$ are relatively small over these reduced time periods. Also, weeks of missing data often cluster by month or season, and so aggregation is not attempted for those months or seasons anyway.

Previous studies using the USNIP database (e.g., Vachon et al., 2010b) typically combined monthly isotope values aggregated from incomplete weekly data with complete monthly climate data despite obvious problems in doing this. In this study, however, climate and isotope data are both initially weekly-resolved, and climate data are only used when isotope data are also available (i.e., the climate data has the same non-continuous nature as the isotope data) so that aggregated climate and isotope values of different completeness are never compared. Although the aggregated monthly and seasonal values calculated using the non-continuous weekly data will differ slightly from what would be expected from a complete and continuous data set, the desired results of this study (trends of correlation and regression change with aggregation) will still be expressed and identifiable.

3.3.2 Temporal grouping of the isotope-climate database

Weekly values were grouped by month or season, (e.g., all June or all autumn data) to analyze characteristics for each month and season. Grouping is different from aggregation because no changes are made to the original weekly data in the grouping process; rather, data are only reorganized into subsets for each site so that regressions and statistics are calculated for each month and season as opposed to calculated using all data as in Chapter 2. The number of weekly data in each month or season varied due to differences in precipitation seasonality and sampling frequency, but generally sample sizes were evenly distributed. References to grouped data are indicated with the phrases 'for each month' and 'for each season' and 'month-to-month' and 'season-to-season' (e.g., slope values for each month, $\delta^{18}O$ variability season-to-season).

3.3.3 Temporal aggregation statistical calculations

Statistical analysis of the $\delta^{18}O$ and PDt relationship were calculated for monthly and seasonal data in the same manner as described for the original weekly data (Chapter 2). Analysis of the relationship between $\delta^{18}O$ and PDa was not performed for the monthly and seasonal aggregates because the original discontinuous USNIP data means that monthly and seasonal precipitation amounts are incomplete. Discontinuous sampling does not affect PDt aggregation because aggregated temperature is a weighted mean and not a summed total as for the precipitation amount. Interpolated values from regression were mapped for visual analysis of spatial trends and distributions, and differences between aggregation levels were calculated for correlation, slope, y-intercept, and fit (r^2).

3.3.4 Temporal grouping statistical calculations

Grouping the weekly data produced 16 data groups per site (twelve months and four seasons), and weighted mean $\delta^{18}O$ averages were calculated for each month and season. Interpolations of these weighted mean $\delta^{18}O$ site values for each month and season (ordinary kriging, spherical semivariogram

model, output cell size = 0.01 decimal degrees) were mapped to track sub-annual changes in $\delta^{18}O$ distributions across the study region. Correlations and linear regressions for $\delta^{18}O$ versus PDt and $\delta^{18}O$ versus PDa were also calculated for each month and season. The original weekly-resolved dataset permits analysis of month-to-month changes in correlation and regression not previously performed with USNIP or GNIP data and provides much greater sample size for season-to-season analysis.

The linear relationship between $\delta^{18}O$ and PDt at a site can be used to predict temperatures for a given $\delta^{18}O$ value (Dansgaard, 1964), although this has limited practical applications in paleoclimate and ecological studies due to the large predictive errors typically calculated. The predictions are useful, however, in visualizing how the relationship between $\delta^{18}O$ and PDt changes on a month-to-month or season-to-season basis. Thus, temperature estimates for a precipitation $\delta^{18}O$ value of -6‰ were calculated for each month and season. This $\delta^{18}O$ value is close to the overall mean $\delta^{18}O$ value observed across the study region. Estimation is also technically possible for the relationship between $\delta^{18}O$ and PDa, but the low correlations of this relationship for the study sites (Chapter 2) precluded implementation.

3.4 Results

3.4.1 Changes to the $\delta^{18}O$ vs. PDt relationship with temporal aggregation

Aggregation does not greatly affect the mean $\delta^{18}O$ vs. PDt regression values at the 25 study sites (Table 6) except for higher r^2 values with increased aggregation to monthly and seasonal data. Aggregation also increases the range of r^2 values at the 25 sites as maximum values increase and minimum values largely do not change. Despite the limited changes in mean regression values with aggregation, individual sites exhibit a greater response (Appendix 5). Overall, aggregation does not radically change the spatial distribution of interpolated slope values for the study region, but aggregation decreases slope values more often than increases them (Figure 12). Slopes decrease most at eastern sites (some sites along the mid-Atlantic have a slope drop of >0.6‰/°C) while western sites have

little change or a small increase in slope value. Y-intercepts are not much affected by aggregation either (Figure 13) and generally show a similar, but inverse, spatial pattern to the changes to slope with aggregation.

Table 6. Weekly, monthly, and seasonal $\delta^{18}O$ vs. PDt regression mean, maximum, and minimum values for the 25 study sites.

$\delta^{18}O$ vs. PDt									
	Slope			***y-Intercept***			***r^2***		
Resolution	***Mean***	***Max***	***Min***	***Mean***	***Max***	***Min***	***Mean***	***Max***	***Min***
Weekly	0.32	0.51	0.12	-11.72	-6.50	-15.99	0.42	0.65	0.08
Monthly	0.30	0.52	0.10	-11.57	-6.56	-16.20	0.45	0.69	0.09
Seasonal	0.31	0.51	0.07	-11.84	-6.07	-16.15	0.51	0.80	0.11

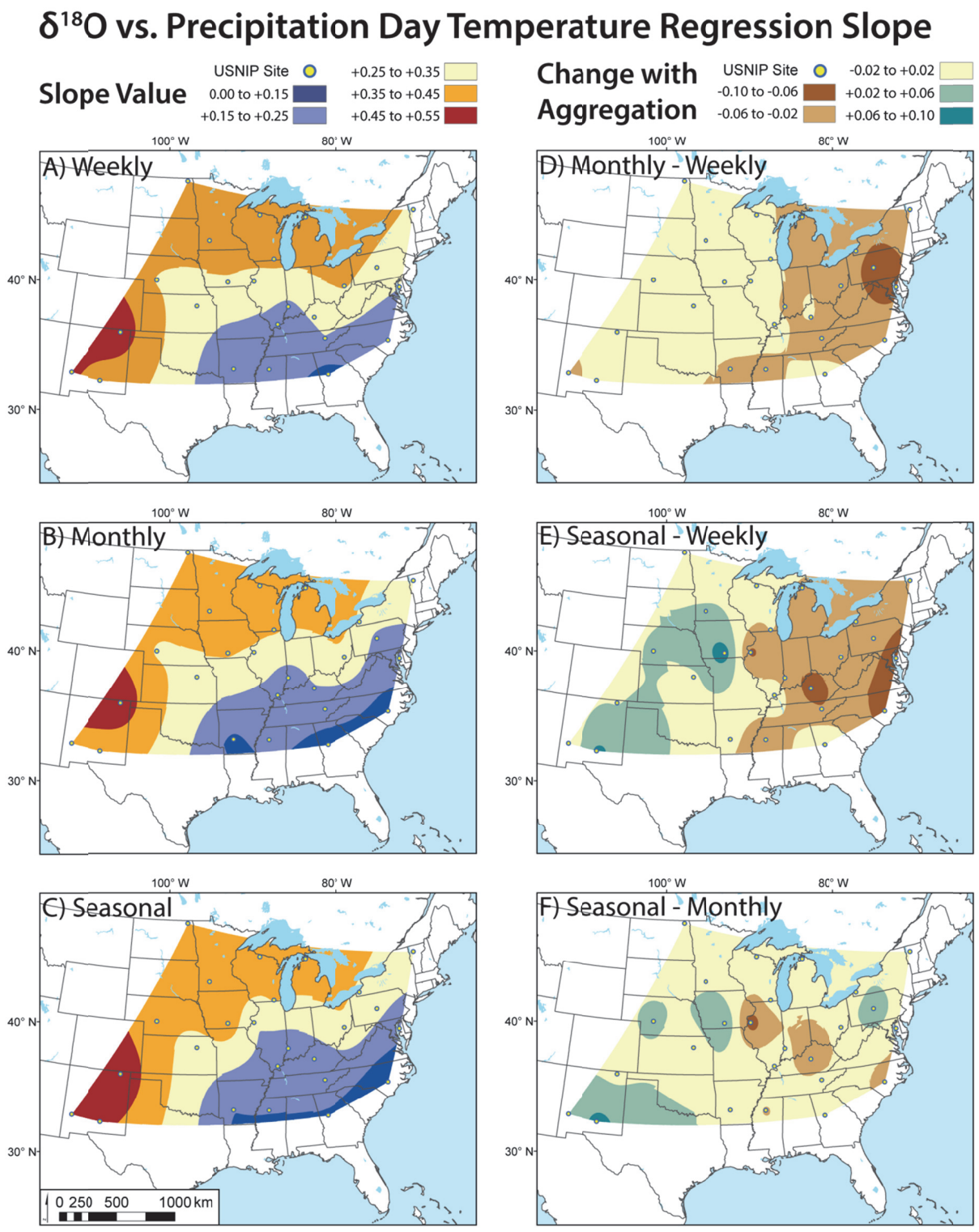

Figure 12. Changes in $\delta^{18}O$ vs. PDt regression slope value with increasing level of aggregation. Maps on the left (A, B, C) show slope values interpolated across the study region while maps on the right (D, E, F) show differences in interpolated values between levels of aggregation.

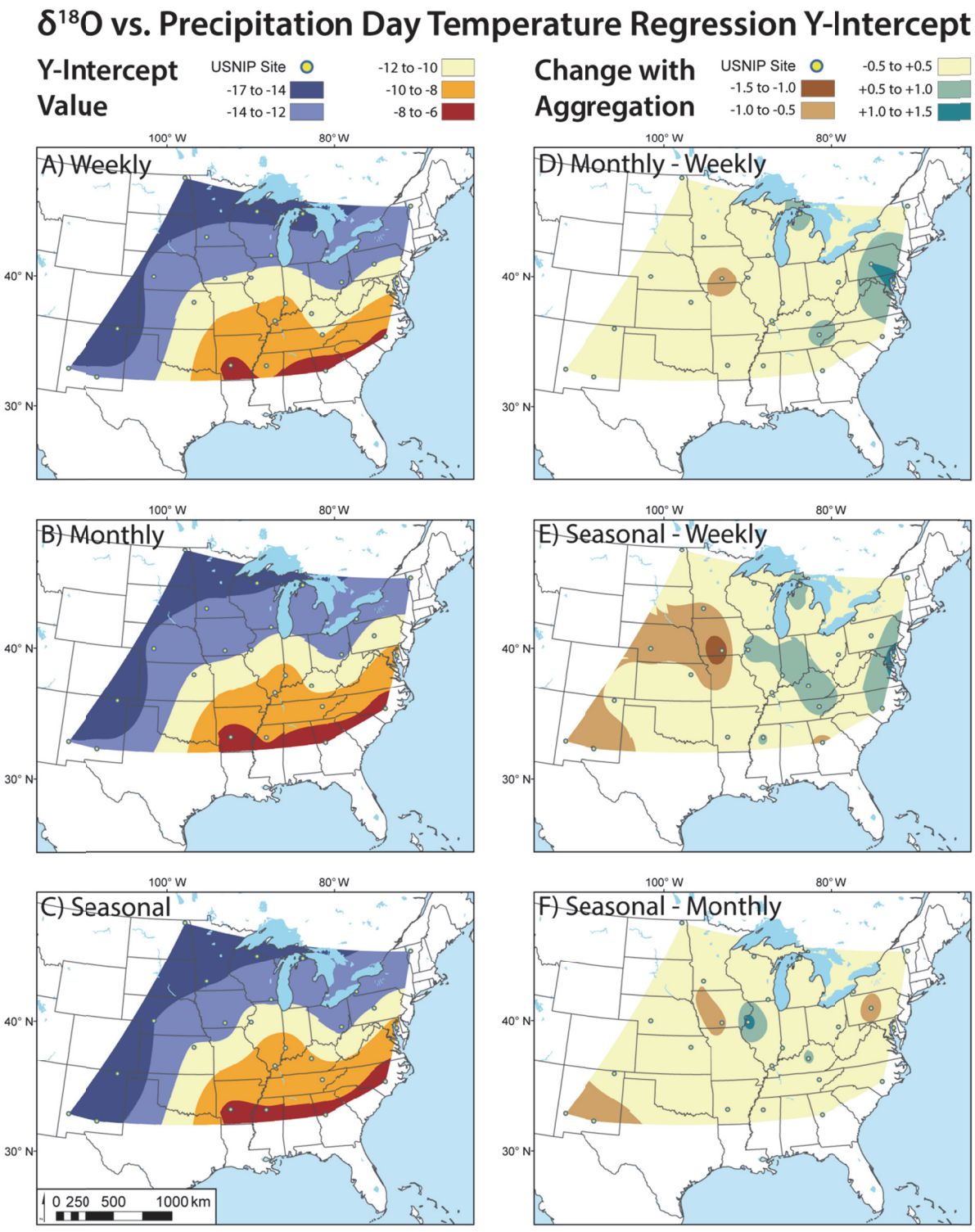

Figure 13. Changes in $\delta^{18}O$ vs. PDt regression y-intercept value with increasing level of aggregation. Figures on the left (A, B, C) show y-intercept values interpolated across the study region while figures on the right (D, E, F) show differences in interpolated values between levels of aggregation.

The r^2 values of the $\delta^{18}O$ vs. PDt regression change much more with temporal aggregation than with either slope or y-intercept (Figure 14). Aggregation generally increases r^2 values, but r^2 values decrease slightly in the Mid-Atlantic region. All fifteen sites where r^2 increases >0.05 in a weekly-to-seasonal aggregation are found north of the Ohio River and/or west of the Mississippi River. Sites where r^2 values decrease also generally show a decrease in slope with aggregation. This fits with the observation that low $\delta^{18}O$ vs. PDt slopes correspond with low correlations since the inherent residual variability is relatively stable across sites (Chapter 2).

Temperatures were estimated using the mean regression of $\delta^{18}O$ vs. PDt (Table 6). Although the exact air temperature estimate varies greatly from site to site (Appendix 5), the standard errors of the estimates are more similar across sites. Errors are consistently large across a wide range of $\delta^{18}O$ values, and aggregation neither improves nor increases the error to a significant degree (Table 7).

Table 7. Mean temperature estimate errors for all 25 sites at weekly, monthly, and seasonal aggregations. The $\delta^{18}O$ value of -6‰ is close to the overall mean $\delta^{18}O$ value.

	Temperature Estimate Error (°C) when Precipitation $\delta^{18}O$ =		
Aggregation	***-20‰***	***-6‰***	***0‰***
Weekly	±12.9	±12.6	±12.7
Monthly	±13.2	±12.3	±12.6
Seasonal	±13.6	±11.2	±12.0

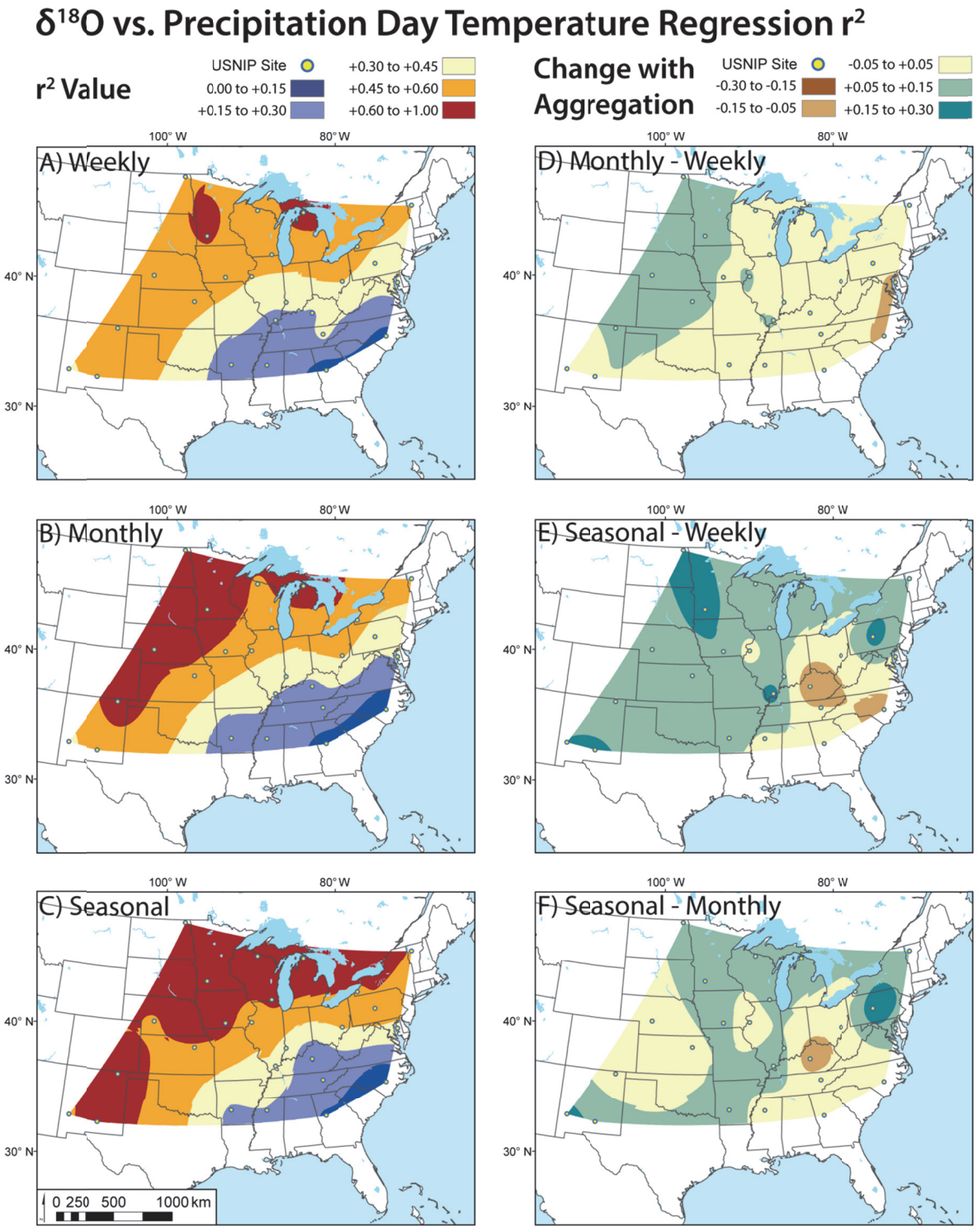

Figure 14. Changes in $\delta^{18}O$ vs. PDt regression r^2 value with increasing level of aggregation. Figures on the left (A, B, C) show y-intercept values interpolated across the study region while figures on the right (D, E, F) show the interpolated values differences between levels of aggregation.

3.4.2 Sub-annual $\delta^{18}O$ variability

When mapped, weighted mean precipitation $\delta^{18}O$ values increase from northwest to southeast in each month (Figure 15) and season (Figure 16). Precipitation $\delta^{18}O$ values vary most in winter (from -22 to -5‰) and vary least in summer (from -8 to -3‰), and the spread of higher $\delta^{18}O$ values northward coincides with the seasonal warming of the northern hemisphere. The climate of the eastern and central United States, including surface air temperatures, varies less from south to north during summer months, and this promotes similar $\delta^{18}O$ values in precipitation. Spatial patterns of $\delta^{18}O$ in spring and autumn are similar to each other and intermediate between the winter and summer extremes, although the range $\delta^{18}O$ values is slightly greater in spring than autumn. An area of higher $\delta^{18}O$ values present along the Mississippi River Valley (most prominent in spring) likely marks the dominant track for Gulf of Mexico moisture advection as well as the generally low regional elevation that limits Rayleigh distillation.

A continental effect is apparent in the spatial distribution of $\delta^{18}O$ values. Moisture reaching the interior Great Plains and upper Midwest travels a long distance over land, and this produces an increasingly lower $\delta^{18}O$ values. Higher elevations in the northern and western parts of the study region may enhance this continental effect by producing lower $\delta^{18}O$ values in the Great Plains and upper Midwest. This elevation effect may manifest along the Appalachian Mountains and Allegheny Plateau to some degree (e.g., May in Figure 15), but the lack of higher elevation sites in the dataset limits the impact of elevation on $\delta^{18}O$ values.

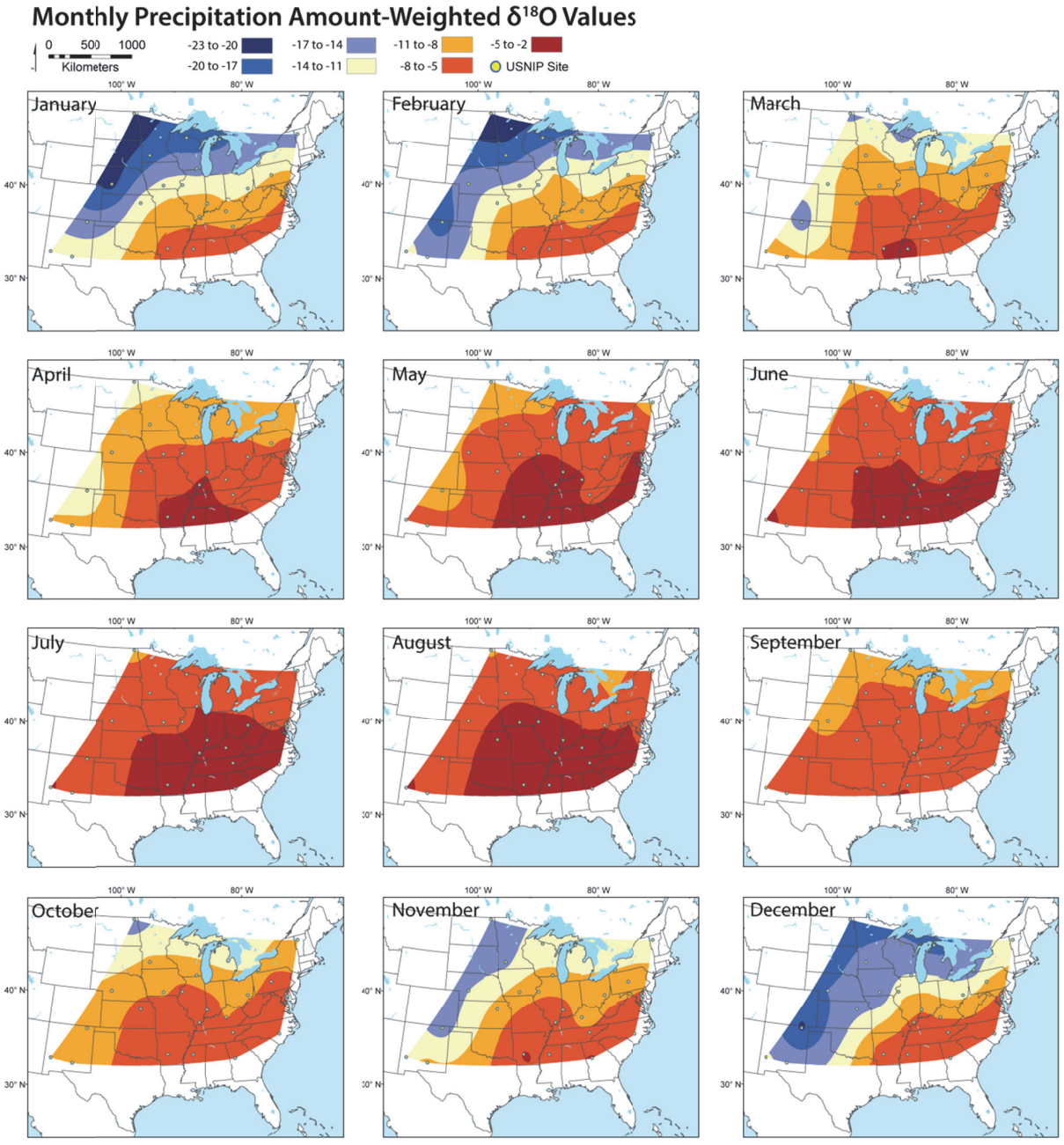

Figure 15. Interpolated spatial variations in weighted mean precipitation $\delta^{18}O$ values for each month across the study region.

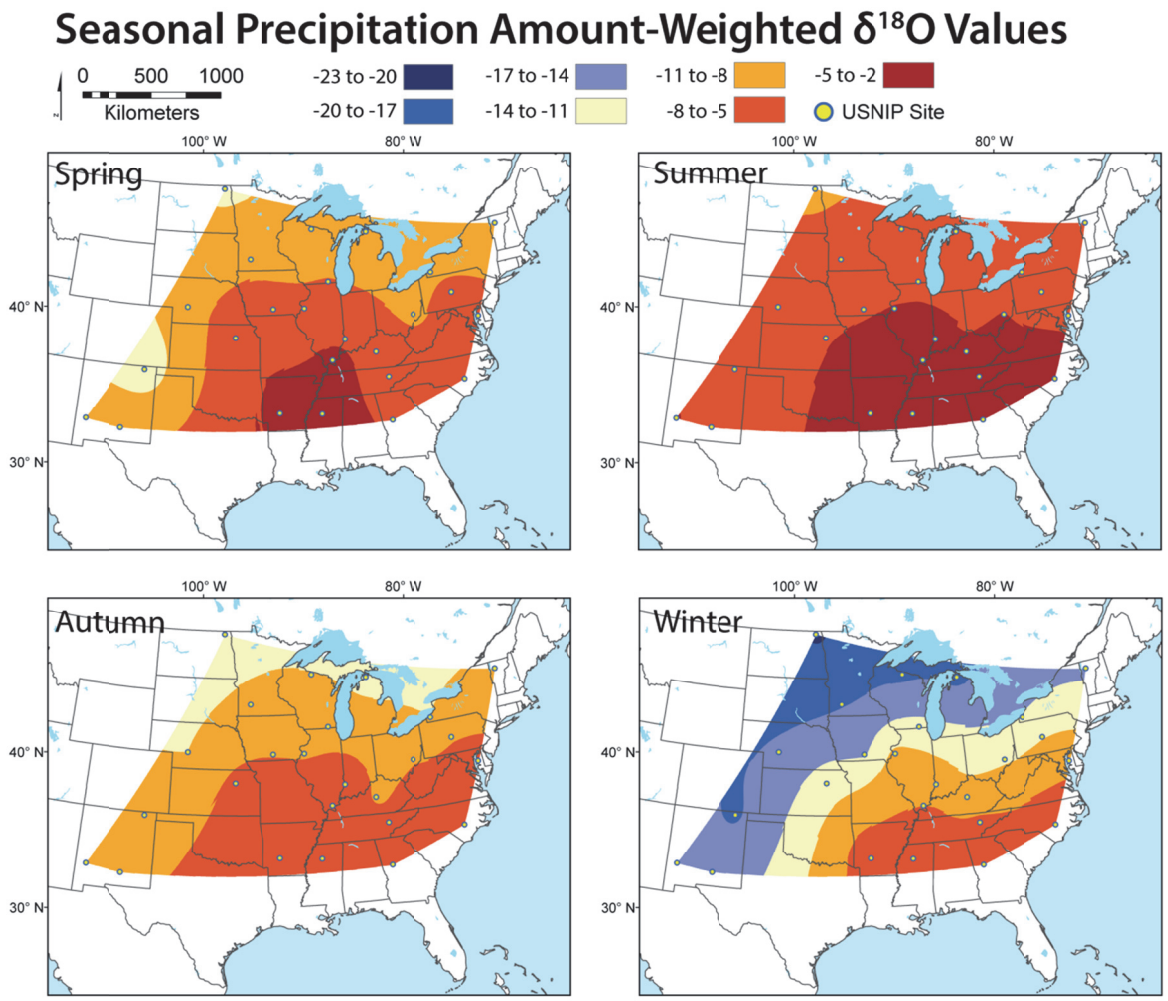

Figure 16. Interpolated spatial variations in weighted mean precipitation $\delta^{18}O$ values for each season across the study region.

3.4.3 Sub-annual relationship changes by month and by season

Slopes, y-intercepts, and r^2 values changed considerably from month-to-month and season-to-season at all sites for both the $\delta^{18}O$ vs. PDt and $\delta^{18}O$ vs. PDa regressions (Figure 17). These values often vary more from month-to-month and from season-to-season at a single site than vary spatially across all mean site values. These sub-annual regression values differ greatly from the values calculated from the entire, non-grouped data (Table 9, Figure 19). Slopes and y-intercepts for the $\delta^{18}O$ vs. PDt relationship

vary month-to-month and season-to-season, but without a clear temporal trend and generally do not stray far from the non-grouped mean slope and y-intercept values. Slope and y-intercept co-vary inversely, and this covariance is likely because the centroids of the precipitation data used to construct the regressions are above 0°C, and thus steeper slopes will have lower y-intercepts.

The strength of the $\delta^{18}O$ vs. PDt relationship is always weaker for each month and season than for the entire, non-grouped data. In contrast, the slope and y-intercept values of the $\delta^{18}O$ vs. PDa relationship show a clear temporal trend with maximum slope and minimum y-intercept in winter and the reverse trend in summer. The clarity of this trend is somewhat surprising, because although the $\delta^{18}O$ vs. PDa relationship is stronger within each temporal unit (particularly in the monthly-grouped data), the fit is still quite weak.

3.4.4 Temperature predictions from $\delta^{18}O$ vs. PDt regressions

Differences between $\delta^{18}O$ vs. PDt regressions calculated for the entire dataset and for each month and season lead to a wide range in temperature predictions for a given $\delta^{18}O$ value (Table 8, Figure 18). Temperatures in Table 8 are calculated with a $\delta^{18}O$ value of -6‰ (close to the overall mean precipitation $\delta^{18}O$ value). The temperature estimates calculated from the entire, non-grouped dataset (14-17°C) are reasonable, but the standard errors are very large (>±10°C). Temperature estimates calculated with the regressions derived from the temporally-grouped data have smaller standard errors, but vary wildly from month-to-month and season-to-season. Temperature estimates follow seasonal temperature changes: summer estimates are higher than winter estimates. Estimation standard errors, in contrast, are inversely related to seasonal temperature changes and are lower in summer likely due to the lower overall $\delta^{18}O$ and temperature variability at this time.

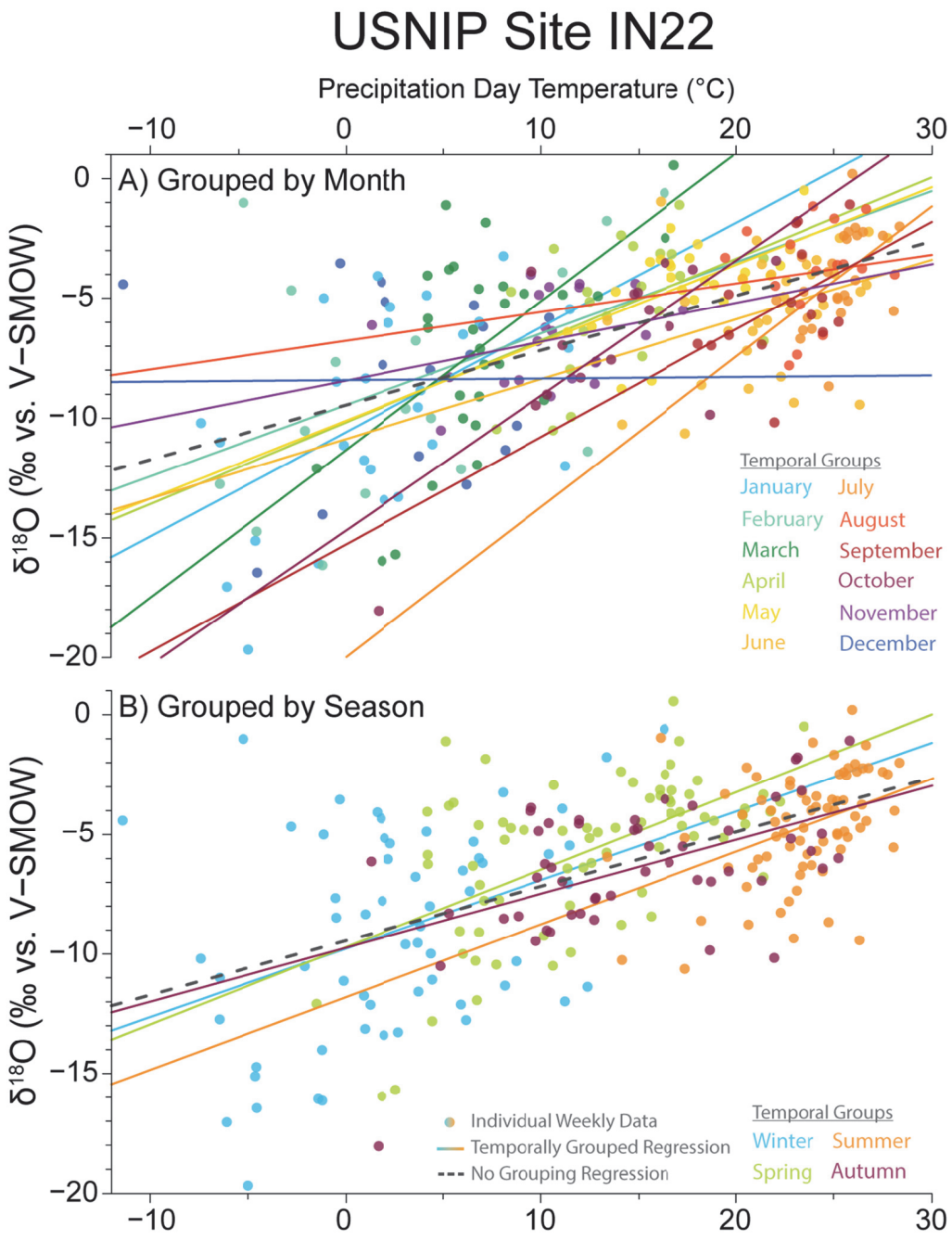

Figure 17. Data regressions for each month (A) and each season (B) for the $\delta^{18}O$ vs. PDt relationship at USNIP site IN22 in southwest Indiana.

Table 8. Temperature estimates for three sites with precipitation $\delta^{18}O$ = -6‰, based on regression analysis for temporally-grouped data.*

	Temperature Estimate (°C) when Precipitation $\delta^{18}O$ = -6‰					
Grouping	***MN27***		***IN22***		***GA41***	
Entire	17.00	±11.67	14.32	±14.75	15.71	±12.72
Jan	-3.69	±25.26	4.37	±9.59	9.57	±9.50
Feb	12.20	±18.48	4.57	±14.84	10.52	±8.79
Mar	6.50	±9.86	7.53	±6.68	12.89	±8.08
Apr	8.87	±8.09	13.69	±7.08	14.66	±8.68
May	15.50	±8.98	16.09	±5.53	21.73	±6.62
Jun	19.74	±6.75	21.63	±6.87	22.26	±6.01
Jul	21.73	±4.67	24.54	±2.89	24.69	±2.52
Aug	20.59	±5.78	23.64	±5.27	24.25	±2.19
Sep	18.38	±7.10	22.02	±5.01	21.70	±6.92
Oct	14.04	±8.83	14.58	±7.78	18.35	±4.72
Nov	3.18	±12.71	10.94	±7.59	15.03	±10.39
Dec	1.14	±5.38	3.13	±12.87	9.02	±7.83
Win	4.04	±12.51	4.10	±10.96	9.67	±8.20
Spr	11.99	±10.90	12.12	±9.58	14.69	±8.45
Sum	20.63	±5.82	22.75	±5.65	23.56	±4.35
Aut	16.67	±11.22	15.34	±10.98	18.42	±8.88

*Red cells represent maximum values while blue cells represent minimum values. Note the inverse relationship between temperature prediction and error.

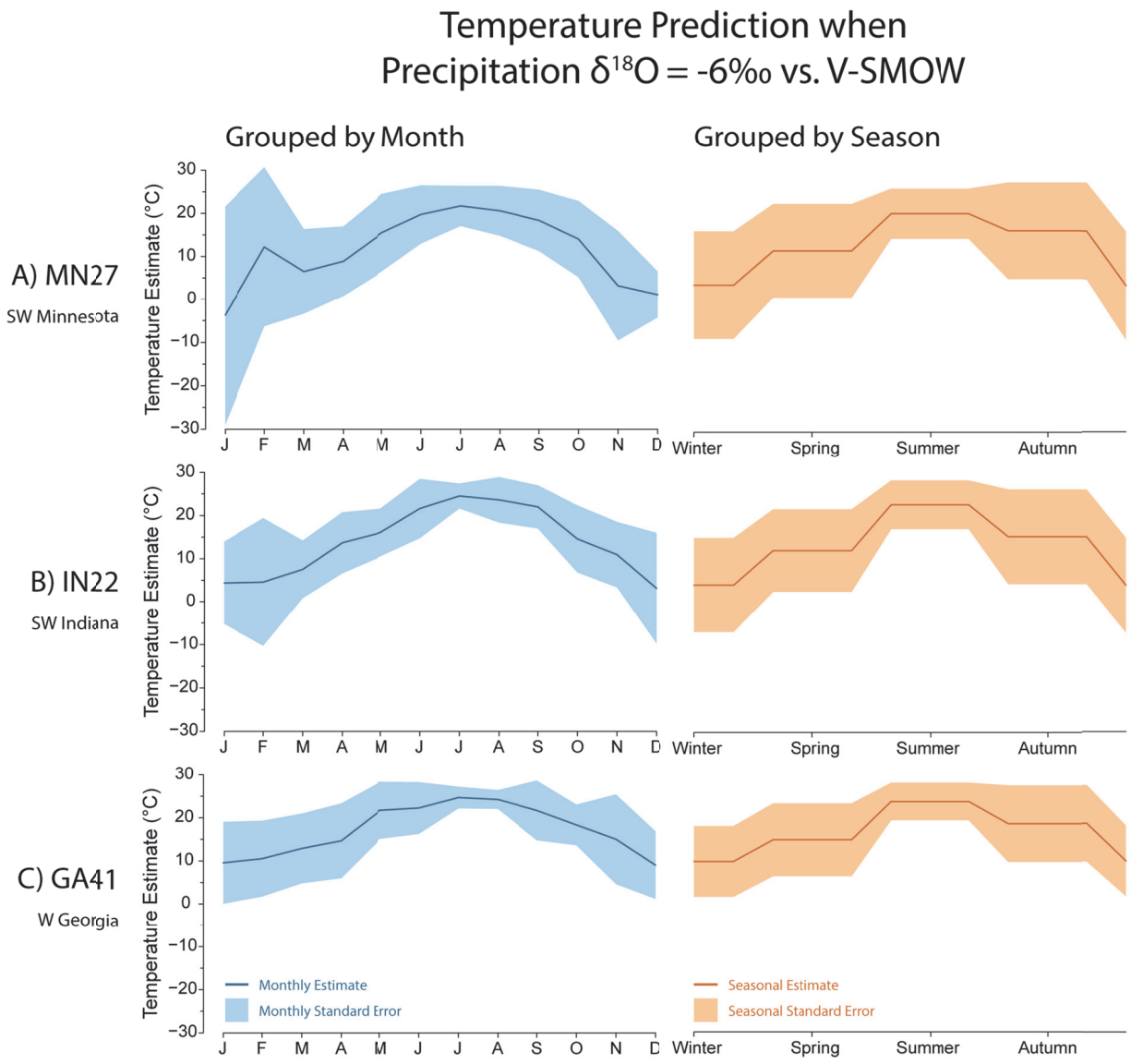

Figure 18. Temperature estimates for $\delta^{18}O$ = -6‰, based on and $\delta^{18}O$ vs. PDt regressions for each month (left, blue) and each season (right, tan). The three USNIP sites shown (A, B, C) fall along a northwest-southeast transect through the study region.

Table 9. Values for isotopic regression relationships for temporally grouped data, averaged for all 25 study sites.*

$\delta^{18}O$ vs. PDt			
Group	**Slope**	**y-Int**	**r^2**
Jan	0.42 ±0.10	-12.50 ±0.77	0.28 ±0.04
Feb	0.43 ±0.04	-12.81 ±0.63	0.24 ±0.03
Mar	0.43 ±0.05	-11.20 ±0.51	0.34 ±0.04
Apr	0.34 ±0.04	-10.58 ±0.54	0.24 ±0.03
May	0.31 ±0.04	-11.00 ±0.82	0.26 ±0.04
Jun	0.22 ±0.05	-9.97 ±1.14	0.12 ±0.02
Jul	0.42 ±0.10	-14.57 ±2.23	0.23 ±0.04
Aug	0.39 ±0.06	-13.74 ±1.44	0.20 ±0.04
Sep	0.42 ±0.05	-14.37 ±0.91	0.28 ±0.04
Oct	0.28 ±0.05	-11.60 ±0.93	0.17 ±0.04
Nov	0.38 ±0.05	-12.17 ±0.65	0.23 ±0.03
Dec	0.36 ±0.09**	-11.74 ±0.69	0.23 ±0.04
Win	0.36 ±0.05	-12.51 ±0.59	0.22 ±0.03
Spr	0.35 ±0.02	-11.08 ±0.47	0.40 ±0.03
Sum	0.31 ±0.02	-12.02 ±0.45	0.12 ±0.01
Aut	0.29 ±0.03	-11.72 ±0.62	0.32 ±0.04
$\delta^{18}O$ vs. PDa			
Group	**Slope**	**y-Int**	**r^2**
Jan	1.55 ±0.68	-16.18 ±1.77	0.18 ±0.04
Feb	-0.11 ±0.57	-11.91 ±1.80	0.14 ±0.04
Mar	-0.15 ±0.27	-9.04 ±1.17	0.06 ±0.02
Apr	-0.22 ±0.15	-7.12 ±0.68	0.05 ±0.01
May	-0.46 ±0.23	-4.77 ±0.72	0.08 ±0.03
Jun	-0.38 ±0.17	-4.47 ±0.55	0.09 ±0.02
Jul	-0.98 ±0.26	-2.12 ±0.93	0.12 ±0.03
Aug	-0.67 ±0.17	-2.97 ±0.63	0.12 ±0.03
Sep	-0.80 ±0.18	-4.22 ±0.74	0.11 ±0.02
Oct	-0.57 ±0.28	-6.86 ±0.82	0.12 ±0.02
Nov	-0.56 ±0.26	-8.00 ±1.06	0.07 ±0.02
Dec	1.32 ±1.47	-15.75 ±4.03	0.16 ±0.04
Win	0.56 ±0.25	-13.74 ±1.25	0.03 ±0.01
Spr	-0.03 ±0.15	-7.60 ±0.73	0.01 ±0.01

Sum	-0.65	±0.10	-3.37	±0.48	0.05	±0.02
Aut	-0.50	±0.14	-6.66	±0.71	0.02	±0.01

*Red cells indicate the value is greater than the mean value in Table 3, and blue cells indicate the value is lower. White cells are equal to the mean value.

**One site was removed in the calculation of the mean value because this site did not have enough samples after the temporal grouping to perform a regression.

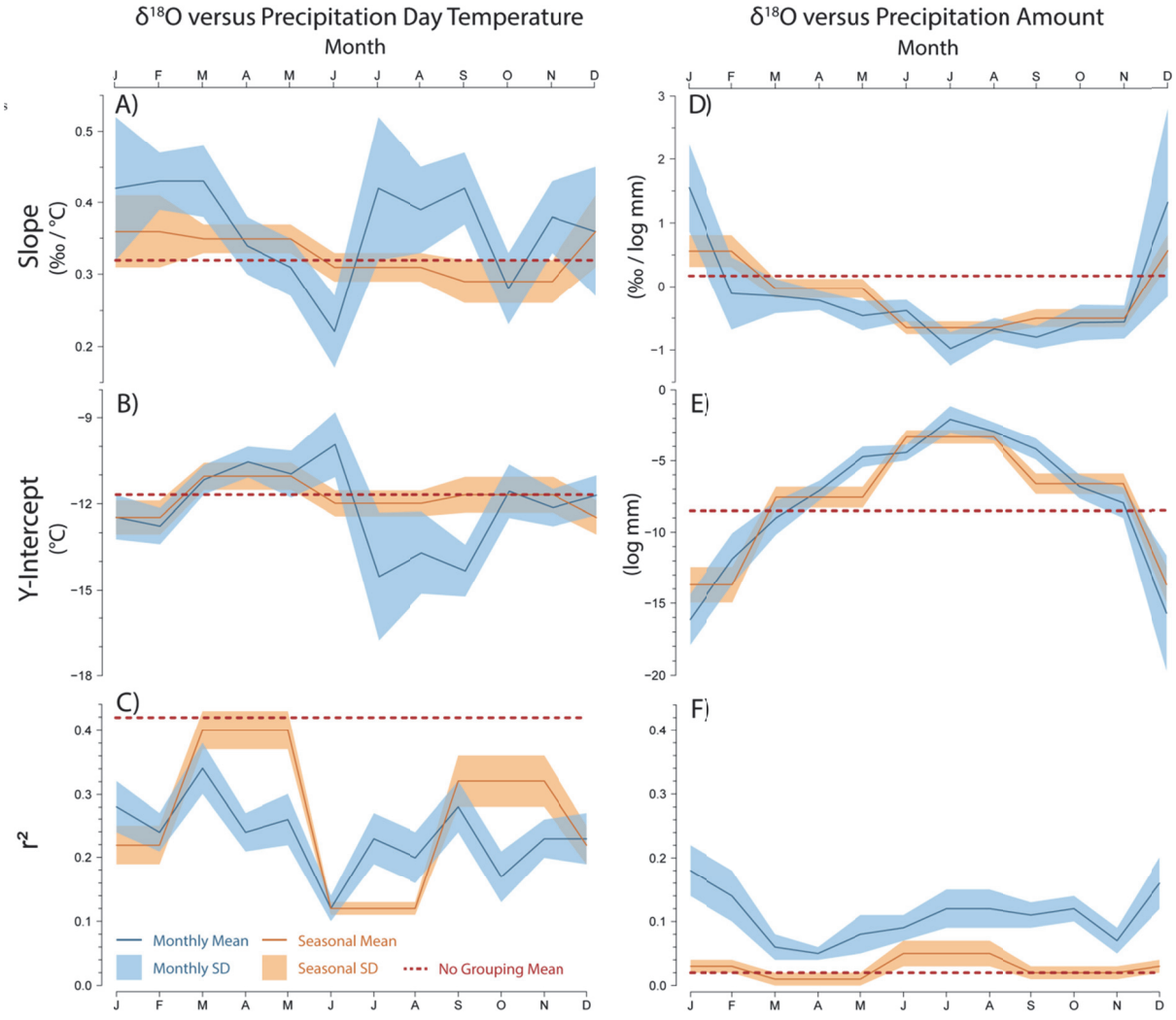

Figure 19. Sub-annual variations in the slope (A & D), y-intercept (B & E), and r^2 (C & F) of the $\delta^{18}O$ vs. PDt and $\delta^{18}O$ vs. PDa regressions, respectively. Mean values are calculated from all 25 USNIP sites to show month-to-month (blue) and season-to-season (tan) variations. These values vary greatly from the entire, non-grouped data's values (red dashed line).

Generally, sites with a stronger relationship between $\delta^{18}O$ and PDt calculated from the entire, non-grouped data have more months and seasons with significant ($p \leq 0.05$) r^2 values. P-values are more useful here as a cutoff of significance than with the weekly data due to the lower sample sizes within each temporal group. However, although many sites have very high r^2 values for the entire dataset, only one site (MI09) has all months and seasons with significant r^2 values (Appendix 5). Statistically significant r^2 values for the $\delta^{18}O$ vs. PDt relationship are most common at sites in spring, and of all 12 months, March and April have significant r^2 values at the most sites (17 and 15, respectively; Table 10). In contrast, June, August, October, and December have significant r^2 values at only 10 sites each.

Table 10. Number of USNIP sites (out of 25) with statistically significant regression r^2 values ($p \leq 0.05$).*

	Number of sites with statistically significant r^2 values	
	$\delta^{18}O$ vs. PDt	***$\delta^{18}O$ vs. PDa***
Jan	11	4
Feb	11	3
Mar	17	2
Apr	15	1
May	12	3
Jun	10	3
Jul	13	6
Aug	10	5
Sep	13	4
Oct	10	4
Nov	13	2
Dec	10	0
Win	19	4
Spr	23	3
Sum	20	10
Aut	21	8

* Colors grade from most sites in red to fewest in blue.

3.5 Discussion

3.5.1 Relationship changes with temporal aggregation

As previously discussed, the $\delta^{18}O$ vs. PDt relationship is not entirely linear and variability increases at lower temperatures. Aggregation appears to improve correlations and raise r^2 values mainly by reducing both the number of extreme values and the broad range of values commonly found at lower temperatures. Since $\delta^{18}O$ residuals tend to be lower than the linear trend at colder temperatures (Figure 5) and these residuals are reduced with aggregation, aggregation 'linearizes' the data. Changes in the spatial pattern of r^2 with aggregation parallels the magnitude of seasonal climate and $\delta^{18}O$ change: sites with greater seasonal change generally see the largest increases in $\delta^{18}O$ vs. PDt r^2 values. Conversely, sites with limited seasonal change, such as the southeastern United States, have little increase in r^2 after aggregation, and some of these sites have a decrease in correlation. The net result of aggregation on the $\delta^{18}O$ vs. PDt relationship is to strengthen the gradient and spatial trends found in the original weekly data, so strong relationships get stronger and weak relationships stay the same or get weaker. This is in contrast to the general lack of spatial change with aggregation for slope and y-intercept values in the $\delta^{18}O$ vs. PDt regression because the relationship stays more or less the same despite a narrower range of values.

3.5.2 Relationship changes by month and by season

Regression slopes, y-intercepts, and r^2 values for the relationship between $\delta^{18}O$ and PDt do not have a clear seasonal trend across the 25 sites, but large monthly variations are still present (Figure 19). Steep slopes and low y-intercepts occur in both winter and late summer, while the opposite is the found in late spring through early summer and October. The high July, August, and September slopes are unusual in that they interrupt what would otherwise be a fairly clear seasonal trend of higher slopes with cooler temperatures. An increase in the degree of moisture recycling or relative dominance of convective precipitation during these months across the study region could increase potential $\delta^{18}O$

variability for a given temperature. With the smaller sample size available within the monthly groupings, a greater $\delta^{18}O$ range in summer would likely result in higher slopes, but with a reduction in r^2 values. This summer drop in r^2 value is indeed present and most notable in the data grouped by season.

The relationship between $\delta^{18}O$ and PDt for each month and season is weaker than the relationship calculated with the entire data. This is likely due to the reduced temperature range in a given temporal grouping and is similar to the observation that sites with reduced annual temperature ranges have lower overall correlation and weaker fit (Chapter 2). There are no clear month-to-month trends in r^2 values, but the spring and autumn seasons have higher r^2 values and lower values are found in the winter season and are particularly low in the summer season. Winter r^2 values may be impacted by the change in fractionation that occurs with frozen precipitation, while low summer values are possibly due to reduced temperature variance and/or convective precipitation.

A surprising result of this research is that temporal grouping reveals a clear seasonal trend in the slope and y-intercept value of the $\delta^{18}O$ vs. PDa relationship, as well as surprisingly high r^2 values in many months. Although no site has a significant relationship between $\delta^{18}O$ and PDa in the overall data, some southeastern sites (MS30, NC35, and TN00) have a relatively strong fit ($r^2 > 0.22$) during the summer months. Summer precipitation in the southeastern United States is dominated by convective precipitation, and it is possible that an amount effect would manifest in these conditions; however, the r^2 value is still rather low even for the sites with the strongest fit. Additionally, a significant relationship between $\delta^{18}O$ and PDa is not seen consistently across the southeastern sites, confounding attempts to conclusively link the amount effect to the southeastern region in summer.

Although most sites show at least one month with a statistically significant (p-value < 0.05) r^2 value for the $\delta^{18}O$ vs. PDa regression, no single site has enough months with a significant r^2 value to identify any seasonal trends. However, the mean slope and y-intercept for all 25 sites clearly shows maximum values in winter and minimum values in summer (Figure 19). The r^2 values follow a bimodal

pattern with highest values in winter and late summer through early fall. The increase in the strength of the relationship between $\delta^{18}O$ and PDa during the summer is understandable as the reduced temperature variability and increased convection in summer could allow an amount effect to emerge in the $\delta^{18}O$ data. Although the amount effect does not emerge enough to dominate the $\delta^{18}O$ variability (maximum r^2 for $\delta^{18}O$ vs. PDa in a summer month in only 0.12), the relationship between $\delta^{18}O$ and PDa does have negative slopes (-0.50 to -0.98‰/log mm) during the summer months with the highest r^2 values as expected from an amount effect. For comparison, the strong amount effect observed in San Salvador, El Salvador, produces a slope of -1.24‰/log mm (IAEA/WMO, 2016). Summer is the most common season for sites to have statistically-significant r^2 values for the $\delta^{18}O$ vs. PDa relationship (ten sites) while July and August are the most common months (six and five sites, respectively).

The increased slopes and r^2 values for $\delta^{18}O$ vs. PDa relationship in winter months may seem counter-intuitive given the importance of the amount effect in tropical climates. However, much winter precipitation, generally from extratropical cyclones, occurs prior to the arrival of the ensuing colder air mass. The heaviest snows are also typically relatively warm and close to 0°C, since colder air cannot hold as much moisture. Additionally, winter rain events during relatively warmer conditions will commonly produce greater liquid precipitation amounts than snow events. It is probable that the positive slopes seen in the $\delta^{18}O$ vs. PDa regression during winter are actually driven by the temperature effect: more precipitation in winter occurs during relatively warmer air temperatures, which produce greater $\delta^{18}O$ values. This temperature control on precipitation amount lessens from spring through autumn when moisture content of air masses is not as restricted by temperature. A similar effect is seen spatially where colder sites have a positive 'amount effect' slope and warmer sites have either negative slopes or slopes near zero (Chapter 2).

Only four sites have a winter season with a statistically significant r^2 for the $\delta^{18}O$ vs. PDa regression, but three of these (MI09, VT99, and WI99) are the study sites with potential lake-effect or

lake-enhanced snow. Lake-effect and enhanced snow occurs after cold wind blows over an open water lake and is recognized as having particularly low $\delta^{18}O$ values (Burnett et al., 2004). Although lake-related snow can sometimes result in large accumulation, most individual events at these sites will not involve a large amount of melted moisture compared to a standard rain event. Thus, lake-effect or lake-enhanced snow will register as low amount events with exceptionally low $\delta^{18}O$ values; this will produce a large positive relationship that enhances the previously stated role of temperature on winter amount effects.

3.5.3 Impacts for paleoclimate and environmental studies

Although $\delta^{18}O$ and climate relationships and spatial trends in the data in this study are similar to the findings of previous studies, the work has documented greater temporal variability than previously recognized in the scientific literature and in the study region. The greater variability uncovered is important because it suggests that care must be taken in selecting the regression relationships for use in paleoclimate and environmental studies. One of the earliest uses of precipitation isotopic data was as a paleotemperature predictor using the global $\delta^{18}O$-temperature equation reported in Dansgaard (1964). This use has fallen out of favor as the complexities of precipitation fractionation typically result in margins of uncertainty much too large to be of use. The research in this chapter also found large uncertainties in predicting temperatures from precipitation $\delta^{18}O$ values using weekly, monthly, and seasonal data and well as data grouped by month and by season (Appendix 5).

Aggregation generally decreases uncertainty slightly due to higher r^2 values, but uncertainties can increase with aggregation towards extreme $\delta^{18}O$ values (e.g., see the -20‰ column in Table 7) and improvement even in the best of cases is not very large. Additionally, these lower uncertainties with aggregation may simply be promoting a false sense of accuracy since the weekly data are more representative of the true spread of climate and isotope values. Thus, aggregated relationships should only be used with proxy values of the same temporal resolution. For example, surface and ground waters may take months to seasons to mix before ending up at a particular depth or surface location

and application of aggregated data relationships would be warranted. However, discharge from small basins or rapid ground water infiltration may reflect weekly or even daily accumulations and associated $\delta^{18}O$ values. In this case, application of a relationship based on aggregated data is ill-advised.

Sub-annual changes in the relationship between $\delta^{18}O$ and PDt pose a dilemma if the $\delta^{18}O$ data is to be used as a temperature proxy. If $\delta^{18}O$ data is a long-term aggregate of precipitation events, using a regression derived from the entire data is probably best with the understanding that any temperature estimate comes with a large uncertainty. For samples of single precipitation events or sub-annual records, modeling with a relationship calculated for a single month or season may be more attractive due to the lower uncertainties (Table 8).

However, the exact month or season must be known in order to select the appropriate regression relationship. In addition, the r^2 values of these sub-annual temperature relationships are not all high and should be independently verified before utilization.

Significant variation in temperature estimates and uncertainties using regressions on data of different temporal scale suggests that caution is needed before application. Even for records where individual $\delta^{18}O$ samples are considered multi-annual deposits, such as many paleoclimate records, deposition seasonality issues may arise (Chapter 5). If a paleoclimate $\delta^{18}O$ record is predominately deposited in the summer, the inferred temperature may follow the summer regression rather than the overall regression. Corrections to aggregated data based on modern precipitation seasonality can be attempted, but will produce erroneous temperatures if seasonality significantly changed in the past. Thus, despite temperature being the clearest control of precipitation $\delta^{18}O$ values in the study region, interpreting $\delta^{18}O$ values as a temperature proxy is rife with problems. Interpretation of $\delta^{18}O$ in paleoclimate records such as those from speleothems should particularly avoid applying a simple transfer from $\delta^{18}O$ to temperature since past alterations in the proxy $\delta^{18}O$ seasonality and temporal mixing are largely unknown and difficult to constrain with any precision.

3.6 Conclusions

3.6.1 Remarks

Aggregation of data from weekly resolution to monthly and seasonal resolutions generally enhanced the spatial gradient of $\delta^{18}O$ vs. PDt regression fit, but did not alter slope or y-intercept values. This suggests that although the regression equation itself may be generally applied across aggregation levels, confidence in the relationship strength may be overstated if a higher level of aggregated data is used to define the relationship. Relationships between $\delta^{18}O$ and both PDt and PDa vary significantly in slope, y-intercept, r^2, and estimation uncertainty throughout a year. These sub-annual variations often result in relationships quite different from the relationship calculated from the overall data and manifest as season trends observed in an overall summary of the 25 sites examined here. These trends reveal much more variability in the relationships between $\delta^{18}O$ and both temperature and precipitation amount than the broad spatial characterizations reported in previous research using entire datasets (Dansgaard, 1964; Rozanski et al., 1993; Vachon et al., 2010a). The wide range of temperature predictions based upon the $\delta^{18}O$ vs. PDt monthly and seasonal regressions illustrate this variability well. The temperature predictions made with regressions calculated for each month and season are generally more accurate than predictions made from the entire dataset. However, applying these more accurate regressions to actual $\delta^{18}O$ data requires precise knowledge of precipitation seasonality and deposition, and temperature reconstructions remain ill-advised for most applications.

3.6.2 Most important findings

- Temporal aggregation produces higher r^2 values due to lower data variance, but does not greatly affect slope or y-intercept values.
- Isotope-climate relationships vary greatly from month-to-month and season-to-season, and are often quite different than the relationships calculated from the entire data.

- Temperature predictions using the regressions for each month and each season have better precision than the predictions made from the entire data regressions, but the difficulty in identifying the exact month or season of $\delta^{18}O$ deposition makes applications problematic

CHAPTER FOUR:

THE EFFECT OF MOISTURE SOURCE ON PRECIPITATION $\delta^{18}O$ VALUES IN THE CENTRAL AND EASTERN UNITED STATES

4.1 Introduction

The role of moisture source in $\delta^{18}O$ variability has become increasingly appreciated and attested in recent years. The precipitation $\delta^{18}O$ and climate database discussed in Chapter 2 offers an opportunity to examine and constrain the effect of moisture source on precipitation $\delta^{18}O$ values. Although moisture source analysis is best suited for daily data, the weekly United States Network for Isotopes in Precipitation (USNIP) database offers excellent spatial coverage and temporal span. The Hybrid Single Particle Lagrangian Integrated Trajectory (HYSPLIT) Model is widely used to track air mass histories and determine moisture sources for precipitation events (Stein et al., 2015) and is utilized here for daily precipitation events at seven USNIP sites to connect moisture sources to the existing precipitation $\delta^{18}O$ and climate database. Quantification of the temperature effect for USNIP sites in Chapter 2 allows the $\delta^{18}O$ data to be detrended for temperature-controlled $\delta^{18}O$ cycles. This detrending allows detection of moisture source effects that otherwise could be overwhelmed by the more dominant air temperature controls. This comparison of the temperature effect regression residuals to moisture source is unprecedented for the central and eastern United States and may help to explain the precipitation $\delta^{18}O$ variability not explained by temperature alone.

4.2 Objectives

- Using weekly data, identify moisture sources for seven sites in the American Midwest for the years 1993 and 2004 using the HYSPLIT model.
- Constrain the meteorological conditions and synoptic setups that are associated with each moisture source identified with HYSPLIT.
- Quantify the effect of different moisture sources on precipitation characteristics, including $\delta^{18}O$ values.

4.3 Background

Seawater $\delta^{18}O$ values are not consistent worldwide; rather, differences in evaporation rates and freshwater input can produce locally higher or lower seawater $\delta^{18}O$ values, respectively (Figure 20). Generally, warmer and saltier marine moisture sources have higher $\delta^{18}O$ values than cooler and fresher sources (Fairbanks et al., 1992; LeGrande and Schmidt, 2006). Since the $\delta^{18}O$ of water vapor evaporating from ocean waters reflects the initial seawater $\delta^{18}O$ value, moisture sourced from waters with distinct $\delta^{18}O$ values will also have distinct $\delta^{18}O$ signatures. Additionally, the temperature and humidity over the moisture source during evaporation can enhance the inherent seawater $\delta^{18}O$ difference in the water vapor as warmer and more humid conditions reduce evaporative fractionation (Dansgaard, 1964; Jouzel et al., 2000; Lachniet, 2009).

The effect of moisture source on precipitation $\delta^{18}O$ values can be significant for regions where water vapor comes from distinctly different sources. Parts of North America, for example, have moisture input from both the Gulf of Mexico and the Pacific Ocean. The Gulf of Mexico has higher seawater $\delta^{18}O$ values than the Pacific, and water vapor arising from the Gulf of Mexico will have higher $\delta^{18}O$ values than the Pacific. Although the $\delta^{18}O$ value of a water vapor parcel will be altered by isotopic effects as it

moves inland (Chapter 2), distinct moisture source $\delta^{18}O$ signatures are commonly identifiable in land-based precipitation (e.g., Fleitmann et al., 2007).

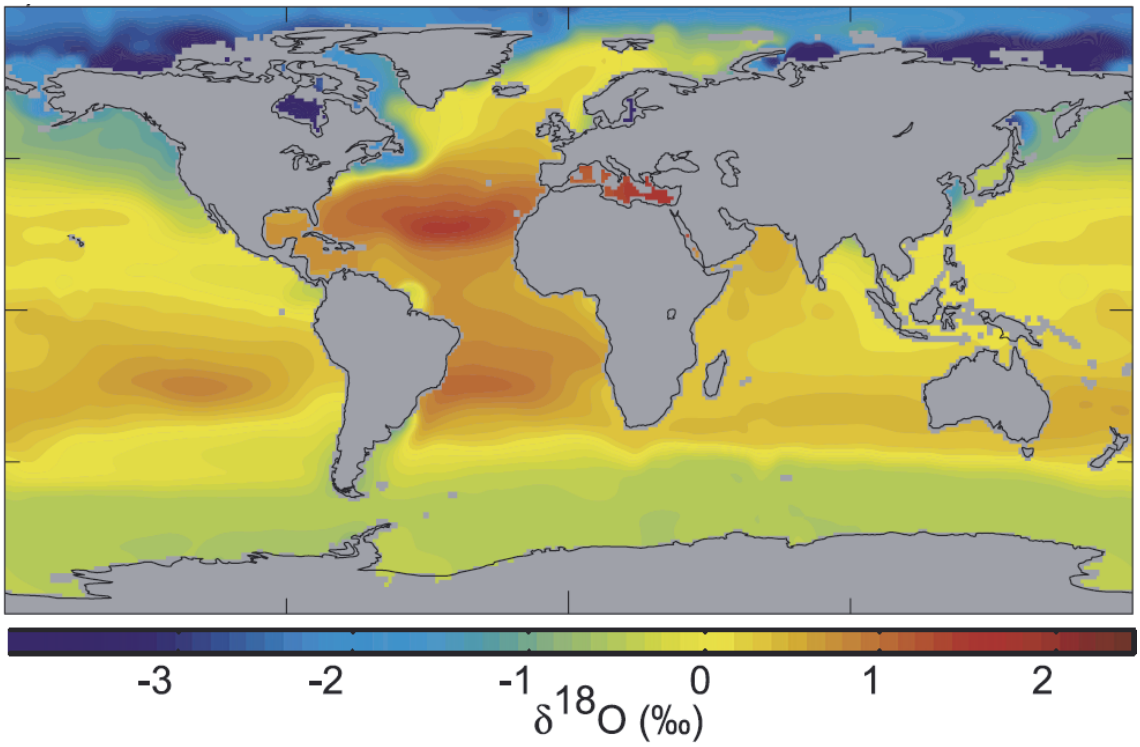

Figure 20. Map of estimated global seawater $\delta^{18}O$ values (from LeGrande and Schmidt, 2006).

The travel path and distance for moisture advection can also create or enhance a moisture source effect. Water vapor from the Pacific Ocean must travel a longer distance over higher elevations to reach the central and eastern United States than moisture from the Gulf of Mexico, and the increased rain-out effect along the Pacific route lowers precipitation $\delta^{18}O$ values beyond the inherently lower Pacific $\delta^{18}O$ values. Gulf of Mexico water vapor, in contrast, has a direct route with few topographic barriers and is less affected by rain-out and Rayleigh distillation. Transpiration and evaporation on land can be a significant source of water vapor during the growing season and warmer months, and this recycled moisture can produce distinctive precipitation $\delta^{18}O$ values (Aemisegger et al., 2014; Matsui et

al., 1983; Worden et al., 2007). Thus, continental-sourced moisture is often treated as a distinct moisture source in precipitation isotope analysis (Sjostrom and Welker, 2009).

A moisture source effect on precipitation $\delta^{18}O$ values must be distinguished from the temperature effect due to seasonal changes in air mass dominance. For example, Pacific air masses are more common in the eastern United States during winter months, and thus Pacific precipitation events will have relatively low $\delta^{18}O$ values due to the lower winter temperatures. However, this is not a true moisture source effect because the low $\delta^{18}O$ values are largely the result of the seasonal temperature effect and not the Pacific sourcing of water vapor. Distinct moisture source effects on isotopic characteristics are best be determined by examining the $\delta^{18}O$ vs. PDt regression residuals that capture the deviation from the predicted temperature effect. Moisture sources with high initial water vapor $\delta^{18}O$ values and short, direct transit paths should have positive residuals, while sources with low initial water vapor $\delta^{18}O$ values and long paths (possibly with significant altitude change) should have negative residuals. Thus, a true Pacific moisture source effect will manifest as lower than expected $\delta^{18}O$ values for a given temperature, and this deviation would be generally consistent across temperatures.

4.4 Methods

4.4.1 Sites and data

Precipitation event moisture sources were investigated for seven USNIP sites in the central and eastern United States (Table 11). These seven sites have similar weekly precipitation amounts in both USNIP and GHCN data, suggesting that the daily Global Historical Climatology Network (GHCN) meteorological data needed for moisture source modeling is well-matched to the weekly USNIP isotope data. A close precipitation amount match is necessary because the daily moisture source data must be aggregated to compare with the weekly isotope data. Only precipitation events in the periods December 1992 to February 1994 and December 2003 to February 2005 were analyzed due to the lengthy time

commitment in running the HYSPLIT model. These periods were chosen because 1993 and 2004 consistently have the highest number of USNIP samples at individual sites and have good data representation from all months. However, all possible precipitation events related to USNIP site IN22 from 1989 to 2004 were analyzed since this site is closest to the cave sampling region.

Table 11. Geographic characteristics of the seven USNIP sites and GHCN stations used for moisture analysis.

USNIP ID	***USNIP Site Name***	***Latitude (°)***	***Longitude (°)***	***Elevation (m)***	***GHCN Station ID***	***GHCN Station Name***
IL78	Monmouth	40.9333	-90.7231	229	USC00115768	Monmouth
IN22	Southwest Purdue Agricultural Center	38.7408	-87.4855	134	USC00129113	Vincennes 5 NE
MN27	Lamberton	44.2370	-95.3011	367	USC00214546	Lamberton SW
NC35	Clinton Crops Research Station	35.0258	-78.2783	41	USC00311881	Clinton 2 NE
NE99	North Platte Agricultural Experiment Station	41.0592	-100.7464	919	USC00256075	North Platte Experimental
PA15	Penn State	40.7883	-77.9458	393	USC00368449	State College
WI36	Trout Lake	46.0512	-89.6541	509	USC00475516	Minocqua

4.4.2 Moisture source categories

Climatology suggests five major moisture source areas for the central and eastern United States: Gulf of Mexico, mid-Atlantic, Pacific, Arctic, and Continental (Figure 21). Preliminary use of the HYSPLIT model suggested that the Pacific category should include three distinct subsets: General Pacific for tracks originating off the Pacific Northwest coast, Pacific-Gulf of California for tracks coming from the eastern subtropical Pacific, and Pacific-Yukon for tracks that travel from offshore the Pacific Northwest far north into northern Canada before heading south to the study sites. Additionally, moisture sources identified as 'continental' were assigned to one of seven geographic subsets: north, east, mid-Atlantic, south, midwest, southwest, and west (Figure 22). Finally, three composite moisture sources were

created by combining all continental sourced data, combining all continental-source data except continental-south, and joining continental-south data with Gulf of Mexico data. These composites were created to better understand the potential difference between HYSPLIT trajectories that clearly began in the Gulf of Mexico and travel northward (identified as Gulf of Mexico-sourced) and the trajectories that travel the same path from the south, but arise on land (identified as continental-south-sourced). The North Atlantic moisture source identified in Sjostrom and Welker (2009) was not viewed as a potential moisture source for any of the sites in this study.

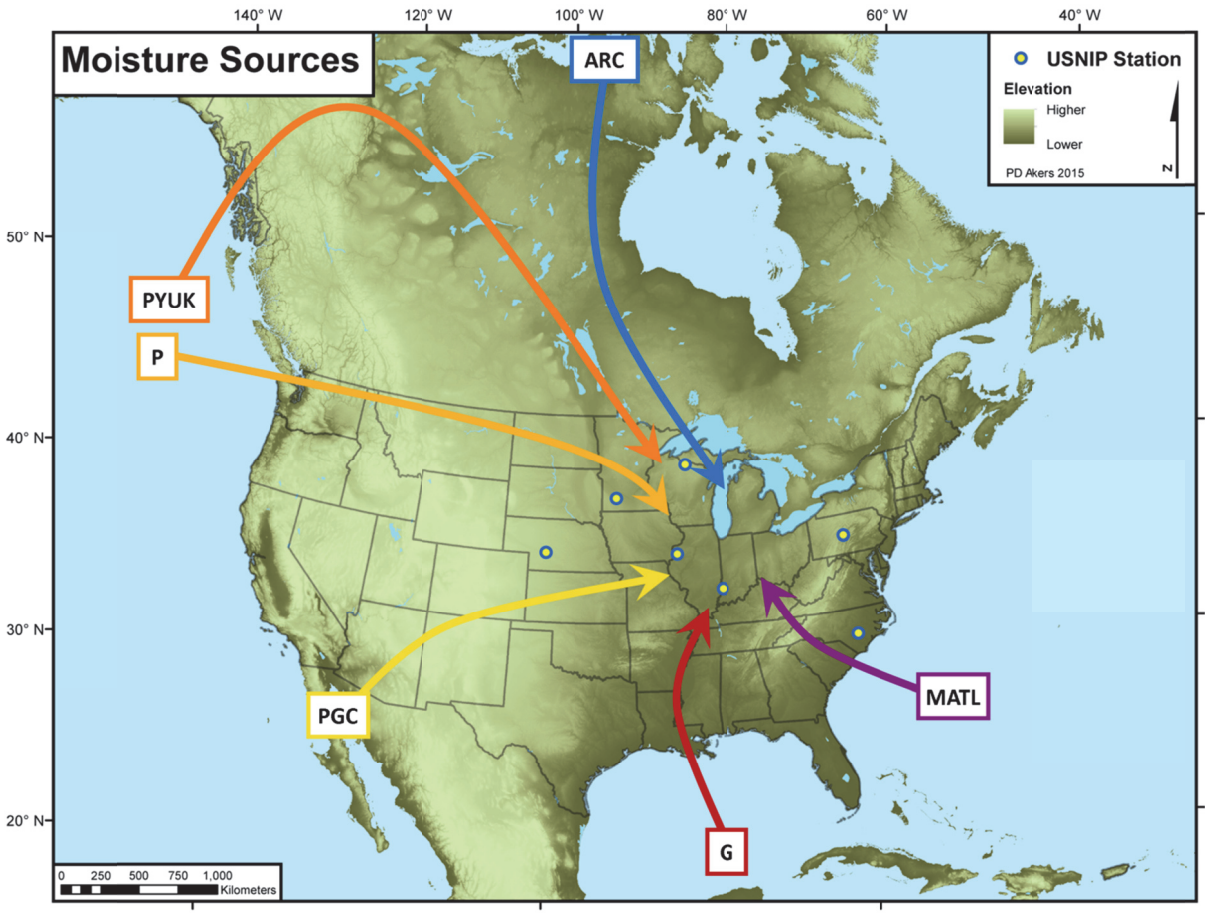

Figure 21. General geographic origin and tracking of marine moisture sources in HYSPLIT model runs and the location of the seven USNIP sites analyzed.

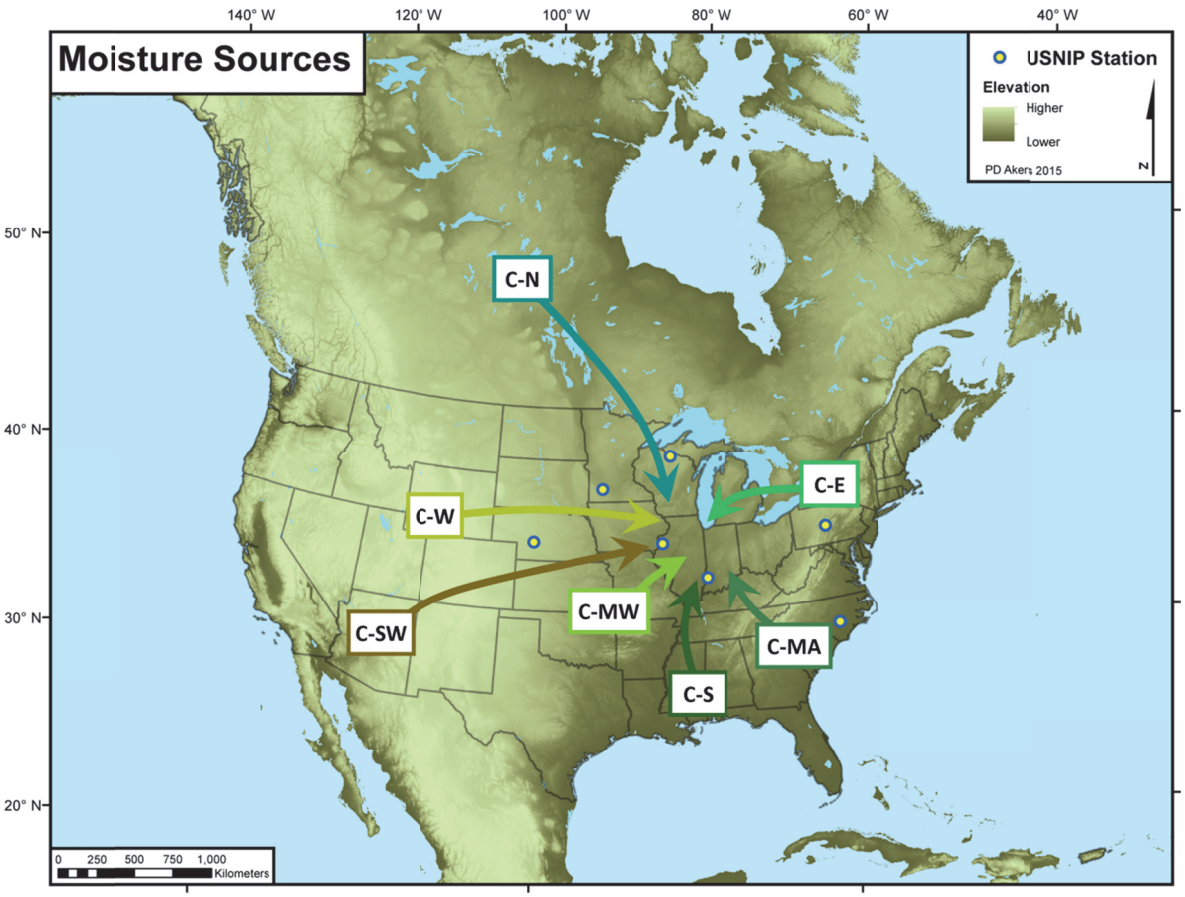

Figure 22. Geographic origin and tracking of continental moisture source subsets in HYSPLIT model runs and the location of the seven USNIP sites analyzed. Exact origin points and tracking of continental moisture sources were often unclear, and these subsets should be seen more as an overlapping continuum than as distinct sources.

4.4.3 HYSPLIT analysis

The identities of moisture sources for daily precipitation events were determined with the website-based Hybrid Single Particle Lagrangian Integrated Trajectory (HYSPLIT) model (HYSPLIT-WEB, 2015). Reanalysis (global, 1948-present) was chosen as the meteorological data input because the meteorological data sets offered by HYSPLIT with higher resolution are not available for the year 1994. Backward trajectory initiation began at the geographic coordinates of the USNIP site for each precipitation event with modeled vertical velocity. Although the latitude and longitude of the USNIP site

were used as source locations for the HYSPLIT model rather than the GHCN stations where daily precipitation events are identified, the distance between the USNIP site and GHCN station is smaller than the spatial resolution of the reanalysis dataset. Trajectories were initiated at 1500 m above ground level (AGL) to approximate the 850 mb level. This level is above the atmospheric boundary level (~500 m) for the sites chosen in this study, and the 850 mb level can be used to track heat and moisture advection. Three sites (NE99, PA15, and WI36) are located at relatively higher elevation, and trajectory initiation heights were lowered to compensate. Trajectories were tracked backward for 100 hours, but longer or shorter runs were initiated if necessary to examine unclear results.

Trajectories were run as ensembles with 27 total members representing fixed grid meteorological data offsets as opposed to single-member normal runs. The 27 ensemble trajectories are more informative than the single trajectory offered in the normal mode because the ensemble model often returns trajectories running in clusters along multiple levels of the atmosphere. Ensemble trajectories during the passage of a cold front show low-level trajectories coming from the south while upper-level trajectories come from the west or north. The single trajectory identified in a normal run may only show the western or northern component, leading to a mistaken identification of Pacific or Arctic moisture source while the ensemble trajectory suite would permit the correct identification of a Gulf of Mexico moisture source.

Most GHCN sites report the previous 24 hours of meteorological data at 8 am eastern standard time (EST), and trajectory onset was started 12 hours prior to data reporting (8 pm EST the previous day). Since exact timing of precipitation with the 24 hour reporting period is unknown in the climate data used, twelve hours prior to reporting was chosen to initiate the trajectories in the middle of the observation period. Sjostrom and Welker (2009) initiated trajectories at the reporting time; however, initiating trajectories at the reporting time commonly results in moisture source assignment to air masses not associated with the precipitation. For example, trajectories initiated after a cold front passes

will usually identify a dry Arctic or Pacific air mass as the moisture source rather than the correct Gulf of Mexico air mass that was earlier driven away. Thus, trajectories initiated at twelve hours prior to reporting are judged to best represent the moist air mass present during or just prior to precipitation. HYSPLIT run initiation times are entered as Coordinated Universal Time (UTC); since 8 pm EST corresponds to 000 UTC, the time of meteorological data reporting and the time of trajectory initiation fall on the same UTC day.

4.4.4 Moisture source assignment

Trajectories were assigned a moisture source by making a best estimate given the ensemble trajectory results. Continental sources are identified as trajectories that dropped below the 500 m boundary layer or lost clear direction while still on continental North America. In cases where multiple potential sources were evident in the HYSPLIT ensemble results, one was chosen as the primary source while a secondary source was recorded. Primary sources were generally easy to identify as possessing the bulk of trajectories and/or trajectories that clearly dropped below the boundary layer at a moisture source. In very unclear situations, primacy was given to the more likely source based upon climatology and precipitation event investigation.

For precipitation events in 2004, context about synoptic set up and precipitation was gained by comparing HYSPLIT trajectory results with archival weather radar images from Plymouth State Weather Center (PSWC, 2015). A radar image was only examined after moisture source was assigned to avoid influencing the assignments. However, if radar or general climatology suggested that a moisture source assignment was potentially wrong, the HYSPLIT model would be run at additional initiation times on the questioned date to determine if a change in moisture source assignment was warranted. Changing the source assignment in light of weather radar information rarely occurred and was typically due to an early frontal passage.

4.4.5 Data aggregation and analysis

Daily moisture sources were aggregated into weekly fractions for comparative analysis with weekly isotope data. Daily moisture sources were weighted by the daily fraction of weekly precipitation they represent and summed across the week. An overall weekly moisture source was assigned if a single source made up more than 80% of the weekly total. Weeks where no single source exceeded the 80% threshold were not included in later analysis. Statistical analysis of weekly moisture sources examined the relationship between moisture source and precipitation day temperature (PDt), precipitation day amount (PDa), $\delta^{18}O$, and the residual of the $\delta^{18}O$ vs. mean PDt regression. Regressions and residuals were calculated on an individual site basis, and not with a single regression using the data combined from all sites. T-tests were attempted to determine whether variable value differences between moisture sources were statistically significant; however, the small sample size for most moisture sources resulted in high p-values for nearly all pairings. Thus, differences between moisture sources are discussed and interpreted here largely on the basis of the mean value difference magnitude.

4.5 Results

A total of 1225 daily moisture sources were identified for the seven USNIP sites used in the moisture source study. Aggregation of the 1225 daily moisture sources produced 377 weekly moisture sources that met the 80% single moisture source threshold. This chapter refers to weeks with an identified moisture source as single precipitation events; for example, a Pacific precipitation event represents a week where >80% of moisture sources were identified as Pacific-sourced. The Pacific-Gulf of California, Pacific-Yukon, Continental-east, and Continental-mid-Atlantic moisture sources had less than five weeks each and are mainly important at only one site; thus, these moisture sources were excluded from later analysis. Composite sources are counted separately from the single-source data, and sample sizes of composite moisture sources do not equal simple addition of individual components

since individual components may not meet the 80% threshold on their own. For example, a week may be comprised of 50% Gulf of Mexico and 50% Continental-south daily events. On an individual basis, neither meets the 80% threshold and thus the week is not assigned a moisture source. However, the composite moisture source Gulf of Mexico + Continental-South does meet the 80% threshold for this week, and would be included in the composite analysis. Moisture source counts and associated isotopic and meteorological data for individual sites are shown in Appendix 2.

Meteorological and isotopic relationships with moisture sources vary from site to site (Appendix 3), which is not unexpected considering the geographic differences across all seven sites. However, some trends and characteristics are identifiable in the overall combined data (Table 12, Figure 23). The Gulf of Mexico is the dominant assignment for precipitation events at individual sites as well as the overall combined data (58% of all individual source identities). The biggest departure from Gulf of Mexico event domination is at site NC35 where mid-Atlantic moisture is equally dominant due to the proximity of the Atlantic Ocean. Continental-south events appear very likely to be Gulf of Mexico moisture, although with a more complicated travel history than normal Gulf of Mexico moisture advection; together, these two moisture sources comprise 69% of all individual moisture sources. If all 'continental' precipitation is actually sourced from the Gulf of Mexico, as seems likely, then the Gulf of Mexico accounts for 86% of all individual moisture sources considered in this study.

Table 12. Mean values for meteorological and isotopic variables by moisture source for all sites*

		Mean Values			
Moisture Source	***n***	***PDa (mm)***	***PDt (°C)***	***$\delta^{18}O$ (‰)***	***$\delta^{18}O$ vs. PDt Residual***
Gulf of Mexico	217	34.2	15.57	-5.93	0.35
Pacific	23	8.9	4.34	-11.19	-0.61
Arctic	5	8.4	9.54	-12.64	-4.94
Mid-Atlantic	23	24.0	14.99	-5.89	-0.45
C-south	43	18.6	11.25	-8.37	-0.10
C-southwest	9	12.8	19.72	-6.53	-0.47
C-west	15	17.1	14.05	-9.82	-1.98
C-midwest	33	14.6	10.66	-9.91	-0.53
C-north	9	11.7	11.02	-10.46	-1.79
All Continental	137	17.6	11.13	-9.59	-0.82
All Continental - C-south	65	14.6	12.31	-9.79	-1.00
Gulf of Mexico + C-south	286	32.3	14.62	-6.43	0.25

*Shading identifies lower (blue) and higher (red) values per column. C = continental sources.

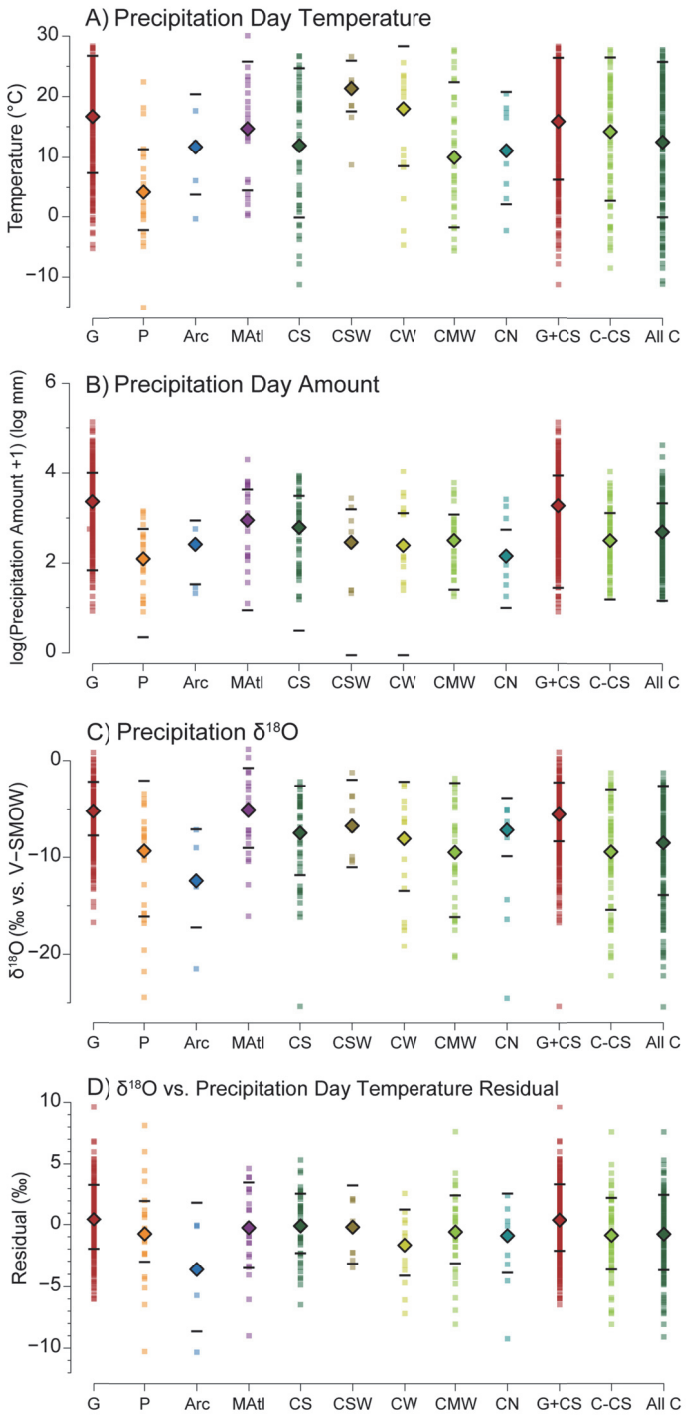

Figure 23. Meteorological and isotopic values from seven USNIP sites plotted by moisture source. Precipitation amount values have undergone a log transformation for visualization purposes. Individual squares represent a week of data, diamonds represent the median value for all weekly data per moisture source, and black bars indicate the median absolute deviation for all weekly data per moisture source.

Gulf of Mexico precipitation events have the highest mean precipitation amount by a large margin while mid-Atlantic events have the second highest amount. These two moisture sources also have relatively warm precipitation events. In contrast, Pacific and Arctic precipitation events have the lowest precipitation amounts, and Pacific events have the coldest temperatures. Continental precipitation events generally have moderate precipitation amounts, but variable temperatures. Continental-west events are relatively warm, and continental-southwest events are the warmest of all moisture sources. In contrast, continental-south, continental-midwest, and continental-north precipitation events are all relatively cool.

The differences in mean $\delta^{18}O$ value between moisture sources appears closely linked to the differences in mean temperature between moisture sources due to the strong temperature effect observed in the study region. Despite Gulf of Mexico dominance in all seasons, the lack of Gulf of Mexico precipitation events below -5°C results in no Gulf of Mexico precipitation event with $\delta^{18}O$ values < -17‰. Rather, these low $\delta^{18}O$ value events are dominated by continental and Pacific precipitation events. The majority of continental precipitation events have $\delta^{18}O$ values that fall within the $\delta^{18}O$ range of Gulf of Mexico events; however, the $\delta^{18}O$ range of continental precipitation extends much lower. These low $\delta^{18}O$ continental precipitation events are related to the low surface temperatures also found in these same events. However, it is worth noting that the difference between the lowest $\delta^{18}O$ value in Gulf of Mexico events and the lowest $\delta^{18}O$ value continental events is much larger than expected based on the difference in minimum temperature. The temperature effect on precipitation $\delta^{18}O$ values must be removed to determine if moisture source truly explains this disparity.

Residuals of the $\delta^{18}O$ vs. PDt regression provide information on the effect of moisture source on $\delta^{18}O$ values without the interference of the temperature effect. Although differences in mean residual $\delta^{18}O$ value exist, the ranges of residual values across moisture sources largely overlap. The only moisture

source with a positive mean residual in the combined data from all sites is the Gulf of Mexico, while Arctic-sourced precipitation has the lowest. Pacific-identified events have a moderate but negative mean residual. Mid-Atlantic precipitation has a negative mean residual, but the mid-Atlantic mean residual is still the third highest of all moisture sources.

The different continental moisture sources have variable $\delta^{18}O$ residual values, but as a group continental moisture has a low mean residual value. Continental-south precipitation has the second highest mean residual value; in contrast, continental-west and continental-north precipitation events have very low mean residual values. Continental-southwest residual values are only moderately low and lack the extreme low residual values present in the other continental events. Continental-midwest residual values are also only moderately low but have a wide variance.

4.6 Discussion

4.6.1 Radar comparisons

A better understanding of the synoptic meaning of moisture source assignments is gained through comparison of HYSPLIT trajectories with weather radar images (Appendix 3). Additionally, since the exact timing of precipitation is unknown in the isotope-climate database, the radar comparison is useful in determining how the relative position of precipitation to the trajectory initiation site (e.g., approaching the site, at the site, past the site) can affect the HYSPLIT back-trajectories. Radar analysis revealed that many precipitation events occurred during the passing of an extratropical cyclone (ETC). Although the bulk of ETC precipitation in the study region is derived from advected Gulf of Mexico water vapor, HYSPLIT trajectories and moisture source identification can vary as an ETC passes depending on the relative location of the site to the ETC. Trajectories clearly indicating a Gulf of Mexico moisture source were commonly found when the trajectory initiation site was south of an ETC core and in the ETC warm sector prior to the passage of the cold front. If trajectory initiation occurred after the cold front

had passed, the model traces the trajectories of the cold and dry air mass behind the cold front and not the actual moisture source; this can lead to erroneous assignments of a Pacific or Arctic moisture source. Repeated comparison viewing of ensemble trajectories with the associated weather radar images made it possible to decide whether an ensemble was likely indicating a wrong moisture source assignment, and it was in these circumstances that additional HYSPLIT model runs were initiated for clarification.

The continental moisture source was originally included to capture the input of moisture from evapotranspiration, but the HYSPLIT model (using the parameters chosen in this study) struggles to trace clear back trajectories for many precipitation events identified as continental. Although evapotranspiration is still believed to play a significant role in determining precipitation $\delta^{18}O$ values in the study region, radar analysis quickly revealed that the HYSPLIT model is not identifying the influence of evapotranspiration when a continental source is suggested. Rather, radar shows that trajectories identified as continental sources are consistently associated with the trajectory initiation site being located near the core of an ETC or in the wrap-around precipitation zone to the north or west of an ETC core (Figure 24, Appendix 3). The complex atmospheric circulation near ETC cores may interfere with the ability of the HYSPLIT model to accurately backtrack moisture history, particularly with the lower resolution of the Reanalysis climate data input.

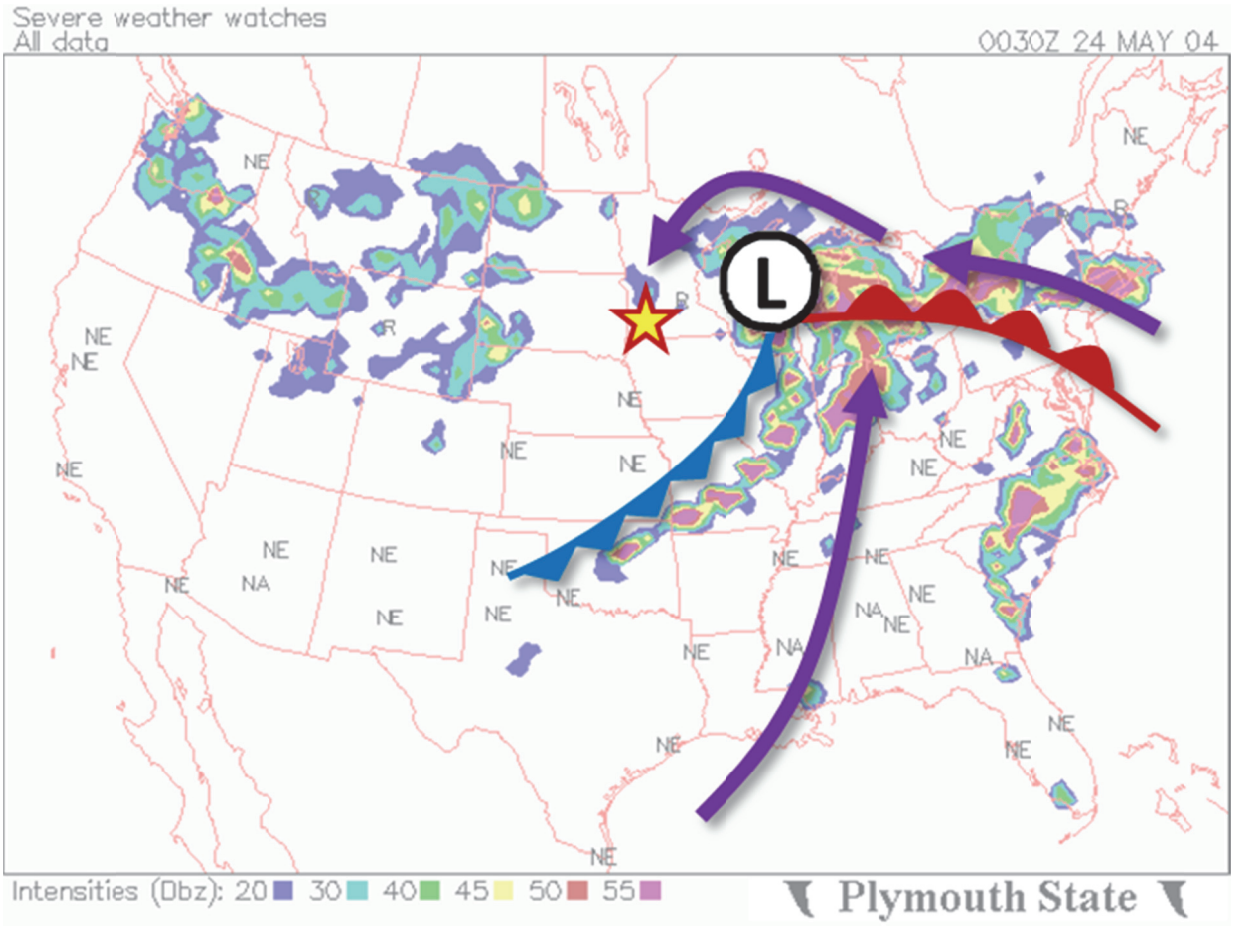

Figure 24. Weather radar indicating a nearby extratropical cyclone for a precipitation event at site MN27 identified as continental-midwest. Purple arrows show the likely routing of water vapor into the wrap-around precipitation zone.

The primary moisture source in these portions of an ETC is believed to be Gulf of Mexico water vapor. However, because wrap-around precipitation has a much different travel path and history than simple southerly advection, the continental sources were still analyzed as a separate entity and not identified as Gulf of Mexico sources. However, it should be made clear that references to 'continental sources' in this chapter are referring to the HYSPLIT identified trajectory and do not necessarily indicate that the moisture in these events was primarily derived from continental evapotranspiration. In hindsight, attempts to mark evapotranspiration as a unique continental moisture source using HYSPLIT

may have been misguided. Many precipitation events with significant influences from evapotranspiration are likely to occur in concert with southerly Gulf of Mexico or mid-Atlantic moisture advection, and separating this mixed process into binary Continental vs. Gulf of Mexico/mid-Atlantic assignments using HYSPLIT does not accurately reflect reality. A more in-depth climatology analysis along the moisture travel path is likely necessary to judge the influence of evapotranspiration rather than a basic HYSPLIT analysis.

4.6.2 Moisture source characteristics

Southerly moisture advection enables Gulf of Mexico and mid-Atlantic precipitation events, and these events are associated with summer convection and ETC squall lines in the weather radar comparison. This agrees well with the warm and wet nature of precipitation events identified as Gulf of Mexico and mid-Atlantic, as warm southerly advection provides abundant moisture for high precipitation amounts. The positive residual values for the Gulf of Mexico events also agree with an expected moisture source effect on $\delta^{18}O$ values, since the Gulf of Mexico water vapor has high initial $\delta^{18}O$ values and a relatively short and simple path to reach the study region. The negative mean residual for mid-Atlantic events is unexpected since the mid-Atlantic has high initial $\delta^{18}O$ values and a relatively simple transit path. However, the bulk of mid-Atlantic precipitation events come from site NC35, which has a fairly weak relationship between $\delta^{18}O$ and PDt. The lack of a strong linear relationship may reduce the usefulness of the residual analysis for this site. Despite this potential analytical issue, mid-Atlantic events still have a relatively high mean residual value (third highest of all moisture sites), behind only the other southerly advection sources: Gulf of Mexico and Continental-south.

While Gulf of Mexico moisture generally produces positive $\delta^{18}O$ residuals in the combined site data, sites MN27, NC35, and NE99 have negative mean residuals for Gulf of Mexico events. For MN27 and NE99, the greater distance Gulf of Mexico moisture must travel to reach these sites may result in a lower residual than found at other sites. The low residuals found at NC35 are more difficult to explain,

but Gulf of Mexico moisture reaching NC35 may have crossed the Appalachian Mountains and suffered rain-out effects. Alternatively, it is also possible that the fairly weak $\delta^{18}O$ vs. PDt relationship at NC35 described above is also a factor in the negative $\delta^{18}O$ residuals for Gulf of Mexico events.

The expected low temperatures and precipitation amounts for Arctic and Pacific precipitation events are realized in the data. These sources are typically most influential in winter months, and the low air mass temperature and long transit paths result in very little water vapor content reaching the study region. Arctic events also have the lowest mean $\delta^{18}O$ residual value, which is not surprising on account the very low initial $\delta^{18}O$ value and lengthy travel distances of Arctic moisture. Pacific events would also be expected to have a low mean residual value due to low initial $\delta^{18}O$ values and a long transit over mountainous western North America, and this agrees with the moderately low residual values observed in this analysis. The wide range and spread in Pacific event residual values, however, suggests that the meteorology associated with Pacific events is complex and quite variable.

Arctic and Pacific precipitation events have lower residual values than Gulf of Mexico events at all sites except NE99. Here, Pacific events have the greatest mean residual value (0.59‰) of the moisture source considered. However, only five Pacific events are recorded at NE99, and one event had an anomalously high residual value (8.10‰). Removing this single data point drops the mean Pacific moisture residual at NE99 to -1.28‰. This value is still slightly higher than the Gulf of Mexico moisture residual at NE99, but fits much better with the mean residual values seen for Pacific moisture at other sites.

Continental precipitation varies greatly in mean meteorological and isotopic values among the continental source subsets, although values generally fall between the extremes of Gulf of Mexico/mid-Atlantic and Arctic/Pacific events. Values observed in this analysis support the conclusion that continental-source identification is actually indicating that an ETC is passing nearby or is positioned to the south or east of the trajectory initiation site. Continental events have precipitation amounts

intermediate between Gulf of Mexico/mid-Atlantic and Arctic/Pacific events. This is likely due to the association of continental events with non-squall line and wrap-around ETC precipitation that leads to steady but moderate precipitation rates. Even in cases when a continental precipitation event is not due to wrap-around precipitation, the convoluted trajectories typically seen in model runs identified as a continental source are a probable sign that the moisture did not travel in a direct manner to reach the point of precipitation. Lacking this direct moisture conduit, potential precipitation amounts are likely to be lower due to greater previous rain-out.

Variability in the different continental geographic subsets is likely due to the wide array of different potential moisture paths and associated rain-out effects for different ETC paths and characteristics. Precipitation events from ETCs tracking well to the north of a study site will likely appear in HYSPLIT analysis as Gulf of Mexico or mid-Atlantic moisture due to clear southerly advection. When ETCs pass closer to the site, this may result in continental-south identification in HYSPLIT analysis. The continental aspect is a result of apparent problems with the HYSPLIT model in tracking air parcel movements in proximity to ETC cores. Continental-north and continental-midwest events are most common when an ETC is passing to the south and/or east of a study site and the site is located in wrap-around precipitation. The complex air mass interactions involved in wrap-around precipitation is a likely cause for the unclear ensemble HYSPLIT trajectories seen in these cases.

The relatively cool temperatures observed in continental-south, continental-midwest, and continental-north precipitation events are a likely result of the cloudy and cool conditions present in the wrap-around precipitation zone. Additionally, wrap-around snow events are typically identified as continental-south and continental-midwest sources in HYSPLIT analysis, further bringing down the temperature average. The continental-south- and continental-midwest events also have the highest temperature variability of any moisture source category. This is likely a result of the complicated weather that occurs with the passage of an ETC and the wide variability in ETC strength and character.

Some ETCs (particularly in winter) may bring about extreme temperature changes while others are much milder. This wide temperature variability supports the concept that many of the continental moisture source designations are not distinct sources in reality, but rather an artifact of the HYSPLIT model struggling with the complicated synoptic patterns around ETCs.

The mean residual values for continental-south, continental-midwest, and continental-north precipitation events potentially reflect a gradient of increased moisture travel and associated rain-out. The continental-south events have a relatively high (although still negative) mean residual. This supports the close association of continental-south events with Gulf of Mexico moisture, and the continental-south identity signifies that the moisture has been modified through interaction with an ETC beyond simple southerly advection. Continental-midwest events have a lower mean residual than continental-south events, suggesting a greater degree of water vapor modification, transit, and rain-out. Finally, continental-north events have the lowest mean residual value of these three sources, in agreement with the association of this source with the ETC backside where precipitation will have traveled the farthest and possibly been altered the most. Continental-north events may also incorporate some low $\delta^{18}O$ residual Pacific or Arctic moisture associated with the colder invading air mass.

Continental-west and continental-southwest precipitation events are more difficult to understand. Weather radar analysis is inconclusive in determining a common meteorological nature among continental-west and continental-southwest events, but they do not appear closely linked to ETC proximity as with the other continental events. Temperatures during continental-west and continental-southwest events are very high, and precipitation amounts are moderate. It does not seem likely that the arid southwestern and western United States is the actual moisture source for these precipitation events, but warm air masses from these regions could produce the high temperatures seen in the data and perhaps trigger precipitation through interacting with evapotranspiration moisture or previously-advected Gulf of Mexico moisture. Surges of monsoonal moisture may also help explain the continental-

west and continental-southwest events, while radar analysis suggests east-to-west trending stationary fronts may be linked to some continental-west precipitation.

Mean residual values differ between continental-west and continental-southwest precipitation events. Continental-west precipitation has a lower mean $\delta^{18}O$ residual than is typical of continental-southwest precipitation. If the connection between continental-west events and east-west stationary fronts is valid, this lower residual value could be the result of moisture traveling east along the southern edge of this front experiencing a great deal of rain-out before reaching the USNIP site. Any monsoonal moisture traveling across the west will likely have had significant rain-out and lower $\delta^{18}O$ residuals. Continental-southwest events, in contrast, have relatively high (although still negative) $\delta^{18}O$ residual values. The reason for this high residual is not entirely clear, although the incorporation of land-derived moisture into warm continental air masses from the southwest could potentially reduce the effect of Rayleigh distillation and rain-out. Although the climatological reason for the relatively higher $\delta^{18}O$ residuals for continental-southwest is not clear, it supports the conclusion that the HYSPLIT trajectories are not showing the actual moisture source for continental-southwest events, since the long travel from the southwest would likely result in low residual values.

When continental precipitation events are grouped together into the 'All Continental' composite, every site has negative mean $\delta^{18}O$ residual values for this composite. Removing continental-south from this composite group results in lower residual values for each site except IN22; this generally supports the idea of continental-south identified moisture being a hybrid between high-residual Gulf of Mexico moisture and the continental moisture which typically has lower $\delta^{18}O$ residuals. The individual sites generally do not have a large number of events identified as these various continental subsets (often $n < 5$), so it is difficult to derive many meaningful conclusions on a site to site basis. The high variance in continental subset residual values from site to site supports the previous concept that these continental subset identities are a result of the HYSPLIT model struggling with ETC circulation.

4.6.3 Moisture source and the overall impact on precipitation $\delta^{18}O$ values

Moisture source has an identifiable effect on weekly $\delta^{18}O$ values for the central and eastern United States. Not including the temperature effect, Gulf of Mexico precipitation $\delta^{18}O$ is on average 1‰ higher than Pacific precipitation and 4.3‰ higher than Arctic precipitation. Precipitation events with moisture sources identified as one of the continental subsets have $\delta^{18}O$ values that are generally 1.3‰ lower than Gulf of Mexico precipitation. Continental events show a great deal of variability related to the unique moisture pathways that differ from one ETC to another at a given site.

Despite moisture sources having distinct effects on precipitation $\delta^{18}O$ values, attributing year-to-year precipitation $\delta^{18}O$ variability in the study region to changing moisture sources is probably not warranted for most sites. Although the weather in the central and eastern United States is often thought of in terms of clashing air masses, the moisture source story is actually much simpler. The majority of moisture is derived from the Gulf of Mexico with relatively little input from Pacific or Arctic sources. Although Pacific and Arctic moisture play a larger role in winter precipitation, absolute precipitation amounts from Pacific or Arctic moisture are typically quite low and overwhelmed by Gulf of Mexico moisture events at seasonal or yearly aggregations. Precipitation events identified as having a continental source are associated with ETC passage and are also largely derived from Gulf of Mexico moisture (although modified by different water vapor travel paths). Thus, the surface waters and groundwater of the central and eastern United States are dominated by Gulf of Mexico-derived precipitation (grading to mid-Atlantic-derived precipitation for more eastern locations). Pacific and Arctic moisture inputs would have to increase dramatically to significantly alter yearly aggregate $\delta^{18}O$ values, which seems highly unlikely due to geographic obstacles preventing high moisture advection from these sources.

A more likely cause of year-to-year $\delta^{18}O$ variations would be changes in general ETC track, strength, and/or frequency. Continental moisture (which indicates a nearby ETC in many cases) has high

variability in all measured parameters. Relationships between specific continental subsets and meteorological trends are sometimes identifiable (for example, the association with warm temperatures for the southwest subset), but generally no clear pattern can be distinguished. The weekly isotope resolution may be responsible for some of this lack of clarity. In a single week, multiple ETCs could influence precipitation at a study site or one ETC could evolve significantly and deliver quite different $\delta^{18}O$-valued precipitation. Daily or even hourly $\delta^{18}O$ and HYSPLIT data are likely necessary to better understand the complexities of HYSPLIT-identified continental moisture sources and the effects of ETC passage on precipitation $\delta^{18}O$ values.

4.6.4 Comparison with the findings of Sjostrom and Welker (2009)

This research on the eastern and central United States found proportionally many fewer Pacific and Arctic precipitation events and more Gulf of Mexico precipitation events than were reported for this area by Sjostrom and Welker (2009). Only one site (PA15) was in common between the studies, and these studies used a different isotope datasets and examined data for different years. However, the general climatology of the eastern and central United States does not vary to the degree suggested by the results of these separate studies. The major methodological differences between the two studies revolve around the parameters entered into the HYSPLIT model. Sjostrom and Welker (2009) used a single trajectory model that increases the likelihood of erroneous moisture source assignments compared with the ensemble trajectory model used in this research. They also initiated their HYSPLIT runs at the end of the 24 hour precipitation accumulation period and started the trajectories at 3000 m ASL, while this study initiated HYSPLIT runs in the middle of the 24 hour precipitation accumulation period and started trajectories at 1500 m AGL. Test runs conducted as part of this research found that initiating a HYSPLIT run at the end of the accumulation period greatly increases the chance of tracking the air mass that came in after a precipitation event and is not representative of the actual moisture source. These post-frontal air masses most often come from the Pacific or Arctic, and the model

initiation at the end of the accumulation period is the likely cause of the Pacific and Arctic moisture source abundance in Sjostrom and Welker (2009).

The trajectory initiation level may also have led to some of the differences in moisture source frequency found in the two studies. The 3000 m level used by Sjostrom and Welker (2009) was found in this research to be a poorer representative of moisture advection than the 1500 m level used in this research. Trajectories at the 3000 m level often follow higher atmospheric flow patterns rather than actual air mass advection nearer the surface. For example, when a site is located in the warm sector of an ETC, Gulf of Mexico trajectories at 1500 m are replaced by Pacific trajectories at 3000 m because the higher trajectories are tracking the westerly flow steering the ETC. Figure 25 illustrates how these differences lead to greater assignments of Pacific and Arctic moisture sources. In searching for moisture sources, the methodology in this chapter would have focused on the 1500 m early run while Sjostrom and Welker (2009) would have used the 3000 m late run. The 1500 m early run offers the best option as it is above the boundary level of the atmosphere, but still captures the Gulf of Mexico advection supported by weather radar analysis. The 3000 m late run, in contrast, suggests a Pacific moisture source. Clearly, the two different methods would result in different conclusions about precipitation event source areas.

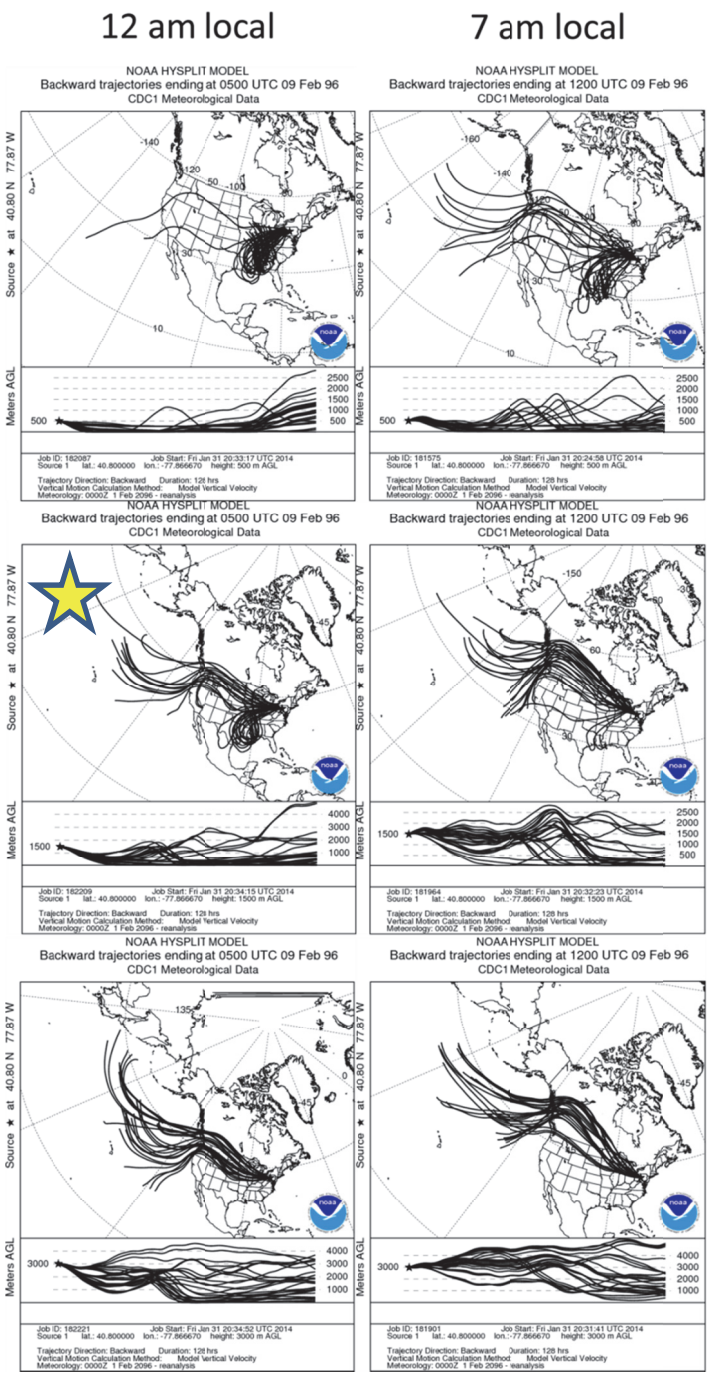

Figure 25. Changes in HYSPLIT ensemble trajectories at different atmospheric levels and initiation times during a frontal passage at site PA15. The 1500 m early run (starred) follows the methods in this chapter, and radar analysis supports a Gulf of Mexico moisture source for this event.

4.7 Conclusions

4.7.1 Remarks

This study illustrates that moisture source analysis is not limited to single event isotope databases, but can be applied to weekly data by aggregating daily moisture source information. However, in order to maintain clear signals, any given week must have the bulk of precipitation from a single moisture source (>80% in this study). This aggregation process, though necessary for analyzing a weekly-resolved isotope dataset, did result in a relatively low number of weekly moisture sources for the effort put into running the HYSPLIT model (1225 individual HYSPLIT runs to produce 377 weekly moisture sources). Additional moisture source work (more daily events run at the sites already in this study as well as the inclusion of new sites) could aid in a better understanding of the isotopic and meteorological characteristics for some of the underrepresented moisture sources (e.g., Arctic and some continental subsets).

Despite the limitations encountered with the use of weekly isotope data, this research did find identifiable moisture source effects on precipitation $\delta^{18}O$ values. Although raw $\delta^{18}O$ values show considerable variation among precipitation across the different moisture sources, this is largely attributable to the temperature effect. Actual moisture source effects are identified by examining the residuals from the $\delta^{18}O$ vs. surface temperature regression, which essentially removes the temperature effect. Precipitation closely associated with southerly advection from warmer moisture sources (Gulf of Mexico, mid-Atlantic, continental-south) had higher than average residuals, while precipitation from distant and colder moisture sources (Pacific and Arctic) had lower than average $\delta^{18}O$ residuals. Precipitation events identified with a continental source are believed to be a sign of moisture incorporated into an ETC. These events generally have moderately negative residuals, and this is thought to be a result of Rayleigh distillation from a longer travel path and greater uplift during ETC incorporation compared to southerly advection.

Seasonal and yearly precipitation across the study region is strongly influenced by the warmer moisture sources (Gulf of Mexico for most of the region, mid-Atlantic in eastern areas). Increasing the input of Pacific and Arctic moisture enough to significantly change the yearly precipitation $\delta^{18}O$ value is not likely due to geographic limitations. Changes in ETC tracking and characteristics are more likely to play a role in explaining some of the variability found in the residuals of the $\delta^{18}O$ vs. surface temperature regression, but weekly isotope data appear too coarsely-resolved to robustly quantify any relationships. These changes in ETC tracking and character may be better examined through climate teleconnection indices and this will be attempted in Chapter 6. Thus, a classic interpretation and clear expression of a moisture source control on precipitation $\delta^{18}O$ values was not identified in this study and is not thought to be an identifiable source of long-term precipitation $\delta^{18}O$ variability for the study region. This is in contrast to many studies that casually cite increases in Pacific and Arctic moisture to explain long-term changes in precipitation $\delta^{18}O$ values, but this modern analysis simply does not support such dramatic increases in alternate moisture sources. While an increase in the dominance of dry Pacific and/or Arctic air masses could drive greater Rayleigh distillation of southerly-sourced moisture, this is not a moisture source effect as commonly-referenced, but rather an effect of changes in atmospheric flow patterns and should be clarified as such**.**

4.7.2 Most important findings

- Different moisture sources do have an identifiable effect on precipitation $\delta^{18}O$ values in the eastern and central United States, but the effect is too small to be a major control on precipitation $\delta^{18}O$ variability.
- Precipitation events identified as continental-sourced in HYSPLIT are likely derived from Gulf of Mexico water vapor, but the moisture is altered by interaction with extratropical cyclones.

CHAPTER FIVE:

THE CREATION AND VERIFICATION OF A NEW PRECIPITATION SEASONALITY METRIC: THE SUMMER SIGNAL ANOMALY (SSA)

5.1 Introduction

Using a $\delta^{18}O$ record for paleoenvironmental interpretation requires an understanding of long-term controls on precipitation $\delta^{18}O$ variability. Chapter 2 quantified the temperature effect on modern precipitation $\delta^{18}O$ values for the eastern and central United States using a weekly database. However, this temperature effect does not apply well to paleoclimate $\delta^{18}O$ records because of the large predictive errors (> ±10°C) and sub-annual changes in the relationship. A direct transfer to air temperature is also difficult to interpret for $\delta^{18}O$ records that are analyzed at multi-annual resolution. A calculated change in air temperature based on precipitation $\delta^{18}O$ values could be a result of a change in annual air temperature, but it could also be from a shift in precipitation seasonality (Hardt et al., 2010; Vachon et al., 2007). If a year has a greater fraction of precipitation during warmer months, the overall annual $\delta^{18}O$ value will reflect the warmer temperatures during precipitation and have a higher $\delta^{18}O$ value and vice versa for winter.

A variable expressing seasonality effects on precipitation $\delta^{18}O$ values has potential use for paleoenvironmental studies in the eastern and central United States. Even southeastern USNIP sites with a weak temperature effect still experience a seasonal cycle in $\delta^{18}O$ values, with lower values in winter and higher values in summer. Changes in the seasonal balance of precipitation will accordingly change the overall $\delta^{18}O$ value of the aggregated precipitation total. Significant changes in precipitation seasonality could lead to large variability in long-term $\delta^{18}O$ records. In contrast, the relatively small

range in mean annual temperature over the Holocene is likely overwhelmed by the natural variance in precipitation seasonality.

A new quantitative metric for interpreting $\delta^{18}O$ values, called the "Summer Signal Anomaly" (SSA) translates precipitation $\delta^{18}O$ values into precipitation seasonality anomalies relative to the modern (1950-2013) precipitation seasonality. This variable is designed for $\delta^{18}O$ records aggregated at an annual or greater resolution. Ideally, applying the SSA to a long-term $\delta^{18}O$ record will identify periods when the precipitation regime was more summer-dominated than modern and when it was more winter-dominated than modern. This chapter explains the creation and verification of the SSA model using southern Indiana as an example. The SSA is later used in Chapter 6 as one possible climate control on interannual precipitation $\delta^{18}O$ variability, and its suitability for interpretation of stalagmite $\delta^{18}O$ will be judged in that chapter.

5.2 Objectives

- Calculate SSAs for modern climate records in southern Indiana.
- Verify the accuracy and precision of the SSA model in representing precipitation seasonality changes.

5.3 Methods

5.3.1 Site seasonal $\delta^{18}O$ signals

Seasonal $\delta^{18}O$ signals were calculated for each USNIP site using the database discussed in Chapters 2 and 3. These signals are the mean $\delta^{18}O$ value (weighted by precipitation amount) of all weekly $\delta^{18}O$ measurements for each season. USNIP site IN22 is the focal site for the verification of the

SSA. Although the $\delta^{18}O$ signals can be calculated for all seasons, the SSA model only requires summer and winter values.

5.3.2 Calculating modern precipitation seasonality

Only three years (1992, 1993, and 2004) of precipitation data in the USNIP database are complete enough at site IN22 to calculate an annual $\delta^{18}O$ value. This is not enough years to define a modern seasonality value, so years of isotope data were created using the seasonal $\delta^{18}O$ signals described above and daily precipitation data for Indianapolis International Airport and Louisville International Airport. The sampled Indiana caves lie along a transect running between these two airports, and airport precipitation data were downloaded from the Global Historic Climate Network for the period 1948 to 2015. Daily precipitation amounts were summed into seasonal totals for each year to calculate the seasonal fractions of annual precipitation for each year. Each seasonal fraction is multiplied by the corresponding seasonal $\delta^{18}O$ signal identified for IN22, and all four seasons are summed to give an estimate of the annual $\delta^{18}O$ value for each year. This produces 67 yearly $\delta^{18}O$ values each for Indianapolis and Louisville. It must be made clear that these $\delta^{18}O$ values are constructed with the assumption that the only factor affecting the yearly $\delta^{18}O$ value is the seasonal distribution of precipitation. Quantifying how close these constructed values approximate real world annual values is not currently possible due to the limited number of yearly $\delta^{18}O$ observations; however, an attempt to calculate potential estimate errors is detailed in the SSA model verification section later in this chapter.

5.3.3 SSA calculation

The SSA assumes that seasonal temperature influences on aggregated precipitation $\delta^{18}O$ values can be simplified into just summer and winter influences. This assumption is made because summer and winter offer extreme $\delta^{18}O$ values which have the greatest effect in shifting the aggregated mean $\delta^{18}O$ value. Since spring and autumn $\delta^{18}O$ signals are similar to the aggregated mean $\delta^{18}O$ value, changes in

their seasonal precipitation fraction amounts have much less effect on aggregated mean $\delta^{18}O$ values. With this simplification, the fraction of summer-signal precipitation relative to winter-signal precipitation can be calculated for a given $\delta^{18}O$ value as follows:

Equation 1:

$$(X_{summer} * \delta^{18}O_{summer.signal}) + ([1-X_{summer}] * \delta^{18}O_{winter.signal}) = \delta^{18}O_{water.sample}$$

where X_{summer} is the summer-signal precipitation fraction and $[1-X_{summer}]$ is the winter-signal precipitation fraction (combined they must equal one because of the seasonal simplification).

It is important to note that the summer-signal precipitation fraction is not equivalent to the fraction of summer precipitation one might calculate based on actual meteorological data. This simple model assumes that all precipitation with a $\delta^{18}O$ value greater than the mean of the summer + winter $\delta^{18}O$ signals is "summer-like" because it pushes the aggregate $\delta^{18}O$ value toward the summer extreme, and vice versa for winter. Results are reported and referenced here in terms of summer-signal fractions rather than winter largely for consistency; it is very simple to calculate winter-signal fractions from any summer-signal fraction if so desired by subtracting the summer-signal fraction from one.

Annual summer-signal fractions were calculated for each year in the Indianapolis and Louisville databases. The *modern mean summer-signal fraction* for each city is defined as the average of all summer-signal fractions from 1948 to 2015. The actual SSA value is the $\delta^{18}O$ deviation from this modern mean summer signal fraction in a given year or given sample and is calculated as follows:

Equation 2:

SSA = [Individual year or sample summer-signal fraction] – [Modern mean summer-signal fraction]

Positive SSAs mean the precipitation is more summer-like than the modern mean, while negative SSAs represent more winter-like precipitation. Once SSAs are calculated for all years in the Indianapolis and

Louisville databases, standard deviations can be calculated to determine the range of expected SSA values for southern Indiana today.

5.3.4 SSA model verification

Potential precision and accuracy errors in SSA estimates are calculated by bootstrapping USNIP precipitation data to construct annual precipitation data for comparison. Bootstrapping is a resampling technique that builds datasets from random sampling of existing data to allow for statistical estimations of measures of accuracy. Because the USNIP database does not have a large enough sample size of complete $\delta^{18}O$ years, using bootstrapped data to make a dataset of constructed precipitation years was judged to be the best alternative. Since the data for bootstrapped years include both $\delta^{18}O$ values and precipitation amounts, SSAs calculated from the $\delta^{18}O$ values can be verified against the actual seasonality calculated from the precipitation amounts. A typical southern Indiana year has approximately 30 weeks with precipitation as estimated from the largely data-complete years of 1992, 1993, and 2004 in the USNIP database (32, 28, and 38 precipitation weeks, respectively), and picking thirty weeks at random from the IN22 data produces precipitation totals (~100 cm/yr) that match well with modern annual climatology. For the verification algorithm, a precipitation aggregation of three years was chosen to test the precision and accuracy of the SSA. Three years was judged large enough to reduce the impact of extreme values, but short enough to approximate what might be captured in a paleoclimate $\delta^{18}O$ record.

Ninety-one precipitation events were picked from the weekly USNIP database for site IN22 to create a constructed precipitation aggregation equal to three years accumulation in southern Indiana. Ninety-one events were chosen rather than an even ninety events due to fractional rounding in the algorithm. A set fraction of the ninety-one precipitation events was randomly picked from summer events and the remainder randomly picked from winter events. Eight pairs of summer and winter balance fractions were chosen to span a range of precipitation seasonality possibilities (Table 13). The

number of events needed to fill a seasonal fraction sometimes exceeded the available number of USNIP data for that season; for this reason, picking repeated values was permitted. One hundred iterations were performed for each fractional pairing for a total of 800 constructed three-year precipitation aggregation dataset.

Table 13. The eight iterated seasonal fractional pairs used to construct precipitation aggregations for both summer and winter events.

	Summer Events		**Winter Events**		**Total Events**
Iteration Set	*Fraction*	*Number*	*Fraction*	*Number*	*Number*
1	0.15	14	0.85	77	91
2	0.25	23	0.75	68	91
3	0.35	32	0.65	59	91
4	0.45	41	0.55	50	91
5	0.55	50	0.45	41	91
6	0.65	59	0.35	32	91
7	0.75	68	0.25	23	91
8	0.85	77	0.15	14	91

An estimated SSA is calculated from the weighted mean $\delta^{18}O$ value for each constructed precipitation aggregation as described previously (Equation 1, Equation 2). Actual summer seasonal fractions are calculated using the precipitation amounts in the constructed precipitation aggregations, and these summer seasonal fractions can be converted to actual SSAs in a similar manner as the estimated SSAs (Equation 2). The accuracy and precision of estimating SSAs from $\delta^{18}O$ values can be judged by comparing the estimated SSAs with the actual SSAs of the constructed precipitation aggregations.

5.4 Results

5.4.1 Site seasonal $\delta^{18}O$ signals

All USNIP sites have statistically distinct summer and winter precipitation $\delta^{18}O$ means as verified by a Welch two sample t-test (all p values < 0.001). However, visual analysis of the kernel density plots

(Appendix 4) shows that many, particularly southern, sites have a large overlap in their summer and winter $\delta^{18}O$ distributions. This overlap increases the potential error in any seasonality prediction. Winter $\delta^{18}O$ values have a greater range than summer $\delta^{18}O$ values resulting in a less peaked winter kernel density distribution. This wide range in winter $\delta^{18}O$ values means that even sites with large seasonal differences in mean $\delta^{18}O$ value have a fair amount of overlap between winter and summer $\delta^{18}O$ value ranges. At site IN22, there is a significant degree of overlap between summer and winter $\delta^{18}O$ values, but the weighted mean values differ enough to produce distinct seasonal signals (Figure 26). Spring and autumn $\delta^{18}O$ distributions and seasonal signals fall between summer and winter values. The winter seasonal signal of -9.0‰ and the summer seasonal signal of -5.7‰ are used in later calculations.

5.4.2 Modern SSAs for southern Indiana

The modern mean summer signal fraction for Indianapolis for the period 1948 to 2014 is 0.659±0.008, while the modern mean summer signal fraction for Louisville during the same period is 0.632±0.008. All calculated annual SSA values for Indianapolis and Louisville fall within a range of ±0.16 (Figure 27). The modern mean summer signal fractions are very similar for both cities, and their average rounded value of 0.65 is taken as the modern mean summer signal fraction for southern Indiana. Standard deviations of the SSA are calculated for each city at both original resolution and with a three-year averaged resolution (Table 14). The three-year averaged standard deviation highlights years of significant SSA deviation and also better approximates the temporal aggregation of the stalagmite $\delta^{18}O$ record analyzed in Chapter 7.

5.4.3 SSA model verification

The SSAs estimated using the bootstrapped aggregated precipitation data under-predict the actual SSAs by a consistent value of 0.06 across the full examined range of seasonal balances (Figure 28, Figure 29). Although estimated mean SSA values have a remarkably consistent offset from actual SSA

values, estimated SSA precision is rather low and decreases with lower SSA values. This decrease in precision is due to the higher percentage of winter events in lower SSAs and their greater $\delta^{18}O$ variability. The 2σ range of estimated SSAs is relatively large (±0.24), and this range is up to 6.5 times larger than the 2σ range of three-year averaged modern SSAs (Table 14). The standard deviation of the estimated SSAs is also twice as large as the standard deviation of actual SSAs. The nature of bootstrapped data means that repeating the analysis will not produce exactly the same results as previous attempts. However, multiple iterations of the verification algorithm were run, and the results presented here are representative of the general values seen in multiple trials.

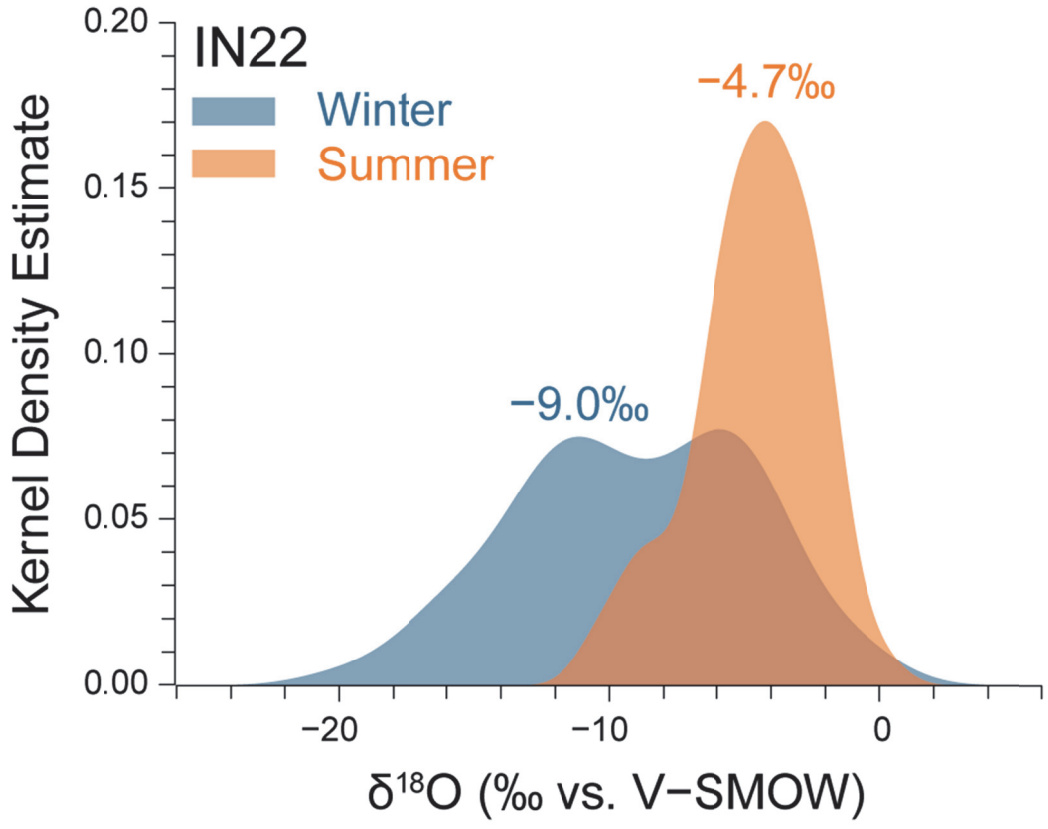

Figure 26. Seasonal kernel density estimates of summer and winter weekly precipitation $\delta^{18}O$ values at USNIP site IN22. The weighted mean value of each season (the seasonal signal) is identified .

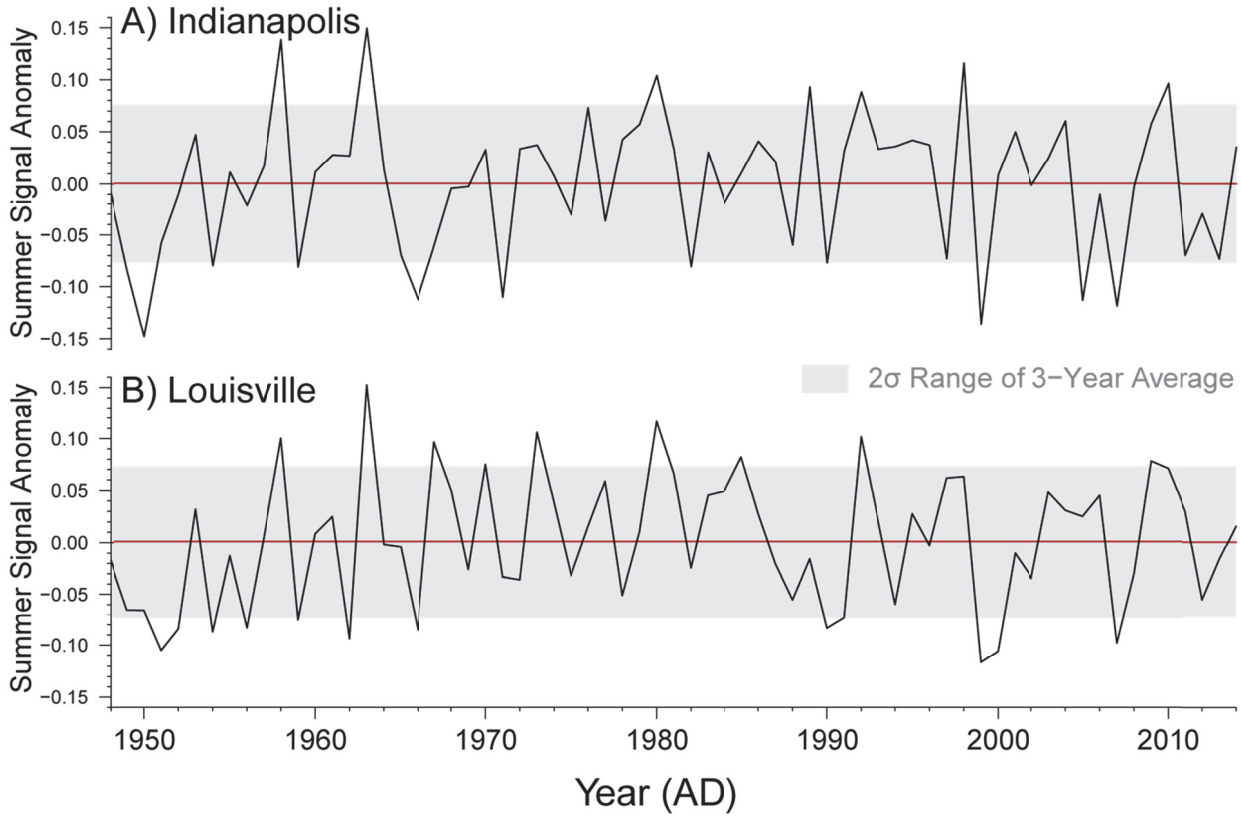

Figure 27. Summer signal anomalies (SSA) calculated for each year using precipitation data from Indianapolis and Louisville International Airports. The gray box illustrates two standard deviations of the three-year averaged data.

Table 14. Annual and three-year averaged standard deviations of SSA values from 1948 to 2014 for Indianapolis and Louisville International Airports.

	SSA Standard Deviation	
Site	***Annual***	***Three-year Averaged***
Indianapolis	0.066	0.038
Louisville	0.064	0.037

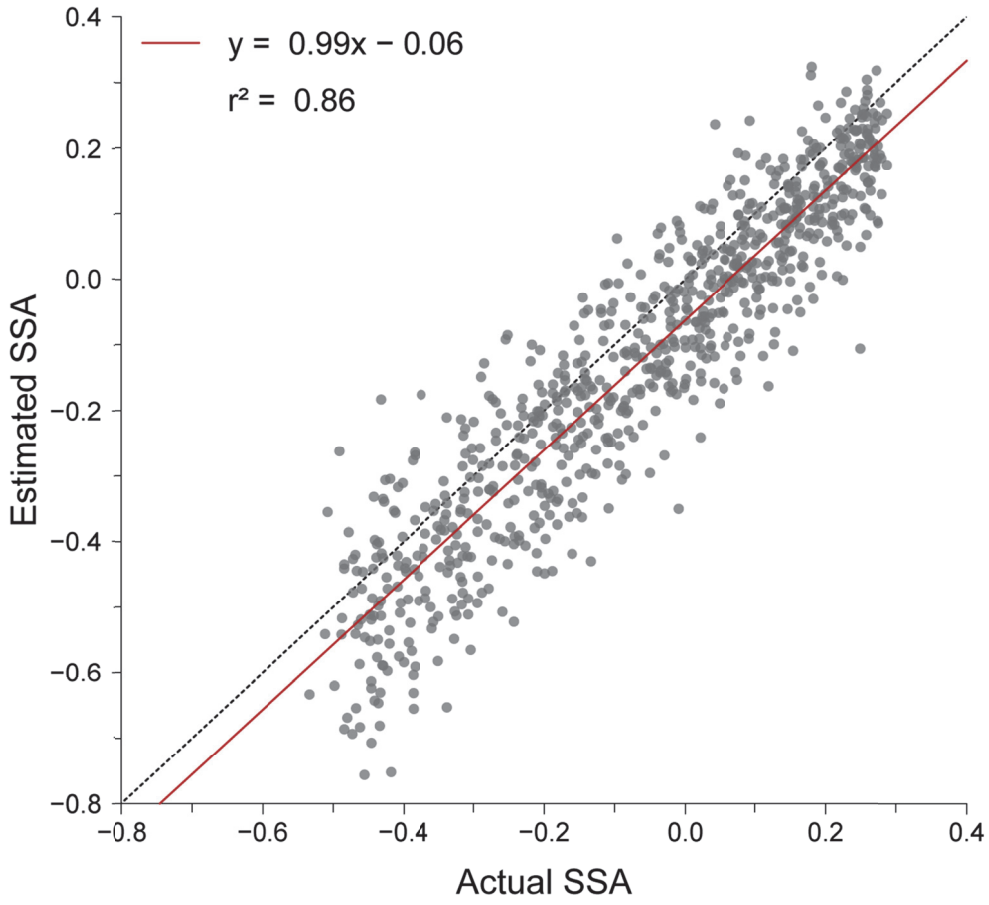

Figure 28. Estimated SSAs calculated from bootstrapped aggregated precipitation $\delta^{18}O$ values compared with the actual SSAs calculated using the precipitation amounts. The relationship between estimated SSAs and actual SSAs is strongly linear (red line) with a slope that consistently under-predicts the expected relationship (dashed black line).

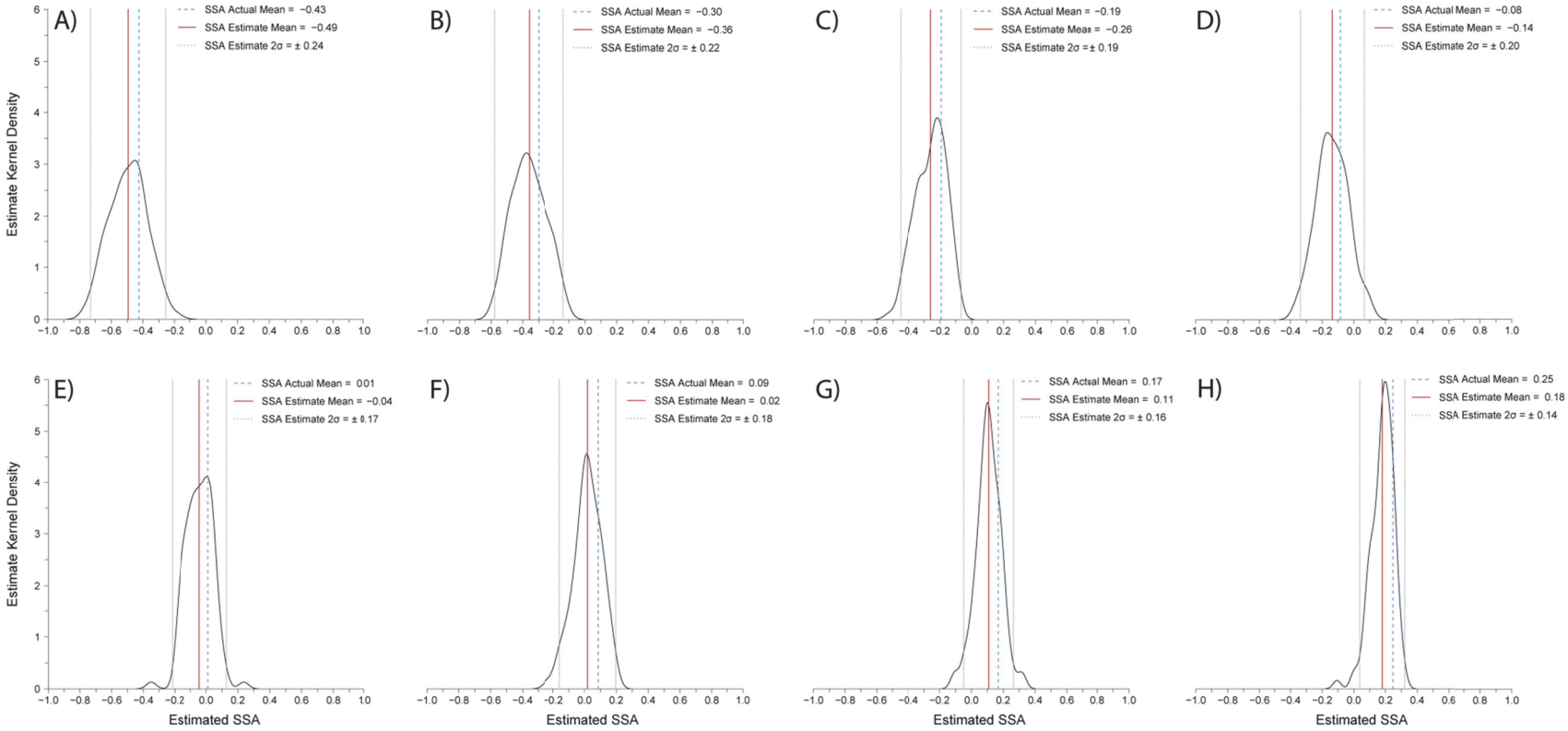

Figure 29. Distributions of SSA estimates calculated from bootstrapped precipitation aggregate $\delta^{18}O$ values. Each individual figure (A:H) represents an iteration set of fractional summer and winter events (Table 13). The actual SSA mean value for each iteration is shown with a blue dashed line, while the estimated SSA mean and two standard deviation range are shown by the red solid and gray dashed lines, respectively.

5.5 Discussion

The SSA model verification suggests that predicting precipitation seasonality from aggregated precipitation $\delta^{18}O$ values is possible. Although an offset of 0.06 exists between the estimated SSAs and the actual SSAs in the example calculated for southern Indiana, this offset is very consistent over the range of SSAs analyzed. A simple correction of 0.06 can be added to the estimated SSAs to improve the prediction accuracy, but any correlations calculated with the estimated SSAs will be the same with or without the correction because it would be applied equally to all values.

The greatest weakness of the SSA model is the lack of precision. The range of estimated SSAs calculated for a single seasonal balance (e.g., 25% summer events, 75% winter events) is larger than the entire range observed in the modern airport data. This suggests that the SSA model is not able to distinguish the level of seasonality variations seen in the modern annual data. A shift in precipitation seasonality would have to be quite large (e.g., perhaps a shift in seasonal fractions of 0.40) to confidently state that the SSA model detected a change. This limits the potential of the SSA as a method of interpreting paleoenvironmental $\delta^{18}O$ records, although applying the SSA algorithm to such records could still provide some insight, although imprecise, into precipitation seasonality changes.

5.6 Conclusions

5.6.1 Remarks

The Summer Signal Anomaly was created as a model to translate $\delta^{18}O$ values into a variable expressing precipitation seasonality fractions relative to modern seasonality. A case study of the SSA model was performed for southern Indiana using the USNIP data from site IN22 and modern climate data from Indianapolis, IN, and Louisville, KY, International Airports. The SSA estimates were verified against actual SSAs using a bootstrapped dataset that contained both precipitation $\delta^{18}O$ values and precipitation amounts. The estimated SSAs are accurate (although with a consistent, correctable offset),

but imprecise. The lack of precision is a limit to constraining and identifying changes in precipitation seasonality in southern Indiana since the potential estimation error is larger than the modern range in precipitation seasonality. However, SSAs may still prove useful as a $\delta^{18}O$ interpretation, and the bootstrapping algorithm will be used to create constructed climate and isotope data to explore controls on interannual $\delta^{18}O$ variability.

This test of the SSA model was performed for southern Indiana and USNIP site IN22; however, the basic principles and findings are applicable to most of the eastern and central United States. Regions to the north and west of IN22 with stronger and more different seasonal signals should have more precise SSA estimates, and use of the SSA model in these regions might be warranted or even favored due to the higher precision. In contrast, sites to the south and east of IN22 will likely have SSA estimates with even lower precision than southern Indiana due to the greater overlap in seasonal signal range.

The greatest benefit of the SSA model in this research may not be its interpretation of $\delta^{18}O$ values, but rather the potential to create constructed $\delta^{18}O$ years through bootstrapping as used in the verification algorithm. The lack of actual yearly precipitation $\delta^{18}O$ data hampers efforts to determine the modern controls on interannual $\delta^{18}O$ variability. Thus, the ability to create substitute annual $\delta^{18}O$ data is a useful tool to explore the correlation between precipitation $\delta^{18}O$ and potential long-term climate controls, as shown in Chapter 6.

5.6.2 Most important finding

- Although the SSA metric accurately reflects the actual precipitation seasonality balance in the verification model, the precision is too low for the SSA to be of much use quantitatively.

CHAPTER SIX:

INTERANNUAL CONTROLS ON PRECIPITATION OXYGEN STABLE ISOTOPE RATIO VARIABILITY IN THE AMERICAN MIDWEST

6.1 Introduction

Analysis of the USNIP database has revealed that precipitation $\delta^{18}O$ values are strongly correlated with precipitation day temperature (PDt) at weekly, monthly, and seasonal aggregations for portions of the eastern and central United States (Chapter 2), and the relationship between precipitation $\delta^{18}O$ and PDt at these aggregations is driven by seasonal changes in air temperature (Chapter 3). However, many paleoenvironmental $\delta^{18}O$ records are aggregated at an annual or multi-annual level, whether through long-term mixing of surface waters or through limits on sampling resolution. Relationships between PDt and precipitation $\delta^{18}O$ at an annual or multi-annual temporal aggregation have been found to be different than the weekly, monthly, and seasonal relationships both in character and strength (Rozanski et al., 1993). At multi-annual scales, environmental and climate factors that are not apparent in weekly, monthly, and seasonal relationships may emerge as major controls on precipitation $\delta^{18}O$ values. Understanding the controls on long-term precipitation $\delta^{18}O$ values is crucial to making proper interpretations of a long-term paleoenvironmental $\delta^{18}O$ record.

Many climate variables could potentially control multi-annual $\delta^{18}O$ variability in the eastern and central United States. Aside from the previously-discussed PDt, other climate variables to be examined include precipitation seasonality and the major climate teleconnections affecting North America. This chapter focuses on identifying and quantifying the multi-annual correlations between possible climate controls and precipitation $\delta^{18}O$ values for the Ohio River Valley and southern Great Lakes region. This chosen region encompasses the stalagmite sampling sites, and the correlations for sites farther from the

stalagmite sampling sites provide a broader sense of regional variability in multi-annual precipitation $\delta^{18}O$ values.

6.2 Objectives

- Construct annual climate and $\delta^{18}O$ records that are reasonably similar in character to available modern records.
- Quantify correlations between annual precipitation $\delta^{18}O$ values and potential climate control variables, and identify those that best explain the interannual variations in precipitation $\delta^{18}O$ values.

6.3 Background

Synoptic and global atmospheric pattern changes are potentially a major control on long-term precipitation $\delta^{18}O$ variability. Periodic and connected changes in geopotential height and related changes in winds, sea surface temperatures, and other meteorological factors have been identified for many locations and are quantitatively described with teleconnection or oscillation indices (Barnston and Livezey, 1987; Sheridan, 2003; Wallace and Gutzler, 1981). These oft-interacting indices have been linked to changes in North American precipitation and hydrology (Table 15), but impacts vary in magnitude and character across North America (McCabe-Glynn et al., 2013; McCabe et al., 2004; Rogers and Coleman, 2003). Teleconnections that affect North America include the North Atlantic Oscillation (NAO) (Hurrell, 1995), the Atlantic Multidecadal Oscillation (AMO) (Enfield et al., 2001), the Pacific Decadal Oscillation (PDO) (Mantua and Hare, 2002), the El Niño-Southern Oscillation (ENSO) (Trenberth, 1997), and the Pacific-North American Teleconnection Pattern (PNA) (Leathers et al., 1991). The Arctic Oscillation (AO) also affects North America, but is very closely linked to the NAO (Thompson and

Wallace, 1998) and is not analyzed separately in this study. Although not a defined oscillation, shifts in the position of the Bermuda High can alter moisture advection routing in eastern and central North America, and a more western position of the Bermuda High has been linked to increased summer precipitation in the central United States (Hardt et al., 2010; Zhu and Liang, 2012). The effect of these oscillations on North American temperatures and precipitation patterns can often alter precipitation $\delta^{18}O$ values in an identifiable way (Berkelhammer and Stott, 2008; Birks and Edwards, 2009; Welker, 2012). Although these climate oscillations are defined through analysis of modern day climate records, their existence and influence have been identified throughout the Holocene using paleoclimate records sensitive to changes in these oscillations (Knudsen et al., 2011; Rimbu et al., 2003).

Previous studies on interannual $\delta^{18}O$ controls in the American Midwest largely focused on the PNA teleconnection (Liu et al., 2011; Liu et al., 2014a; Liu et al., 2014b). This is not surprising as the PNA has very clear effects on Midwestern seasonal precipitation amounts, and the relationships between Midwestern climate variables and the other teleconnections are generally weaker and less apparent. The positive phase of the PNA consists of a meridional atmospheric flow with a ridge of high pressure over the western United States and a trough of low pressure over the eastern United States. This trough blocks moisture advection from the Gulf of Mexico and results in a drier than average winter in the Midwest. In contrast, a negative PNA phase consists of a more zonal atmospheric flow and a wetter than average Midwest from increased Gulf of Mexico moisture advection (Coleman and Rogers, 2003; Leathers et al., 1991). The correlation of the PNA index with winter precipitation amount is strongest ($r < -0.7$) in southern Indiana (Coleman and Rogers, 2003). A proposed relationship between the PNA and precipitation $\delta^{18}O$ values has been used to interpret a Holocene stalagmite $\delta^{18}O$ record from West Virginia (Liu et al., 2014a), and re-evaluation of this interpretation is one goal of this analysis.

Table 15. Information on teleconnections analyzed in this study to determine possible relationships with precipitation $\delta^{18}O$ values.

Teleconnection	**Abbreviation**	**Brief Description**	**Periodicity**	**Atmospheric Flow**		**Impact on Southern Indiana**	
				Positive Index	*Negative Index*	*Positive Index*	*Negative Index*
North Atlantic Oscillation	NAO	Barometric pressure difference between Icelandic low and Azores high	Sub-annual	Zonal	Meridional	Warmer winter	Colder winter
Atlantic Multidecadal Oscillation	AMO	Sea surface temperature anomaly of North Atlantic	Multi-annual	*	*	Drier	Wetter
El Niño-Southern Oscillation (Multivariate ENSO Index)	ENSO (MEI)	Six Pacific variable composite: sea-level pressure, zonal and meridional surface wind components, sea surface temperature, surface air temperature, and total cloudiness	Multi-annual	Zonal	Meridional	Warmer and drier winter	Cooler and wetter winter
Pacific Decadal Oscillation	PDO	Sea surface temperature anomaly of North Pacific	Multi-annual	Meridional	Zonal	Colder and drier winter	Warmer and wetter winter
Pacific-North American Teleconnection	PNA	Barometric pressure difference between Hawaii/intermountain North America and Aleutian Islands/southeastern United States	Sub-annual	Meridional	Zonal	Colder and drier winter	Warmer and wetter winter
Bermuda High Index	BHI	Barometric pressure difference between the Gulf of Mexico and the southern Great Plains	Sub-annual	*	*	Wetter	Drier

*The AMO and BHI are not generally associated with a zonal-meridional binary atmospheric flow.

6.4 Methods

6.4.1 Climate teleconnections data

Monthly climate teleconnection indices from 1950-2014 for the NAO, AMO, ENSO (specifically the Multivariate ENSO Index, or MEI), PDO, and PNA were downloaded from the NOAA Earth System Research Laboratory website (NOAA, 2015a). Additionally, monthly BHI indices as defined by Zhu and Liang (2012) were created from barometric pressure data downloaded by Jordan McLeod from the Royal Netherlands Meteorological Institute Climate Explorer website (KNMI, 2015). These monthly teleconnection indices were adjoined to the GNIP and USNIP climate data described below.

6.4.2 Multi-annual climate and precipitation $\delta^{18}O$ records

The paucity of long-term, complete precipitation $\delta^{18}O$ records for the United States is a hindrance to determining multi-annual controls on $\delta^{18}O$ variability. The precipitation $\delta^{18}O$ databases of GNIP and USNIP are two potential sources of multi-annual $\delta^{18}O$ data. Of the GNIP stations in the eastern and central United States, only the Chicago station offers a sufficiently long and sufficiently complete record of precipitation $\delta^{18}O$ for multi-annual $\delta^{18}O$ analysis. The Chicago GNIP data are a monthly dataset that began in 1962 and ended in 1979. This dataset is largely complete, although 24 months have no data and only six years have data for all months. To maximize the number of annual $\delta^{18}O$ records, a 'year' was defined as any period when twelve consecutive months had data, following the analysis of Liu et al. (2011). Unlike Liu et al., this study only uses periods with all 12 months present, while Liu accepted periods with up to two missing months. Although most of the 'years' in this consecutive 12-month dataset share their monthly data with other 'years,' this is necessary to produce enough data for correlation analysis.

The second method of constructing a multi-annual $\delta^{18}O$ database is through bootstrapping USNIP and Chicago GNIP data to create many 'years' of climate and precipitation $\delta^{18}O$ data. This same method was used in Chapter 5 to verify the predictive ability of the Summer Signal Anomaly (SSA)

model. Five USNIP sites (IL78, IN22, KY03, OH49, and WI99) were chosen for bootstrapping along with the Chicago GNIP data. The monthly-aggregated USNIP database was used instead of the original weekly-resolved database because the teleconnection indices are monthly-resolved. A constructed 'year' of climate and $\delta^{18}O$ data was created by randomly selecting one of each month (January, February, March, etc.) from each USNIP site data or from the Chicago GNIP data (Table 16). One thousand iterations created 1000 bootstrapped years of climate and precipitation $\delta^{18}O$ data for each USNIP site and the Chicago GNIP station.

Table 16. Number of individual months in the GNIP or USNIP database for each site.

	GNIP	**USNIP**				
	Chicago	*IL78*	*IN22*	*KY03*	*OH49*	*WI99*
Jan	14	8	12	8	14	12
Feb	16	11	11	7	10	11
Mar	17	12	10	10	13	13
Apr	16	12	10	10	9	11
May	17	9	10	9	8	15
Jun	16	12	12	10	11	14
Jul	16	10	10	9	10	12
Aug	16	8	8	9	10	12
Sep	16	9	8	9	8	12
Oct	17	8	8	9	11	13
Nov	16	8	7	7	7	11
Dec	15	5	7	4	8	10

Daily climate data were downloaded for the five major airports closest to the USNIP sites (Table 17) to determine actual means and standard deviations for annual temperature and SSA over the years 1950 to 2014. These statistics are compared to the bootstrapped data to see how close the bootstrapped climate data compare with real world data. Annual precipitation day temperature (PDt) means were calculated from daily temperature means over the period January-November and December of the previous year (to keep the winter months consecutive) and weighted by precipitation

amount. The airport data were used rather than Global Historical Climate Network (GHCN) data because the airport data are complete (or very nearly so) while the GHCN data used in Chapter 2 have many missing values. Filling missing daily data for the GHCN data over the years 1950 to 2014 was not feasible in any reasonable amount of time, and many GHCN stations did not exist over the whole 1950 to 2014 period. Thus, although the airports are not as close to the USNIP sites as the GHCN stations, they are close enough to be adequate for annual temperature and SSA comparison.

Table 17. Airports matched to USNIP sites for comparison with bootstrapping data.

USNIP Site	**Airport Location**
IL78	Moline, IL
IN22	Indianapolis, IN
KY03	Louisville, KY
OH49	Charleston, WV
WI99	Chicago (Midway), IL

6.4.3 Data analysis

Yearly data for the consecutive 12-month Chicago GNIP years and the bootstrapped years were analyzed in the same manner. Precipitation amount-weighted annual means were calculated for all monthly-resolved variables ($\delta^{18}O$, PDt, and teleconnection indices), and SSAs were calculated for each year following the method described in Chapter 5. Rather than use airport climate data to calculate a modern mean summer-signal fraction (the baseline to express the SSA anomalies), the mean summer-signal fraction of the 1000 bootstrapped years was substituted. In addition to annual means, seasonal means weighted by seasonal precipitation amount were calculated for each teleconnection index (e.g., Spring PDO, Summer PDO, Autumn PDO, Winter PDO, and Year PDO). Overall, 32 climate variables were compared with precipitation $\delta^{18}O$ values (Table 18). Pearson correlations were calculated between annual precipitation $\delta^{18}O$ weighted means and the climate variables. Thirty iterations of the bootstrapping were run to check for variance between iterations. Use of Chicago GNIP data for both

consecutive 12-month and bootstrapping permitted comparative analysis of the two techniques for creating multi-annual precipitation $\delta^{18}O$ data.

Table 18. List of climate variables correlated with annual weighted mean precipitation $\delta^{18}O$ values.

Climate Variable	**Temporal Sub-variable**
Precipitation day temperature	Annual weighted mean
Summer signal anomaly	Annual calculated value
North Atlantic Oscillation (NAO)	Annual weighted mean
	Spring weighted mean
	Summer weighted mean
	Autumn weighted mean
	Winter weighted mean
Atlantic Multidecadal Oscillation (AMO)	Annual weighted mean
	Spring weighted mean
	Summer weighted mean
	Autumn weighted mean
	Winter weighted mean
El Niño-Southern Oscillation (MEI)	Annual weighted mean
	Spring weighted mean
	Summer weighted mean
	Autumn weighted mean
	Winter weighted mean
Pacific Decadal Oscillation (PDO)	Annual weighted mean
	Spring weighted mean
	Summer weighted mean
	Autumn weighted mean
	Winter weighted mean
Pacific-North American Teleconnection (PNA)	Annual weighted mean
	Spring weighted mean
	Summer weighted mean
	Autumn weighted mean
	Winter weighted mean
Bermuda High Index (BHI)	Annual weighted mean
	Spring weighted mean
	Summer weighted mean
	Autumn weighted mean
	Winter weighted mean

6.5 Results

Mean annual PDt for the bootstrapped data are generally similar (less than ±1.2°C) to actual mean annual PDt estimated from the airport climate data (Table 19). However, the PDt difference between Chicago Midway Airport and both site WI99 and the Chicago GNIP is more than double (±2.6°C) the difference in other pairings. Mean annual PDt deviations are largely explained by latitudinal or elevation differences between the USNIP sites and the airports. The mean SSA is zero for all USNIP sites and airports because the SSA is defined here as the difference from the mean value. Standard deviations of both bootstrapped mean annual PDt and SSAs are similar to actual airport data but are slightly larger for the bootstrapped data.

Table 19. Comparison of annual temperatures and SSAs between one iteration of bootstrapped 1000 years and airport climate data recorded from 1950-2014.

Bootstrapped Data (1000 years)					**Measured Airport Data (1950-2014)**				
	Annual PDt		**SSA**			**Annual PDt**		**SSA**	
USNIP Site	*Mean*	*SD*	*Mean*	*SD*	*Airport*	*Mean*	*SD*	*Mean*	*SD*
IL78	14.39	1.89	0.00	0.06	Moline, IL	14.55	1.47	0.00	0.06
IN22	15.45	1.55	0.00	0.07	Indianapolis, IN	14.37	1.25	0.00	0.06
KY03	14.49	1.57	0.00	0.08	Louisville, KY	15.69	1.31	0.00	0.06
OH49	13.72	1.96	0.00	0.09	Charleston, WV	14.92	1.01	0.00	0.05
WI99	11.71	1.68	0.00	0.06	Chicago (Midway), IL	14.30	1.75	0.00	0.06
Chicago (GNIP)	12.13	1.55	0.00	0.06	Chicago (Midway), IL	14.30	1.75	0.00	0.06

Annual precipitation $\delta^{18}O$ values are correlated ($|r| > 0.2$) with some of the climate variables examined in this analysis (Table 20). Although a correlation of 0.2 is not very strong, this value is considered high enough to suggest a true, though weak, relationship. All sites examined have some correlations where $|r| > 0.2$; however, there are major correlation discrepancies between the consecutive 12-month Chicago data and the bootstrapped data. Most teleconnection variables have relatively strong correlations with the consecutive 12-month Chicago data, while SSA and PDt have low

correlations. In contrast, SSA and PDt have the highest correlations in the bootstrapped data across all sites, while correlations with teleconnection variables are much lower.

The bootstrapped correlations are similar across all 30 iterations of 1000 years, with the maximum standard deviation of any correlation across the iterations being 0.04. All bootstrapped stations show good agreement with strong correlations between $\delta^{18}O$ and the yearly BHI indices, PDt, and SSA. Slightly weaker correlations between $\delta^{18}O$ and the spring PNA and the spring BHI are also consistent across all bootstrapped stations. Some sites have relatively strong correlations between $\delta^{18}O$ and various seasons of the MEI, PDO, and PNA although no consensus is found across sites. The NAO and AMO are not well-correlated with $\delta^{18}O$ at any bootstrapped site.

The annual climate and precipitation $\delta^{18}O$ records created in this analysis permit examination of the possible climate controls on multi-annual precipitation $\delta^{18}O$ variability. While not as ideal as having actual multi-annual $\delta^{18}O$ records, the lack of such records for the eastern and central United States necessitates the use of these constructed $\delta^{18}O$ data. The bootstrapping technique is particularly flexible in design, and adaptive changes to the bootstrap algorithm can be made for different data as needed in future use.

Table 20. Correlations between climate variables and precipitation $\delta^{18}O$ values.*

	GNIP		**USNIP**					**Mean**
	12-Month	Boot-strapped	Boot-strapped	Boot-strapped	Boot-strapped	Boot-strapped	Boot-strapped	Boot-strapped
Variable	Chicago	Chicago	IL78	IN22	KY03	OH49	WI99	
PDt	0.16	0.43	0.63	0.50	0.36	0.43	0.53	0.48
SSA	0.00	0.31	0.47	0.39	0.40	0.27	0.38	0.37
NAO.yr	0.31	0.23	-0.01	0.08	0.17	-0.03	0.02	0.08
NAO.win	0.21	0.09	0.02	-0.12	0.21	0.21	-0.15	0.04
NAO.spr	0.15	0.15	-0.06	-0.06	-0.02	-0.13	0.14	0.00
NAO.sum	-0.01	0.08	0.08	0.11	-0.03	-0.09	-0.05	0.02
NAO.aut	0.52	0.07	0.06	0.13	0.27	0.07	0.09	0.12
AMO.yr	-0.45	-0.19	-0.05	-0.05	0.04	-0.07	-0.14	-0.08
AMO.win	-0.36	-0.16	0.09	-0.03	0.01	-0.13	0.00	-0.04
AMO.spr	-0.51	-0.11	-0.06	0.01	0.18	0.17	0.00	0.03
AMO.sum	-0.45	-0.06	-0.08	0.09	0.00	-0.12	-0.11	-0.05
AMO.aut	-0.39	-0.05	0.01	-0.23	-0.13	-0.04	-0.12	-0.09
MEI.yr	-0.45	0.00	-0.31	-0.19	-0.17	-0.17	0.14	-0.12
MEI.win	-0.53	-0.04	0.01	-0.12	-0.16	-0.27	-0.05	-0.11
MEI.spr	-0.39	-0.21	-0.29	0.00	0.03	0.03	0.19	-0.04
MEI.sum	-0.04	0.16	0.01	-0.28	-0.01	-0.09	0.00	-0.04
MEI.aut	-0.52	-0.01	-0.23	0.04	-0.23	-0.05	-0.01	-0.08
PDO.yr	-0.57	-0.11	0.21	-0.11	-0.05	-0.13	0.12	-0.01
PDO.win	-0.59	-0.10	-0.04	-0.16	-0.31	-0.35	0.03	-0.16
PDO.spr	-0.52	-0.24	-0.08	0.19	-0.06	0.05	0.07	-0.01
PDO.sum	-0.39	0.12	0.09	-0.34	0.16	0.03	0.02	0.01
PDO.aut	-0.33	-0.07	0.13	0.03	-0.19	-0.14	0.03	-0.04
PNA.yr	-0.53	-0.14	0.02	-0.18	-0.17	-0.38	-0.14	-0.17
PNA.win	-0.43	-0.05	0.23	0.08	0.16	-0.18	0.04	0.05
PNA.spr	-0.08	-0.08	-0.26	-0.19	-0.27	-0.30	-0.11	-0.20
PNA.sum	-0.35	-0.06	-0.01	-0.15	0.06	-0.09	-0.03	-0.05
PNA.aut	-0.39	-0.21	0.04	-0.12	-0.33	-0.15	-0.11	-0.15
BHI.yr	0.47	0.18	0.29	0.24	0.39	0.31	0.37	0.30
BHI.win	0.26	-0.05	0.06	0.02	-0.05	-0.01	0.07	0.01
BHI.spr	0.36	0.23	0.17	0.10	0.13	0.31	0.25	0.20
BHI.sum	0.25	-0.01	-0.02	0.02	0.10	0.10	0.18	0.06
BHI.aut	0.52	-0.03	0.01	0.04	0.25	0.14	0.11	0.09

*Red cells show where $|r| > 0.3$ and orange cells show where $0.2 < |r| < 0.3$.

6.6 Discussion

6.6.1 Consecutive 12 month data

The consecutive 12-month Chicago GNIP data generated some concern for its interpretation, because many of the 'years' in this data greatly overlap. For example, the first three years in the database are January 1962-December 1962, February 1962-January 1963, and March 1962-February 1963. This raises the risk of artificially increasing the magnitude of any correlation found, because similar pairs of $\delta^{18}O$ and climate values are repeatedly found in the database due to 'years' sharing up to 11 months of data. This risk appears borne out in the results, where 26 of the 32 variables have an absolute r value greater than 0.2. The consistently high correlations found between $\delta^{18}O$ and all the teleconnection indices is particularly alarming, because it is highly unlikely that every teleconnection has such a strong influence on precipitation $\delta^{18}O$ values.

Despite such problems, the relationships between climate variables and precipitation $\delta^{18}O$ values in the consecutive 12-month data do not seem random or completely erroneous. The sign of the correlation is consistent within a teleconnection, suggesting that the consecutive 12-month data can at least tell which way different teleconnections force the $\delta^{18}O$ values. Increases in annual precipitation $\delta^{18}O$ value are associated with positive NAO and BHI indices and with negative AMO, MEI, PDO, and PNA indices. This set of index signs reflects a more zonal atmospheric flow (+NAO, -PDO, -PNA) that allows for greater Gulf of Mexico moisture advection (+BHI, -PNA) and a lessened risk of summer drought (-AMO coupled with -PDO). This favorable set up for heightened Gulf of Mexico moisture transport promotes higher precipitation $\delta^{18}O$ values due to the positive $\delta^{18}O$ residuals and warmer temperatures found with Gulf of Mexico-sourced precipitation (Chapter 4). Additionally, the lack of strong temperature gradients in the Midwest during the conditions suggested by these indices reduces the rain-out effect on $\delta^{18}O$ values, particularly in winter. In contrast, the teleconnection index signs correlated with lower precipitation $\delta^{18}O$ values reflect meridional flow with a deep trough over the

eastern United States and reduced Gulf of Mexico advection. A trough offers a greater chance for low $\delta^{18}O$ Pacific or Arctic moisture to reach the Midwest and blocks the higher $\delta^{18}O$ Gulf of Mexico moisture advection. This trough can also force extratropical cyclone (ETC) tracks farther south and increase the chance of the Midwest being affected by the cooler wrap-around precipitation zone north of the ETC. This more southerly storm track enhances the rain-out effect on water vapor reaching the Midwest and produces lower precipitation $\delta^{18}O$ values.

6.6.2 Bootstrapped data

Correlations between teleconnection indices and precipitation $\delta^{18}O$ values in the bootstrapped data are much weaker. On average, only 5.5 indices out of a possible 30 have a correlation greater than 0.2 at each bootstrapped site. The lack of relatively strong ($|r| > 0.3$) NAO and AMO correlations at any of the USNIP sites studied suggests the North Atlantic has less of a forcing effect on Midwestern precipitation $\delta^{18}O$ values than the Pacific, where the PDO, MEI, and PNA show variable, but generally stronger, correlations. The annual BHI index is the only teleconnection with relatively strong correlations at all USNIP sites (all $r > 0.24$), and the positive correlation suggests higher annual precipitation $\delta^{18}O$ values when Gulf of Mexico moisture advection is favored (similar to the BHI conclusion from the consecutive 12-month data). Teleconnection indices that have an $|r| > 0.1$ at all USNIP sites include the BHI spring index and the PNA spring index. The BHI spring index has a positive correlation with precipitation $\delta^{18}O$ values, likely due again to increased Gulf of Mexico advection. The PNA spring index is a negative correlation because a positive PNA index reflects an eastern trough that blocks Gulf of Mexico advection, leading to lower precipitation $\delta^{18}O$ values. The relatively strong negative correlations between the PDO winter index and precipitation $\delta^{18}O$ values observed at KY03 and OH49 is likely because of a similar atmospheric setup as the positive PNA index.

Although the teleconnection indices have low correlations overall, the correlations between precipitation $\delta^{18}O$ and both PDt and SSA are quite high (all $r > 0.27$) at all bootstrapped sites. While

these correlations may be accurate, they may reflect a drawback of the bootstrapping technique for creating constructed multi-annual data. The bootstrapping process by nature removes the longer-term climate context and trends that would exist in actual annual data. For example, teleconnections with a slow rate of change such as the PDO typically show less variability in index value during an actual year than a bootstrapped year where data are picked from the span of a decade. The full range of variability in the multi-decadal teleconnections (PDO, AMO) may not be fully captured in the original data because it only covers the years from 1989 to 2006. Mean annual temperatures and SSAs also show a greater range of values in the bootstrapped data than in modern climate data (Table 19), again likely attributable to the removal of longer-term climate trends.

The high correlation between PDt and precipitation $\delta^{18}O$ in the bootstrapped data is likely partially explained by this wider than actual range in mean annual PDt. Actual mean annual temperatures not weighted by precipitation amount (for example, those reported in generic climate statistics) do not vary greatly from year-to-year in the central and eastern United States, and this lack of variability limits correlative relationships. Other climate variables, such as precipitation seasonality and climate teleconnections, show greater interannual variability, and their effects on $\delta^{18}O$ would be expected to overwhelm any interannual temperature effect. However, it is important to note that the PDt values used in this analysis are weighted by precipitation amount, and precipitation-weighted annual temperatures vary much more than non-weighted temperatures (Table 21). Previous studies that found annual temperature to lack significant correlation with precipitation $\delta^{18}O$ values used unweighted temperature data, and it is possible that the precipitation-weighted temperatures of the PDt actually do have an identifiable correlation with annual $\delta^{18}O$ values. The PDt and unweighted temperature data have low correlations, and thus the relationship between $\delta^{18}O$ and PDt may be significantly different that relationships with standard unweighted temperature data. Multi-annual PDt variation is likely to be

driven by changes in atmospheric flow and storm tracking, with eastern troughs and more southerly storm tracks promoting colder annual precipitation-weighted temperatures.

Table 21. Difference between precipitation-weighted and unweighted mean annual temperature and standard deviation over the years 1950 to 2014 for airport climate data.

	Precipitation-weighted Annual Temperature		**Unweighted Annual Temperature**		**Correlation of Weighted and Unweighted Data**
Airport	*Mean*	*SD*	*Mean*	*SD*	*r*
Moline, IL	14.55	1.47	10.10	0.86	0.28
Indianapolis, IN	14.37	1.25	11.57	0.80	0.39
Louisville, KY	15.69	1.31	13.96	0.84	0.14
Charleston, WV	14.92	1.01	13.01	0.67	0.28
Chicago (Midway), IL	14.30	1.75	10.67	0.89	0.12

Correlations between SSA and precipitation $\delta^{18}O$ are positive at all sites, reflecting the concept that a greater summer precipitation fraction will produce a higher annual precipitation $\delta^{18}O$ value. Whether the SSA correlations accurately reflect the actual role of seasonality on interannual $\delta^{18}O$ values is not entirely clear. While the logic behind seasonality as a major $\delta^{18}O$ control is sound (Chapter 5), the bootstrapped data likely overestimate the actual correlation since the bootstrapped SSA variability is greater than calculated for the airport data (similar to PDt). However, the difference in variability between the bootstrapped and airport data is very small for most sites, and no variability difference exists for the Moline and Chicago airports. Thus, while the correlations may be slightly overestimated, the SSA does appear to have validly-strong correlations with the bootstrapped annual precipitation $\delta^{18}O$ values.

6.6.3 Comparison of consecutive 12-month and bootstrapped data

The Chicago GNIP data produce very different correlations with climate variables depending on whether the data are transformed into consecutive 12-month yearly data or bootstrapped yearly data (Table 20). This seems unusual since both annual data transformations are drawing from the same initial

dataset. Teleconnection indices have much stronger correlations in the consecutive 12-month data (although the potential overestimation of these correlations has been discussed previously), and only five indices have an $|r| > 0.2$ in both the 12-month and bootstrapped data: annual NAO, spring MEI, spring PDO, autumn PNA, and spring BHI. Despite the difference in correlation magnitude, the sign of the correlation is the same for most indices between the two datasets suggesting that the effect of the teleconnection on precipitation $\delta^{18}O$ values is in the same direction and is valid.

The lack of a strong correlation between $\delta^{18}O$ and both annual PDt and SSA in the 12-month data is in sharp contrast to the strong correlations seen with these variables in the bootstrapped data. This difference appears due to two factors in the bootstrapped data: 1) the greater number of 'years' and 2) the wider range of mean annual temperatures and SSAs (Figure 30). The consecutive 12-month data distributions overlap entirely within the larger bootstrapped distributions, but a much clearer linear relationship is evident in the bootstrapped data. The reduced range of annual PDt and SSAs in the consecutive 12-month data is likely due to its inherent creation from only a few actual years of data, while the bootstrapping may also produce annual PDt and SSAs beyond what would actually be seen in reality. However, the greater sample size in the bootstrapped data suggests that conclusions drawn from it are likely more robust and accurate than is the case for the consecutive 12-month data. Thus, it appears likely that mean annual PDt and SSAs are indeed correlated with annual precipitation $\delta^{18}O$ values in the American Midwest.

6.6.4 Overall consensus

No single climate variable is a clear dominant control on multi-annual precipitation $\delta^{18}O$ variability across all sites and techniques examined. However, this lack of a single dominant control should not be a surprise in the climatologically-diverse American Midwest. Although no single variable stands out, a common thread of atmospheric flow pattern unites all the correlations observed. Higher annual precipitation $\delta^{18}O$ values occur in the Midwest when a flow dominates that allows for ample

moisture advection from the Gulf of Mexico. ETC tracks are displaced farther north than average, favoring precipitation directly from warm-core moisture advection over wrap-around precipitation. This promotes higher precipitation $\delta^{18}O$ values from warmer precipitation temperatures due to increased southerly advection and the positive $\delta^{18}O$ vs. PDt residuals of Gulf of Mexico precipitation (Chapter 4). Multiple teleconnections favor this set-up, including the negative PDO and PNA as well as the positive NAO and BHI.

In contrast, lower annual precipitation $\delta^{18}O$ values occur in the Midwest when a meridional flow, specifically an eastern North American trough, dominates. This blocks Gulf of Mexico moisture advection and directs ETC tracks farther south. This increases the likelihood of wrap-around precipitation whose negative $\delta^{18}O$ vs. PDt residuals and generally cooler temperatures favor lower precipitation $\delta^{18}O$ values (see discussion in Chapter 4). Additionally, the steeper temperature gradient in this flow pattern between moisture source and precipitation site increases the rain-out effect. The positive PDO and PNA and the negative NAO are associated with an eastern trough, while the positive AMO is associated with summer drought and thus an increase in winter fraction of annual precipitation.

The wider range in winter precipitation $\delta^{18}O$ values (and spring and autumn $\delta^{18}O$ values to a lesser extent), compared to summer $\delta^{18}O$ values, suggests that cool-season weather has a larger effect on annual precipitation $\delta^{18}O$ values than warm-season weather. The limited range of both precipitation $\delta^{18}O$ values and general climate variability in summer means that there is relatively little interannual variation in mean summer $\delta^{18}O$ values. Teleconnection impacts on climate are strongest in the cooler months, and extratropical cyclones are more frequent from autumn to spring. This may explain why summer teleconnection indices are best correlated ($|r| > 0.2$) with annual precipitation $\delta^{18}O$ less frequently than other seasons in the bootstrapped data (Table 22).

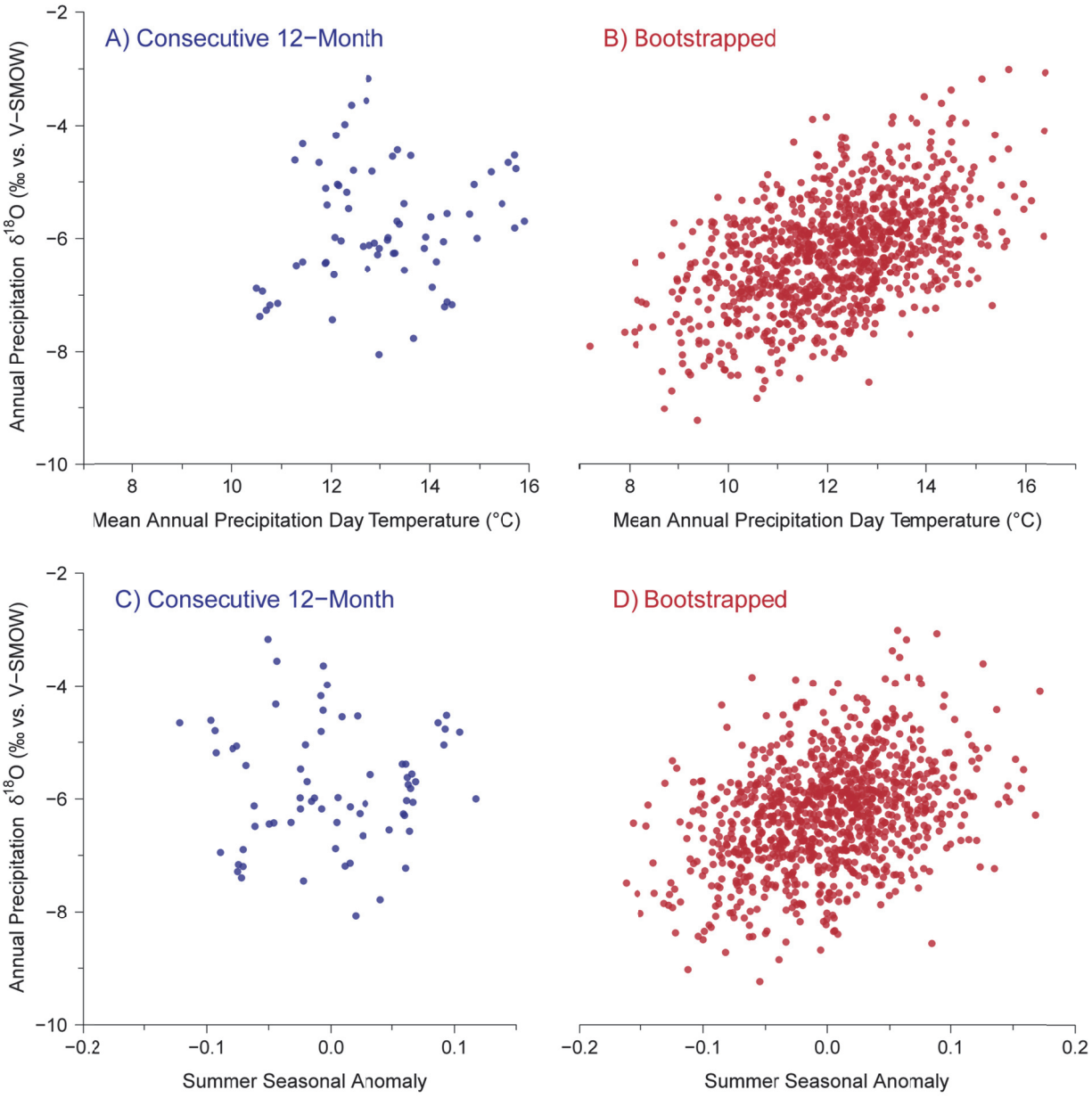

Figure 30. Difference between consecutive 12-month years and bootstrapped years derived from the Chicago GNIP data in the distribution of annual precipitation $\delta^{18}O$ vs. annual PDt (A, B) and annual precipitation $\delta^{18}O$ vs. SSA (C, D).

Table 22. Robust correlations (|r| > 0.2) between teleconnection index and annual precipitation $\delta^{18}O$ value for the bootstrapped data, sorted by temporal group of the index.

Teleconnection Index Temporal Group	**Number of Robust Correlations**
Year	9
Winter	6
Spring	9
Summer	2
Autumn	7

Precipitation seasonality as represented by SSA has a complicated relationship with the other climate variables. In a straightforward sense, higher SSAs mean that more precipitation has fallen in the warmer months, and not surprisingly this leads to higher annual precipitation $\delta^{18}O$ values. The SSA thus agrees well with the previous connections between atmospheric flow and precipitation $\delta^{18}O$ values in the warm season. However, contradictions and competing effects between precipitation seasonality and atmospheric flow become apparent in the cool season. A trough over the eastern United States in winter is associated with lower precipitation $\delta^{18}O$ values due to reduced Gulf of Mexico moisture advection and increased rain-out due to greater temperature contrast. Yet, this trough serves to limit winter precipitation amounts, which increases the summer fraction of annual precipitation and leads to higher SSAs. Higher SSAs should correspond to higher annual precipitation $\delta^{18}O$ values, but the trough promotes lower annual precipitation $\delta^{18}O$ values.

This discrepancy between the SSA and other climate effects cannot be resolved easily, especially with the lack of actual long-term climate and precipitation $\delta^{18}O$ records. However, the variability of the SSA is generally quite small (the standard deviation of SSAs from 1950 to 2014 is only 0.06). Using the seasonal $\delta^{18}O$ means for USNIP site IN22, this is equivalent to a potential $\delta^{18}O$ range of 0.27‰. In contrast, the standard deviation of winter $\delta^{18}O$ values in the seasonally-aggregated IN22 database is 2.54‰ (Chapter 3). The effect of seasonality (at least as measured by the SSA) is likely overwhelmed by

the larger potential change in winter $\delta^{18}O$ values from atmospheric flow changes. Seasonality, in effect, is better identified as a source of $\delta^{18}O$ noise, reducing the precision of interannual relationships between precipitation $\delta^{18}O$ and atmospheric flow. However, major shifts in precipitation seasonality that exceed anything in the modern record have the potential to have a greater impact on interannual precipitation $\delta^{18}O$ values.

The identification of atmospheric flow patterns as the dominate control on interannual precipitation $\delta^{18}O$ values for the Midwest follows on the conclusions drawn in Liu et al. (2011; 2014b). However, the Liu et al. papers single out the PNA as a singularly dominant control, partially based on conclusions drawn from a consecutive 12-month Chicago GNIP database. Connecting interannual precipitation $\delta^{18}O$ variability to a single teleconnection factor is neither accurate nor prudent according to the analysis conducted here. While the PNA affects atmospheric flow patterns in a manner consistent with the conclusions presented here, other teleconnections can also produce similar flow patterns and the covariance of many teleconnection indices makes singling out a lone teleconnection rather than the general resulting atmospheric effect ill-advised.

6.7 Conclusions

6.7.1 Remarks

Understanding the interannual and long-term controls on precipitation $\delta^{18}O$ variability is critical to accurately interpreting paleoclimate $\delta^{18}O$ records. Quantifying potential climate controls on $\delta^{18}O$ values is difficult for most of the United States due to a lack of long and complete precipitation $\delta^{18}O$ data. This analysis created constructed years of climate and $\delta^{18}O$ data from the two most complete and long databases available: GNIP and USNIP. This constructed dataset was examined for correlations between precipitation $\delta^{18}O$ and climate variables including mean annual precipitation air temperature, seasonality, and teleconnection indices.

The two techniques of creating constructed years (consecutive 12-month and bootstrapping) produced significantly different correlation magnitudes. Bootstrapping is believed to provide more accurate results, due to the greater sample size available, but the sign of the consecutive 12 month correlations still describes the effect of a teleconnection on precipitation $\delta^{18}O$ values. While no single climate variable dominates the correlations, together the various correlations offer a clear picture of the atmospheric conditions that control precipitation $\delta^{18}O$ values over multi-annual timescales in the American Midwest. Years have higher precipitation $\delta^{18}O$ values when the atmospheric flow promotes the advection of water vapor from the Gulf of Mexico. Lower precipitation $\delta^{18}O$ values result during meridional flow when a trough over eastern North America enhances the latitudinal temperature gradient and reduces Gulf of Mexico moisture advection. These atmospheric conditions can arise through multiple teleconnections that often co-vary; thus, identifying a single teleconnection as the major control on precipitation $\delta^{18}O$ is not warranted. Although the oft-desired direct translation from $\delta^{18}O$ to a teleconnection index does not appear applicable for the American Midwest, such a transfer function would likely lack precision due to the large amount of noise present in the $\delta^{18}O$ values available for the region due to complex climate and seasonality factors. Although a quantitative identification of the controls on precipitation $\delta^{18}O$ was not achieved, the understanding of atmospheric flow as the dominant modern control is a powerful tool for interpreting regional paleoclimate $\delta^{18}O$ records.

6.7.2 Most important findings

- High annual or multi-annual precipitation $\delta^{18}O$ values are associated with ample southerly moisture advection while low $\delta^{18}O$ values are associated with an eastern North American trough and reduced southerly moisture advection.
- Multiple climate teleconnections can result in similar atmospheric flow patterns that control precipitation $\delta^{18}O$ values; focusing on a single teleconnection is not advised.

- Precipitation seasonality is likely to influence precipitation $\delta^{18}O$ values to a lesser degree on short timescales, but is itself affected by atmospheric flow patterns and teleconnections.

CHAPTER SEVEN:

A HOLOCENE PALEOENVIRONMENTAL RECORD FROM UPPER PORTER CAVE STALAGMITES

7.1 Introduction

Stalagmites US-INUP3 and US-INUP4 (hereafter referred to as UP3 and UP4) were collected from Upper Porter Cave, IN, on July 23, 2013. UP4 was chosen for high-resolution paleoenvironmental analysis on account of its relatively long length of Holocene record and interesting petrography. A parallel paleoenvironmental analysis at lower resolution was performed on UP3 for comparison with the UP4 record. US-INUP7 (UP7), a small stalagmite from Upper Porter Cave, was also dated to provide an additional estimate of stalagmite growth timing. The findings of research discussed in Chapters 2-6 will be used to interpret the stalagmite stable oxygen isotope ratio ($\delta^{18}O$) time series to detect past climate changes. Additional environmental proxies will place the $\delta^{18}O$ record in a broader paleoenvironmental context and provide distinct records of their own. The timing of stalagmite growth, and cessation of growth in particular, emerged as an important record of past climate changes. Combined, the narrative from the Upper Porter Cave stalagmites provides a revealing insight into environmental changes occurring in southern Indiana during the Holocene.

7.2 Objectives

- Constrain the periods of growth and hiatus for Upper Porter Cave stalagmites and determine the environmental drivers of these depositional cycles.
- Integrate paleoenvironmental proxies into a single narrative that describes changes in weather patterns and hydroclimate in southern Indiana during the Holocene.

- Compare the Upper Porter Cave paleoenvironmental narrative with other paleoenvironmental records to develop a regional climate explanation for the changes observed.

7.3 Background

Seven environmental proxies were examined in UP4: stable oxygen and carbon isotope ratios ($\delta^{18}O$, $\delta^{13}C$), ultraviolet-stimulated luminescence (UVL), petrography, reflectance, tone, and clarity. The paleoenvironmental interpretation of these proxies is not universal and must be understood in context of the study region. Currently, two unpublished stalagmite records exist for southern Indiana (Chirienco, 2010; Zhang et al., 2007), but the data has not been vetted or made generally available. Thus, the interpretation of stalagmite paleoenvironmental proxies for southern Indiana has been largely unaddressed in scientific literature.

Previous studies offer varied interpretations of stalagmite $\delta^{18}O$ values. Broadly, cave drip water $\delta^{18}O$ values are assumed to reflect the complex system beginning with precipitation $\delta^{18}O$ values and any fractionation effects that may occur from evaporation during transit through the soil zone and epikarst (Lachniet, 2009). If water infiltration is rapid and transit to the cave direct, drip water $\delta^{18}O$ values can vary at the temporal scale of precipitation-events. In contrast, other waters may have slow or diffuse infiltration and transit that promotes longer-period temporal mixing, resulting in a smoothing of $\delta^{18}O$ variability (Baker et al., 2007; Baker and Brunsdon, 2003; Fairchild et al., 2006; Perrin et al., 2003). The deposition of calcium carbonate ($CaCO_3$) from drip water involves a temperature-controlled $\delta^{18}O$ fractionation; however, drip water $\delta^{18}O$ value may not be accurately preserved in the $CaCO_3$ if the system is not at equilibrium due to non-ideal CO_2 or humidity levels (Feng et al., 2012; Hendy, 1971; Lachniet, 2009). Seasonal cave ventilation in continental temperate climates favors stalagmite growth

during winter due to lower CO_2 concentrations, and this may cause bias in the stalagmite $\delta^{18}O$ record if the drip water has seasonal $\delta^{18}O$ variability (James et al., 2015).

Multi-annual precipitation $\delta^{18}O$ variability for southern Indiana is largely controlled by atmospheric flow patterns (Chapter 6). High $\delta^{18}O$ values occur during times of more northern storm track and ample Gulf of Mexico moisture advection. Low $\delta^{18}O$ values occur during times of an eastern North American trough, more southern storm track, and suppressed Gulf of Mexico moisture advection. These atmospheric patterns can often be linked to global changes in climate teleconnection (e.g., Leathers et al., 1991; Mantua and Hare, 2002; Wallace and Gutzler, 1981). Modern annual precipitation, river water, and tap water $\delta^{18}O$ values for southern Indiana and the Ohio River Valley fall between -6 and -8‰ (Bowen et al., 2007; Dutton et al., 2005). Cave drip water in the eastern United States has been found to correlate with the annual precipitation $\delta^{18}O$ value (Harmon, 1979; Yonge et al., 1985); however, groundwater recharge at some locations may be seasonally-biased toward winter precipitation due to increased evapotranspiration in the summer (Lachniet, 2009). The effect of precipitation seasonality on interannual $\delta^{18}O$ variability in southern Indiana is inconclusive (Chapter 6), but major changes in seasonal precipitation or groundwater recharge balance would likely be recorded in a stalagmite due to the sheer magnitude of the effect.

Stable carbon isotope ratios ($\delta^{13}C$) in stalagmites primarily reflect changes in the vegetation and soil above the cave as well as the drip water history prior to reaching the stalagmite (McDermott, 2004). Biogenic CO_2 has a lower $\delta^{13}C$ value than atmospheric CO_2. Drier surface conditions reduce vegetative cover and biological activity in the soil zone, which results in a lower proportion of biogenic CO_2 relative to atmospheric CO_2 and a rise in the $\delta^{13}C$ value of soil CO_2 (Baldini et al., 2005; Hesterberg and Siegenthaler, 1991). Drier surface conditions are associated with lower cave humidity and CO_2 concentration, and this promotes increased degassing of drip water CO_2 and deposition of $CaCO_3$ prior to dripping onto a growing stalagmite. Carbon-12 is preferentially removed in degassed CO_2 and prior

$CaCO_3$ deposition, resulting in higher $\delta^{13}C$ values in the remaining drip water (Cross et al., 2015; Dreybrodt and Scholz, 2011). Changes in the dominant vegetation photosynthetic pathway between C_3 and C_4 plants can also affect soil CO_2 $\delta^{13}C$ values. C_4-plant dominated vegetation, such as prairies, has higher soil CO_2 $\delta^{13}C$ values than C_3-plant dominated vegetation, such as hardwood forest (Bender, 1971; Schwartz et al., 1986). C_4 plants and prairie vegetation are favored under warmer, drier conditions in the American Midwest, while cooler and wetter conditions favor forest growth. Crucially, all of these potential controls on stalagmite $\delta^{13}C$ values produce higher $\delta^{13}C$ values with drier conditions.

However, increased water infiltration speed may result in increased stalagmite $\delta^{13}C$ values due to soil water not fully equilibrating with soil CO_2 (Baker et al., 1997). Soil CO_2 concentrations and $\delta^{13}C$ values often exhibit seasonal cycles where the growing season has higher soil CO_2 concentrations and lower $\delta^{13}C$ values (Kiefer and Amey, 1992; Rightmire, 1978). If the seasonal composition of water in the soil zone and epikarst changes, the mean $\delta^{13}C$ value may change as well. Increased cave ventilation can increase stalagmite $\delta^{13}C$ values by reducing CO_2 concentrations and thus increasing drip water CO_2 degassing (Meyer et al., 2014). Thus, the interpretation of $\delta^{13}C$ values in a speleothem should be made within the context of environmental data derived from the other proxies.

Fulvic and humic acids can travel with drip water from the soil zone and be deposited alongside $CaCO_3$ in a growing stalagmite. These organic acids are biologically produced, and the concentration of these acids in drip water and stalagmites is related to overall soil productivity. When a cut stalagmite is exposed to ultraviolet light, the trapped organic acids will fluoresce between 410 and 460 nm (McGarry and Baker, 2000; Shopov et al., 1994; van Beynen et al., 2001). Changes in peak emission wavelength can be utilized as a proxy for soil humification (Baker et al., 1998). Variations in the luminescence intensity emitted can be recorded as a UVL record, but this intensity can be altered by changes in past drip water flow rates, detrital grain presence, and petrographic changes (Baker et al., 1996). High detrital content can block UVL emission, and in some cases UVL may be a better proxy for detrital

content than soil productivity. Thus, UVL records are best utilized in context with other paleoclimate proxies rather than interpreted as stand-alone records.

Petrographic changes in stalagmites are a lesser-utilized proxy, yet can offer physical evidence of past climate and environmental changes (Belli et al., 2013; Boch et al., 2011; Railsback et al., 2014; Turgeon and Lundberg, 2001). The mineral $CaCO_3$ can be deposited as two polymorphs: aragonite and calcite. Deposition of aragonite is more common in drier environmental conditions, but properly identifying the mineralogy of a stalagmite is important because stable isotope ratios are fractionated differently for aragonite and calcite (Frisia et al., 2002; Railsback et al., 1994). Identification of transitional layer boundaries and growth hiatuses is particularly important for proper chronology creation and paleoclimate interpretation. Two petrographic surface types that signify important paleoenvironmental changes are Type E and Type L surfaces. Type E surfaces show evidence of layer erosion associated with increased water flow and solutional drilling of previously-deposited $CaCO_3$. Layers that rapidly thin progressing from the stalagmite apex are associated with reduced $CaCO_3$ deposition and water flow (Railsback et al., 2013).

The color of stalagmites has been given relatively low attention in scientific literature. Early work established organic components as the major source of color variations (Lauritzen et al., 1986), yet color is rarely mentioned in modern stalagmite-based paleoclimate interpretations. Recent work by this author and others at the University of Georgia (UGA) has illustrated links between visual color, petrography, stable isotopes, and UVL with implications for paleoclimate interpretation. In one study, layers of a stalagmite that appear pale in reflected light and opaque in transmitted light had higher organic acid content, while layers that are dark in reflected light and translucent in transmitted light had lower organic acid content (Railsback et al., 2014). Comparing changes in stalagmite reflectance, tone, and clarity with other better-understood paleoenvironmental proxies may help in properly interpreting the color changes found in stalagmites.

7.4 Methods

7.4.1 Field sampling

The Upper Porter Cave stalagmites UP3, UP4, and UP7 were removed at their base with hammer and chisel in July 2013 (Figure 31, Appendix 1). UP3 is 220 mm tall and grew with a single growth axis while UP4 is 230 mm tall but has two growth axes. The main UP4 growth axis is 215 mm from base to apex, while the secondary growth axis began on the side of the main axis and grew 120 mm. UP7 is a small 70 mm stalagmite that grew 5 cm from UP4 and shares some growth layers. Seventeen water samples were taken from Lower Porter Cave, Johnson Cave, and Indiana Caverns during three visits in June 2014, December 2014, and June 2015. Water samples were analyzed for $\delta^{18}O$ and δD at the Center for Applied Isotope Studies at UGA.

Four Hobo® Pro v2 temperature and relative humidity data loggers were placed in caves in December 2014 and set to record cave air temperature and relative humidity at hourly intervals. Two loggers were placed in Lower Porter Cave at roughly 8 m and 30 m from the entrance zone. Another logger was placed in Johnson Cave and a fourth in Indiana Caverns near the collection sites of US-INJN2 and US-INIC6, respectively. An attempt to retrieve data loggers in June 2015 recovered only the Indiana Caverns data logger, and the reason for the loss of the other loggers is unknown.

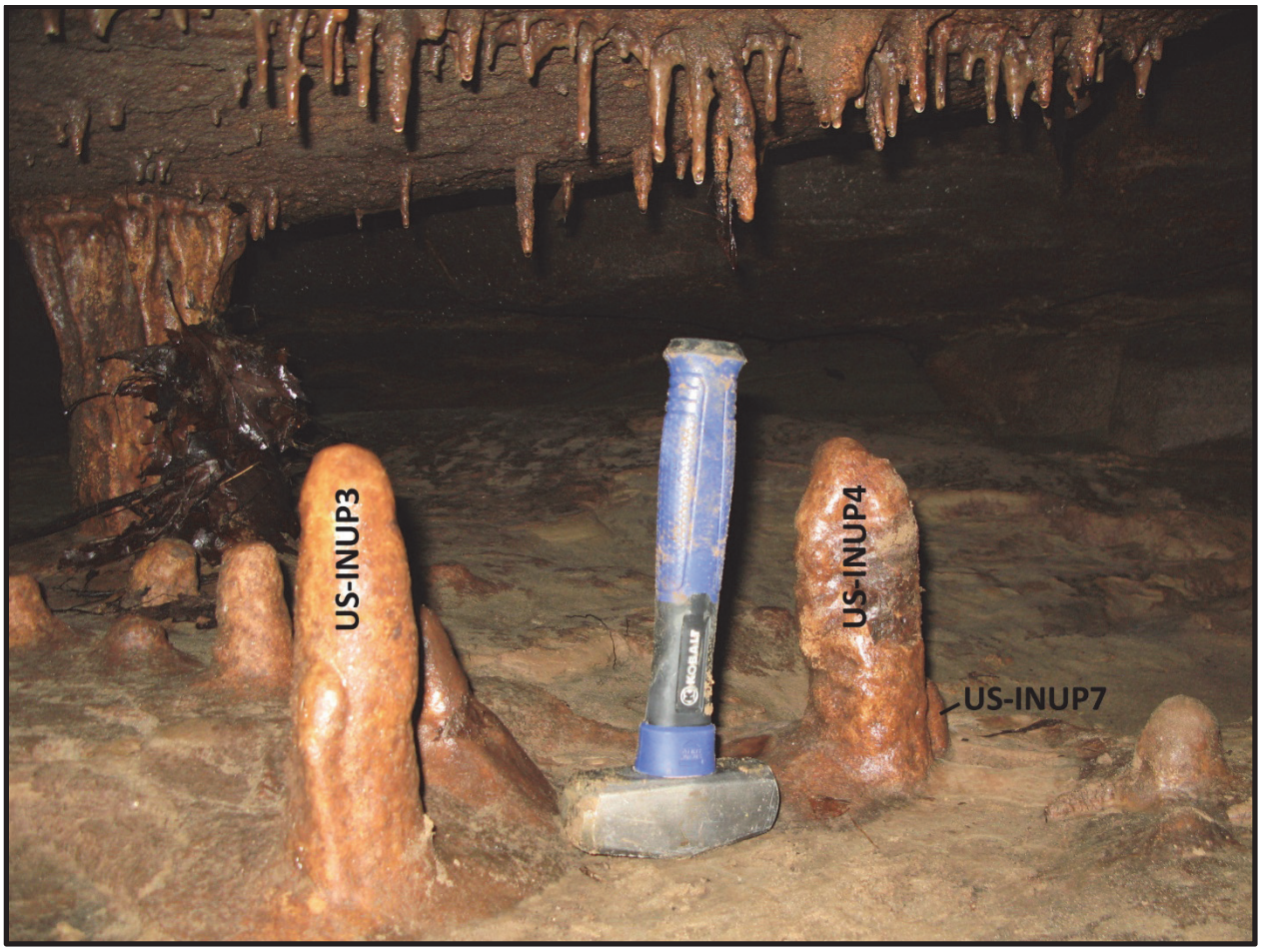

Figure 31. Three Upper Porter Cave stalagmites in growth position prior to collection. Leaves piled up against the rear column and sandy material on the floor are evidence of relatively recent flooding.

7.4.2 Laboratory analysis

Stalagmites were processed in the Sedimentary Petrology/Geochemistry Laboratory at UGA. UP3 and UP4 were cut in half and cut faces polished with graded sandpaper. One half was preserved for reference and visual analysis while the other half was quartered. One quarter was cut into small slabs and sent for thin section processing at Quality Thin Sections in Tucson, Arizona. Thin sections were analyzed at UGA with a petrographic microscope. A 1-2 cm thick slab was cut from the remaining

stalagmite quarter for stable isotope sampling. UP7 was cut in half and polished, but not quartered for isotope analysis or thin sections.

Samples for U-Th dating were drilled with a hand-held dental drill avoiding detrital material if at all possible. The first age samples contained approximately 150 mg of $CaCO_3$ powder, but later samples were reduced to 40-60 mg based on the ^{238}U content of the stalagmite. Ages were determined at the Minnesota Isotope Laboratory at the University of Minnesota by Fuyuan Liang using an inductively coupled plasma mass spectrometric Neptune following methods described in Edwards et al. (1987) and Shen et al. (2002). Ages were calculated using half-lives determined by Cheng et al. (2000) and are reported with analytical errors of two standard deviations of the mean. Thirty ages were produced: nine ages for UP3, eighteen ages for UP4, and three ages for UP7. An age-depth model was constructed for each stalagmite through a combination of the StalAge model (Scholz and Hoffmann, 2011) and linear regression extrapolation.

Samples for stable isotope analysis were drilled using a CNC Taig Micro Mill with servo motors (Figure 32) and computer-controlled through the SuperCamXP program. For UP4, a total of 906 stable isotope samples were drilled from both growth axes representing the full growth of UP4. Each stable isotope sample contained 50-100 µg of $CaCO_3$ powder drilled from a trough typically 0.5-1 mm long and 0.2-0.4 mm deep oriented parallel with stalagmite laminae. Troughs were drilled at an interval of 0.3 mm on the main axis and 0.5 mm on the secondary axis. At this resolution, trough widths overlap and thus the stable isotope sampling produces a continuous record.

Seventy stable isotope samples were drilled from UP3 with a similar length and depth to the troughs in UP4, but at a much lower resolution that does not produce overlapping troughs. For UP3, the drilled troughs were spaced by 5 mm, although two regions of interest were drilled at a 1 mm interval. An additional three samples were drilled to capture detritus-rich layers missed by the 5 mm and 1 mm sampling. No systematic isotope sample was done on UP7, but a single sample was taken from the very

top of the stalagmite to determine the isotope characteristics of the youngest layers (Chapter 8). All stable isotope samples were analyzed at the University of Alabama Stable Isotope Laboratory using methods described in Lambert and Aharon (2011).

A UVL image of each stalagmite was produced by exposing a cut and polished stalagmite face to ultraviolet light and photographing the resulting luminescence with a digital camera equipped with an ultraviolet filter. The green channel of the UVL image was converted to grayscale where higher pixel values represent greater luminescence intensity. Changes in pixel value were recorded along a transect parallel to the isotope sampling paths. Stalagmite reflectance images were created from digital scans of cut and polished stalagmite halves. The scanned images were converted to grayscale and analyzed in a manner similar to that described for UVL images. UVL and reflectance images of UP3 and UP4 were taken of the isotope sampling slab rather than the intact stalagmite half to allow high precision matching between stable isotope, UVL , and reflectance data.

Tone and clarity were recorded for each stable isotope sample drilled. Tone is a description of the relative color of a sampled lamina on a gradient from very dark to very light, while clarity describes whether the lamina is translucent, partially-translucent, or opaque. Tone is inferred from the natural reflected light appearance of the stalagmite, while clarity is determined by transmitting light through the stalagmite from a small LED flashlight. Both measures are subjective and often relative, but all tone and clarity assignments were made solely by the author and should be consistent across a stalagmite.

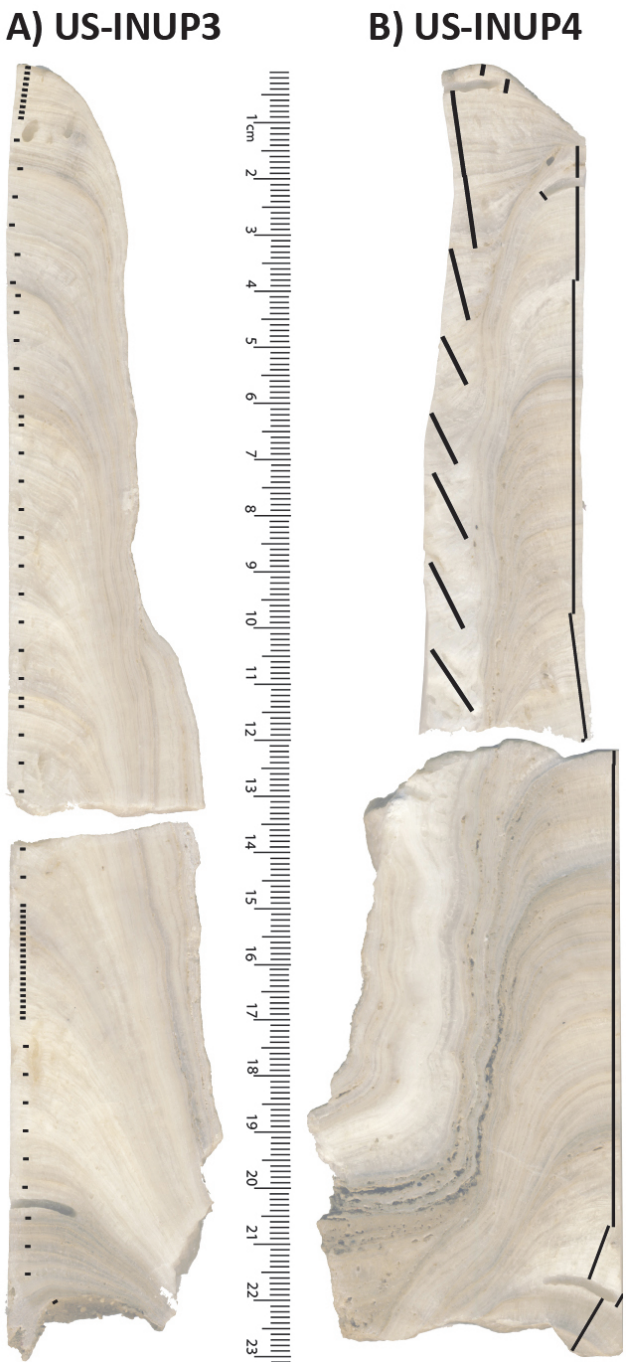

Figure 32. Stable isotope sampling for stalagmites UP3 (A) and UP4 (B). Black dashes and lines represent stable isotope samples. Samples on UP4 appear as solid lines because individual samples overlap. The angled nature of some sampling paths is a result of drilling individual samples along stalagmite laminae.

7.4.3 Statistical analysis

Spearman rank correlations were calculated for paired combinations of the quantitative proxies ($\delta^{18}O$, $\delta^{13}C$, UVL, reflectance) for both UP3 and UP4. Because Spearman correlation coefficients (rho) can only be calculated between proxy variables of matching sample size, UVL and reflectance data were run through a reduction algorithm to reduce the number of values to match the sample size and interval of the stable isotope data. The reduction algorithm calculates the mean value of all UVL or reflectance values within the interval of each stable isotope sample. For example, if an isotope sample spanned from 10.00 mm to 10.25 mm in depth on the stalagmite, the reduction algorithm would average all UVL or reflectance values that fell within that depth range into a single UVL or reflectance value. The continuous stable isotope sampling of UP4 is ideal for comparing all four proxies, but the discontinuous stable isotope sampling on UP3 reduces the potential accuracy of any correlations calculated between the stable isotope and visual proxies. However, correlations for UP3 are included for comparison.

7.5 Results

7.5.1 Chronology

Twenty-eight of the 30 U-Th ages date between 2000 and 9000 calendar years before present (cal yr BP). The other two ages are from UP4 and were judged unreliable due to detrital contamination and excessive error (Table 23, Figure 33). High ^{232}Th values suggest that most samples were contaminated by detrital thorium, despite careful sampling aimed at avoiding detritus (Table 23). Most ages are in correct stratigraphic order and considered accurate, but precision is commonly quite low due because corrections were needed to account for the detrital thorium. Both UP3 and UP4 began growing around 8.5 thousand calendar years before present (ka BP) and stopped growing between 7.0 and 7.5 ka BP. UP7 was deposited between 7.3 and 7.9 ka BP. Although UP3 and UP7 never grew again after the growth stoppage around 7.3 ka BP, there was further growth of UP4 from 4.9 ka BP to 2.3 ka BP.

However, three growth hiatuses in this later UP4 growth phase are indicated by two detrital layers and a shift in the growth axis.

An age-depth model was created for UP3 using the StalAge model (Figure 34). The ages lie in stratigraphic order when including uncertainty; however, the UP3-84 age was excluded from the age-depth model as an outlier because it lies out of correct stratigraphic order and suggests a significant slowdown in growth rate (or a hiatus) before age UP3-70. However, petrographic analysis does not support a growth rate change here. The growth rate estimated by StalAge for UP3 is approximately 0.17 mm/yr.

Table 23. Uranium-thorium ages data for Upper Porter Cave stalagmites.*

Sample ID	Depth (mm)	^{238}U (ppb)	^{232}Th (ppt)	$^{230}Th/^{232}Th$ (atomic x 10^{-6})	$\delta^{234}U$ (measured)	$^{230}Th/^{238}U$ (activity)	^{230}Th age (±2σ) (uncorrected)	^{230}Th age (±2σ) (corrected BP)
UP3-3	3	466.4 ±0.9	17076 ±343	38 ±1	141.3 ±2.2	0.0848 ±0.0003	8402 ±37	**7405 ±662**
UP3-21	21	418.6 ±0.9	13965 ±281	43 ±1	182.2 ±2.4	0.0862 ±0.0004	8237 ±39	**7352 ±582**
UP3-47	47	560.3 ±1.1	2961 ±60	253 ±5	172.4 ±2.1	0.0811 ±0.0004	7806 ±44	**7611 ±102**
UP3-70	70	619.1 ±1.0	6858 ±138	124 ±3	187.9 ±1.7	0.0835 ±0.0002	7938 ±26	**7603 ±193**
UP3-84	*84*	*761.2 ±1.8*	*3441 ±69*	*306 ±6*	*163.5 ±2.2*	*0.0839 ±0.0004*	*8144 ±43*	*7968 ±90*
UP3-119	119	654.4 ±1.3	4188 ±84	219 ±5	178.3 ±2.1	0.0848 ±0.0004	8133 ±45	**7911 ±120**
UP3-152	156	531.2 ±0.8	6718 ±135	117 ±2	197.2 ±1.7	0.0900 ±0.0003	8506 ±31	**8135 ±219**
UP3-174	178	505.2 ±1.0	5958 ±120	125 ±3	169.4 ±2.0	0.0897 ±0.0005	8687 ±49	**8330 ±213**
UP3-193	197	728.3 ±1.7	34103 ±687	36 ±1	181.0 ±2.5	0.1012 ±0.0003	9744 ±39	**8526 ±818**
UP4-210	*3*	*426.8 ±1.0*	*228566 ±4602*	*3 ±0*	*131.7 ±2.6*	*0.1064 ±0.0009*	*10749 ±96*	*-4016 ±10500*
UP4-233	16	354.9 ±0.7	6378 ±128	27 ±1	147.3 ±2.7	0.0299 ±0.0003	2877 ±31	**2357 ±324**
UP4-258	47	386.6 ±0.5	5925 ±119	32 ±1	124.6 ±1.7	0.0295 ±0.0004	2901 ±37	**2440 ±283**
UP4-309	92.5	315.5 ±0.6	385 ±8	378 ±10	126.0 ±2.0	0.0280 ±0.0005	2742 ±48	**2646 ±53**
UP4-3	*106.5*	*332.5 ±0.7*	*26778 ±538*	*7 ±0*	*127.6 ±2.4*	*0.0352 ±0.0003*	*3453 ±32*	*1295 ±1484*
UP4-3b	106.5	286.8 ±0.6	4290 ±86	38 ±1	126.3 ±2.2	0.0342 ±0.0005	3363 ±53	**2914 ±279**
UP4-17	125.5	325.7 ±0.3	2516 ±50	72 ±2	133.1 ±1.5	0.0336 ±0.0003	3283 ±27	**3023 ±143**
UP4-31	138.5	374.7 ±0.7	2282 ±46	90 ±2	134.6 ±2.1	0.0332 ±0.0004	3239 ±39	**3019 ±117**
UP4-40	148	424.6 ±0.9	16174 ±325	20 ±0	138.7 ±2.7	0.0469 ±0.0005	4586 ±50	**3545 ±693**
UP4-61	169.5	419.5 ±1.0	5453 ±110	55 ±1	132.7 ±2.2	0.0430 ±0.0004	4217 ±39	**3821 ±239**
UP4-67	175.5	429.7 ±1.0	9571 ±193	35 ±1	145.1 ±3.0	0.0470 ±0.0003	4567 ±32	**3937 ±402**
UP4-101	207.5	415.2 ±1.0	4166 ±84	74 ±2	126.4 ±2.7	0.0450 ±0.0005	4443 ±48	**4120 ±189**
UP4-111	217	461.0 ±1.2	5978 ±121	67 ±1	134.5 ±2.4	0.0528 ±0.0004	5189 ±41	**4795 ±239**
UP4-119	228	534.9 ±1.1	9612 ±193	50 ±1	132.9 ±2.3	0.0540 ±0.0002	5324 ±24	**4800 ±328**
UP4-142	252.5	602.4 ±1.5	4636 ±94	177 ±4	164.6 ±2.4	0.0827 ±0.0004	8017 ±47	**7761 ±144**
UP4-165	247	535.5 ±1.1	8658 ±174	92 ±2	205.5 ±2.3	0.0898 ±0.0003	8421 ±36	**7968 ±278**

UP4-166	275	503.8	±1.1	5169	±104	146	±3	208.3	±2.2	0.0906	±0.0003	8484	±35	**8173**	**±178**
UP4-198	305.5	777.3	±2.0	1436	±29	792	±16	184.8	±2.5	0.0888	±0.0003	8476	±34	**8369**	**±46**
UP7-4	4	572.9	±4.5	9347	±201	80	±2	146.3	±4.2	0.0787	±0.0008	7744	±83	**7266**	**±303**
UP7-45	45	704.0	±5.7	1656	±36	573	±13	164.0	±4.7	0.0818	±0.0008	7930	±86	**7807**	**±95**
UP7-66	66	*50.1*	*±0.1*	*1749*	*±35*	*41*	*±1*	*165.7*	*±2.1*	*0.0865*	*±0.0003*	*8389*	*±33*	*7455*	*±618*

*Corrected ^{230}Th ages assume the initial ^{230}Th/^{232}Th atomic ratio of 4.4 ± 2.2 x 10^{-6}, which is the value for a material at secular equilibrium, with the bulk earth ^{232}Th/^{238}U value of 3.8. Errors are arbitrarily assumed to be 50%. The gray and italicized ages are not included in the age-depth models because of very high ^{232}Th concentrations or because they deviate significantly from the expected age for their stratigraphic position.

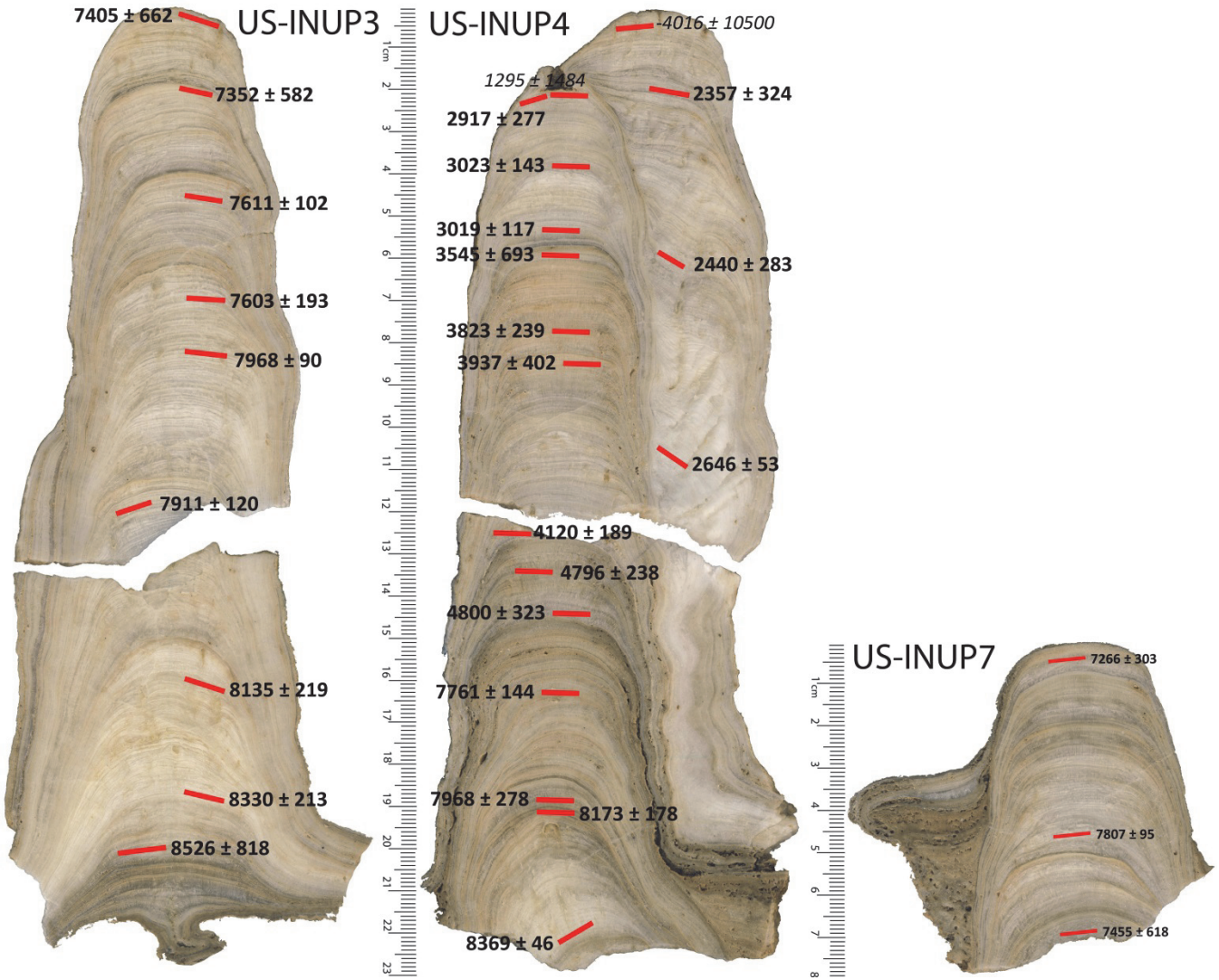

Figure 33. Uranium-thorium ages for the three Upper Porter stalagmites illustrating the location sampled.

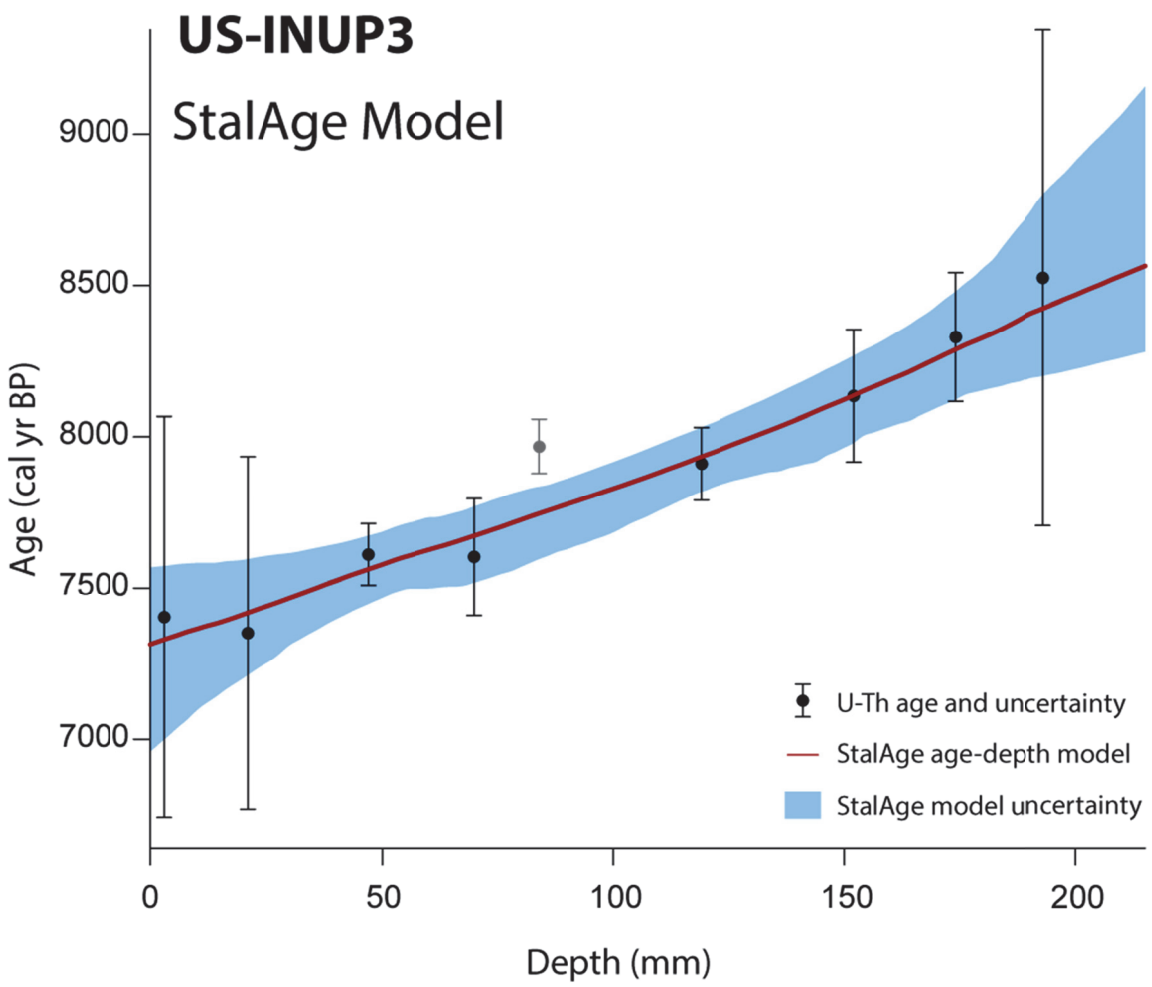

Figure 34. The StalAge-created age-depth model for US-INUP3. One age (gray) was excluded from the model as an outlier.

StalAge age-depth modeling was not used on the UP4 age data because this stalagmite has four growth hiatuses that are difficult for the modeling process. Instead linear regression analysis was used to model age-depth relationships in each of the five sections separated by growth hiatuses that date to 2.7-2.9, 3.1-3.6, 4.2-4.7, and 4.9-7.5 ka BP (Figure 35,Table 24). The age data show that stalagmite growth was slower in the early Holocene and three times faster after 3.1 ka BP. The growth that dates from 4.7 to 4.9 ka BP only has two U-Th dates that are nearly identical when uncertainties are

considered, so the growth rate estimated for the 3.6-4.2 ka BP section (judged to be similar petrographically and visually) was applied to the 4.7-4.9 ka BP section.

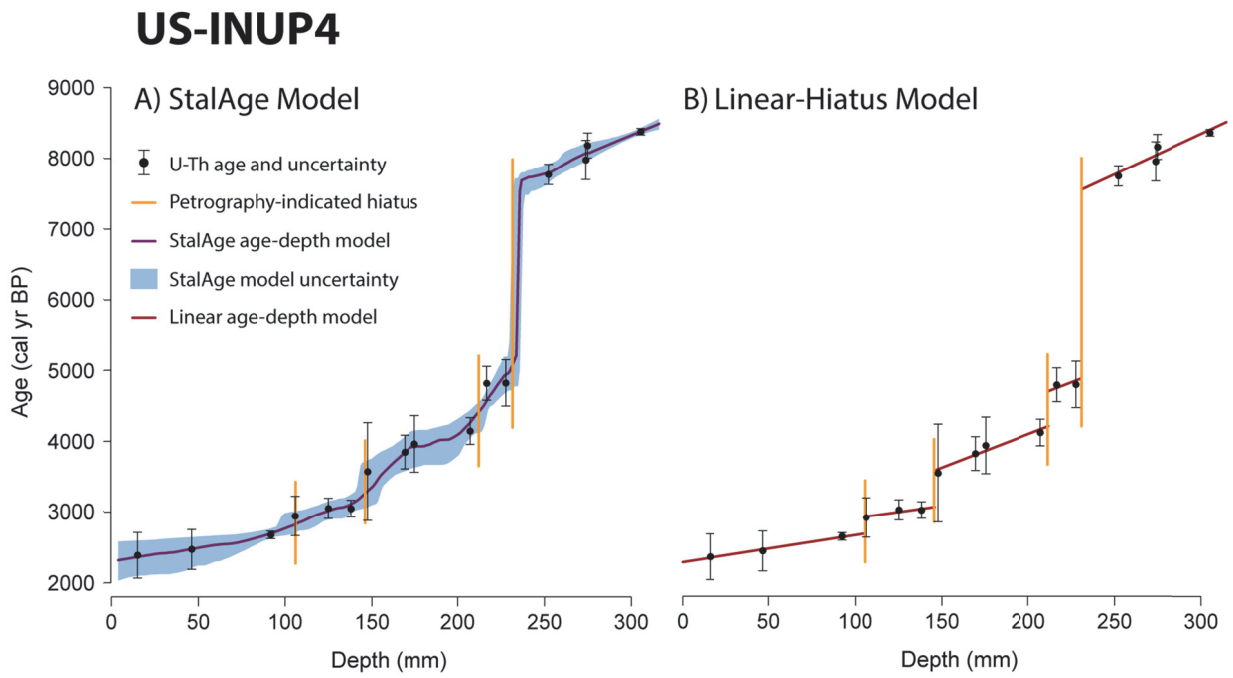

Figure 35. U-Th age-depth models for UP4. The StalAge model (A) assumes generally continuous growth and does not take into account four major growth hiatuses. An age-depth model based on linear regression within each growth section (B) is judged more realistic.

Table 24. Beginning and ending ages for the growth and hiatus phases of UP4 based on linear regression. Note that the growth rate for section 3 was applied to section 2.

UP4 Section	**Start Age (cal yr BP)**	**End Age (cal yr BP)**	**Growth Rate (mm/yr)**
Section 1	8520	7550	0.09
Hiatus 1	7550	4880	-
Section 2	4880	4690	*0.11 (applied)*
Hiatus 2	4690	4200	-
Section 3	4200	3570	0.11
Hiatus 3	3570	3060	-
Section 4	3060	2920	0.29
Hiatus 4	2920	2690	-
Section 5	2690	2280	0.26

7.5.2 Paleoenvironmental proxies

Paleoenvironmental proxy records for UP3 and UP4 are shown in Figure 36 and Figure 37, respectively. Values for stalagmite $\delta^{18}O$ fall between -3.8 and -6.5‰ with a mean value of -5.0‰. Stalagmite $\delta^{13}C$ values have a larger and generally lower range, falling between -5.5 and -11.0‰ with a mean value of -8.6‰ (Table 25). The $\delta^{18}O$ values are highest in the early Holocene and are lowest approaching the late Holocene, while $\delta^{13}C$ values are lowest in the early Holocene and have higher, but more variable, values after 4.9 ka BP. Maximum $\delta^{13}C$ values are found near the detritus-rich layers immediately preceding a growth hiatus, and $\delta^{13}C$ values are 2-3‰ lower following a hiatus.

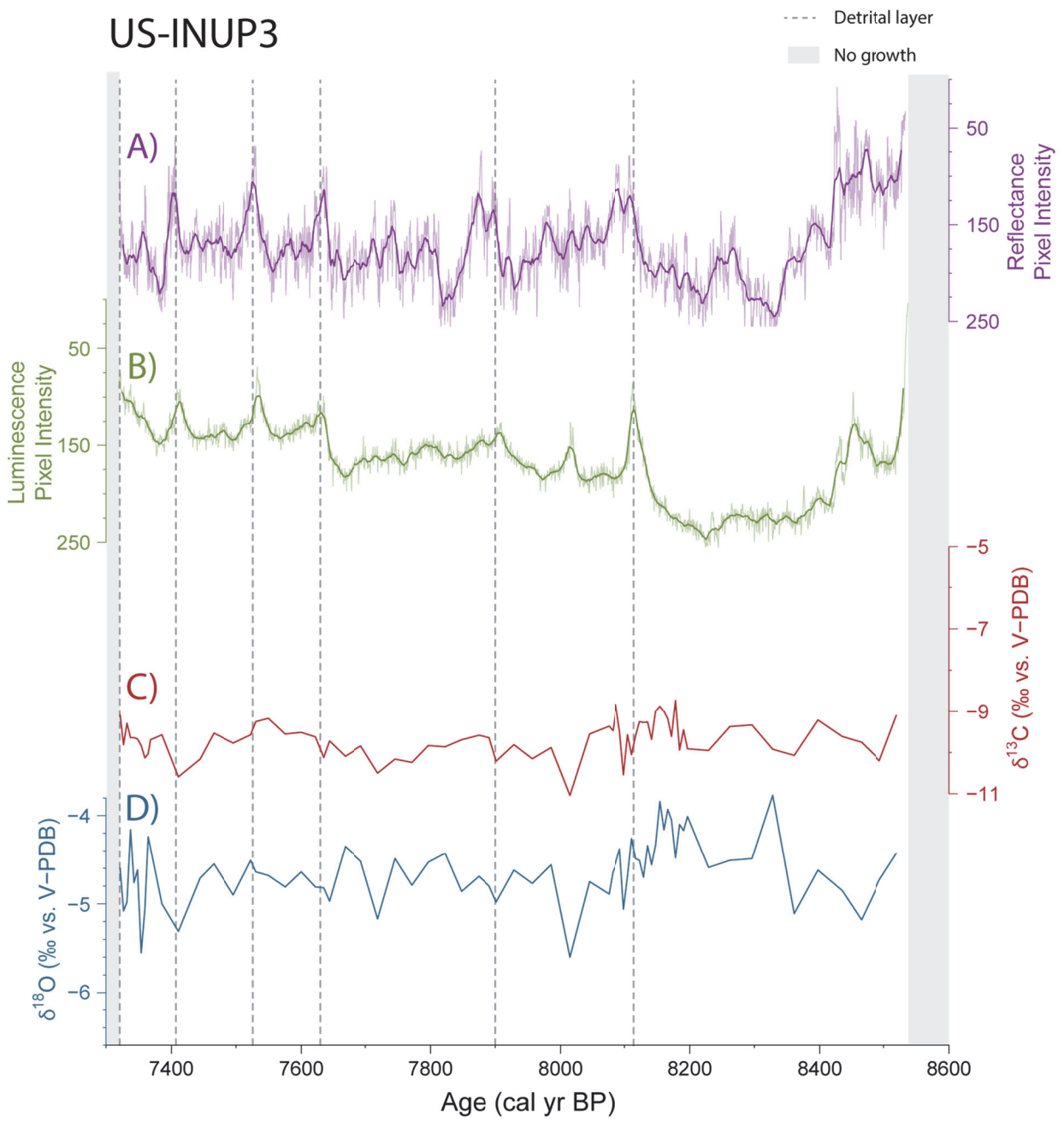

Figure 36. Paleoclimate proxy records for UP3: A) reflectance, B) UVL, C) $\delta^{13}C$, and D) $\delta^{18}O$. Dashed vertical lines show the locations of detrital-rich layers.

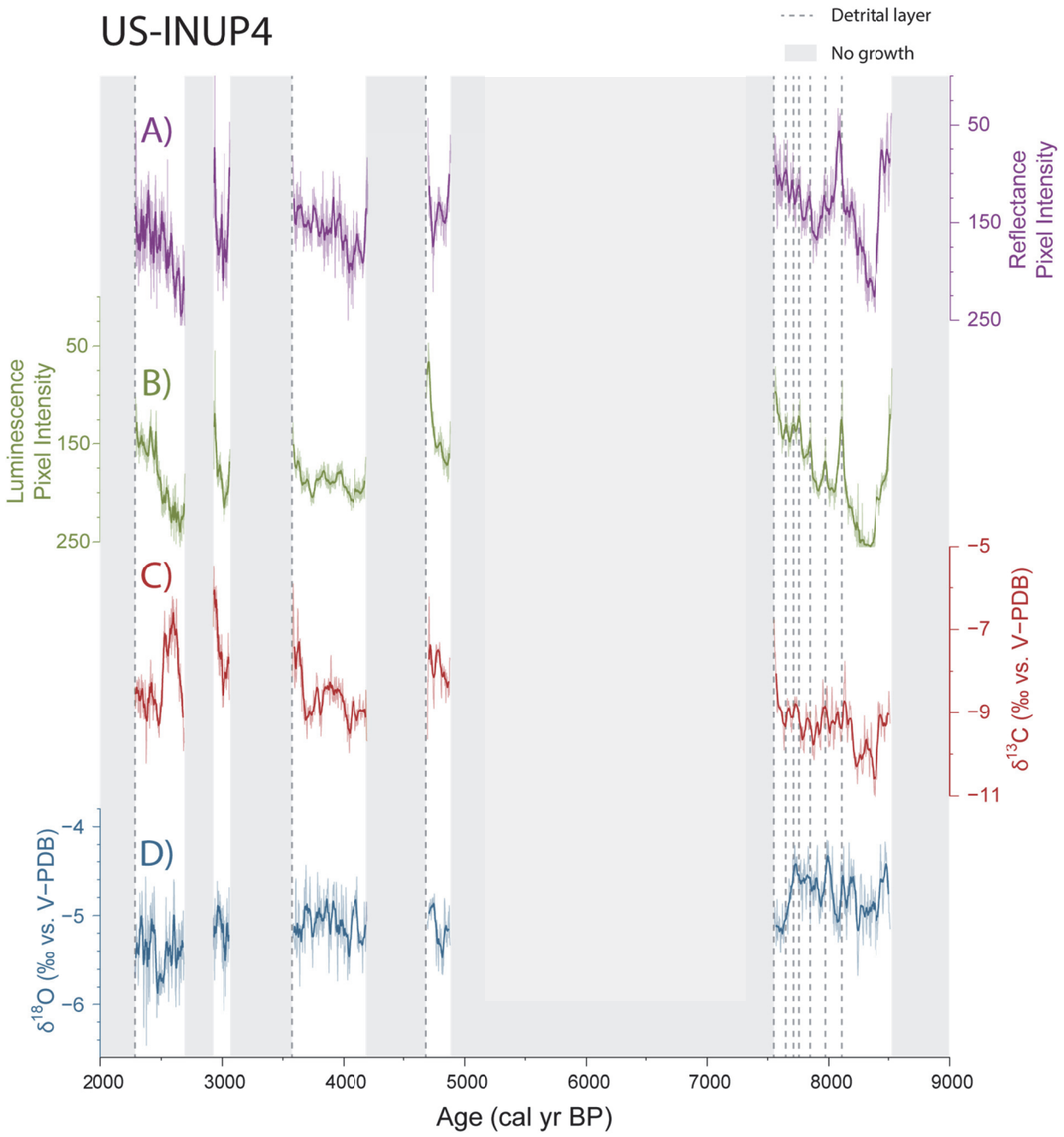

Figure 37. Paleoclimate proxy records for UP4: A) reflectance, B) UVL, C) $\delta^{13}C$, and D) $\delta^{18}O$. The stalagmite grew in five phases, separated by long periods of no growth (gray boxes). Dashed lines show the locations of detritus-rich layers.

Table 25. Changes in mean stable isotope value in UP3 and UP4 during the Holocene.

	Mean $\delta^{18}O$ (‰ vs. V-PDB)		**Mean $\delta^{13}C$ (‰ vs. V-PDB)**	
Period (ka BP)	*UP3*	*UP4*	*UP3*	*UP4*
Entire Record	-4.6	-5.1	-9.7	-8.6
7.3-8.5	-4.6	-4.8	-9.7	-9.3
4.7-4.9	-	-5.1	-	-7.9
3.6-4.2	-	-5.1	-	-8.6
2.9-3.1	-	-5.1	-	-7.5
2.3-2.7	-	-5.4	-	-8.2

UVL and reflectance data show similar trends in both UP3 and UP4 although the reflectance data are more variable (Figures 36-38). UVL values have a clearer relationship with detrital layers than do reflectance and show a pattern of extreme values similar to that of the $\delta^{13}C$ record in UP4. The darkest UVL values (lowest pixel values) occur in the detritus-rich layers immediately before a growth hiatus, and UVL is brighter with the resumption of deposition after a hiatus. Short-term UVL variability is largely attributable to changes in detrital content. Longer-term variability and base-level UVL values may contain a signal for soil productivity, but changes in low-level detrital concentrations also affect these longer-term values.

The tone of both UP3 and UP4 is largely classified as dark or medium, although UP4 is generally darker than UP3 (Table 26). Approximately 20% of UP3 and UP4 isotope samples come from light or very light lamina. Lighter tones in UP3 are associated with higher $\delta^{18}O$ and lower $\delta^{13}C$ values, while no pattern is distinguishable between stable isotopes and clarity in UP3 (Figure 39). For UP4, $\delta^{13}C$ values do not show a trend with tone, but $\delta^{18}O$ has a slight decrease in value with lighter tones. While $\delta^{13}C$ does not show a trend with tone in the overall data from UP4, individual growth phases have $\delta^{13}C$ values that decrease with lighter tones except during the 2.7-2.9 ka BP growth phase when the opposite relationship is observed. The absence of a trend in the total dataset is because each growth phase has a different mean $\delta^{13}C$ value that blurs any longer-term relationship. Additionally, the inverse trend

exhibited in the 2.7-2.9 ka BP phase also obscures the otherwise dominant relationship of lower $\delta^{13}C$ with lighter tones during other growth periods. For the clarity classification, over half of all isotope samples come from translucent lamina in both stalagmites, and less than 6% of all samples come from opaque lamina. No trend is apparent between stable isotopes and clarity in UP4.

Table 26. Tone and clarity statistical data for UP3 and UP4.

	UP3				**UP4**			
Tone	**Count***	**Percent**	**Mean $\delta^{13}C$ (‰)**	**Mean $\delta^{18}O$ (‰)**	**Count***	**Percent**	**Mean $\delta^{13}C$ (‰)**	**Mean $\delta^{18}O$ (‰)**
Very dark	2	2.9%	-9.43	-4.80	24	2.7%	-9.05	-4.81
Very dark-dark border	0	0.0%	-	-	3	0.3%	-8.13	-5.00
Dark	14	20.3%	-9.60	-4.71	324	36.8%	-8.53	-5.01
Dark-medium border	3	4.3%	-9.78	-4.68	46	5.2%	-8.84	-4.98
Medium	35	50.7%	-9.69	-4.69	257	29.2%	-8.78	-5.05
Medium-light border	1	1.4%	-8.99	-4.33	36	4.1%	-8.16	-5.29
Light	12	17.4%	-9.76	-4.43	126	14.3%	-8.42	-5.18
Light-very light border	0	0.0%	-	-	0	0.0%	-	-
Very light	2	2.9%	-9.93	-4.18	65	7.4%	-7.88	-5.33
Clarity								
Opaque	4	5.8%	-9.39	-4.64	42	4.8%	-8.68	-4.93
Opaque-partially transparent border	0	0.0%	-	-	9	1.0%	-7.96	-4.96
Partially translucent	25	36.2%	-9.73	-4.51	215	24.3%	-8.41	-5.07
Partially translucent-translucent border	5	7.2%	-9.68	-4.65	105	11.9%	-7.99	-5.23
Translucent	35	50.7%	-9.62	-4.72	513	59.0%	-8.73	-5.06

*The counts do not add up to the total number of isotope samples taken because some samples did not have a classifiable tone or clarity.

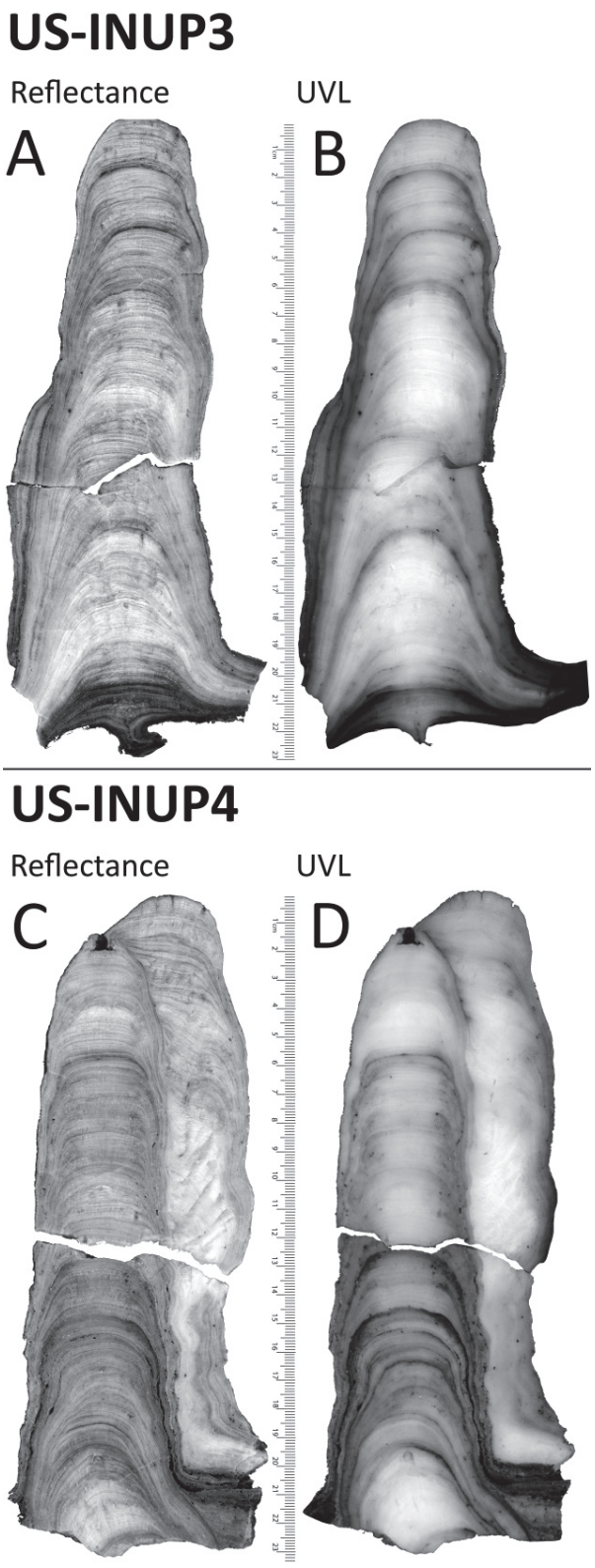

Figure 38. Grayscale reflectance and UVL images for cross sections of UP3 (A, B) and UP4 (C, D).

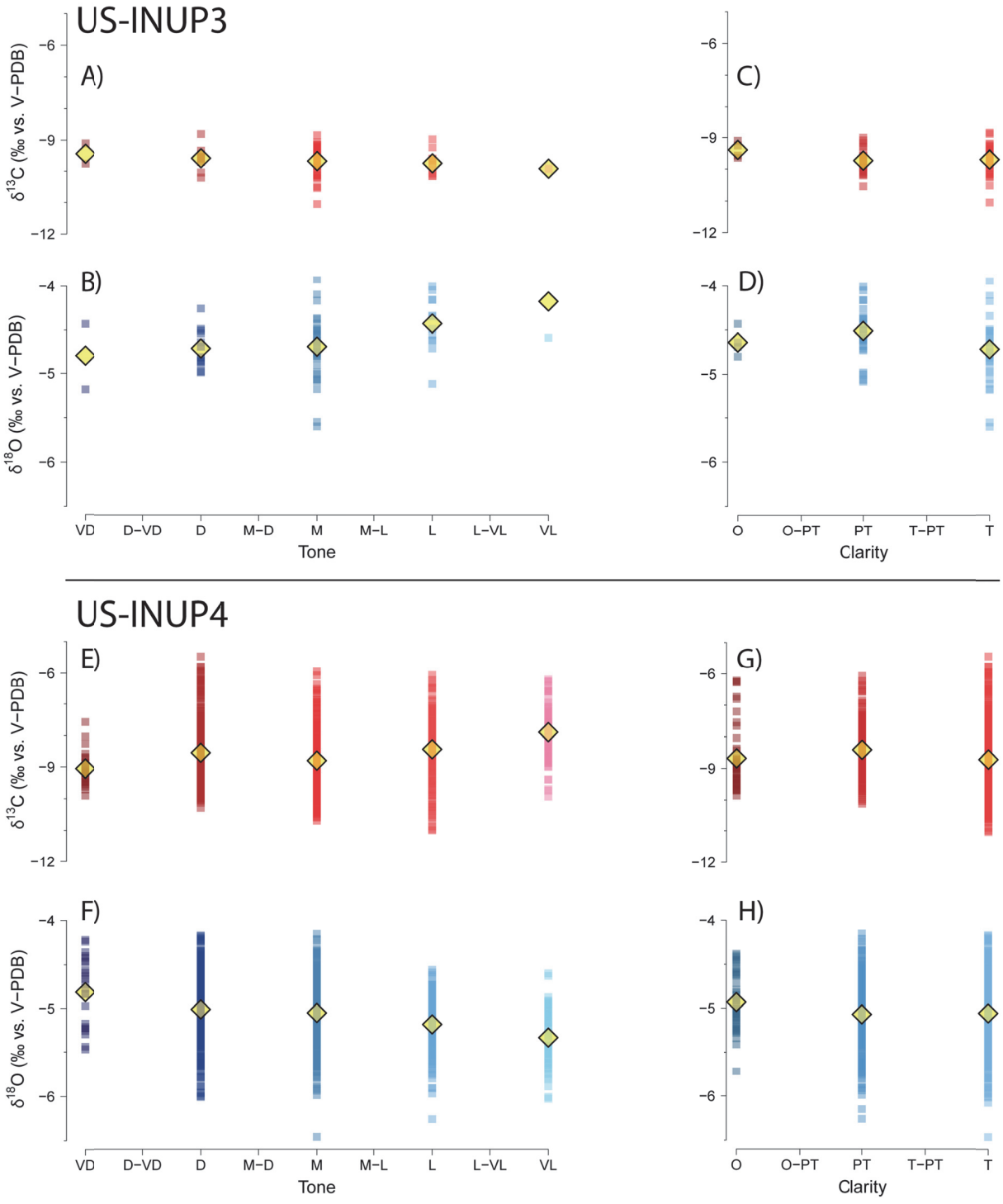

Figure 39. Values for $\delta^{18}O$ (blue) and $\delta^{13}C$ (red) sorted by tone (A, B, E, F) and clarity (C, D, G, H). Squares indicate individual stable isotope values, while yellow diamonds indicate the mean stable isotope value for a category.

Petrographic analysis shows that the three stalagmites consist entirely of calcite. There are six major detrital layers in UP3 and ten in UP4. Four detrital layers in UP4 coincide with long stoppages in stalagmite growth (three hiatuses and the final cessation). No significant growth hiatuses were identified in UP3 despite the presence of six detrital layers. While it is possible that the detrital layers in UP3 indicate short hiatuses, the U-Th ages are not precise enough to confirm this. However, it is clear that any hiatuses in the growth of UP3 were not of the same magnitude as the multi-century hiatuses that affected UP4.

The detrital layers occur at petrographic boundaries that are visible to the unaided eye but are not clearly type L or type E surfaces. Detrital content generally increases in the layers directly below the petrographic boundary and culminates in a nearly opaque detritus layer at the petrographic surface itself. Calcite deposited above the petrographic boundary contains much less detrital content. The detritus is mostly fine (clay, possibly silt), but in UP4 sand grains are sometimes present in detrital layers along the flanks of the stalagmite (Figure 40a). Additionally, the boundary associated with the major 4.9-7.5 ka BP hiatus in UP4 has several sand grains near even the lamina apex (Figure 41). This detritus is likely washed onto the stalagmite during cave flooding events as the small entrance and tortuous passage makes aeolian input extremely unlikely. Detritus is not restricted to these petrographic boundaries or major detrital layers as low-level detrital content is present for most of UP4 and multiple detritus-rich layers are found from 7.5-8.0 ka.

Laminae thickness and extent appear to decline below many of the petrographic boundaries, suggesting type L layering. However, the petrographic surface boundary itself is irregular either because of erosion or because detritus has blocked calcite growth, and so are best classified as type E surfaces (Figures 40 and 41). This juxtaposition of type L and type E characteristics is most obvious in UP4 at the 3.1-3.6, 4.2-4.7, and 4.9-7.5 ka BP hiatuses. In contrast, the UP3 surfaces do not show as much evidence

of erosion. This difference may be because hiatuses in UP4 were longer than in UP3, thus allowing more erosion to occur.

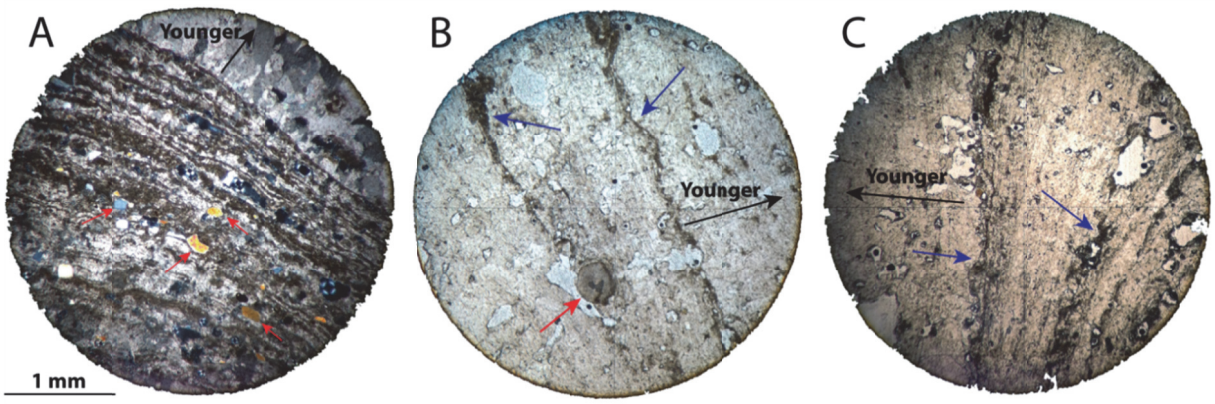

Figure 40. Images of major petrographic surfaces in UP4: A) the 4.9-7.5 ka BP hiatus in crossed-polarized light, B) the flanks of the 4.2-4.7 ka BP hiatus, and C) the flanks of the 3.1-3.6 ka BP hiatus. Images are oriented as actually deposited (i.e., image 'up' is higher in the stalagmite), and the stratigraphic order is indicated. Opaque brown material is largely fine detritus. Sand grains are marked with red arrows in image A, and the red arrow in image B points to an echinoderm grain eroded from limestone bedrock. Blue arrows in images B and C point to irregular, eroded petrographic surfaces.

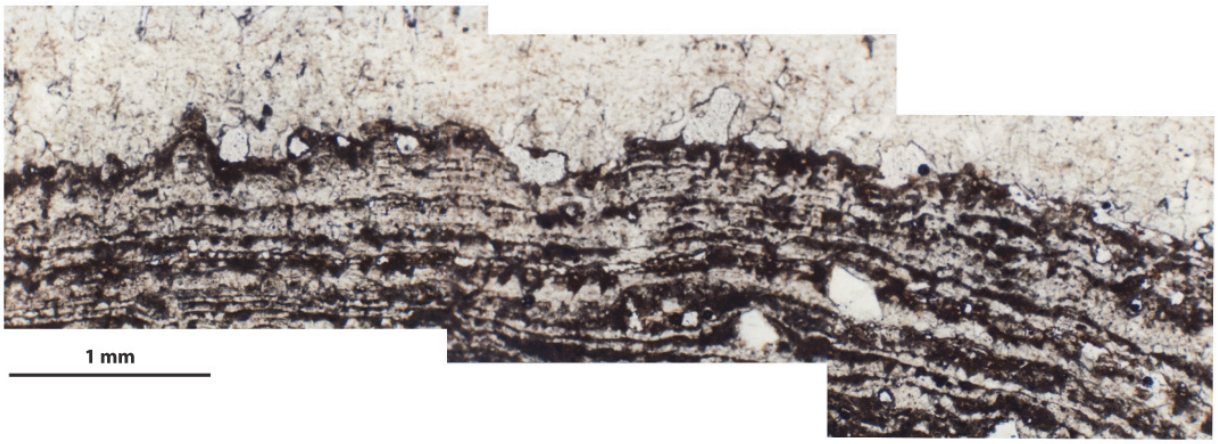

Figure 41. A type E surface in UP4 showing evidence of laminae erosion. The darker deposits shown in the photomicrograph are detritus-rich, including sand grains, and date to approximately 7.5 ka BP. The overlying lighter and cleaner deposits date to approximately 4.9 ka BP. The type E surface lies at the interface of these sections of different age.

The 2.7-2.9 ka BP hiatus in UP4 lacks a significant detrital layer and stalagmite growth after the hiatus is diverted to the side of the original stalagmite. The apex of the original stalagmite culminates in an odd detrital-coated cylindrical hollow with a small amount of deposition on the outside of this hollow. It appears that this hollow is the remnant of a soda straw or stalactite that met with UP4 around 2900 cal yr BP and formed a column. This column formation and blocking of the primary path of the drip water may have led to the diversion of the drip point to the side of UP4. At some point between 2300 and 2700 cal yr BP, the connecting upper stalactite broke off as evidenced by the youngest layers of UP4 overtopping the apex of the original growth axis. Thus, it appears that the 2.7-2.9 ka BP hiatus is simply an artifact of the depositional changes occurring at this time.

7.5.3 Statistical analysis of paleoenvironmental proxy data

Spearman correlations between paleoenvironmental proxies are generally low with the exception of a strong positive correlation between UVL and reflectance (Table 27). The strong correlation between these two proxies in both UP3 and UP4 is expected because petrographic changes

and detrital content captured in the reflectance data are a strong control on luminescence emission. The other paired proxy correlations are quite different for UP3 and UP4 with the exception of the correlations between $\delta^{13}C$ and reflectance. In fact, all correlations involving $\delta^{18}O$ and the correlation between $\delta^{13}C$ and UVL have opposite signs for UP3 and UP4. This difference in correlation when comparing the stable isotope and visual data is possibly due to differences in differences in continuous (UP4) and non-continuous (UP3) stable isotope sampling. However, the inverse correlation in the two stalagmites between carbon and oxygen stable isotopes is surprising. However, when only the early Holocene UP4 data (that grew contemporaneously with UP3) is compared with UP3, the $\delta^{18}O$ and $\delta^{13}C$ correlations are more similar and any difference may be due to the coarser resolution of UP3 data. The $\delta^{18}O$ and $\delta^{13}C$ correlation calculated from the full UP4 data is more negative than UP3 because middle Holocene stable isotope data in UP4 have opposite long-term trends ($\delta^{18}O$ = negative, $\delta^{13}C$ = positive) toward the present.

Table 27. Spearman rank correlation coefficients for paleoclimate proxies in UP3 (n=70) and UP4 (n=904). Correlations from the 7.5-8.5 ka zone of UP4 are also given for better comparison with UP3.

	Spearman rank correlation coefficient (rho)		
Proxy pairing	*UP4*	*UP4 (7.5-8.5 ka)*	*UP3*
$\delta^{18}O$ and $\delta^{13}C$	-0.29	+0.08	+0.36
$\delta^{18}O$ and UVL	-0.10	-0.06	+0.39
$\delta^{18}O$ and reflectance	-0.27	-0.04	+0.34
$\delta^{13}C$ and UVL	-0.16	-0.56	+0.16
$\delta^{13}C$ and reflectance	+0.05	-0.56	+0.03
UVL and reflectance	+0.58	+0.67	+0.38

7.5.4 Cave water geochemistry and cave temperature

Sampled cave waters (Table 28) have a mean $\delta^{18}O$ value of -8.11‰ vs. V-SMOW. The mean values for drip water and fracture flows are slightly lower (-8.28‰ and -8.44‰, respectively) while

stream values are higher (-7.40‰). Water sampled in June is about 1‰ higher than water sampled in December, although this is enhanced by the low $\delta^{18}O$ values in June streamflow, which was sampled shortly after a rain event and likely was not reflecting groundwater values. The deuterium excesses calculated ($d = \delta D - 8 * \delta^{18}O$) are similar to values observed in Indiana precipitation (Appendix 5), and thus significant evaporative effects are not believed to have affected the cave water stable isotopes.

However, the cave water $\delta^{18}O$ values illustrate a significant bias toward winter precipitation. Based upon modern seasonal means of Indiana precipitation $\delta^{18}O$, 80% of the cave water fell in 'winter' conditions and 20% in 'summer' conditions. This is a much higher winter signal than the modern balance of 35% winter-65% summer predicted by airport data (Chapter 5). The highest drip water $\delta^{18}O$ value observed (-7.11‰) only represents a 59% winter-41% summer balance. This suggests that modern groundwater recharge at the sampled caves is dominated by winter precipitation, and much of the summer precipitation is likely lost to evapotranspiration.

Cave water $\delta^{18}O$ values can be converted into calcite $\delta^{18}O$ values for comparison with speleothem $\delta^{18}O$ values. This conversion assumes calcite deposition in equilibrium conditions and follows the equation defined in Kim and O'Neil (1997) at an estimated Upper Porter Cave temperature of 12.1°C (based upon Indiana climate data). Predicted $\delta^{18}O$ values for calcite that would form from the cave water samples are all lower than any $\delta^{18}O$ value observed in UP3 or UP4. Although non-equilibrium conditions can result in kinetic fractionation that results in calcite $\delta^{18}O$ values higher than expected, the lack of strong positive covariance between $\delta^{18}O$ and $\delta^{13}C$ suggests kinetic fractionation does not significantly alter the UP3 or UP4 calcite $\delta^{18}O$ values. Rather, modern day cave water may truly have a greater winter component than the cave waters that existed during the growth of UP3 and UP4.

The mean cave temperature in Indiana Caverns from December 10, 2014, through June 17, 2015, was 13.4°C and relative humidity was always above the logger limit of 95%. A total temperature range of 0.5°C was observed but the bulk of this variation was due to a single precipitation event on

March 3, 2015, when the cave temperature dropped 0.4°C in 24 hours. This precipitation event consisted of 7.5-12.0 cm total liquid precipitation and 25-40 cm of snow in the Indiana Caverns region, approaching records for snowfall in March. Although no active stream flows in the chamber where the data logger was located, the chamber is connected to the trunk passage of the cave which contains a large stream, and the rapid infiltration of cold water into the cave system during this precipitation event was significant enough to drop the overall temperature. Temperatures largely recovered after six days to only 0.1°C below mean temperature, but full return to the mean cave temperature was very gradual.

Table 28. Stable isotope characteristics for cave water samples. Predicted $\delta^{18}O$ values for calcite are calculated with the equation of Kim and O'Neil (1997) based on an estimated Porter Cave temperature of 12.1°C.

Sample	Month	Year	Cave	Water Source	$\delta^{18}O$ (vs. V-SMOW)	δD (vs. V-SMOW)	Deuterium Excess	Predicted calcite $\delta^{18}O$ (vs. V-PDB)
WS-INIC-Drip1	June	2014	Indiana Caverns	Drip water	-8.42 ±0.01	-54 ±1	13	-8.21
WS-INIC-Drip2	December	2014	Indiana Caverns	Drip water	-8.98 ±0.01	-43 ±1	29	-8.77
WS6-ICDW1	June	2015	Indiana Caverns	Drip water	-7.88 ±0.22	-41 ±1	22	-7.67
WS7-ICDW2	June	2015	Indiana Caverns	Drip water	-7.11 ±0.19	-39 ±1	18	-6.90
WS-INIC-FrZo2	December	2014	Indiana Caverns	Fracture flow	-8.40 ±0.01	-46 ±1	21	-8.19
WS8-ICST	June	2015	Indiana Caverns	Stream	-6.71 ±0.10	-48 ±0	6	-6.49
WS-INJN-Drip1	June	2014	Johnson Cave	Drip water	-7.63 ±0.01	-57 ±3	4	-7.42
WS-INJN-Drip2	December	2014	Johnson Cave	Drip water	-8.70 ±0.11	-52 ±6	18	-8.49
WS2-JNDW1	June	2015	Johnson Cave	Drip water	-8.91 ±0.29	-46 ±1	25	-8.70
WS3-JNDW2	June	2015	Johnson Cave	Drip water	-7.83 ±0.28	-46 ±2	17	-7.62
WS-INJN-FrZo1	June	2014	Johnson Cave	Fracture flow	-8.67 ±0.01	-52 ±7	17	-8.46
WS-INJN-FrZo2	December	2014	Johnson Cave	Fracture flow	-8.65 ±0.02	-53 ±4	16	-8.44
WS4-JNFR	June	2015	Johnson Cave	Fracture flow	-8.04 ±0.12	-44 ±2	20	-7.83
WS5-JNST	June	2015	Johnson Cave	Stream	-8.10 ±0.39	-42 ±0	23	-7.89
WS1-LPDW	December	2014	Lower Porter Cave	Drip water	-9.03 ±0.34	-54 ±0	18	-8.82
WS9-LPST1	June	2015	Lower Porter Cave	Stream	-7.30 ±0.37	-41 ±1	17	-7.09
WS10-LPST2	June	2015	Lower Porter Cave	Stream	-7.48 ±0.21	-48 ±1	12	-7.27
Mean					-8.11 ±0.16	-47 ±2	17	-7.89
SD					0.70 ±0.14	5 ±2	6	0.70

7.6 Discussion

7.6.1 Comparison of the UP3 and UP4 records

Both UP3 and UP4 began growing around 8.5 ka BP and the two stalagmites display similar variations in tone and petrography over time. In both stalagmites, a dark, translucent base is topped with a very light zone that has the brightest UVL values and lowest $\delta^{13}C$ values in each record. A detrital layer is located 10-15 mm above the light zone and dates to 8.1 ka BP. Above this detrital layer the stalagmites are generally medium- or dark-toned and have several additional detrital layers. Both stalagmites stopped growing around 7.0-7.5 ka BP, and petrographic similarities between the two stalagmites suggest they stopped growing at nearly the same time. Five of the six detrital layers in UP4 from 7.5-8.0 ka BP match very well with the five detrital layers in UP3. The age-depth model for the early Holocene could be adjusted for UP3 or UP4 in light of this petrographic matching, but without better age constraints, it is unclear which stalagmite should be adjusted. Obtaining a precise date for growth cessation is difficult due to high levels of detritus in the deposits preceding this hiatus. However, the fact that both UP3 and UP4 (and also UP7) stopped growing at this time suggests an environmental cause.

Mean stable isotope values in UP3 and UP4 are similar during the shared period of growth. Stable isotope value trends appear slightly different for the stalagmites, but matching the stalagmites by detrital layers reveals possible broad covariance between the stalagmite $\delta^{13}C$ records (Figure 42). However, similarities in stable isotope trends between UP3 and UP4 are not strong, and the difference in sampling resolution makes definitive comparisons and conclusions difficult.

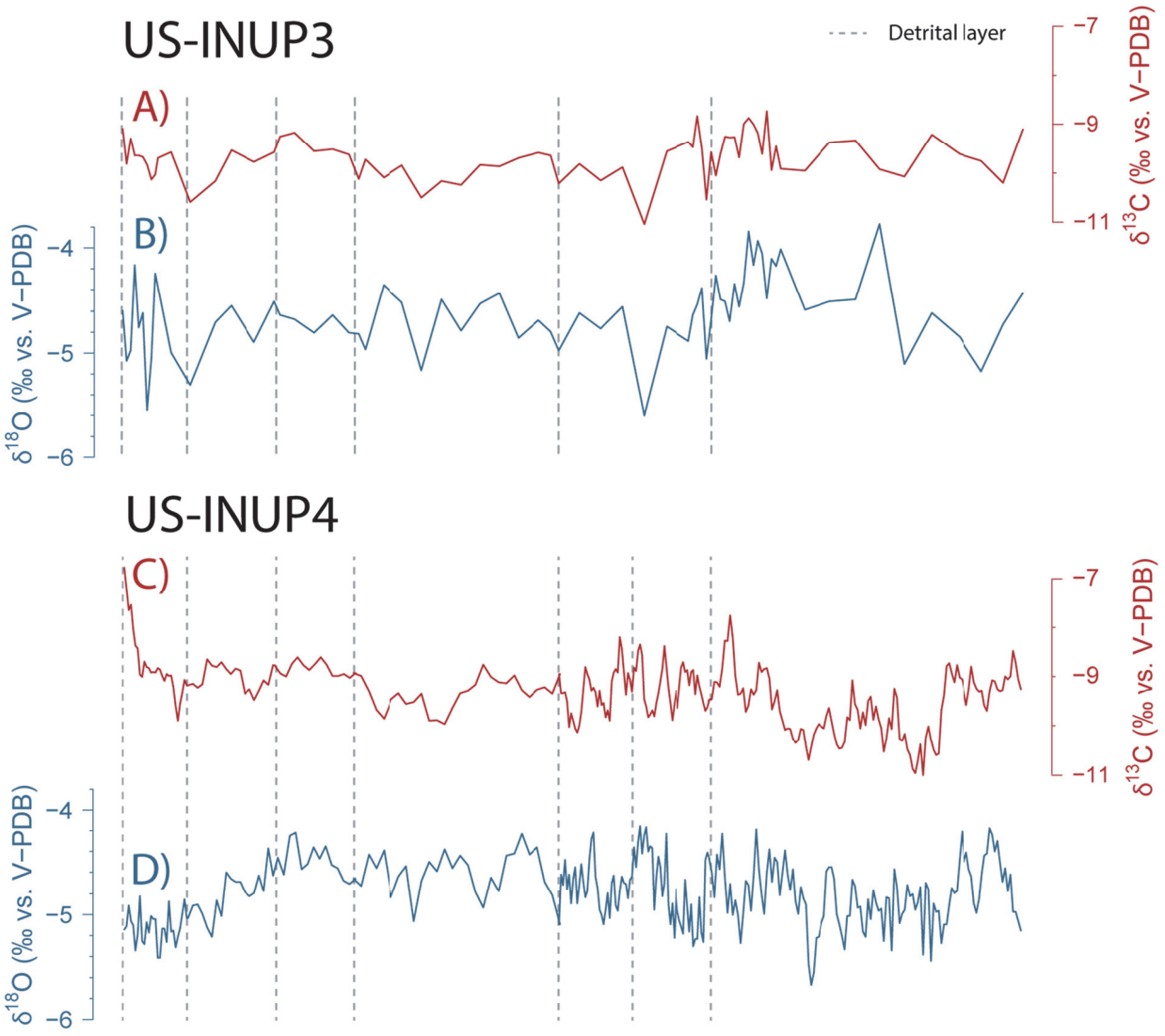

Figure 42. Values for $\delta^{18}O$ (B, D) and $\delta^{13}C$ (A, C) during the early Holocene period of shared growth between UP3 and UP4. The stable isotope records have been matched using parallel detrital layers (dashed vertical lines) found in both stalagmites.

7.6.2 Growth hiatuses and petrographic surfaces

The environmental condition that produced the petrographic boundaries and associated growth hiatuses in UP3 and UP4 is difficult to determine due to multiple, often conflicting, lines of evidence. The detrital content and evidence of erosion suggests increased cave flooding, but the gradually declining

deposition below the boundaries has been interpreted as drying evidence in other published literature (Railsback et al., 2013). The UVL minima associated with the petrographic boundaries are very likely a reflection of high detrital content and should not be viewed as a soil productivity proxy. However, $\delta^{13}C$ values increase significantly upwards towards these petrographic surfaces and hiatuses, and this typically would be interpreted as a reduction in vegetative cover and/or productivity. The $\delta^{18}O$ values do not show consistently significant trends at the boundaries, although a slight drop in $\delta^{18}O$ value before a boundary is common. Finally, the stalagmites are in a growth hiatus today, and the modern climate and environment are not dry. Upper Porter Cave has active drip water, including above UP3 and UP4 (Figure 31), but no modern or recent speleothem growth is apparent. This suggests the modern hiatus is not due to a lack of available moisture, but rather an excess of moisture and/or undersaturation of $CaCO_3$ in the drip water (note that references to undersaturated waters in this dissertation are always with respect to $CaCO_3$).

Thus, the hiatuses in UP4 appear to be recording a shift to a wetter and stormier precipitation regime that produces less favorable conditions for stalagmite growth in Upper Porter Cave. An increase in precipitation intensity and/or infiltration rate can reduce aqueous $CaCO_3$ concentrations by limiting the available time for water to dissolve CO_2 in the soil and $CaCO_3$ from the bedrock and lead to undersaturated cave drip waters (Railsback et al., 2013). The wetter climate may be due to an increase in winter precipitation events and/or amounts as suggested by the modern drip water $\delta^{18}O$ values and the decrease in stalagmite $\delta^{18}O$ value before the petrographic boundaries. Stalagmite growth at all Indiana caves sampled appears favored during times of high northern hemisphere summer insolation and low winter insolation when seasonality is enhanced relative to modern climate (Chapter 8). Winters during these times would likely be dry and cold while modern day winters are probably wetter due to greater winter insolation (Shuman and Donnelly, 2006). A shift in the seasonal precipitation balance toward winter could also limit stalagmite growth. Soil CO_2 concentrations are lower in winter due to

decreased biological respiration (Rightmire, 1978), and increasing the winter fraction of the temporally-mixed water entering a cave would also reduce CO_2 concentrations in water, reducing its acidity. Less dissolution of $CaCO_3$ due to less acidic water can limit or stop speleothem growth (Baldini et al., 2005). Winter precipitation events are more likely to lead to rapid infiltration and flooding as the reduced vegetation coverage in winter both lessens water capture and increases runoff.

A major shift in the rainfall intensity and/or seasonal balance of soil and cave water can also explain the 'drying' signals observed in $\delta^{13}C$ and petrography. The $\delta^{13}C$ values show a rapid rise in values shortly before a hiatus. Higher $\delta^{13}C$ values are produced when water residence time in soil is short, as would be the case in stormier, wetter conditions (Baker et al., 1997). Additionally, if the drip water is fed more and more from winter precipitation, then $\delta^{13}C$ values should rise because the $\delta^{13}C$ of soil CO_2 is higher in winter (Rightmire, 1978). The 'type L' surfaces identified in UP3 and UP4 below a hiatus do not show the degree of apex narrowing of 'classic' surfaces of this type (Railsback et al., 2013), but do appear to record declining $CaCO_3$ deposition. A reduction in aqueous $CaCO_3$ saturation due to wetter conditions could reduce speleothem deposition and produce pseudo-type L layering. Additionally, the detrital content embedded within these pseudo-type L layers may be limiting $CaCO_3$ deposition by reducing the area of exposed $CaCO_3$ crystals upon which new $CaCO_3$ growth can take place. This blocking of $CaCO_3$ crystal growth by detritus is observed at these petrographic surfaces as disruptions in the growth of same-phase $CaCO_3$ crystals in crossed-polarized light.

With these ideas in mind, a paleoenvironmental interpretation of the petrographic surfaces and associated hiatuses can be developed. The stalagmite UP3 and UP4 grow during periods of relatively low precipitation amount and intensity. The lower soil water input allows for slower infiltration and equilibration with soil CO_2. Drip waters may be derived more from diffuse flow than conduit flow in drier periods, and diffuse flow is more likely to be saturated in $CaCO_3$ than conduit flow (Shuster and White, 1972). Slower-dripping cave water is also generally more saturated in $CaCO_3$ than fast-dripping water

(Baldini et al., 2006). A reduction in winter precipitation is most likely the driver of this change since summer precipitation is somewhat mitigated by higher evapotranspiration rates, and higher summer soil CO_2 concentrations increase the amount of $CaCO_3$ delivered to the stalagmites in drip water.

A shift to a stormier, more winter-dominated precipitation regime increases flood events in Upper Porter Cave that deposit detrital material on UP3 and UP4, and this is recorded in the stalagmites as increasing levels of detritus approaching a hiatus boundary. Stalagmite growth slows as drip water chemistry becomes less favorable to $CaCO_3$ deposition due to lower aqueous CO_2 and $CaCO_3$ concentrations. If the trend toward more winter-dominated precipitation and precipitation intensity continues, the drip water chemistry becomes incapable of depositing $CaCO_3$ mineral and stalagmite growth stops. For UP3 and the longer growth portions of UP4, the climate appears to oscillate between favorable and less favorable conditions for stalagmite growth with only limited periods when growth stops entirely. However, climate shifted far enough toward unfavorable growth conditions on four occasions (2.3, 3.6, 4.7, and ~7.4 ka BP) to stop stalagmite deposition for over a century. During these hiatuses, water continued to drip onto the stalagmites due to the wet climate, but the undersaturated water could not deposit $CaCO_3$ and even dissolved away some prior deposits to produce the type E petrographic surfaces observed at hiatus boundaries.

7.6.3 Paleoenvironmental interpretation

The complex depositional history of UP3 and UP4 precludes standard interpretation of the paleoenvironmental proxies. Additionally, the stalagmites in Upper Porter Cave are from a relatively shallow cave with changing surface conditions sometimes directly transferred into the stalagmite passages by means of the cave stream. As such, it should not be surprising that the Upper Porter Cave stalagmites do not appear to record paleoenvironmental proxies in a similar manner to stalagmites in deep caves typically chosen for paleoenvironmental reconstruction. Long-term (>centennial) changes in stalagmite stable isotope values may reflect broad environmental changes such as soil productivity and

atmospheric flow or precipitation seasonality. However, since the drip water source appears to have been responsive to short-term precipitation events and not a steady drip from a well-mixed aquifer, short-term stable isotope variability likely contains a fair amount of noise due to additional controls on stable isotopes that can overwhelm the long-term controls on short timescales. For example, high, short-lived extremes in $\delta^{13}C$ values are believed to reflect rapid water infiltration and not lower vegetation and soil productivity that would be expected in a more typical $\delta^{13}C$ interpretation. However, the changes in long-term mean $\delta^{13}C$ values in the Holocene are still taken to represent changes in vegetation cover and productivity.

The $\delta^{18}O$ record in general shows greater short-term variability relative to overall value range than the other paleoenvironmental proxies. However, longer-term $\delta^{18}O$ trends appear to reflect changes in seasonal water balance. Thus, the general drop in $\delta^{18}O$ values around 7.5-7.7 ka BP and the overall decline in $\delta^{18}O$ values over the Holocene signify greater input of winter moisture, while the short-term noise is likely due to the many meteorological factors that can influence interannual $\delta^{18}O$ values such as storm tracking and moisture source balances. The causes for this short-term noise would not be expected to impact the other paleoenvironmental proxies as much and explains the generally weak correlations and lack of similar trends observed between $\delta^{18}O$ and the other paleoenvironmental proxies. Stalagmite $\delta^{18}O$ values typically decrease in detritus-rich layers, and this decrease supports the conclusions drawn from petrography and $\delta^{13}C$ of a shift toward a more winter-dominated water source at these times.

The UVL record largely reflects detrital content in the stalagmite, and high detritus zones are found immediately below hiatuses. High background levels of detritus and intermittent detrital layers are found in the periods 3.6-4.0, 4.7-4.8, and 7.5-8.0 ka in UP4, suggesting increased flooding from stormier conditions. However, UP4 continued to grow through these times suggesting precipitation was not intense enough and not sufficiently plentiful to stop stalagmite deposition. Zones in the stalagmites

with lighter tones generally have lower $\delta^{13}C$ values. The lighter colors may be due to higher concentrations of organic acids that scatter light and would be associated with higher soil productivity and lower $\delta^{13}C$ values.

7.6.4 Early Holocene

UP3 and UP4 have similar petrographic and tone characteristics in the period from 8.0 to 8.5 ka BP. An initial dark translucent base layer is topped by very light, detritus-free calcite with bright UVL and relatively low $\delta^{18}O$ and $\delta^{13}C$ values. The low $\delta^{13}C$ values, bright UVL, and lack of detritus suggest a high input of summer-dominated soil water and infrequent cave flooding, consistent with a dry early Holocene observed in the Midwest (Williams et al., 2009). However, the low $\delta^{18}O$ values in UP4 suggest a high winter precipitation component or more southerly storm track, and neither of these scenarios agrees well with the other proxy interpretations. In contrast, UP3 has relatively higher $\delta^{18}O$ values in the light zone that agree better with the other proxies. The reason for the difference between the UP3 and UP4 $\delta^{18}O$ records is unclear. This light calcite dates to approximately 8150-8400 cal yr BP and darkens before culminating in a detrital layer dating to 8115 ± 170 cal yr BP. This light zone and detrital layer fall within uncertainty to the age of the 8.2 ka climate event at 8175 ± 30 cal yr BP (Kobashi et al., 2007). The 8.2 ka event is a global, abrupt climate event believed to have been triggered by the drainage of proglacial Lake Agassiz that brought cold, dry, and windy conditions to many regions of the world (Alley and Ágústsdóttir, 2005; Morrill and Jacobsen, 2005) including the upper Midwest (Dean et al., 2002).

Although the detrital layer is closer in estimated age to the 8.2 ka event, the characteristics of the light zone may better match the expected climate changes experienced in the Midwest during the 8.2 ka event. The southerly displacement of storm tracks and jet streams at this time would be most significant in winter, as the high northern hemisphere summer insolation would likely somewhat offset the impacts in summer. A southerly displacement of the jet would result in a dry winter for southern Indiana from strong northwest air flow and continental anticyclone dominance. This would greatly favor

summer precipitation dominance of soil and cave drip waters and promote stalagmite growth while reducing the risk of cave flooding. The $\delta^{13}C$ values would be low as drip water is primarily-derived from the summer growing season. The detrital layer may mark the end of the 8.2 ka event and an increase in winter precipitation. Similar wetter conditions are reported for southern Michigan shortly after the 8.2 ka event (Nelson et al., 2009).

Stalagmite deposition may have been favored in the early Holocene due to atmospheric conditions that favored summer-dominant precipitation and drier winters. The North American subtropical and polar jets may have merged over 30-35°N in response to heightened latitudinal temperature gradients from increased summer insolation and a remnant Laurentide Ice Sheet (LaMoreaux et al., 2009). This merged jet would have left the northern Midwest relatively dry while the southeastern United States was wet. This spatial moisture pattern is evidenced by the lack of larger Upper Mississippi flood events before 7.0 ka BP (Knox, 1985, 2000) coincident with evidence for wet conditions in peat cores from the southeastern United States (Goman and Leigh, 2004; LaMoreaux et al., 2009). Southern Indiana, located between these spatial extremes, would likely have seen a seasonal migration of the storm track directing precipitation toward Upper Porter Cave in summer months but remaining drier in winter as precipitation stayed to the south.

The increased detrital content and marked detrital layers deposited in both UP3 and UP4 in the period from 7.4 to 8.0 ka BP represents the transition into a wet middle Holocene for southern Indiana. Southerly moisture advection appears to have increased in magnitude or seasonal duration after 8.0 ka BP, as evidenced by more cave flooding events and the eventual cessation of growth for UP3, UP4, and UP7 between 7.2 and 7.5 ka BP. Although the middle Holocene is well-recognized as being dry in the Great Plains and upper Midwest (Denniston et al., 1999a; King and Allen Jr, 1977; Winkler et al., 1986), sites to the south and east of southern Indiana typically record a wet middle Holocene (Goman and Leigh, 2004; McFadden et al., 2005). This is commonly understood to have resulted from the

development of a steeper precipitation gradient between central and eastern North America during the early to middle Holocene transition. Southern Indiana appears to have been located in the wet middle Holocene zone and east of the wet-dry boundary from 4.9 to 7.5 ka BP based on both the lack of deposition on UP3 and UP4 and evidence of floods and stalagmite erosion during this period. This steep precipitation contrast suggests very focused Gulf of Mexico moisture advection, perhaps driven by a very stable Bermuda High and a general lack of eastern North American troughs. This period of stalagmite growth hiatus and wet conditions in southern Indiana coincides with the warmest northern Hemisphere temperatures observed in the Holocene, variously termed the Holocene Altithermal, Hypsithermal, Climate Optimum, or Thermal Maximum (Marcott et al., 2013).

7.6.5 Middle Holocene

The series of growth periods and hiatuses in UP4 from 2.3 to 4.9 ka BP suggests that Upper Porter Cave was located at this time near the boundary between the drier and wetter conditions that favored/disfavored stalagmite growth. Many of these growth cycles share timing with globally-identified climate changes in the Holocene (Mayewski et al., 2004; Wanner et al., 2008; Wanner et al., 2011). Parallel wet-dry phases in northern Michigan broadly agree with the timing of the growth cycles in UP4 (Booth et al., 2004; Jackson et al., 2014), and the period from 2.3 to 4.9 ka BP when UP4 intermittently grows because of drier conditions is also reported as dry across much of the eastern and central United States (Forman et al., 2001; Hanson et al., 2010; Knox, 2000; Naughton et al., 2015; Springer et al., 2008). The period from 3.3 to 5.5 ka BP had a low frequency of small flood events in Wisconsin, and evidence of a dry, warm climate is observed in soils (Knox, 2000). The $\delta^{13}C$ values in UP4 are variable but mean values are relatively high in growth periods during the middle Holocene, supportive of drier conditions. The $\delta^{18}O$ values show a long-term decline beginning around 3.9 ka BP, perhaps reflecting a gradual increase in winter precipitation coinciding with increasing winter insolation.

An eastward expansion of midcontinent dryness is observed with the migration of the prairie-forest boundary over the middle Holocene (Denniston et al., 1999b; Nelson et al., 2006), and this eastward progression of drier climate appears to reached southern Indiana at 4.9 ka BP when UP4 restarted growth. Detrital content increased approaching the next hiatus at 4.7 ka BP, suggesting cave flooding and precipitation increased until conditions became too wet again for stalagmite growth.

UP4 began growing again at 4.2 ka BP and deposition continued until 3.6 ka BP. The timing and duration of this growth period corresponds with the 4.2 ka BP abrupt climate event and its lingering impact on North America. Evidence of a rapid climate change event around 4200 cal yr BP has been identified at sites around the world including southwest Asia (Arz et al., 2006; Cullen et al., 2000; Staubwasser et al., 2003; Weiss et al., 1993), Africa (Rijsdijk et al., 2011; Stanley et al., 2003), the Mediterranean region (Kuzucuoğlu et al., 2011; Magny et al., 2009), China (Huang et al., 2011; Huang et al., 2010), and South America (Tripaldi and Forman, 2007). In North America, the Pacific Northwest became wetter and glaciers advanced (Menounos et al., 2008) while dry conditions prevailed across much of the midcontinent (Booth et al., 2005) and into northern Michigan (Booth et al., 2004).

This abrupt climate event have been linked to a weakening in monsoonal strength and changes in overall global circulation patterns, but the global climate driver for this event has not been positively identified. Generally, explanations include persistent La Niña conditions and/or abnormally cold North Atlantic sea surface temperatures (Booth et al., 2005; Gupta et al., 2003; Ju and Slingo, 1995). Many studies have suggested a link between such North Atlantic cold events and climate change in North America (Springer et al., 2008; Viau et al., 2002). However, the magnitude and even existence of strong links between North Atlantic temperature changes and North American climate is debated (Viau et al., 2006; Wanner et al., 2008; Wanner et al., 2011), possibly due to greater complexity of North Atlantic drift ice patterns than previously acknowledged (Moros et al., 2006). A potential link between the aridity seen in southwest Asia, Africa, and North America is the positioning of the Bermuda High. Dry conditions

in the Sahel region are linked to a weaker South Asian Low and an east-displaced Bermuda High (Hameed and Riemer, 2012). A weaker South Asian Low generally means a weaker southwestern Asian monsoon, and eastward displacement of the Bermuda High reduces midcontinent precipitation in North America (Zhu and Liang, 2012). An east-shifted Bermuda High could direct southerly moisture advection farther to the east and promote drying conditions in southern Indiana.

In a similar pattern to the 4.7-4.9 growth zone, detritus was increasingly deposited until the stalagmite stopped growing at 3.6 ka BP, and this hiatus in growth coincides with a very wet period recorded in upper Michigan (Booth et al., 2004). This wet period may signify a return of southerly moisture advection as the Bermuda High shifted to the west. An abrupt climate event at 3.2 ka BP has been proposed based upon dry conditions in the Middle East (Kaniewski et al., 2008; Kaniewski et al., 2013). A 3.2 ka event is not globally identified or widely-recognized. However, a parallel drying of midcontinent North America and the Middle East similar to the 4.2 ka event may be represented by the growth resumption in UP4 at 3.1 ka BP when deposited calcite was relatively free of detritus, which likely signifies a low frequency of cave flooding.

As stated previously, the hiatus from 2.9 to 2.7 ka BP in UP4 is probably due to the stalagmite top connecting to a stalactite and new deposition eventually being forced to the side of the original growth axis. This side growth is initially very light-colored (almost white) and of low density with almost no detritus. The petrography suggests that this light section was a period of very rapid stalagmite growth, and subtle banding may reflect annual deposition cycles. The $\delta^{13}C$ record shows a sustained period of high values around 2.6 ka BP, but the other paleoenvironmental proxy data do not support low vegetation productivity or heavy precipitation at this time. The high $\delta^{13}C$ values may be related to the unusual petrography in this zone and a higher rate of CO_2 degassing during the rapid growth. The $\delta^{13}C$ values drop to more normal values when stalagmite color and petrography return to a form more similar to the rest of UP4. The lowest $\delta^{18}O$ values from either UP3 or UP4 are in this final growth phase of UP4,

suggesting an increase in winter precipitation and/or increased shift of the storm track south relative to the early and middle Holocene. The $\delta^{18}O$ values are also much more variable in the last 200 years of deposition on UP4 than the older stalagmite portions, perhaps related to a more active and variable winter precipitation regime.

Stalagmite UP4 stopped growing for a final time at 2.3 ka BP. When collected, the stalagmite surface was coated in a layer of fine detritus, and the apex had solutional pitting as evidence of erosion since the last $CaCO_3$ deposition. If stalagmite deposition would have resumed in the future, the current stalagmite surface layer would look very similar to the petrographic surfaces at 3.1-3.6, 4.2-4.7, and 4.9-7.5 ka BP. This final growth hiatus that has lasted until present coincides with a general drop in global temperature and a northern hemisphere winter insolation maximum (Berger, 1992; Marcott et al., 2013). Winter precipitation during the late Holocene is thought to have increased in the eastern United States, due in part to warmer winters from increased insolation (Shuman and Donnelly, 2006). This additional winter precipitation is more likely to infiltrate rapidly into the cave and be undersaturated due to lower evapotranspiration and less capture by biomass compared to summer precipitation.

The fact that the current climate is not producing stalagmite growth in Upper Porter Cave suggests that past periods of stalagmite growth must have been markedly drier than today or any climate of the past 2300 years. Modern climate in southern Indiana has a nearly equal seasonal precipitation balance (although winter months are slightly drier), but flood frequency is greatest in winter and spring due to snowmelt and reduced evapotranspiration. An increase in winter anticyclone dominance and a southern displacement of the storm track due to atmospheric flow changes during times of stalagmite growth appears the most likely cause of drier winters in southern Indiana. Abnormally dry conditions that led to stalagmite growth in the middle Holocene may also have been aided by dominant La Niña conditions in the Pacific (Cobb et al., 2013; Conroy et al., 2008). However, La Niña conditions were dominant for a large portion of the Holocene, including the wetter periods in

Indiana, so tropical Pacific conditions do not appear to fully explain climate variability observed in UP3 and UP4. Severe dry episodes in southern Indiana during the middle Holocene may have been triggered by colder conditions in the North Atlantic that pushed the winter storm track south of the region and reduced southerly advection by shifting the Bermuda High to the east. Most likely, a complex atmospheric situation involving both Atlantic and Pacific forcing is required to replicate the very different climate experienced in southern Indiana during times of stalagmite growth.

7.6.6 Comparison with other Midwestern Holocene stalagmites

Data from three other caves in or near the Midwest with long-term Holocene stalagmite stable isotope data were compared with the record from UP4 (Table 29). While additional stalagmite records are available from other Midwestern caves (Denniston et al., 2007; Denniston et al., 1999a), these records are too short for the desired Holocene comparison. For each of the three caves with long-term records, a single stalagmite record was chosen that was high-quality and, if multiple quality records were available, representative of the narrative from the cave. Data from the caves were simplified into wet and dry phases for comparative purposes. These caves lie along a west-east transect across much of the Midwest, stretching from Minnesota in the west to West Virginia in the east.

Table 29. Stalagmite records used in the regional comparison of stalagmite stable isotope data.

Stalagmite	**Cave**	**Period of Record (ka BP)**	**Source**
US-INUP4	Porter Cave, IN	2.3-8.5	This study
BCC-2	Buckeye Creek Cave, WV	0.0-7.0	Springer et al. (2008)
CWC 3L	Cold Water Cave, IA	1.9-8.6	Denniston et al. (1999a)
SV-1	Spring Valley Cave, MN	0.0-8.5	Denniston et al. (1999a)

The stalagmite from Minnesota and the Iowa stalagmite both shift to drier conditions after a wetter early Holocene (Denniston et al., 1999a). This drying occurs at 8.0 ka BP in Minnesota, but does not begin until 6.0 ka BP in Iowa (Figure 43). The drier Minnesota conditions after 8.0 ka BP coincide

with the onset of the wet middle Holocene hiatus in UP4, perhaps related to the focusing of precipitation toward the east and the development of the steep west-east precipitation gradient at this time. The resumption of UP4 deposition after 4.9 ka BP coincides with the period of highest $\delta^{13}C$ values in Iowa, supporting the conclusion of an eastward expansion of a drier climate at this time. The eastward expansion of midcontinent aridity in the middle Holocene does not appear to have reached West Virginia to the degree of southern Indiana, likely due to more precipitation being directed to the eastern United States and away from the west. A sustained eastward shift in the location of the Bermuda High in the middle Holocene may explain this eastward expansion of drier climate. From 2.3 to 4.9 ka BP, conditions in Indiana alternated between being dry enough for stalagmite growth and too wet for growth. This alternation suggests that the boundary between the wet east and dry west was very near southern Indiana and migrated back and forth across Upper Porter Cave multiple times. Climate during the later Holocene (2.0 ka BP to present) is less clear as two of the stalagmites stopped growing, but it appears that western cave sites became wetter reflecting a more moderated precipitation gradient from west to east. Overall, the regional stalagmite data support the conclusions made from the UP4 data concerning Midwestern climate patterns over the Holocene.

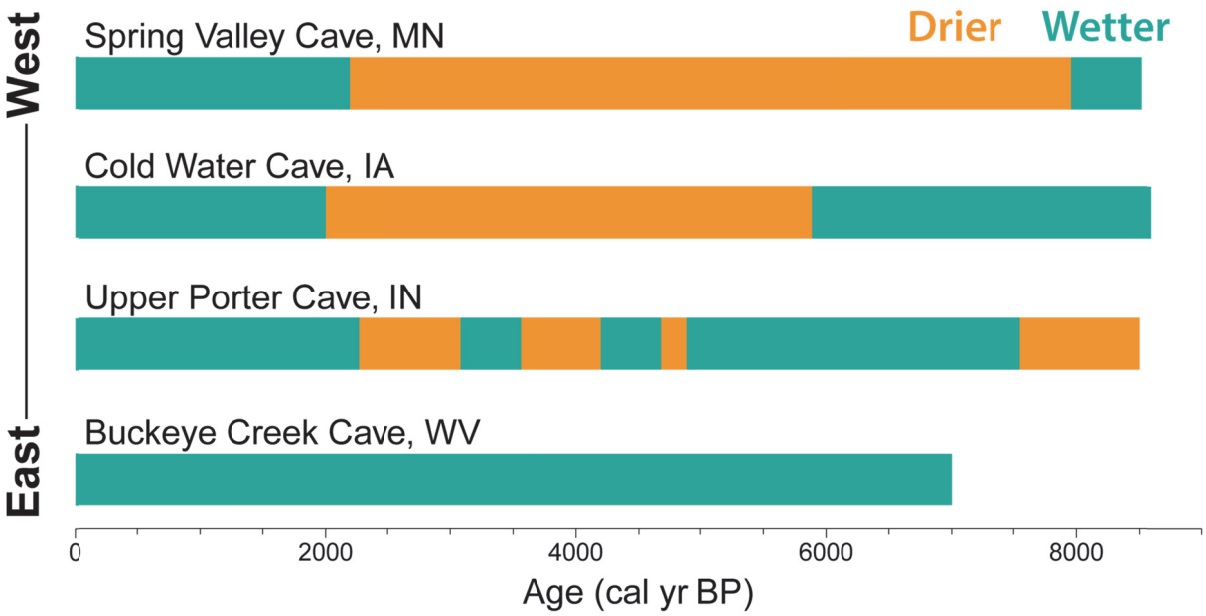

Figure 43. The timing of Midwestern wet and dry phases indicated by stalagmites from four caves using data reported in this study, Denniston et al. (1999a), and Springer et al. (2008).

7.7 Conclusions

7.7.1 Remarks

The stalagmites collected from Upper Porter Cave in south-central Indiana have provided a series of paleoenvironmental proxies spanning portions of the Holocene. The environment in which the stalagmites were deposited (near-surface, flood-prone, dirty) would not be seen as ideal for a classic speleothem paleoclimate study. However, this changeable setting has produced stalagmites that are very sensitive to varying environmental and climate shifts. Although the data from UP3 and UP4 have been difficult to interpret, in the end they have produced a valuable paleoclimate record for a little-studied region. Additionally, the paleoenvironmental records have generated many additional questions about the nature of early and middle Holocene climates of the central and eastern United States. In particular, these stalagmites highlight the complexity of middle Holocene aridity at the fringes of the

more intensively-studied Great Plains and suggest a general assumption of dry conditions for the Midwest during the middle Holocene is not warranted for all regions.

The data retrieved from the stalagmites also validate the merit and necessity of multi-proxy analysis. Although petrography is not commonly mentioned in stalagmite literature, it is critical for properly interpretation of the stable isotope and UVL data in UP3 and UP4 as well as for constructing accurate age-depth models. If the $\delta^{18}O$ records from UP3 and UP4 were analyzed and interpreted alone, as is common in stalagmite research, it is highly likely that erroneous interpretations and conclusions about the paleoenvironment of southern Indiana would have been made. Combined, the suite of paleoenvironmental proxies offers a more complete narrative of past climate changes in Indiana than is possible with individual proxy data. The lessons learned in the high-resolution study of UP3 and UP4 offer an important baseline to investigate the potential paleoenvironmental records contained in other stalagmites collected from southern Indiana (Chapter 8).

7.7.2 Most important findings

- Stalagmites in Upper Porter Cave, Indiana, grow during periods of relatively drier climate and stop growing during wetter periods.
- Southern Indiana was wet in the first part of the middle Holocene (4.9-7.5 ka), unlike the drier conditions to the west.
- Between 2.3 and 4.9 ka BP, the climate of southern Indiana oscillated between conditions dry enough to allow stalagmite growth and wetter conditions that stopped growth, and these oscillations coincide with global, abrupt climate events and possible shifts in the position of the Bermuda High.
- Wetter conditions for the past 2300 years prevented stalagmite growth, and portions of the Holocene were drier than modern conditions in southern Indiana.

CHAPTER EIGHT:

PALEOENVIRONMENTAL IMPLICATIONS OF INTERMITTENT STALAGMITE DEPOSITION IN SOUTHERN INDIANA DURING THE PAST 90,000 YEARS

8.1 Introduction

Fifteen stalagmites were collected for paleoenvironmental study during field work in four southern Indiana cave systems in the years 2013 to 2015 (Appendix 1). Thirteen of the stalagmites have been dated by 91 total uranium-thorium (U-Th) ages, and these stalagmites grew for brief portions of the last 90,000 years. Although only two stalagmites, US-INUP3 and US-INUP4, provided detailed paleoenvironmental data (Chapter 7), the timing of growth and hiatus of all collected stalagmites has provided information for this little-known period in southern Indiana. A small number of samples taken from the stalagmites for stable isotope analysis have also given a glimpse of how stable oxygen and carbon isotopes ($\delta^{18}O$ and $\delta^{13}C$) varied over the past 90,000 years. This expanded paleoenvironmental investigation also places the Holocene record from UP3 and UP4 into a longer temporal context and examines the environmental responses in southern Indiana to the global climate changes from the Late Pleistocene to present-day.

8.2 Objectives

- Constrain the times of growth and hiatuses for thirteen southern Indiana stalagmites.
- Determine which regional and global climates promote or hinder stalagmite growth in southern Indiana.

- Describe the paleoenvironmental history of southern Indiana over the past 90,0000 years based upon the aggregated stalagmite records.

8.3 Background

8.3.1 Regional millennial-scale climate change

The global climate of the Quaternary Period is dominated by alternating glacial and interglacial periods driven by changes in the orbit and rotational axis of the Earth (Imbrie, 1984; Shackleton and Opdyke, 1973). These astronomical changes shift the balance and timing of solar radiation across the globe, leading to dramatic changes in continental ice volumes and sea levels (Broecker and van Donk, 1970). The cyclical growth and decay of continental ice volumes is reflected in ocean $\delta^{18}O$ values, and a numbered list of these 'marine isotope stages' is commonly used as a chronological reference and anchor (Railsback et al., 2015b). The globally colder and drier glacial periods have lasted much longer than the warmer interglacials for the past 800,000 years (Andersen et al., 2004; Jouzel et al., 2007), and the climate and environment of a given location often changed drastically between glacial and interglacial times. This is particularly true in higher latitudes where the growth of continental ice sheets altered global atmospheric circulation patterns and cooled nearby regions (Bromwich et al., 2005; Lee et al., 2008; Lofverstrom et al., 2014; Merz et al., 2015).

Glacial periods were not consistently cold, but varied between relatively warmer and cooler conditions. A series of approximately 25 interstadials, also known as Dansgaard-Oeschger events, have been identified during the last glacial period. These interstadials were relatively warm periods expressed in the Greenland ice core data with a rapid onset of warming and a gradual cooling (Andersen et al., 2004; Dansgaard et al., 1993; Johnsen et al., 1992). These events are also recorded in Antarctic ice cores, although they are more muted in magnitude, have a gradual onset, and tend to lead the Greenland

changes (Jouzel et al., 2007). The reason for this non-synchronous timing between Greenland and Antarctic data is poorly understood, and portions of the North Atlantic even appear to have operated on Antarctic timing (Rasmussen et al., 2016). Despite the regional differences in interstadial expression, it is clear that these dramatic changes in climate had global ramifications (Genty et al., 2003; Leuschner and Sirocko, 2000; Litwin et al., 2013; Spötl and Mangini, 2002).

Large portions of the American Midwest were covered by the Laurentide Ice Sheet (LIS) during glacial periods, and the ice sheet reached south of 40°N latitude in southern Indiana at its greatest extent during glacial maxima. The sampled southern Indiana caves were never glaciated in the Quaternary with the exception of Porter Cave. Porter Cave was ice-free in the Last Glacial Maximum (LGM) from 19 to 23 thousand years before present (ka BP), but just north of the ice margin and glaciated during the penultimate glaciation. During glacial maxima, southern Indiana was dominated by tundra and muskeg vegetation (French and Millar, 2013; Heusser et al., 2002); however, climate gradients were likely very steep south of the LIS margin (Bromwich et al., 2005) and boreal forest invaded the southern Indiana tundra quickly when the ice sheet retreated (Heusser et al., 2002). This rapidly changing environment is valuable for paleoenvironmental studies because even minor global changes in climate can significantly affect such climate-sensitive regions.

8.3.2 Stalagmite paleoenvironmental proxy interpretation

Earlier chapters of this dissertation have focused on the interpretation of $\delta^{18}O$ variations in modern precipitation, and a framework for interpreting Holocene stalagmite $\delta^{18}O$ and $\delta^{13}C$ was described in Chapter 7. However, when extending stalagmite records into the Pleistocene, the extreme environmental changes experienced at millennial timescales negates many of the assumptions and interpretations for paleoenvironmental proxies developed from modern-day analogs. During the LGM, mean annual temperatures were 12 to 17°C colder than modern in southern Indiana with the greatest deviation from modern temperatures in winter (Annan and Hargreaves, 2013; Jackson et al., 2000).

These colder conditions (perhaps similar to modern-day central Manitoba) and the influence of the LIS significantly altered atmospheric flow patterns and vegetation away from anything experienced during the Holocene. Changes during the LGM are likely to have resulted in different environmental controls on stalagmite growth and stable isotope values than during the Holocene.

Changes to the mean stalagmite $\delta^{18}O$ value for a given location over millennial timescales are governed by multiple environmental factors with conflicting directions of forcing. Since stalagmite $\delta^{18}O$ values reflect precipitation $\delta^{18}O$ values, the changes to precipitation $\delta^{18}O$ values due to radically different climate during glacial periods must be estimated. While global circulation modeling has produced estimates of LGM precipitation $\delta^{18}O$ spatial distributions, these models are generally too coarsely-resolved to capture the steep climate gradients that must have existed in southern Indiana during the LGM (Charles et al., 2001; Lee et al., 2008; Tharammal et al., 2013). Mean ocean and Gulf of Mexico $\delta^{18}O$ values were 1.0-1.2‰ higher during glacial maxima due to low $\delta^{18}O$ water being locked up in continental ice sheets (Lachniet, 2009; Whitaker, 2008), and this ice-volume effect would be transferred into higher precipitation $\delta^{18}O$ values. However, much of the ice-volume effect on precipitation $\delta^{18}O$ values is mitigated by kinetic effects on $\delta^{18}O$ from cooler and drier evaporative conditions at the sea surface; these kinetic effects during ocean evaporation in the LGM may have reduced precipitation $\delta^{18}O$ values by approximately 1.9‰ (Lachniet, 2009).

Colder conditions in southern Indiana during the LGM would increase rain-out and Rayleigh distillation to produce lower precipitation $\delta^{18}O$ values. Assuming a mean annual temperature in southern Indiana around 0.5°C (a value within regional temperature estimates and still warm enough for stalagmite deposition), the temperature effect alone would result in annual precipitation $\delta^{18}O$ values approximately 2.7‰ lower than modern at USNIP site IN22 (Chapter 2). This is, of course, a rough estimate as the temperature effect at IN22 is determined from modern observations and the slope of the temperature effect in southern Indiana is very likely to have changed on millennial timescales.

Additionally, the very cold winters during the LGM likely reduced winter precipitation in southern Indiana, and a shift to a more summer-dominated precipitation regime (with comparatively higher precipitation $\delta^{18}O$ values) during the LGM would reduce the magnitude of precipitation $\delta^{18}O$ value drop due to lower annual temperature in a glacial setting compared to modern.

Cave temperature controls the kinetic fractionation of oxygen isotopes when the $CaCO_3$ in a stalagmite is deposited (Kim and O'Neil, 1997). During the Holocene, mean annual temperatures, and thus cave temperatures, did not vary enough in southern Indiana to be a major control on stalagmite $\delta^{18}O$ variability. However, cave temperatures have a much greater magnitude of change over millennial timescales and must be accounted for in any Pleistocene stalagmite $\delta^{18}O$ interpretation. Stalagmites growing in southern Indiana during the LGM with a cave temperature of 0.5°C would have calcite $\delta^{18}O$ values 2.75‰ higher than with modern cave temperatures (Kim and O'Neil, 1997). Combined together, estimated effects of the LGM environment on stalagmite $\delta^{18}O$ values in southern Indiana largely offset each other (Table 30) with a predicted overall difference well within the modern range of stalagmite $\delta^{18}O$ variability (Chapter 7). Additional climate factors not well constrained over millennial timescales (e.g., atmospheric flow patterns, precipitation seasonality, transpiration and evaporation, etc.) potentially alter mean precipitation $\delta^{18}O$ values as well, and thus a standard $\delta^{18}O$ correction factor based on these calculations is not advisable. Stalagmite carbon isotope ratios were probably higher during the LGM and glacial periods as a result of reduced vegetative cover and productivity due to the colder and drier conditions in southern Indiana (Baldini et al., 2005; Hesterberg and Siegenthaler, 1991; McDermott, 2004).

Table 30. Environmental effects on stalagmite $\delta^{18}O$ values for southern Indiana during the LGM.

Environmental Forcing	**Precipitation $\delta^{18}O$ difference between LGM and modern day**
Ice volume effect	+1.2‰
Conditions at moisture source evaporation	-1.9‰
Temperature effect in southern Indiana	-2.7‰
Cave temperature effect on calcite fractionation	+2.8‰
Summed together	-0.6‰

An individual stalagmite is rarely able to grow during all environmental conditions experienced in millennial-scale climate shifts from glacial to interglacial periods. More commonly, a stalagmite will grow only during a distinct set of environmental conditions and cease growth when the favorable growth conditions disappear. However, the stalagmite may resume growth if favorable conditions reappear, and some stalagmites reflect millennial-scale glacial-interglacial cycles in their growth and hiatus cycles (Ersek et al., 2009; Railsback et al., 2015a). A shift to wetter conditions (either during glacial or interglacial periods, depending on location) is commonly inferred to activate stalagmite growth, although drier conditions may also favor stalagmite growth as shown in Chapter 7. Dramatic vegetation changes recorded over millennial timescales can also control the growth of stalagmites: limited vegetation due to colder and/or drier conditions reduces soil water CO_2 concentrations and may not permit stalagmite growth (Baldini et al., 2005).

The stalagmite DC20 discussed in Chirienco (2010) is unique among reported Indiana stalagmites in that it grew over at least a portion of the deglaciation period. The stable isotopes reported for DC20 have a sustained and abrupt drop in values that likely coincides with the beginning of deglaciation during the Bølling-Allerød period. Values for stalagmite $\delta^{18}O$ in DC20 are approximately 0.7‰ higher in the glacial period than after deglaciation, and mean $\delta^{13}C$ values are 3.5‰ higher during the glacial period. While the drop in $\delta^{13}C$ values with deglaciation is expected due to increasing vegetation with

deglaciation, the $\delta^{18}O$ values have the opposite direction of change than might be expected (Table 30). Possible explanations for the higher stalagmite $\delta^{18}O$ values in glacial periods could be lower cave humidity enhancing disequilibrium fractionation, a strongly summer-dominant precipitation regime, or a more dominant-than-predicted effect of the cave temperature during calcite deposition. The sustained difference in $\delta^{18}O$ values from deglaciation values during the glacial period suggests that the cause of this shift should be intrinsic to the difference between glacial and post-glacial environments. This suggests that changes in the cave temperature are the most likely reason for lower stalagmite $\delta^{18}O$ values after deglaciation. If this theory is correct, then the mean stalagmite $\delta^{18}O$ value might be a rough proxy for mean annual air temperature, at least on millennial timescales. Shorter-term variability in $\delta^{18}O$ values is likely still heavily influenced by atmospheric flow and seasonality changes.

8.3.2 Comparison of stalagmite record between caves

Differences in drip water routing and local cave environment can make quantitative comparisons between stalagmite paleoenvironmental records difficult at times even within a single cave. Aggregation and quantitative comparison of stalagmite records between different caves is not often performed due to inherent cave differences in geology, local climate, and vegetation composition that may mimic desired environmental and climate signals. However, the spotty nature of stalagmite growth periods in southern Indiana, coupled with the desire not to oversample any single cave for conservation purposes, necessitates comparing paleoenvironmental records from multiple caves to capture a more complete understanding of millennial-scale environmental change. Some inherent environmental differences between caves, such as mean annual air temperature and bedrock $\delta^{13}C$, can be mitigated through standardization factors drawn from modern observations. Time periods when stalagmite records from different caves overlap can be used to estimate inherent paleoenvironmental proxy biases between caves as well. Broad and sustained changes in mean stable isotope value are most useful in deriving regional paleoenvironmental information from multiple caves, as short-term isotopic

variations are more likely responding to local climate and cave changes than to a regional environmental signal. Periods of stalagmite growth and hiatus may be the best paleoenvironmental records to compare between caves because the growth-hiatus cycles can often be distilled to simple wetter or drier conditions without the complicating factors found with stable isotope records.

8.4 Methods

8.4.1 Field sampling

Fifteen stalagmites were collected by hammer and chisel from four Indiana caves between July 2013 and June 2015 (Table 31,). All stalagmites are identified with the prefix US-IN to signify their United States-Indiana origin. The remainder of each stalagmite identification is comprised of a two letter abbreviation of the home cave and a number indicating the order collected. In this chapter, stalagmite names will be truncated to their cave abbreviation and number signifier (e.g., US-INJN1 is referenced as JN1). Actively-growing stalagmites were always targeted for sampling; however, only one stalagmite appeared potentially active in all caves visited. This stalagmite was collected (IC14) but initial ages suggest it was not actively growing upon collection. Details on cave environment, setting, and sampling locations are found in Appendix 1.

8.4.2 Laboratory analysis

The 15 stalagmites were cut and processed , and samples for U-Th dating and stable isotope analysis were obtained and analyzed as described in Chapter 7. The mean weight of samples for U-Th dating varied between stalagmites depending upon inherent ^{238}U concentration but typically ranged between 20 and 100 mg. Age-depth models were produced using linear regression and extrapolation due to relatively low number of ages per stalagmite and high age uncertainties. Stalagmite growth periods were determined from U-Th ages, but the exact timing of growth initiation and cessation were

estimated based upon the general distribution of ages in the stalagmite and evidence from global and regional climate changes.

Thirty-seven samples for oxygen and carbon stable isotope analysis were drilled from nine stalagmites, beyond the 976 stable isotope samples drilled from UP3 and UP4 (Table 31). These additional stable isotope samples were taken to offer a glimpse of how stable isotope values varied from stalagmite to stalagmite. Although only a few samples were drilled from each stalagmite, sample locations were chosen to best represent both the full growth of a stalagmite and potential stable isotope extremes as judged from petrography.

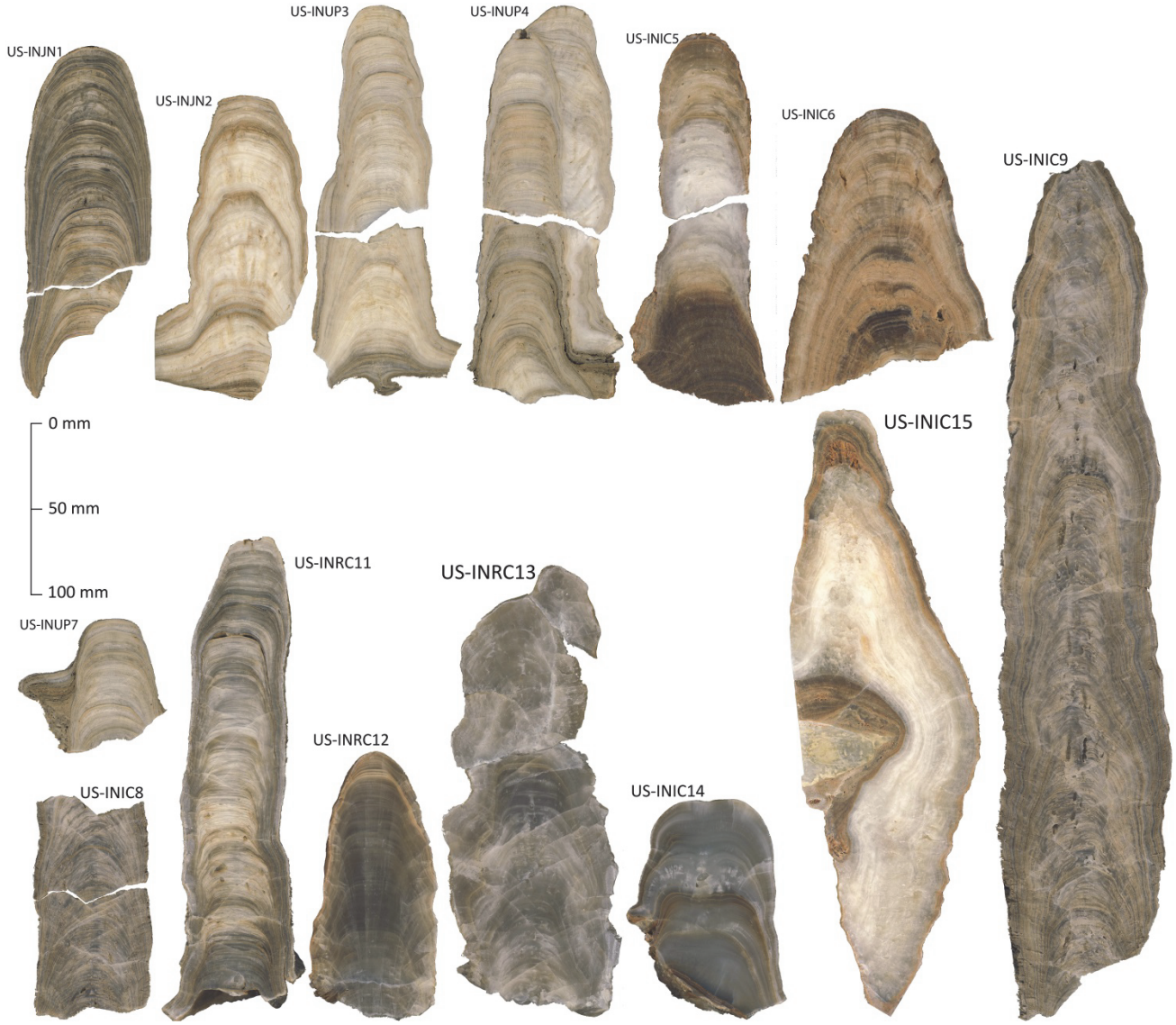

Figure 44. Stalagmites, shown to scale, collected as part of this research, with the exception of US-INLP10 which was not processed for paleoenvironmental analysis.

Table 31. Summary of characteristics and data for stalagmites collected from southern Indiana.

Stalagmite	*Cave*	*Collection year*	*Height (mm)*	*U-Th ages*	*Age range (ka)*	*Stable isotope samples*	*Thin sections*
US-INJN1	Johnson's Cave	2013	160	10	5-7 (est)	-	-
US-INJN2	Johnson's Cave	2013	165	9	8.7-9.2	3	-
US-INUP3	Upper Porter Cave	2013	220	9	7.4-8.5	70	Yes
US-INUP4	Upper Porter Cave	2013	315	18	2.3-8.5	906	Yes
US-INIC5	Indiana Caverns	2013	200	7	80-85	5	-
US-INIC6	Indiana Caverns	2013	155	7	80-85	3	-
US-INUP7	Upper Porter Cave	2013	65	3	7.3-7.9	1	-
US-INIC8	Indiana Caverns	2014	100	4	3.0-4.0 (est)	-	-
US-INIC9	Indiana Caverns	2014	400	7	1.5-4.0 (est)	-	-
US-INLP10	Lower Porter Cave	2014	70	-	Unknown	-	-
US-INRC11	Roadcut Cave	2014	260	7	8.4-12.0	7	Yes
US-INRC12	Roadcut Cave	2014	145	3	57-59	5	-
US-INRC13	Roadcut Cave	2014	245	4	57-59	3	-
US-INIC14	Indiana Caverns	2015	105	3	6.0-12.0 (est); base 27	7	-
US-INIC15	Indiana Caverns	2015	190	-	80-85 (est)	3	-

8.4.3 Cave record aggregation

Stalagmite stable isotope data from all caves were combined into a single dataset and analyzed as both original data and standardized data. In the first case, the original, unaltered data were used. In the second case, the data were adjusted based upon precipitation $\delta^{18}O$ differences between sites in modern observations and mean value offsets identified in temporally-overlapping records from different caves. Stable isotope data from stalagmite DC20 from Donnehue's Cave, Bedford, IN (Chirienco, 2010), were added to the cave dataset. This cave is located very close (<3 km) to Roadcut Cave, and DC20 offers stable isotope data dating to a period not covered by the stalagmites in this study. Although Chirienco (2010) reports that DC20 grew continuously from 12.8 to 55.8 ka BP, the U-Th ages and photographs of the stalagmite indicate that significant hiatuses in stalagmite growth likely exist between 12.8 and 46.5 ka BP and the reported ages of stable isotope values in this interval are probably wrong. For this reason, only DC20 data from 46.5 to 55.8 ka BP are considered here.

8.5 Results

8.5.1 Periods of stalagmite growth and hiatus

Seventy-two of the 91 U-Th ages obtained from the southern Indiana stalagmites are believed to be accurate, although precision is low for many of the ages (Table 32). The 19 excluded ages are believed to be affected by the addition of detrital thorium, which is also the reason for the high uncertainties in the reliable ages. The southern Indiana stalagmites grew during three distinct intervals: 1.5-12.0, 57-59, and 80-85 ka BP. Growth during the 57-59 ka BP period is only observed in Roadcut Cave stalagmites, and growth during the 80-85 ka BP period is only observed in Indiana Caverns stalagmites. Stalagmite growth was occurring in all four caves for at least a portion of time from 7.5 to 9.0 ka BP. During the Holocene, the onset and cessation of growth in different stalagmites are often very similar. For example, JN2 and RC11 stopped growing around 8.6 ka BP, just before UP3, UP4, and UP7

started to grow. Growth of JN1 is difficult to determine with precision due to high thorium content, but it appears to have grown during long middle Holocene hiatus of UP4. Stalagmite JN1 stopped growing around 5.0 ka BP shortly before UP4 began growing again and before the first growth of IC8 and IC9.

Table 32. Uranium-thorium age data for southern Indiana stalagmites.*

Sample ID	Depth (mm)	^{238}U (ppb)		^{232}Th (ppt)		^{230}Th/^{232}Th (atomic x 10^{-6})		δ^{234}U (measured)		^{230}Th/^{238}U (activity)		^{230}Th age (±2σ) (uncorrected)		^{230}Th age (±2σ) (corrected BP)	
JN1-3	*3*	*806.1*	*±2.6*	*30466*	*±618*	*64*	*±1*	*466.3*	*±3.1*	*0.1476*	*±0.0005*	*11507*	*±50*	*10700*	*±529*
JN1-7	7	929.2	±2.2	26751	±539	43	±1	438.4	±3.3	0.0744	±0.0003	5778	±29	**5133**	**±412**
JN1-16	16	577.9	±1.1	18014	±362	45	±1	439.9	±3.6	0.0844	±0.0004	6564	±36	**5874**	**±446**
JN1-35	35	935.7	±2.1	23867	±480	53	±1	514.0	±3.2	0.0824	±0.0003	6085	±25	**5534**	**±347**
JN1-60	60	750.5	±1.9	34990	±705	31	±1	502.3	±3.2	0.0882	±0.0003	6580	±29	**5616**	**±639**
JN1-90	*90*	*1201.5*	*±1.9*	*29405*	*±590*	*100*	*±2*	*521.7*	*±2.1*	*0.1477*	*±0.0003*	*11072*	*±29*	*10546*	*±330*
JN1-103	103	860.5	±2.2	38154	±769	35	±1	448.6	±3.0	0.0948	±0.0003	7359	±29	**6408**	**±630**
JN1-118	118	1103.7	±2.4	38525	±775	48	±1	552.1	±2.9	0.1015	±0.0003	7346	±25	**6632**	**±462**
JN1-140	*140*	*632.2*	*±1.1*	*110211*	*±2213*	*6*	*±0*	*529.3*	*±2.9*	*0.0652*	*±0.0004*	*4742*	*±31*	*1322*	*±2381*
JN1-156	*156*	*1422.8*	*±4.9*	*20662*	*±420*	*62*	*±1*	*512.6*	*±3.2*	*0.0545*	*±0.0002*	*3992*	*±18*	*3652*	*±198*
JN2-5	*5*	*767.6*	*±1.6*	*16943*	*±341*	*84*	*±2*	*361.4*	*±2.7*	*0.1119*	*±0.0003*	*9316*	*±34*	*8784*	*±334*
JN2-12	12	988.5	±1.2	10404	±209	171	±4	369.3	±1.6	0.1090	±0.0005	9009	±46	**8723**	**±164**
JN2-31	*31*	*911.5*	*±2.3*	*5368*	*±108*	*314*	*±6*	*355.8*	*±2.6*	*0.1121*	*±0.0004*	*9373*	*±37*	*9185*	*±96*
JN2-52	52	1169.5	±1.7	2072	±42	985	±20	367.7	±1.7	0.1058	±0.0004	8749	±33	**8647**	**±42**
JN2-80	80	796.4	±0.9	2331	±47	597	±12	338.6	±1.6	0.1059	±0.0006	8961	±52	**8834**	**±68**
JN2-115	*115*	*1028.3*	*±1.9*	*9123*	*±183*	*218*	*±4*	*419.2*	*±2.1*	*0.1173*	*±0.0003*	*9366*	*±27*	*9123*	*±131*
JN2-138	138	1082.2	±1.6	4512	±91	433	±9	344.4	±1.8	0.1096	±0.0004	9242	±35	**9088**	**±72**
JN2-143	143	795.0	±1.6	11595	±233	123	±2	349.5	±2.1	0.1089	±0.0003	9147	±29	**8772**	**±223**
JN2-163	163	107.6	±0.3	4473	±91	50	±1	374.6	±2.9	0.1262	±0.0004	10453	±44	**9514**	**±622**
UP3-3	3	466.4	±0.9	17076	±343	38	±1	141.3	±2.2	0.0848	±0.0003	8402	±37	**7405**	**±662**
UP3-21	21	418.6	±0.9	13965	±281	43	±1	182.2	±2.4	0.0862	±0.0004	8237	±39	**7352**	**±582**
UP3-47	47	560.3	±1.1	2961	±60	253	±5	172.4	±2.1	0.0811	±0.0004	7806	±44	**7611**	**±102**
UP3-70	70	619.1	±1.0	6858	±138	124	±3	187.9	±1.7	0.0835	±0.0002	7938	±26	**7603**	**±193**
UP3-84	*84*	*761.2*	*±1.8*	*3441*	*±69*	*306*	*±6*	*163.5*	*±2.2*	*0.0839*	*±0.0004*	*8144*	*±43*	*7968*	*±90*

UP3-119	119	654.4	±1.3	4188	±84	219	±5	178.3	±2.1	0.0848	±0.0004	8133	±45	**7911**	**±120**
UP3-152	156	531.2	±0.8	6718	±135	117	±2	197.2	±1.7	0.0900	±0.0003	8506	±31	**8135**	**±219**
UP3-174	178	505.2	±1.0	5958	±120	125	±3	169.4	±2.0	0.0897	±0.0005	8687	±49	**8330**	**±213**
UP3-193	197	728.3	±1.7	34103	±687	36	±1	181.0	±2.5	0.1012	±0.0003	9744	±39	**8526**	**±818**
UP4-210	*3*	*426.8*	*±1.0*	*228566*	*±4602*	*3*	*±0*	*131.7*	*±2.6*	*0.1064*	*±0.0009*	*10749*	*±96*	*-4016*	*±10500*
UP4-233	16	354.9	±0.7	6378	±128	27	±1	147.3	±2.7	0.0299	±0.0003	2877	±31	**2357**	**±324**
UP4-258	47	386.6	±0.5	5925	±119	32	±1	124.6	±1.7	0.0295	±0.0004	2901	±37	**2440**	**±283**
UP4-309	92.5	315.5	±0.6	385	±8	378	±10	126.0	±2.0	0.0280	±0.0005	2742	±48	**2646**	**±53**
UP4-3	*106.5*	*332.5*	*±0.7*	*26778*	*±538*	*7*	*±0*	*127.6*	*±2.4*	*0.0352*	*±0.0003*	*3453*	*±32*	*1295*	*±1484*
UP4-3b	106.5	286.8	±0.6	4290	±86	38	±1	126.3	±2.2	0.0342	±0.0005	3363	±53	**2914**	**±279**
UP4-17	125.5	325.7	±0.3	2516	±50	72	±2	133.1	±1.5	0.0336	±0.0003	3283	±27	**3023**	**±143**
UP4-31	138.5	374.7	±0.7	2282	±46	90	±2	134.6	±2.1	0.0332	±0.0004	3239	±39	**3019**	**±117**
UP4-40	148	424.6	±0.9	16174	±325	20	±0	138.7	±2.7	0.0469	±0.0005	4586	±50	**3545**	**±693**
UP4-61	169.5	419.5	±1.0	5453	±110	55	±1	132.7	±2.2	0.0430	±0.0004	4217	±39	**3821**	**±239**
UP4-67	175.5	429.7	±1.0	9571	±193	35	±1	145.1	±3.0	0.0470	±0.0003	4567	±32	**3937**	**±402**
UP4-101	207.5	415.2	±1.0	4166	±84	74	±2	126.4	±2.7	0.0450	±0.0005	4443	±48	**4120**	**±189**
UP4-111	217	461.0	±1.2	5978	±121	67	±1	134.5	±2.4	0.0528	±0.0004	5189	±41	**4795**	**±239**
UP4-119	228	534.9	±1.1	9612	±193	50	±1	132.9	±2.3	0.0540	±0.0002	5324	±24	**4800**	**±328**
UP4-142	252.5	602.4	±1.5	4636	±94	177	±4	164.6	±2.4	0.0827	±0.0004	8017	±47	**7761**	**±144**
UP4-165	247	535.5	±1.1	8658	±174	92	±2	205.5	±2.3	0.0898	±0.0003	8421	±36	**7968**	**±278**
UP4-166	275	503.8	±1.1	5169	±104	146	±3	208.3	±2.2	0.0906	±0.0003	8484	±35	**8173**	**±178**
UP4-198	305.5	777.3	±2.0	1436	±29	792	±16	184.8	±2.5	0.0888	±0.0003	8476	±34	**8369**	**±46**
IC5-5	5	202.2	±0.2	5197	±104	455	±9	316.1	±1.7	0.7098	±0.0012	81337	±255	**80739**	**±456**
IC5-44	44	233.7	±0.3	2706	±54	981	±20	276.2	±2.0	0.6888	±0.0012	81709	±284	**81396**	**±333**
IC5-72	72	236.7	±0.5	249	±5	11421	±241	361.9	±2.5	0.7294	±0.0021	80208	±403	**80123**	**±403**
IC5-121	121	219.9	±0.3	2363	±47	1147	±23	380.8	±2.4	0.7474	±0.0016	81321	±332	**81048**	**±363**
IC5-147	147	247.9	±0.3	7699	±154	396	±8	350.7	±1.8	0.7452	±0.0015	83779	±296	**83087**	**±532**
IC5-174	174	264.2	±0.6	14062	±283	235	±5	361.6	±2.5	0.7598	±0.0023	85105	±445	**83974**	**±873**

IC5-196	*196*	*271.7*	*±0.4*	*56215*	*±1127*	*65*	*±1*	*364.5*	*±2.3*	*0.8210*	*±0.0018*	*95180*	*±417*	*90954*	*±2978*
IC6-4	4	285.4	±0.4	21529	±431	176	±4	478.4	±2.2	0.8035	±0.0014	81205	±267	**79762**	**±1012**
IC6-18	18	179.7	±0.4	3625	±73	609	±12	379.4	±2.6	0.7449	±0.0021	81049	±404	**80586**	**±491**
IC6-37	37	203.3	±0.3	6051	±121	416	±8	375.8	±2.7	0.7505	±0.0015	82249	±344	**81597**	**±538**
IC6-81	81	143.4	±0.1	4735	±95	366	±7	323.2	±1.7	0.7324	±0.0016	84392	±324	**83644**	**±581**
IC6-93	93	185.0	±0.2	29503	±591	74	±1	257.1	±2.1	0.7169	±0.0015	88769	±361	**85156**	**±2539**
IC6-122	122	89.9	±0.1	5466	±110	185	±4	216.3	±2.2	0.6809	±0.0020	86731	±459	**85270**	**±1086**
IC6-153	*153*	*117.8*	*±0.2*	*31681*	*±635*	*47*	*±1*	*288.0*	*±2.6*	*0.7729*	*±0.0020*	*95557*	*±497*	*89646*	*±4177*
UP7-4	4	572.9	±4.5	9347	±201	80	±2	146.3	±4.2	0.0787	±0.0008	7744	±83	**7266**	**±303**
UP7-45	45	704.0	±5.7	1656	±36	573	±13	164.0	±4.7	0.0818	±0.0008	7930	±86	**7807**	**±95**
UP7-66	*66*	*50.1*	*±0.1*	*1749*	*±35*	*41*	*±1*	*165.7*	*±2.1*	*0.0865*	*±0.0003*	*8389*	*±33*	*7455*	*±618*
IC8-05	*5*	*339.3*	*±0.5*	*4695*	*±94*	*109*	*±2*	*380.6*	*±2.5*	*0.0911*	*±0.0003*	*7424*	*±31*	*7071*	*±208*
IC8-25	25	496.5	±1.3	10644	±215	43	±1	735.3	±3.0	0.0557	±0.0003	3553	±23	**3130**	**±255**
IC8-90	90	448.0	±1.1	18794	±379	25	±1	510.1	±2.8	0.0639	±0.0004	4706	±31	**3834**	**±573**
IC8-100	*100*	*427.4*	*±0.5*	*49531*	*±992*	*11*	*±0*	*550.5*	*±2.0*	*0.0767*	*±0.0003*	*5518*	*±22*	*3269*	*±1549*
IC9-33	*33*	*371.6*	*±0.7*	*9267*	*±186*	*29*	*±1*	*557.2*	*±2.9*	*0.0433*	*±0.0003*	*3067*	*±21*	*2539*	*±330*
IC9-56	56	498.2	±0.8	1663	±33	113	±3	492.3	±1.8	0.0228	±0.0003	1681	±25	**1552**	**±52**
IC9-158	158	363.6	±0.8	19971	±402	13	±0	551.7	±3.0	0.0445	±0.0005	3166	±39	**2070**	**±732**
IC9-173	*173*	*633.1*	*±1.4*	*21864*	*±440*	*13*	*±0*	*637.1*	*±3.3*	*0.0277*	*±0.0002*	*1862*	*±14*	*1186*	*±435*
IC9-292	292	536.2	±0.9	3537	±71	143	±3	635.7	±2.5	0.0571	±0.0004	3868	±28	**3687**	**±87**
IC9-392	392	606.0	±1.6	25196	±509	28	±1	627.6	±3.0	0.0707	±0.0004	4832	±29	**4026**	**±526**
IC9-397	*397*	*406.4*	*±1.1*	*61167*	*±1237*	*8*	*±0*	*601.9*	*±4.3*	*0.0742*	*±0.0004*	*5158*	*±33*	*2338*	*±1955*
RC11-5	5	248.0	±0.5	5681	±114	62	±1	74.2	±2.3	0.0865	±0.0006	9144	±65	**8461**	**±444**
RC11-16	*16*	*255.6*	*±0.6*	*35043*	*±706*	*12*	*±0*	*70.0*	*±2.9*	*0.0976*	*±0.0008*	*10419*	*±92*	*6567*	*±2683*
RC11-54	54	348.1	±0.8	52463	±1055	14	±0	101.8	±2.1	0.1261	±0.0007	13233	±83	**9129**	**±2863**

RC11-108	108	243.3	±0.7	8605	±174	54	±1	130.8	±2.9	0.1154	±0.0008	11713	±90	**10739**	**±650**
RC11-153	153	210.3	±0.3	4205	±84	97	±2	134.9	±2.0	0.1182	±0.0009	11966	±95	**11390**	**±374**
RC11-257	257	322.0	±0.6	7439	±149	90	±2	169.2	±2.2	0.1267	±0.0007	12476	±73	**11838**	**±412**
RC11-257X	257	322.1	±0.5	8079	±162	84	±2	165.2	±2.1	0.1285	±0.0006	12712	±65	**12023**	**±447**
RC12-43	43	90.3	±0.1	1096	±22	599	±12	73.2	±2.4	0.4411	±0.0023	57317	±422	**56927**	**±479**
RC12-102	102	110.6	±0.2	18995	±381	46	±1	75.5	±2.3	0.4823	±0.0023	64341	±466	**59592**	**±3347**
RC12-144	144	83.6	±0.1	21658	±434	31	±1	83.3	±2.0	0.4926	±0.0026	65527	±507	**58378**	**±5047**
RC13-36	36	105.5	±0.2	1147	±23	668	±14	84.5	±2.1	0.4403	±0.0020	56363	±362	**56011**	**±414**
RC13-118	118	89.1	±0.1	3692	±74	183	±4	76.6	±2.4	0.4589	±0.0028	60120	±530	**58944**	**±945**
RC13-191	191	73.6	±0.1	948	±19	578	±12	77.1	±1.8	0.4512	±0.0025	58756	±450	**58348**	**±510**
RC13-244	244	89.8	±0.1	1087	±22	619	±13	83.7	±2.2	0.4545	±0.0022	58815	±415	**58430**	**±472**
IC14-23	23	1031.0	±2.8	490	±10	3756	±77	660.8	±2.3	0.1082	±0.0004	7318	±27	**7248**	**±27**
IC14-51	51	2945.9	±12.5	298	±6	19496	±412	514.2	±2.8	0.1198	±0.0006	8949	±47	**8885**	**±47**
IC14-101	101	1660.2	±4.4	4478	±91	2086	±42	530.2	±2.3	0.3413	±0.0011	27116	±106	**27004**	**±112**

*Corrected ^{230}Th ages assume the initial $^{230}Th/^{232}Th$ atomic ratio of 4.4 ± 2.2 x 10^{-6}. Those are the values for a material at secular equilibrium, with the bulk earth $^{232}Th/^{238}U$ value of 3.8. Errors are arbitrarily assumed to be 50%. Gray and italicized ages are considered inaccurate and were not included in age-depth models because of excessive ^{232}Th concentrations or deviation from a clear age-depth trend.

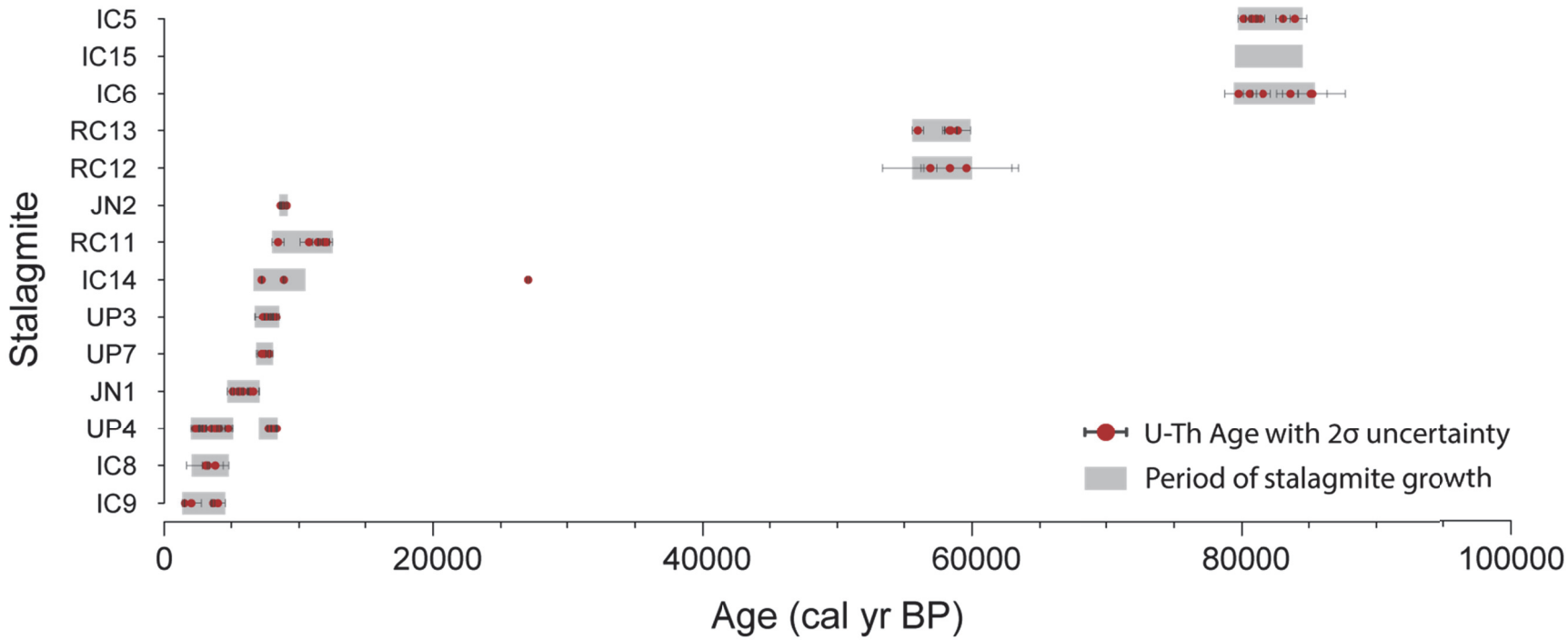

Figure 45. Southern Indiana stalagmite U-Th ages and estimated periods of growth. Stalagmites have been sorted by the age of final growth. IC14 has a thin basal layer dated to 27 ka, but the bulk of stalagmite growth began in the Holocene. Stalagmite IC15 does not have any U-Th ages, but petrography, color changes, and stable isotope results match it to IC5, and a similar growth period is assumed.

8.5.2 Stable isotope data

Stable isotope data for the eleven sampled stalagmites and the DC20 stalagmite were combined into a single dataset covering portions of the past 90,000 years (Figure 46). Values for $\delta^{18}O$ ranged from -6.5 to -3.0‰ over all the stalagmites. The highest $\delta^{18}O$ values were from the DC20 data, and lowest values were from the youngest part of UP4. The $\delta^{13}C$ values ranged from -11.3 to +2.5‰ with highest values consistently in stalagmites from Indiana Caverns. Low $\delta^{13}C$ values were found in a number of stalagmites deposited during the early Holocene.

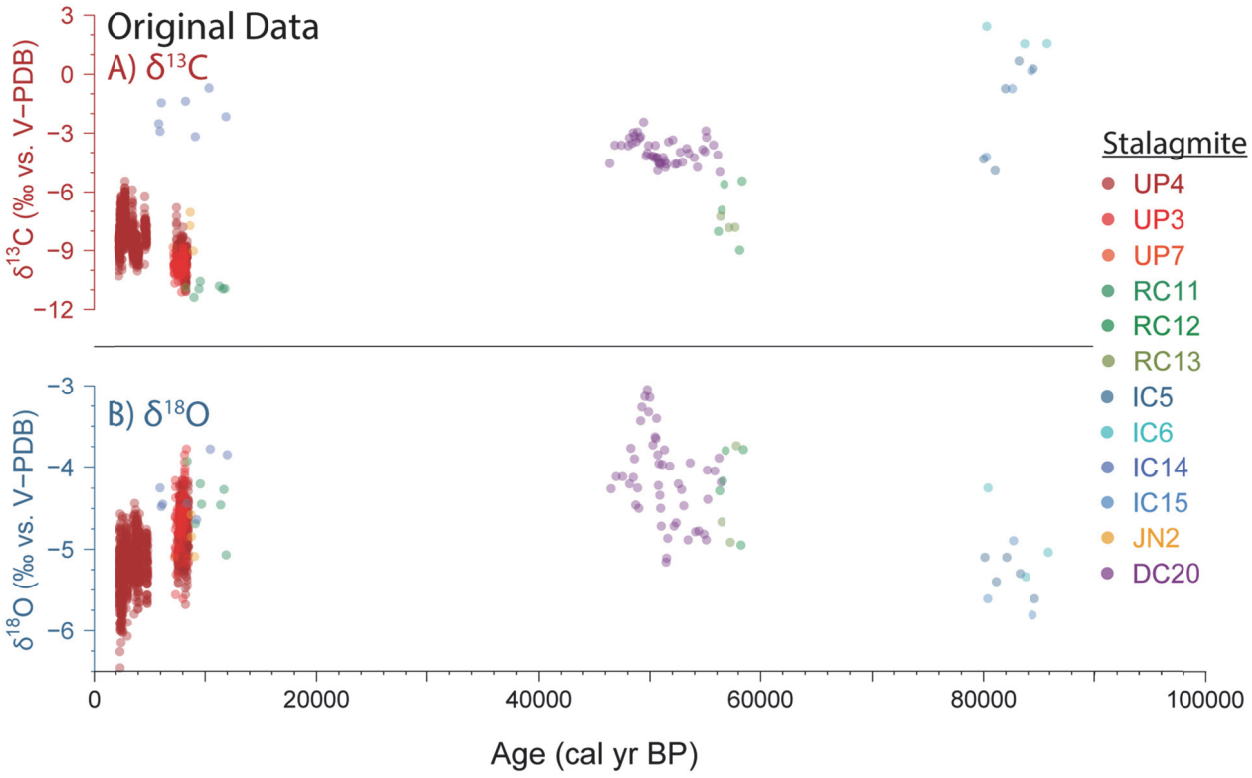

Figure 46. Stalagmite $\delta^{13}C$ (A) and $\delta^{18}O$ (B) values for twelve southern Indiana stalagmites. Data have not been adjusted for potential mean stable isotope bias between caves.

8.5.3 Stable isotope data adjustments

Mean annual cave temperatures for the four caves were estimated using the latitudinal gradient of 0.0092°C/km derived from mean annual air temperatures at Indianapolis, IN, and Bloomington, IN, (NOAA, 2015c) and the cave temperature recorded with the climate logger in Indiana Caverns (Table 33). Using the precipitation temperature effect regression from USNIP site IN22 (Appendix 5) and the calcite temperature fractionation equation of Kim and O'Neil (1997), the net effect of the temperature differences on stalagmite $\delta^{18}O$ can be estimated between caves. Porter Cave and Indiana Caverns have the greatest difference in mean temperature, but the net effect of the precipitation temperature effect (-0.29‰) and the calcite temperature fractionation (+0.30‰) is less than 0.01‰. Thus, a standardization factor does not appear warranted for the modern mean temperature differences between the study caves based on modern observations.

Table 33. Mean annual cave temperatures estimated from nearby city climate records and the temperature data from Indiana Caverns.

Cave	**Mean Annual Cave Temperature (°C)**
Porter Cave	12.1
Roadcut Cave	12.6
Johnson Cave	12.7
Indiana Caverns	13.4

A bias in precipitation $\delta^{18}O$ may arise from the continental effect due to latitudinal differences between the caves. Today, the mean precipitation $\delta^{18}O$ isolines in southern Indiana run north-northwest to south-southeast, and a transect running through the four caves lies roughly parallel with these isolines (Chapter 3). This limits the potential continental effect to a maximum difference of 0.5‰ between Porter Cave and Indiana Caverns. Sharper climate gradients during glacial periods may have increased this continental effect in southern Indiana, but quantifying the changes in the continental

effect over time is difficult without overlapping stalagmite records from multiple caves. Thus, a single standardization factor cannot be applied based on the modern precipitation $\delta^{18}O$ data; however, the continental effect remains a possible explanation for higher $\delta^{18}O$ values in stalagmites from the more southerly caves.

Although the stalagmite records from different caves do not share many periods of growth, at least one stalagmite in Upper Porter Cave, Roadcut Cave, and Indiana Caverns was each growing around 8300-8500 cal yr BP. Standardization factors for $\delta^{18}O$ and $\delta^{13}C$ can be calculated from the coeval stalagmite stable isotope data to permit cross-cave comparison (Table 34). Many assumptions are made for the standardization factors, and the adjusted stable isotope data should be viewed as an exploratory exercise and not a definitive correction. Primarily, the standardization factors assume that the environment above each cave was generally the same at 8360 cal yr BP when the stable isotope data are shared. Applying the standardization factor calculated for a cave to all samples assumes that the $\delta^{18}O$ and $\delta^{13}C$ offsets are static over time, and that the standardization factor calculated from a single stable isotope value is accurate for the entire cave. These assumptions are not likely to be wholly true, but they offer a glimpse into how intrinsic stable isotope biases between caves can dramatically alter a paleoenvironmental interpretation of data aggregated from multiple caves.

Table 34. Standardization factors calculated for stalagmite stable isotope data based on values during a shared period of stalagmite growth. The standardization factors for Roadcut Cave are applied to nearby Donnehue's Cave.

	Value at 8360 cal yr BP		**Standardization Factor**	
Cave	*$\delta^{18}O$ (‰ vs. V-PDB)*	*$\delta^{13}C$ (‰ vs. V-PDB)*	*$\delta^{18}O$ (‰)*	*$\delta^{13}C$ (‰)*
Upper Porter Cave	-5.0	-10.1	-	-
Roadcut Cave	-3.9	-10.8	-1.1	+0.7
Donnehue's Cave	-	-	-1.1	+0.7
Indiana Caverns	-4.4	-1.3	-0.6	-8.8

Upper Porter Cave was used as the standard cave on which to base the standardization factors because of available high-resolution stable isotope records from UP3 and UP4. The standardization factor for Roadcut Cave was also applied to the data from Donnehue's Cave due to the very close proximity of the two caves. No standardization factor could be estimated for Johnson Cave because stalagmites from that cave do not coincide with a period of stalagmite growth in Upper Porter Cave. The $\delta^{18}O$ standardization factors for Roadcut Cave and Indiana Caverns are relatively small and negative, and these adjustments are likely a partial response to the continental effect (both caves are farther south than Upper Porter Cave). The $\delta^{13}C$ standardization factors are quite different between caves and are probably related to bedrock and drip water travel distance differences. The -8.8‰ adjustment for Indiana Caverns seems quite extreme, but $\delta^{13}C$ values in all four Indiana Caverns stalagmites are consistently much higher than stalagmites from other caves and a significant geologic difference in cave setting appears likely to explain the major $\delta^{13}C$ discrepancy. By standardizing $\delta^{13}C$ values between caves, it is hoped that relative changes in vegetation coverage and productivity can be detected more easily.

Applying the standardization factors reduces the overall range of stable isotope values observed across all stalagmites (Figure 47). The range of adjusted $\delta^{18}O$ is generally the same across all caves, but DC20 no longer has the highest $\delta^{18}O$ values. The $\delta^{18}O$ standardization factor applied to Roadcut Cave and Donnehue's Cave may be too extreme since the growth of DC20 occurs in what should be coldest period (and thus highest $\delta^{18}O$ values) in which there was stalagmite growth. The adjusted $\delta^{13}C$ data distribution are very different from the original data due to the large drop in Indiana Caverns stalagmite $\delta^{13}C$ values, but the adjusted Indiana Caverns data fit much better with the general range in $\delta^{13}C$ observed at the other caves. The potential error with the standardization factors makes drawing definitive conclusions about changes in stable isotope values over time somewhat risky. However, analysis of both the original and corrected data has the potential to reveal important clues about the environmental history of southern Indiana.

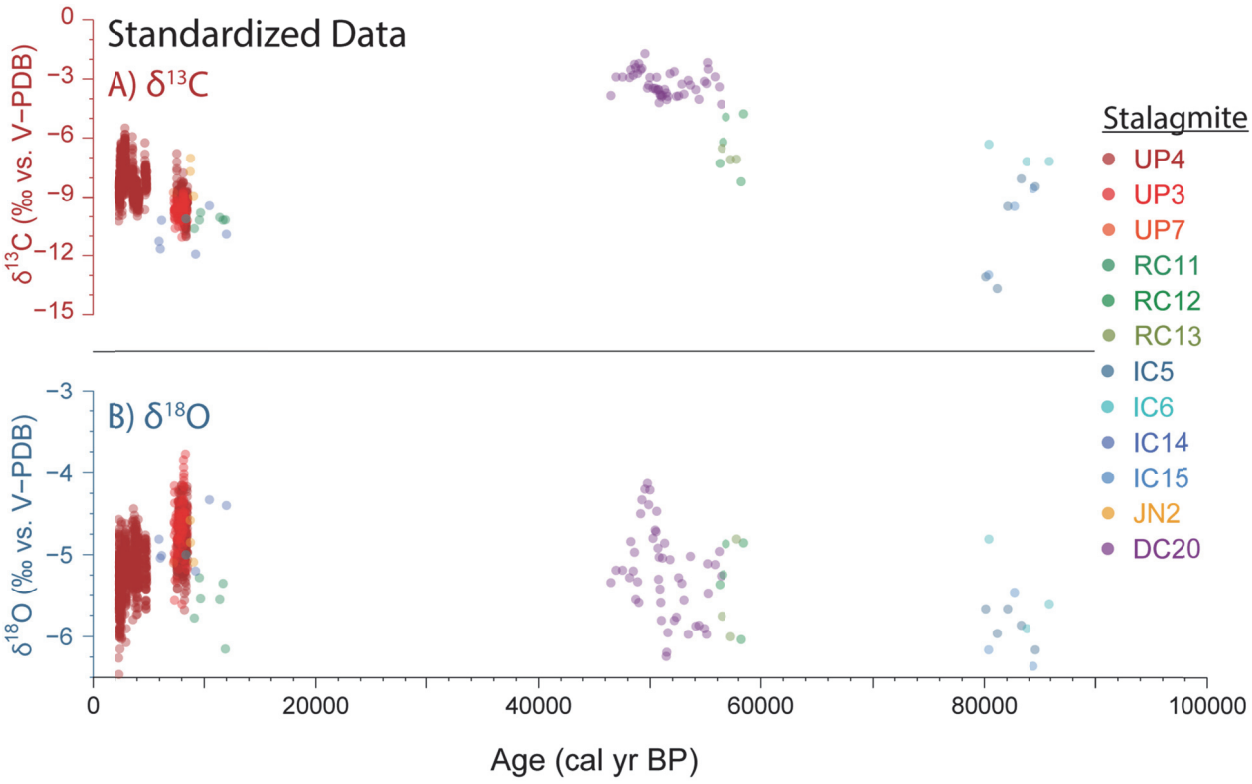

Figure 47. Stalagmite $\delta^{13}C$ (A) and $\delta^{18}O$ (B) values for twelve southern Indiana stalagmites adjusted for potential mean stable isotope bias between caves.

8.6 Discussion

8.6.1 Favorable environment for stalagmite growth

The distinct periods of stalagmite growth in southern Indiana coincide with globally-warmer periods and peaks in northern hemisphere summer insolation (Figure 48). Stalagmites grew during MIS 1, 3c, and 5a, and the two periods of growth prior to the Holocene coincide with Greenland interstadials 16-17 and 21. Stalagmite growth in the four southern Indiana caves examined here was likely controlled in part by the presence of vegetation and the production of biogenic CO_2 in soil. Vegetation in southern Indiana would increase in globally-warmer periods due to warmer local conditions and higher

precipitation from increased southerly advection, and this vegetation is necessary to enable stalagmite growth (Baldini et al., 2005). Stalagmites generally begin to form at or slightly after peak insolation and grow as insolation declines. This is expected as climate and vegetation responses generally lag behind insolation, and peak warmth arrives sometime after maxima in summer insolation. In contrast, cold periods would have a reduced cover of vegetation particularly when the LIS advanced into the Midwest, and the decline in vegetation and biogenic CO_2 might have ended stalagmite growth. During glacial maxima, discontinuous permafrost could limit stalagmite growth; however, the extent of permafrost in southern Indiana is poorly known. Excessively wet conditions or too much winter precipitation may also stop stalagmite growth as reported in Chapter 7. In fact, evidence of drip water undersaturated in $CaCO_3$, either from reduced biogenic CO_2 or excessive water runoff and infiltration, is present as type E surfaces in some stalagmites (Figure 49).

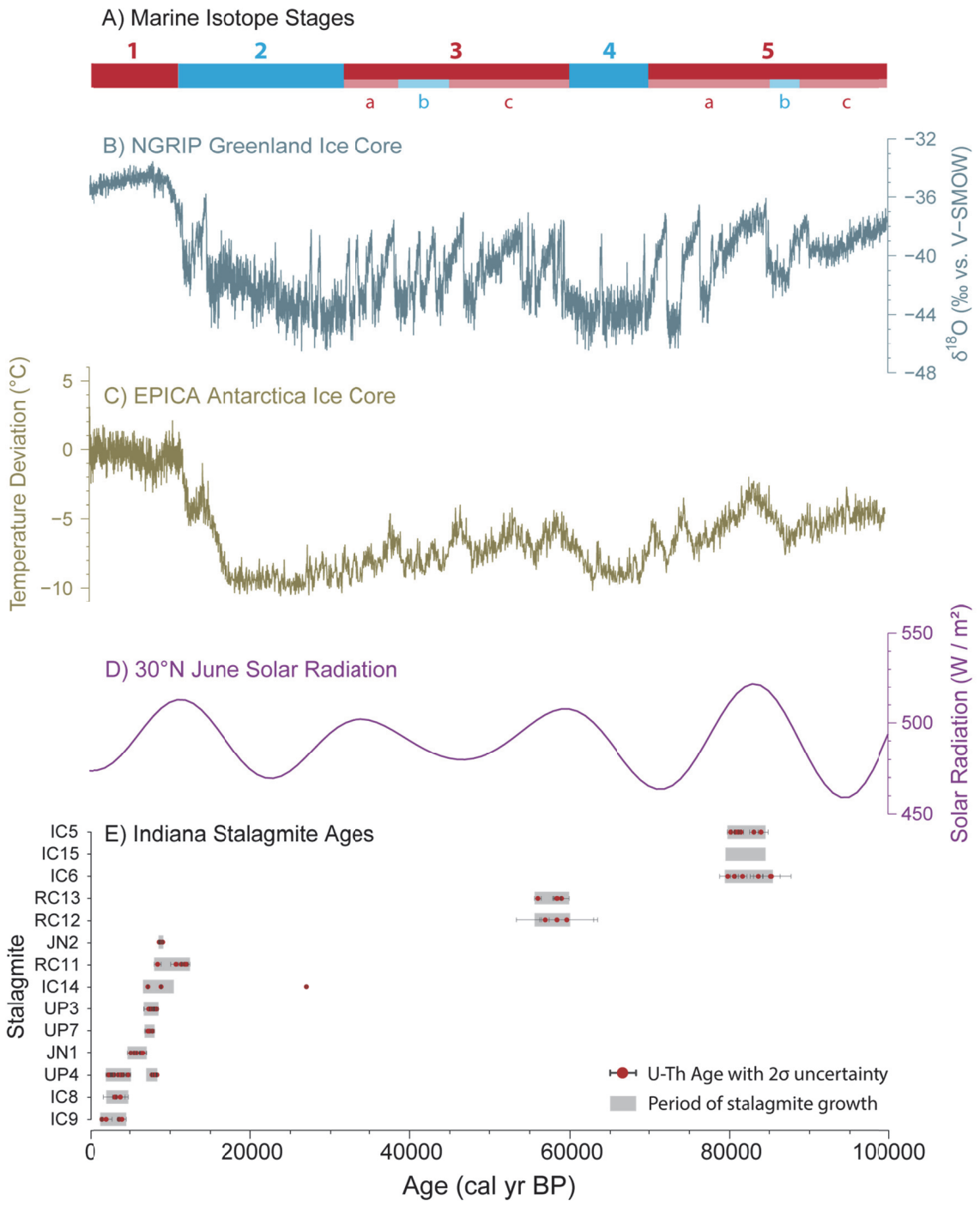

Figure 48. Periods of southern Indiana stalagmite growth (E) compared with millennial-scale global climate changes categorized by A) marine isotope stages and substages (Railsback et al., 2015b) and recorded in the B) NGRIP ice core (Andersen et al., 2004), C) EPICA ice core (Jouzel et al., 2007), and D) solar radiation hitting 30°N latitude in June (Berger, 1992).

Figure 49. Features on the apex of IC5 indicating erosion by unsaturated drip water. Note the solutional pitting on the top surface of the stalagmite and truncation of the prominent orange layers on the flanks of the stalagmite.

Warm interstadials during the glacial period were too brief to produce full-scale deglaciation, and a remnant Laurentide Ice Sheet was present in Canada throughout the Pleistocene and into the early Holocene. This promoted a very seasonal climate in southern Indiana during periods of stalagmite growth. Summers were likely quite warm due to the high summer insolation, but winters would likely be cold and dry due to the influence of the continental ice sheet to the north. This could have produced ideal conditions for stalagmite growth, with enough summer moisture to supply water to the caves, but not enough annual or winter moisture to produce undersaturated drip water. The high summer insolation appears key to stalagmite growth in the Pleistocene, as other warm interstadials that lacked high summer insolation did not bring about stalagmite deposition in the studied caves. The only stalagmite growth during low summer insolation periods was in the later Holocene (with the possible exception of DC20), and two of the three stalagmites growing at this time (IC8, IC9) grew in a cave

passage that was probably not connected to the main cave ventilation until the later Holocene. There has been no observed stalagmite growth in the past millennium when insolation seasonality has been at a minimum.

Major shifts in the climate of southern Indiana are suggested at around 8.6, 7.3, and 5.0 ka BP. At these times, multiple stalagmites either began or stopped growing, and the synchronized timing of these starts and stops suggests that the climate shifted substantially enough to trigger stalagmite growth at some locations and to stop growth at other locations. For example, UP4 grew during relatively dry conditions (Chapter 7) but did not grow from 5.0 to 7.5 ka BP due to excessively wet conditions. In contrast, JN1 started growing when UP4 was not growing and then stopped growing shortly before UP4 began to grow again. This suggests that JN1 only grew during relatively wetter periods. Thus, the timing of stalagmite growth can prove to be a valuable paleoenvironmental proxy on its own.

7.6.2 Paleoenvironmental information from stable isotopes

Although directly comparing stable isotope values from different caves comes with uncertainty due to inherent biases in cave stable isotope values, some general conclusions can be reached about changes in the southern Indiana environment over the past 90,000 years. The $\delta^{13}C$ values from 46.5 to 59.0 ka BP are greater than the Holocene values even when a standardization factor is applied. The interstadial warmth at this time and insolation are weaker than in the other stalagmite growth periods, and it is probable that vegetation was not as dense or productive at this time resulting in higher $\delta^{13}C$ values. In contrast, $\delta^{13}C$ values are lowest in the transitional period from the Younger Dryas to the early Holocene and vegetation may have thrived at this time. However, it should be kept in mind that the Holocene stalagmites UP3 and UP4 apparently only grew during drier periods of time and this would likely result in higher $\delta^{13}C$ values than during the wetter Holocene periods when there was no stalagmite growth.

The $\delta^{18}O$ values do not vary a great deal across stalagmites, even in the original unaltered data. This supports the conclusion that broad changes in precipitation $\delta^{18}O$ due to colder conditions in the Pleistocene are largely canceled out by competing forcings and fractionation during $CaCO_3$ deposition. However, the DC20 stable isotope data suggest that $CaCO_3$ deposited during glacial times may have been 0.7‰ higher. The relatively similar range of stalagmite $\delta^{18}O$ values (generally within a 3‰ range) across multiple growth periods suggests that the climate in southern Indiana during the interstadials was not so different from Holocene conditions. The $\delta^{18}O$ data from 80-84 ka BP are very similar to Holocene $\delta^{18}O$ values for both original and standardized data, and it is possible that temperatures and climate were actually somewhat similar to modern, at least in summer. However, more definitive conclusions are not possible without better constraints on standardization factors and higher-resolution stable isotope data.

8.7 Conclusions

8.7.1 Remarks

Ages of stalagmites from four southern Indiana caves document brief periods of growth and long periods of no-growth in the caves. There are no active stalagmites in the caves today, and most of the older, inactive stalagmites (other than UP4) grew during only one time period in the past before becoming permanently inactive. However, the timing of stalagmite growth is generally restricted to periods of relatively high global temperature and high summer insolation in the northern hemisphere. This suggests that the environment in southern Indiana at 57-59 and 80-84 ka BP was relatively similar to Holocene conditions as these are the only periods when stalagmite growth is recorded in the four sampled caves.

The data obtained cannot be used to conclude that stalagmites in caves throughout Indiana only grew in the time periods defined by these stalagmite ages. Stalagmites growing at other times even in

the sampled caves may simply not have been collected, and other regional caves may have different suites of deposition ages. That said, the ages determined for the collected stalagmites show remarkable consistency in the timing of growth and hiatus as well as a clear connection to northern hemisphere insolation changes. Thus, even if future studies in other southern Indiana caves find stalagmites growing during the LGM or globally cold periods, it will not refute findings detailed in this chapter.

Although the standardization factors estimated here are not well constrained or robust, they offer a potential method to aggregate stalagmite records from different caves and compare stable isotope data. Ideal calculation of standardization factors would come from stalagmites with a relatively long period of co-eval growth and high resolution stable isotope data that allow comparisons of mean stable isotope values between caves. Applying standardization factors beyond the period of overlapping growth would still involve some uncertainty and risk, but the adjusted data would very likely be more informative than the original, uncorrected data. In the absence of high-quality standardization factors, comparing stalagmite stable isotope records from different caves must be done with the acknowledgment of the many factors that may affect the mean stable isotope values of a stalagmite beyond regional and global climate changes.

8.7.2 Most important findings

- Stalagmites in sampled southern Indiana caves grew only for relatively brief periods over the past 90,000 years, suggesting environmental conditions favorable for stalagmite growth are rare.
- Stalagmites grew during periods of high summer insolation, low winter insolation, and relative global warmth, likely due to a strongly summer-dominant seasonal precipitation regime.
- Climate and environment in southern Indiana during the periods 57-59 and 80-85 ka BP may have been similar to early Holocene conditions based upon similar $\delta^{18}O$ values.

CHAPTER NINE:

OVERALL CONCLUSIONS

9.1 Introduction

Although the individual chapters contained within this dissertation are effective and important on their own, they draw their true strength from the close integration between the chapters. Trends and relationships identified in the initial investigation into modern controls on oxygen isotope ($\delta^{18}O$) variations are repeatedly drawn upon to understand the impact of climate teleconnections, interpret long-term climate changes, and aggregate data from different cave environments. Analysis of stalagmite $\delta^{18}O$ values in light of other paleoclimate proxies has likewise helped in constraining which of the various climate controls on $\delta^{18}O$ are most likely to be expressed in long-term paleoclimate data. The end result is a much-improved understanding of environmental change for a region in the American Midwest largely lacking any previous paleoenvironmental research.

9.2 Summary of objective goals achieved

9.2.1 Better constrain and quantify the climate controls on modern precipitation $\delta^{18}O$ variability in the eastern and central United States with a focus on southern Indiana

Thorough analysis of a paired climate and precipitation $\delta^{18}O$ database produced spatial and temporal trends and quantified relationships for the eastern and central United States (Chapter 2). Calculating climate and precipitation $\delta^{18}O$ relationships at a weekly temporal resolution using daily climate data weighted by precipitation amount is an unprecedented methodology for wide spatial-scale analysis in the eastern and central United States. While this new method did not dramatically improve

relationship strength over previous research, the higher variability and weaker relationships observed with weekly data are thought to be a more accurate estimate of actual relationships than those calculated from more aggregated data. The weekly data permitted temporal aggregation to identify changes to climate and $\delta^{18}O$ relationships that occur when using aggregated data, and this offers a bridge between temporally-aggregated but spatially-broad studies and shorter-term but spatially-limited studies. The weekly data also allowed quantification of changes to climate and $\delta^{18}O$ relationships that occur on a sub-annual basis with the discovery that many well-known controls on precipitation $\delta^{18}O$ such as the temperature effect vary dramatically in strength and effect on a month-to-month and season-to-season basis.

Further analysis examined the effects that changes in moisture source (Chapter 4) and precipitation seasonality (Chapter 5) have on precipitation $\delta^{18}O$ values in the American Midwest. Although changes in moisture source as classically thought (i.e., Pacific versus Gulf of Mexico moisture) was not found to be a likely major control on southern Indiana precipitation $\delta^{18}O$ values, the research did accomplish a great deal in connecting moisture back-trajectory ensembles to synoptic-scale weather patterns. In particular, the path and relative location of extratropical cyclones emerged as a major influence on moisture source back-trajectories and prompted a re-evaluation of moisture sources previously identified as continental-sourced. A new metric to quantify precipitation seasonality called the Summer Signal Anomaly (SSA) was created as a potential way to interpret long-term $\delta^{18}O$ records, but a lack of precision in the SSA estimates limits the ability to use the SSA as a quantitative transfer function for $\delta^{18}O$ values. However, the SSA accuracy was found to be quite good in a test using bootstrapped yearly climate and $\delta^{18}O$ data, and the SSA was retained for later analysis as a quantified measure of precipitation seasonality.

Research into precipitation $\delta^{18}O$ variability culminated in an analysis of climate controls on multi-annual $\delta^{18}O$ variability (Chapter 6). This required creating years of $\delta^{18}O$ and climate data as no

modern United States precipitation $\delta^{18}O$ database is long-enough or complete enough for rigorous statistical analysis. Although both methods of creating constructed yearly data (consecutive 12-month and bootstrapping) have their own drawbacks, this work enabled what may be the first 'long-term' analysis of climate controls on annual $\delta^{18}O$ values for the American Midwest and possibly United States. While no single climate factor appears as a dominant control, a clear picture of atmospheric flow patterns that control moisture advection and $\delta^{18}O$ values in the American Midwest emerged in the analysis. Climate teleconnections and atmospheric conditions that favor uninhibited southerly moisture advection are associated with high precipitation $\delta^{18}O$ values while teleconnections that favor a trough over eastern North America and blocks on southerly advection result in lower precipitation $\delta^{18}O$ values. Changes in mean annual temperature weighted by precipitation amount and precipitation seasonality balance also show evidence of controlling precipitation $\delta^{18}O$ values on multi-annual scales, but their forcings sometimes conflict with and sometimes support the effects from atmospheric flow patterns.

The overall conclusion from this research on precipitation $\delta^{18}O$ variability in the American Midwest is that while the climate factors that change $\delta^{18}O$ values can generally be identified and perhaps even have their magnitude of control estimated, attempts to frame Midwestern $\delta^{18}O$ variability in terms of a single dominant control (such as a specific teleconnection index) are misguided and not warranted. Although a quantitative connection between precipitation $\delta^{18}O$ values and climate variables is a commonly-cited goal of precipitation isotope research, the climate of the American Midwest may simply be too complex to distill into such basic terms and mathematics. This complexity is compounded when the goal is to apply these findings to paleorecords of $\delta^{18}O$. Simply transferring $\delta^{18}O$ values in terms of Pacific-North American (PNA) teleconnection indices, for example, not only ignores the possible contribution from other climate variables but also restricts the ability to recognize if the climate variables shifted in their relative dominance in the past. Thus, it is immensely important to acknowledge

the actual complexity of Midwestern precipitation $\delta^{18}O$ variability and recognize that multiple climate factors could potentially produce an observed change in $\delta^{18}O$ values.

9.2.2 Determine how to best apply the findings from modern precipitation $\delta^{18}O$ studies to stalagmite-based paleoenvironmental data

The modern precipitation $\delta^{18}O$ research identified atmospheric flow and precipitation seasonality as the most likely controls on long-term $\delta^{18}O$ variability, and theoretically an ideal stalagmite $\delta^{18}O$ record should reflect these controls. In reality, many processes in the soil, epikarst, and cave environment can affect the $\delta^{18}O$ of water dripping onto a growing stalagmite, and the effects of these processes must be constrained as much as possible for a quality interpretation of stalagmite $\delta^{18}O$ values. Connecting the modern day $\delta^{18}O$ findings to stalagmite $\delta^{18}O$ values is complicated by the absence of modern calcium carbonate ($CaCO_3$) deposition in the sampled caves. Cave drip water samples have a lower $\delta^{18}O$ value than the estimated $\delta^{18}O$ of drip water calculated from the stalagmite $\delta^{18}O$ data, suggesting that modern climate is different than the climate when the stalagmites were actively growing. However, the main factors controlling stalagmite $\delta^{18}O$ values are still believed to be those identified in the modern-day multi-annual $\delta^{18}O$ study (Chapter 6).

At millennial timescales, the major controls on long-term mean stalagmite $\delta^{18}O$ values are likely to be different than that those affecting modern data. Estimates of changes in $\delta^{18}O$ controls due to colder global conditions during the Last Glacial Maximum (LGM) suggest stalagmite $\delta^{18}O$ values should be slightly lower in the LGM, but actual stalagmite $\delta^{18}O$ data from southern Indiana are 0.7‰ higher in the LGM than during deglaciation. These higher values are best explained by the increased importance of the temperature-controlled $\delta^{18}O$ fractionation during $CaCO_3$ deposition, although a significant change in precipitation seasonality to less winter precipitation in glacial periods may have added to this effect. Thus, changes in mean stalagmite $\delta^{18}O$ value in southern Indiana at millennial-timescales may be used

as relative cave temperature proxy, but much variability (particularly on shorter timescales) is still likely attributable to changes in atmospheric flow and precipitation seasonality.

9.2.3 Identify and describe changes in the climate and environment of southern Indiana in the Holocene and Pleistocene based upon stalagmite paleoenvironmental data

High-resolution paleoenvironmental analysis of two stalagmites and coarser-resolution data from twelve other stalagmites have produced a new paleoenvironmental narrative for southern Indiana and the American Midwest over the Holocene and late Pleistocene (Chapters 7 and 8). The stalagmites collected in this research each grew for only a short time, and stalagmite growth occurred only during particular time periods at 1.5-12.0, 57-59, and 80-85 thousand calendar years before present (ka BP). These periods coincide with high northern hemisphere insolation seasonality and globally warmer temperatures. The lack of stalagmite growth during other times in the Pleistocene suggests that the climate during 57-59 and 80-85 ka BP may have been relatively similar to the early Holocene or at least similar enough to permit stalagmite growth. If mean stalagmite $\delta^{18}O$ values truly do reflect cave temperatures, then the period 80-85 ka BP was nearly as warm as the Holocene while the period from 46-59 ka BP was cooler. However, this interpretation requires comparing stalagmite stable isotope values from different caves, and although preliminary standardization factors for inherent cave stable isotope biases have been applied, a great deal of uncertainty remains when comparing stalagmite data across caves. Vegetation, as indicated by stable carbon isotope ($\delta^{13}C$) values, was most productive during the very early Holocene, but since the later Holocene stalagmites only grew during drier periods, the $\delta^{13}C$ record may not capture more productive periods in the Holocene. The $\delta^{13}C$ values suggest less productive vegetation from 46-59 ka BP that agrees with the indicated cooler climate at that time, but the relative productivity during 80-85 ka BP is difficult to estimate due to a very large potential $\delta^{13}C$ standardization factor needed for those stalagmites.

High-resolution stable isotope sampling, and the development of a paleoenvironmental record, focused on two Holocene stalagmites from Upper Porter Cave, Indiana. Interpreting the stalagmite paleoenvironmental proxy data was not straight-forward due to a complex depositional history and multiple climate signals imbedded in the stable isotope data. However, once the climatological conditions that promote stalagmite growth in Upper Porter Cave were understood, an important paleoenvironmental narrative emerged. Results from the stalagmite analysis suggest that southern Indiana experienced dramatic changes in precipitation in the Holocene as a sharp boundary between a wet region to the east and a dry region to the west migrated across the region multiple times. A drier period in the early Holocene may have set in around 8.5 ka BP when the stalagmites in Upper Porter Cave began growing, but stalagmites in Roadcut Cave and Johnson's Cave stopped growing at this time. Increased precipitation, likely focused in winter, around 7.3 ka BP resulted in periodic cave flooding and eventual stalagmite cessation of stalagmite growth in Upper Porter Cave. The increased precipitation resulted in rapid infiltration of unsaturated water into the cave and onto the stalagmites as evidenced by solutional pitting, layer truncation, and spikes in $\delta^{13}C$ values along type E surfaces. The period from 5.0 to 7.3 ka BP was likely consistently wet as there was no stalagmite deposition in Upper Porter Cave; however, a stalagmite in Johnson's Cave was deposited during this wet interval and may have required wetter conditions to grow. This wet period in southern Indiana coincides with a drier climate to the west in the Great Plains and may be a result of a stable Bermuda High location that directed moisture into southern Indiana and the eastern United States at the expense of more western locations.

Beginning at 4.9 ka BP, there was intermittent growth on one Upper Porter Cave stalagmite. The cycles of stalagmite growth and hiatus appear linked to alternating drier and wetter climates, respectively. This suggests that the location of the Bermuda High may have become more variable or at least shifted to the east after 5.0 ka BP and brought periodically drier conditions to southern Indiana. Periods of stalagmite growth beginning around 4.2 and 3.1 ka BP may be related to abrupt climate

changes observed both in the Middle East and globally. The growth in this stalagmite ceased at around 2.3 ka BP, and there has been no growth to the present day, suggesting modern climate is wetter than during past periods of stalagmite growth. This wetter modern climate may be due to an increase in winter northern hemisphere insolation that brings warmer winters with greater precipitation.

9.2.4 Examine what the new paleoenvironmental data may suggest about the climate connections beyond the American Midwest and future climate change in southern Indiana

The alternating wet and dry periods in southern Indiana during the early and middle Holocene correspond with similar climate changes in the Middle East and North Africa. The wet period from 5-7 ka BP in southern Indiana roughly coincides with the timing of greatly enhanced precipitation over the Sahara and Arabian Peninsula. Abrupt drying events in the Middle East at 3.2 and 4.2 ka BP also have parallel drier periods in southern Indiana. This suggests a possible link between American Midwest precipitation regimes and global changes in monsoon strength. The location of the Bermuda High is a likely mediator and connection between the parallel climate changes observed in southern Indiana and the Middle East. As described in Chapter 7, changes in monsoon strength in Asia and Africa affects the positon of the Bermuda High, and changes in northern hemisphere insolation patterns and/or changes in North Atlantic circulation would likely result in a linked response on opposite sides of the Atlantic.

Southern Indiana may be ideally located to record paleoenvironmental evidence of this possible climate connection. In contrast to the wet and dry cycles observed in southern Indiana, the better studied western regions of the American Midwest were generally drier than today for much of the early and middle Holocene. While evidence of a severe drying at the 4.2 ka event is reported for some sites across the Midwest, the location of southern Indiana near the steep precipitation boundary between wet east and dry west appears to have emphasized the climate changes occurring in North America during the middle Holocene. The presence and location of this Midwestern precipitation boundary are not well-known or reported in current literature, but this new stalagmite data presented here and

future paleoenvironmental records from southern Indiana could help fill in this gap in our knowledge. The factors responsible for the abrupt climate changes in the middle Holocene are generally poorly understood, and a better understanding of the North American expression of these climate events may prove valuable for future modeling and data synthesis.

This cave research in southern Indiana revealed very little, if any, modern stalagmite growth suggesting that environmental conditions during growth phases in the past must have been quite different from those of today. The ages of the stalagmites that were studied confirmed this observation and indicated that stalagmites grow during times of warm global climate and high northern hemisphere seasonality. During the Holocene, climate was generally drier than present from 8.5 to 7.3 and from 4.9 to 2.3 ka BP. These drier intervals bracket the period of warmest Holocene temperatures in North America when southern Indiana was quite wet. This wet Indiana climate during warmer conditions agrees with the predictions for a generally wetter Indiana in the coming century due to anthropogenic climate change (PCCRC, 2008). However, it should be of some concern that the transitional period from the warmer middle Holocene to modern climate was a time of wide climate variability in southern Indiana. The deposition of the Upper Porter Cave stalagmite suggests that multiple periods of this transition had climates markedly drier than any experienced in the past 2300 years. A return to a warmer climate in the future holds the potential risk of a return to climate instability and centennial-length drier periods until the climate stabilizes into a generally wet regime. This climate instability and dryness would have dire consequences for the modern agricultural and forestry industries of Indiana and the Midwest.

Overall, however, it is difficult to use climate conclusions from the stalagmites as analogs for a future warmer climate. Climate projections suggest regional warming beyond anything seen in the Pleistocene and Holocene, and thus, no analog exists of a similar climate. Additionally, the warmer climates of the past most often used as future climate analogs, such as the middle and early Holocene

and the last interglacial, had very different insolation regimes than today. Previous warm periods in the northern hemisphere, including when the majority of southern Indiana stalagmites grew, had enhanced seasonal differences due to high summer insolation and low winter insolation. Today, insolation seasonality is at a minimum and atmospheric CO_2-driven warming may not result in climates analogous to previous ones driven by insolation changes. Despite the potential lack of strong analogs, it is clear that previous changes in global climates resulted in significant variability in precipitation amounts and seasonality in southern Indiana. Climate mitigation strategies that assume a generally wetter future climate in Indiana should take heed of the potential for long periods of drier than modern climate as global climate systems reorganize in light of anthropogenic climate change. Political institutions and parties with a vested interest in Indiana agriculture, forestry, and other precipitation-dependent industries would be wise to have contingency plans in place if predictive climate models have overlooked the risk of a drier future for Indiana.

9.3 Overall most important findings

- The choice of temporal aggregation and sub-annual timing of precipitation stable isotope data is critical to accurate calculation and application of relationships between isotopes and climate variables.
- The impact of moisture source changes on Midwestern precipitation $\delta^{18}O$ values is overemphasized in scientific literature, but the potentially more-important role of extratropical cyclones on precipitation $\delta^{18}O$ alteration is less acknowledged and understood.
- During the Holocene, multi-annual precipitation $\delta^{18}O$ variability is largely controlled by changes in atmospheric flow patterns and changes in precipitation seasonality.
- Stalagmite growth in the southern Indiana caves sampled is favored during periods of global warmth and high insolation seasonality, likely due to a reduction in winter precipitation.

- Although the warmest period of the Holocene was wet in southern Indiana, the transitions into and out of this warm period were drier than the climate of the past 2300 years.
- The position of the Bermuda High, perhaps coupled with influences from the Pacific, appears most likely to explain the middle Holocene shifts in the boundary between the dry North American midcontinent and the wet eastern region.

9.4 Concluding statements

The research detailed here is an important contribution to our knowledge of paleoenvironmental change in North America and offers a strong foundation for future work. Although the study of modern precipitation $\delta^{18}O$ variability was focused on southern Indiana, the conclusions drawn are applicable to the broader Midwestern and eastern North American regions. The atmospheric flow patterns that control the multi-annual precipitation $\delta^{18}O$ values in southern Indiana also affect much of mid-latitude North America, and related $\delta^{18}O$ responses to changes in large-scale atmospheric conditions are expected. The algorithms and computer programming scripts written for this research (Appendix 6) are easily adapted for new data, and thus future data updates and expansions are a relatively simple affair.

The stalagmite paleoenvironmental records developed reveal the need for a concerted effort to synthesize existing Midwestern paleoenvironmental data into a more unified narrative that acknowledges spatial differences in climate change over the Holocene. Focused modeling efforts could then begin to unravel the broader regional and global atmospheric patterns that led to the observed spatial trends in Midwestern climate change. Understanding what factors drove the middle Holocene shifts in the spatial pattern of dry west and wet east in eastern and central North America would greatly benefit efforts to predict future climate changes and mitigate potential impacts. This is particularly important for southern Indiana, which appears to be located at a critical spatial juncture between a

warmer climate bringing either wetter or drier conditions. The analyses detailed in this dissertation are an important step toward a better understanding of past and future Midwestern climate, and this research and follow-up paleoenvironmental studies in southern Indiana may prove essential in adequately planning for and adapting to future climates in the American Midwest.

REFERENCES

Aemisegger, F., Pfahl, S., Sodemann, H., Lehner, I., Seneviratne, S. I., and Wernli, H., 2014, Deuterium excess as a proxy for continental moisture recycling and plant transpiration: Atmospheric Chemistry and Physics, v. 14, no. 8, p. 4029-4054.

Alley, R. B., and Ágústsdóttir, A. M., 2005, The 8k event: cause and consequences of a major Holocene abrupt climate change: Quaternary Science Reviews, v. 24, no. 10–11, p. 1123-1149.

Alley, R. B., and Cuffey, K. M., 2001, Oxygen- and hydrogen-isotopic ratios of water in precipitation: beyond paleothermometry: Reviews in Mineralogy and Geochemistry, v. 43, no. 1, p. 527-553.

Andersen, K. K., Azuma, N., Barnola, J. M., Bigler, M., Biscaye, P., Caillon, N., Chappellaz, J., Clausen, H. B., DahlJensen, D., Fischer, H., Fluckiger, J., Fritzsche, D., Fujii, Y., Goto-Azuma, K., Gronvold, K., Gundestrup, N. S., Hansson, M., Huber, C., Hvidberg, C. S., Johnsen, S. J., Jonsell, U., Jouzel, J., Kipfstuhl, S., Landais, A., Leuenberger, M., Lorrain, R., Masson-Delmotte, V., Miller, H., Motoyama, H., Narita, H., Popp, T., Rasmussen, S. O., Raynaud, D., Rothlisberger, R., Ruth, U., Samyn, D., Schwander, J., Shoji, H., Siggard-Andersen, M. L., Steffensen, J. P., Stocker, T., Sveinbjornsdottir, A. E., Svensson, A., Takata, M., Tison, J. L., Thorsteinsson, T., Watanabe, O., Wilhelms, F., White, J. W. C., and Project, N. G. I. C., 2004, High-resolution record of Northern Hemisphere climate extending into the last interglacial period: Nature, v. 431, no. 7005, p. 147-151.

Annan, J. D., and Hargreaves, J. C., 2013, A new global reconstruction of temperature changes at the Last Glacial Maximum: Climate of the Past, v. 9, no. 1, p. 367-376.

Arz, H. W., Lamy, F., and Patzold, J., 2006, A pronounced dry event recorded around 4.2 ka in brine sediments from the northern Red Sea: Quaternary Research, v. 66, no. 3, p. 432-441.

Baker, A., Asrat, A., Fairchild, I. J., Leng, M. J., Wynn, P. M., Bryant, C., Genty, D., and Umer, M., 2007, Analysis of the climate signal contained within δ18O and growth rate parameters in two Ethiopian stalagmites: Geochimica et Cosmochimica Acta, v. 71, no. 12, p. 2975-2988.

Baker, A., Barnes, W. L., and Smart, P. L., 1996, Speleothem luminescence intensity and spectral characteristics: Signal calibration and a record of palaeovegetation change: Chemical Geology, v. 130, no. 1-2, p. 65-76.

Baker, A., and Brunsdon, C., 2003, Non-linearities in drip water hydrology: an example from Stump Cross Caverns, Yorkshire: Journal of Hydrology, v. 277, no. 3–4, p. 151-163.

Baker, A., Genty, D., and Smart, P. L., 1998, High-resolution records of soil humification and paleoclimate change from variations in speleothem luminescence excitation and emission wavelengths: Geology, v. 26, no. 10, p. 903-906.

Baker, A., Ito, E., Smart, P. L., and McEwan, R. F., 1997, Elevated and variable values of 13C in speleothems in a British cave system: Chemical Geology, v. 136, no. 3–4, p. 263-270.

Baker, R. G., Bettis, E. A., Denniston, R. F., Gonzalez, L. A., Strickland, L. E., and Krieg, J. R., 2002, Holocene paleoenvironments in southeastern Minnesota - chasing the prairie-forest ecotone: Palaeogeography, Palaeoclimatology, Palaeoecology, v. 177, no. 1-2, p. 103-122.

Baldini, J. U. L., McDermott, F., Baker, A., Baldini, L. M., Mattey, D. P., and Railsback, L. B., 2005, Biomass effects on stalagmite growth and isotope ratios: A 20th century analogue from Wiltshire, England: Earth and Planetary Science Letters, v. 240, no. 2, p. 486-494.

Baldini, J. U. L., McDermott, F., and Fairchild, I. J., 2006, Spatial variability in cave drip water hydrochemistry: Implications for stalagmite paleoclimate records: Chemical Geology, v. 235, no. 3–4, p. 390-404.

Barnston, A. G., and Livezey, R. E., 1987, Classification, Seasonality and Persistence of Low-Frequency Atmospheric Circulation Patterns: Monthly Weather Review, v. 115, no. 6, p. 1083-1126.

Belli, R., Frisia, S., Borsato, A., Drysdale, R., Hellstrom, J., Zhao, J. X., and Spotl, C., 2013, Regional climate variability and ecosystem responses to the last deglaciation in the northern hemisphere from stable isotope data and calcite fabrics in two northern Adriatic stalagmites: Quaternary Science Reviews, v. 72, p. 146-158.

Bender, M. M., 1971, Variations in the 13C/12C ratios of plants in relation to the pathway of photosynthetic carbon dioxide fixation: Phytochemistry, v. 10, no. 6, p. 1239-1244.

Berger, A., 1992, Orbital variations and insolation database, IGBP PAGES/World Data Center-A for Paleoclimatology Data Contribution Series #92-007, NOAA/NGDC Paleoclimatology Program, Boulder, CO.

Berkelhammer, M. B., and Stott, L. D., 2008, Recent and dramatic changes in Pacific storm trajectories recorded in delta O-18 from Bristlecone Pine tree ring cellulose: Geochemistry Geophysics Geosystems, v. 9.

Birks, S. J., and Edwards, T. W. D., 2009, Atmospheric circulation controls on precipitation isotope-climate relations in western Canada: Tellus Series B-Chemical and Physical Meteorology, v. 61, no. 3, p. 566-576.

Boch, R., Spotl, C., and Frisia, S., 2011, Origin and palaeoenvironmental significance of lamination in stalagmites from Katerloch Cave, Austria: Sedimentology, v. 58, no. 2, p. 508-531.

Booth, R. K., Jackson, S. T., Forman, S. L., Kutzbach, J. E., Bettis, E. A., Kreig, J., and Wright, D. K., 2005, A severe centennial-scale drought in mid-continental North America 4200 years ago and apparent global linkages: Holocene, v. 15, no. 3, p. 321-328.

Booth, R. K., Jackson, S. T., and Gray, C. E. D., 2004, Paleoecology and high-resolution paleohydrology of a kettle peatland in upper Michigan: Quaternary Research, v. 61, no. 1, p. 1-13.

Bowen, G. J., Ehleringer, J. R., Chesson, L. A., Stange, E., and Cerling, T. E., 2007, Stable isotope ratios of tap water in the contiguous United States: Water Resources Research, v. 43, no. 3, p. 12.

Broecker, W. S., and van Donk, J., 1970, Insolation changes, ice volumes, and the O18 record in deep-sea cores: Rev. Geophys., v. 8, no. 1, p. 169-198.

Bromwich, D. H., Toracinta, E. R., Oglesby, R. J., Fastook, J. L., and Hughes, T. J., 2005, LGM summer climate on the southern margin of the Laurentide Ice Sheet: wet or dry?: Journal of Climate, v. 18, no. 16, p. 3317-3338.

Bryson, R. A., and Hare, F. K., 1974, Climates of North America, World Survey of Climatology, Volume 11: Amsterdam, Elsevier Scientific Publishing Company.

Burnett, A. W., Mullins, H. T., and Patterson, W. P., 2004, Relationship between atmospheric circulation and winter precipitation delta O-18 in central New York State: Geophysical Research Letters, v. 31, no. 22.

Charles, D. C., Rind, D., Healy, R., and Webb, R., 2001, Tropical cooling and the isotopic composition of precipitation in general circulation model simulations of the ice age climate: Climate Dynamics, v. 17, no. 7, p. 489-502.

Cheng, H., Edwards, R. L., Hoff, J., Gallup, C. D., Richards, D. A., and Asmerom, Y., 2000, The half-lives of uranium-234 and thorium-230: Chemical Geology, v. 169, no. 1-2, p. 17-33.

Chirienco, M. I., 2010, Interpretations of paleoclimate and speleogenesis from speleothems in Donnehue's Cave, Indiana, Master of Science, Department of Geology, University of Illinois at Urbana-Champaign: Urbana, Illinois.

Clark, I. D., and Fritz, P., 1997, Environmental Isotopes in Hydrogeology, New York, Lewis Publishers.

Clark, J. S., Carpenter, S. R., Barber, M., Collins, S., Dobson, A., Foley, J. A., Lodge, D. M., Pascual, M., Jr., R. P., Pizer, W., Pringle, C., Reid, W. V., Rose, K. A., Sala, O., Schlesinger, W. H., Wall, D. H., and Wear, D., 2001, Ecological forecasts: an emerging imperative: Science, v. 293, no. 5530, p. 657-660.

Clark, P. U., Webb, R. S., and Keigwin, L. D., 1999, Mechanisms of global climate change at millenial time scales: Washington, DC, American Geophysical Union.

Cobb, K. M., Westphal, N., Sayani, H. R., Watson, J. T., Di Lorenzo, E., Cheng, H., Edwards, R. L., and Charles, C. D., 2013, Highly variable El Niño–Southern Oscillation throughout the Holocene: Science, v. 339, no. 6115, p. 67-70.

Cole, K. L., and Taylor, R. S., 1995, Past and current trends of change in a dune prairie/oak savanna reconstructed through a multiple-scale history: Journal of Vegetation Science, v. 6, no. 3, p. 399-410.

Coleman, J. S. M., and Rogers, J. C., 2003, Ohio River Valley winter moisture conditions associated with the Pacific-North American teleconnection pattern: Journal of Climate, v. 16, no. 6, p. 969-981.

Conroy, J. L., Overpeck, J. T., Cole, J. E., Shanahan, T. M., and Steinitz-Kannan, M., 2008, Holocene changes in eastern tropical Pacific climate inferred from a Galapagos lake sediment record: Quaternary Science Reviews, v. 27, no. 11-12, p. 1166-1180.

Craig, H., 1961a, Isotopic Variations in Meteoric Waters: Science, v. 133, no. 3465, p. 1702-1703.

-, 1961b, Standard for reporting concentrations of deuterium and oxygen-18 in natural waters: Science, v. 133, no. 346, p. 1833-&.

Cross, M., McGee, D., Broecker, W. S., Quade, J., Shakun, J. D., Cheng, H., Lu, Y., and Edwards, R. L., 2015, Great Basin hydrology, paleoclimate, and connections with the North Atlantic: A speleothem stable isotope and trace element record from Lehman Caves, NV: Quaternary Science Reviews, v. 127, p. 186-198.

Cullen, H. M., deMenocal, P. B., Hemming, S., Hemming, G., Brown, F. H., Guilderson, T., and Sirocko, F., 2000, Climate change and the collapse of the Akkadian empire: Evidence from the deep sea: Geology, v. 28, no. 4, p. 379-382.

Curry, B. B., and Filippelli, G. M., 2010, Episodes of low dissolved oxygen indicated by ostracodes and sediment geochemistry at Crystal Lake, Illinois, USA: Limnology and Oceanography, v. 55, no. 6, p. 2403-2423.

Curry, B. B., Gonzales, L. M., and Grimm, E. C., 2013, Correspondence regarding "Atmospheric changes in North America during the last deglaciation from dune wetland records in the Midwestern United States" by Wang, H., Stumpf, A.J., Miao, X., Lowell, T.V. (2012), Quaternary Science Reviews 58, 124–134: Quaternary Science Reviews, v. 70, p. 176-178.

Dansgaard, W., 1964, Stable isotopes in precipitation: Tellus, v. 16, no. 4, p. 436-468.

Dansgaard, W., Johnsen, S. J., Clausen, H. B., Dahljensen, D., Gundestrup, N. S., Hammer, C. U., Hvidberg, C. S., Steffensen, J. P., Sveinbjornsdottir, A. E., Jouzel, J., and Bond, G., 1993, Evidence for general instability of past climate from a 250-kyr ice-core record: Nature, v. 364, no. 6434, p. 218-220.

Dean, W. E., Forester, R. M., and Bradbury, J. P., 2002, Early Holocene change in atmospheric circulation in the Northern Great Plains: an upstream view of the 8.2 ka cold event: Quaternary Science Reviews, v. 21, no. 16–17, p. 1763-1775.

Delcourt, P. A., and Delcourt, H. R., 1984, Late Quaternary paleoclimates and biotic responses in eastern North America and the western North Atlantic Ocean: Palaeogeography, Palaeoclimatology, Palaeoecology, v. 48, no. 2, p. 263-284.

Denniston, R. F., DuPree, M., Dorale, J. A., Asmerom, Y., Polyak, V. J., and Carpenter, S. J., 2007, Episodes of late Holocene aridity recorded by stalagmites from Devil's Icebox Cave, central Missouri, USA: Quaternary Research, v. 68, no. 1, p. 45-52.

Denniston, R. F., González, L. A., Baker, R. G., Asmerom, Y., Reagan, M. K., Edwards, R. L., and Alexander, E. C., 1999a, Speleothem evidence for Holocene fluctuations of the prairie-forest ecotone, north-central USA: The Holocene, v. 9, no. 6, p. 671-676.

Denniston, R. F., Gonzalez, L. A., Semken, H. A., Asmerom, Y., Baker, R. G., Recelli-Snyder, H., Reagan, M. K., and Bettis, E. A., 1999b, Integrating stalagmite, vertebrate, and pollen sequences to investigate holocene vegetation and climate change in the Southern Midwestern United States: Quaternary Research, v. 52, no. 3, p. 381-387.

Denniston, R. F., Gonzalez, L. A., Semken Jr, H. A., Asmerom, Y., Baker, R. G., Recelli-Snyder, H., Reagan, M. K., and Bettis Iii, E. A., 1999c, Integrating Stalagmite, Vertebrate, and Pollen Sequences to Investigate Holocene Vegetation and Climate Change in the Southern Midwestern United States: Quaternary Research, v. 52, no. 3, p. 381-387.

Dorale, J. A., Wozniak, L. A., Bettis, E. A., Carpenter, S. J., Mandel, R. D., Hajic, E. R., Lopinot, H., and Ray, J. H., 2010, Isotopic evidence for Younger Dryas aridity in the North American midcontinent: Geology, v. 38, no. 6, p. 519-522.

Dreybrodt, W., and Scholz, D., 2011, Climatic dependence of stable carbon and oxygen isotope signals recorded in speleothems: From soil water to speleothem calcite: Geochimica et Cosmochimica Acta, v. 75, no. 3, p. 734-752.

Drysdale, R. N., Spötl, C., Hellstrom, J. C., and Richards, D. A., 2012, New advances in the dating of speleothems – An introduction: Quaternary Geochronology, v. 14, p. 1-4.

Dutton, A., Wilkinson, B. H., Welker, J. M., Bowen, G. J., and Lohmann, K. C., 2005, Spatial distribution and seasonal variation in O-18/O-16 of modern precipitation and river water across the conterminous USA: Hydrological Processes, v. 19, no. 20, p. 4121-4146.

Edwards, R. L., Chen, J. H., and Wasserburg, G. J., 1987, U-238- U-234- TH-230- TH-232 systematics and the precise measurement of time over the past 500000 years: Earth and Planetary Science Letters, v. 81, no. 2-3, p. 175-192.

Emiliani, C., 1955, Pleistocene temperatures: Journal of Geology, v. 63, p. 538-578.

Enfield, D. B., Mestas-Nunez, A. M., and Trimble, P. J., 2001, The Atlantic multidecadal oscillation and its relation to rainfall and river flows in the continental US: Geophysical Research Letters, v. 28, no. 10, p. 2077-2080.

Ersek, V., Hostetler, S. W., Cheng, H., Clark, P. U., Anslow, F. S., Mix, A. C., and Edwards, R. L., 2009, Environmental influences on speleothem growth in southwestern Oregon during the last 380 000 years: Earth and Planetary Science Letters, v. 279, no. 3–4, p. 316-325.

Fairbanks, R., Charles, C., and Wright, J., 1992, Origin of Global Meltwater Pulses, *in* Taylor, R. E., Long, A., and Kra, R., eds., Radiocarbon After Four Decades, Springer New York, p. 473-500.

Fairchild, I. J., Smith, C. L., Baker, A., Fuller, L., Spötl, C., Mattey, D., McDermott, F., and E.I.M.F, 2006, Modification and preservation of environmental signals in speleothems: Earth-Science Reviews, v. 75, no. 1–4, p. 105-153.

Feng, W., Banner, J. L., Guilfoyle, A. L., Musgrove, M., and James, E. W., 2012, Oxygen isotopic fractionation between drip water and speleothem calcite: A 10-year monitoring study, central Texas, USA: Chemical Geology, v. 304–305, p. 53-67.

Fleitmann, D., Burns, S. J., Mangini, A., Mudelsee, M., Kramers, J., Villa, I., Neff, U., Al-Subbary, A. A., Buettner, A., Hippler, D., and Matter, A., 2007, Holocene ITCZ and Indian monsoon dynamics recorded in stalagmites from Oman and Yemen (Socotra): Quaternary Science Reviews, v. 26, no. 1–2, p. 170-188.

Forman, S. L., Oglesby, R., and Webb, R. S., 2001, Temporal and spatial patterns of Holocene dune activity on the Great Plains of North America: megadroughts and climate links: Global and Planetary Change, v. 29, no. 1–2, p. 1-29.

Frelich, L. E., and Reich, P. B., 2010, Will environmental changes reinforce the impact of global warming on the prairie–forest border of central North America?: Frontiers in Ecology and the Environment, v. 8, no. 7, p. 371-378.

French, H. M., and Millar, S. W. S., 2013, Permafrost at the time of the Last Glacial Maximum (LGM) in North America: Boreas, p. n/a-n/a.

Frisia, S., Borsato, A., Fairchild, I. J., McDermott, F., and Selmo, E. M., 2002, Aragonite-calcite relationships in speleothems (Grotte de Clamouse, France): Environment, fabrics, and carbonate geochemistry: Journal of Sedimentary Research, v. 72, no. 5, p. 687-699.

Fuchs, B. A., Wood, D. A., and Ebbeka, D., 2013, From too much to too little: how the central U.S. drought of 2012 evolved out of one of the most devastating floods on record in 2011, National Drought Mitigation Center, University of Nebraska-Lincoln; Lincoln, NE.

Gat, J. R., 1996, Oxygen and hydrogen isotopes in the hydrologic cycle: Annual Review of Earth and Planetary Sciences, v. 24, p. 225-262.

Gat, J. R., and Matsui, E., 1991, Atmospheric water-balance in the Amazon Basin- an isotopic evapotranspiration model: Journal of Geophysical Research-Atmospheres, v. 96, no. D7, p. 13179-13188.

Genty, D., Blamart, D., Ouahdi, R., Gilmour, M., Baker, A., Jouzel, J., and Van-Exter, S., 2003, Precise dating of Dansgaard-Oeschger climate oscillations in western Europe from stalagmite data: Nature, v. 421, no. 6925, p. 833-837.

Glover, K. C., Lowell, T. V., Wiles, G. C., Pair, D., Applegate, P., and Hajdas, I., 2011, Deglaciation, basin formation and post-glacial climate change from a regional network of sediment core sites in Ohio and eastern Indiana: Quaternary Research, v. 76, no. 3, p. 401-410.

Goman, M., and Leigh, D. S., 2004, Wet early to middle Holocene conditions on the upper Coastal Plain of North Carolina, USA: Quaternary Research, v. 61, no. 3, p. 256-264.

Gonfiantini, R., 1978, Standards for stable isotope measurements in natural compounds: Nature, v. 271, no. 5645, p. 534-536.

-, 1986, Environmental isotopes in lake studies, *in* Fritz, P., and Fontes, J.-C., eds., Handbook of Environmental Isotope Geochemistry: Amsterdam, Netherlands, Elsevier, p. 113-168.

Grimm, E. C., and Jacobson Jr., G. L., 2003, Late-Quaternary vegetation history of the eastern United States, *in* A.R. Gillespie, S. C. P., and Atwater, B. F., eds., Developments in Quaternary Sciences, Volume Volume 1, Elsevier, p. 381-402.

Gupta, A. K., Anderson, D. M., and Overpeck, J. T., 2003, Abrupt changes in the Asian southwest monsoon during the Holocene and their links to the North Atlantic Ocean: Nature, v. 421, no. 6921, p. 354-357.

Guyette, R. P., Dey, D. C., and Stambaugh, M. C., 2003, Fire and human history of a barren-forest mosaic in southern Indiana: American Midland Naturalist, v. 149, no. 1, p. 21-34.

Hameed, S., and Riemer, N., 2012, Relationship of Sahel precipitation and atmospheric centers of action: Advances in Meteorology, v. 2012, p. 8.

Hansen, A. J., Neilson, R. P., Dale, V. H., Flather, C. H., Iverson, L. R., Currie, D. J., Shafer, S., Cook, R., and Bartlein, P. J., 2001, Global Change in Forests: Responses of Species, Communities, and Biomes: BioScience, v. 51, no. 9, p. 765.

Hanson, P. R., Arbogast, A. F., Johnson, W. C., Joeckel, R. M., and Young, A. R., 2010, Megadroughts and late Holocene dune activation at the eastern margin of the Great Plains, north-central Kansas, USA: Aeolian Research, v. 1, no. 3–4, p. 101-110.

Hardt, B., Rowe, H. D., Springer, G. S., Cheng, H., and Edwards, R. L., 2010, The seasonality of east central North American precipitation based on three coeval Holocene speleothems from southern West Virginia: Earth and Planetary Science Letters, v. 295, no. 3–4, p. 342-348.

Harmon, R. S., 1979, An isotopic study of groundwater seepage in the central Kentucky Karst: Water Resources Research, v. 15, no. 2, p. 476-480.

Harvey, F. E., and Welker, J. M., 2000, Stable isotopic composition of precipitation in the semi-arid north-central portion of the US Great Plains: Journal of Hydrology, v. 238, no. 1-2, p. 90-109.

Hays, J. D., Imbrie, J., and Shackleton, N. J., 1976, Variations in the Earth's orbit: pacemaker of the Ice Ages: Science, v. 194, no. 4270, p. 1121-1132.

Hendy, C. H., 1971, The isotopic geochemistry of speleothems—I. The calculation of the effects of different modes of formation on the isotopic composition of speleothems and their applicability as palaeoclimatic indicators: Geochimica et Cosmochimica Acta, v. 35, no. 8, p. 801-824.

Hendy, C. H., and Wilson, A. T., 1968, Palaeoclimatic data from speleothems: Nature, v. 219, no. 5149, p. 48-&.

Hesterberg, R., and Siegenthaler, U., 1991, Production and stable isotopic composition of CO2 in a soil near Bern, Switzerland: Tellus B, v. 43, no. 2, p. 197-205.

Heusser, L., Maenza-Gmelch, T., Lowell, T., and Hinnefeld, R., 2002, Late Wisconsin periglacial environments of the southern margin of the Laurentide Ice Sheet reconstructed from pollen analyses: Journal of Quaternary Science, v. 17, no. 8, p. 773-780.

Huang, C. C., Pang, J. L., Zha, X. C., Su, H. X., and Jia, Y. F., 2011, Extraordinary floods related to the climatic event at 4200 a BP on the Qishuihe River, middle reaches of the Yellow River, China: Quaternary Science Reviews, v. 30, no. 3-4, p. 460-468.

Huang, C. C., Pang, J. L., Zha, X. C., Zhou, Y. L., Su, H. X., and Li, Y. G., 2010, Extraordinary Floods of 4100-4000 BP recorded at the Late Neolithic Ruins in the Jinghe River Gorges, Middle Reach of the Yellow River, China: Palaeogeography Palaeoclimatology Palaeoecology, v. 289, no. 1-4, p. 1-9.

Hurrell, J. W., 1995, Decadal trends in the North Atlantic Oscillation- regional temperatures and precipitation: Science, v. 269, no. 5224, p. 676-679.

HYSPLIT-WEB, 2015, Hybrid Single Particle Lagrangian Integrated Trajectory (HYSPLIT) model: http://ready.arl.noaa.gov/HYSPLIT.php.

IAEA/WMO, 2016, Global Network of Isotopes in Precipitation. The GNIP Database: http://www.iaea.org/water.

IBRC, 2015, Beyond the farm: a state and regional report on the economic contribution of farms, forests, and related industries: Indiana Business Research Center, Kelly School of Business, Indiana University; Bloomington, IN.

Imbrie, J. H., J. D.; Martinson, D. G.; McIntyre, A.; Mix, A. C.; Morley, J. J.; Pisias, N. G.; Prell, W. L.; Shackleton, N. J., 1984, The orbital theory of Pleistocene climate : support from a revised chronology of the marine δ18 O record, *in* Proceedings Milankovitch and Climate: Understanding the Response to Astronomical Forcing, Palisades, NY, 1984, D. Reidel Publishing, p. 269.

Jackson, S. T., Booth, R. K., Reeves, K., Andersen, J. J., Minckley, T. A., and Jones, R. A., 2014, Inferring local to regional changes in forest composition from Holocene macrofossils and pollen of a small lake in central Upper Michigan: Quaternary Science Reviews, v. 98, p. 60-73.

Jackson, S. T., Webb, R. S., Anderson, K. H., Overpeck, J. T., Webb Iii, T., Williams, J. W., and Hansen, B. C. S., 2000, Vegetation and environment in Eastern North America during the Last Glacial Maximum: Quaternary Science Reviews, v. 19, no. 6, p. 489-508.

James, E. W., Banner, J. L., and Hardt, B., 2015, A global model for cave ventilation and seasonal bias in speleothem paleoclimate records: Geochemistry Geophysics Geosystems, v. 16, no. 4, p. 1044-1051.

Johnsen, S. J., Clausen, H. B., Dansgaard, W., Fuhrer, K., Gundestrup, N., Hammer, C. U., Iversen, P., Jouzel, J., Stauffer, B., and Steffensen, J. P., 1992, Irregular glacial interstadials recorded in a new Greenland ice core: Nature, v. 359, no. 6393, p. 311-313.

Johnson, W. H., Hansel, A. K., Bettis Iii, E. A., Karrow, P. F., Larson, G. J., Lowell, T. V., and Schneider, A. F., 1997, Late Quaternary Temporal and Event Classifications, Great Lakes Region, North America: Quaternary Research, v. 47, no. 1, p. 1-12.

Jouzel, J., Hoffmann, G., Koster, R. D., and Masson, V., 2000, Water isotopes in precipitation: data/model comparison for present-day and past climates: Quaternary Science Reviews, v. 19, no. 1–5, p. 363-379.

Jouzel, J., Masson-Delmotte, V., Cattani, O., Dreyfus, G., Falourd, S., Hoffmann, G., Minster, B., Nouet, J., Barnola, J. M., Chappellaz, J., Fischer, H., Gallet, J. C., Johnsen, S., Leuenberger, M., Loulergue, L., Luethi, D., Oerter, H., Parrenin, F., Raisbeck, G., Raynaud, D., Schilt, A., Schwander, J., Selmo, E., Souchez, R., Spahni, R., Stauffer, B., Steffensen, J. P., Stenni, B., Stocker, T. F., Tison, J. L., Werner, M., and Wolff, E. W., 2007, Orbital and millennial Antarctic climate variability over the past 800,000 years: Science, v. 317, no. 5839, p. 793-796.

Jouzel, J., and Merlivat, L., 1984, Deuterium and oxygen 18 in precipitation: Modeling of the isotopic effects during snow formation: Journal of Geophysical Research: Atmospheres, v. 89, no. D7, p. 11749-11757.

Ju, J., and Slingo, J., 1995, The Asian summer monsoon and ENSO: Quarterly Journal of the Royal Meteorological Society, v. 121, no. 525, p. 1133-1168.

Kaniewski, D., Paulissen, E., Van Campo, E., Al-Maqdissi, M., Bretschneider, J., and Van Lerberghe, K., 2008, Middle East coastal ecosystem response to middle-to-late Holocene abrupt climate changes: Proceedings of the National Academy of Sciences of the United States of America, v. 105, no. 37, p. 13941-13946.

Kaniewski, D., Van Campo, E., Guiot, J., Le Burel, S., Otto, T., and Baeteman, C., 2013, Environmental roots of the Late Bronze Age crisis: Plos One, v. 8, no. 8, p. 10.

Kawamura, K., Parrenin, F., Lisiecki, L., Uemura, R., Vimeux, F., Severinghaus, J. P., Hutterli, M. A., Nakazawa, T., Aoki, S., Jouzel, J., Raymo, M. E., Matsumoto, K., Nakata, H., Motoyama, H., Fujita, S., Goto-Azuma, K., Fujii, Y., and Watanabe, O., 2007, Northern Hemisphere forcing of climatic cycles in Antarctica over the past 360,000 years: Nature, v. 448, no. 7156, p. 912-U914.

Kiefer, R. H., and Amey, M. R. G., 1992, Concentrations and controls of soil carbon dioxide in sandy soil in the North Carolina coastal plain: CATENA, v. 19, no. 6, p. 539-559.

Kilibarda, Z., and Blockland, J., 2011, Morphology and origin of the Fair Oaks Dunes in NW Indiana, USA: Geomorphology, v. 125, no. 2, p. 305-318.

Kim, S.-T., and O'Neil, J. R., 1997, Equilibrium and nonequilibrium oxygen isotope effects in synthetic carbonates: Geochimica et Cosmochimica Acta, v. 61, no. 16, p. 3461-3475.

King, J. E., and Allen Jr, W. H., 1977, A Holocene vegetation record from the Mississippi River Valley, southeastern Missouri: Quaternary Research, v. 8, no. 3, p. 307-323.

KNMI, 2015, Climate Explorer Web Application: http://climexp.knmi.nl/, Royal Netherlands Meteorological Institute.

Knox, J. C., 1985, Responses of floods to Holocene climatic change in the upper Mississippi Valley: Quaternary Research, v. 23, no. 3, p. 287-300.

-, 2000, Sensitivity of modern and Holocene floods to climate change: Quaternary Science Reviews, v. 19, no. 1–5, p. 439-457.

Knudsen, M. F., Seidenkrantz, M.-S., Jacobsen, B. H., and Kuijpers, A., 2011, Tracking the Atlantic Multidecadal Oscillation through the last 8,000 years: Nat Commun, v. 2, p. 178.

Kobashi, T., Severinghaus, J. P., Brook, E. J., Barnola, J. M., and Grachev, A. M., 2007, Precise timing and characterization of abrupt climate change 8200 years ago from air trapped in polar ice: Quaternary Science Reviews, v. 26, no. 9-10, p. 1212-1222.

Kohn, M. J., and Welker, J. M., 2005, On the temperature correlation of delta O-18 in modern precipitation: Earth and Planetary Science Letters, v. 231, no. 1-2, p. 87-96.

Kuzucuoğlu, C., Dörfler, W., Kunesch, S., and Goupille, F., 2011, Mid- to late-Holocene climate change in central Turkey: The Tecer Lake record: The Holocene, v. 21, no. 1, p. 173-188.

Lachniet, M. S., 2009, Climatic and environmental controls on speleothem oxygen-isotope values: Quaternary Science Reviews, v. 28, no. 5-6, p. 412-432.

Lachniet, M. S., Burns, S. J., Piperno, D. R., Asmerom, Y., Polyak, V. J., Moy, C. M., and Christenson, K., 2004, A 1500-year El Nino/Southern Oscillation and rainfall history for the Isthmus of Panama from speleothem calcite: Journal of Geophysical Research-Atmospheres, v. 109, no. D20.

Lambert, W. J., and Aharon, P., 2011, Controls on dissolved inorganic carbon and delta C-13 in cave waters from DeSoto Caverns: Implications for speleothem delta C-13 assessments: Geochimica Et Cosmochimica Acta, v. 75, no. 3, p. 753-768.

LaMoreaux, H. K., Brook, G. A., and Knox, J. A., 2009, Late Pleistocene and Holocene environments of the Southeastern United States from the stratigraphy and pollen content of a peat deposit on the Georgia Coastal Plain: Palaeogeography, Palaeoclimatology, Palaeoecology, v. 280, no. 3–4, p. 300-312.

Lauritzen, S.-E., Ford, D. C., and Schwarcz, H. P., Humic substances in speleothem matrix- paleoclimate significance, *in* Proceedings Proceedings of the 9th International Speleological Congress, Barcelona, Spain, 1986, p. 77-79.

Leathers, D. J., Yarnal, B., and Palecki, M. A., 1991, The Pacific-North American teleconnection pattern and United States Climate: 1. Regional temperature and precipitation associations: Journal of Climate, v. 4, no. 5, p. 517-528.

Lee, J.-E., Fung, I., DePaolo, D. J., and Otto-Bliesner, B., 2008, Water isotopes during the Last Glacial Maximum: New general circulation model calculations: Journal of Geophysical Research: Atmospheres, v. 113, no. D19, p. n/a-n/a.

LeGrande, A. N., and Schmidt, G. A., 2006, Global gridded data set of the oxygen isotopic composition in seawater: Geophysical Research Letters, v. 33, no. 12.

Leuschner, D. C., and Sirocko, F., 2000, The low-latitude monsoon climate during Dansgaard–Oeschger cycles and Heinrich Events: Quaternary Science Reviews, v. 19, no. 1–5, p. 243-254.

Litwin, R. J., Smoot, J. P., Pavich, M. J., Markewich, H. W., Brook, G., and Durika, N. J., 2013, 100,000-year-long terrestrial record of millennial-scale linkage between eastern North American mid-latitude paleovegetation shifts and Greenland ice-core oxygen isotope trends: Quaternary Research, v. 80, no. 2, p. 291-315.

Liu, Z., Bowen, G. J., and Welker, J. M., 2010, Atmospheric circulation is reflected in precipitation isotope gradients over the conterminous United States: Journal of Geophysical Research-Atmospheres, v. 115.

Liu, Z., Kennedy, C. D., and Bowen, G. J., 2011, Pacific/North American teleconnection controls on precipitation isotope ratios across the contiguous United States: Earth and Planetary Science Letters, v. 310, no. 3-4, p. 319-326.

Liu, Z., Yoshimura, K., Bowen, G. J., Buenning, N. H., Risi, C., Welker, J. M., and Yuan, F., 2014a, Paired oxygen isotope records reveal modern North American atmospheric dynamics during the Holocene: Nat Commun, v. 5.

Liu, Z., Yoshmura, K., Bowen, G. J., and Welker, J. M., 2014b, Pacific-North American teleconnection controls on precipitation isotopes (delta O-18) across the contiguous United States and adjacent regions: a GCM-based analysis: Journal of Climate, v. 27, no. 3, p. 1046-1061.

Lofverstrom, M., Caballero, R., Nilsson, J., and Kleman, J., 2014, Evolution of the large-scale atmospheric circulation in response to changing ice sheets over the last glacial cycle: Climate of the Past, v. 10, no. 4, p. 1453-1471.

Magny, M., Vanniere, B., Zanchetta, G., Fouache, E., Touchais, G., Petrika, L., Coussot, C., Walter-Simonnet, A. V., and Arnaud, F., 2009, Possible complexity of the climatic event around 4300-3800 cal. BP in the central and western Mediterranean: Holocene, v. 19, no. 6, p. 823-833.

Mallya, G., Zhao, L., Song, X. C., Niyogi, D., and Govindaraju, R. S., 2013, 2012 Midwest Drought in the United States: Journal of Hydrologic Engineering, v. 18, no. 7, p. 737-745.

Mantua, N. J., and Hare, S. R., 2002, The Pacific Decadal Oscillation: Journal of Oceanography, v. 58, no. 1, p. 35-44.

Marcott, S. A., Shakun, J. D., Clark, P. U., and Mix, A. C., 2013, A reconstruction of regional and global temperature for the past 11,300 years: Science, v. 339, no. 6124, p. 1198-1201.

Matsui, E., Salati, E., Ribeiro, M. N. G., Reis, C. M., Tancredi, A. C. S. N. F., and Gat, J. R., 1983, Precipitation in the central Amazon Basin: the isotopic composition of rain and atmospheric moisture at Belem and Manaus, Brazil: Acta Amazonica, v. 13, no. 2, p. 307-370.

Mayewski, P. A., Rohling, E. E., Curt Stager, J., Karlén, W., Maasch, K. A., David Meeker, L., Meyerson, E. A., Gasse, F., van Kreveld, S., Holmgren, K., Lee-Thorp, J., Rosqvist, G., Rack, F., Staubwasser, M., Schneider, R. R., and Steig, E. J., 2004, Holocene climate variability: Quaternary Research, v. 62, no. 3, p. 243-255.

McCabe-Glynn, S., Johnson, K. R., Strong, C., Berkelhammer, M., Sinha, A., Cheng, H., and Edwards, R. L., 2013, Variable North Pacific influence on drought in southwestern North America since AD 854: Nature Geoscience, v. 6, no. 8, p. 617-621.

McCabe, G. J., Palecki, M. A., and Betancourt, J. L., 2004, Pacific and Atlantic Ocean influences on multidecadal drought frequency in the United States: Proceedings of the National Academy of Sciences of the United States of America, v. 101, no. 12, p. 4136-4141.

McDermott, F., 2004, Palaeo-climate reconstruction from stable isotope variations in speleothems: a review: Quaternary Science Reviews, v. 23, no. 7-8, p. 901-918.

McFadden, M. A., Patterson, W. P., Mullins, H. T., and Anderson, W. T., 2005, Multi-proxy approach to long- and short-term Holocene climate-change: evidence from eastern Lake Ontario: Journal of Paleolimnology, v. 33, no. 3, p. 371-391.

McGarry, S. F., and Baker, A., 2000, Organic acid fluorescence: applications to speleothem palaeoenvironmental reconstruction: Quaternary Science Reviews, v. 19, no. 11, p. 1087-1101.

Menounos, B., Clague, J. J., Osborn, G., Luckman, B. H., Lakeman, T. R., and Minkus, R., 2008, Western Canadian glaciers advance in concert with climate change circa 4.2 ka: Geophysical Research Letters, v. 35, no. 7.

Merz, N., Raible, C. C., and Woollings, T., 2015, North Atlantic eddy-driven jet in interglacial and glacial winter climates: Journal of Climate, v. 28, no. 10, p. 3977-3997.

Meyer, K. W., Feng, W. M., Breecker, D. O., Banner, J. L., and Guilfoyle, A., 2014, Interpretation of speleothem calcite delta C-13 variations: Evidence from monitoring soil CO2, drip water, and modern speleothem calcite in central Texas: Geochimica Et Cosmochimica Acta, v. 142, p. 281-298.

Moros, M., Andrews, J. T., Eberl, D. D., and Jansen, E., 2006, Holocene history of drift ice in the northern North Atlantic: Evidence for different spatial and temporal modes: Paleoceanography, v. 21, no. 2, p. 10.

Morrill, C., and Jacobsen, R. M., 2005, How widespread were climate anomalies 8200 years ago?: Geophysical Research Letters, v. 32, no. 19, p. n/a-n/a.

Naughton, F., Keigwin, L., Peteet, D., Costas, S., Desprat, S., Oliveira, D., de Vernal, A., Voelker, A., and Abrantes, F., 2015, A 12,000-yr pollen record off Cape Hatteras - Pollen sources and mechanisms of pollen dispersion: Marine Geology, v. 367, p. 118-129.

Nelson, D. M., Hu, F. S., Grimm, E. C., Curry, B. B., and Slate, J. E., 2006, The influence of aridity and fire on Holocene Prairie communities in the eastern Prairie Peninsula: Ecology, v. 87, no. 10, p. 2523-2536.

Nelson, J. A., Licht, K., Yansa, C., and Filippelli, G., 2009, Climate-related cyclic deposition of carbonate and organic matter in Holocene lacustrine sediment, Lower Michigan, USA: Journal of Paleolimnology, v. 44, no. 1, p. 1-13.

NOAA, 2015a, Earth System Research Laboratory Climate Indices: Monthly Atmospheric and Ocean Time Series: http://www.esrl.noaa.gov/psd/data/climateindices/list/, National Oceanic and Atmospheric Administration.

-, 2015b, National Centers for Environmental Information: 1981-2010 U.S. Climate Normals: https://www.ncdc.noaa.gov/data-access/land-based-station-data/land-based-datasets/climate-normals/1981-2010-normals-data, National Oceanic and Atmospheric Administration.

-, 2015c, National Centers for Environmental Information: Daily Observational Data Mapping Tool, https://gis.ncdc.noaa.gov/map/viewer/#app=cdo&cfg=cdo&theme=daily&layers=111, National Oceanic and Atmospheric Administration.

-, 2015d, NOAA Paleoclimatology Program, www.ncdc.noaa.gov/paleo/paleo.html, NCDC Paleoclimatology Branch.

-, 2016, CPC - Climate Weather Linkage: Teleconnections, http://www.cpc.ncep.noaa.gov/products/precip/CWlink/daily_ao_index/teleconnections.shtml, Volume 2016, National Oceanic and Atmospheric Administration.

Pachauri, R. K., and Reisinger, A., 2008, Climate change 2007: Synthesis report. Contribution of Working Groups I, II and III to the fourth assessment report: Geneva, Switzerland, IPCC, p. 104.

PCCRC, 2008, Impacts of climate change for the state of Indiana: Purdue Climate Change Research Center, Purdue University, West Lafayette, IN.

Peixóto, J. P., and Oort, A. H., 1983, The atmospheric branch of the hydrological cycle and climate, *in* Street-Perrott, A., Beran, M., and Ratcliffe, R., eds., Variations in the Global Water Budget, Springer Netherlands, p. 5-65.

Perrin, J., Jeannin, P.-Y., and Zwahlen, F., 2003, Epikarst storage in a karst aquifer: a conceptual model based on isotopic data, Milandre test site, Switzerland: Journal of Hydrology, v. 279, no. 1–4, p. 106-124.

PRISM, 2004, PRISM Climate Group, Oregon State University, http://prism.oregonstate.edu.

PSWC, 2015, Plymouth State Weather Center WXP Radar Map Generator, http://vortex.plymouth.edu/rad-u.html, Plymouth State University, Plymouth, NH.

Railsback, L. B., Akers, P. D., Wang, L., Holdridge, G. A., and Voarintsoa, N. R., 2013, Layer-bounding surfaces in stalagmites as keys to better paleoclimatological histories and chronologies: International Journal of Speleology, v. 42, no. 3, p. 13.

Railsback, L. B., Brook, G. A., Chen, J., Kalin, R., and Fleisher, C. J., 1994, Environmental controls on the petrology of a late Holocene speleothem from Botswana with annual layers of aragonite and calcite: Journal of Sedimentary Research Section a-Sedimentary Petrology and Processes, v. 64, no. 1, p. 147-155.

Railsback, L. B., Brook, G. A., Ellwood, B. B., Liang, F. Y., Cheng, H., and Edwards, R. L., 2015a, A record of wet glacial stages and dry interglacial stages over the last 560 kyr from a standing massive stalagmite in Carlsbad Cavern, New Mexico, USA: Palaeogeography Palaeoclimatology Palaeoecology, v. 438, p. 256-266.

Railsback, L. B., Gibbard, P. L., Head, M. J., Voarintsoa, N. R. G., and Toucanne, S., 2015b, An optimized scheme of lettered marine isotope substages for the last 1.0 million years, and the climatostratigraphic nature of isotope stages and substages: Quaternary Science Reviews, v. 111, p. 94-106.

Railsback, L. B., Xiao, H., Liang, F., Akers, P. D., Brook, G. A., Dennis, W. M., Lanier, T. E., Tan, M., Cheng, H., and Edwards, R. L., 2014, A stalagmite record of abrupt climate change and possible Westerlies-derived atmospheric precipitation during the Penultimate Glacial Maximum in northern China: Palaeogeography, Palaeoclimatology, Palaeoecology, v. 393, no. 0, p. 30-44.

Rasmussen, T. L., Thomsen, E., and Moros, M., 2016, North Atlantic warming during Dansgaard-Oeschger events synchronous with Antarctic warming and out-of-phase with Greenland climate: Scientific Reports, v. 6, p. 20535.

Rightmire, C. T., 1978, Seasonal variation in pCO2 and 13C content of soil atmosphere: Water Resources Research, v. 14, no. 4, p. 691-692.

Rijsdijk, K. F., Zinke, J., de Louw, P. G. B., Hume, J. P., van der Plicht, H., Hooghiemstra, H., Meijer, H. J. M., Vonhof, H. B., Porch, N., Florens, F. B. V., Baider, C., van Geel, B., Brinkkemper, J., Vernimmen, T., and Janoo, A., 2011, Mid-Holocene (4200 kyr BP) mass mortalities in Mauritius (Mascarenes): Insular vertebrates resilient to climatic extremes but vulnerable to human impact: Holocene, v. 21, no. 8, p. 1179-1194.

Rimbu, N., Lohmann, G., Kim, J. H., Arz, H. W., and Schneider, R., 2003, Arctic/North Atlantic Oscillation signature in Holocene sea surface temperature trends as obtained from alkenone data: Geophysical Research Letters, v. 30, no. 6.

Rogers, J. C., and Coleman, J. S. M., 2003, Interactions between the Atlantic Multidecadal Oscillation, El Nino/La Nina, and the PNA in winter Mississippi valley stream flow: Geophysical Research Letters, v. 30, no. 10.

Rozanski, K., Araguás-Araguás, L., and Gonfiantini, R., 1993, Isotopic Patterns in Modern Global Precipitation, Climate Change in Continental Isotopic Records, American Geophysical Union, p. 1-36.

Scholl, M. A., Shanley, J. B., Zegarra, J. P., and Coplen, T. B., 2009, The stable isotope amount effect: New insights from NEXRAD echo tops, Luquillo Mountains, Puerto Rico: Water Resources Research, v. 45, p. 14.

Scholz, D., and Hoffmann, D. L., 2011, StalAge – An algorithm designed for construction of speleothem age models: Quaternary Geochronology, v. 6, no. 3–4, p. 369-382.

Schwartz, D., Mariotti, A., Lanfranchi, R., and Guillet, B., 1986, 13C/12C ratios of soil organic matter as indicators of vegetation changes in the Congo: Geoderma, v. 39, no. 2, p. 97-103.

Seifert, C. L., Cox, R. T., Forman, S. L., Foti, T. L., Wasklewicz, T. A., and McColgan, A. T., 2009, Relict nebkhas (pimple mounds) record prolonged late Holocene drought in the forested region of south-central United States: Quaternary Research, v. 71, no. 3, p. 329-339.

Semken, H. A. J., Graham, R. W., and Stafford Jr., T. W., 2010, AMS 14C analysis of Late Pleistocene non-analog faunal components from 21 cave deposits in southeastern North America: Quaternary International, v. 217, no. 1–2, p. 240-255.

Shackleton, N. J., Berger, A., and Peltier, W. R., 1990, An alternative astronomical calibration of the lower Pleistocene timescale based on ODP site 677: Transactions of the Royal Society of Edinburgh-Earth Sciences, v. 81, p. 251-261.

Shackleton, N. J., and Opdyke, N. D., 1973, Oxygen isotope and palaeomagnetic stratigraphy of Equatorial Pacific core V28-238: Oxygen isotope temperatures and ice volumes on a 105 year and 106 year scale: Quaternary Research, v. 3, no. 1, p. 39-55.

Shen, C.-C., Lawrence Edwards, R., Cheng, H., Dorale, J. A., Thomas, R. B., Bradley Moran, S., Weinstein, S. E., and Edmonds, H. N., 2002, Uranium and thorium isotopic and concentration

measurements by magnetic sector inductively coupled plasma mass spectrometry: Chemical Geology, v. 185, no. 3–4, p. 165-178.

Sheridan, S. C., 2003, North American weather-type frequency and teleconnection indices: International Journal of Climatology, v. 23, no. 1, p. 27-45.

Shinker, J. J., Bartlein, P. J., and Shuman, B., 2006, Synoptic and dynamic climate controls of North American mid-continental aridity: Quaternary Science Reviews, v. 25, no. 13–14, p. 1401-1417.

Shopov, Y. Y., Ford, D. C., and Schwarcz, H. P., 1994, Luminescent microbanding in speleothems: High-resolution chronology and paleoclimate: Geology, v. 22, no. 5, p. 407-410.

Shuman, B., and Donnelly, J. P., 2006, The influence of seasonal precipitation and temperature regimes on lake levels in the northeastern United States during the Holocene: Quaternary Research, v. 65, no. 1, p. 44-56.

Shuster, E. T., and White, W. B., 1972, Source areas and climatic effects in carbonate groundwaters determined by saturation indices and carbon dioxide pressures: Water Resources Research, v. 8, no. 4, p. 1067-1073.

Singer, D. K., Jackson, S. T., Madsen, B. J., and Wilcox, D. A., 1996, Differentiating climatic and successional influences on long-term development of a marsh: Ecology, v. 77, no. 6, p. 1765-1778.

Sjostrom, D. J., and Welker, J. M., 2009, The influence of air mass source on the seasonal isotopic composition of precipitation, eastern USA: Journal of Geochemical Exploration, v. 102, no. 3, p. 103-112.

Spötl, C., and Mangini, A., 2002, Stalagmite from the Austrian Alps reveals Dansgaard–Oeschger events during isotope stage 3:: Implications for the absolute chronology of Greenland ice cores: Earth and Planetary Science Letters, v. 203, no. 1, p. 507-518.

Springer, G. S., Rowe, H. D., Hardt, B., Cheng, H., and Edwards, R. L., 2014, East central North America climates during marine isotope stages 3-5: Geophysical Research Letters, v. 41, no. 9, p. 3233-3237.

Springer, G. S., Rowe, H. D., Hardt, B., Edwards, R. L., and Cheng, H., 2008, Solar forcing of Holocene droughts in a stalagmite record from West Virginia in east-central North America: Geophysical Research Letters, v. 35, no. 17, p. n/a-n/a.

Stanley, J. D., Krom, M. D., Cliff, R. A., and Woodward, J. C., 2003, Short contribution: Nile flow failure at the end of the old kingdom, Egypt: Strontium isotopic and petrologic evidence: Geoarchaeology-an International Journal, v. 18, no. 3, p. 395-402.

Staubwasser, M., Sirocko, F., Grootes, P. M., and Segl, M., 2003, Climate change at the 4.2 ka BP termination of the Indus valley civilization and Holocene south Asian monsoon variability: Geophysical Research Letters, v. 30, no. 8.

Stein, A. F., Draxler, R. R., Rolph, G. D., Stunder, B. J. B., Cohen, M. D., and Ngan, F., 2015, NOAA's HYSPLIT Atmospheric Transport and Dispersion Modeling System: Bulletin of the American Meteorological Society, v. 96, no. 12, p. 2059-2077.

Steinman, B. A., Abbott, M. B., Mann, M. E., Stansell, N. D., and Finney, B. P., 2012, 1,500 year quantitative reconstruction of winter precipitation in the Pacific Northwest: Proceedings of the National Academy of Sciences.

Tharammal, T., Paul, A., Merkel, U., and Noone, D., 2013, Influence of Last Glacial Maximum boundary conditions on the global water isotope distribution in an atmospheric general circulation model: Clim. Past, v. 9, no. 2, p. 789-809.

Thompson, D. W. J., and Wallace, J. M., 1998, The Arctic Oscillation signature in the wintertime geopotential height and temperature fields: Geophysical Research Letters, v. 25, no. 9, p. 1297-1300.

Trenberth, K. E., 1997, The definition of El Nino: Bulletin of the American Meteorological Society, v. 78, no. 12, p. 2771-2777.

Tripaldi, A., and Forman, S. L., 2007, Geomorphology and chronology of Late Quaternary dune fields of western Argentina: Palaeogeography Palaeoclimatology Palaeoecology, v. 251, no. 2, p. 300-320.

Trouet, V., and Taylor, A., 2010, Multi-century variability in the Pacific North American circulation pattern reconstructed from tree rings: Climate Dynamics, v. 35, no. 6, p. 953-963.

Turgeon, S., and Lundberg, J., 2001, Chronology of discontinuities and petrology of speleothems as paleoclimatic indicators of the Klamath Mountains, Southwest Oregon, USA: Carbonates and Evaporites, v. 16, no. 2, p. 153-167.

Vachon, R. W., Welker, J. M., White, J. W. C., and Vaughn, B. H., 2010a, Moisture source temperatures and precipitation delta O-18-temperature relationships across the United States: Water Resources Research, v. 46.

-, 2010b, Monthly precipitation isoscapes (delta O-18) of the United States: Connections with surface temperatures, moisture source conditions, and air mass trajectories: Journal of Geophysical Research-Atmospheres, v. 115.

Vachon, R. W., White, J. W. C., Gutmann, E., and Welker, J. M., 2007, Amount-weighted annual isotopic (delta O-18) values are affected by the seasonality of precipitation: A sensitivity study: Geophysical Research Letters, v. 34, no. 21.

van Beynen, P., Bourbonniere, R., Ford, D., and Schwarcz, H., 2001, Causes of colour and fluorescence in speleothems: Chemical Geology, v. 175, no. 3–4, p. 319-341.

Viau, A. E., Gajewski, K., Fines, P., Atkinson, D. E., and Sawada, M. C., 2002, Widespread evidence of 1500 yr climate variability in North America during the past 14 000 yr: Geology, v. 30, no. 5, p. 455-458.

Viau, A. E., Gajewski, K., Sawada, M. C., and Fines, P., 2006, Millennial-scale temperature variations in North America during the Holocene: Journal of Geophysical Research: Atmospheres, v. 111, no. D9, p. n/a-n/a.

Voelker, S. L., Stambaugh, M. C., Guyette, R. P., Feng, X., Grimley, D. A., Leavitt, S. W., Panyushkina, I., Grimm, E. C., Marsicek, J. P., Shuman, B., and Brandon Curry, B., 2015, Deglacial hydroclimate of midcontinental North America: Quaternary Research, v. 83, no. 2, p. 336-344.

Wahl, E. R., Diaz, H. F., and Ohlwein, C., 2012, A pollen-based reconstruction of summer temperature in central North America and implications for circulation patterns during medieval times: Global and Planetary Change, v. 84–85, no. 0, p. 66-74.

Wallace, J. M., and Gutzler, D. S., 1981, Teleconnections in the Geopotential Height Field during the Northern Hemisphere Winter: Monthly Weather Review, v. 109, no. 4, p. 784-812.

Wang, H., Stumpf, A. J., and Miao, X., 2013, Reply to comments by Curry et al. (2013) on "Atmospheric changes in North America during the last deglaciation from dune-wetland records in the Midwestern United States": Quaternary Science Reviews, v. 80, p. 200-203.

Wang, H., Stumpf, A. J., Miao, X., and Lowell, T. V., 2012, Atmospheric changes in North America during the last deglaciation from dune-wetland records in the Midwestern United States: Quaternary Science Reviews, v. 58, p. 124-134.

Wang, Y., 2013, Vegetation and climate changes at Spicer Lake, Indiana, during the Holocene: Master of Science, Department of Geography, University of Wisconsin-Madison: Madison, Wisconsin.

Wanner, H., Beer, J., Buetikofer, J., Crowley, T. J., Cubasch, U., Flueckiger, J., Goosse, H., Grosjean, M., Joos, F., Kaplan, J. O., Kuettel, M., Mueller, S. A., Prentice, I. C., Solomina, O., Stocker, T. F., Tarasov, P., Wagner, M., and Widmann, M., 2008, Mid- to Late Holocene climate change: an overview: Quaternary Science Reviews, v. 27, no. 19-20, p. 1791-1828.

Wanner, H., Solomina, O., Grosjean, M., Ritz, S. P., and Jetel, M., 2011, Structure and origin of Holocene cold events: Quaternary Science Reviews, v. 30, no. 21–22, p. 3109-3123.

Weiss, H., Courty, M.-A., Wetterstrom, W., Guichard, F., Senior, L., Meadow, R., and Curnow, A., 1993, The Genesis and Collapse of Third Millennium North Mesopotamian Civilization: Science, v. 261, no. 5124, p. 995-1004.

Welker, J. M., 2000, Isotopic (delta O-18) characteristics of weekly precipitation collected across the USA: an initial analysis with application to water source studies: Hydrological Processes, v. 14, no. 8, p. 1449-1464.

Welker, J. M., 2012, ENSO effects on delta O-18, delta H-2 and d-excess values in precipitation across the U.S. using a high-density, long-term network (USNIP): Rapid Communications in Mass Spectrometry, v. 26, no. 17, p. 1893-1898.

Whitaker, J. L., 2008, Orbital- to millennial-scale variability in Gulf of Mexico sea surface temperature and salinity during the late Pleistocene: Master of Science, College of Marine Science, University of South Florida, Tampa, FL.

Whitehead, D. R., Jackson, S. T., Sheehan, M. C., and Leyden, B. W., 1982, Late-glacial vegetation associated with caribou and mastodon in central Indiana: Quaternary Research, v. 17, no. 2, p. 241-257.

Williams, J. W., and Jackson, S. T., 2007, Novel climates, no-analog communities, and ecological surprises: Frontiers in Ecology and the Environment, v. 5, no. 9, p. 475-482.

Williams, J. W., Shuman, B., and Bartlein, P. J., 2009, Rapid responses of the prairie-forest ecotone to early Holocene aridity in mid-continental North America: Global and Planetary Change, v. 66, no. 3-4, p. 195-207.

Winkler, M. G., Swain, A. M., and Kutzbach, J. E., 1986, Middle Holocene dry period in the northern Midwestern United States: lake levels and pollen stratigraphy: Quaternary Research, v. 25, no. 2, p. 235-250.

Winnick, M. J., Chamberlain, C. P., Caves, J. K., and Welker, J. M., 2014, Quantifying the isotopic 'continental effect': Earth and Planetary Science Letters, v. 406, p. 123-133.

Wood, J. R., Forman, S. L., Everton, D., Pierson, J., and Gomez, J., 2010a, Lacustrine sediments in Porter Cave, Central Indiana, USA and possible relation to Laurentide ice sheet marginal positions in the middle and late Wisconsinan: Palaeogeography, Palaeoclimatology, Palaeoecology, v. 298, no. 3–4, p. 421-431.

Wood, J. R., Forman, S. L., Pierson, J., and Gomez, J., 2010b, New insights on Illinoian deglaciation from deposits of Glacial Lake Quincy, central Indiana: Quaternary Research, v. 73, no. 2, p. 374-384.

Worden, J., Noone, D., Bowman, K., and Tropospheric Emission, S., 2007, Importance of rain evaporation and continental convection in the tropical water cycle: Nature, v. 445, no. 7127, p. 528-532.

Wu, H., Zhang, X., Li, X., Li, G., and Huang, Y., 2015, Seasonal variations of deuterium and oxygen-18 isotopes and their response to moisture source for precipitation events in the subtropical monsoon region: Hydrological Processes, v. 29, no. 1, p. 90-102.

Yonge, C. J., Ford, D. C., Gray, J., and Schwarcz, H. P., 1985, Stable isotope studies of cave seepage water: Chemical Geology: Isotope Geoscience section, v. 58, no. 1–2, p. 97-105.

Zhang, R., Schwarcz, H. P., Ford, D. C., and Beddows, P. A., 2007, Paleoclimate variations from 0 to 12.3 ka BP inferred from three coeval calcite and aragonite speleothems from Marengo Cave, Indiana, USA: Geological Society of America Abstracts with Programs, v. 39, no. 6.

Zhu, J., and Liang, X.-Z., 2012, Impacts of the Bermuda High on Regional Climate and Ozone over the United States: Journal of Climate, v. 26, no. 3, p. 1018-1032.

APPENDIX ONE:

DESCRIPTIONS OF SAMPLED CAVES IN SOUTHERN INDIANA

This appendix contains physical descriptions of the environmental setting and appearance of the caves sampled in this dissertation research. It also includes specifics on stalagmite sampling locations and images from the caves.

Lower Porter Cave

US-INLP

Porter Cave (39.429°N 86.630°W, 230 masl) is located 9.2 km northeast of Gosport, IN, and consists of two sections with three known entrances. The lower section is the most known and heavily visited portion. The main entrance is a large opening (~3 m high by 10 m wide) on a limestone scarp at the head of a valley. The entrance is 8-10 m above the valley floor and clearly exposed. A small stream < 1 m deep flows throughout the lower cave portion and exits the main entrance as a waterfall. The cave is a major drainage channel for water during heavy rain and the stream can approach 2 m in depth and span most of the main passage. The cave is located on Devore Ridge which separates the Proglacial Lake Quincy deposits to the north from the West Fork of the White River Valley in the south. Several deeply incised valleys with misfit streams run N-S along Devore Ridge, created from drainage of Lake Quincy.

Much of Lower Porter Cave is a wide, apparently stream-cut channel at least 1 m wide and 3 m high. Only a single active flowstone deposit can be found immediately inside the entrance, but older and non-active flowstone deposits can be seen within 10 m of the entrance. Deeper in the cave, flowstone deposits of various ages decorate the walls of the passage. Most are inactive, but some are currently or

very recently active. These flowstones are largely over 1.5 m above the floor and out of the typical influence of the stream. No significant stalagmites are visible in Lower Porter Cave. The presence of perched sediments dating back to MIS 4 suggests that the cave is never completely flooded, and no large woody deposits or other signs of regular flooding are visible at levels higher than 2 m. Approximately 30 m into the cave, a large active flowstone deposit blocks the main route, and a large quantity of the stream flow passes over this flowstone. Beyond the large blocking flowstone, the passage continues until the stream emits from a passage too small for humans. Exit is possible at this point in a second entrance with a ladder.

Seven flowstone samples of both active and inactive deposits were collected at points stretching from the entrance to the passage blocking flowstone. A hammer and chisel broke off some deposits, although some older deposits were already loose and simply collected by hand. A small stalagmite, US-INLP10, was collected in a secondary passage running below the main passage that runs over the blocking flowstone. US-INLP10 was the only stalagmite-like speleothem seen in lower Porter Cave, although it grew nearly on the base level within 1 m of the stream. During high water events, US-INLP10 certainly was covered by water. Although uniquely stalagmite-type, US-INLP10 was still small, non-descript, and very much out of view of any visitors to the cave, and collection of this stalagmite was not seen as impacting the aesthetics of Porter Cave at all. Lower Porter Cave was visited multiple times for sampling and monitoring purposes from July 2013 through April 2016.

Two climate data loggers were placed in Lower Porter Cave in December 2014: one in a side alcove ~10 m from the entrance and the other on a shelf above the blocking waterfall. The entrance logger was missing upon attempted retrieval in June 2015. Lower Porter Cave is not open to visitors, but appears heavily used by locals and the loss of the data loggers within, while unexpected, is not surprising. A chance discussion with local boys in Lower Porter Cave suggests at least the near-entrance data logger was present until nearly the retrieval date as the boys mentioned recently seeing a ‘camera’

(mistaken identity because of the blinking LED on the logger) at the logger site only a few weeks prior. The local boys insisted they did not disturb the logger, but it is likely some cave visitor removed this logger and perhaps the other logger deeper in the cave. Alternatively, the deeper logger may have been knocked into the stream or flooded away during the major June 2015 flood event. This logger's disappearance is not verified, as travel to the logger site was blocked by floodwaters on the June 2015 trip, but the boys mentioned to never have seen any 'camera' in that area. While the logger was somewhat camouflaged, it seems likely that these boys would have seen the logger if it still had been present. A cursory search of the stream bed outside the cave entrance did not reveal the loggers. A final trip to Lower Porter Cave is scheduled for late spring 2016 with priority on verifying the loss of the second logger.

Upper Porter Cave

US-INUP

The upper portion of Porter Cave is hydrologically linked to the lower portion, but direct human travel between the two is not possible. Upon exiting the second entrance of the lower portion, a relatively short (~300 m) walk through a dry streambed leads to a third entrance. This entrance, the only entrance to Upper Porter Cave, lies at the end of a dry stream channel. A nearly horizontal passage extends from the cave entrance for ~10 m and is choked with large amounts of washed-in woody debris. Some of the wood is quite large (>3 m in length, 30 cm diameter), and their presence along with tires and plastic barrels indicates that flow rates into the cave can be quite high, presumably during storm events.

A small opening (~1 m wide by 0.5 m tall) on the right side of the opening passage leads to a wet and stream-cut portion. This portion is initially quite wide (~3 m) but only ~0.75 m tall. This low ceiling necessitates crawling for ~10 m, half of which is in water. Eventually, the passage opens up into a

keyhole-style passage with a walking path usually <1 m wide. The ceiling is quite high (>5 m) and typically one or both sides of the passage has elevated terraces ~2 m above the passage floor. Small stalagmites are present along these terraces. None of the formations appear currently active, although the presence of drip water indicates that some may simply be slowly growing. In general, speleothems are relatively sparse and no major flowstone or draperies are present.

This keyhole passage eventually ceases to travel through terraces with speleothems, and was thus no longer traveled by this author. However, testimony from a fellow caver indicates that the passage simply ceases to become navigable beyond the stalagmite terrace area. Presumably, the stream travels from the end of Upper Porter Cave and later emerges near the secondary entrance to Lower Porter Cave. Sticks are wedged in multiple places near the highest ceilings of Upper Porter Cave, and a tire was found relatively deep along the main passage near the stalagmite terraces. High water flows must nearly fill the entire passage at times, though it is unclear how often this happens. High floods do not appear to be too frequent, since the speleothems appear relatively unmarred, but much of the wood and organic debris wedged in the cave appears fairly fresh, and the tire was relatively recent in make (<50 years).

Approximately halfway through the passage with stalagmite terraces, three stalagmites in close proximity to each other (US-INUP3, US-INUP4, US-INUP7) were collected from a terrace ~2 m above the main passage's floor in July 2013. The cave ceiling is less than 1 m above the terrace level at the stalagmite collection location. US-INUP3 and US-INUP4 were the largest stalagmites seen in the cave, although they were not significantly larger than other stalagmites not collected. US-INUP7 was a small stalagmite adjacent to US-INUP4 and collected along with US-INUP4 as a single piece. Due to the difficulty in accessing Upper Porter Cave, the only visit made was the original stalagmite sampling trip in July 2013.

Johnson Cave

US-INJN

Johnson Cave (38.734°N, 86.370°W, 205 masl) is a privately-owned cave located 4 km east of Spring Mill State Park, Mitchell, IN. The cave entrance was not accessible to humans until 2004 when the then-owner removed boulders from the entrance with a tractor. The entrance is small (<1 m high and <1.5 m wide) and drops along a slope approximately 2-3 m until reaching a passage floor. The main cave path is a stream cut, keyhole-type passage extending back >50 m with few side branches and little speleothem development. Near the end of the cave, a small room is adjacent to the main passage with a floor elevated 2 m above the passage floor. This room's ceiling is <2 m above the room floor, and some limited stalagmite growth is present throughout the room and along the periphery. A major fracture flow of water exists along a penetrating root.

None of the speleothems in Johnson Cave appear actively growing. Two stalagmites (US-INJN1 and US-INJN2) were collected from the stalagmite room in July 2013. US-INJN1 is a very symmetrical stalagmite that grew near the rear intersection of the room ceiling and floor. US-INJN2 grew in the middle of the room only 15 cm from another stalagmite left uncollected. A small drapery-like stalactite with twin points exists above US-INJN2 and its adjacent stalagmite. A soda straw and small, cap-like floor deposit were collected in June 2015 in an attempt to get a modern speleothem sample, but the cap-like formation shows signs of apex dissolution and was likely inactive and relatively old when sampled.

A climate data logger was placed in Johnson Cave at the sampling location of US-INJN2 in December 2014, but the logger was missing upon attempted retrieval in June 2015. The loss of the Johnson Cave logger is a surprise as this cave has restricted-access and is on private property. The data logger was placed well above any potential flood levels, and no signs of unexpected surface flow were seen at the logger’s former location. A search of where the logger potentially may have rolled if disturbed did not reveal the logger.

Roadcut Cave

US-INRC

Roadcut Cave (38.830°N, 86.507°W, 170 m masl) is a small cave exposed along the base of a road cut limestone scarp on the right side of southbound US 50 south of Bedford, IN. The entrance is very small (0.5 m high, 1 m wide) and remains that small for 2 m into the cave. This entrance was dug out and enlarged by Dave Everton in 200X. After navigating the initial tight entrance squeeze, the cave opens slightly into a passage 1 m wide and 1.5 m tall. This appears to be the top of a keyhole-type passage, with the lower portion of the passage too narrow to reach. The cave is <15 m long, and air quality seems poor due to high CO_2 and/or trapped automobile exhaust. Some stalagmite growth is evident on the walls and projecting shelves. Most surfaces in the cave were covered in a layer of wet clay sediment.

Three stalagmites were collected from Roadcut Cave on December 12, 2014. All three stalagmites were located within a 3 m stretch of the cave near the end of the passage (at least the portion navigable by humans). US-INRC11 was collected from an open shelf on the south side of the passage and was the farthest stalagmite from the entrance. US-INRC12 was a small stalagmite growing on a projecting shelf on the north side of the passage over a narrow slot in the passage floor of unknown depth (>2 m). US-INRC13 was a medium-sized stalagmite growing on the south side of the main passage floor. Although covered in clay mud and notably irregular in shape, the light from a flashlight clearly illuminated the stalagmite, suggesting a clean, detritus-free formation. A broken stalagmite was discovered laying in sediment along the passage floor, but was not removed from the cave because the gear pack was already full and quite heavy for the arduous crawl back out. A future trip in 2016 may collect this stalagmite as well as look for other potential specimens not collected in the initial, somewhat hasty sampling trip. This cave is ideal for speleothem sampling because it was likely completely sealed

from the surface until the creation of the road cut. Additionally, aesthetic impacts from speleothem removal are limited since the cave hosts little to no human visitors and is little more than a wide fracture in the bedrock.

Indiana Caverns

US-INIC

Indiana Caverns (38.183°N 86.150°W, 210 masl) is a tourist cave portion of the Binkley Cave system located 4 km southwest of Corydon, IN. At 68.4 km of mapped passages, Binkley Cave is the 7th longest cave system in the United States and the longest in Indiana. Active mapping is ongoing, and water flows and air movement suggest a very large amount of cave remains undiscovered. Geological details and a history of Binkley Cave exploration can be found in XXXXX. Indiana Caverns began with the discovery of a large bone deposit found in a large room deep within Binkley Cave. Access to the bones initially required a long 4+ hour trip from the nearest entrance, but a later shortcut enabled a paleontologist to review the bones. The bulk of bones are from the extinct flat-headed peccary (*Playgonus compressus*), although bear, bison, and many smaller animal bones have also been identified. Bear wallows and claw marks are also evident in the mud banks along a cave stream. Two bones have been radiocarbon dated to 40695-41865 cal yr BP (black bear) and 38060-42760 cal yr BP (peccary). A large entrance to the surface apparently existed in or near the bone room in the Late Pleistocene, but became blocked and filled later. The lack of any human artifacts suggests entrance closure occurred prior to the Holocene. Current access to this portion of Binkley Cave is by means of a tunnel bored through the limestone bedrock. Much of the bone room is now a tourist attraction with improved walkways and guided tours.

Stalagmites were collected from three areas accessed through Indiana Caverns. The first two stalagmites were collected in June 2013 in a speleothem-decorated room off one of the main cave

passages leading away from the Indiana Caverns portion of Binkley Cave. This room is accessed by kayaking down a passage partially flooded for the tourist cave and then walking along a large (usually at least 5 m wide by 4 m tall) stream passage for a significant distance (at least 200 m). A small side passage is present on the left side of the main passage. Crawling is necessary for a brief distance in the side passage (~10 m) before opening into a small room. US-INIC5 was collected on a large breakdown boulder, and the non-perpendicular angle of the stalagmite suggests that the breakdown has shifted or fallen since the stalagmite stopped growing. US-INIC6 was found growing on the room floor near the rear of the room. US-INIC6 was difficult to remove, and unfortunately a large portion of the base was left behind. A climate data logger was left in this room from December 2014 to June 2015. Upon recovery of the data logger, the stalagmite US-INIC15 was found lying with other breakdown rubble in the room. This stalagmite clearly grew on the edge of a projecting shelf, as indicated by the drapery deposit located below the stalagmite proper, and a secondary stalagmite was also found on the same breakdown piece 10 cm from US-INIC15. This secondary stalagmite was largely filled with detritus and not removed from the cave.

Speleothem growth is also found on a sediment slope along the main cave passage after the kayaking portion but before entering the small side passage. Most of these formations are either too large or too small for sampling, but stalagmite US-INIC14 was collected from this area in June 2015. Although small, this stalagmite was pristinely white, translucent, and appeared to be actively growing in contrast to nearly every other stalagmite seen in any Indiana cave. Although this stalagmite was noted on the first sampling trip to Indiana Caverns, it was not collected until the last sampling trip in the hopes it could provide a modern calcite record.

Initial disappointment with the age ranges of the first set of stalagmites collected from Indiana led to a second sampling trip to Indiana Caverns on June 20, 2014. A drainage chute (1 m tall by 1.5 m wide) off part of the tourist path contains several large stalagmites growing along the chute's wall.

Water drains from this level of the cave into a lower level, and the chute is likely a fairly geologically-recent creation. A broken stalagmite piece was found in the stream and named US-INIC8. The large stalagmite US-INIC9, connected to the ceiling by a cemented soda straw, was removed in whole.

APPENDIX TWO:

MOISTURE SOURCE ANALYSIS DATA FOR INDIVIDUAL USNIP SITES

This appendix contains tables of meteorological and isotopic data calculated during moisture source analysis for each of the seven USNIP sites studied. Note that deuterium and *d-excess* values are included here for reference, although they are not covered in Chapter 4.

Table A2.1. Mean values for meteorological and isotopic variables per moisture source for IL78. Shading identifies lower (blue) and higher (red) values per column.

IL78		***Mean Values***					
Moisture Source	***n***	***PDa (mm)***	***PDt (°C)***	***$\delta^{18}O$ (‰)***	***δD (‰)***	***d-excess (‰)***	***$\delta^{18}O$ vs. PDt Residual***
Gulf of Mexico	27	39.5	16.8	-5.84	-32.51	14.19	0.34
Pacific	1	6.4	8.1	-9.35	-57.82	16.98	-0.34
Arctic	0	—	—	—	—	—	—
Mid-Atlantic	0	—	—	—	—	—	—
C-South	5	11.7	7.9	-8.84	-56.05	14.67	0.21
C-Southwest	0	—	—	—	—	—	—
C-West	1	23.9	3.1	-16.70	-120.69	12.91	-6.09
C-Midwest	5	9.4	8.8	-8.66	-57.05	12.23	0.11
C-North	2	5.6	7.2	-10.34	-66.45	16.31	-1.06
Gulf of Mexico + C-South	41	32.6	14.2	-6.68	-39.42	14.05	0.33
All Continental	16	14.8	8.2	-9.26	-61.01	13.08	-0.28
All Continental - C-South	6	11.8	7.9	-10.00	-67.66	12.34	-0.92

Table A2.2. Mean values for meteorological and isotopic variables per moisture source for IN22. Shading identifies lower (blue) and higher (red) values per column.

IN22		***Mean Values***					
Moisture Source	***n***	***PDa (mm)***	***PDt (°C)***	***$\delta^{18}O$ (‰)***	***δD (‰)***	***d-excess (‰)***	***$\delta^{18}O$ vs. PDt Residual***
Gulf of Mexico	132	35.8	15.3	-5.44	-31.30	12.22	0.52
Pacific	10	9.7	6.2	-7.98	-51.88	11.96	0.07
Arctic	0	—	—	—	—	—	—
Mid-Atlantic	4	12.4	14.7	-7.05	-44.19	12.21	-0.96
C-South	17	24.2	13.5	-6.98	-42.24	13.60	-0.60
C-Southwest	3	10.3	18.9	-6.12	-36.89	12.07	-0.98
C-West	5	18.7	19.7	-4.60	-24.81	11.99	0.37
C-Midwest	5	10.1	20.6	-5.13	-28.16	12.85	-0.36
C-North	3	9.7	16.4	-6.43	-39.59	11.85	-0.70
Gulf of Mexico + C-South	160	35.5	14.9	-5.71	-33.27	12.43	0.35
All Continental	38	18.2	15.6	-7.09	-43.59	13.10	-1.20
All Continental - C-South	13	13.4	19.9	-5.15	-28.89	12.34	-0.22

Table A2.3. Mean values for meteorological and isotopic variables per moisture source for MN27. Shading identifies lower (blue) and higher (red) values per column.

MN27		***Mean Values***					
Moisture Source	***n***	***PDa (mm)***	***PDt (°C)***	***$\delta^{18}O$ (‰)***	***δD (‰)***	***d-excess (‰)***	***$\delta^{18}O$ vs. PDt Residual***
Gulf of Mexico	13	33.0	17.4	-7.10	-42.98	13.86	-0.27
Pacific	5	6.4	3.5	-13.38	-102.24	4.80	-1.15
Arctic	3	8.1	11.9	-14.33	-108.17	6.44	-5.34
Mid-Atlantic	0	—	—	—	—	—	—
C-South	4	25.1	3.7	-12.80	-89.01	13.43	-0.64
C-Southwest	0	—	—	—	—	—	—
C-West	5	13.5	14.9	-9.89	-68.24	10.90	-2.09
C-Midwest	6	21.6	9.8	-9.01	-59.28	12.82	0.79
C-North	2	27.1	17.4	-6.59	-40.65	12.03	0.25
Gulf of Mexico + C-South	19	31.7	14.9	-8.20	-51.66	13.96	-0.39
All Continental	19	18.6	8.5	-10.65	-72.48	12.70	-0.34
All Continental - C-South	12	17.0	12.3	-9.34	-63.31	11.39	-0.54

Table A2.4. Mean values for meteorological and isotopic variables per moisture source for NC35. Shading identifies lower (blue) and higher (red) values per column.

NC35		***Mean Values***					
Moisture Source	***n***	***PDa (mm)***	***PDt (°C)***	***$\delta^{18}O$ (‰)***	***δD (‰)***	***d-excess (‰)***	***$\delta^{18}O$ vs. PDt Residual***
Gulf of Mexico	18	27.3	18.2	-4.93	-25.70	13.71	-0.44
Pacific	0	—	—	—	—	—	—
Arctic	1	2.8	-0.3	-7.18	-33.39	24.05	-0.06
Mid-Atlantic	18	25.9	14.3	-5.56	-31.21	13.27	-0.52
C-South	3	15.0	16.2	-3.17	-13.75	11.64	1.59
C-Southwest	0	—	—	—	—	—	—
C-West	0	—	—	—	—	—	—
C-Midwest	0	—	—	—	—	—	—
C-North	0	—	—	—	—	—	—
Gulf of Mexico + C-South	22	27.6	18.2	-4.78	-24.98	13.27	-0.30
All Continental	5	35.6	16.6	-3.55	-16.33	12.07	1.16
All Continental - C-South	0	—	—	—	—	—	—

Table A2.5. Mean values for meteorological and isotopic variables per moisture source for NE99. Shading identifies lower (blue) and higher (red) values per column.

NE99		***Mean Values***					
Moisture Source	***n***	***PDa (mm)***	***PDt (°C)***	***$\delta^{18}O$ (‰)***	***δD (‰)***	***d-excess (‰)***	***$\delta^{18}O$ vs. PDt Residual***
Gulf of Mexico	11	33.7	15.3	-9.65	-65.00	12.22	-1.47
Pacific	5	11.1	5.4	-10.99	-79.98	7.94	0.59
Arctic	0	—	—	—	—	—	—
Mid-Atlantic	0	—	—	—	—	—	—
C-South	5	13.8	15.9	-8.77	-61.58	8.56	-0.78
C-Southwest	6	14.1	20.1	-6.74	-47.45	6.49	-0.22
C-West	3	21.6	13.1	-13.64	-99.35	9.77	-4.71
C-Midwest	4	12.4	5.5	-12.18	-84.88	12.56	-0.63
C-North	0	—	—	—	—	—	—
Gulf of Mexico + C-South	16	27.5	15.5	-9.38	-63.93	11.08	-1.26
All Continental	24	14.7	13.9	-9.34	-65.62	9.10	-0.66
All Continental - C-South	16	15.0	13.6	-9.88	-69.39	9.67	-1.10

Table A2.6. Mean values for meteorological and isotopic variables per moisture source for PA15. Shading identifies lower (blue) and higher (red) values per column.

PA15		***Mean Values***					
Moisture Source	***n***	***PDa (mm)***	***PDt (°C)***	***$\delta^{18}O$ (‰)***	***δD (‰)***	***d-excess (‰)***	***$\delta^{18}O$ vs. PDt Residual***
Gulf of Mexico	6	25.8	13.6	-7.26	-43.92	14.13	0.36
Pacific	0	—	—	—	—	—	—
Arctic	0	—	—	—	—	—	—
Mid-Atlantic	1	14.0	5.8	-7.21	-46.53	11.15	2.95
C-South	1	22.1	3.7	-7.70	-34.66	26.94	3.13
C-Southwest	0	—	—	—	—	—	—
C-West	0	—	—	—	—	—	—
C-Midwest	1	18.3	19.9	-6.77	-40.03	14.13	-1.19
C-North	0	—	—	—	—	—	—
Gulf of Mexico + C-South	7	25.3	12.2	-7.32	-42.60	15.96	0.76
All Continental	5	22.9	7.6	-10.52	-64.40	19.79	-0.94
All Continental - C-South	1	18.3	19.9	-6.77	-40.03	14.13	-1.19

Table A2.7. Mean values for meteorological and isotopic variables per moisture source for WI36. Shading identifies lower (blue) and higher (red) values per column.

WI36		***Mean Values***					
Moisture Source	***n***	***PDa (mm)***	***PDt (°C)***	***$\delta^{18}O$ (‰)***	***δD (‰)***	***d-excess (‰)***	***$\delta^{18}O$ vs. PDt Residual***
Gulf of Mexico	10	19.6	10.1	-8.01	-51.08	13.02	2.35
Pacific	2	7.0	-7.2	-23.16	-173.20	12.03	-5.80
Arctic	1	14.7	12.4	-13.04	-96.27	8.05	-3.60
Mid-Atlantic	0	—	—	—	—	—	—
C-South	8	11.5	8.6	-10.60	-70.29	14.47	0.40
C-Southwest	0	—	—	—	—	—	—
C-West	1	6.9	-4.6	-17.17	-124.80	12.56	-0.88
C-Midwest	12	13.0	8.7	-12.39	-86.45	12.67	-1.44
C-North	2	5.4	0.5	-20.48	-149.97	13.83	-6.21
Gulf of Mexico + C-South	21	18.4	9.7	-9.03	-58.61	13.63	1.51
All Continental	30	16.1	6.2	-13.32	-93.38	13.15	-1.38
All Continental - C-South	17	14.3	6.5	-13.68	-97.02	12.44	-1.85

APPENDIX THREE:

COMPARATIVE IMAGE EXAMPLES OF HYSPLIT ENSEMBLE TRAJECTORIES AND COINCIDING WEATHER RADAR IMAGERY

This appendix contains pairs of images showing the weather radar over the United States during times of HYSPLIT model initiation. These selected images offer examples of how radar was used to understand HYSPLIT back trajectories in terms of synoptic-scale weather patterns.

Gulf Moisture Source

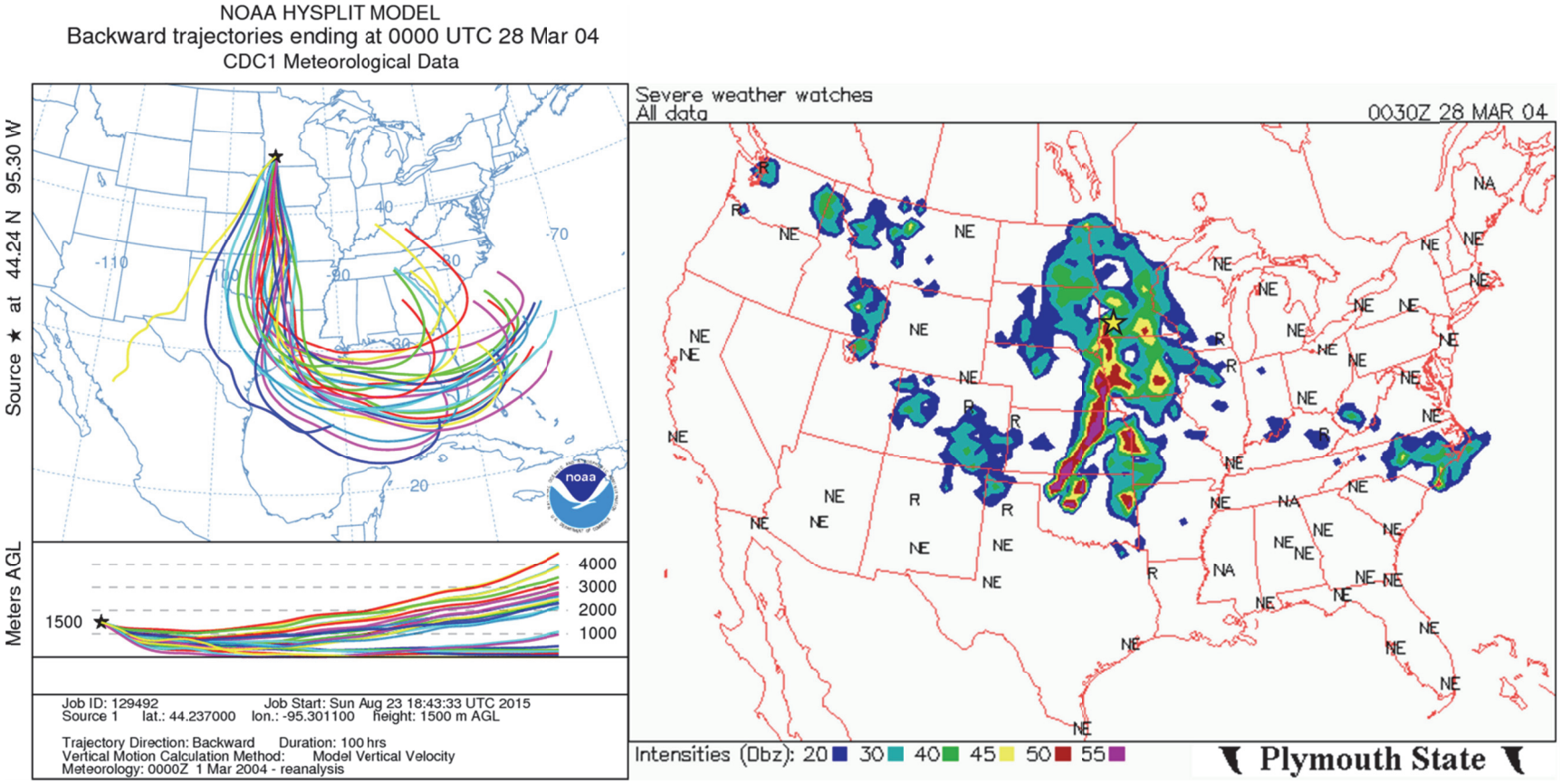

Figure A3.1. Gulf of Mexico moisture source determined for MN27 on March 28, 2004. HYSPLIT trajectories agree on a southerly advection from the Gulf of Mexico. RADAR indicates MN27 is in the warm sector of an extratropical cyclone ahead of an approaching cold front.

Gulf Moisture Source

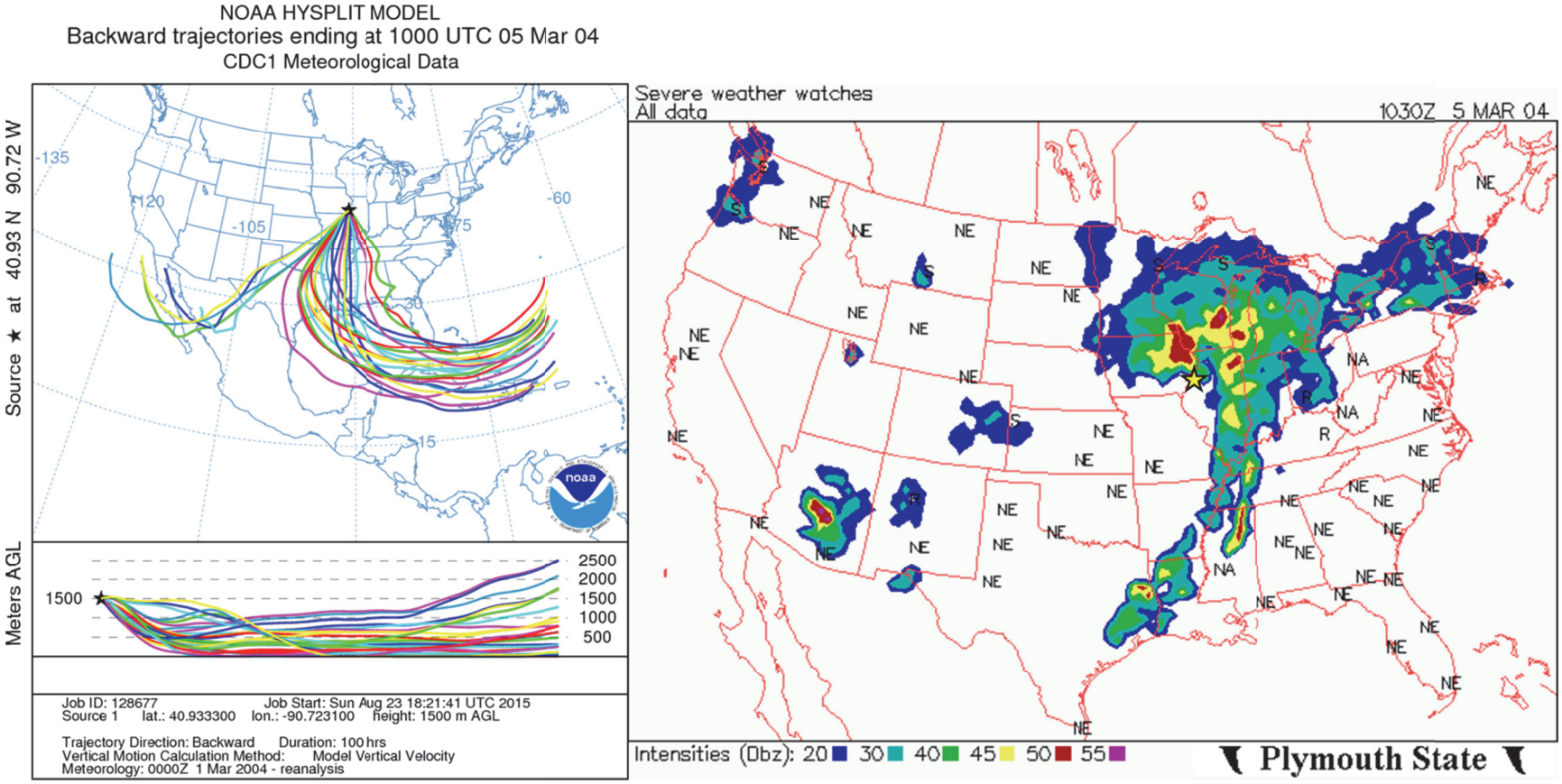

Figure A3.2. Gulf of Mexico moisture source determined for IL78 on March 5, 2004. HYSPLIT trajectories agree on a southerly advection from the Gulf of Mexico aside from a five western trajectories. RADAR indicates the recent passage of an extratropical cyclone cold front which supports the previous Gulf moisture advection. The five western trajectories are likely tracking the incoming air mass behind the cold front.

Pacific Moisture Source

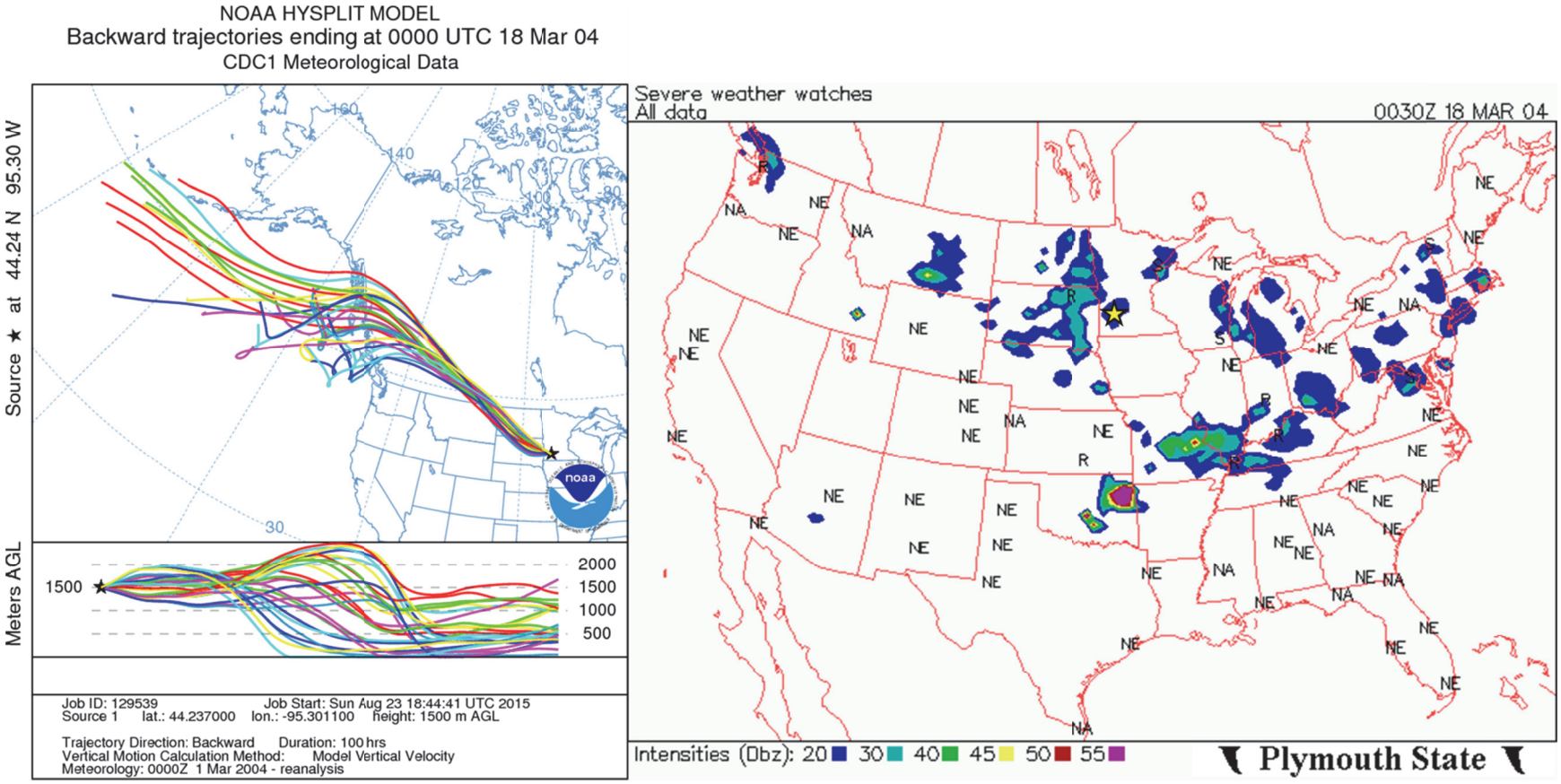

Figure A3.3. Pacific moisture source determined for MN27 on March 18, 2004. HYSPLIT trajectories agree on a westerly advection from the Pacific Northwest. RADAR indicates the present of light precipitation. Combined with daily temperatures below freezing, this suggests series of snow showers coming from the northwest.

Arctic Moisture Source

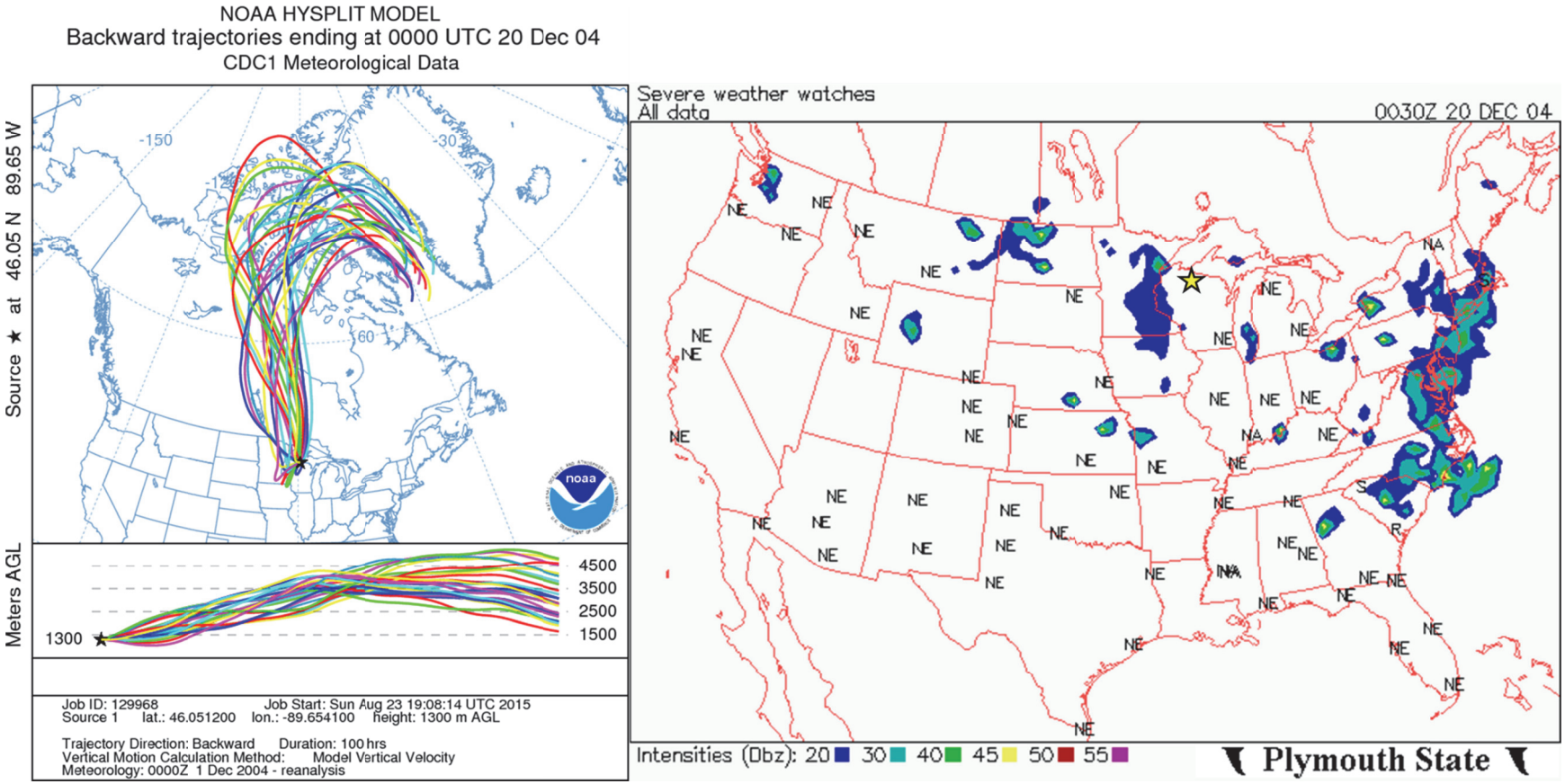

Figure A3.4. Pacific moisture source determined for WI36 on December 20, 2004. HYSPLIT trajectories agree on a northerly advection from the Canadian Archipelago. RADAR indicates the present of light precipitation. Combined with daily temperatures below freezing, this suggests series of snow showers coming from the north and northwest

.

Mid-Atlantic Moisture Source

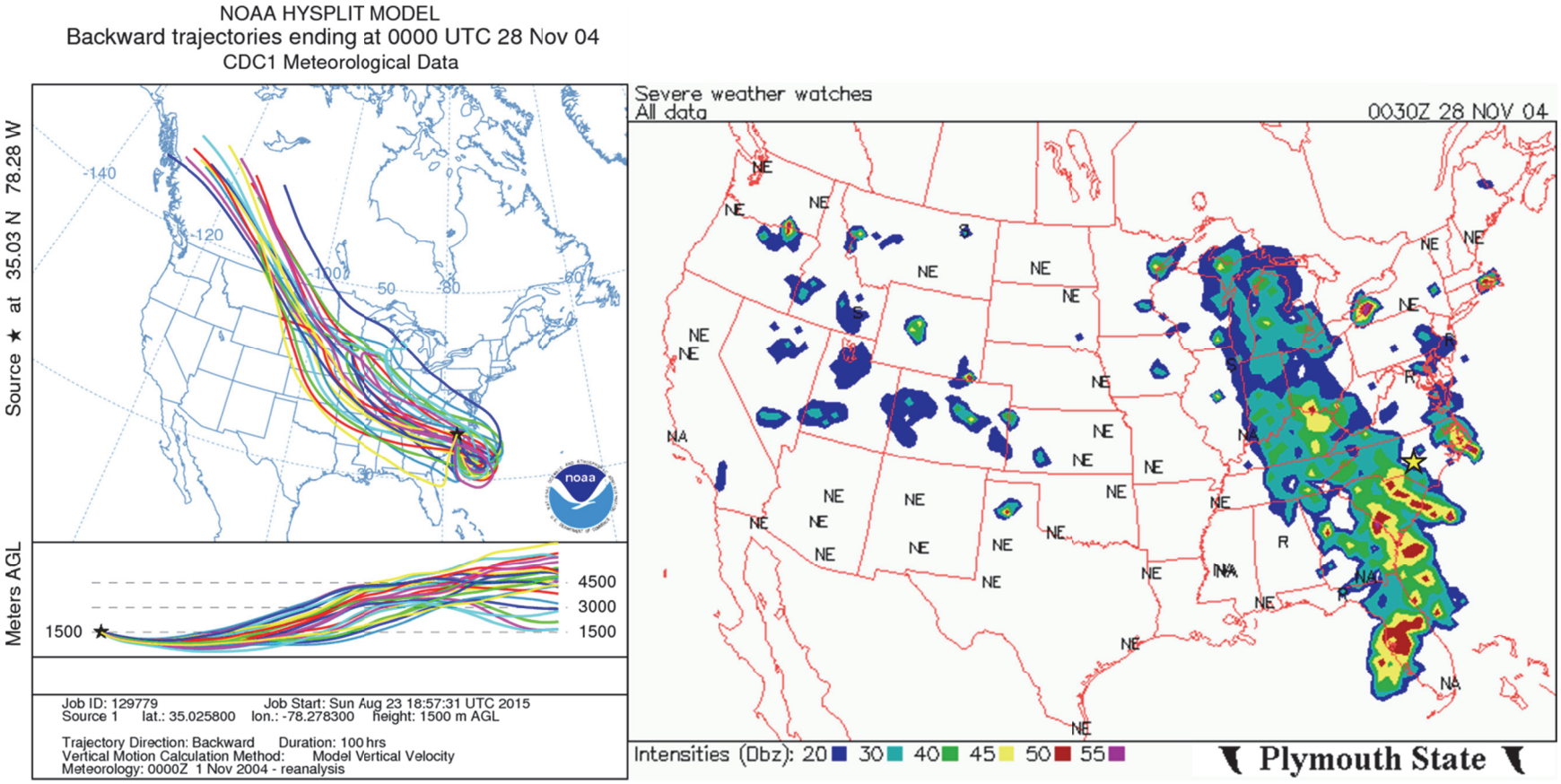

Figure A3.5. Mid-Atlantic moisture source determined for NC35 on November 28, 2004. HYSPLIT trajectories agree on a southerly advection from just offshore in the Atlantic. Note that the drop below the boundary level occurs very quickly which indicates the moisture retrieval came shortly before precipitation. The long tail of trajectories from the northwest represents pre-moisture source time. RADAR indicates the approach of heavy precipitation likely associated with an extratropical cyclone cold front. While this synoptic setup typically produces Gulf of Mexico moisture source assignments for the study region, the position of NC35 relative to the Atlantic Ocean coast draws Atlantic moisture from southerly advection, not Gulf of Mexico moisture.

Continental-South Moisture Source

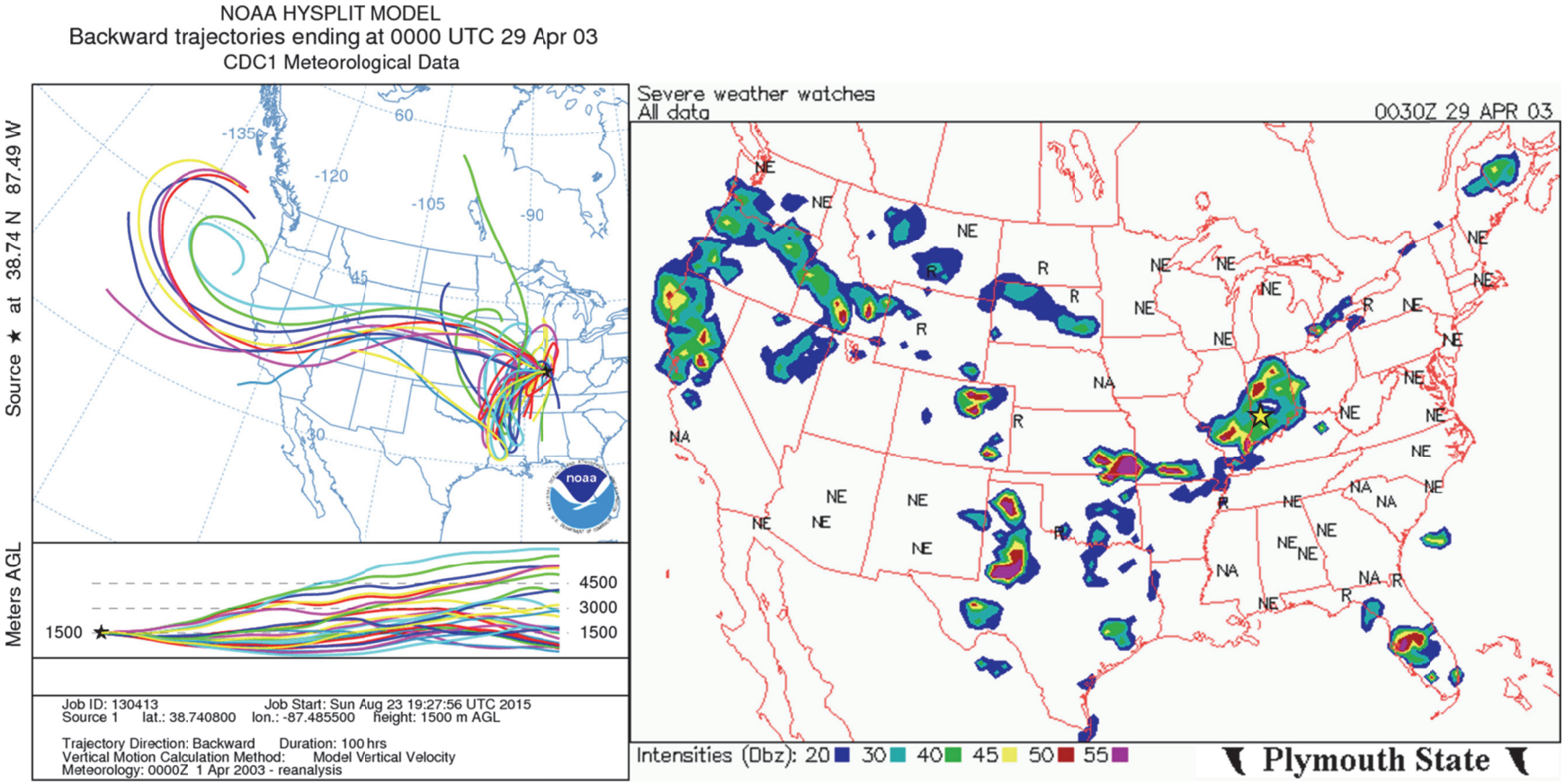

Figure A3.6. Continental-south moisture source determined for IN22 on April 29, 2003. HYSPLIT trajectories are somewhat unclear (as is common with continental assignments) but trajectories dropping below the boundary level do so over Arkansas and Louisiana. Pacific trajectories are linked to upper level circulation and are not indicative of moisture source. RADAR indicates locally heavy precipitation that may be the result of a stationary front or mesoscale convective complex; actual moisture is probably Gulf of Mexico derived with evapotranspiration additions.

Continental-South Moisture Source

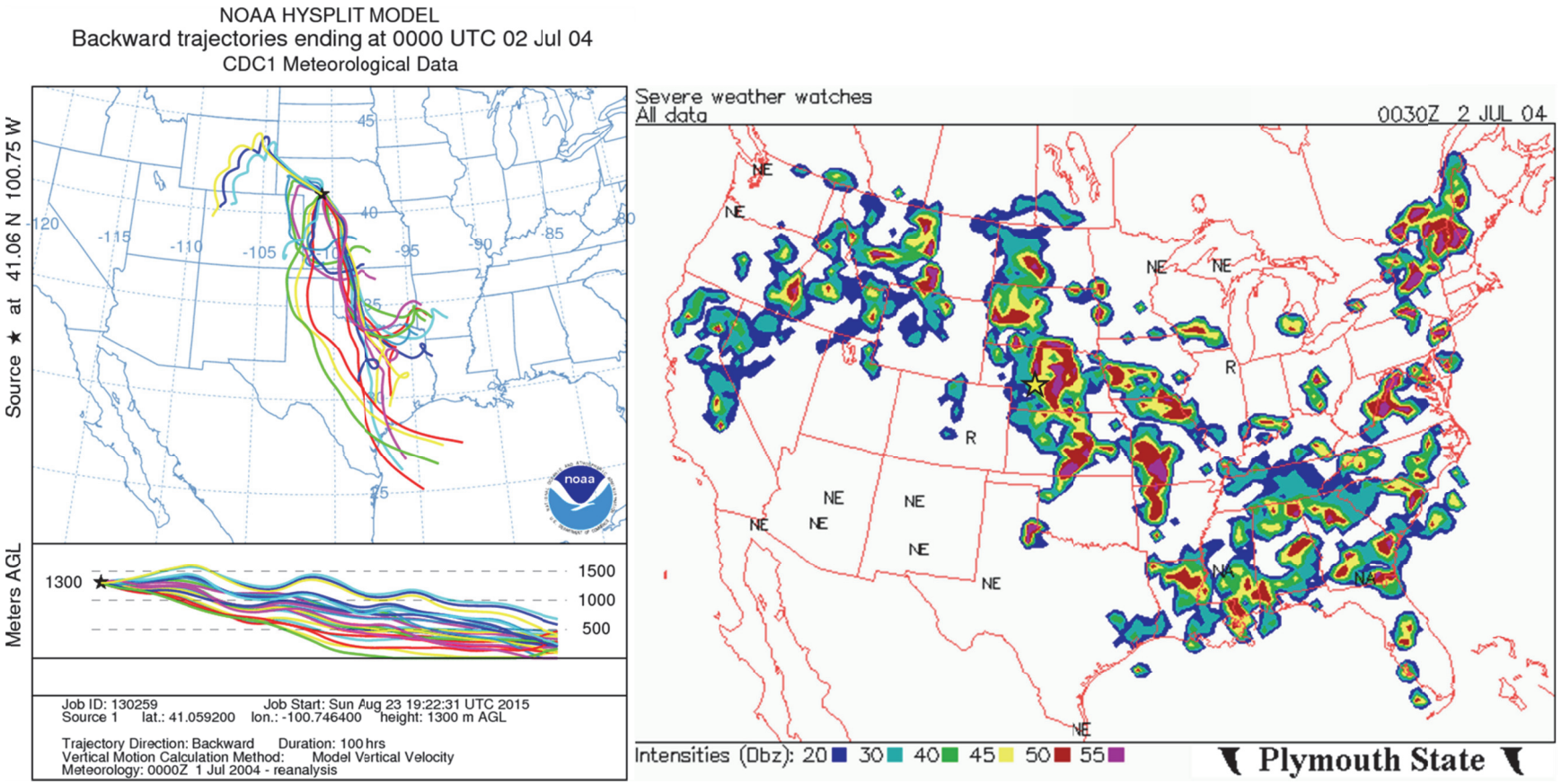

Figure A3.7. Continental-south moisture source determined for NE99 on July 2, 2004. HYSPLIT trajectories are somewhat unclear (as is common with continental assignments) but generally end on land to the south of NE99. The limited distance traveled in 100 hours suggests a locally source moisture with slow rates of advection. RADAR indicates locally heavy precipitation that may be from local summer convection or a mesoscale convective complex; actual moisture is probably originally Gulf of Mexico derived with evapotranspiration additions.

Continental-Southwest Moisture Source

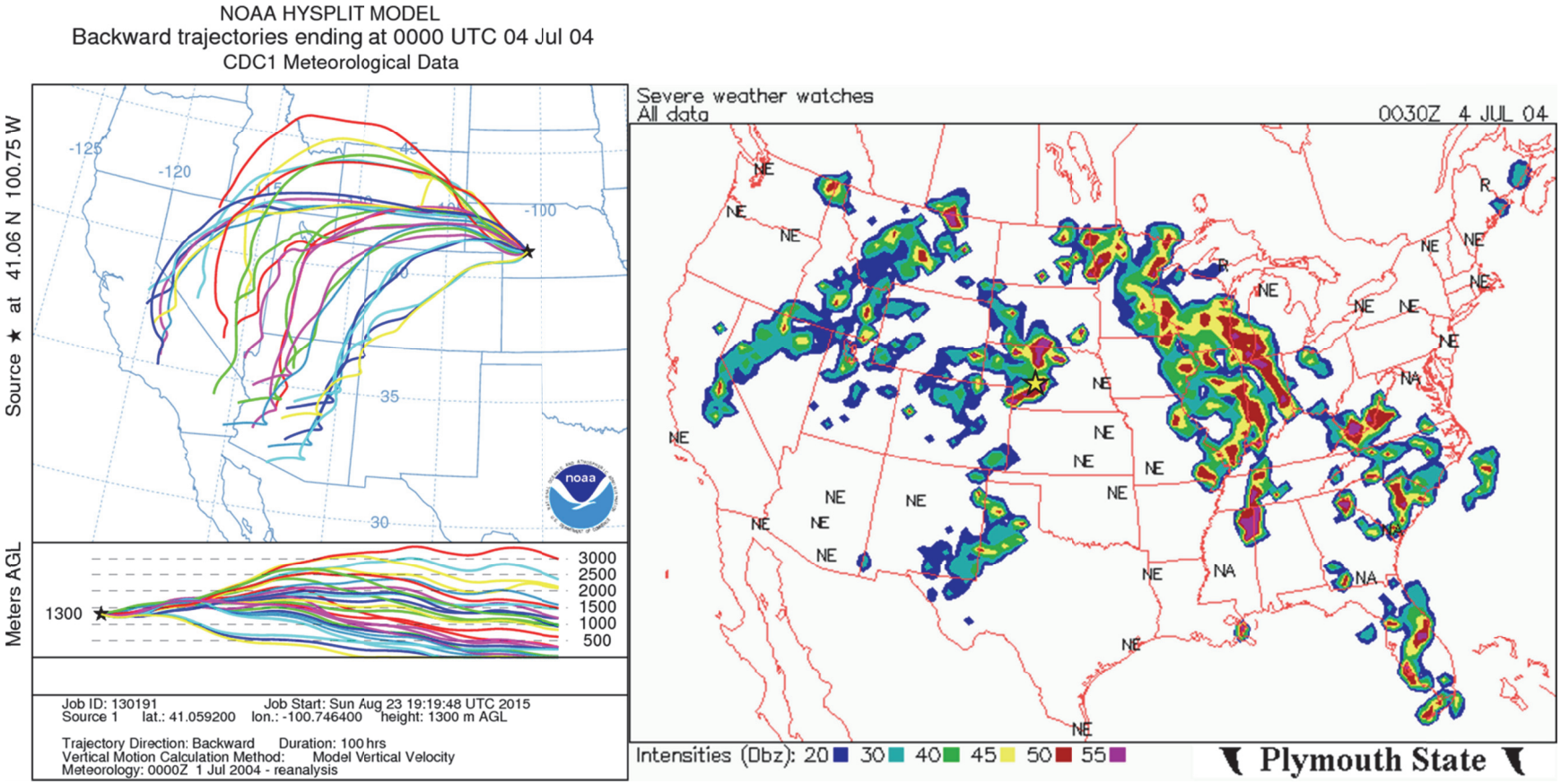

Figure A3.8. Continental-southwest moisture source determined for NE99 on July 4, 2004. HYSPLIT trajectories track to the desert southwest: an unlikely source of any moisture. Trajectories are more likely tracking the source of the disturbance that gave rise to the precipitation. RADAR indicates locally heavy precipitation that may be from local summer convection or a mesoscale convective complex; actual moisture is probably originally Gulf of Mexico derived with evapotranspiration additions.

Continental-West Moisture Source

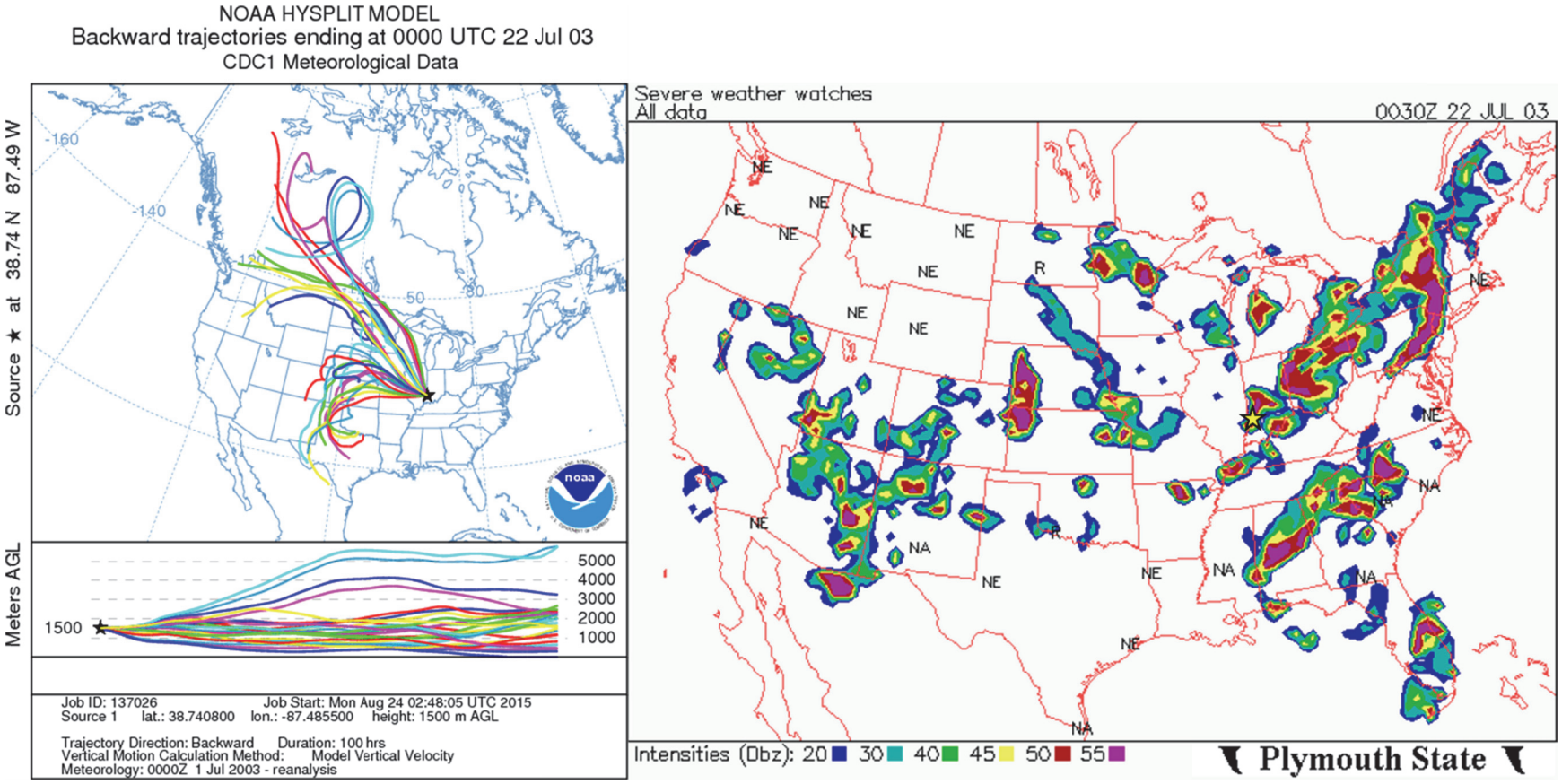

Figure A3.9. Continental-west moisture source determined for IN22 on July 22, 2003. Lower level HYSPLIT trajectories track to the western Great Plains. RADAR indicates locally heavy precipitation that may be from a passing extratropical cyclone, trough, or a mesoscale convective complex; actual moisture is probably originally Gulf of Mexico derived with evapotranspiration additions. Western trajectories may be a result of timing after the squall line passage.

Continental-Midwest Moisture Source

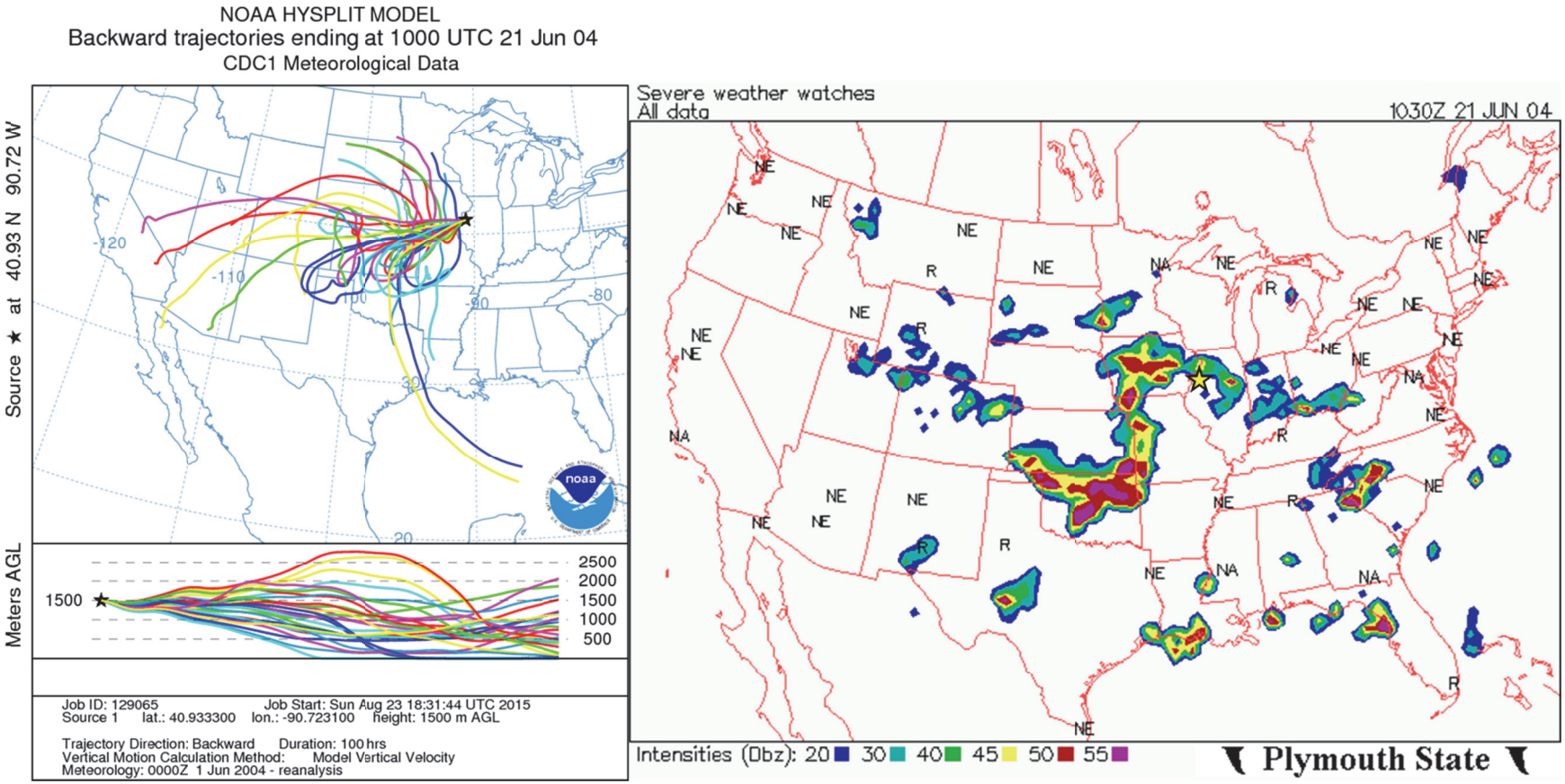

Figure A3.10. Continental-midwest moisture source determined for IL78 on June 21, 2004. HYSPLIT trajectories drop below the boundary level largely over Missouri and Kansas. RADAR indicates precipitation possibly associated with a warm front of an extratropical cyclone.

Continental-Midwest Moisture Source

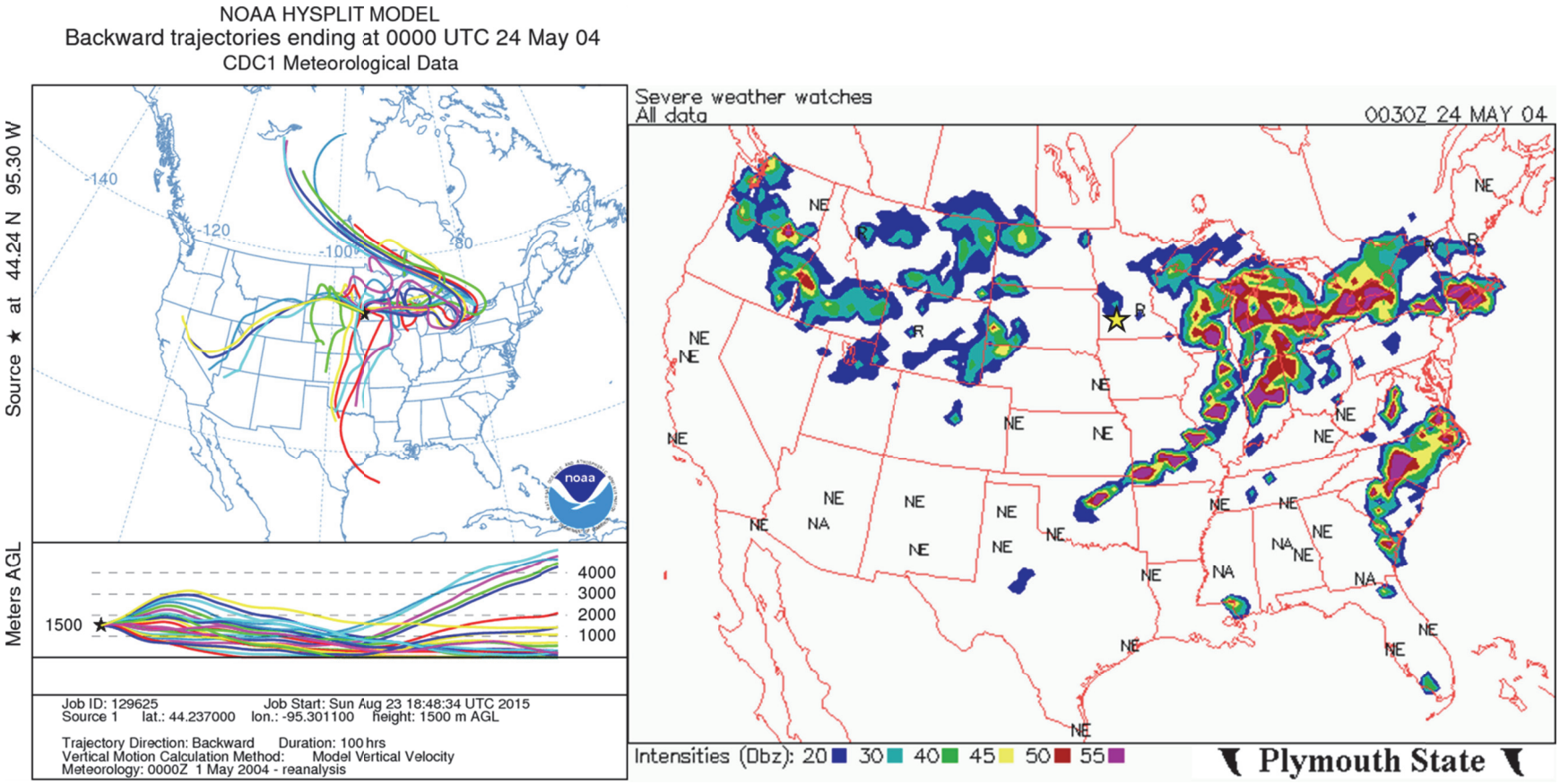

Figure A3.11. Continental-midwest moisture source determined for MN27 on May 24, 2004. HYSPLIT trajectories are unclear and spiral out over the Midwest. RADAR indicates light precipitation probably from extratropical cyclone wrap-around precipitation. This moisture was likely originally Gulf of Mexico derived, but has been transported and altered a great deal more than simple southerly advection.

Continental-North Moisture Source

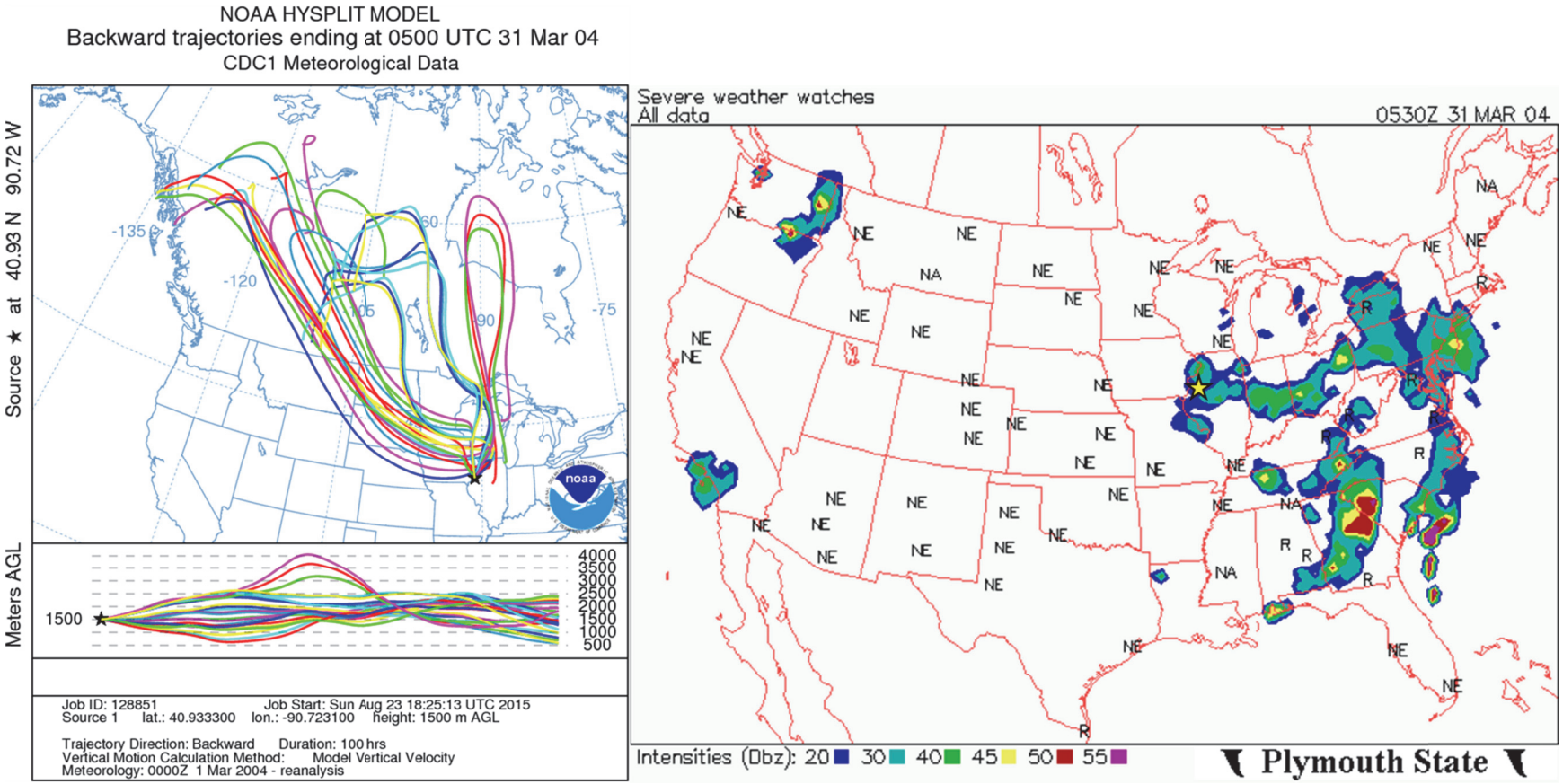

Figure A3.12. Continental-north moisture source determined for IL78 on March 31, 2004. HYSPLIT trajectories stall out over the Canadian landmass. RADAR indicates light precipitation associated with extratropical cyclone wraparound precipitation. This moisture was likely originally Gulf of Mexico derived, but has been transported and altered a great deal more than simple southerly advection.

APPENDIX FOUR:

SEASONAL PRECIPITATION OXYGEN ISOTOPE DISTRIBUTIONS FOR EACH USNIP SITE

This appendix contains plots illustrating the winter and summer distribution and means of precipitation $\delta^{18}O$ values as calculated for each USNIP site. These seasonal means can be used to calculate Seasonal Signal Anomalies (SSAs) as described in Chapter 5.

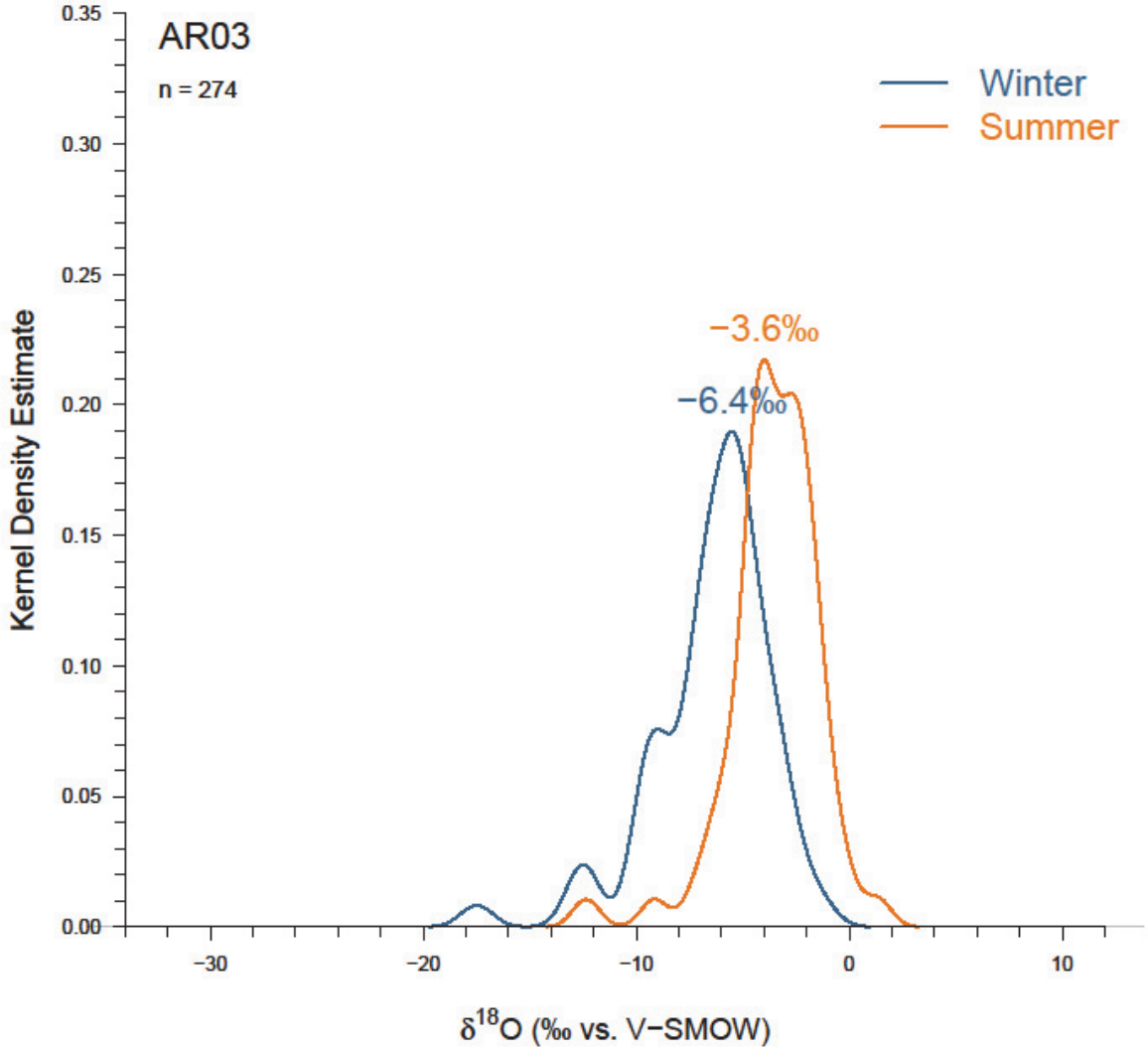

Figure A4.1. Kernel density estimate of AR03 $\delta^{18}O$ values for winter and summer seasons. The written number above the density peak is the weighted mean $\delta^{18}O$ value for each season.

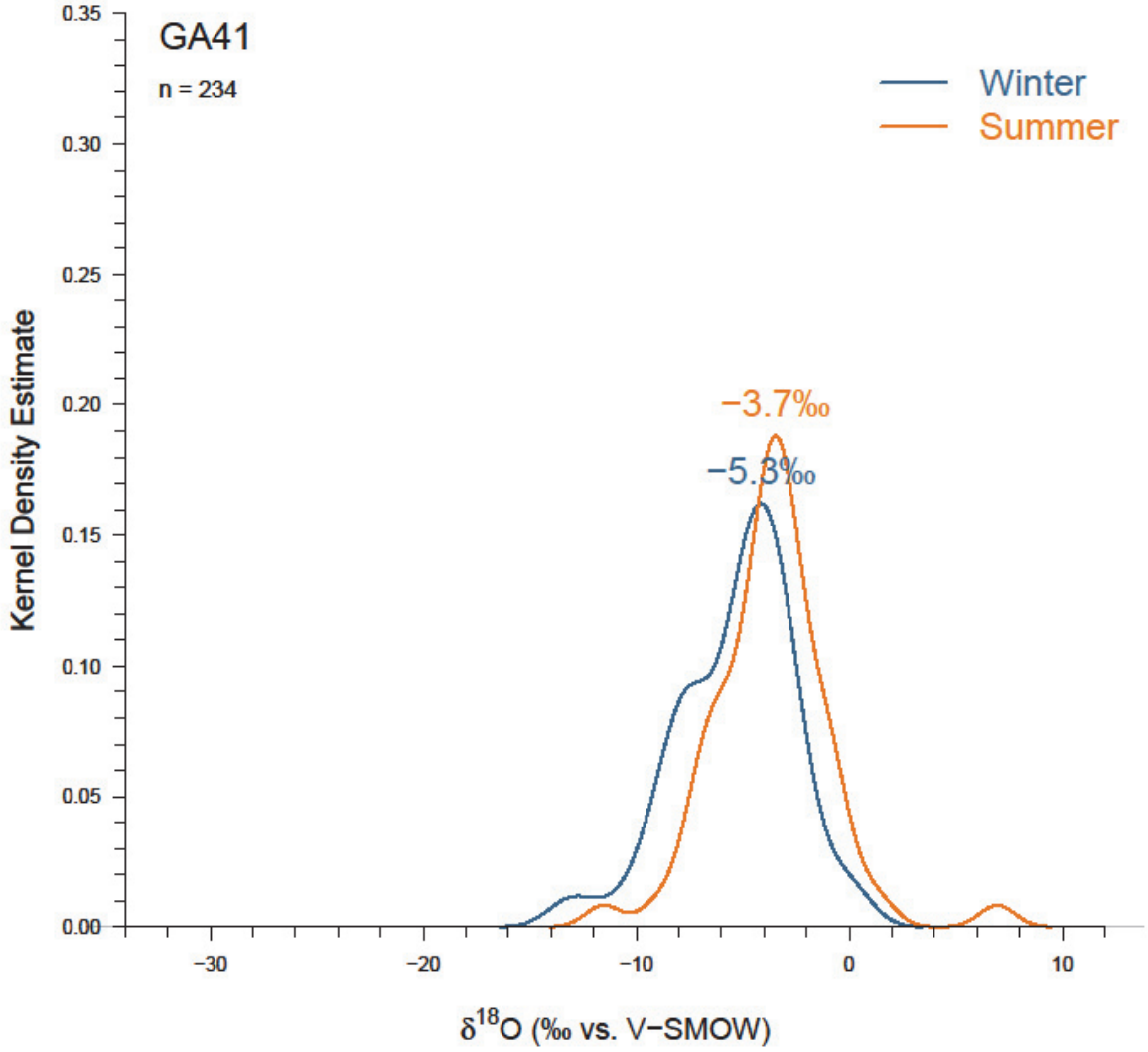

Figure A4.2. Kernel density estimate of GA41 $\delta^{18}O$ values for winter and summer seasons. The written number above the density peak is the weighted mean $\delta^{18}O$ value for each season.

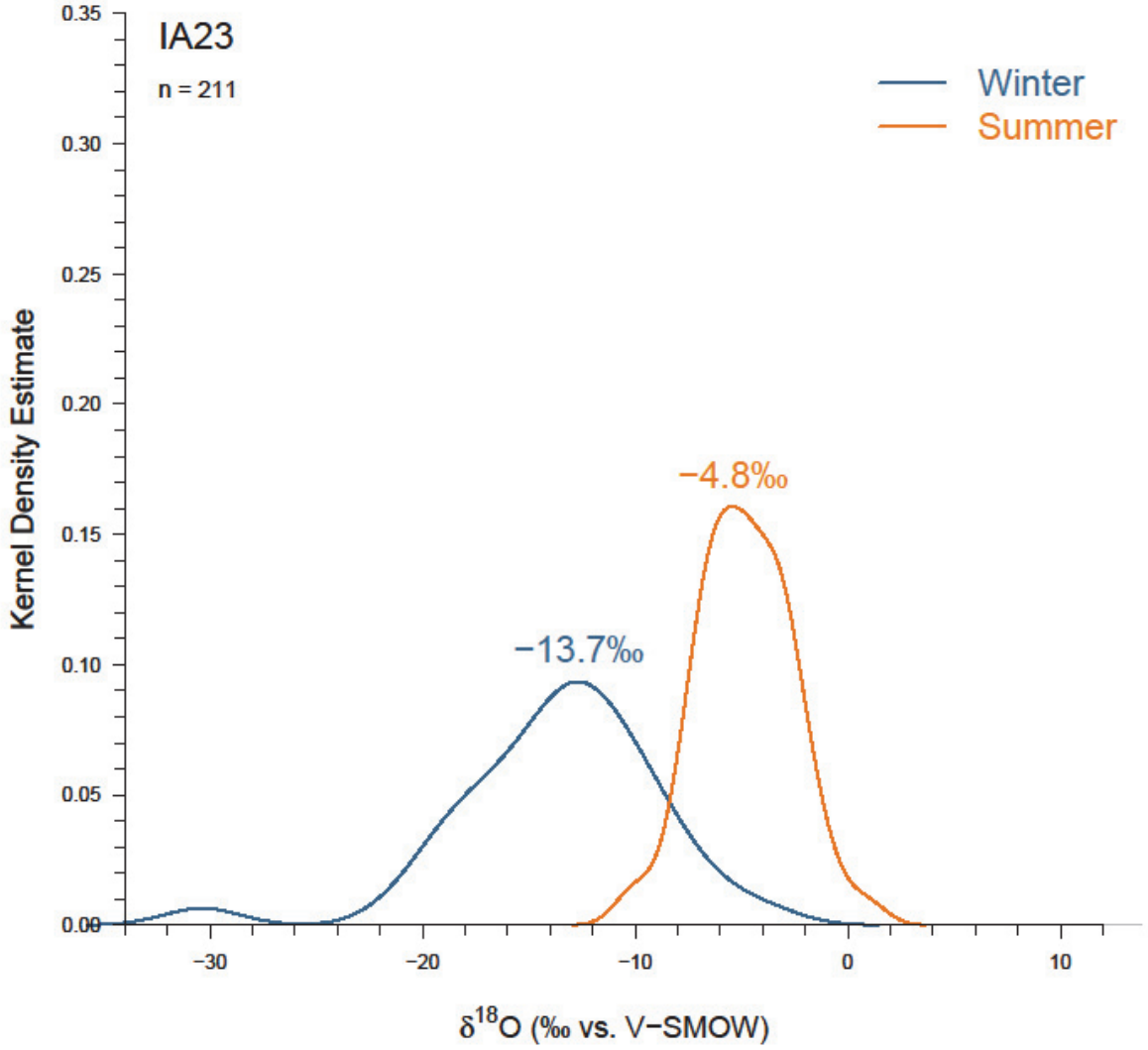

Figure A4.3. Kernel density estimate of IA23 $\delta^{18}O$ values for winter and summer seasons. The written number above the density peak is the weighted mean $\delta^{18}O$ value for each season.

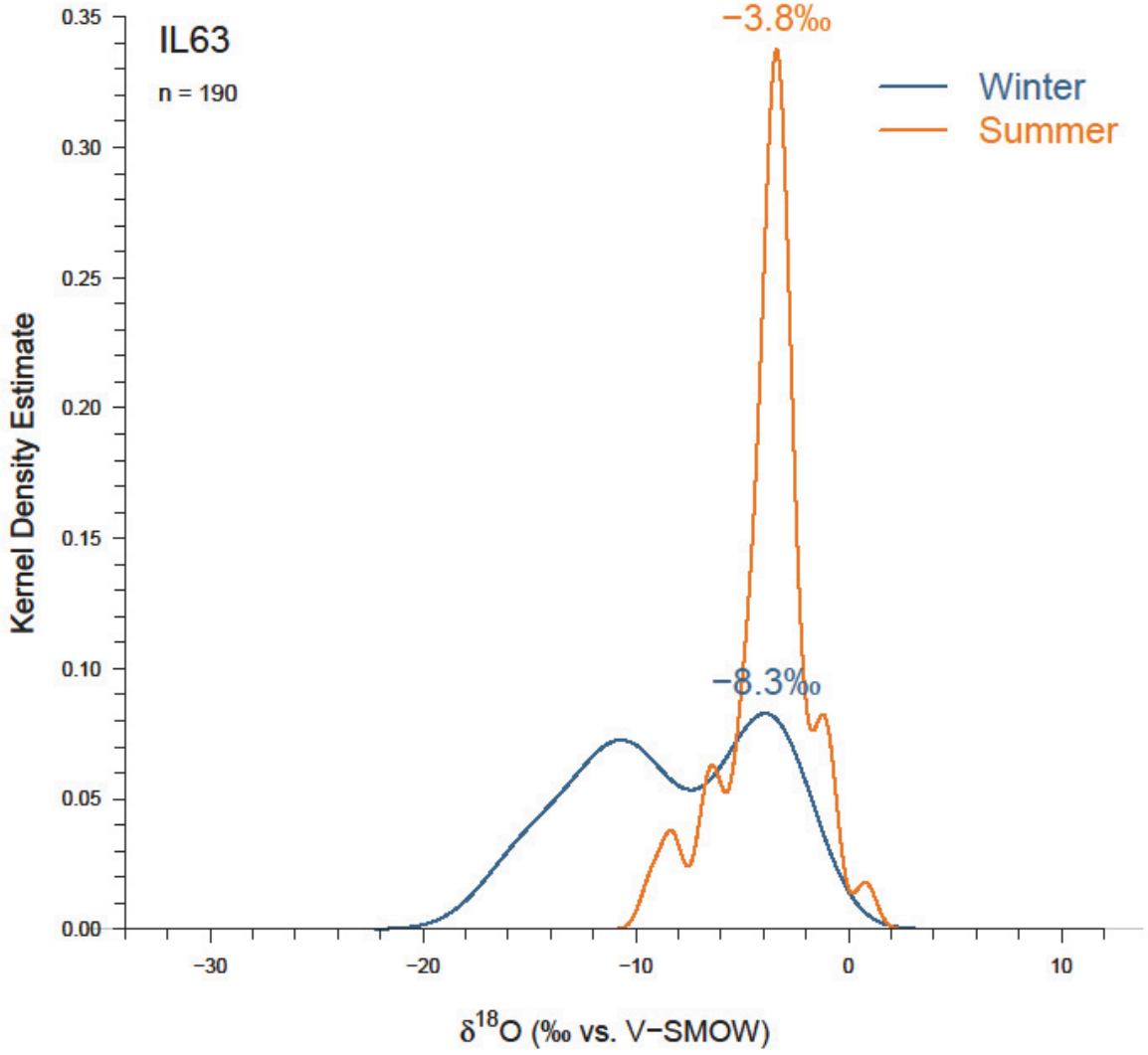

Figure A4.4. Kernel density estimate of IL63 $\delta^{18}O$ values for winter and summer seasons. The written number above the density peak is the weighted mean $\delta^{18}O$ value for each season.

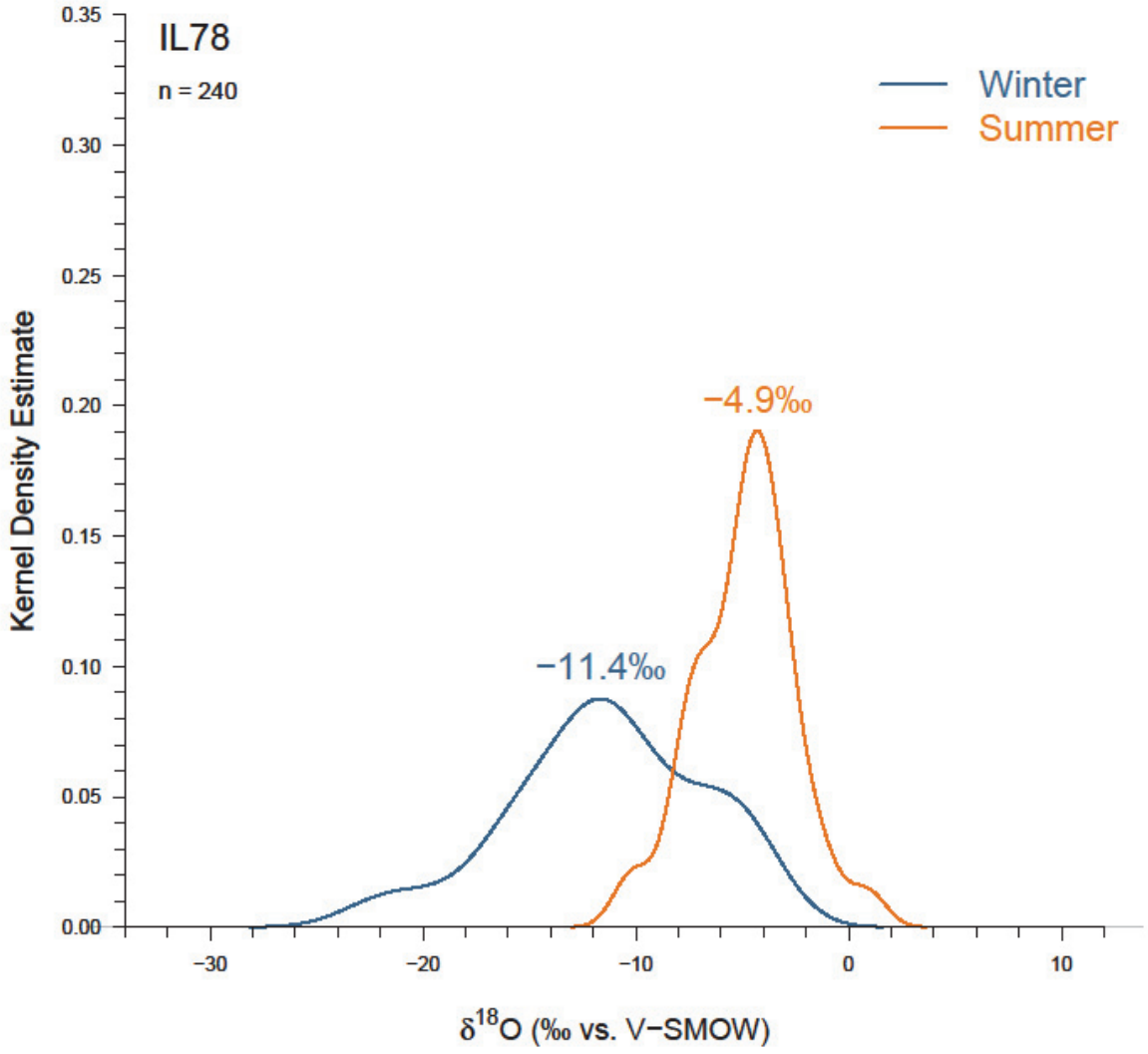

Figure A4.5. Kernel density estimate of IL78 $\delta^{18}O$ values for winter and summer seasons. The written number above the density peak is the weighted mean $\delta^{18}O$ value for each season.

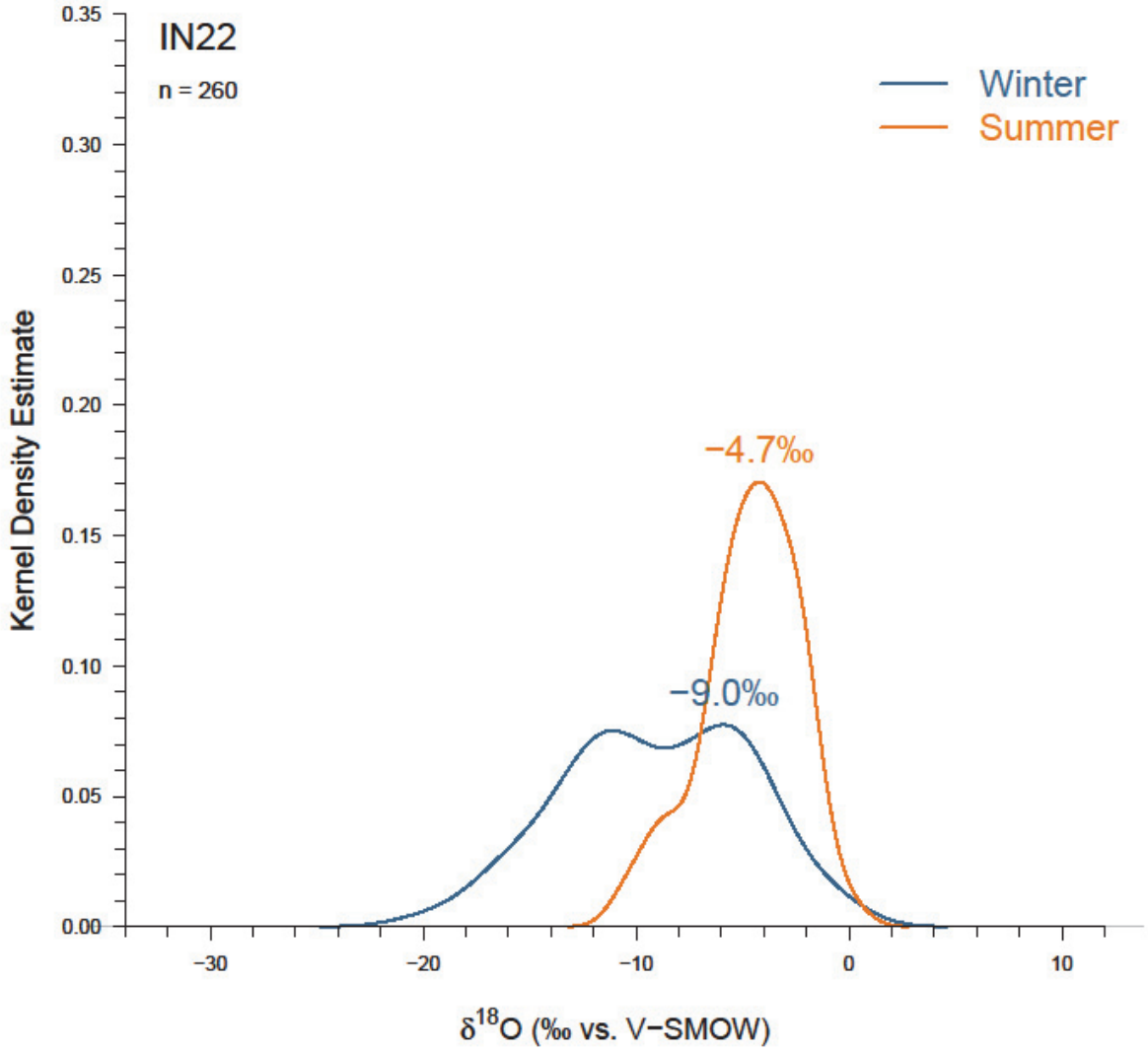

Figure A4.6. Kernel density estimate of IN22 $\delta^{18}O$ values for winter and summer seasons. The written number above the density peak is the weighted mean $\delta^{18}O$ value for each season.

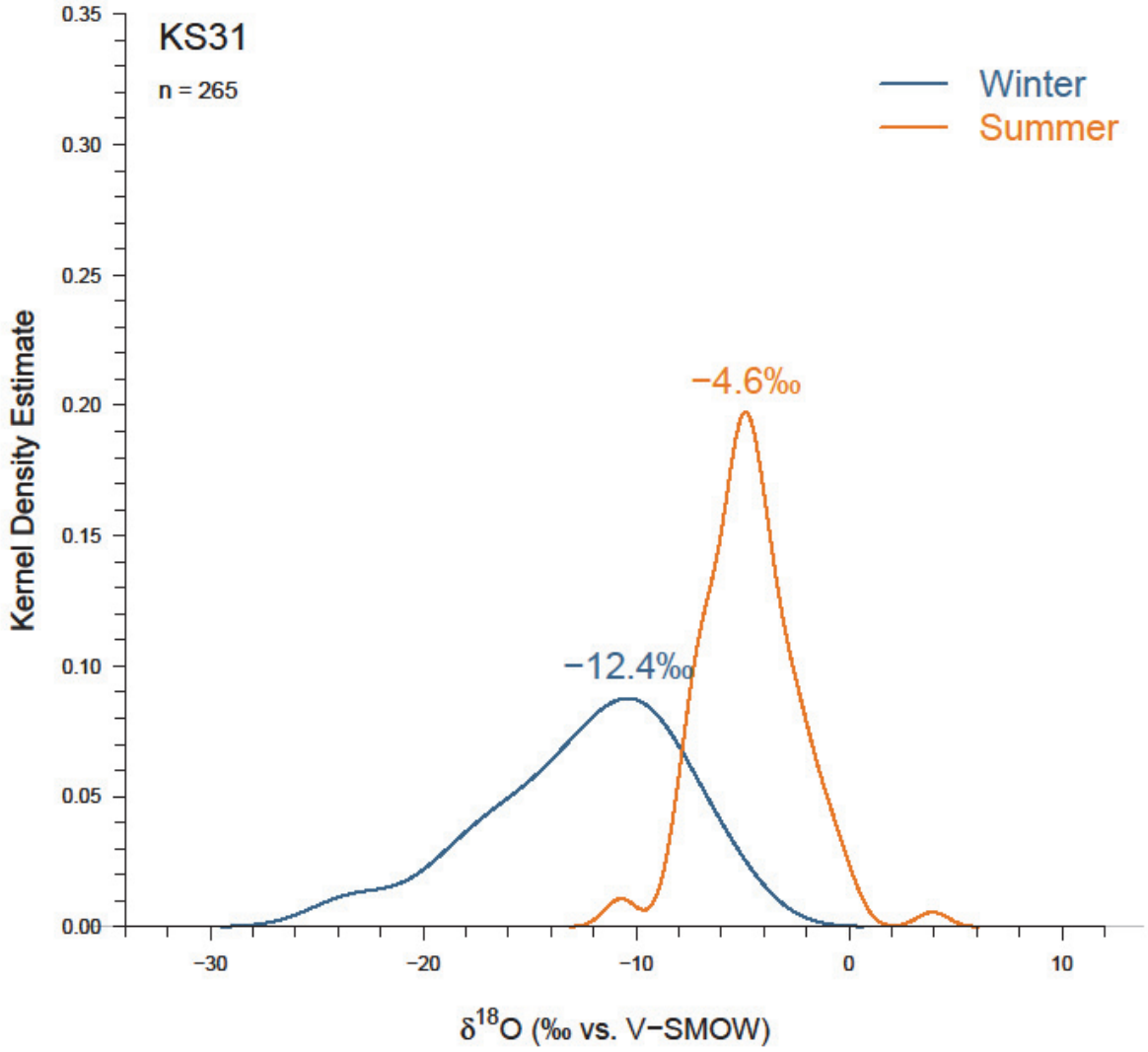

Figure A4.7. Kernel density estimate of KS31 $\delta^{18}O$ values for winter and summer seasons. The written number above the density peak is the weighted mean $\delta^{18}O$ value for each season.

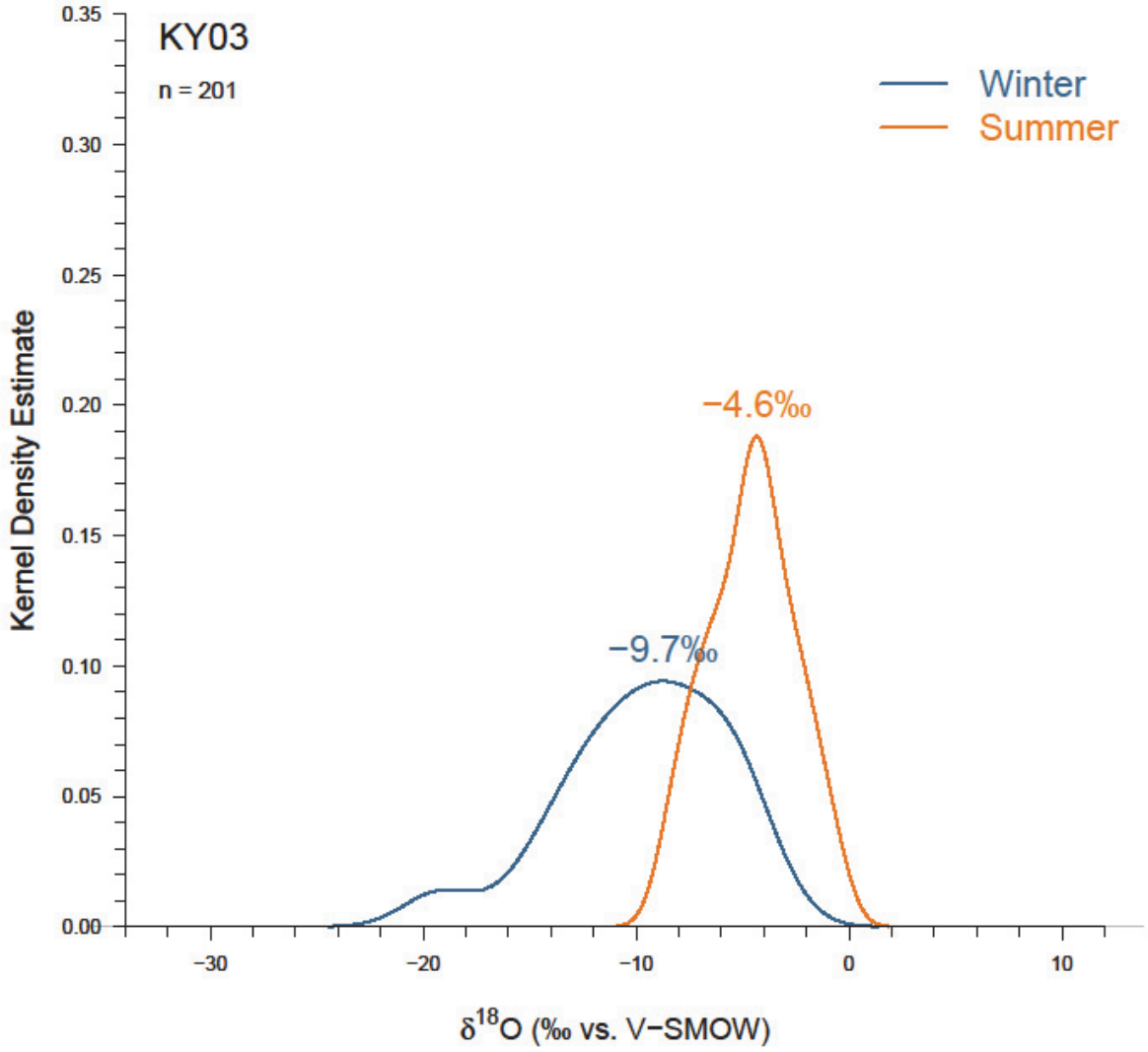

Figure A4.8. Kernel density estimate of KY03 $\delta^{18}O$ values for winter and summer seasons. The written number above the density peak is the weighted mean $\delta^{18}O$ value for each season.

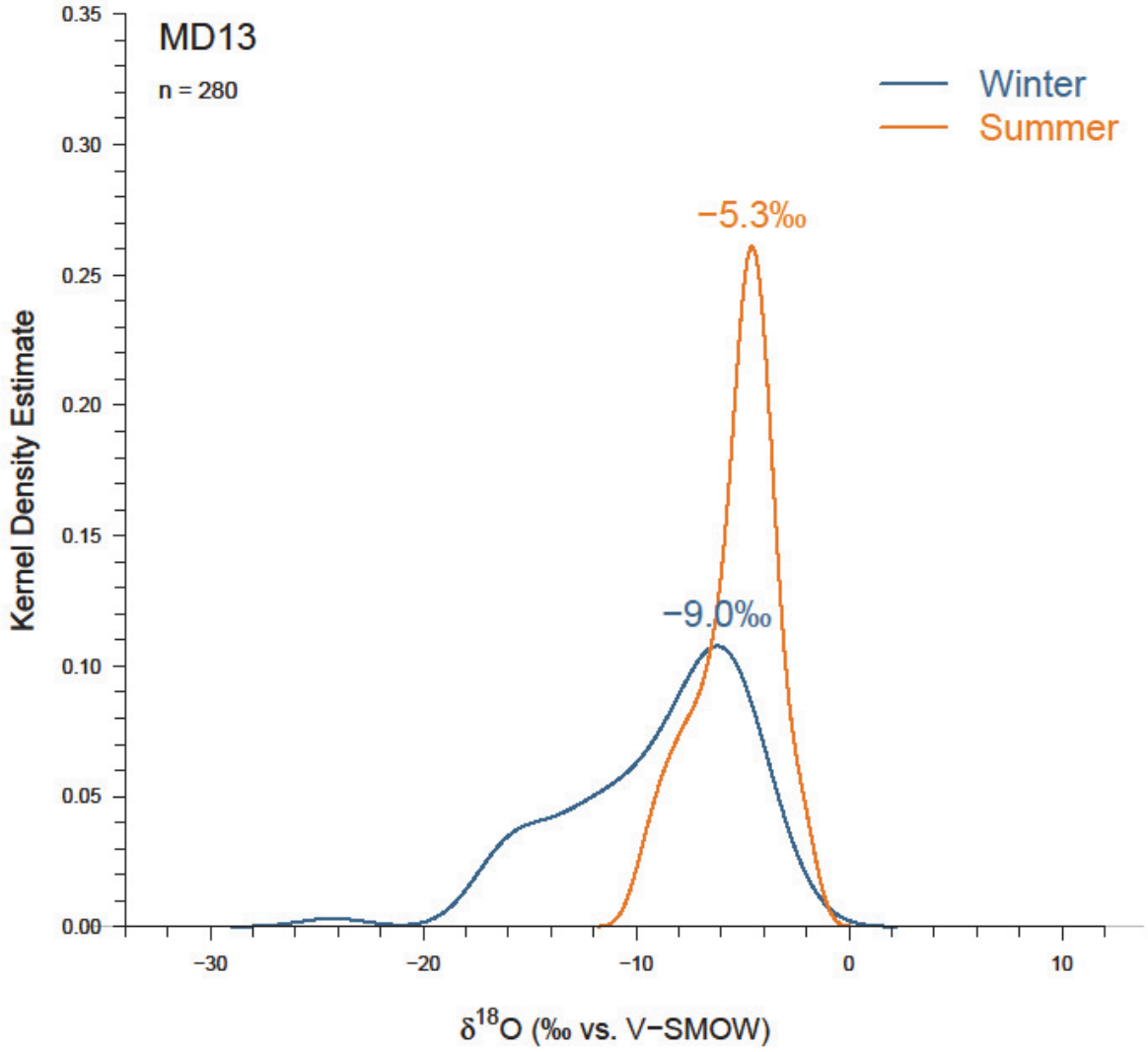

Figure A4.9. Kernel density estimate of MD13 $\delta^{18}O$ values for winter and summer seasons. The written number above the density peak is the weighted mean $\delta^{18}O$ value for each season.

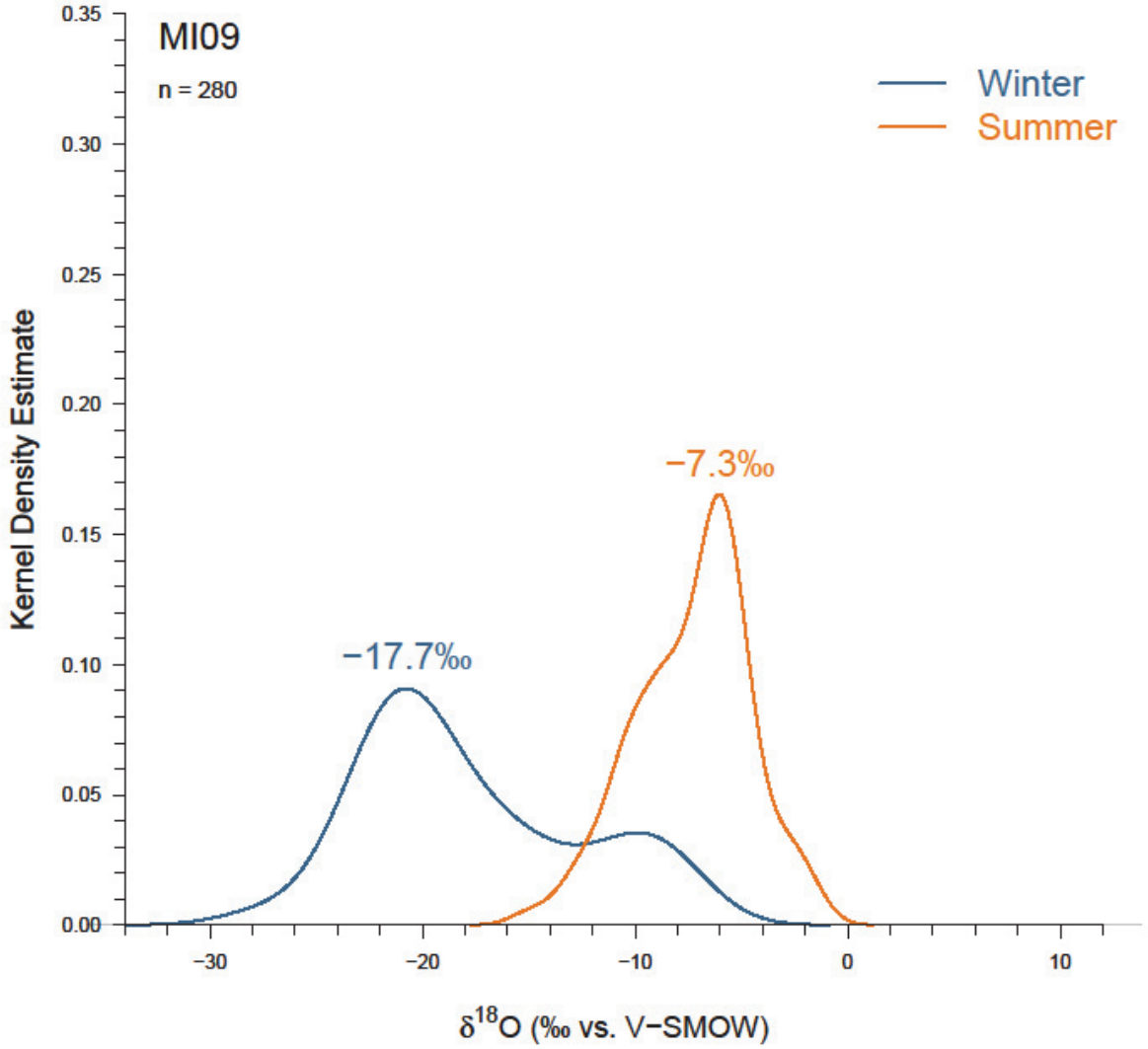

Figure A4.10. Kernel density estimate of MI09 $\delta^{18}O$ values for winter and summer seasons. The written number above the density peak is the weighted mean $\delta^{18}O$ value for each season.

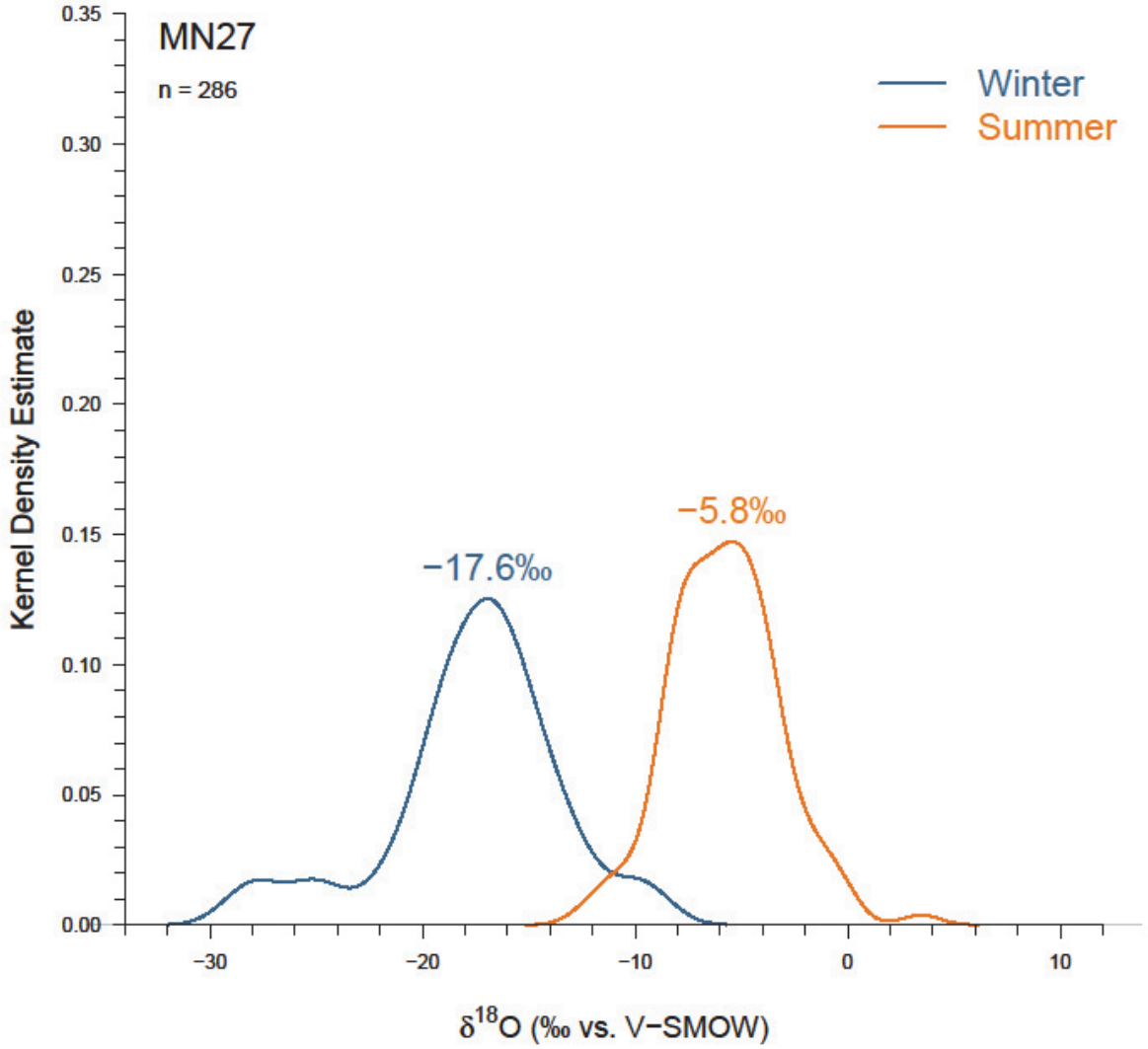

Figure A4.11. Kernel density estimate of MN27 $\delta^{18}O$ values for winter and summer seasons. The written number above the density peak is the weighted mean $\delta^{18}O$ value for each season.

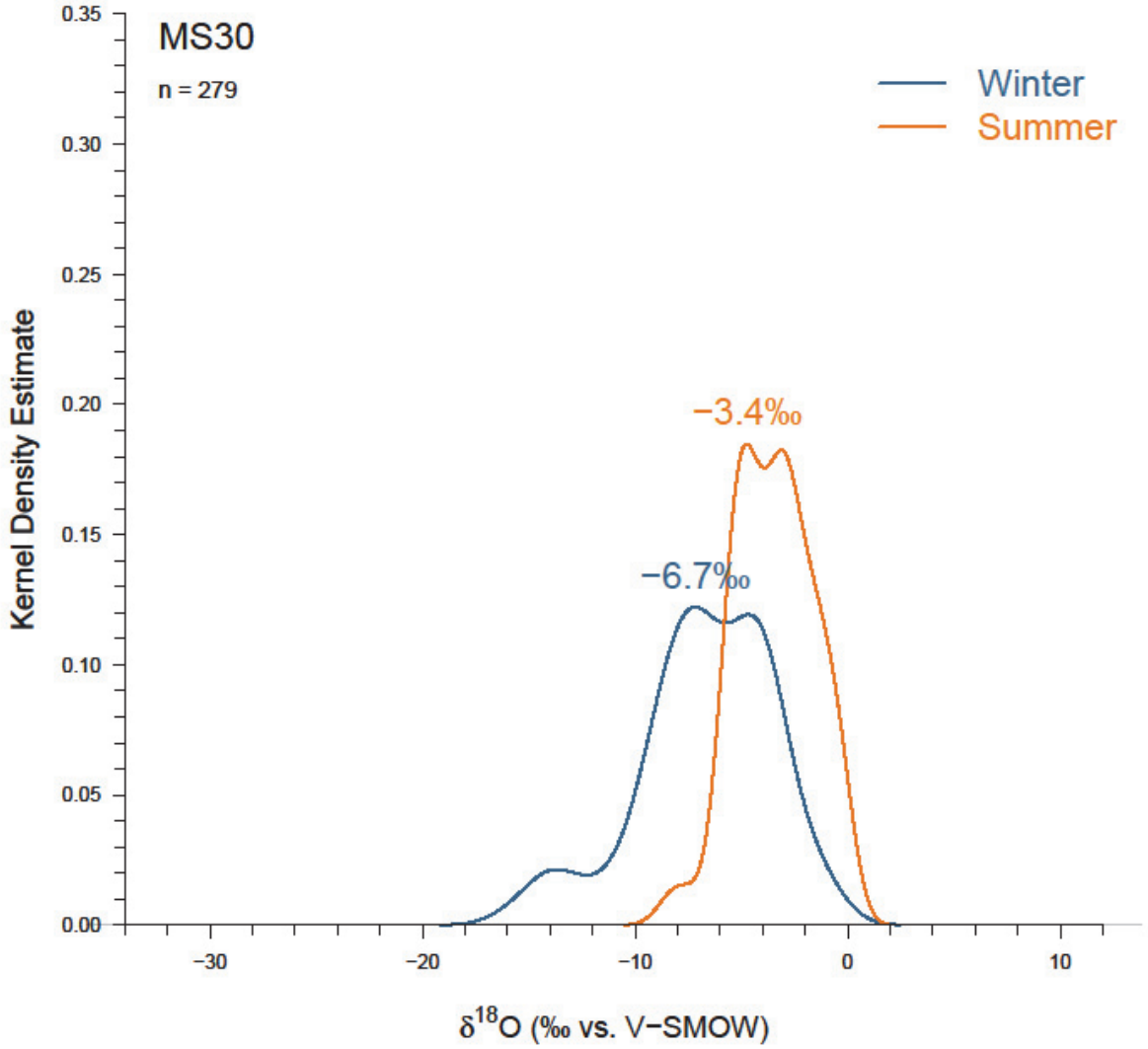

Figure A4.12. Kernel density estimate of MS30 $\delta^{18}O$ values for winter and summer seasons. The written number above the density peak is the weighted mean $\delta^{18}O$ value for each season.

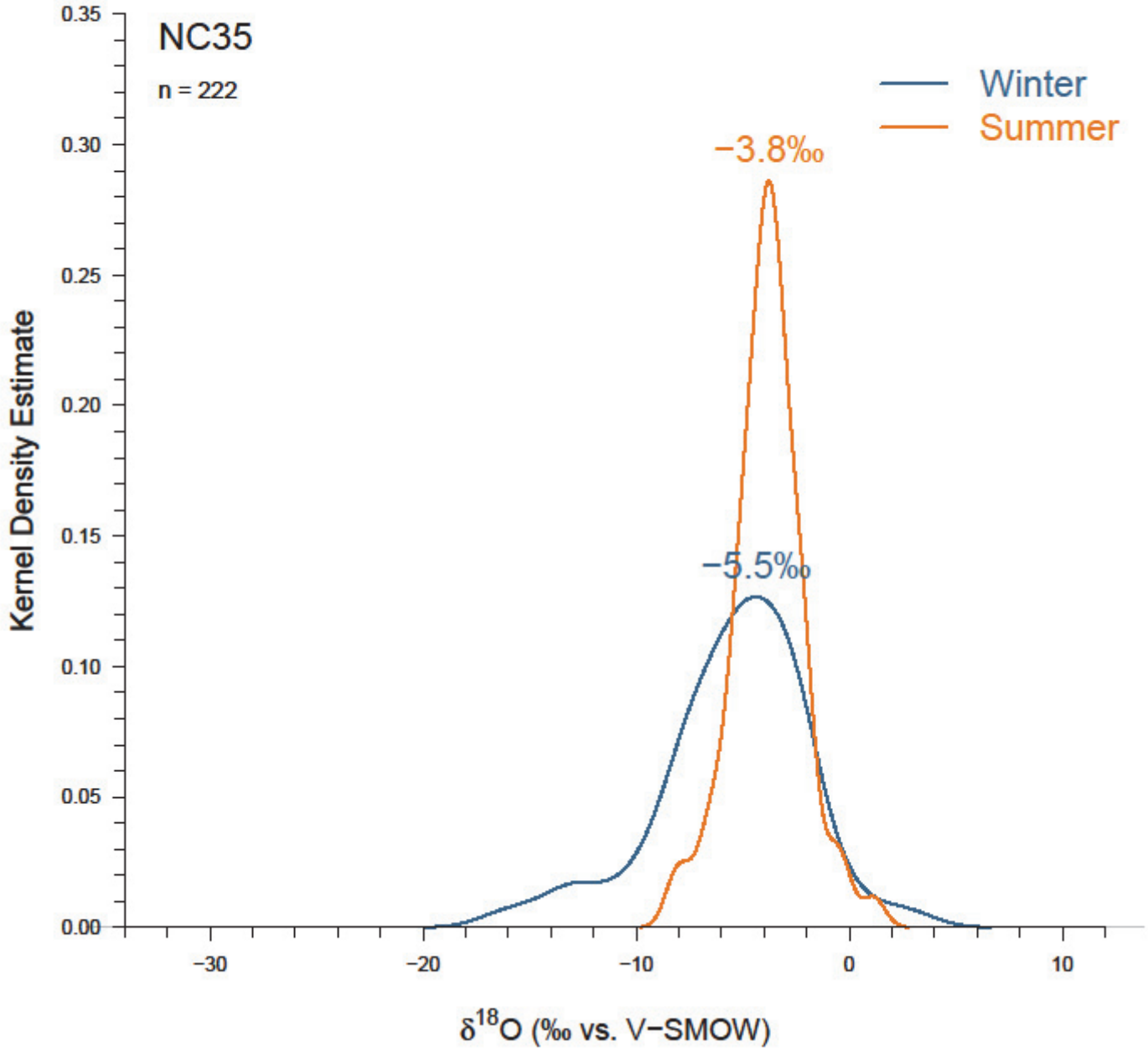

Figure A4.13. Kernel density estimate of NC35 $\delta^{18}O$ values for winter and summer seasons. The written number above the density peak is the weighted mean $\delta^{18}O$ value for each season.

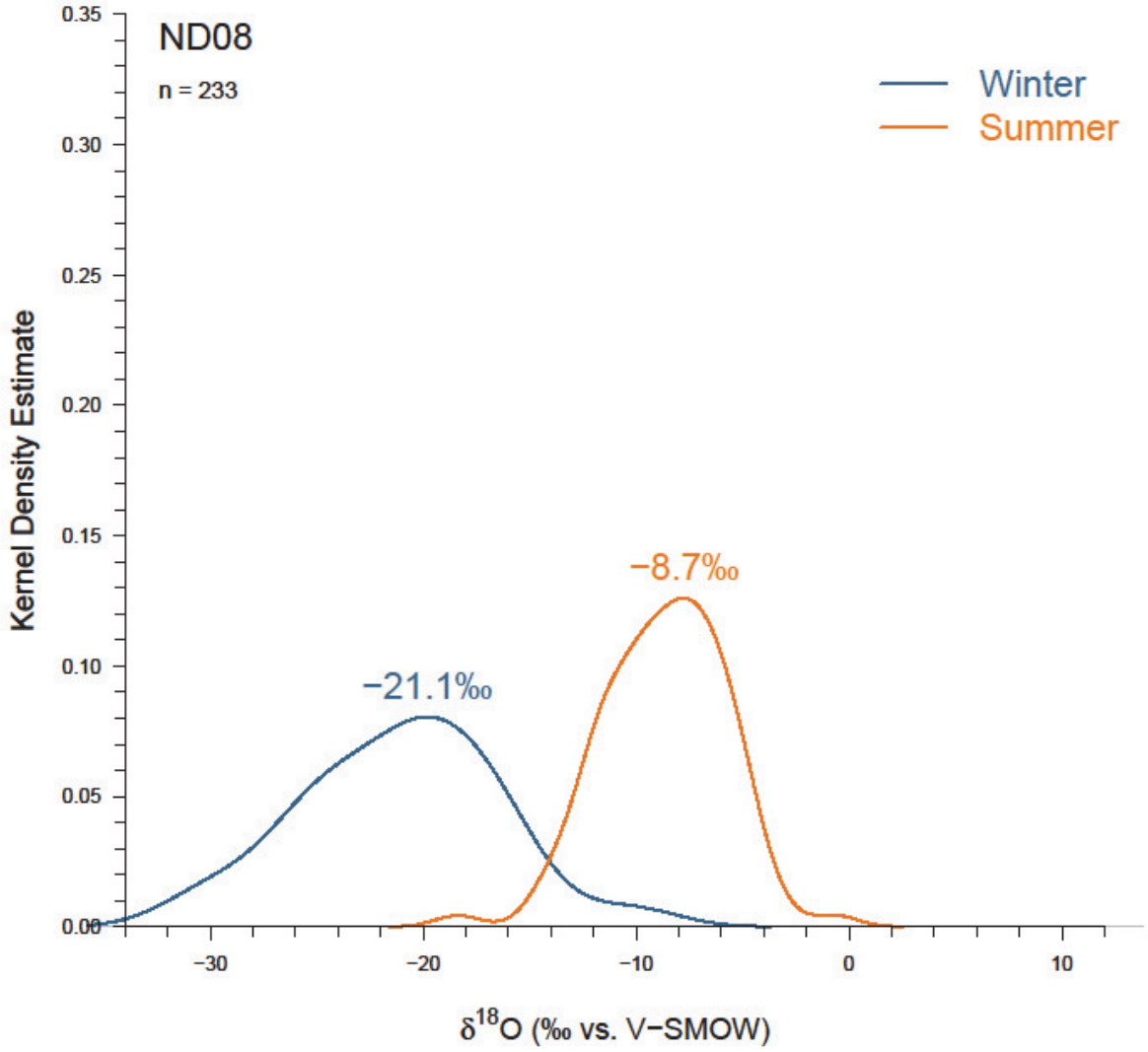

Figure A4.14. Kernel density estimate of ND08 $\delta^{18}O$ values for winter and summer seasons. The written number above the density peak is the weighted mean $\delta^{18}O$ value for each season.

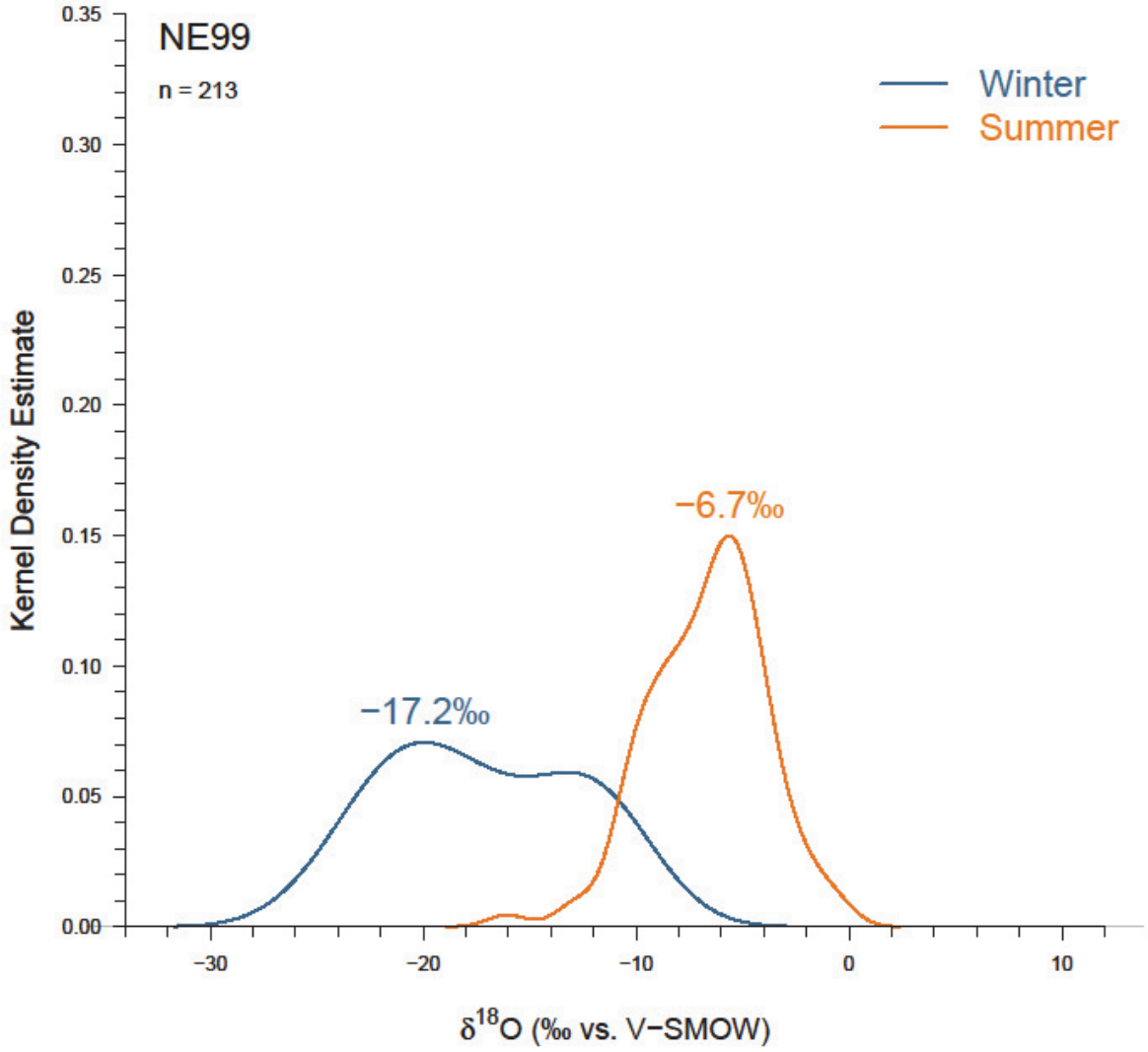

Figure A4.15. Kernel density estimate of NE99 $\delta^{18}O$ values for winter and summer seasons. The written number above the density peak is the weighted mean $\delta^{18}O$ value for each season.

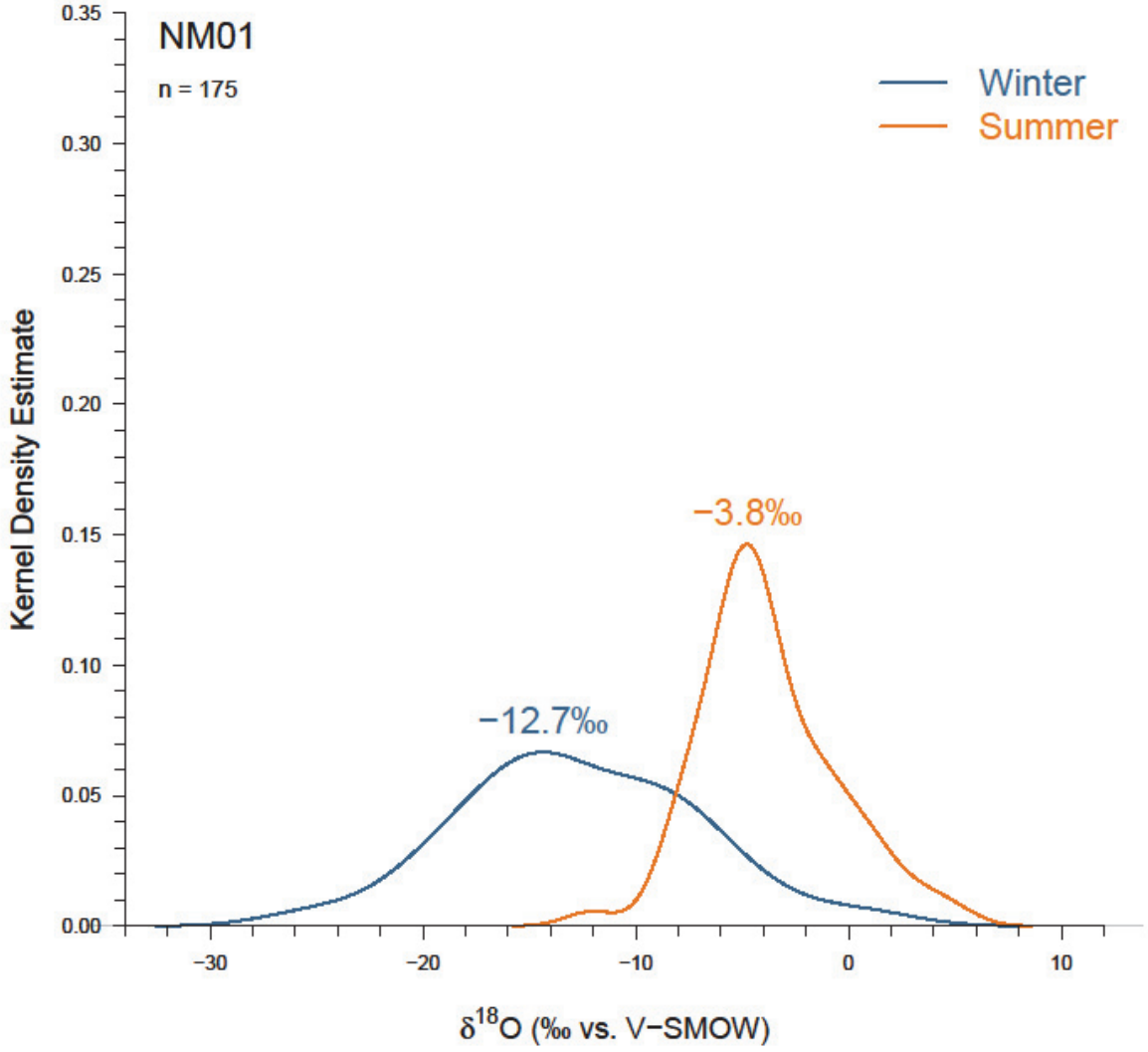

Figure A4.16. Kernel density estimate of NM01 $\delta^{18}O$ values for winter and summer seasons. The written number above the density peak is the weighted mean $\delta^{18}O$ value for each season.

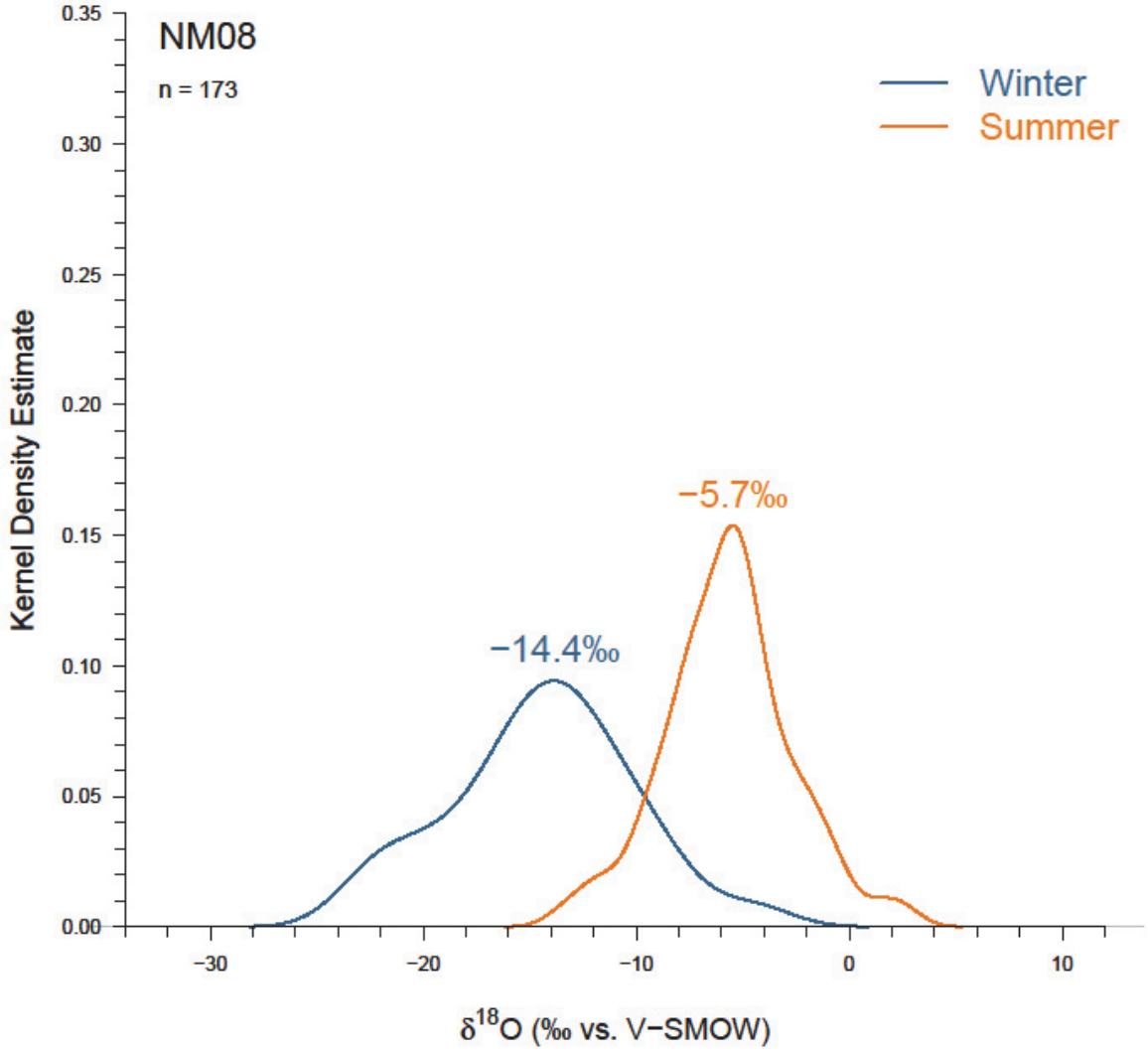

Figure A4.17. Kernel density estimate of NM08 $\delta^{18}O$ values for winter and summer seasons. The written number above the density peak is the weighted mean $\delta^{18}O$ value for each season.

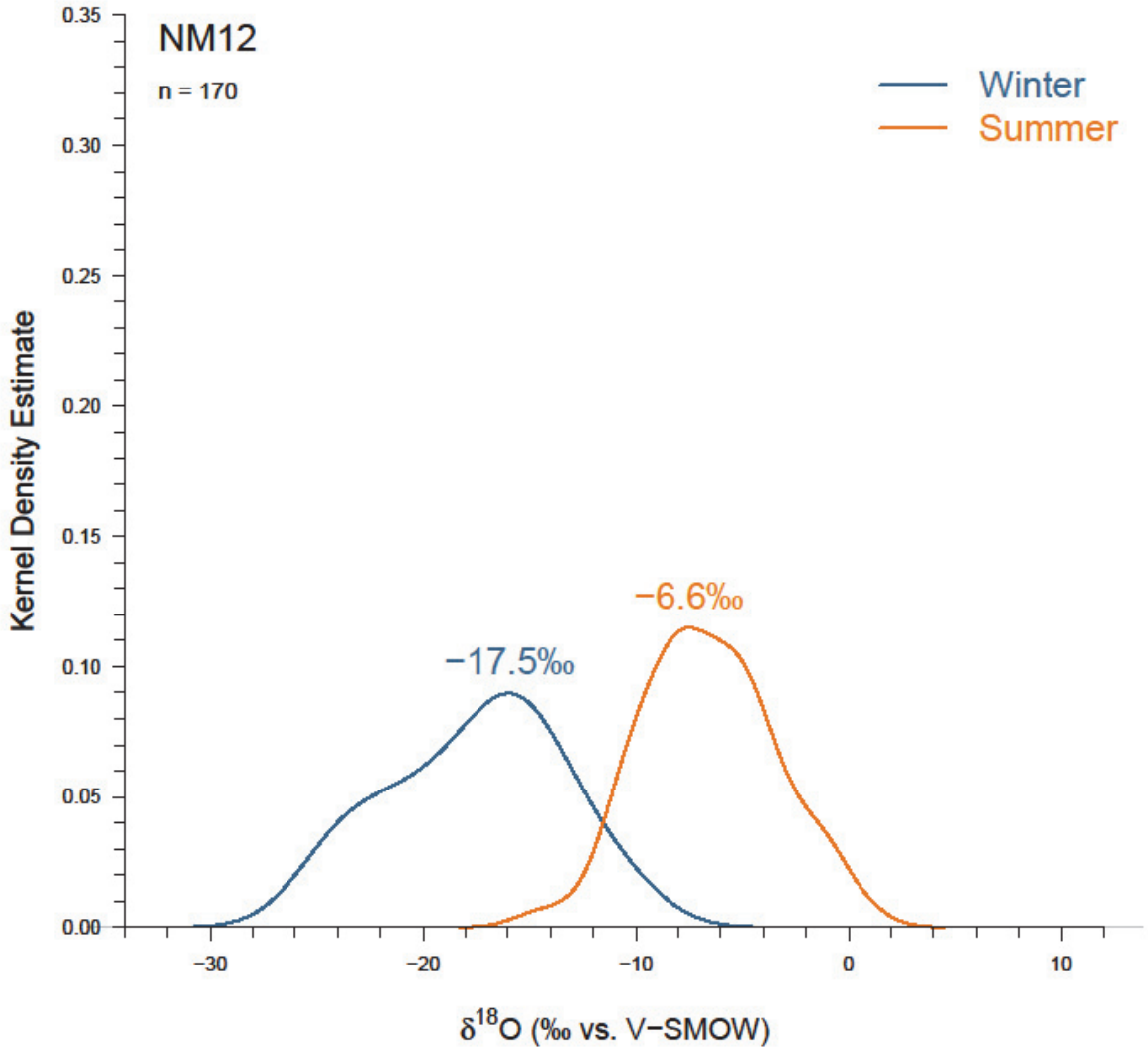

Figure A4.18. Kernel density estimate of NM12$\delta^{18}O$ values for winter and summer seasons. The written number above the density peak is the weighted mean $\delta^{18}O$ value for each season.

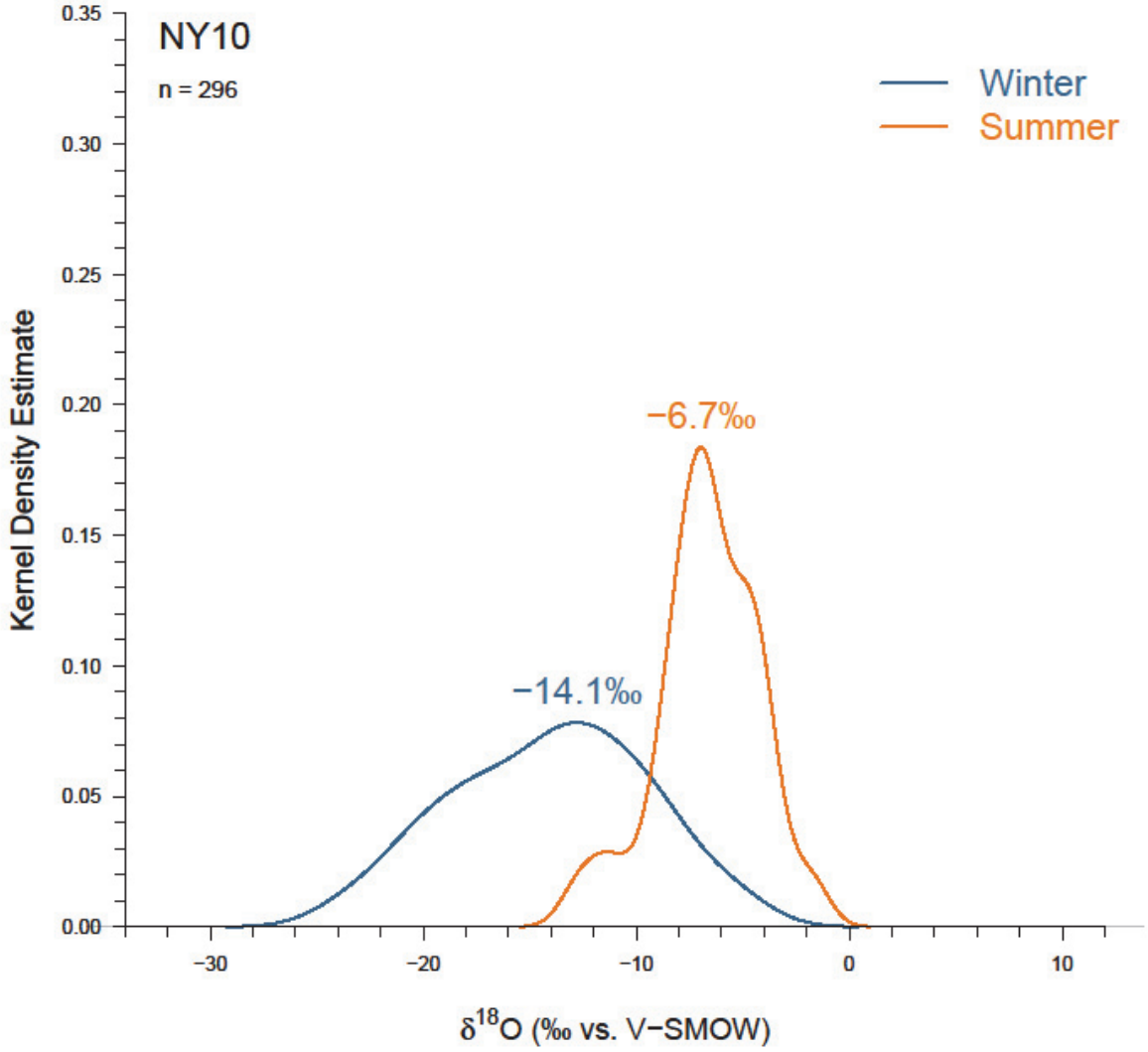

Figure A4.19. Kernel density estimate of NY10 $\delta^{18}O$ values for winter and summer seasons. The written number above the density peak is the weighted mean $\delta^{18}O$ value for each season.

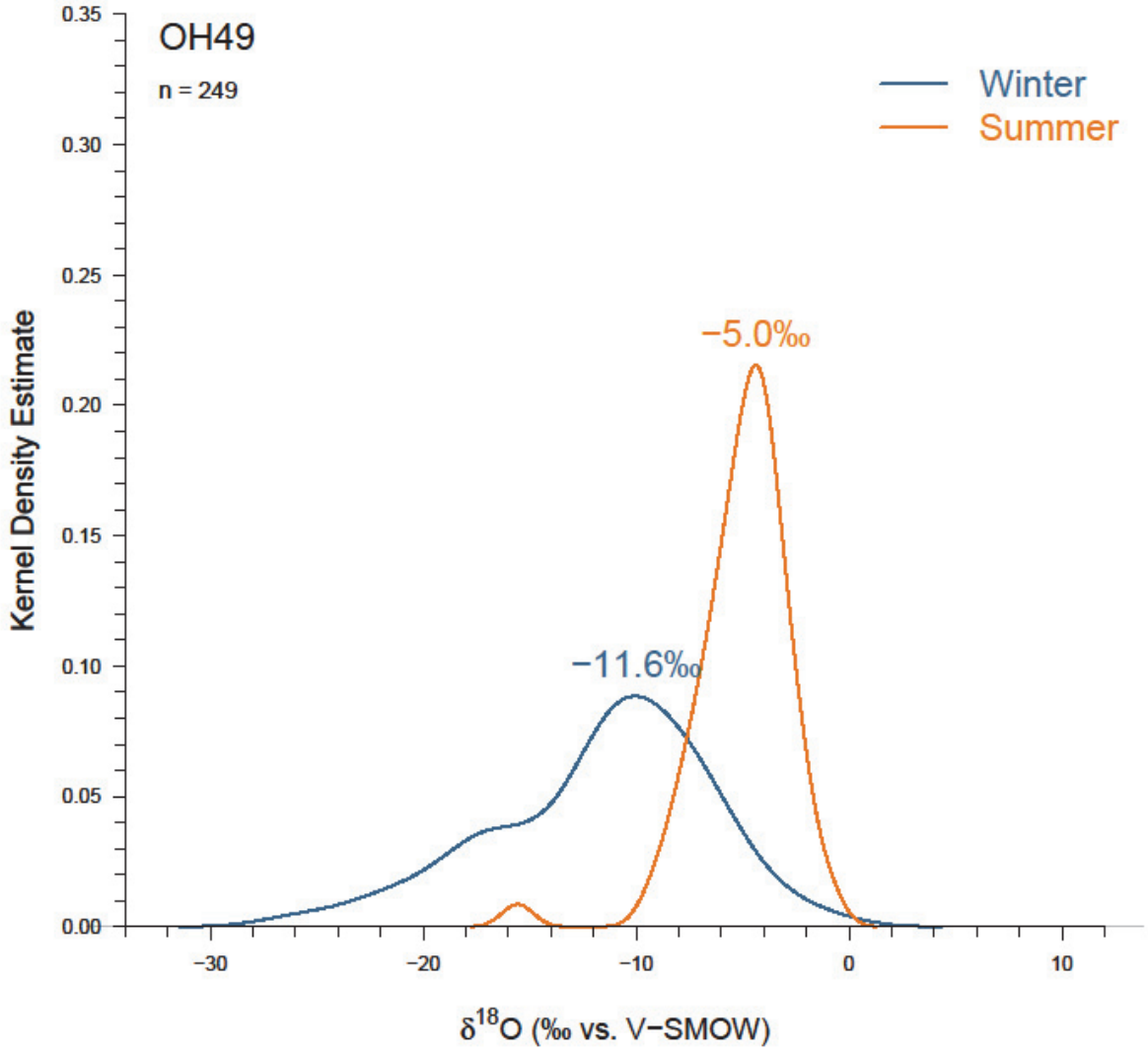

Figure A4.20. Kernel density estimate of OH49 $\delta^{18}O$ values for winter and summer seasons. The written number above the density peak is the weighted mean $\delta^{18}O$ value for each season.

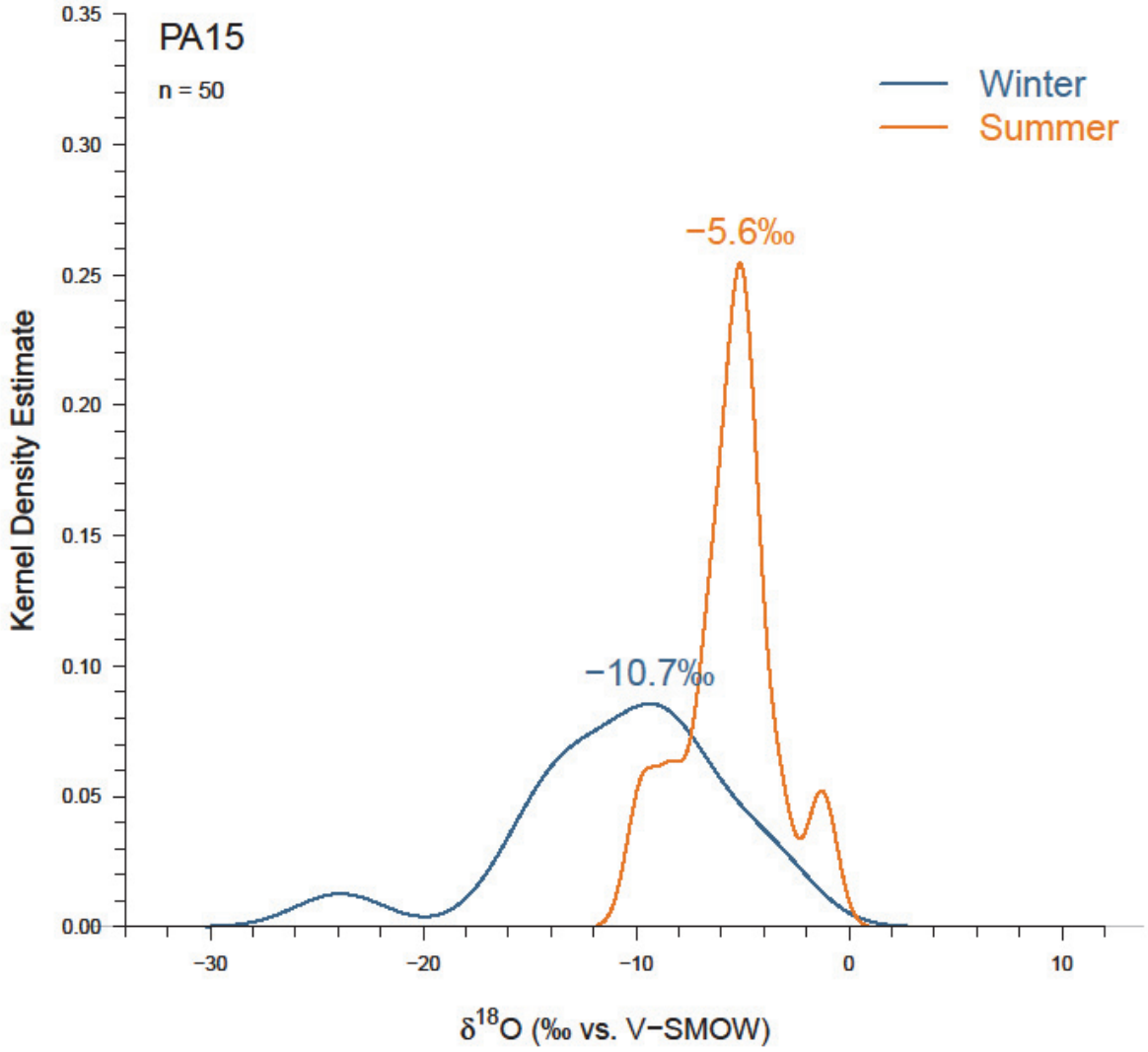

Figure A4.21. Kernel density estimate of PA15 $\delta^{18}O$ values for winter and summer seasons. The written number above the density peak is the weighted mean $\delta^{18}O$ value for each season.

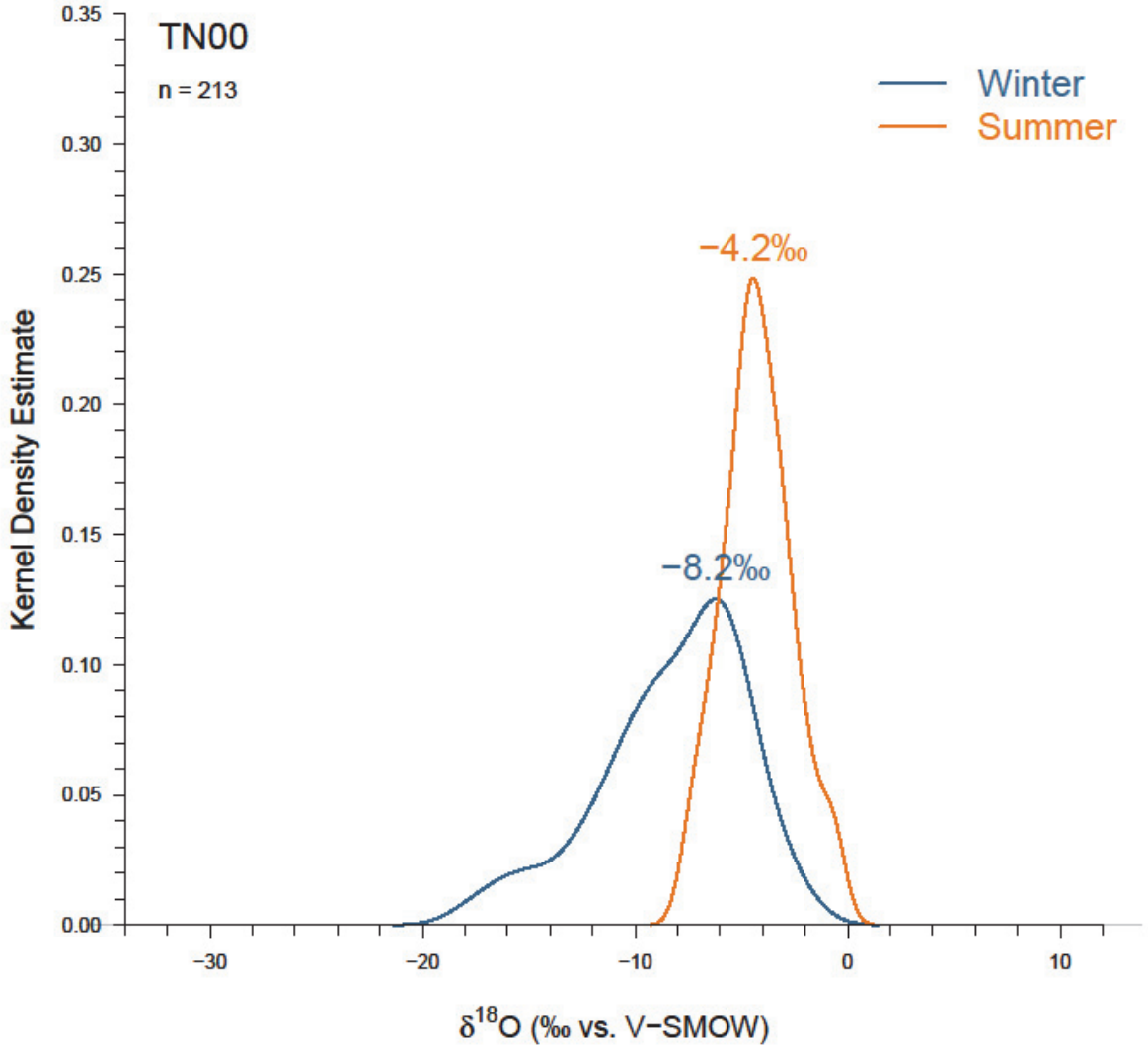

Figure A4.22. Kernel density estimate of TN00 $\delta^{18}O$ values for winter and summer seasons. The written number above the density peak is the weighted mean $\delta^{18}O$ value for each season.

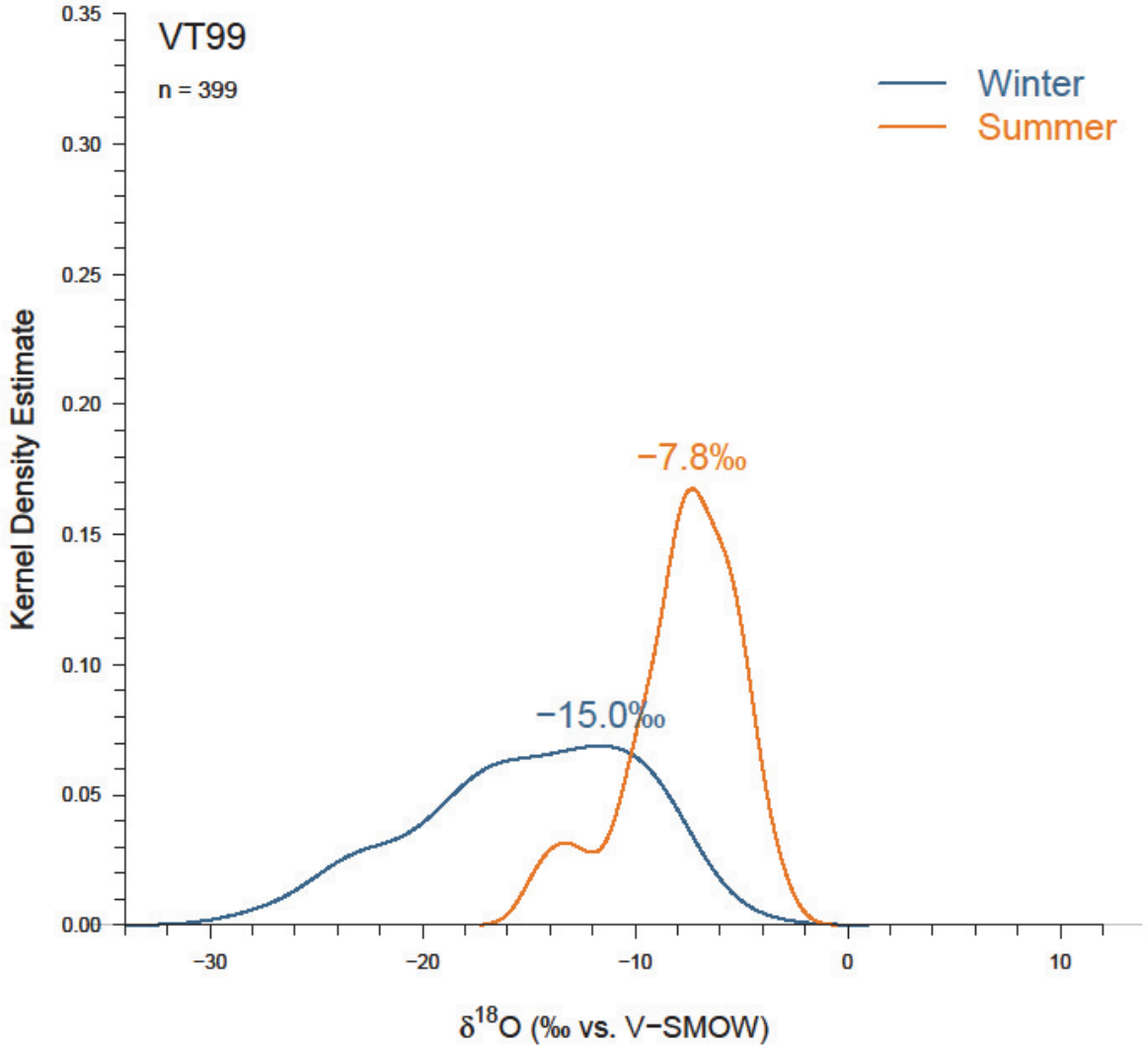

Figure A4.23. Kernel density estimate of VT99 $\delta^{18}O$ values for winter and summer seasons. The written number above the density peak is the weighted mean $\delta^{18}O$ value for each season.

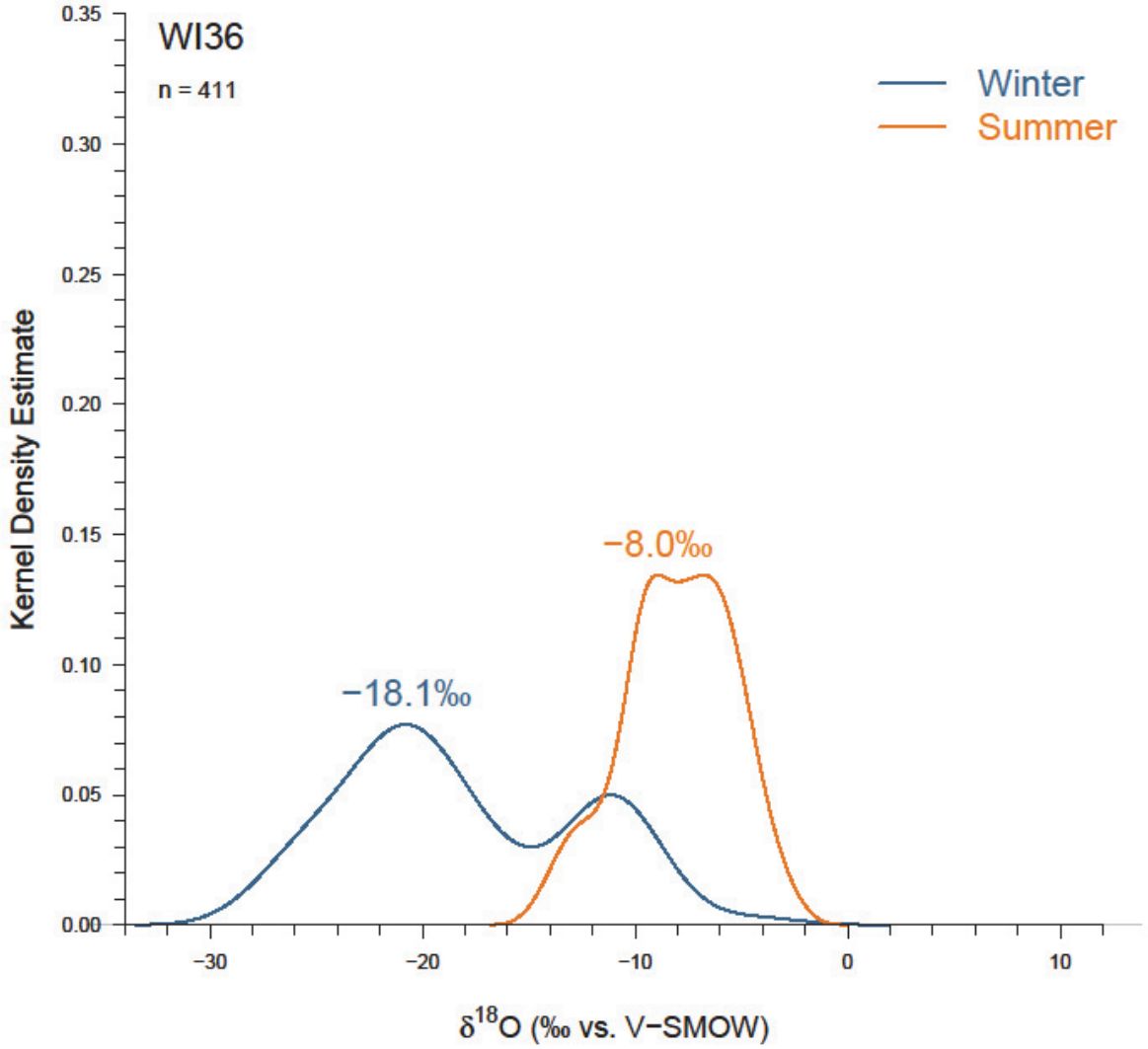

Figure A4.24. Kernel density estimate of WI36 $\delta^{18}O$ values for winter and summer seasons. The written number above the density peak is the weighted mean $\delta^{18}O$ value for each season.

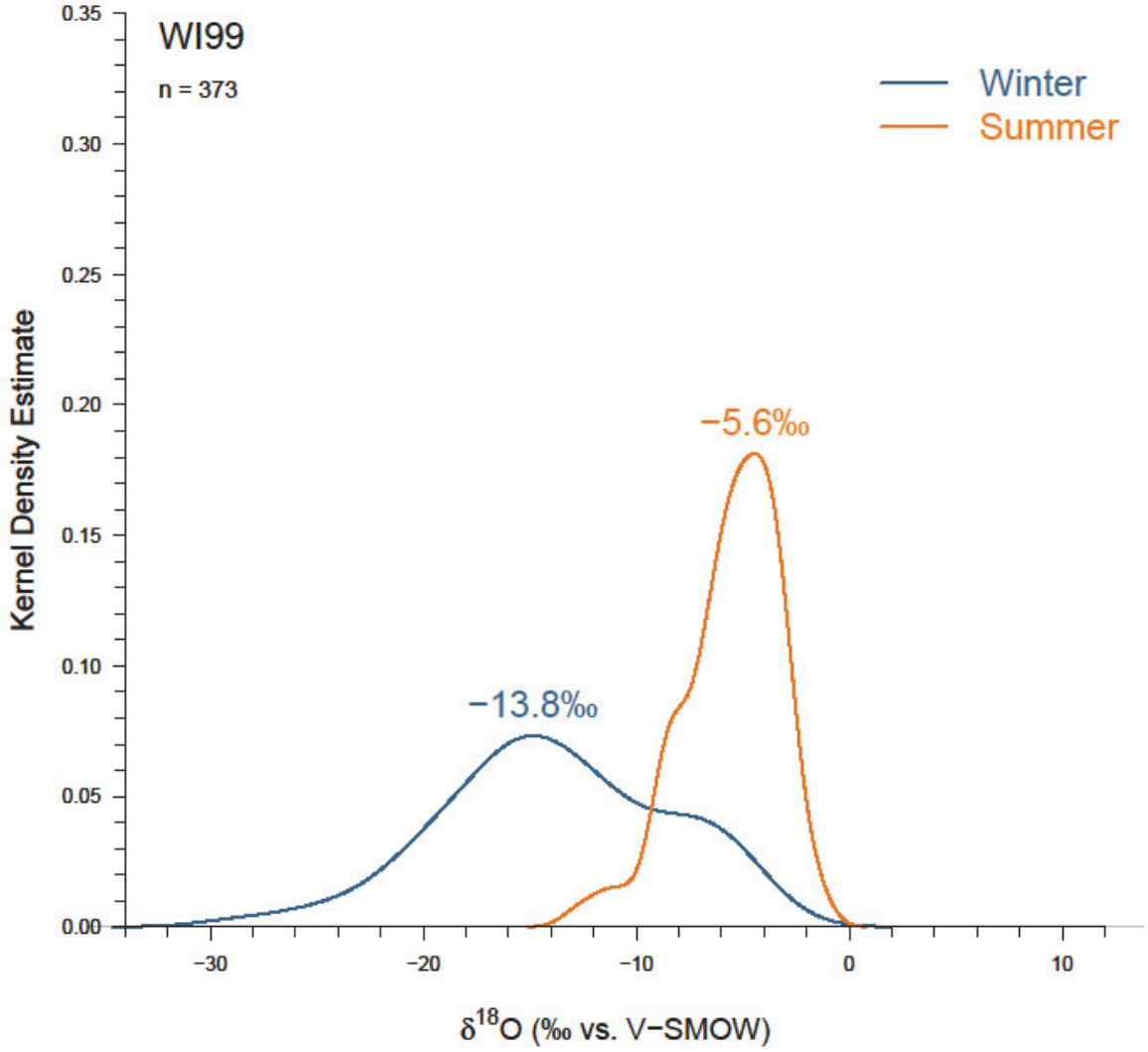

Figure A4.25. Kernel density estimate of WI99 $\delta^{18}O$ values for winter and summer seasons. The written number above the density peak is the weighted mean $\delta^{18}O$ value for each season.

APPENDIX FIVE:

TABLES AND FIGURES FOR INDIVIDUAL USNIP SITE PRECIPTATION STABLE ISOTOPE AND CLIMATE RELATIONSHIPS

This appendix contains tables and figures for isotopic and climate relationships for each individual USNIP site studied. Note that this appendix includes data for deuterium, *d-excess*, and local mean water lines (LMWL) that is not covered in Chapter 1, but are included here for reference.

AR03

Table A5.A1. Regression results for AR03 at weekly, monthly, and seasonal resolutions. Significant results ($p \leq 0.05$) are bolded, while insignificant results are italicized. Actual precipitation amounts were normalized by a log transformation. Precipitation amount data cannot be weight-averaged for aggregation, and thus regression was only performed at weekly resolution.

LMWL (δD vs. $\delta^{18}O$)							
Resolution	***n***	***Slope***		***y-Int***		***r^2***	***p-value***
Weekly	**274**	**7.05**	**±0.14**	**6.84**	**±0.76**	**0.90**	**0.00**
Monthly	**124**	**6.81**	**±0.22**	**5.35**	**±1.15**	**0.89**	**0.00**
Seasonal	**59**	**6.74**	**±0.33**	**4.93**	**±1.67**	**0.88**	**0.00**
$\delta^{18}O$ vs.							
Resolution	***n***	***Slope***		***y-Int***		***r^2***	***p-value***
Weekly	**274**	**0.16**	**±0.02**	**-7.57**	**±0.36**	**0.21**	**0.00**
Monthly	**124**	**0.14**	**±0.03**	**-7.13**	**±0.49**	**0.19**	**0.00**
Seasonal	**59**	**0.15**	**±0.03**	**-7.43**	**±0.61**	**0.27**	**0.00**
$\delta^{18}O$ vs. PDa							
Resolution	***n***	***Slope***		***y-Int***		***r^2***	***p-value***
Weekly	*274*	*-0.12*	*±0.16*	*-4.37*	*±0.57*	*0.00*	*0.47*

Table A5.A2. Percent change in AR03 regression values (Table A5.A1) due to aggregation.

LMWL (δD vs. $\delta^{18}O$)					
Aggregation	***Slope***	***Slope Error***	***y-Int***	***y-Int Error***	***r^2***
Weekly-Monthly	-3%	58%	-22%	52%	-2%
Weekly-Seasonal	-5%	85%	-36%	79%	-3%
Monthly-Seasonal	-1%	33%	-9%	31%	-1%
$\delta^{18}O$ vs. PDt					
Aggregation	***Slope***	***Slope Error***	***y-Int***	***y-Int Error***	***r^2***
Weekly-Monthly	-16%	35%	-6%	36%	-11%
Weekly-Seasonal	-10%	52%	-2%	53%	31%
Monthly-Seasonal	8%	21%	4%	21%	30%

Table A5.A3. AR03 temperature estimates and standard errors for three $\delta^{18}O$ values (vs. V-SMOW) at weekly, monthly, and seasonal resolutions. The three $\delta^{18}O$ values span much of the natural range of precipitation $\delta^{18}O$ in the study region, and -6‰ is close to the mean $\delta^{18}O$ value of all sites.

	Temperature Estimate (°C) when Precipitation $\delta^{18}O$ =		
Resolution	***-20‰***	***-6‰***	***0‰***
Weekly	-2.6 ±13.6	15.7 ±12.8	23.5 ±12.9
Monthly	-3.4 ±14.6	16.0 ±12.3	24.3 ±12.6
Seasonal	-9.8 ±16.1	15.7 ±10.7	26.7 ±11.3

Table A5.A4. Weight-averaged weekly values of $\delta^{18}O$ and average surface temperature for AR03 grouped by month and season. Blue (red) cells show low (high) values of note.

Group	***n***	***$\delta^{18}O_{wt}$***	***PDt***
Jan	23	-6.82 ±0.53	9.8 ±1.0
Feb	23	-5.90 ±0.72	9.6 ±1.0
Mar	31	-4.80 ±0.50	11.7 ±0.8
Apr	23	-4.10 ±0.45	17.9 ±0.8
May	35	-3.40 ±0.28	20.8 ±0.6
Jun	24	-4.05 ±0.56	23.4 ±0.4
Jul	21	-3.03 ±0.29	26.9 ±0.3
Aug	15	-3.05 ±0.38	25.5 ±0.4
Sep	18	-4.99 ±0.60	24.8 ±0.9
Oct	19	-5.51 ±0.47	20.2 ±0.7
Nov	24	-4.87 ±0.35	14.3 ±1.1
Dec	18	-5.88 ±0.48	9.1 ±1.1
Win	64	-6.15 ±0.35	9.8 ±0.6
Spr	89	-3.95 ±0.24	17.7 ±0.5
Sum	60	-3.71 ±0.27	25.0 ±0.3
Aut	61	-5.32 ±0.27	19.5 ±0.8

Table A5.A5. Regression results for AR03 when weekly data is grouped by month and by season. Significant results ($p \leq 0.05$) are bolded, while insignificant results are italicized. Actual precipitation amounts were normalized by a log transformation. Blue (red) cells show low (high) values of note.

LMWL (δD vs. $\delta^{18}O$)							
Group	***n***	***Slope***		***y-Int***		***r^2***	***p-value***
Jan	**23**	**7.26**	**±0.42**	**9.16**	**±3.14**	**0.93**	**0.00**
Feb	**23**	**7.94**	**±0.37**	**9.79**	**±2.61**	**0.96**	**0.00**
Mar	**31**	**7.47**	**±0.27**	**11.40**	**±1.56**	**0.96**	**0.00**
Apr	**23**	**5.54**	**±0.65**	**0.29**	**±2.91**	**0.78**	**0.00**
May	**35**	**6.42**	**±0.62**	**2.94**	**±2.33**	**0.76**	**0.00**
Jun	**24**	**6.26**	**±0.42**	**2.36**	**±2.14**	**0.91**	**0.00**
Jul	**21**	**7.35**	**±0.97**	**6.61**	**±3.06**	**0.75**	**0.00**
Aug	**15**	**7.29**	**±0.61**	**8.46**	**±2.15**	**0.92**	**0.00**
Sep	**18**	**7.85**	**±0.64**	**10.21**	**±3.58**	**0.90**	**0.00**
Oct	**19**	**7.47**	**±0.43**	**8.58**	**±2.49**	**0.95**	**0.00**
Nov	**24**	**7.63**	**±0.51**	**12.58**	**±2.76**	**0.91**	**0.00**
Dec	**18**	**6.51**	**±1.09**	**5.35**	**±6.85**	**0.69**	**0.00**
Win	**64**	**7.50**	**±0.32**	**9.58**	**±2.21**	**0.90**	**0.00**
Spr	**89**	**6.57**	**±0.27**	**4.89**	**±1.28**	**0.87**	**0.00**
Sum	**60**	**6.64**	**±0.32**	**4.78**	**±1.31**	**0.88**	**0.00**
Aut	**61**	**7.68**	**±0.32**	**10.85**	**±1.77**	**0.91**	**0.00**
$\delta^{18}O$ vs. PDt							
Group	***n***	***Slope***		***y-Int***		***r^2***	***p-value***
Jan	*23*	*0.16*	*±0.12*	*-8.41*	*±1.12*	*0.09*	*0.17*
Feb	**23**	**0.31**	**±0.13**	**-9.27**	**±1.47**	**0.20**	**0.03**
Mar	*31*	*0.18*	*±0.11*	*-7.44*	*±1.49*	*0.09*	*0.09*
Apr	*23*	*0.13*	*±0.13*	*-6.08*	*±2.16*	*0.05*	*0.33*
May	**35**	**0.30**	**±0.07**	**-9.61**	**±1.42**	**0.38**	**0.00**
Jun	*24*	*0.51*	*±0.30*	*-16.29*	*±7.10*	*0.11*	*0.11*
Jul	*21*	*0.28*	*±0.18*	*-10.45*	*±4.93*	*0.11*	*0.14*
Aug	*15*	*0.19*	*±0.26*	*-8.20*	*±6.76*	*0.04*	*0.48*
Sep	*18*	*0.01*	*±0.18*	*-5.26*	*±4.24*	*0.00*	*0.95*
Oct	*19*	*0.10*	*±0.16*	*-7.31*	*±3.18*	*0.02*	*0.54*
Nov	*24*	*0.09*	*±0.06*	*-6.41*	*±0.93*	*0.09*	*0.16*
Dec	*18*	*-0.03*	*±0.11*	*-5.73*	*±1.02*	*0.00*	*0.79*
Win	**64**	**0.16**	**±0.07**	**-7.92**	**±0.72**	**0.08**	**0.02**
Spr	**89**	**0.21**	**±0.04**	**-7.66**	**±0.78**	**0.21**	**0.00**

Sum	**60**	**0.41**	**±0.12**	**-13.97**	**±2.92**	**0.18**	**0.00**
Aut	*61*	*0.04*	*±0.04*	*-5.96*	*±0.86*	*0.02*	*0.33*
δ^{18}O vs. PDa							
Group	***n***	***Slope***		***y-Int***		***r^2***	***p-value***
Jan	*23*	*-0.41*	*±0.65*	*-5.62*	*±2.21*	*0.02*	*0.53*
Feb	*23*	*0.39*	*±0.85*	*-7.55*	*±2.90*	*0.01*	*0.65*
Mar	*31*	*-0.80*	*±0.59*	*-2.25*	*±2.10*	*0.06*	*0.19*
Apr	*23*	*-0.18*	*±0.58*	*-3.35*	*±2.00*	*0.00*	*0.76*
May	*35*	*-0.08*	*±0.33*	*-3.08*	*±1.20*	*0.00*	*0.80*
Jun	*24*	*0.67*	*±0.72*	*-6.71*	*±2.58*	*0.04*	*0.36*
Jul	*21*	*-0.45*	*±0.29*	*-1.32*	*±1.02*	*0.11*	*0.13*
Aug	*15*	*0.11*	*±0.36*	*-3.55*	*±1.11*	*0.01*	*0.77*
Sep	**18**	**-1.19**	**±0.50**	**-1.13**	**±1.70**	**0.26**	**0.03**
Oct	*19*	*-0.43*	*±0.39*	*-4.04*	*±1.28*	*0.07*	*0.28*
Nov	*24*	*0.01*	*±0.36*	*-5.16*	*±1.24*	*0.00*	*0.98*
Dec	*18*	*0.57*	*±0.47*	*-7.77*	*±1.58*	*0.08*	*0.25*
Win	*64*	*0.18*	*±0.39*	*-7.04*	*±1.32*	*0.00*	*0.64*
Spr	*89*	*-0.32*	*±0.29*	*-3.00*	*±1.05*	*0.01*	*0.29*
Sum	*60*	*-0.02*	*±0.28*	*-3.50*	*±0.99*	*0.00*	*0.95*
Aut	**61**	**-0.49**	**±0.24**	**-3.59**	**±0.80**	**0.07**	**0.04**

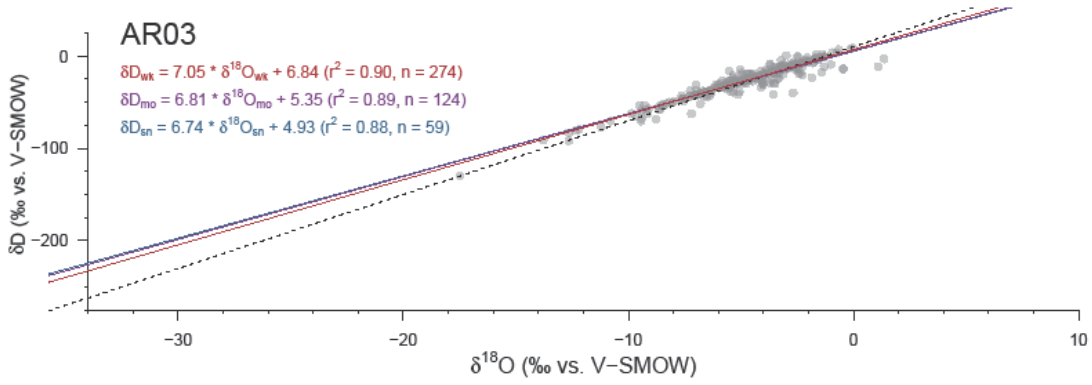

Figure A5.A1. Local meteoric water line for AR03. Gray circles represent values at their original weekly resolution while linear trends are plotted for weekly (red), aggregated monthly (violet), and aggregated seasonal (blue) resolutions. The dashed black line represents the global meteoric water line.

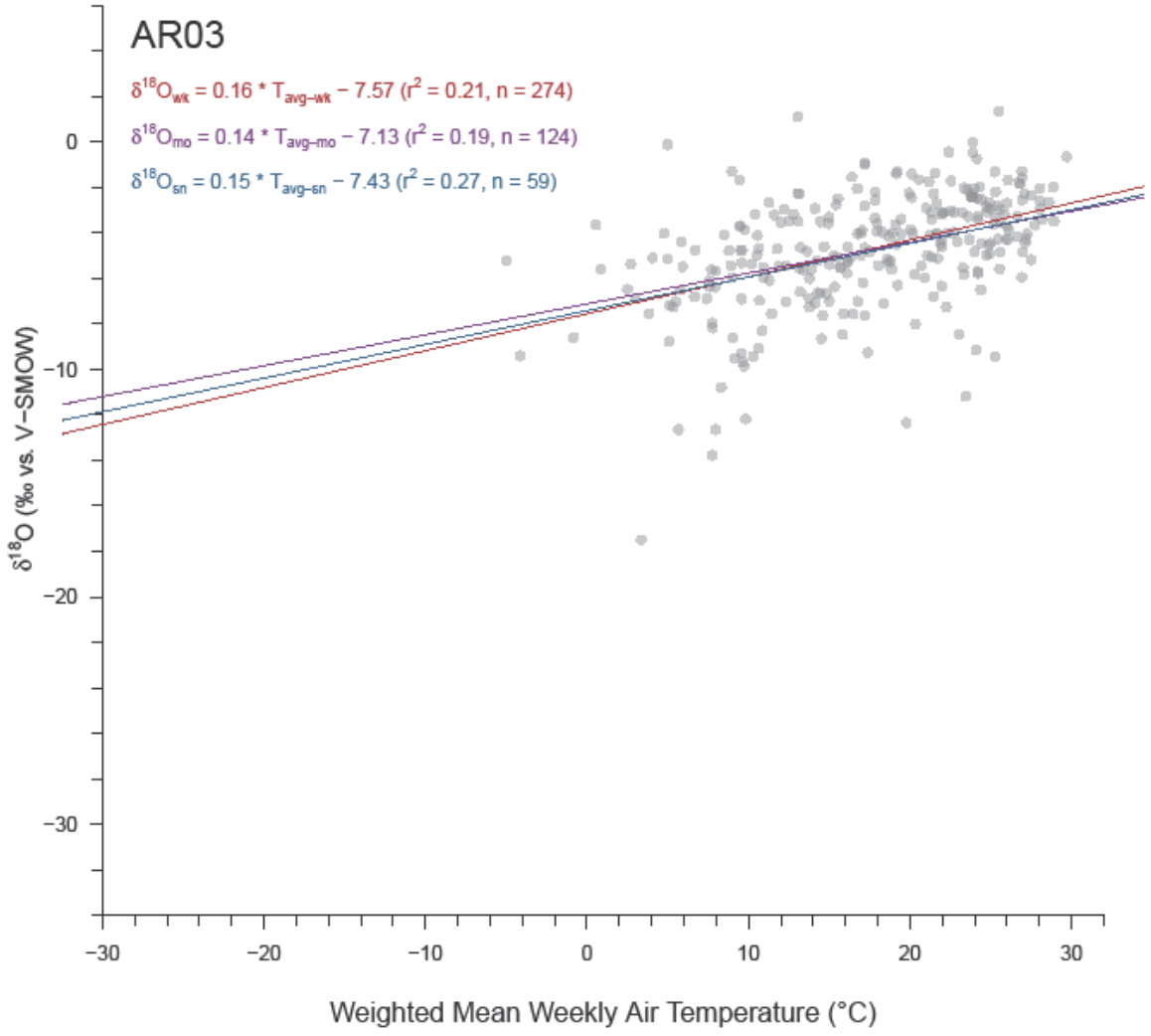

Figure A5.A2. Relationship between precipitation $\delta^{18}O$ and mean PDt at site AR03. Gray circles represent values at their original weekly resolution while linear trends are plotted for weekly (red), aggregated monthly (violet), and aggregated seasonal (blue) resolutions.

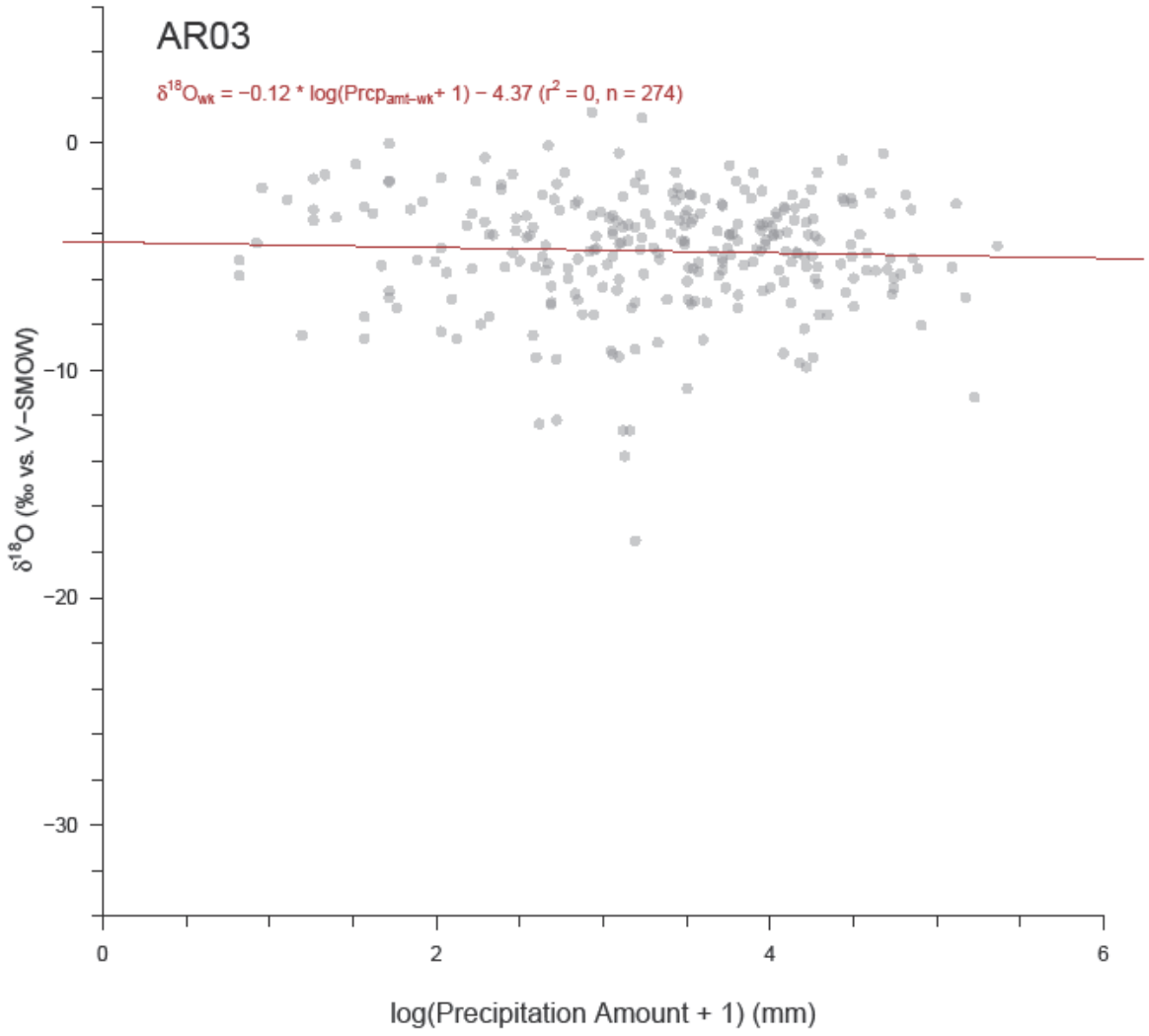

Figure A5.A3. Relationship between precipitation $\delta^{18}O$ and PDa at site AR03. Actual precipitation amounts were normalized by a log transformation. Gray circles represent values at their original weekly resolution with the weekly linear trend plotted in red. Precipitation amount data cannot be weight-averaged for aggregation, and thus regression was only performed at weekly resolution.

GA41

Table A5.B1. Regression results for GA41 at weekly, monthly, and seasonal resolutions. Significant results ($p \leq 0.05$) are bolded, while insignificant results are italicized. Actual precipitation amounts were normalized by a log transformation. Precipitation amount data cannot be weight-averaged for aggregation, and thus regression was only performed at weekly resolution.

LMWL (δD vs. $\delta^{18}O$)							
Resolution	**n**	**Slope**		**y-Int**		**r^2**	**p-value**
Weekly	**234**	**7.34**	**±0.13**	**10.47**	**±0.71**	**0.93**	**0.00**
Monthly	**113**	**6.96**	**±0.16**	**8.48**	**±0.89**	**0.94**	**0.00**
Seasonal	**48**	**7.33**	**±0.18**	**10.45**	**±1.02**	**0.97**	**0.00**
$\delta^{18}O$ vs. *PDt*							
Resolution	**n**	**Slope**		**y-Int**		**r^2**	**p-value**
Weekly	**234**	**0.12**	**±0.03**	**-6.50**	**±0.47**	**0.08**	**0.00**
Monthly	**113**	**0.13**	**±0.04**	**-6.95**	**±0.71**	**0.09**	**0.00**
Seasonal	**48**	**0.14**	**±0.06**	**-7.48**	**±1.01**	**0.13**	**0.01**
$\delta^{18}O$ vs. PDa							
Resolution	**n**	**Slope**		**y-Int**		**r^2**	**p-value**
Weekly	**234**	**-0.77**	**±0.18**	**-2.15**	**±0.61**	**0.07**	**0.00**

Table A5.B2. Percent change in GA41 regression values (Table A5.B1) due to aggregation.

LMWL (δD vs. $\delta^{18}O$)					
Aggregation	***Slope***	***Slope Error***	***y-Int***	***y-Int Error***	***r^2***
Weekly-Monthly	-5%	21%	-19%	25%	2%
Weekly-Seasonal	0%	31%	0%	35%	5%
Monthly-Seasonal	5%	12%	19%	13%	3%
$\delta^{18}O$ vs. PDt					
Aggregation	***Slope***	***Slope Error***	***y-Int***	***y-Int Error***	***r^2***
Weekly-Monthly	8%	49%	7%	52%	9%
Weekly-Seasonal	22%	77%	14%	75%	56%
Monthly-Seasonal	13%	30%	7%	29%	32%

Table A5.B3. GA41 temperature estimates and standard errors for three $\delta^{18}O$ values (vs. V-SMOW) at weekly, monthly, and seasonal resolutions. The three $\delta^{18}O$ values span much of the natural range of precipitation $\delta^{18}O$ in the study region, and -6‰ is close to the mean $\delta^{18}O$ value of all sites.

	Temperature Estimate (°C) when Precipitation $\delta^{18}O$ =		
Aggregation	***-20‰***	***-6‰***	***0‰***
Weekly	6.2 ±13.5	15.7 ±12.7	19.8 ±12.8
Monthly	6.8 ±13.8	16.4 ±12.3	20.6 ±12.4
Seasonal	3.9 ±15.4	16.2 ±11.5	21.5 ±12.0

Table A5.B4. Weight-averaged weekly values of $\delta^{18}O$ and average surface temperature for GA41 grouped by month and season. Blue (red) cells show low (high) values of note.

Group	***n***	***$\delta^{18}O_{wt}$***	***PDt***
Jan	28	-4.78 ±0.55	9.8 ±0.8
Feb	21	-5.53 ±0.50	10.1 ±0.9
Mar	19	-6.82 ±0.70	12.0 ±0.9
Apr	17	-4.18 ±0.53	16.8 ±1.0
May	13	-2.72 ±0.44	21.5 ±0.7
Jun	22	-3.31 ±0.59	22.7 ±0.6
Jul	23	-3.46 ±0.56	25.1 ±0.2
Aug	13	-3.67 ±0.77	24.7 ±0.3
Sep	18	-5.32 ±0.70	22.4 ±0.8
Oct	19	-6.93 ±0.70	18.2 ±0.5
Nov	17	-4.77 ±0.54	16.0 ±1.1
Dec	24	-5.58 ±0.60	9.3 ±0.7
Win	73	-5.73 ±0.32	9.7 ±0.5
Spr	49	-5.46 ±0.37	16.0 ±0.7
Sum	58	-3.60 ±0.36	23.7 ±0.3
Aut	54	-5.42 ±0.38	19.5 ±0.6

Table A5.B5. Regression results for GA41 when weekly data is grouped by month and by season. Significant results ($p \leq 0.05$) are bolded, while insignificant results are italicized. Actual precipitation amounts were normalized by a log transformation. Blue (red) cells show low (high) values of note.

LMWL (δD vs. $\delta^{18}O$)							
Group	***n***	***Slope***		***y-Int***		***r^2***	***p-value***
Jan	**28**	**8.28**	**±0.47**	**16.65**	**±2.78**	**0.92**	**0.00**
Feb	**21**	**7.77**	**±0.62**	**13.82**	**±3.65**	**0.89**	**0.00**
Mar	**19**	**7.62**	**±0.30**	**13.92**	**±1.86**	**0.97**	**0.00**
Apr	**17**	**7.68**	**±0.32**	**12.07**	**±1.39**	**0.97**	**0.00**
May	**13**	**5.35**	**±0.95**	**2.33**	**±3.14**	**0.74**	**0.00**
Jun	**22**	**5.70**	**±0.38**	**1.91**	**±1.82**	**0.92**	**0.00**
Jul	**23**	**7.50**	**±0.51**	**7.73**	**±2.02**	**0.91**	**0.00**
Aug	**13**	**7.18**	**±0.22**	**9.41**	**±1.15**	**0.99**	**0.00**
Sep	**18**	**7.56**	**±0.23**	**10.22**	**±1.19**	**0.99**	**0.00**
Oct	**19**	**7.51**	**±0.23**	**13.04**	**±1.40**	**0.98**	**0.00**
Nov	**17**	**7.66**	**±0.28**	**12.96**	**±1.42**	**0.98**	**0.00**
Dec	**24**	**8.40**	**±0.53**	**17.23**	**±3.16**	**0.92**	**0.00**
Win	**73**	**8.22**	**±0.30**	**16.32**	**±1.76**	**0.92**	**0.00**
Spr	**49**	**7.13**	**±0.24**	**9.86**	**±1.21**	**0.95**	**0.00**
Sum	**58**	**6.67**	**±0.26**	**5.86**	**±1.21**	**0.92**	**0.00**
Aut	**54**	**7.49**	**±0.15**	**11.68**	**±0.81**	**0.98**	**0.00**
$\delta^{18}O$ vs. PDt							
Group	***n***	***Slope***		***y-Int***		***r^2***	***p-value***
Jan	*28*	*-0.03*	*±0.13*	*-4.94*	*±1.33*	*0.00*	*0.80*
Feb	*21*	*0.02*	*±0.13*	*-5.73*	*±1.49*	*0.00*	*0.86*
Mar	*19*	*0.31*	*±0.17*	*-9.58*	*±2.34*	*0.16*	*0.09*
Apr	*17*	*0.21*	*±0.13*	*-7.16*	*±2.15*	*0.15*	*0.12*
May	*13*	*-0.15*	*±0.18*	*0.21*	*±3.76*	*0.06*	*0.41*
Jun	*22*	*0.15*	*±0.22*	*-7.27*	*±5.06*	*0.02*	*0.52*
Jul	*23*	*0.44*	*±0.50*	*-13.88*	*±12.43*	*0.04*	*0.39*
Aug	*13*	*1.15*	*±0.76*	*-32.65*	*±18.53*	*0.17*	*0.16*
Sep	*18*	*0.36*	*±0.20*	*-12.39*	*±4.60*	*0.16*	*0.10*
Oct	*19*	*0.25*	*±0.34*	*-9.93*	*±6.32*	*0.03*	*0.48*
Nov	*17*	*0.07*	*±0.12*	*-5.79*	*±1.97*	*0.02*	*0.57*
Dec	*24*	*0.07*	*±0.17*	*-5.84*	*±1.69*	*0.01*	*0.71*
Win	*73*	*0.00*	*±0.08*	*-5.36*	*±0.83*	*0.00*	*0.96*
Spr	**49**	**0.27**	**±0.07**	**-8.54**	**±1.22**	**0.23**	**0.00**

Sum	*58*	*0.26*	*±0.17*	*-9.83*	*±3.98*	*0.04*	*0.13*
Aut	*54*	*0.13*	*±0.08*	*-7.35*	*±1.63*	*0.05*	*0.12*
$\delta^{18}O$ vs. PDa							
Group	***n***	***Slope***		***y-Int***		***r^2***	***p-value***
Jan	*28*	*0.26*	*±0.71*	*-6.04*	*±2.23*	*0.01*	*0.72*
Feb	*21*	*-0.90*	*±0.55*	*-2.44*	*±1.92*	*0.12*	*0.12*
Mar	**19**	**-1.30**	**±0.49**	**-1.69**	**±1.58**	**0.29**	**0.02**
Apr	*17*	*-0.76*	*±0.64*	*-1.53*	*±1.94*	*0.08*	*0.26*
May	*13*	*-0.41*	*±0.54*	*-1.68*	*±1.74*	*0.05*	*0.46*
Jun	*22*	*0.14*	*±0.74*	*-4.41*	*±2.48*	*0.00*	*0.85*
Jul	**23**	**-2.17**	**±0.72**	**4.49**	**±2.51**	**0.30**	**0.01**
Aug	*13*	*-0.82*	*±0.70*	*-1.56*	*±2.57*	*0.11*	*0.27*
Sep	*18*	*-1.20*	*±0.66*	*-0.57*	*±2.16*	*0.17*	*0.09*
Oct	*19*	*-0.97*	*±0.52*	*-2.55*	*±1.64*	*0.17*	*0.08*
Nov	*17*	*-0.90*	*±0.55*	*-1.81*	*±1.83*	*0.15*	*0.12*
Dec	*24*	*-1.10*	*±0.64*	*-1.85*	*±2.07*	*0.12*	*0.10*
Win	*73*	*-0.60*	*±0.37*	*-3.42*	*±1.20*	*0.04*	*0.11*
Spr	**49**	**-0.96**	**±0.35**	**-1.36**	**±1.10**	**0.14**	**0.01**
Sum	*58*	*-0.78*	*±0.42*	*-1.02*	*±1.47*	*0.06*	*0.07*
Aut	**54**	**-0.97**	**±0.32**	**-1.84**	**±1.05**	**0.15**	**0.00**

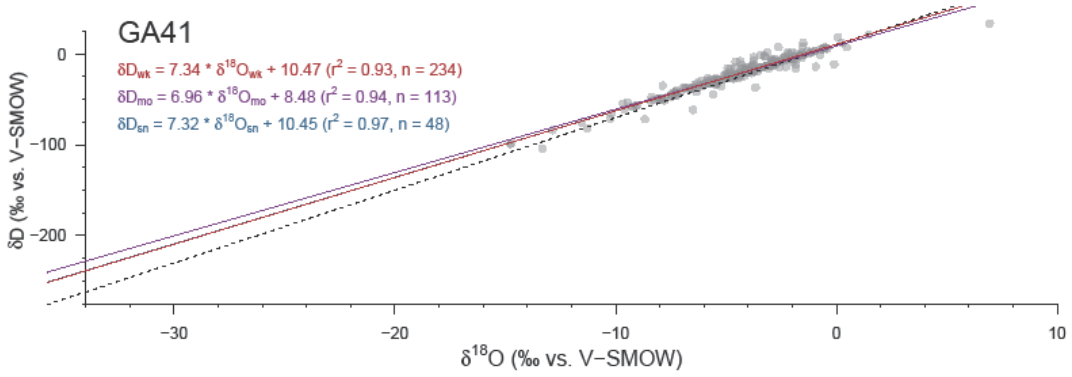

Figure A5.B1. Local meteoric water line for GA41. Gray circles represent values at their original weekly resolution while linear trends are plotted for weekly (red), aggregated monthly (violet), and aggregated seasonal (blue) resolutions. The dashed black line represents the global meteoric water line.

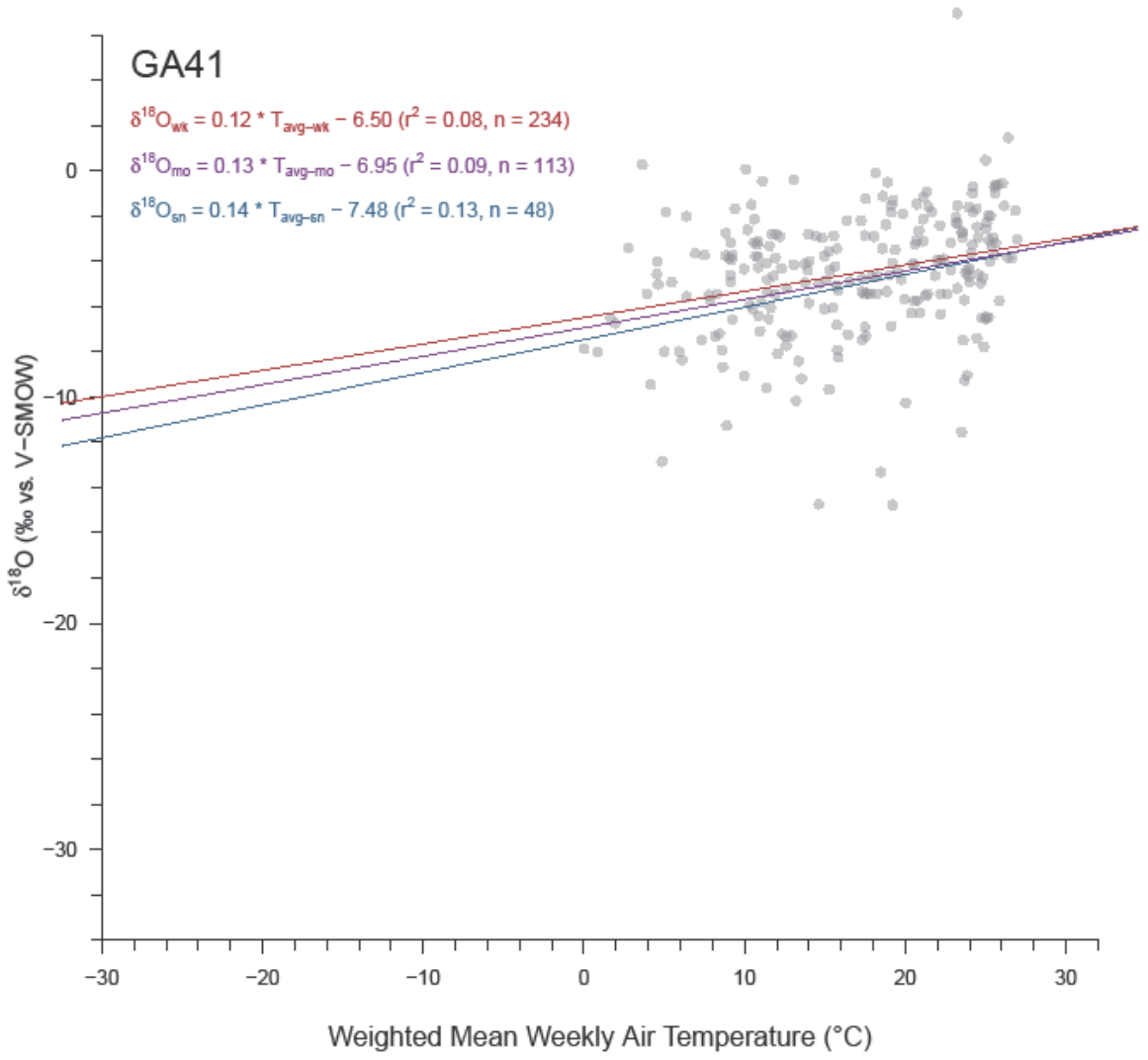

Figure A5.B2. Relationship between precipitation $\delta^{18}O$ and mean PDt at site GA41. Gray circles represent values at their original weekly resolution while linear trends are plotted for weekly (red), aggregated monthly (violet), and aggregated seasonal (blue) resolutions.

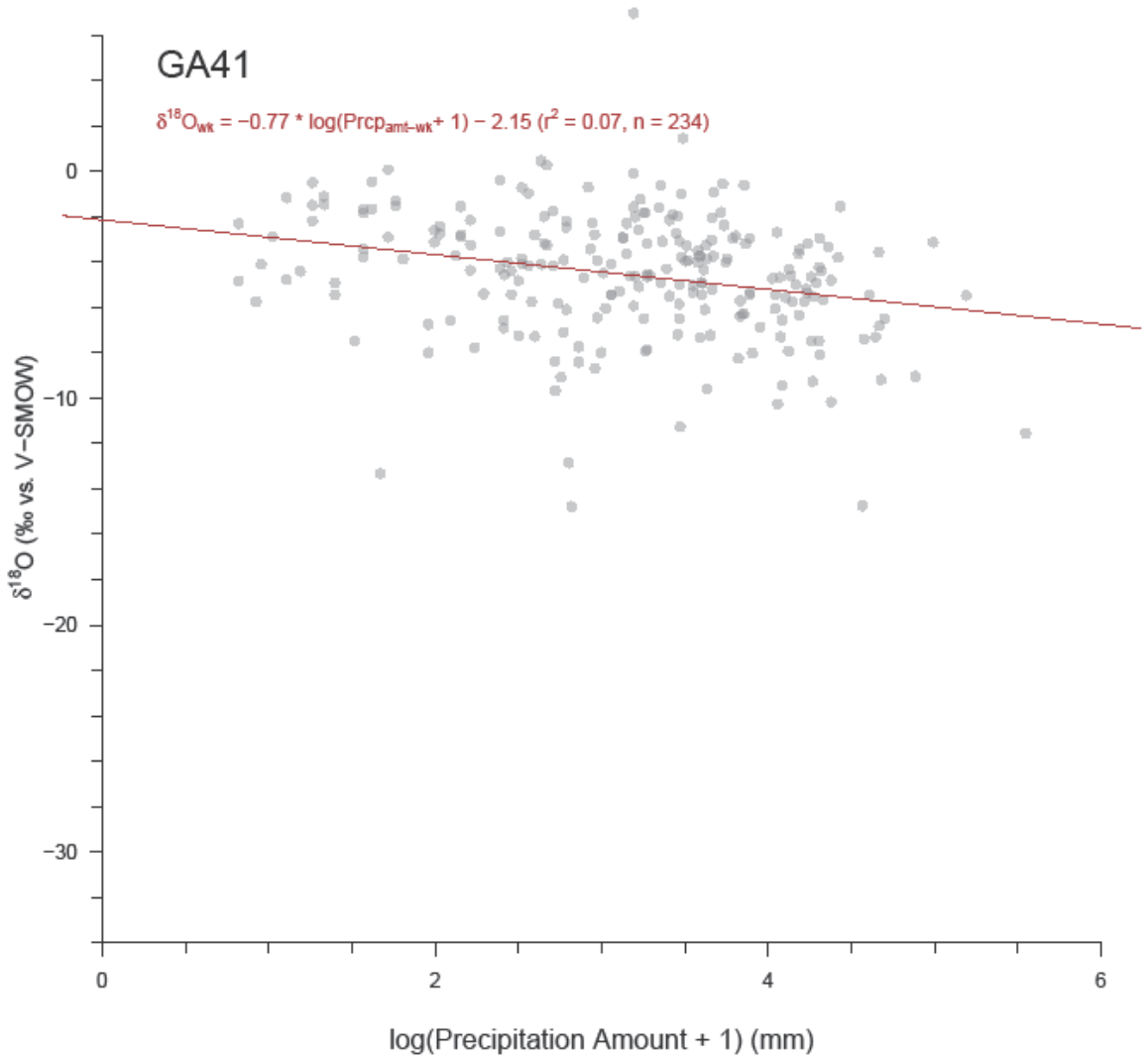

Figure A5.B3. Relationship between precipitation $\delta^{18}O$ and PDa at site GA41. Actual precipitation amounts were normalized by a log transformation. Gray circles represent values at their original weekly resolution with the weekly linear trend plotted in red. Precipitation amount data cannot be weight-averaged for aggregation, and thus regression was only performed at weekly resolution.

IA23

Table A5.C1. Regression results for IA23 at weekly, monthly, and seasonal resolutions. Significant results ($p \leq 0.05$) are bolded, while insignificant results are italicized. Actual precipitation amounts were normalized by a log transformation. Precipitation amount data cannot be weight-averaged for aggregation, and thus regression was only performed at weekly resolution.

LMWL (δD vs. $\delta^{18}O$)							
Resolution	***n***	***Slope***		***y-Int***		***r^2***	***p-value***
Weekly	**211**	**7.95**	**±0.07**	**11.41**	**±0.62**	**0.98**	**0.00**
Monthly	**99**	**8.01**	**±0.08**	**12.04**	**±0.78**	**0.99**	**0.00**
Seasonal	**45**	**8.13**	**±0.08**	**13.14**	**±0.80**	**1.00**	**0.00**
$\delta^{18}O$ vs. PDt							
Resolution	***n***	***Slope***		***y-Int***		***r^2***	***p-value***
Weekly	**211**	**0.34**	**±0.02**	**-11.89**	**±0.34**	**0.52**	**0.00**
Monthly	**99**	**0.36**	**±0.03**	**-12.56**	**±0.46**	**0.59**	**0.00**
Seasonal	**45**	**0.41**	**±0.05**	**-13.25**	**±0.68**	**0.64**	**0.00**
$\delta^{18}O$ vs. PDa							
Resolution	***n***	***Slope***		***y-Int***		***r^2***	***p-value***
Weekly	**211**	**0.94**	**±0.35**	**-10.55**	**±1.08**	**0.03**	**0.01**

Table A5.C2. Percent change in IA23 regression values (Table A5.C1) due to aggregation.

LMWL (δD vs. $\delta^{18}O$)					
Aggregation	***Slope***	***Slope Error***	***y-Int***	***y-Int Error***	***r^2***
Weekly-Monthly	1%	18%	6%	27%	1%
Weekly-Seasonal	2%	14%	14%	23%	1%
Monthly-Seasonal	2%	-2%	8%	2%	1%
$\delta^{18}O$ vs. PDt					
Aggregation	***Slope***	***Slope Error***	***y-Int***	***y-Int Error***	***r^2***
Weekly-Monthly	7%	37%	6%	33%	12%
Weekly-Seasonal	21%	80%	11%	73%	21%
Monthly-Seasonal	13%	34%	5%	33%	9%

Table A5.C3. IA23 temperature estimates and standard errors for three $\delta^{18}O$ values (vs. V-SMOW) at weekly, monthly, and seasonal resolutions. The three $\delta^{18}O$ values span much of the natural range of precipitation $\delta^{18}O$ in the study region, and -6‰ is close to the mean $\delta^{18}O$ value of all sites.

	Temperature Estimate (°C) when Precipitation $\delta^{18}O$ =		
Aggregation	***-20‰***	***-6‰***	***0‰***
Weekly	-6.7 ±12.9	14.9 ±12.7	24.1 ±12.8
Monthly	-7.4 ±12.7	15.3 ±12.3	25.1 ±12.5
Seasonal	-6.6 ±12.2	15.2 ±11.6	24.5 ±11.9

Table A5.C4. Weight-averaged weekly values of $\delta^{18}O$ and average surface temperature for IA23 grouped by month and season. Blue (red) cells show low (high) values of note.

Group	***n***	***$\delta^{18}O_{wt}$***	***PDt***
Jan	8	-12.93 ±1.61	-1.6 ±1.8
Feb	17	-13.29 ±0.96	-0.6 ±1.4
Mar	18	-9.05 ±1.05	3.2 ±1.6
Apr	26	-7.38 ±0.53	9.1 ±0.7
May	30	-5.31 ±0.39	15.6 ±0.7
Jun	25	-5.92 ±0.46	19.9 ±0.6
Jul	18	-5.40 ±0.39	22.7 ±0.5
Aug	16	-3.57 ±0.60	23.6 ±0.4
Sep	13	-7.82 ±0.72	18.9 ±1.1
Oct	18	-8.26 ±0.89	13.9 ±0.8
Nov	13	-9.66 ±0.63	6.7 ±1.0
Dec	9	-17.04 ±2.09	-2.2 ±2.1
Win	34	-14.34 ±0.83	-1.7 ±1.0
Spr	74	-7.04 ±0.38	10.6 ±0.8
Sum	59	-5.46 ±0.29	21.6 ±0.4
Aut	44	-8.11 ±0.46	14.0 ±0.9

Table A5.C5. Regression results for IA23 when weekly data is grouped by month and by season. Significant results ($p \leq 0.05$) are bolded, while insignificant results are italicized. Actual precipitation amounts were normalized by a log transformation. Blue (red) cells show low (high) values of note.

LMWL (δD vs. $\delta^{18}O$)							
Group	***n***	***Slope***		***y-Int***		***r^2***	***p-value***
Jan	**8**	**8.09**	**±0.21**	**14.10**	**±2.79**	**1.00**	**0.00**
Feb	**17**	**8.04**	**±0.22**	**12.07**	**±3.01**	**0.99**	**0.00**
Mar	**18**	**8.39**	**±0.30**	**16.64**	**±2.96**	**0.98**	**0.00**
Apr	**26**	**7.43**	**±0.30**	**8.13**	**±2.26**	**0.96**	**0.00**
May	**30**	**7.62**	**±0.35**	**8.99**	**±2.09**	**0.95**	**0.00**
Jun	**25**	**7.16**	**±0.38**	**6.48**	**±2.21**	**0.94**	**0.00**
Jul	**18**	**8.05**	**±0.58**	**10.25**	**±3.11**	**0.92**	**0.00**
Aug	**16**	**7.22**	**±0.36**	**8.26**	**±1.58**	**0.97**	**0.00**
Sep	**13**	**8.38**	**±0.29**	**15.52**	**±2.48**	**0.99**	**0.00**
Oct	**18**	**7.98**	**±0.39**	**11.42**	**±3.52**	**0.96**	**0.00**
Nov	**13**	**9.20**	**±0.44**	**25.94**	**±4.13**	**0.98**	**0.00**
Dec	**9**	**8.66**	**±0.20**	**22.60**	**±3.37**	**1.00**	**0.00**
Win	**34**	**8.30**	**±0.13**	**16.11**	**±1.83**	**0.99**	**0.00**
Spr	**74**	**7.87**	**±0.16**	**11.11**	**±1.26**	**0.97**	**0.00**
Sum	**59**	**7.43**	**±0.23**	**7.99**	**±1.24**	**0.95**	**0.00**
Aut	**44**	**8.19**	**±0.24**	**14.46**	**±2.19**	**0.96**	**0.00**
$\delta^{18}O$ vs. PDt							
Group	***n***	***Slope***		***y-Int***		***r^2***	***p-value***
Jan	*8*	*0.39*	*±0.32*	*-11.90*	*±1.70*	*0.19*	*0.28*
Feb	*17*	*0.32*	*±0.16*	*-12.85*	*±0.88*	*0.21*	*0.06*
Mar	**18**	**0.55**	**±0.09**	**-10.97**	**±0.71**	**0.68**	**0.00**
Apr	**26**	**0.31**	**±0.13**	**-9.83**	**±1.28**	**0.18**	**0.03**
May	**30**	**0.39**	**±0.06**	**-11.60**	**±1.00**	**0.57**	**0.00**
Jun	*25*	*0.24*	*±0.15*	*-10.12*	*±2.93*	*0.10*	*0.12*
Jul	*18*	*0.36*	*±0.18*	*-13.28*	*±4.13*	*0.20*	*0.06*
Aug	*16*	*-0.19*	*±0.38*	*0.77*	*±9.07*	*0.02*	*0.63*
Sep	**13**	**0.40**	**±0.16**	**-15.43**	**±2.98**	**0.36**	**0.03**
Oct	*18*	*-0.02*	*±0.28*	*-7.98*	*±3.97*	*0.00*	*0.94*
Nov	*13*	*-0.07*	*±0.19*	*-8.79*	*±1.33*	*0.01*	*0.74*
Dec	**9**	**0.76**	**±0.25**	**-14.26**	**±1.53**	**0.58**	**0.02**
Win	**34**	**0.47**	**±0.13**	**-13.08**	**±0.72**	**0.31**	**0.00**
Spr	**74**	**0.36**	**±0.04**	**-10.65**	**±0.48**	**0.54**	**0.00**

Sum	**59**	**0.26**	**±0.09**	**-10.46**	**±2.05**	**0.12**	**0.01**
Aut	*44*	*0.09*	*±0.08*	*-9.73*	*±1.09*	*0.03*	*0.24*
$\delta^{18}O$ vs. PDa							
Group	***n***	***Slope***		***y-Int***		***r^2***	***p-value***
Jan	*8*	*3.23*	*±3.13*	*-20.87*	*±8.08*	*0.15*	*0.34*
Feb	*17*	*-0.85*	*±1.32*	*-10.80*	*±3.54*	*0.03*	*0.53*
Mar	*18*	*-0.77*	*±1.71*	*-6.58*	*±5.18*	*0.01*	*0.66*
Apr	*26*	*0.08*	*±0.61*	*-7.30*	*±1.79*	*0.00*	*0.90*
May	*30*	*0.77*	*±0.45*	*-8.26*	*±1.58*	*0.09*	*0.10*
Jun	*25*	*-1.25*	*±0.66*	*-1.27*	*±2.20*	*0.14*	*0.07*
Jul	*18*	*0.09*	*±0.42*	*-5.38*	*±1.37*	*0.00*	*0.84*
Aug	*16*	*-0.28*	*±0.56*	*-2.84*	*±1.75*	*0.02*	*0.62*
Sep	*13*	*-0.29*	*±1.04*	*-7.37*	*±3.31*	*0.01*	*0.79*
Oct	*18*	*0.82*	*±1.25*	*-10.40*	*±3.34*	*0.03*	*0.52*
Nov	*13*	*-0.24*	*±0.84*	*-8.48*	*±2.53*	*0.01*	*0.78*
Dec	*9*	*3.92*	*±3.64*	*-25.84*	*±9.55*	*0.14*	*0.32*
Win	*34*	*0.71*	*±1.28*	*-15.50*	*±3.40*	*0.01*	*0.58*
Spr	*74*	*0.54*	*±0.44*	*-8.60*	*±1.41*	*0.02*	*0.22*
Sum	*59*	*-0.48*	*±0.32*	*-3.31*	*±1.04*	*0.04*	*0.14*
Aut	*44*	*0.12*	*±0.60*	*-8.88*	*±1.75*	*0.00*	*0.84*

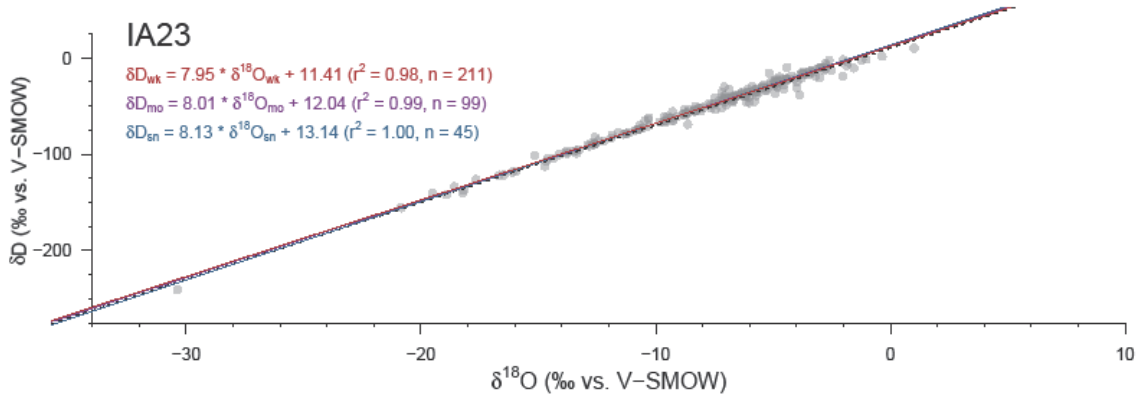

Figure A5.C1. Local meteoric water line for IA23. Gray circles represent values at their original weekly resolution while linear trends are plotted for weekly (red), aggregated monthly (violet), and aggregated seasonal (blue) resolutions. The dashed black line represents the global meteoric water line.

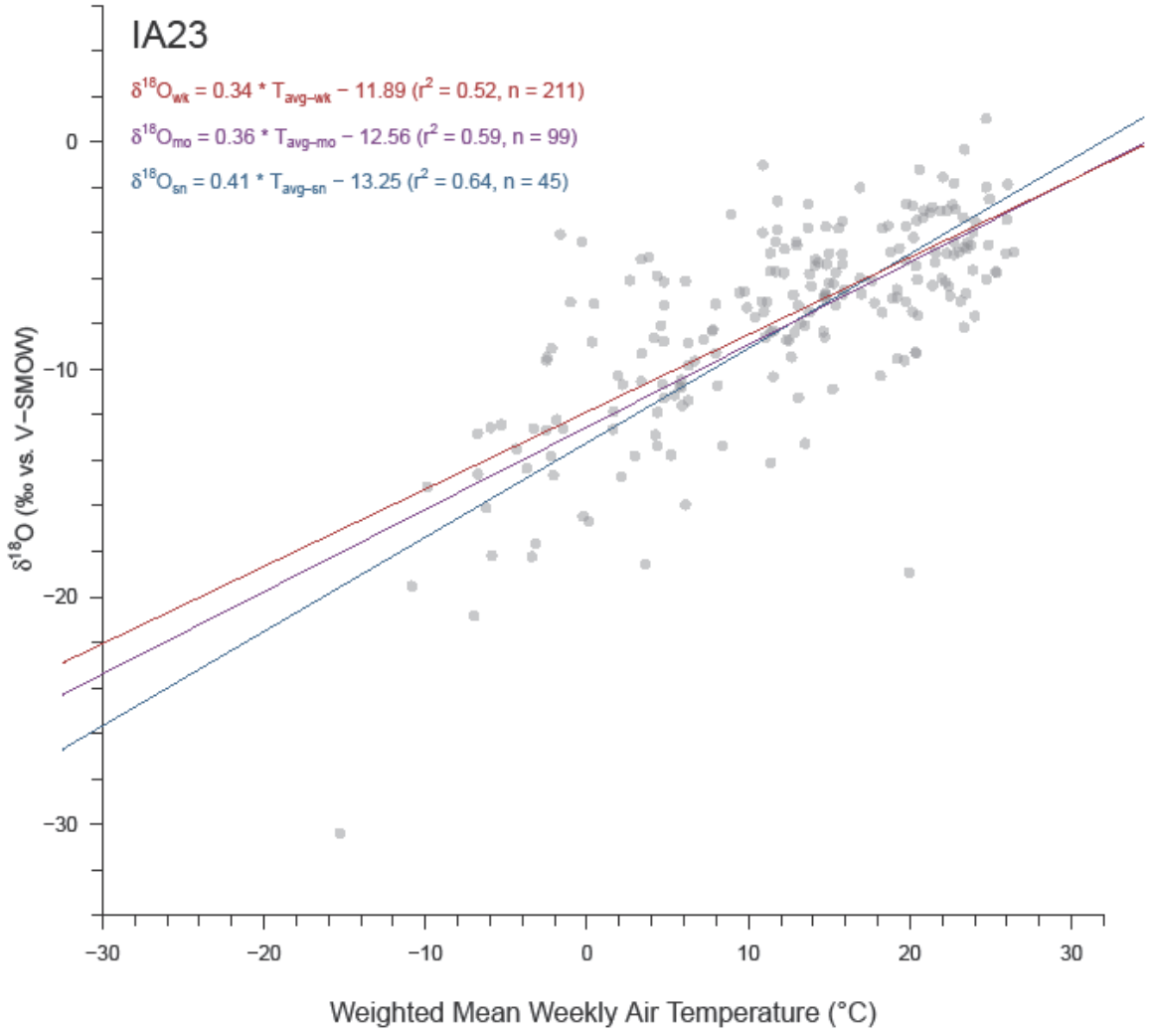

Figure A5.C2. Relationship between precipitation $\delta^{18}O$ and mean PDt at site IA23. Gray circles represent values at their original weekly resolution while linear trends are plotted for weekly (red), aggregated monthly (violet), and aggregated seasonal (blue) resolutions.

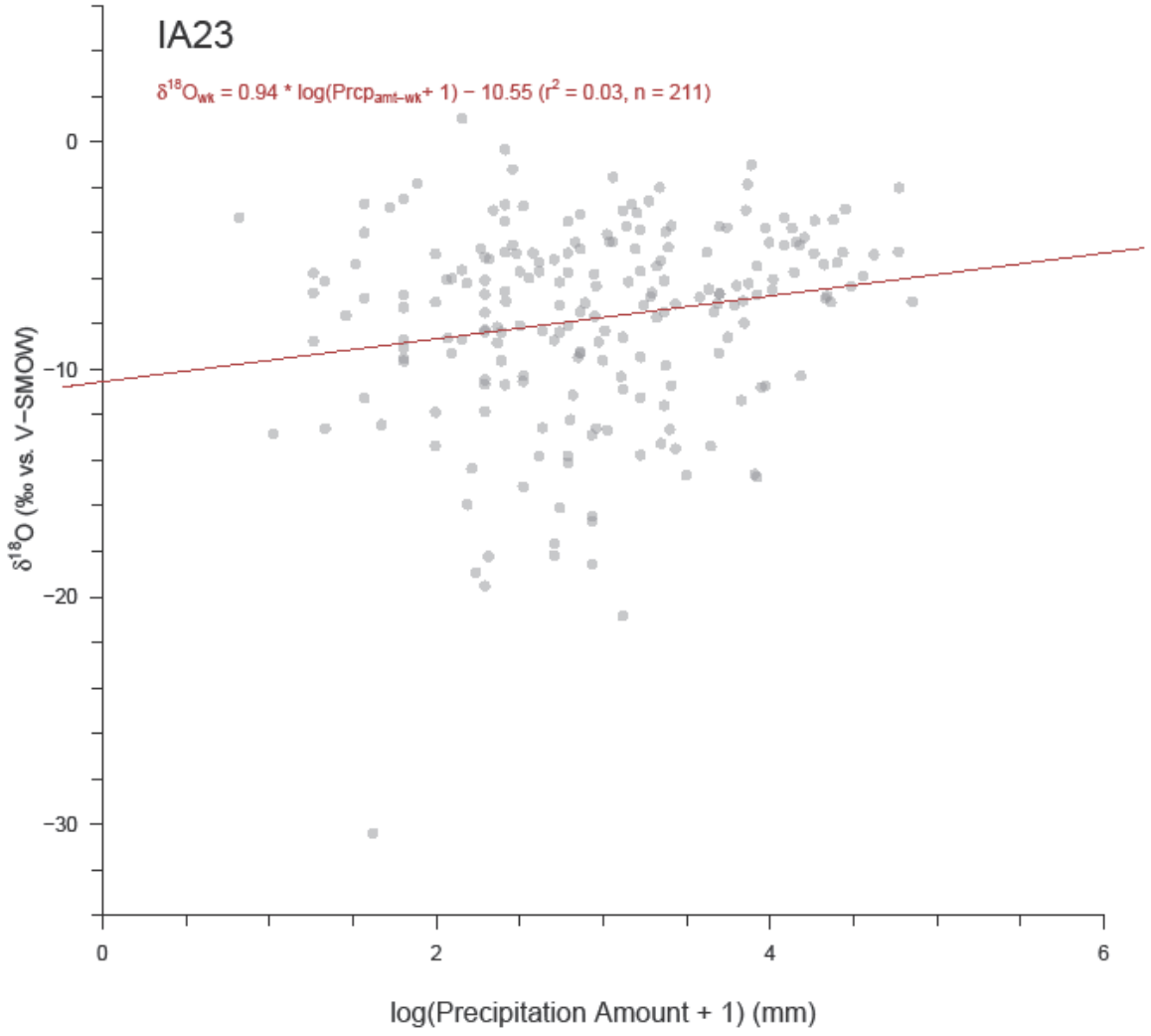

Figure A5.C3. Relationship between precipitation $\delta^{18}O$ and PDa at site IA23. Actual precipitation amounts were normalized by a log transformation. Gray circles represent values at their original weekly resolution with the weekly linear trend plotted in red. Precipitation amount data cannot be weight-averaged for aggregation, and thus regression was only performed at weekly resolution.

IL63

Table A5.D1. Regression results for IL63 at weekly, monthly, and seasonal resolutions. Significant results ($p \leq 0.05$) are bolded, while insignificant results are italicized. Actual precipitation amounts were normalized by a log transformation. Precipitation amount data cannot be weight-averaged for aggregation, and thus regression was only performed at weekly resolution.

LMWL (δD vs. $\delta^{18}O$)							
Resolution	***n***	***Slope***		***y-Int***		***r^2***	***p-value***
Weekly	**190**	**7.19**	**±0.19**	**3.17**	**±1.26**	**0.88**	**0.00**
Monthly	**72**	**6.73**	**±0.35**	**0.31**	**±2.15**	**0.84**	**0.00**
Seasonal	**29**	**6.22**	**±0.61**	**-1.69**	**±3.66**	**0.80**	**0.00**
$\delta^{18}O$ vs. PDt							
Resolution	***n***	***Slope***		***y-Int***		***r^2***	***p-value***
Weekly	**190**	**0.22**	**±0.03**	**-8.79**	**±0.46**	**0.26**	**0.00**
Monthly	**72**	**0.22**	**±0.03**	**-8.97**	**±0.55**	**0.41**	**0.00**
Seasonal	**29**	**0.20**	**±0.05**	**-8.82**	**±0.85**	**0.39**	**0.00**
$\delta^{18}O$ vs. PDa							
Resolution	***n***	***Slope***		***y-Int***		***r^2***	***p-value***
Weekly	*190*	*0.07*	*±0.30*	*-5.72*	*±1.00*	*0.00*	*0.82*

Table A5.D2. Percent change in IL63 regression values (Table A5.D1) due to aggregation.

LMWL (δD vs. $\delta^{18}O$)					
Aggregation	***Slope***	***Slope Error***	***y-Int***	***y-Int Error***	***r^2***
Weekly-Monthly	-6%	80%	-90%	71%	-4%
Weekly-Seasonal	-14%	119%	-1557%	112%	-10%
Monthly-Seasonal	-8%	43%	118%	41%	-6%
$\delta^{18}O$ vs. PDt					
Aggregation	***Slope***	***Slope Error***	***y-Int***	***y-Int Error***	***r^2***
Weekly-Monthly	2%	18%	2%	19%	58%
Weekly-Seasonal	-7%	70%	0%	70%	31%
Monthly-Seasonal	-9%	35%	-2%	35%	-6%

Table A5.D3. IL63 temperature estimates and standard errors for three $\delta^{18}O$ values (vs. V-SMOW) at weekly, monthly, and seasonal resolutions. The three $\delta^{18}O$ values span much of the natural range of precipitation $\delta^{18}O$ in the study region, and -6‰ is close to the mean $\delta^{18}O$ value of all sites.

	Temperature Estimate (°C) when Precipitation $\delta^{18}O$ =		
Aggregation	***-20‰***	***-6‰***	***0‰***
Weekly	-2.2 ±14.7	14.7 ±14.1	21.9 ±14.2
Monthly	-11.4 ±14.6	14.7 ±12.4	26.0 ±12.8
Seasonal	-11.7 ±18.1	15.2 ±11.7	26.8 ±12.9

Table A5.D4. Weight-averaged weekly values of $\delta^{18}O$ and average surface temperature for IL63 grouped by month and season. Blue (red) cells show low (high) values of note.

Group	***n***	***$\delta^{18}O_{wt}$***		***PDt***	
Jan	20	-8.73	±0.84	4.6	±1.3
Feb	15	-8.83	±1.33	6.8	±1.2
Mar	25	-5.22	±0.54	11.0	±0.8
Apr	21	-4.22	±0.43	16.2	±0.8
May	20	-3.95	±0.68	20.5	±0.7
Jun	17	-4.34	±0.66	23.1	±0.9
Jul	15	-3.74	±0.39	25.5	±0.5
Aug	12	-2.95	±0.36	25.7	±0.5
Sep	9	-6.42	±1.66	23.6	±1.2
Oct	15	-5.90	±0.49	16.3	±1.1
Nov	10	-5.09	±0.71	13.1	±1.7
Dec	11	-6.79	±0.97	7.8	±1.1
Win	46	-7.69	±0.64	6.9	±0.7
Spr	66	-4.32	±0.32	16.2	±0.7
Sum	44	-4.05	±0.30	24.2	±0.5
Aut	34	-6.46	±0.51	16.9	±1.0

Table A5.D5. Regression results for IL63 when weekly data is grouped by month and by season. Significant results ($p \leq 0.05$) are bolded, while insignificant results are italicized. Actual precipitation amounts were normalized by a log transformation. Blue (red) cells show low (high) values of note.

LMWL (δD vs. $\delta^{18}O$)							
Group	***n***	***Slope***		***y-Int***		***r^2***	***p-value***
Jan	**20**	**8.54**	**±0.40**	**19.09**	**±3.94**	**0.96**	**0.00**
Feb	**15**	**7.97**	**±0.62**	**6.74**	**±6.48**	**0.93**	**0.00**
Mar	**25**	**5.73**	**±0.83**	**-3.94**	**±4.94**	**0.67**	**0.00**
Apr	**21**	**7.27**	**±0.99**	**4.87**	**±4.83**	**0.74**	**0.00**
May	**20**	**6.90**	**±0.80**	**-0.60**	**±3.92**	**0.81**	**0.00**
Jun	**17**	**7.18**	**±0.50**	**4.56**	**±2.44**	**0.93**	**0.00**
Jul	**15**	**6.41**	**±1.01**	**1.95**	**±4.14**	**0.76**	**0.00**
Aug	**12**	**4.24**	**±1.74**	**-4.14**	**±6.09**	**0.37**	**0.04**
Sep	**9**	**6.87**	**±0.35**	**-5.87**	**±2.62**	**0.98**	**0.00**
Oct	**15**	**6.59**	**±1.65**	**-2.24**	**±9.61**	**0.55**	**0.00**
Nov	**10**	**4.40**	**±1.09**	**-9.93**	**±6.58**	**0.67**	**0.00**
Dec	**11**	**6.18**	**±0.64**	**-3.51**	**±4.06**	**0.91**	**0.00**
Win	**46**	**7.78**	**±0.33**	**8.15**	**±3.05**	**0.93**	**0.00**
Spr	**66**	**6.42**	**±0.48**	**-0.55**	**±2.53**	**0.74**	**0.00**
Sum	**44**	**6.77**	**±0.46**	**3.40**	**±1.97**	**0.84**	**0.00**
Aut	**34**	**6.46**	**±0.57**	**-3.01**	**±3.62**	**0.80**	**0.00**
$\delta^{18}O$ vs. PDt							
Group	***n***	***Slope***		***y-Int***		***r^2***	***p-value***
Jan	*20*	*0.27*	*±0.13*	*-10.38*	*±0.99*	*0.18*	*0.06*
Feb	**15**	**0.71**	**±0.24**	**-13.21**	**±1.76**	**0.39**	**0.01**
Mar	*25*	*0.20*	*±0.13*	*-7.46*	*±1.48*	*0.10*	*0.13*
Apr	*21*	*0.13*	*±0.12*	*-6.50*	*±1.90*	*0.06*	*0.30*
May	*20*	*0.00*	*±0.23*	*-3.85*	*±4.64*	*0.00*	*0.99*
Jun	*17*	*0.12*	*±0.18*	*-6.91*	*±4.21*	*0.03*	*0.51*
Jul	*15*	*0.38*	*±0.19*	*-13.45*	*±4.81*	*0.24*	*0.07*
Aug	*12*	*0.03*	*±0.22*	*-3.97*	*±5.75*	*0.00*	*0.91*
Sep	*9*	*-0.12*	*±0.50*	*-3.06*	*±11.12*	*0.01*	*0.82*
Oct	*15*	*0.10*	*±0.12*	*-7.00*	*±1.86*	*0.05*	*0.42*
Nov	*10*	*0.08*	*±0.14*	*-6.52*	*±1.83*	*0.03*	*0.61*
Dec	*11*	*0.07*	*±0.29*	*-6.06*	*±2.42*	*0.01*	*0.81*
Win	**46**	**0.41**	**±0.11**	**-10.59**	**±0.86**	**0.22**	**0.00**
Spr	**66**	**0.14**	**±0.06**	**-6.80**	**±0.95**	**0.08**	**0.02**

Sum	*44*	*0.17*	*±0.10*	*-7.96*	*±2.50*	*0.06*	*0.10*
Aut	*34*	*0.02*	*±0.09*	*-5.97*	*±1.51*	*0.00*	*0.80*
$\delta^{18}O$ vs. PDa							
Group	***n***	***Slope***		***y-Int***		***r^2***	***p-value***
Jan	*20*	*2.10*	*±1.07*	*-15.61*	*±3.39*	*0.18*	*0.07*
Feb	*15*	*1.23*	*±1.53*	*-13.02*	*±4.96*	*0.05*	*0.44*
Mar	*25*	*-1.53*	*±0.86*	*-0.62*	*±2.70*	*0.12*	*0.09*
Apr	*21*	*0.77*	*±0.55*	*-7.11*	*±1.90*	*0.09*	*0.18*
May	*20*	*0.92*	*±1.15*	*-7.27*	*±4.28*	*0.03*	*0.44*
Jun	*17*	*-1.09*	*±0.84*	*-0.15*	*±3.15*	*0.10*	*0.22*
Jul	*15*	*-0.20*	*±0.56*	*-3.26*	*±1.58*	*0.01*	*0.72*
Aug	*12*	*-0.32*	*±0.37*	*-2.39*	*±1.10*	*0.07*	*0.41*
Sep	*9*	*-2.59*	*±1.87*	*3.78*	*±7.03*	*0.22*	*0.21*
Oct	*15*	*-0.52*	*±0.48*	*-4.03*	*±1.47*	*0.08*	*0.30*
Nov	*10*	*0.04*	*±0.78*	*-5.75*	*±2.74*	*0.00*	*0.96*
Dec	*11*	*-1.27*	*±1.31*	*-1.39*	*±4.37*	*0.10*	*0.36*
Win	*46*	*1.18*	*±0.80*	*-11.99*	*±2.60*	*0.05*	*0.15*
Spr	*66*	*0.35*	*±0.47*	*-5.78*	*±1.59*	*0.01*	*0.46*
Sum	*44*	*-0.55*	*±0.32*	*-2.07*	*±1.03*	*0.07*	*0.09*
Aut	*34*	*-0.72*	*±0.50*	*-3.28*	*±1.69*	*0.06*	*0.16*

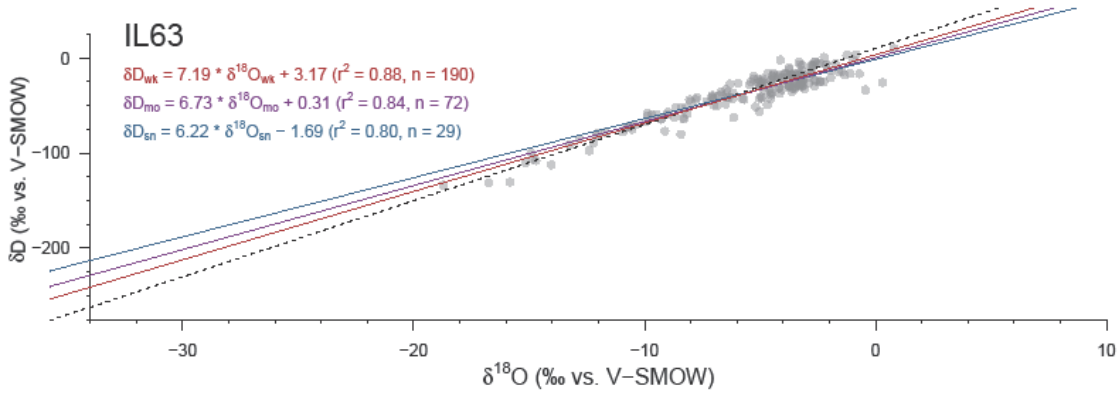

Figure A5.D1. Local meteoric water line for IL63. Gray circles represent values at their original weekly resolution while linear trends are plotted for weekly (red), aggregated monthly (violet), and aggregated seasonal (blue) resolutions. The dashed black line represents the global meteoric water line.

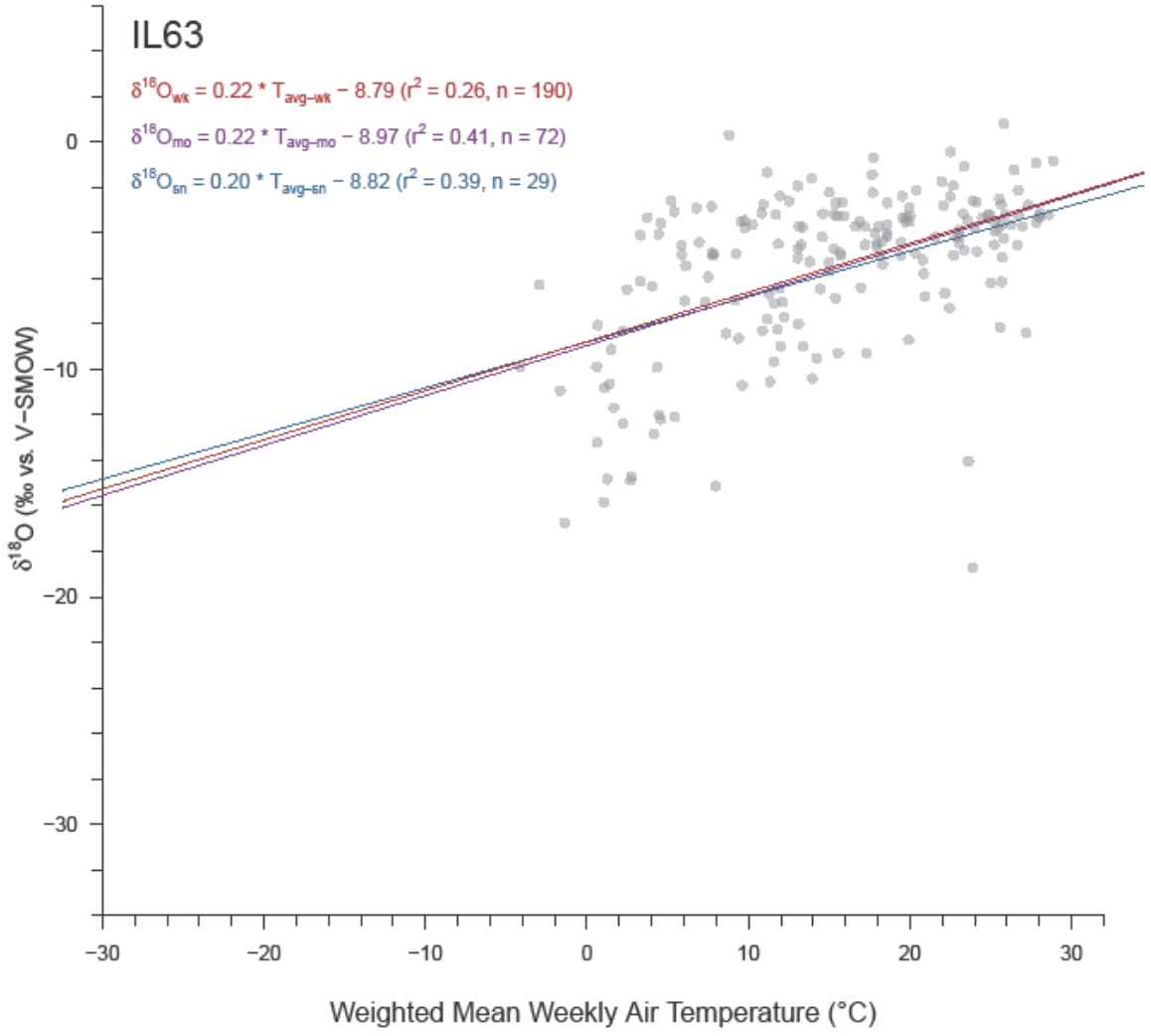

Figure A5.D2. Relationship between precipitation $\delta^{18}O$ and mean PDt at site IL63. Gray circles represent values at their original weekly resolution while linear trends are plotted for weekly (red), aggregated monthly (violet), and aggregated seasonal (blue) resolutions.

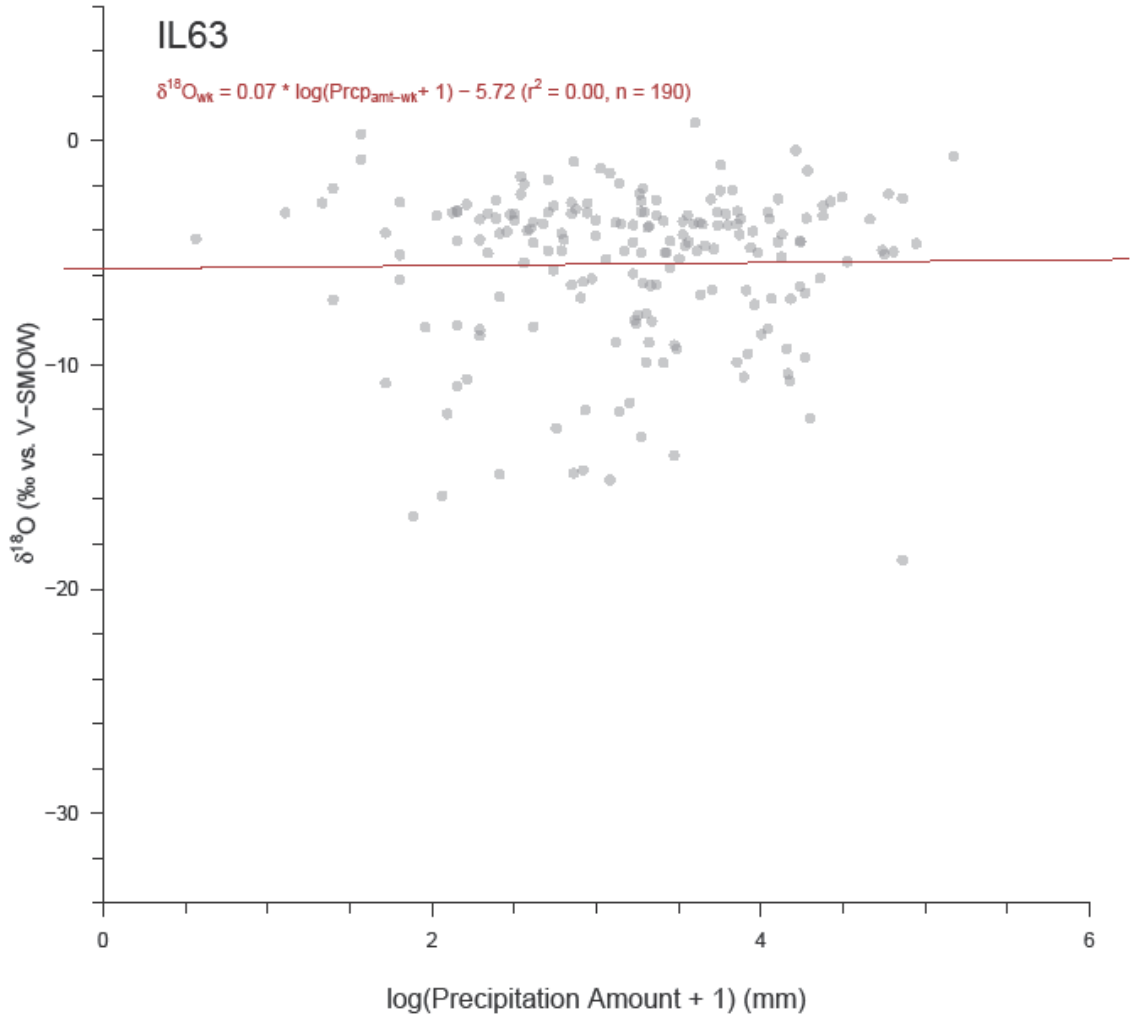

Figure A5.D3. Relationship between precipitation $\delta^{18}O$ and PDa at site IL63. Actual precipitation amounts were normalized by a log transformation. Gray circles represent values at their original weekly resolution with the weekly linear trend plotted in red. Precipitation amount data cannot be weight-averaged for aggregation, and thus regression was only performed at weekly resolution.

IL78

Table A5.E1. Regression results for IL78 at weekly, monthly, and seasonal resolutions. Significant results ($p \leq 0.05$) are bolded, while insignificant results are italicized. Actual precipitation amounts were normalized by a log transformation. Precipitation amount data cannot be weight-averaged for aggregation, and thus regression was only performed at weekly resolution.

LMWL (δD vs. $\delta^{18}O$)							
Resolution	***n***	***Slope***		***y-Int***		***r^2***	***p-value***
Weekly	**240**	**7.92**	**±0.07**	**12.15**	**±0.60**	**0.98**	**0.00**
Monthly	**112**	**7.96**	**±0.09**	**12.43**	**±0.75**	**0.99**	**0.00**
Seasonal	**48**	**7.81**	**±0.16**	**12.01**	**±1.28**	**0.98**	**0.00**
$\delta^{18}O$ vs. PDt							
Resolution	***n***	***Slope***		***y-Int***		***r^2***	***p-value***
Weekly	**240**	**0.32**	**±0.02**	**-11.61**	**±0.35**	**0.46**	**0.00**
Monthly	**112**	**0.33**	**±0.03**	**-12.03**	**±0.49**	**0.50**	**0.00**
Seasonal	**48**	**0.25**	**±0.04**	**-10.68**	**±0.62**	**0.46**	**0.00**
$\delta^{18}O$ vs. PDa							
Resolution	***n***	***Slope***		***y-Int***		***r^2***	***p-value***
Weekly	**240**	**0.82**	**±0.29**	**-9.79**	**±0.89**	**0.03**	**0.01**

Table A5.E2. Percent change in IL78 regression values (Table A5.E1) due to aggregation.

LMWL (δD vs. $\delta^{18}O$)					
Aggregation	***Slope***	***Slope Error***	***y-Int***	***y-Int Error***	***r^2***
Weekly-Monthly	1%	22%	2%	26%	1%
Weekly-Seasonal	-1%	104%	-1%	91%	0%
Monthly-Seasonal	-2%	46%	-3%	41%	-1%
$\delta^{18}O$ vs. PDt					
Aggregation	***Slope***	***Slope Error***	***y-Int***	***y-Int Error***	***r^2***
Weekly-Monthly	4%	39%	4%	38%	10%
Weekly-Seasonal	-21%	56%	-8%	54%	0%
Monthly-Seasonal	-32%	22%	-13%	21%	-10%

Table A5.E3. IL78 temperature estimates and standard errors for three $\delta^{18}O$ values (vs. V-SMOW) at weekly, monthly, and seasonal resolutions. The three $\delta^{18}O$ values span much of the natural range of precipitation $\delta^{18}O$ in the study region, and -6‰ is close to the mean $\delta^{18}O$ value of all sites.

	Temperature Estimate (°C) when Precipitation $\delta^{18}O$ =		
Aggregation	***-20‰***	***-6‰***	***0‰***
Weekly	-4.9 ±12.7	15.0 ±12.4	23.5 ±12.5
Monthly	-5.7 ±12.7	15.4 ±12.2	24.4 ±12.4
Seasonal	-9.9 ±14.5	15.5 ±12.5	26.4 ±13.2

Table A5.E4. Weight-averaged weekly values of $\delta^{18}O$ and average surface temperature for IL78 grouped by month and season. Blue (red) cells show low (high) values of note.

Group	***n***	***$\delta^{18}O_{wt}$***	***PDt***
Jan	13	-12.37 ±1.42	-0.3 ±0.9
Feb	16	-12.04 ±1.15	1.8 ±1.4
Mar	25	-8.87 ±0.81	7.0 ±1.0
Apr	29	-7.13 ±0.69	12.5 ±0.9
May	23	-5.02 ±0.48	15.8 ±0.8
Jun	27	-5.11 ±0.47	20.1 ±0.6
Jul	18	-5.59 ±0.54	24.0 ±0.4
Aug	20	-3.96 ±0.43	23.4 ±0.4
Sep	19	-6.97 ±0.70	20.3 ±0.9
Oct	17	-7.15 ±0.57	14.1 ±0.7
Nov	21	-8.62 ±0.75	7.9 ±0.9
Dec	12	-12.33 ±1.17	1.9 ±1.0
Win	41	-10.25 ±0.71	1.8 ±0.7
Spr	77	-6.84 ±0.44	12.2 ±0.7
Sum	65	-4.94 ±0.29	21.9 ±0.4
Aut	57	-8.24 ±0.42	14.6 ±0.8

Table A5.E5. Regression results for IL78 when weekly data is grouped by month and by season. Significant results ($p \leq 0.05$) are bolded, while insignificant results are italicized. Actual precipitation amounts were normalized by a log transformation. Blue (red) cells show low (high) values of note.

LMWL (δD vs. $\delta^{18}O$)							
Group	***n***	***Slope***		***y-Int***		***r^2***	***p-value***
Jan	**13**	**8.86**	**±0.30**	**24.93**	**±3.56**	**0.99**	**0.00**
Feb	**16**	**8.20**	**±0.20**	**14.76**	**±2.59**	**0.99**	**0.00**
Mar	**25**	**8.11**	**±0.24**	**14.20**	**±2.45**	**0.98**	**0.00**
Apr	**29**	**7.98**	**±0.23**	**11.95**	**±1.80**	**0.98**	**0.00**
May	**23**	**7.63**	**±0.47**	**8.64**	**±2.58**	**0.93**	**0.00**
Jun	**27**	**7.72**	**±0.30**	**9.28**	**±1.79**	**0.96**	**0.00**
Jul	**18**	**7.85**	**±0.24**	**11.45**	**±1.34**	**0.99**	**0.00**
Aug	**20**	**6.50**	**±0.34**	**5.64**	**±1.44**	**0.95**	**0.00**
Sep	**19**	**7.93**	**±0.22**	**13.12**	**±1.62**	**0.99**	**0.00**
Oct	**17**	**8.13**	**±0.27**	**14.51**	**±2.04**	**0.98**	**0.00**
Nov	**21**	**8.24**	**±0.19**	**17.10**	**±1.82**	**0.99**	**0.00**
Dec	**12**	**8.81**	**±0.51**	**24.80**	**±5.98**	**0.97**	**0.00**
Win	**41**	**8.62**	**±0.19**	**21.42**	**±2.27**	**0.98**	**0.00**
Spr	**77**	**7.87**	**±0.14**	**11.01**	**±1.14**	**0.98**	**0.00**
Sum	**65**	**7.55**	**±0.18**	**9.18**	**±0.97**	**0.97**	**0.00**
Aut	**57**	**8.03**	**±0.12**	**14.32**	**±0.99**	**0.99**	**0.00**
$\delta^{18}O$ vs. PDt							
Group	***n***	***Slope***		***y-Int***		***r^2***	***p-value***
Jan	*13*	*0.84*	*±0.41*	*-10.60*	*±1.28*	*0.27*	*0.07*
Feb	**16**	**0.52**	**±0.18**	**-12.84**	**±0.99**	**0.38**	**0.01**
Mar	**25**	**0.53**	**±0.13**	**-13.07**	**±1.04**	**0.43**	**0.00**
Apr	*29*	*0.23*	*±0.15*	*-9.65*	*±1.76*	*0.09*	*0.12*
May	**23**	**0.43**	**±0.10**	**-11.92**	**±1.60**	**0.48**	**0.00**
Jun	*27*	*0.24*	*±0.15*	*-10.20*	*±3.08*	*0.09*	*0.13*
Jul	**18**	**1.09**	**±0.24**	**-31.63**	**±5.76**	**0.57**	**0.00**
Aug	*20*	*0.31*	*±0.27*	*-11.09*	*±6.21*	*0.07*	*0.26*
Sep	*19*	*0.30*	*±0.17*	*-12.37*	*±3.32*	*0.16*	*0.10*
Oct	*17*	*0.30*	*±0.18*	*-11.24*	*±2.51*	*0.15*	*0.12*
Nov	**21**	**0.39**	**±0.17**	**-12.05**	**±1.48**	**0.22**	**0.03**
Dec	*12*	*0.53*	*±0.31*	*-12.69*	*±1.43*	*0.22*	*0.12*
Win	**41**	**0.51**	**±0.14**	**-12.11**	**±0.65**	**0.25**	**0.00**
Spr	**77**	**0.43**	**±0.06**	**-12.02**	**±0.74**	**0.41**	**0.00**

Sum	**65**	**0.30**	**±0.10**	**-11.54**	**±2.15**	**0.13**	**0.00**
Aut	**57**	**0.26**	**±0.06**	**-11.16**	**±0.89**	**0.25**	**0.00**
δ^{18}O vs. PDa							
Group	***n***	***Slope***		***y-Int***		***r^2***	***p-value***
Jan	**13**	**3.75**	**±1.39**	**-20.69**	**±3.79**	**0.40**	**0.02**
Feb	*16*	*1.53*	*±1.56*	*-15.70*	*±4.01*	*0.06*	*0.34*
Mar	*25*	*0.81*	*±1.15*	*-11.89*	*±3.35*	*0.02*	*0.49*
Apr	*29*	*0.43*	*±0.74*	*-8.21*	*±2.11*	*0.01*	*0.56*
May	*23*	*-0.09*	*±0.52*	*-4.75*	*±1.71*	*0.00*	*0.87*
Jun	*27*	*-0.12*	*±0.77*	*-5.00*	*±2.50*	*0.00*	*0.87*
Jul	*18*	*-0.70*	*±0.58*	*-2.96*	*±1.94*	*0.08*	*0.25*
Aug	*20*	*-0.22*	*±0.47*	*-3.22*	*±1.46*	*0.01*	*0.65*
Sep	*19*	*-0.42*	*±0.84*	*-5.26*	*±2.79*	*0.01*	*0.62*
Oct	*17*	*0.36*	*±0.75*	*-8.13*	*±2.05*	*0.02*	*0.64*
Nov	*21*	*0.89*	*±0.88*	*-11.64*	*±2.73*	*0.05*	*0.33*
Dec	*12*	*-1.96*	*±1.15*	*-6.11*	*±3.13*	*0.22*	*0.12*
Win	*41*	*0.97*	*±0.85*	*-13.83*	*±2.26*	*0.03*	*0.26*
Spr	*77*	*0.57*	*±0.50*	*-8.90*	*±1.49*	*0.02*	*0.26*
Sum	*65*	*-0.46*	*±0.35*	*-3.43*	*±1.13*	*0.03*	*0.19*
Aut	*57*	*0.30*	*±0.48*	*-8.56*	*±1.49*	*0.01*	*0.54*

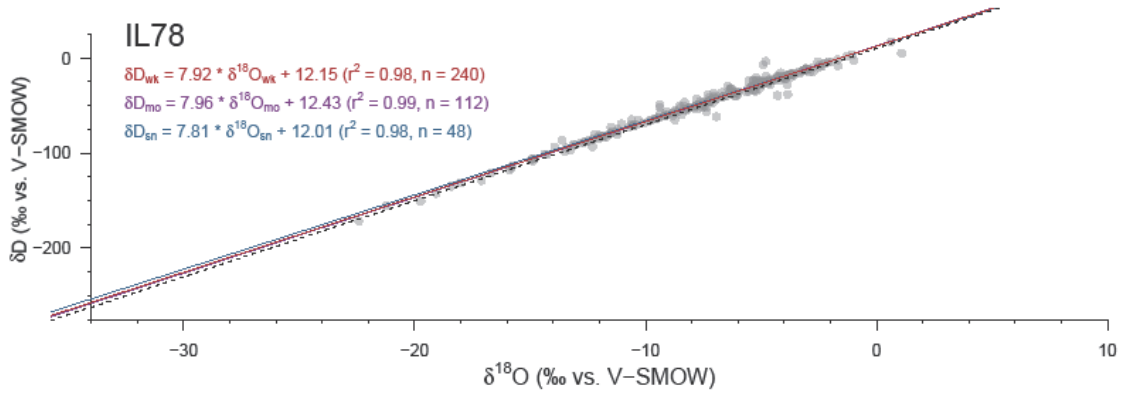

Figure A5.E1. Local meteoric water line for IL78. Gray circles represent values at their original weekly resolution while linear trends are plotted for weekly (red), aggregated monthly (violet), and aggregated seasonal (blue) resolutions. The dashed black line represents the global meteoric water line.

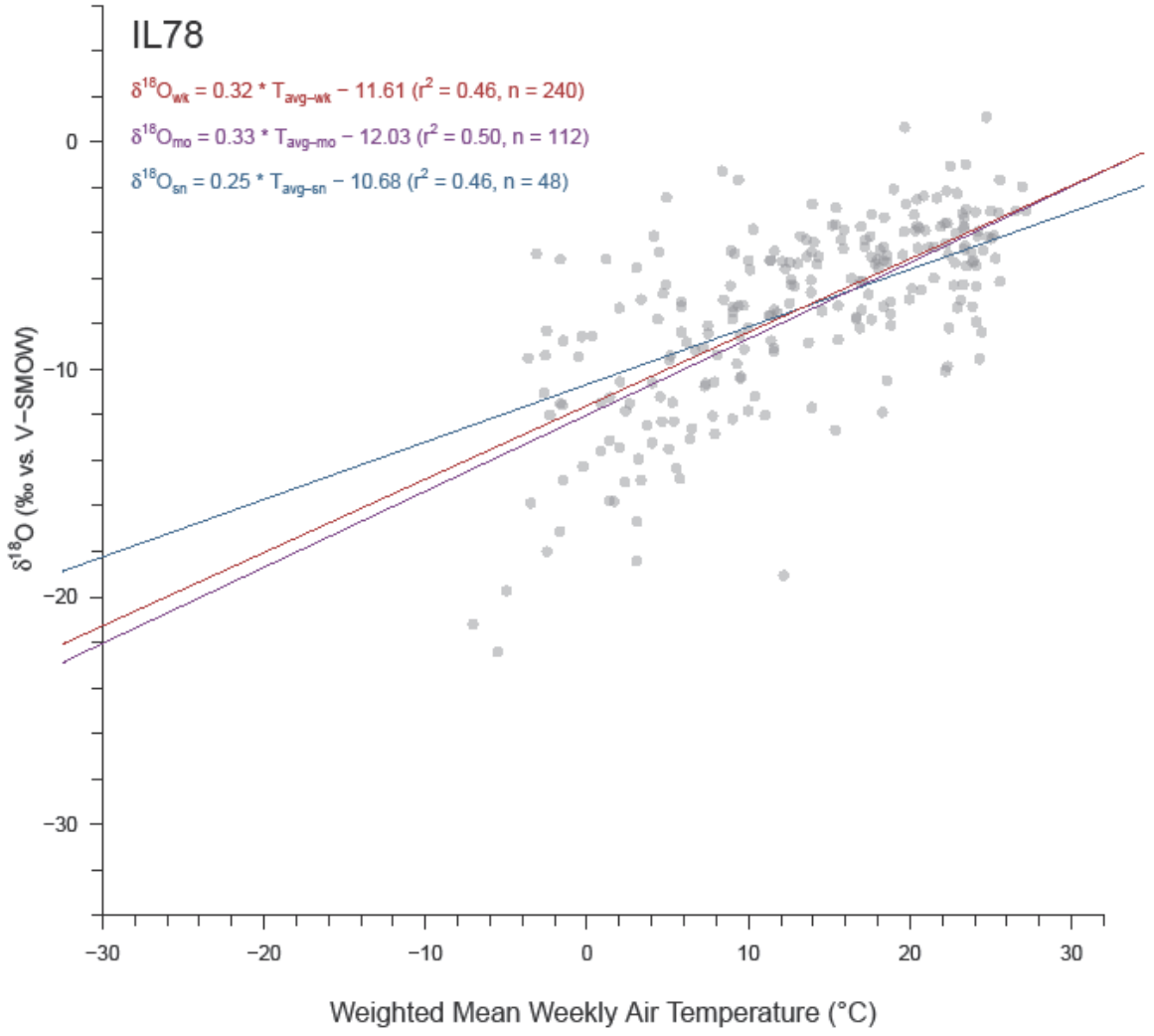

Figure A5.E2. Relationship between precipitation $\delta^{18}O$ and mean PDt at site IL78. Gray circles represent values at their original weekly resolution while linear trends are plotted for weekly (red), aggregated monthly (violet), and aggregated seasonal (blue) resolutions.

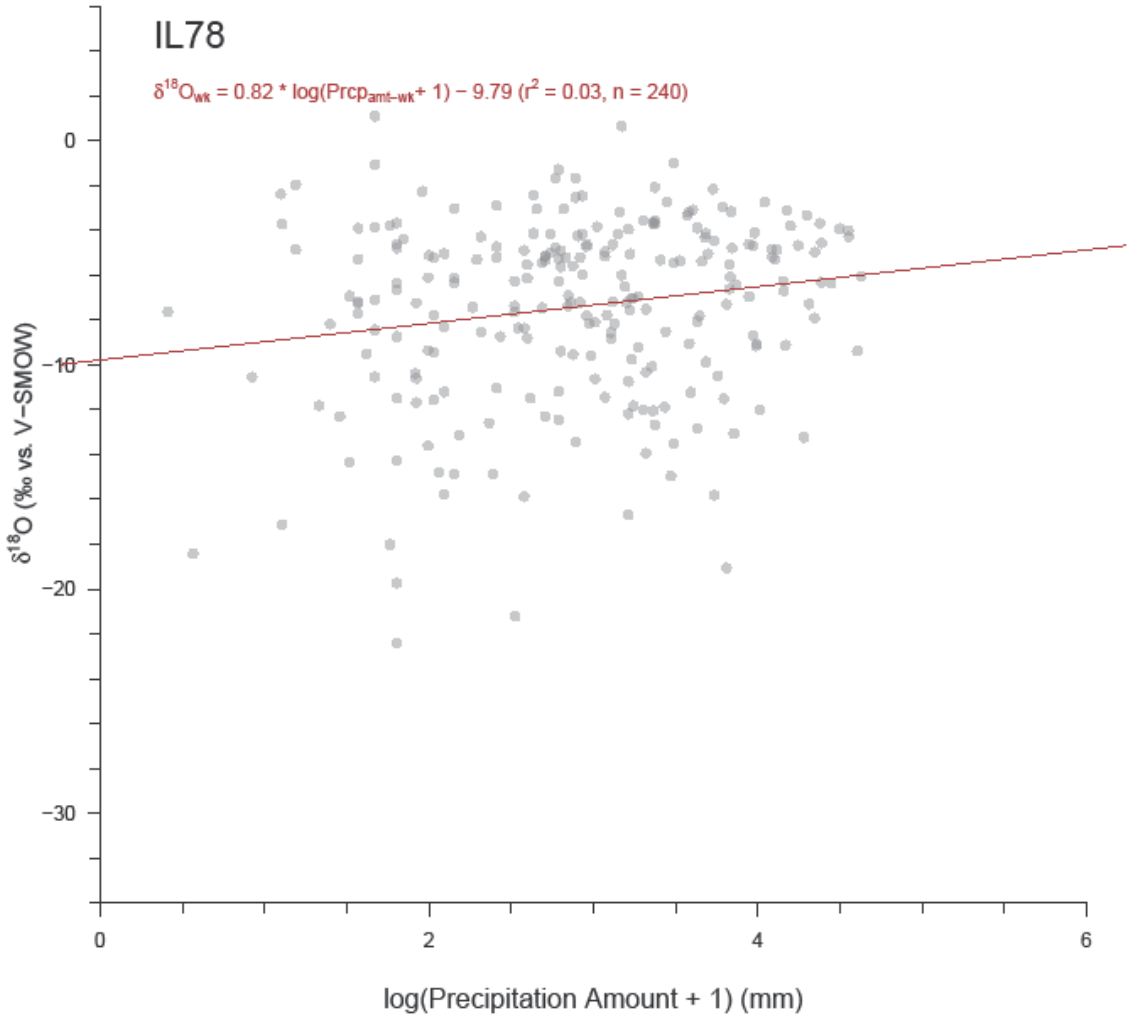

Figure A5.E3. Relationship between precipitation $\delta^{18}O$ and PDa at site IL78. Actual precipitation amounts were normalized by a log transformation. Gray circles represent values at their original weekly resolution with the weekly linear trend plotted in red. Precipitation amount data cannot be weight-averaged for aggregation, and thus regression was only performed at weekly resolution.

IN22

Table A5.F1. Regression results for IN22 at weekly, monthly, and seasonal resolutions. Significant results ($p \leq 0.05$) are bolded, while insignificant results are italicized. Actual precipitation amounts were normalized by a log transformation. Precipitation amount data cannot be weight-averaged for aggregation, and thus regression was only performed at weekly resolution.

LMWL (δD vs. $\delta^{18}O$)							
Resolution	***n***	***Slope***		***y-Int***		***r^2***	***p-value***
Weekly	**260**	**7.74**	**±0.07**	**10.50**	**±0.51**	**0.98**	**0.00**
Monthly	**113**	**7.72**	**±0.13**	**10.24**	**±0.85**	**0.97**	**0.00**
Seasonal	**52**	**7.57**	**±0.19**	**9.31**	**±1.25**	**0.97**	**0.00**
$\delta^{18}O$ vs. PDt							
Resolution	***n***	***Slope***		***y-Int***		***r^2***	***p-value***
Weekly	**260**	**0.23**	**±0.02**	**-9.45**	**±0.33**	**0.34**	**0.00**
Monthly	**113**	**0.20**	**±0.03**	**-8.95**	**±0.44**	**0.34**	**0.00**
Seasonal	**52**	**0.20**	**±0.03**	**-8.97**	**±0.53**	**0.42**	**0.00**
$\delta^{18}O$ vs. PDa							
Resolution	***n***	***Slope***		***y-Int***		***r^2***	***p-value***
Weekly	*260*	*0.30*	*±0.25*	*-7.20*	*±0.79*	*0.01*	*0.22*

Table A5.F2. Percent change in IN22 regression values (Table A5.F1) due to aggregation.

LMWL (δD vs. $\delta^{18}O$)					
Aggregation	***Slope***	***Slope Error***	***y-Int***	***y-Int Error***	***r^2***
Weekly-Monthly	0%	77%	-2%	67%	-1%
Weekly-Seasonal	-2%	92%	-12%	86%	-1%
Monthly-Seasonal	-2%	32%	-10%	31%	0%
$\delta^{18}O$ vs. PDt					
Aggregation	***Slope***	***Slope Error***	***y-Int***	***y-Int Error***	***r^2***
Weekly-Monthly	-12%	36%	-5%	34%	-1%
Weekly-Seasonal	-14%	50%	-5%	45%	24%
Monthly-Seasonal	0%	19%	0%	16%	20%

Table A5.F3. IN22 temperature estimates and standard errors for three $\delta^{18}O$ values (vs. V-SMOW) at weekly, monthly, and seasonal resolutions. The three $\delta^{18}O$ values span much of the natural range of precipitation $\delta^{18}O$ in the study region, and -6‰ is close to the mean $\delta^{18}O$ value of all sites.

	Temperature Estimate (°C) when Precipitation $\delta^{18}O$ =		
Aggregation	***-20‰***	***-6‰***	***0‰***
Weekly	-6.6 ±15.2	14.3 ±14.7	23.3 ±14.8
Monthly	-9.2 ±15.4	14.3 ±14.1	24.3 ±14.4
Seasonal	-15.4 ±16.0	14.2 ±12.8	26.8 ±13.5

Table A5.F4. Weight-averaged weekly values of $\delta^{18}O$ and average surface temperature for IN22 grouped by month and season. Blue (red) cells show low (high) values of note.

Group	***n***	***$\delta^{18}O_{wt}$***	***PDt***
Jan	27	-9.18 ±0.82	3.2 ±1.0
Feb	16	-8.08 ±1.24	3.9 ±1.8
Mar	29	-6.41 ±0.76	7.9 ±0.7
Apr	21	-5.08 ±0.59	14.3 ±0.8
May	24	-4.63 ±0.36	17.6 ±0.6
Jun	34	-5.39 ±0.42	22.1 ±0.6
Jul	26	-4.13 ±0.38	25.4 ±0.3
Aug	16	-3.59 ±0.50	23.9 ±0.6
Sep	15	-5.51 ±0.63	22.7 ±0.6
Oct	15	-6.44 ±0.98	14.2 ±1.3
Nov	21	-6.64 ±0.41	10.6 ±0.8
Dec	16	-8.13 ±0.97	3.7 ±1.4
Win	59	-8.97 ±0.57	3.3 ±0.8
Spr	74	-5.26 ±0.38	13.2 ±0.7
Sum	76	-4.47 ±0.26	23.8 ±0.4
Aut	51	-6.14 ±0.39	14.5 ±0.9

Table A5.F5. Regression results for IN22 when weekly data is grouped by month and by season. Significant results ($p \leq 0.05$) are bolded, while insignificant results are italicized. Actual precipitation amounts were normalized by a log transformation. Blue (red) cells show low (high) values of note.

LMWL (δD vs. $\delta^{18}O$)							
Group	***n***	***Slope***		***y-Int***		***r^2***	***p-value***
Jan	**27**	**8.10**	**±0.16**	**15.24**	**±1.73**	**0.99**	**0.00**
Feb	**16**	**7.99**	**±0.31**	**11.06**	**±3.04**	**0.98**	**0.00**
Mar	**29**	**7.36**	**±0.33**	**6.76**	**±2.67**	**0.95**	**0.00**
Apr	**21**	**7.78**	**±0.38**	**10.34**	**±2.29**	**0.96**	**0.00**
May	**24**	**7.83**	**±0.37**	**10.19**	**±1.72**	**0.95**	**0.00**
Jun	**34**	**8.06**	**±0.15**	**11.91**	**±0.88**	**0.99**	**0.00**
Jul	**26**	**7.72**	**±0.20**	**10.31**	**±0.90**	**0.98**	**0.00**
Aug	**16**	**7.98**	**±0.38**	**11.64**	**±1.67**	**0.97**	**0.00**
Sep	**15**	**8.01**	**±0.32**	**11.58**	**±1.81**	**0.98**	**0.00**
Oct	**15**	**7.64**	**±0.17**	**10.29**	**±1.33**	**0.99**	**0.00**
Nov	**21**	**7.25**	**±0.23**	**8.24**	**±1.63**	**0.98**	**0.00**
Dec	**16**	**7.93**	**±0.36**	**14.42**	**±3.29**	**0.97**	**0.00**
Win	**59**	**8.01**	**±0.15**	**13.70**	**±1.48**	**0.98**	**0.00**
Spr	**74**	**7.55**	**±0.19**	**8.64**	**±1.25**	**0.96**	**0.00**
Sum	**76**	**7.96**	**±0.11**	**11.39**	**±0.58**	**0.99**	**0.00**
Aut	**51**	**7.61**	**±0.12**	**10.15**	**±0.86**	**0.99**	**0.00**
$\delta^{18}O$ vs. PDt							
Group	***n***	***Slope***		***y-Int***		***r^2***	***p-value***
Jan	**27**	**0.44**	**±0.14**	**-10.57**	**±0.76**	**0.29**	**0.00**
Feb	*16*	*0.30*	*±0.17*	*-9.44*	*±1.27*	*0.18*	*0.10*
Mar	**29**	**0.62**	**±0.17**	**-11.31**	**±1.34**	**0.33**	**0.00**
Apr	**21**	**0.34**	**±0.15**	**-10.17**	**±2.20**	**0.21**	**0.04**
May	**24**	**0.32**	**±0.11**	**-10.10**	**±1.88**	**0.30**	**0.01**
Jun	**34**	**0.25**	**±0.12**	**-10.86**	**±2.59**	**0.12**	**0.04**
Jul	**26**	**0.63**	**±0.23**	**-19.97**	**±5.84**	**0.24**	**0.01**
Aug	*16*	*0.12*	*±0.24*	*-6.77*	*±5.69*	*0.02*	*0.62*
Sep	*15*	*0.45*	*±0.25*	*-15.26*	*±5.61*	*0.20*	*0.10*
Oct	**15**	**0.56**	**±0.15**	**-14.68**	**±2.14**	**0.53**	**0.00**
Nov	*21*	*0.16*	*±0.11*	*-8.43*	*±1.24*	*0.10*	*0.17*
Dec	*16*	*0.01*	*±0.19*	*-8.42*	*±1.16*	*0.00*	*0.97*
Win	**59**	**0.29**	**±0.09**	**-9.78**	**±0.58**	**0.15**	**0.00**
Spr	**74**	**0.32**	**±0.05**	**-9.71**	**±0.75**	**0.33**	**0.00**

Sum	**76**	**0.30**	**±0.08**	**-11.81**	**±1.88**	**0.17**	**0.00**
Aut	**51**	**0.23**	**±0.05**	**-9.74**	**±0.88**	**0.26**	**0.00**
δ^{18}O vs. PDa							
Group	***n***	***Slope***		***y-Int***		***r^2***	***p-value***
Jan	*27*	*1.62*	*±0.92*	*-14.57*	*±2.87*	*0.11*	*0.09*
Feb	**16**	**-4.28**	**±1.28**	**3.93**	**±3.84**	**0.45**	**0.00**
Mar	*29*	*1.17*	*±0.87*	*-10.27*	*±2.57*	*0.06*	*0.19*
Apr	*21*	*0.59*	*±0.65*	*-7.25*	*±2.14*	*0.04*	*0.37*
May	**24**	**-1.25**	**±0.44**	**-0.14**	**±1.53**	**0.27**	**0.01**
Jun	*34*	*-0.31*	*±0.45*	*-4.45*	*±1.45*	*0.01*	*0.50*
Jul	**26**	**-0.83**	**±0.41**	**-1.45**	**±1.37**	**0.15**	**0.05**
Aug	*16*	*0.45*	*±0.56*	*-5.43*	*±1.94*	*0.05*	*0.43*
Sep	*15*	*0.92*	*±0.65*	*-7.87*	*±1.97*	*0.13*	*0.18*
Oct	*15*	*0.28*	*±1.19*	*-7.81*	*±3.61*	*0.00*	*0.82*
Nov	*21*	*-0.03*	*±0.50*	*-6.63*	*±1.70*	*0.00*	*0.95*
Dec	*16*	*-1.80*	*±1.09*	*-4.03*	*±2.80*	*0.16*	*0.12*
Win	*59*	*-0.76*	*±0.66*	*-6.90*	*±1.93*	*0.02*	*0.25*
Spr	*74*	*0.73*	*±0.43*	*-7.95*	*±1.39*	*0.04*	*0.09*
Sum	*76*	*-0.24*	*±0.28*	*-3.88*	*±0.94*	*0.01*	*0.39*
Aut	*51*	*0.27*	*±0.44*	*-7.21*	*±1.39*	*0.01*	*0.54*

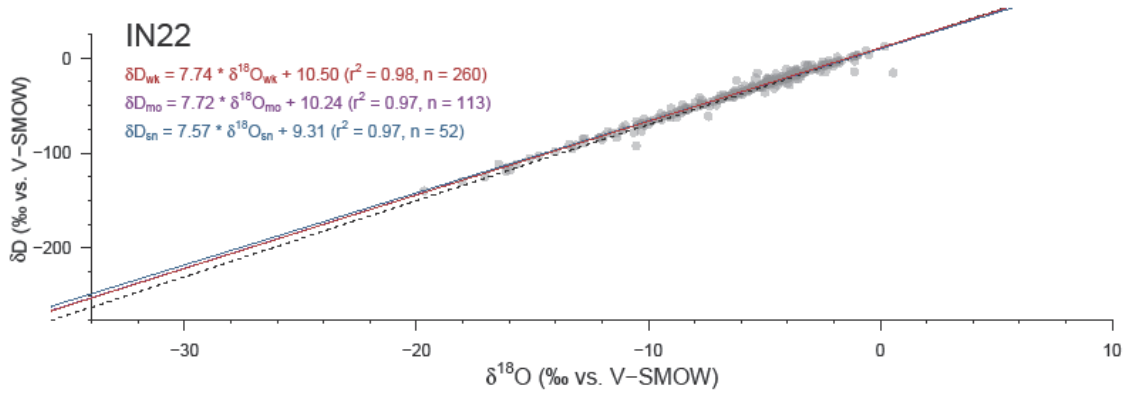

Figure A5.F1. Local meteoric water line for IN22. Gray circles represent values at their original weekly resolution while linear trends are plotted for weekly (red), aggregated monthly (violet), and aggregated seasonal (blue) resolutions. The dashed black line represents the global meteoric water line.

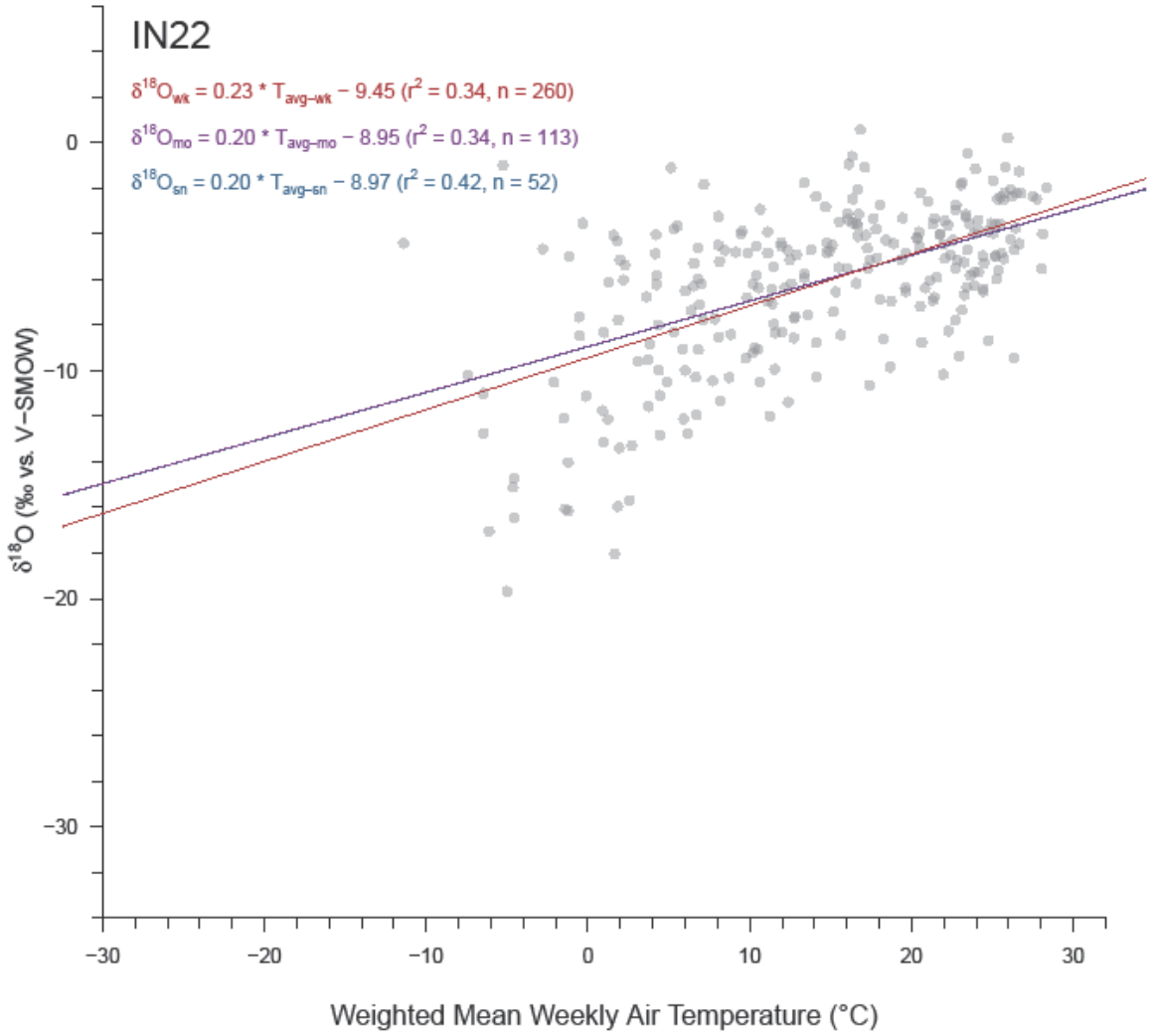

Figure A5.F2. Relationship between precipitation $\delta^{18}O$ and mean PDt at site IN22. Gray circles represent values at their original weekly resolution while linear trends are plotted for weekly (red), aggregated monthly (violet), and aggregated seasonal (blue) resolutions.

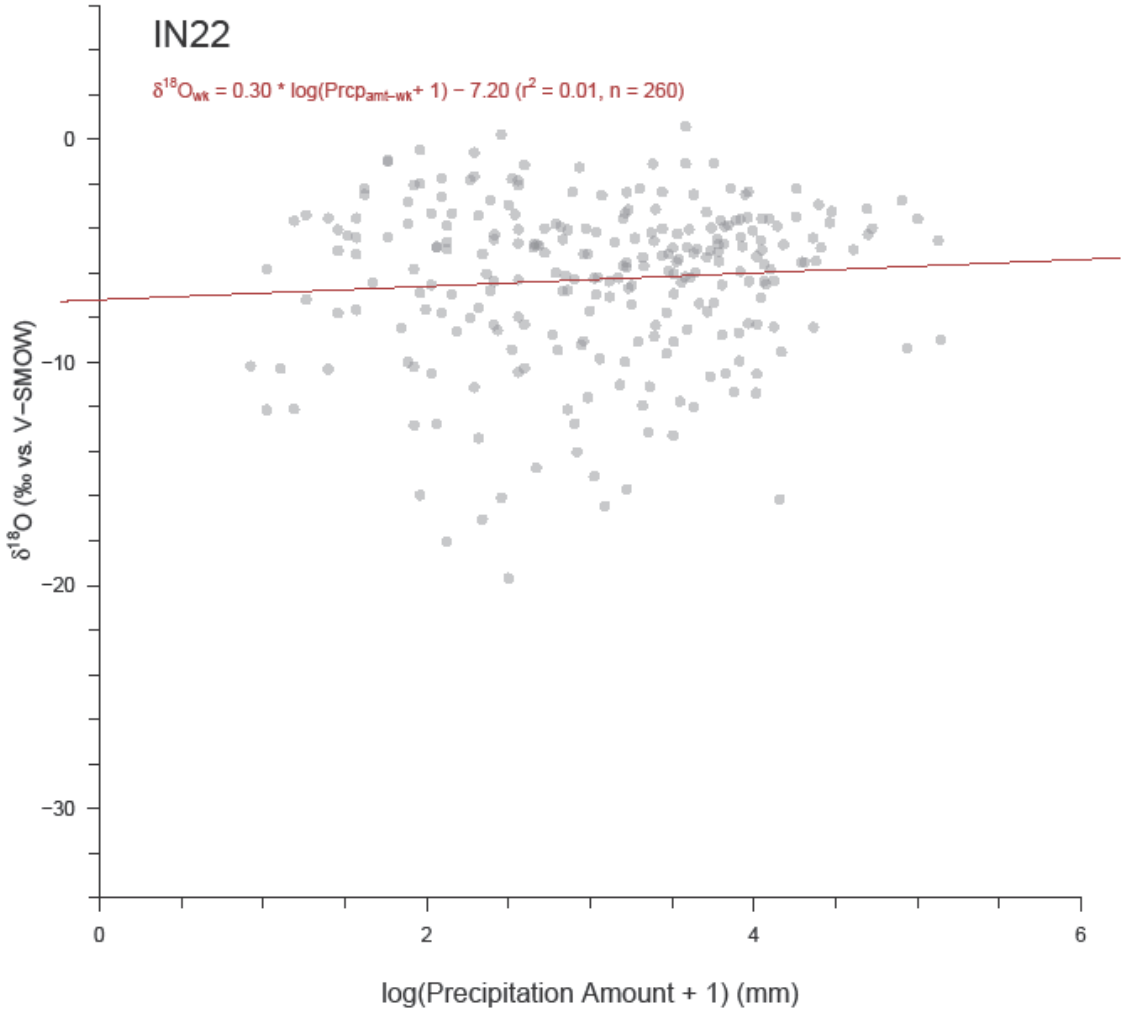

Figure A5.F3. Relationship between precipitation $\delta^{18}O$ and PDa at site IN22. Actual precipitation amounts were normalized by a log transformation. Gray circles represent values at their original weekly resolution with the weekly linear trend plotted in red. Precipitation amount data cannot be weight-averaged for aggregation, and thus regression was only performed at weekly resolution.

KS31

Table A5.G1. Regression results for KS31 at weekly, monthly, and seasonal resolutions. Significant results ($p \leq 0.05$) are bolded, while insignificant results are italicized. Actual precipitation amounts were normalized by a log transformation. Precipitation amount data cannot be weight-averaged for aggregation, and thus regression was only performed at weekly resolution.

LMWL (δD vs. $\delta^{18}O$)							
Resolution	***n***	***Slope***		***y-Int***		***r^2***	***p-value***
Weekly	**265**	**7.64**	**±0.07**	**8.77**	**±0.52**	**0.98**	**0.00**
Monthly	**125**	**7.72**	**±0.09**	**9.52**	**±0.74**	**0.99**	**0.00**
Seasonal	**55**	**8.00**	**±0.12**	**12.25**	**±1.06**	**0.99**	**0.00**
$\delta^{18}O$ vs. PDt							
Resolution	***n***	***Slope***		***y-Int***		***r^2***	***p-value***
Weekly	**265**	**0.30**	**±0.02**	**-11.39**	**±0.33**	**0.50**	**0.00**
Monthly	**125**	**0.32**	**±0.02**	**-11.86**	**±0.41**	**0.58**	**0.00**
Seasonal	**55**	**0.32**	**±0.04**	**-11.78**	**±0.56**	**0.58**	**0.00**
$\delta^{18}O$ vs. PDa							
Resolution	***n***	***Slope***		***y-Int***		***r^2***	***p-value***
Weekly	**265**	**0.67**	**±0.28**	**-8.93**	**±0.86**	**0.02**	**0.02**

Table A5.G2. Percent change in KS31 regression values (Table A5.G1) due to aggregation.

LMWL (δD vs. $\delta^{18}O$)					
Aggregation	***Slope***	***Slope Error***	***y-Int***	***y-Int Error***	***r^2***
Weekly-Monthly	1%	32%	9%	41%	0%
Weekly-Seasonal	5%	65%	37%	73%	1%
Monthly-Seasonal	4%	29%	22%	31%	0%
$\delta^{18}O$ vs. PDt					
Aggregation	***Slope***	***Slope Error***	***y-Int***	***y-Int Error***	***r^2***
Weekly-Monthly	7%	34%	4%	25%	16%
Weekly-Seasonal	5%	73%	3%	57%	14%
Monthly-Seasonal	-2%	32%	-1%	27%	1%

Table A5.G3. KS31 temperature estimates and standard errors for three $\delta^{18}O$ values (vs. V-SMOW) at weekly, monthly, and seasonal resolutions. The three $\delta^{18}O$ values span much of the natural range of precipitation $\delta^{18}O$ in the study region, and -6‰ is close to the mean $\delta^{18}O$ value of all sites.

	Temperature Estimate (°C) when Precipitation $\delta^{18}O$ =		
Aggregation	***-20‰***	***-6‰***	***0‰***
Weekly	-7.0 ±13.6	16.4 ±13.3	26.4 ±13.4
Monthly	-9.1 ±13.1	16.2 ±12.6	27.0 ±12.8
Seasonal	-10.2 ±13.2	15.8 ±12.1	26.9 ±12.6

Table A5.G4. Weight-averaged weekly values of $\delta^{18}O$ and average surface temperature for KS31 grouped by month and season. Blue (red) cells show low (high) values of note.

Group	***n***	***$\delta^{18}O_{wt}$***	***PDt***
Jan	12	-12.65 ±1.60	-0.7 ±1.7
Feb	16	-11.50 ±0.94	0.5 ±1.5
Mar	26	-8.32 ±0.70	6.8 ±1.1
Apr	22	-7.20 ±0.64	10.6 ±0.8
May	28	-5.79 ±0.60	16.4 ±0.7
Jun	38	-4.77 ±0.35	22.6 ±0.5
Jul	29	-4.70 ±0.45	23.7 ±0.5
Aug	31	-4.04 ±0.41	24.7 ±0.5
Sep	21	-6.39 ±0.85	19.0 ±1.2
Oct	19	-7.15 ±0.51	15.1 ±1.0
Nov	16	-9.79 ±0.85	5.9 ±1.3
Dec	7	-14.71 ±1.69	-0.3 ±2.2
Win	35	-12.36 ±0.77	0.4 ±1.0
Spr	76	-6.70 ±0.39	11.9 ±0.7
Sum	98	-5.03 ±0.23	23.0 ±0.3
Aut	56	-7.36 ±0.47	13.8 ±1.0

Table A5.G5. Regression results for KS31 when weekly data is grouped by month and by season. Significant results ($p \leq 0.05$) are bolded, while insignificant results are italicized. Actual precipitation amounts were normalized by a log transformation. Blue (red) cells show low (high) values of note.

LMWL (δD vs. $\delta^{18}O$)							
Group	***n***	***Slope***		***y-Int***		***r^2***	***p-value***
Jan	**12**	**8.13**	**±0.22**	**16.20**	**±2.90**	**0.99**	**0.00**
Feb	**16**	**7.93**	**±0.26**	**11.17**	**±3.14**	**0.99**	**0.00**
Mar	**26**	**7.97**	**±0.16**	**12.70**	**±1.44**	**0.99**	**0.00**
Apr	**22**	**7.34**	**±0.29**	**6.84**	**±2.12**	**0.97**	**0.00**
May	**28**	**7.65**	**±0.16**	**9.18**	**±1.06**	**0.99**	**0.00**
Jun	**38**	**7.01**	**±0.44**	**4.36**	**±2.22**	**0.88**	**0.00**
Jul	**29**	**7.54**	**±0.27**	**7.39**	**±1.49**	**0.97**	**0.00**
Aug	**31**	**6.73**	**±0.34**	**5.07**	**±1.72**	**0.93**	**0.00**
Sep	**21**	**7.57**	**±0.26**	**9.49**	**±1.87**	**0.98**	**0.00**
Oct	**19**	**7.84**	**±0.50**	**10.47**	**±3.62**	**0.94**	**0.00**
Nov	**16**	**7.95**	**±0.33**	**12.80**	**±3.31**	**0.98**	**0.00**
Dec	**7**	**8.12**	**±0.12**	**13.48**	**±1.80**	**1.00**	**0.00**
Win	**35**	**8.07**	**±0.13**	**13.77**	**±1.78**	**0.99**	**0.00**
Spr	**76**	**7.66**	**±0.11**	**9.43**	**±0.84**	**0.99**	**0.00**
Sum	**98**	**7.11**	**±0.21**	**5.59**	**±1.11**	**0.92**	**0.00**
Aut	**56**	**7.71**	**±0.17**	**10.12**	**±1.39**	**0.97**	**0.00**
$\delta^{18}O$ vs. PDt							
Group	***n***	***Slope***		***y-Int***		***r^2***	***p-value***
Jan	**12**	**0.62**	**±0.22**	**-11.77**	**±1.26**	**0.44**	**0.02**
Feb	*16*	*0.16*	*±0.16*	*-11.73*	*±0.94*	*0.07*	*0.33*
Mar	**26**	**0.33**	**±0.10**	**-10.61**	**±0.89**	**0.30**	**0.00**
Apr	**22**	**0.39**	**±0.15**	**-10.67**	**±1.70**	**0.25**	**0.02**
May	**28**	**0.64**	**±0.10**	**-16.24**	**±1.68**	**0.61**	**0.00**
Jun	*38*	*0.20*	*±0.12*	*-8.98*	*±2.78*	*0.06*	*0.12*
Jul	*29*	*0.15*	*±0.16*	*-8.58*	*±3.98*	*0.03*	*0.36*
Aug	**31**	**0.40**	**±0.12**	**-14.35**	**±3.11**	**0.26**	**0.00**
Sep	**21**	**0.51**	**±0.12**	**-15.72**	**±2.40**	**0.47**	**0.00**
Oct	*19*	*-0.10*	*±0.12*	*-5.39*	*±1.93*	*0.04*	*0.42*
Nov	**16**	**0.38**	**±0.14**	**-11.62**	**±1.06**	**0.35**	**0.02**
Dec	*7*	*0.32*	*±0.31*	*-14.80*	*±1.69*	*0.18*	*0.35*
Win	**35**	**0.34**	**±0.12**	**-12.48**	**±0.71**	**0.19**	**0.01**
Spr	**76**	**0.35**	**±0.05**	**-10.84**	**±0.63**	**0.39**	**0.00**

Sum	**98**	**0.21**	**±0.07**	**-9.69**	**±1.73**	**0.08**	**0.00**
Aut	**56**	**0.28**	**±0.05**	**-11.24**	**±0.82**	**0.34**	**0.00**
δ^{18}O vs. PDa							
Group	***n***	***Slope***		***y-Int***		***r^2***	***p-value***
Jan	*12*	*2.09*	*±3.12*	*-16.64*	*±6.74*	*0.04*	*0.52*
Feb	*16*	*-1.87*	*±1.36*	*-7.07*	*±3.43*	*0.12*	*0.19*
Mar	*26*	*-0.40*	*±1.22*	*-7.29*	*±3.72*	*0.00*	*0.74*
Apr	*22*	*-1.09*	*±0.95*	*-3.44*	*±2.84*	*0.06*	*0.27*
May	*28*	*-0.66*	*±0.80*	*-3.67*	*±2.82*	*0.03*	*0.42*
Jun	*38*	*-0.34*	*±0.40*	*-3.56*	*±1.32*	*0.02*	*0.41*
Jul	*29*	*-0.17*	*±0.45*	*-4.30*	*±1.57*	*0.01*	*0.71*
Aug	*31*	*-0.41*	*±0.50*	*-3.07*	*±1.75*	*0.02*	*0.42*
Sep	*21*	*-0.91*	*±0.90*	*-3.73*	*±2.63*	*0.05*	*0.33*
Oct	*19*	*0.17*	*±0.58*	*-7.39*	*±1.63*	*0.01*	*0.77*
Nov	*16*	*-0.73*	*±1.03*	*-7.62*	*±2.77*	*0.03*	*0.49*
Dec	*7*	*1.21*	*±2.47*	*-17.72*	*±6.60*	*0.05*	*0.64*
Win	*35*	*-0.31*	*±1.18*	*-11.72*	*±2.87*	*0.00*	*0.80*
Spr	*76*	*-0.32*	*±0.55*	*-6.00*	*±1.77*	*0.00*	*0.57*
Sum	*98*	*-0.28*	*±0.25*	*-3.71*	*±0.85*	*0.01*	*0.26*
Aut	*56*	*-0.35*	*±0.52*	*-6.45*	*±1.46*	*0.01*	*0.50*

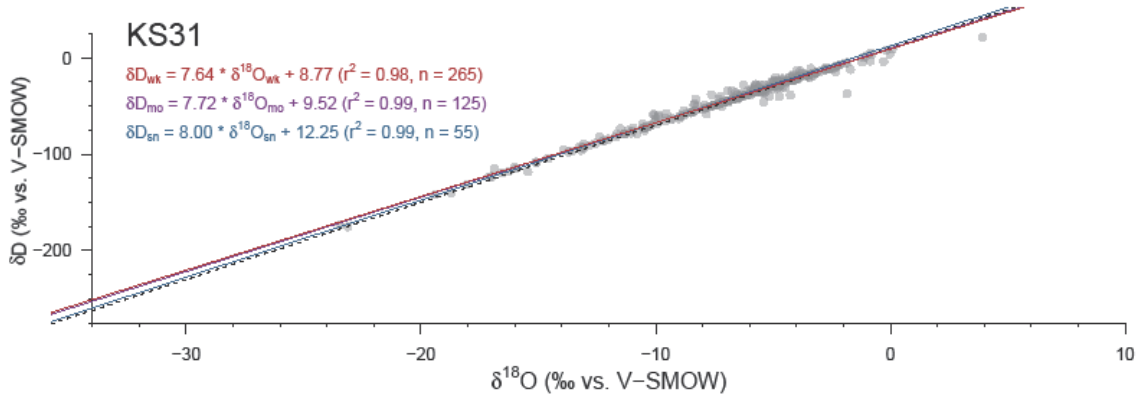

Figure A5.G1. Local meteoric water line for KS31. Gray circles represent values at their original weekly resolution while linear trends are plotted for weekly (red), aggregated monthly (violet), and aggregated seasonal (blue) resolutions. The dashed black line represents the global meteoric water line.

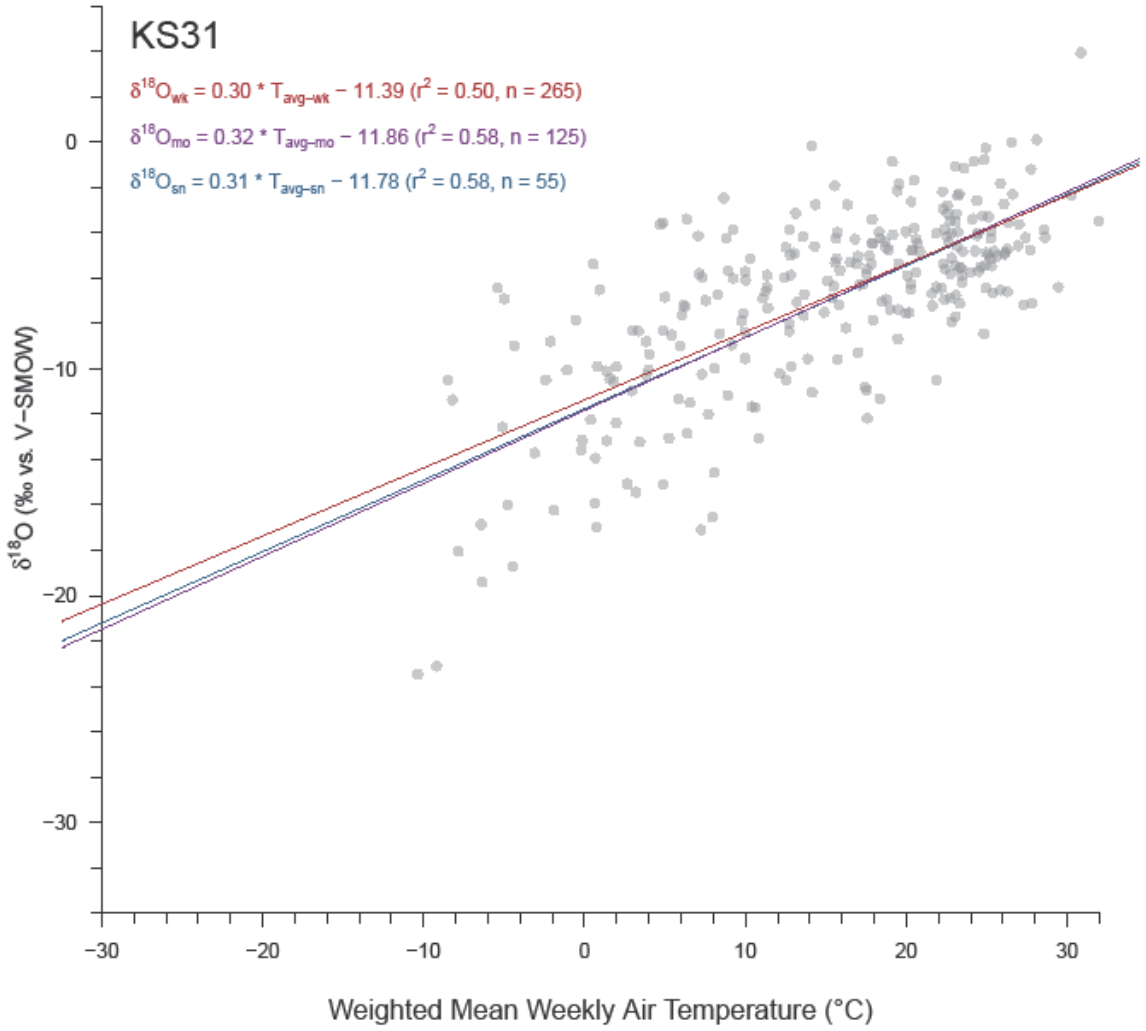

Figure A5.G2. Relationship between precipitation $\delta^{18}O$ and mean PDt at site KS31. Gray circles represent values at their original weekly resolution while linear trends are plotted for weekly (red), aggregated monthly (violet), and aggregated seasonal (blue) resolutions.

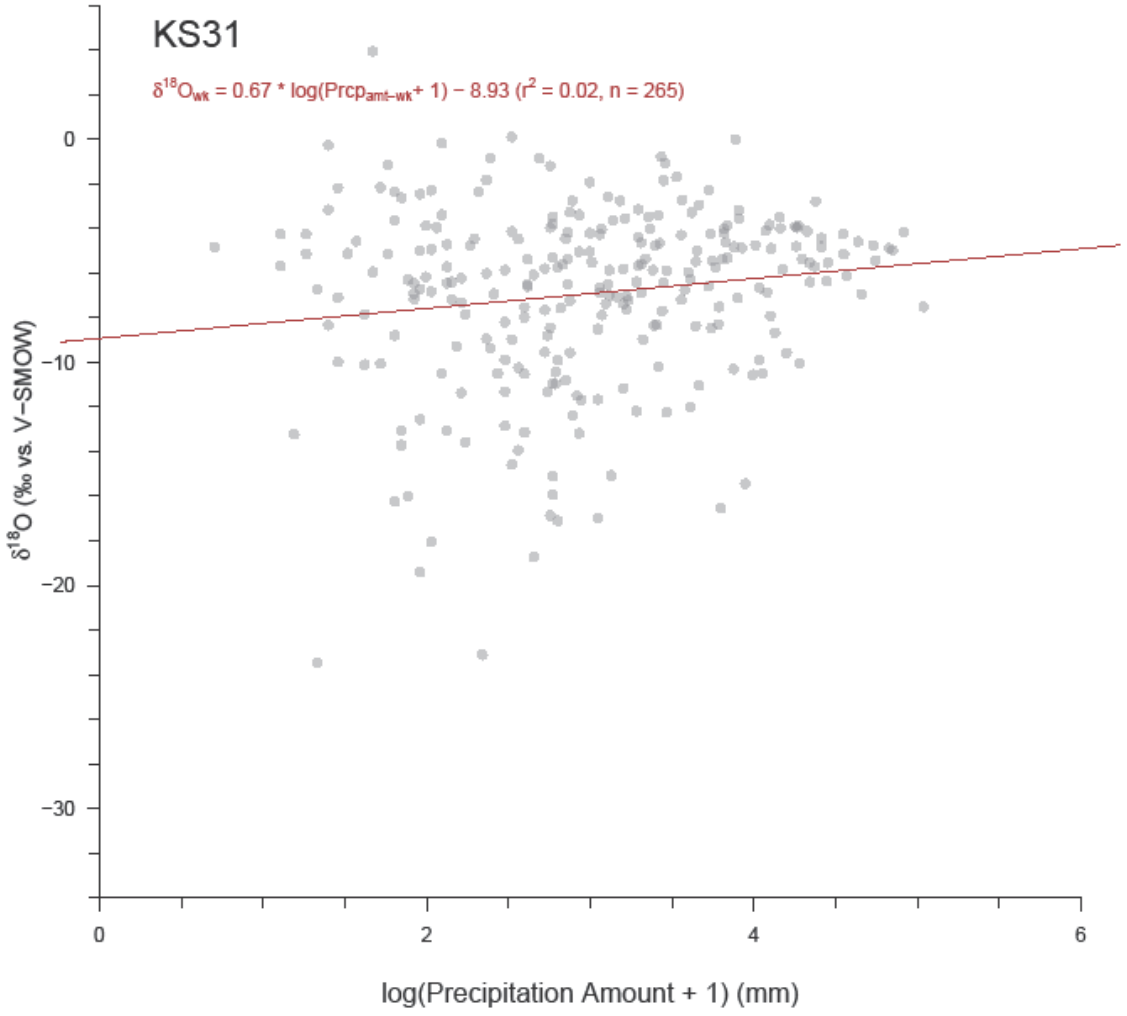

Figure A5.G3. Relationship between precipitation $\delta^{18}O$ and PDa at site KS31. Actual precipitation amounts were normalized by a log transformation. Gray circles represent values at their original weekly resolution with the weekly linear trend plotted in red. Precipitation amount data cannot be weight-averaged for aggregation, and thus regression was only performed at weekly resolution.

KY03

Table A5.H1. Regression results for KY03 at weekly, monthly, and seasonal resolutions. Significant results ($p \leq 0.05$) are bolded, while insignificant results are italicized. Actual precipitation amounts were normalized by a log transformation. Precipitation amount data cannot be weight-averaged for aggregation, and thus regression was only performed at weekly resolution.

LMWL (δD vs. $\delta^{18}O$)							
Resolution	***n***	***Slope***		***y-Int***		***r^2***	***p-value***
Weekly	**201**	**8.07**	**±0.07**	**11.61**	**±0.50**	**0.99**	**0.00**
Monthly	**101**	**8.09**	**±0.09**	**11.68**	**±0.68**	**0.99**	**0.00**
Seasonal	**53**	**8.08**	**±0.12**	**11.75**	**±0.96**	**0.99**	**0.00**
$\delta^{18}O$ vs. PDt							
Resolution	***n***	***Slope***		***y-Int***		***r^2***	***p-value***
Weekly	**201**	**0.26**	**±0.03**	**-10.47**	**±0.49**	**0.28**	**0.00**
Monthly	**101**	**0.24**	**±0.04**	**-10.36**	**±0.67**	**0.26**	**0.00**
Seasonal	**53**	**0.18**	**±0.06**	**-9.79**	**±1.01**	**0.13**	**0.01**
$\delta^{18}O$ vs. PDa							
Resolution	***n***	***Slope***		***y-Int***		***r^2***	***p-value***
Weekly	*201*	*-0.39*	*±0.33*	*-5.46*	*±1.02*	*0.01*	*0.23*

Table A5.H2. Percent change in KY03 regression values (Table A5.H1) due to aggregation.

LMWL (δD vs. $\delta^{18}O$)					
Aggregation	***Slope***	***Slope Error***	***y-Int***	***y-Int Error***	***r^2***
Weekly-Monthly	0%	36%	1%	37%	0%
Weekly-Seasonal	0%	61%	1%	67%	0%
Monthly-Seasonal	0%	26%	1%	29%	0%
$\delta^{18}O$ vs. PDt					
Aggregation	***Slope***	***Slope Error***	***y-Int***	***y-Int Error***	***r^2***
Weekly-Monthly	-8%	39%	-1%	38%	-9%
Weekly-Seasonal	-33%	86%	-7%	78%	-58%
Monthly-Seasonal	-32%	37%	-6%	34%	-92%

Table A5.H3. KY03 temperature estimates and standard errors for three $\delta^{18}O$ values (vs. V-SMOW) at weekly, monthly, and seasonal resolutions. The three $\delta^{18}O$ values span much of the natural range of precipitation $\delta^{18}O$ in the study region, and -6‰ is close to the mean $\delta^{18}O$ value of all sites.

	Temperature Estimate (°C) when Precipitation $\delta^{18}O$ =		
Aggregation	***-20‰***	***-6‰***	***0‰***
Weekly	0.2 ±13.1	15.4 ±12.7	21.9 ±12.8
Monthly	0.6 ±13.6	15.6 ±12.8	22.0 ±13.0
Seasonal	4.7 ±14.8	15.0 ±13.2	19.4 ±13.8

Table A5.H4. Weight-averaged weekly values of $\delta^{18}O$ and average surface temperature for KY03 grouped by month and season. Blue (red) cells show low (high) values of note.

Group	***n***	***$\delta^{18}O_{wt}$***	***PDt***
Jan	17	-10.25 ±0.96	4.7 ±1.1
Feb	11	-10.39 ±1.33	5.4 ±0.9
Mar	19	-6.96 ±0.71	8.7 ±1.0
Apr	22	-5.85 ±0.77	11.7 ±0.9
May	15	-4.59 ±0.32	17.6 ±0.6
Jun	20	-5.31 ±0.44	21.1 ±0.7
Jul	18	-4.44 ±0.42	24.6 ±0.5
Aug	21	-4.41 ±0.49	22.5 ±0.5
Sep	17	-7.03 ±0.80	20.3 ±0.7
Oct	17	-8.11 ±0.79	14.6 ±1.2
Nov	17	-9.54 ±1.31	9.7 ±1.0
Dec	7	-8.21 ±1.19	5.6 ±1.8
Win	35	-10.06 ±0.65	5.7 ±0.7
Spr	56	-5.94 ±0.42	11.5 ±0.7
Sum	59	-4.95 ±0.26	22.5 ±0.4
Aut	51	-8.21 ±0.58	15.9 ±0.8

Table A5.H5. Regression results for KY03 when weekly data is grouped by month and by season. Significant results ($p \leq 0.05$) are bolded, while insignificant results are italicized. Actual precipitation amounts were normalized by a log transformation. Blue (red) cells show low (high) values of note.

LMWL (δD vs. $\delta^{18}O$)							
Group	***n***	***Slope***		***y-Int***		***r^2***	***p-value***
Jan	**17**	**8.29**	**±0.23**	**13.92**	**±2.36**	**0.99**	**0.00**
Feb	**11**	**7.59**	**±0.13**	**5.72**	**±1.45**	**1.00**	**0.00**
Mar	**19**	**8.61**	**±0.22**	**16.28**	**±1.76**	**0.99**	**0.00**
Apr	**22**	**7.83**	**±0.23**	**9.83**	**±1.69**	**0.98**	**0.00**
May	**15**	**7.90**	**±0.70**	**10.83**	**±3.24**	**0.91**	**0.00**
Jun	**20**	**7.56**	**±0.23**	**9.27**	**±1.30**	**0.98**	**0.00**
Jul	**18**	**7.09**	**±0.48**	**6.77**	**±2.21**	**0.93**	**0.00**
Aug	**21**	**8.33**	**±0.26**	**12.44**	**±1.23**	**0.98**	**0.00**
Sep	**17**	**8.49**	**±0.15**	**12.87**	**±1.00**	**1.00**	**0.00**
Oct	**17**	**8.08**	**±0.40**	**12.16**	**±3.52**	**0.96**	**0.00**
Nov	**17**	**8.21**	**±0.19**	**13.61**	**±1.87**	**0.99**	**0.00**
Dec	**7**	**8.33**	**±0.52**	**15.81**	**±5.01**	**0.98**	**0.00**
Win	**35**	**8.05**	**±0.16**	**11.57**	**±1.61**	**0.99**	**0.00**
Spr	**56**	**8.09**	**±0.15**	**11.87**	**±1.04**	**0.98**	**0.00**
Sum	**59**	**7.77**	**±0.18**	**10.06**	**±0.92**	**0.97**	**0.00**
Aut	**51**	**8.18**	**±0.14**	**12.44**	**±1.17**	**0.99**	**0.00**
$\delta^{18}O$ vs. PDt							
Group	***n***	***Slope***		***y-Int***		***r^2***	***p-value***
Jan	*17*	*0.14*	*±0.23*	*-10.29*	*±1.54*	*0.03*	*0.54*
Feb	*11*	*0.19*	*±0.48*	*-11.31*	*±3.26*	*0.02*	*0.71*
Mar	**19**	**0.40**	**±0.14**	**-10.45**	**±1.23**	**0.33**	**0.01**
Apr	**22**	**0.45**	**±0.16**	**-11.71**	**±2.01**	**0.28**	**0.01**
May	*15*	*0.27*	*±0.13*	*-9.10*	*±2.27*	*0.25*	*0.06*
Jun	*20*	*-0.17*	*±0.14*	*-1.68*	*±3.10*	*0.07*	*0.26*
Jul	*18*	*0.08*	*±0.21*	*-6.16*	*±5.23*	*0.01*	*0.73*
Aug	**21**	**0.70**	**±0.18**	**-20.08**	**±4.11**	**0.44**	**0.00**
Sep	*17*	*0.05*	*±0.31*	*-7.07*	*±6.40*	*0.00*	*0.87*
Oct	*17*	*0.16*	*±0.17*	*-10.38*	*±2.56*	*0.05*	*0.37*
Nov	*17*	*0.61*	*±0.29*	*-13.70*	*±2.95*	*0.22*	*0.06*
Dec	*7*	*-0.02*	*±0.30*	*-9.01*	*±2.18*	*0.00*	*0.94*
Win	*35*	*0.10*	*±0.17*	*-10.25*	*±1.15*	*0.01*	*0.54*
Spr	**56**	**0.36**	**±0.06**	**-10.48**	**±0.82**	**0.37**	**0.00**

Sum	*59*	*0.15*	*±0.10*	*-8.08*	*±2.22*	*0.04*	*0.12*
Aut	**51**	**0.24**	**±0.09**	**-10.96**	**±1.46**	**0.12**	**0.01**
δ^{18}O vs. PDa							
Group	***n***	***Slope***		***y-Int***		***r^2***	***p-value***
Jan	*17*	*0.44*	*±1.24*	*-10.78*	*±3.57*	*0.01*	*0.73*
Feb	*11*	*-0.85*	*±1.96*	*-7.33*	*±6.62*	*0.02*	*0.67*
Mar	*19*	*-0.25*	*±0.81*	*-6.59*	*±2.51*	*0.01*	*0.76*
Apr	*22*	*0.46*	*±1.06*	*-7.83*	*±3.36*	*0.01*	*0.67*
May	*15*	*0.46*	*±0.67*	*-5.89*	*±2.10*	*0.03*	*0.51*
Jun	*20*	*-0.38*	*±0.55*	*-3.94*	*±1.95*	*0.03*	*0.49*
Jul	*18*	*-0.72*	*±0.41*	*-2.24*	*±1.24*	*0.16*	*0.10*
Aug	*21*	*-0.11*	*±0.74*	*-3.86*	*±2.30*	*0.00*	*0.88*
Sep	**17**	**-2.25**	**±0.84**	**-0.04**	**±2.35**	**0.32**	**0.02**
Oct	*17*	*-0.89*	*±1.00*	*-5.41*	*±3.18*	*0.05*	*0.39*
Nov	*17*	*-1.86*	*±1.72*	*-2.67*	*±5.22*	*0.07*	*0.30*
Dec	*7*	*2.43*	*±1.57*	*-16.61*	*±4.93*	*0.32*	*0.18*
Win	*35*	*0.28*	*±0.84*	*-10.51*	*±2.62*	*0.00*	*0.74*
Spr	*56*	*0.20*	*±0.56*	*-6.81*	*±1.77*	*0.00*	*0.73*
Sum	*59*	*-0.57*	*±0.30*	*-2.80*	*±0.99*	*0.06*	*0.07*
Aut	**51**	**-1.84**	**±0.68**	**-2.10**	**±2.04**	**0.13**	**0.01**

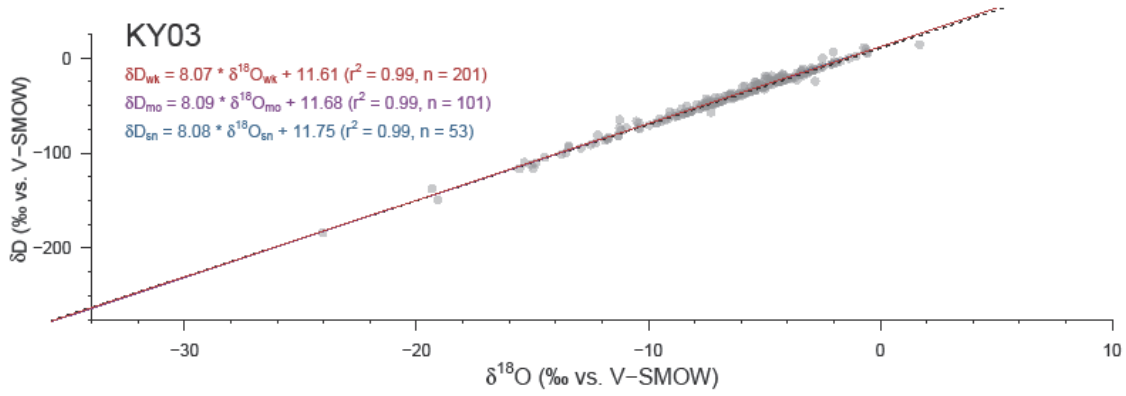

Figure A5.H1. Local meteoric water line for KY03. Gray circles represent values at their original weekly resolution while linear trends are plotted for weekly (red), aggregated monthly (violet), and aggregated seasonal (blue) resolutions. The dashed black line represents the global meteoric water line.

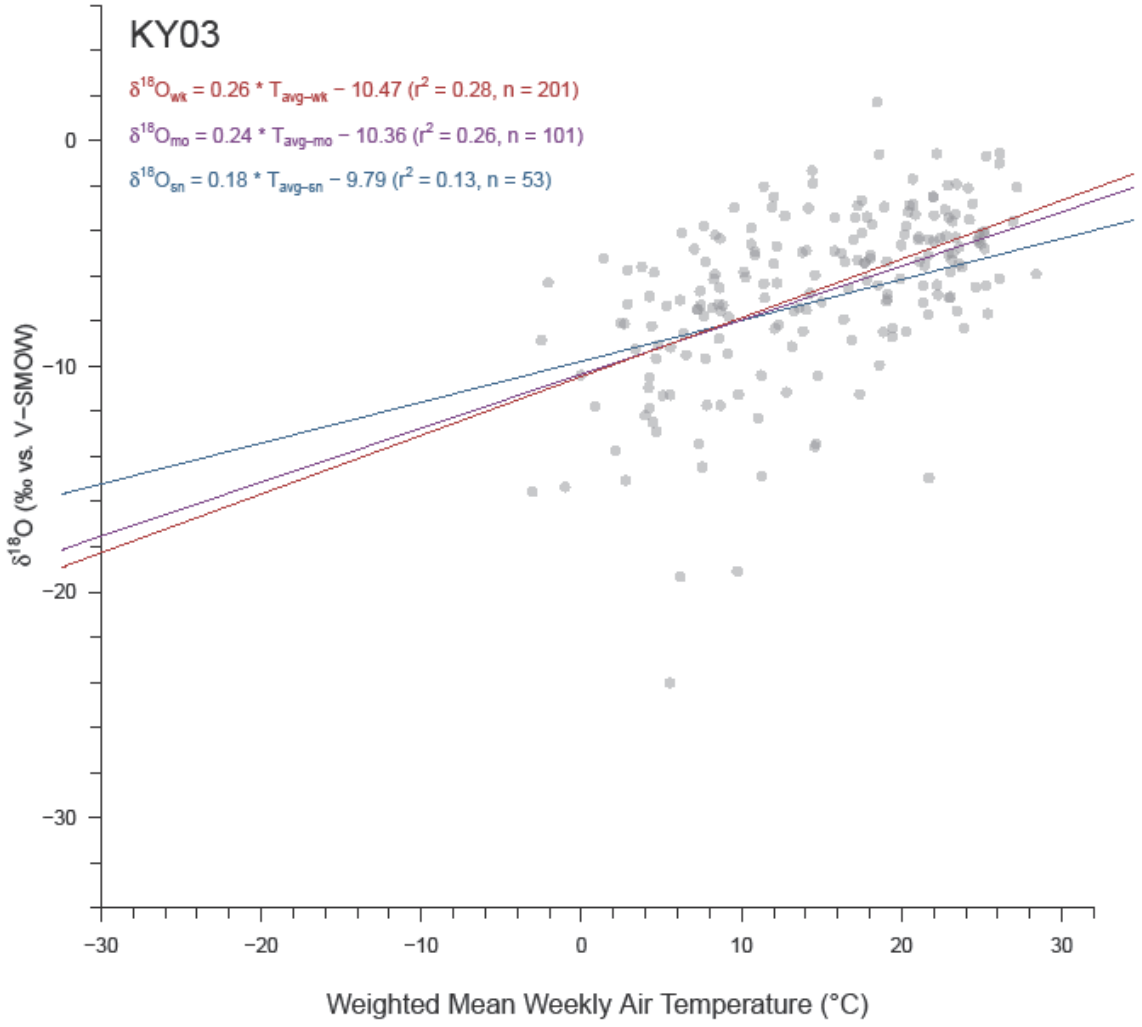

Figure A5.H2. Relationship between precipitation $\delta^{18}O$ and mean PDt at site KY03. Gray circles represent values at their original weekly resolution while linear trends are plotted for weekly (red), aggregated monthly (violet), and aggregated seasonal (blue) resolutions.

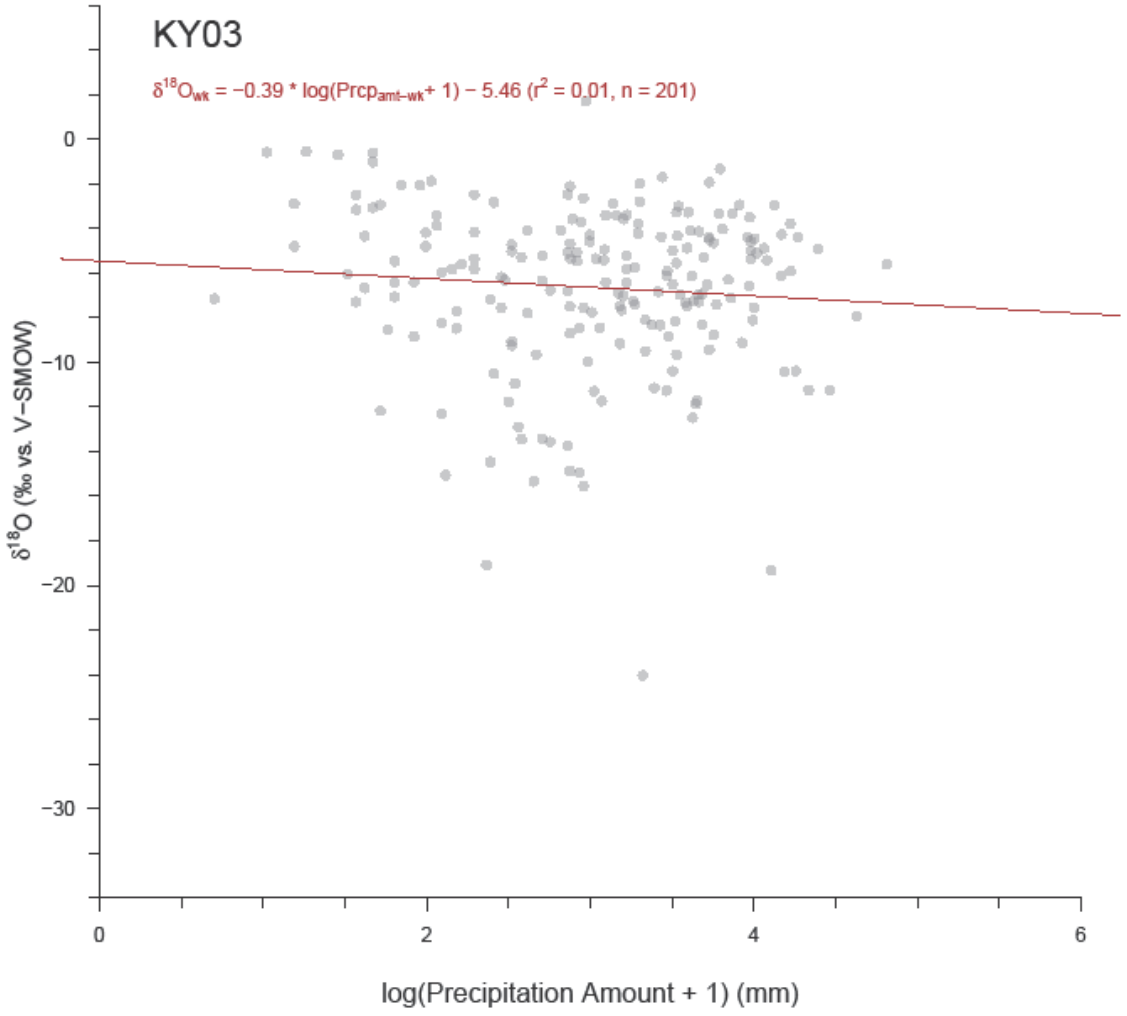

Figure A5.H3. Relationship between precipitation $\delta^{18}O$ and PDa at site KY03. Actual precipitation amounts were normalized by a log transformation. Gray circles represent values at their original weekly resolution with the weekly linear trend plotted in red. Precipitation amount data cannot be weight-averaged for aggregation, and thus regression was only performed at weekly resolution.

MD13

Table A5.I1. Regression results for MD13 at weekly, monthly, and seasonal resolutions. Significant results ($p \leq 0.05$) are bolded, while insignificant results are italicized. Actual precipitation amounts were normalized by a log transformation. Precipitation amount data cannot be weight-averaged for aggregation, and thus regression was only performed at weekly resolution.

LMWL (δD vs. $\delta^{18}O$)							
Resolution	***n***	***Slope***		***y-Int***		***r^2***	***p-value***
Weekly	**280**	**7.85**	**±0.08**	**13.58**	**±0.60**	**0.97**	**0.00**
Monthly	**130**	**7.88**	**±0.13**	**13.57**	**±0.88**	**0.97**	**0.00**
Seasonal	**55**	**7.54**	**±0.15**	**11.31**	**±1.07**	**0.98**	**0.00**
$\delta^{18}O$ vs. PDt							
Resolution	***n***	***Slope***		***y-Int***		***r^2***	***p-value***
Weekly	**280**	**0.25**	**±0.02**	**-10.35**	**±0.32**	**0.37**	**0.00**
Monthly	**130**	**0.19**	**±0.02**	**-9.24**	**±0.40**	**0.32**	**0.00**
Seasonal	**55**	**0.18**	**±0.03**	**-9.16**	**±0.47**	**0.41**	**0.00**
$\delta^{18}O$ vs. PDa							
Resolution	***n***	***Slope***		***y-Int***		***r^2***	***p-value***
Weekly	*280*	*0.06*	*±0.25*	*-7.00*	*±0.78*	*0.00*	*0.82*

Table A5.I2. Percent change in MD13 regression values (Table A5.I1) due to aggregation.

LMWL (δD vs. $\delta^{18}O$)					
Aggregation	***Slope***	***Slope Error***	***y-Int***	***y-Int Error***	***r^2***
Weekly-Monthly	0%	62%	0%	48%	-1%
Weekly-Seasonal	-4%	60%	-17%	53%	1%
Monthly-Seasonal	-5%	18%	-20%	17%	1%
$\delta^{18}O$ vs. PDt					
Aggregation	***Slope***	***Slope Error***	***y-Int***	***y-Int Error***	***r^2***
Weekly-Monthly	-24%	24%	-11%	27%	-14%
Weekly-Seasonal	-39%	40%	-13%	38%	11%
Monthly-Seasonal	-7%	17%	-1%	15%	21%

Table A5.I3. MD13 temperature estimates and standard errors for three $\delta^{18}O$ values (vs. V-SMOW) at weekly, monthly, and seasonal resolutions. The three $\delta^{18}O$ values span much of the natural range of precipitation $\delta^{18}O$ in the study region, and -6‰ is close to the mean $\delta^{18}O$ value of all sites.

	Temperature Estimate (°C) when Precipitation $\delta^{18}O$ =		
Aggregation	***-20‰***	***-6‰***	***0‰***
Weekly	-5.5 ±13.4	15.3 ±13.0	24.1 ±13.1
Monthly	-8.3 ±14.3	15.4 ±13.0	25.5 ±13.3
Seasonal	-16.5 ±15.8	15.7 ±12.1	29.5 ±13.1

Table A5.I4. Weight-averaged weekly values of $\delta^{18}O$ and average surface temperature for MD13 grouped by month and season. Blue (red) cells show low (high) values of note.

Group	***n***	***$\delta^{18}O_{wt}$***	***PDt***
Jan	24	-8.05 ±1.03	5.7 ±1.1
Feb	29	-9.16 ±0.72	3.5 ±0.8
Mar	26	-7.39 ±0.75	8.7 ±0.7
Apr	30	-5.61 ±0.49	12.6 ±0.7
May	17	-4.65 ±0.43	19.3 ±0.9
Jun	30	-5.19 ±0.35	23.2 ±0.6
Jul	20	-4.73 ±0.36	25.1 ±0.3
Aug	19	-5.58 ±0.44	24.1 ±0.5
Sep	17	-6.15 ±0.47	20.7 ±0.7
Oct	21	-6.05 ±0.35	17.5 ±0.7
Nov	21	-7.23 ±0.73	12.5 ±0.9
Dec	26	-7.41 ±0.75	7.6 ±0.9
Win	79	-8.65 ±0.48	5.0 ±0.5
Spr	73	-6.14 ±0.38	11.7 ±0.6
Sum	69	-5.25 ±0.22	23.9 ±0.3
Aut	59	-6.31 ±0.32	17.4 ±0.6

Table A5.I5. Regression results for MD13 when weekly data is grouped by month and by season. Significant results ($p \leq 0.05$) are bolded, while insignificant results are italicized. Actual precipitation amounts were normalized by a log transformation. Blue (red) cells show low (high) values of note.

LMWL (δD vs. $\delta^{18}O$)							
Group	***n***	***Slope***		***y-Int***		***r^2***	***p-value***
Jan	**24**	**7.47**	**±0.28**	**9.06**	**±2.87**	**0.97**	**0.00**
Feb	**29**	**8.25**	**±0.20**	**17.25**	**±1.98**	**0.99**	**0.00**
Mar	**26**	**8.29**	**±0.17**	**17.86**	**±1.51**	**0.99**	**0.00**
Apr	**30**	**7.59**	**±0.39**	**10.30**	**±2.56**	**0.93**	**0.00**
May	**17**	**7.86**	**±0.56**	**13.76**	**±2.75**	**0.93**	**0.00**
Jun	**30**	**7.66**	**±0.33**	**11.15**	**±1.87**	**0.95**	**0.00**
Jul	**20**	**8.46**	**±0.54**	**16.65**	**±2.78**	**0.93**	**0.00**
Aug	**19**	**8.13**	**±0.30**	**14.36**	**±1.74**	**0.98**	**0.00**
Sep	**17**	**7.13**	**±0.48**	**8.66**	**±2.99**	**0.94**	**0.00**
Oct	**21**	**8.24**	**±0.33**	**16.61**	**±2.07**	**0.97**	**0.00**
Nov	**21**	**8.12**	**±0.27**	**16.10**	**±2.15**	**0.98**	**0.00**
Dec	**26**	**8.16**	**±0.23**	**19.57**	**±2.15**	**0.98**	**0.00**
Win	**79**	**7.93**	**±0.15**	**15.11**	**±1.47**	**0.97**	**0.00**
Spr	**73**	**7.93**	**±0.17**	**13.68**	**±1.23**	**0.97**	**0.00**
Sum	**69**	**8.00**	**±0.22**	**13.59**	**±1.22**	**0.95**	**0.00**
Aut	**59**	**7.93**	**±0.19**	**14.36**	**±1.28**	**0.97**	**0.00**
$\delta^{18}O$ vs. PDt							
Group	***n***	***Slope***		***y-Int***		***r^2***	***p-value***
Jan	**24**	**0.67**	**±0.13**	**-12.11**	**±0.90**	**0.56**	**0.00**
Feb	**29**	**0.60**	**±0.14**	**-11.92**	**±0.80**	**0.41**	**0.00**
Mar	**26**	**0.51**	**±0.20**	**-11.83**	**±1.71**	**0.21**	**0.02**
Apr	**30**	**0.43**	**±0.11**	**-11.43**	**±1.46**	**0.35**	**0.00**
May	*17*	*0.12*	*±0.13*	*-6.94*	*±2.46*	*0.06*	*0.35*
Jun	**30**	**0.22**	**±0.10**	**-10.25**	**±2.22**	**0.15**	**0.03**
Jul	*20*	*0.29*	*±0.26*	*-12.29*	*±6.61*	*0.06*	*0.28*
Aug	*19*	*0.20*	*±0.23*	*-10.29*	*±5.61*	*0.04*	*0.41*
Sep	**17**	**0.48**	**±0.12**	**-16.01**	**±2.59**	**0.51**	**0.00**
Oct	*21*	*0.16*	*±0.10*	*-8.66*	*±1.71*	*0.11*	*0.14*
Nov	**21**	**0.58**	**±0.12**	**-14.36**	**±1.59**	**0.55**	**0.00**
Dec	**26**	**0.46**	**±0.15**	**-11.50**	**±1.21**	**0.28**	**0.01**
Win	**79**	**0.58**	**±0.08**	**-11.93**	**±0.53**	**0.43**	**0.00**
Spr	**73**	**0.33**	**±0.06**	**-10.44**	**±0.77**	**0.33**	**0.00**

Sum	**69**	**0.21**	**±0.08**	**-10.18**	**±1.80**	**0.10**	**0.01**
Aut	**59**	**0.30**	**±0.05**	**-11.28**	**±0.93**	**0.34**	**0.00**
δ^{18}O vs. PDa							
Group	***n***	***Slope***		***y-Int***		***r^2***	***p-value***
Jan	**24**	**2.74**	**±1.34**	**-17.10**	**±4.00**	**0.16**	**0.05**
Feb	*29*	*-0.99*	*±0.82*	*-6.49*	*±2.50*	*0.05*	*0.24*
Mar	*26*	*1.19*	*±0.84*	*-11.50*	*±2.68*	*0.08*	*0.17*
Apr	*30*	*-0.57*	*±0.66*	*-4.31*	*±1.95*	*0.03*	*0.40*
May	*17*	*-0.44*	*±0.55*	*-3.32*	*±1.66*	*0.04*	*0.44*
Jun	*30*	*-0.38*	*±0.54*	*-4.17*	*±1.71*	*0.02*	*0.49*
Jul	*20*	*-0.46*	*±0.39*	*-3.40*	*±1.33*	*0.07*	*0.25*
Aug	**19**	**-1.24**	**±0.46**	**-1.63**	**±1.50**	**0.30**	**0.01**
Sep	*17*	*-1.16*	*±0.64*	*-1.63*	*±2.42*	*0.18*	*0.09*
Oct	*21*	*-0.30*	*±0.37*	*-5.23*	*±1.09*	*0.03*	*0.43*
Nov	*21*	*-0.37*	*±1.10*	*-6.04*	*±3.39*	*0.01*	*0.74*
Dec	*26*	*0.22*	*±1.00*	*-9.00*	*±2.99*	*0.00*	*0.83*
Win	*79*	*0.31*	*±0.60*	*-9.88*	*±1.81*	*0.00*	*0.61*
Spr	*73*	*0.06*	*±0.46*	*-6.48*	*±1.42*	*0.00*	*0.90*
Sum	**69**	**-0.63**	**±0.27**	**-3.26**	**±0.88**	**0.08**	**0.02**
Aut	*59*	*-0.32*	*±0.37*	*-5.43*	*±1.20*	*0.01*	*0.40*

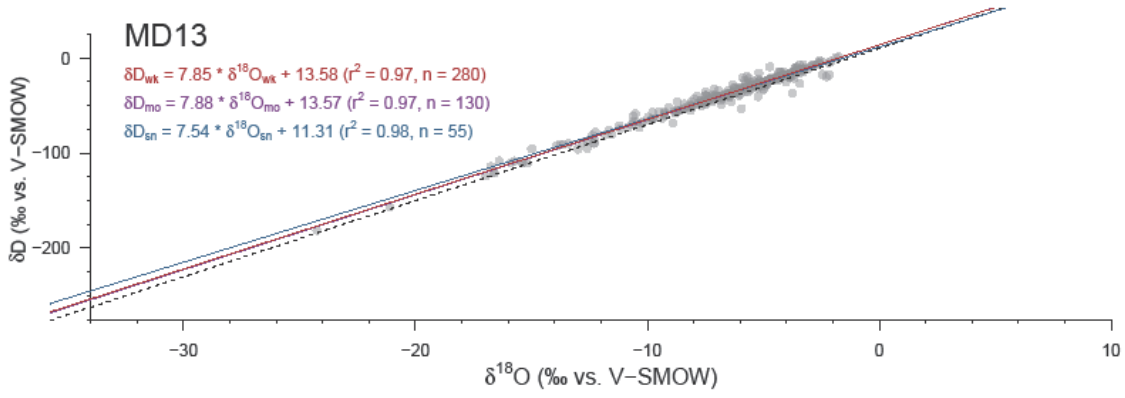

Figure A5.I1. Local meteoric water line for MD13. Gray circles represent values at their original weekly resolution while linear trends are plotted for weekly (red), aggregated monthly (violet), and aggregated seasonal (blue) resolutions. The dashed black line represents the global meteoric water line.

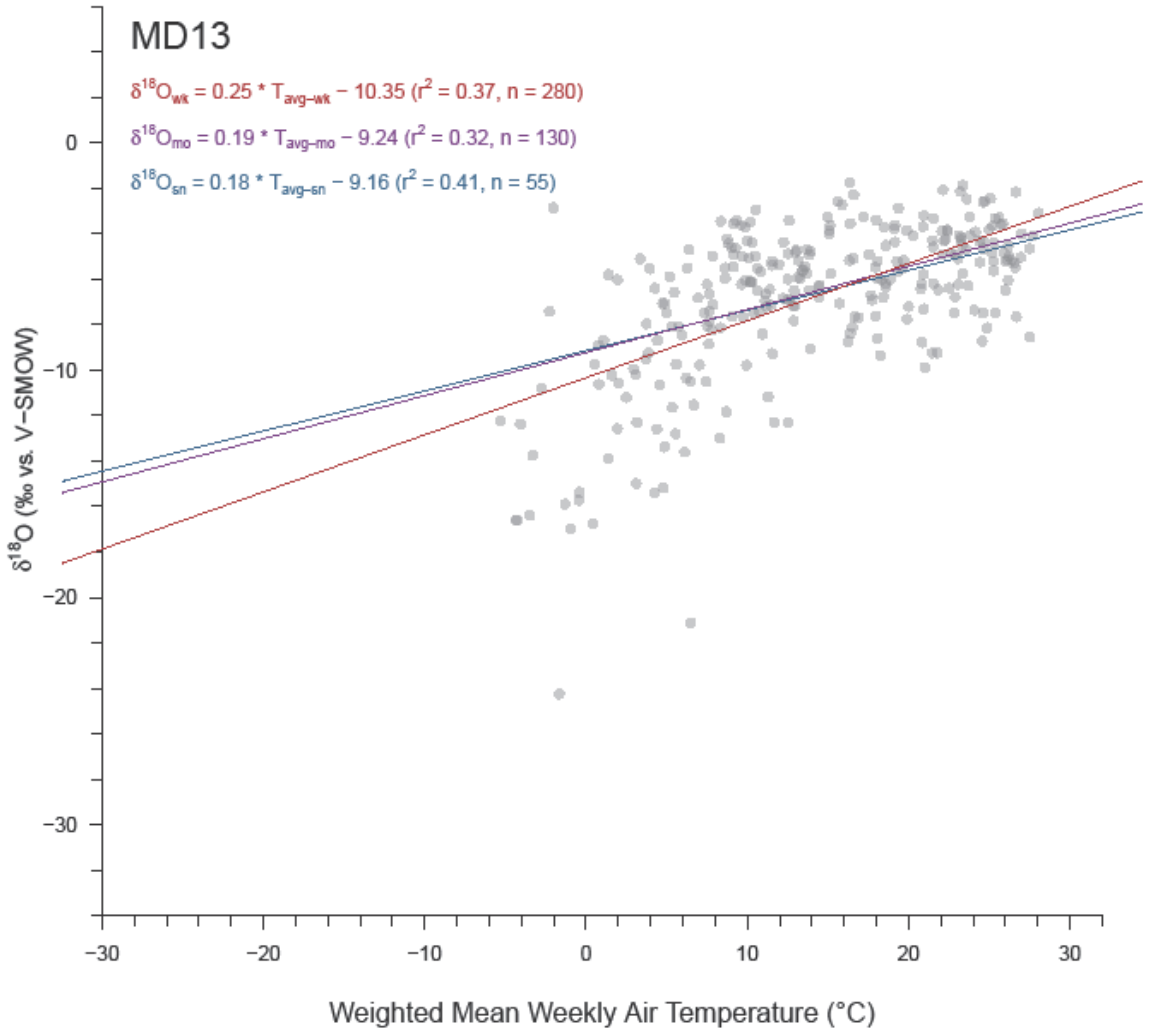

Figure A5.I2. Relationship between precipitation $\delta^{18}O$ and mean PDt at site MD13. Gray circles represent values at their original weekly resolution while linear trends are plotted for weekly (red), aggregated monthly (violet), and aggregated seasonal (blue) resolutions.

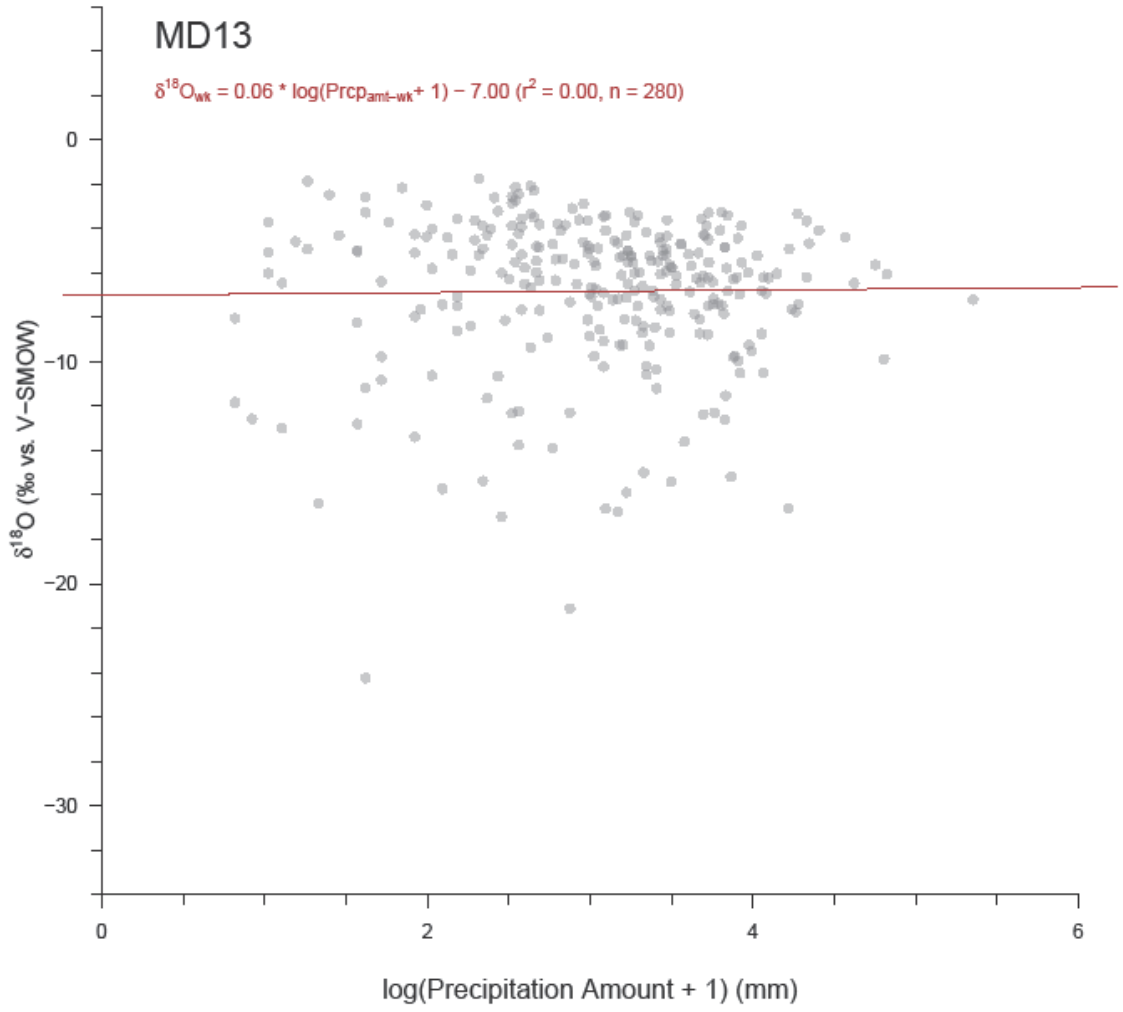

Figure A5.I3. Relationship between precipitation $\delta^{18}O$ and PDa at site MD13. Actual precipitation amounts were normalized by a log transformation. Gray circles represent values at their original weekly resolution with the weekly linear trend plotted in red. Precipitation amount data cannot be weight-averaged for aggregation, and thus regression was only performed at weekly resolution.

MI09

Table A5.J1. Regression results for MI09 at weekly, monthly, and seasonal resolutions. Significant results ($p \leq 0.05$) are bolded, while insignificant results are italicized. Actual precipitation amounts were normalized by a log transformation. Precipitation amount data cannot be weight-averaged for aggregation, and thus regression was only performed at weekly resolution.

LMWL (δD vs. $\delta^{18}O$)							
Resolution	***n***	***Slope***		***y-Int***		***r^2***	***p-value***
Weekly	**280**	**7.78**	**±0.05**	**10.78**	**±0.61**	**0.99**	**0.00**
Monthly	**118**	**7.77**	**±0.06**	**10.87**	**±0.69**	**0.99**	**0.00**
Seasonal	**53**	**7.80**	**±0.07**	**11.43**	**±0.89**	**1.00**	**0.00**
$\delta^{18}O$ vs. PDt							
Resolution	***n***	***Slope***		***y-Int***		***r^2***	***p-value***
Weekly	**280**	**0.44**	**±0.02**	**-14.69**	**±0.25**	**0.65**	**0.00**
Monthly	**118**	**0.40**	**±0.03**	**-14.02**	**±0.33**	**0.65**	**0.00**
Seasonal	**53**	**0.42**	**±0.03**	**-14.14**	**±0.34**	**0.79**	**0.00**
$\delta^{18}O$ vs. PDa							
Resolution	***n***	***Slope***		***y-Int***		***r^2***	***p-value***
Weekly	*280*	*0.80*	*±0.42*	*-13.63*	*±1.21*	*0.01*	*0.06*

Table A5.J2. Percent change in MI09 regression values (Table A5.J1) due to aggregation.

LMWL (δD vs. $\delta^{18}O$)					
Aggregation	***Slope***	***Slope Error***	***y-Int***	***y-Int Error***	***r^2***
Weekly-Monthly	0%	18%	1%	14%	0%
Weekly-Seasonal	0%	42%	6%	41%	1%
Monthly-Seasonal	0%	21%	5%	22%	0%
$\delta^{18}O$ vs. PDt					
Aggregation	***Slope***	***Slope Error***	***y-Int***	***y-Int Error***	***r^2***
Weekly-Monthly	-11%	37%	-5%	34%	1%
Weekly-Seasonal	-7%	38%	-4%	30%	23%
Monthly-Seasonal	5%	10%	1%	5%	18%

Table A5.J3. MI09 temperature estimates and standard errors for three $\delta^{18}O$ values (vs. V-SMOW) at weekly, monthly, and seasonal resolutions. The three $\delta^{18}O$ values span much of the natural range of precipitation $\delta^{18}O$ in the study region, and -6‰ is close to the mean $\delta^{18}O$ value of all sites.

	Temperature Estimate (°C) when Precipitation $\delta^{18}O$ =					
Aggregation	***-20‰***		***-6‰***		***0‰***	
Weekly	-5.2	±11.9	15.3	±11.9	24.1	±12.0
Monthly	-7.4	±12.0	15.7	±11.9	25.6	±12.1
Seasonal	-9.9	±9.5	16.8	±9.3	28.3	±9.7

Table A5.J4. Weight-averaged weekly values of $\delta^{18}O$ and average surface temperature for MI09 grouped by month and season. Blue (red) cells show low (high) values of note.

Group	***n***	***$\delta^{18}O_{wt}$***		***PDt***	
Jan	24	-17.63	±1.04	-6.9	±0.9
Feb	21	-16.65	±1.12	-6.2	±1.0
Mar	25	-13.33	±0.94	-2.1	±1.0
Apr	23	-9.69	±0.85	5.1	±1.0
May	28	-7.11	±0.62	12.4	±0.7
Jun	27	-6.27	±0.48	15.6	±0.8
Jul	22	-6.75	±0.59	19.8	±0.8
Aug	27	-7.74	±0.55	19.8	±0.6
Sep	22	-9.18	±0.87	16.0	±0.9
Oct	23	-13.05	±0.77	7.7	±0.7
Nov	25	-13.54	±0.65	3.2	±0.8
Dec	13	-17.80	±1.55	-4.1	±1.8
Win	58	-17.50	±0.68	-6.3	±0.7
Spr	76	-10.50	±0.56	4.4	±0.9
Sum	76	-6.57	±0.31	18.6	±0.4
Aut	70	-11.97	±0.48	8.3	±0.7

Table A5.J5. Regression results for MI09 when weekly data is grouped by month and by season. Significant results ($p \leq 0.05$) are bolded, while insignificant results are italicized. Actual precipitation amounts were normalized by a log transformation. Blue (red) cells show low (high) values of note.

LMWL (δD vs. $\delta^{18}O$)							
Group	***n***	***Slope***		***y-Int***		***r^2***	***p-value***
Jan	**24**	**8.02**	**±0.21**	**15.59**	**±4.02**	**0.98**	**0.00**
Feb	**21**	**7.47**	**±0.30**	**4.49**	**±5.52**	**0.97**	**0.00**
Mar	**25**	**8.11**	**±0.17**	**15.23**	**±2.49**	**0.99**	**0.00**
Apr	**23**	**7.79**	**±0.21**	**11.38**	**±2.28**	**0.98**	**0.00**
May	**28**	**8.50**	**±0.23**	**13.95**	**±1.93**	**0.98**	**0.00**
Jun	**27**	**8.03**	**±0.31**	**11.07**	**±2.25**	**0.96**	**0.00**
Jul	**22**	**7.56**	**±0.26**	**8.24**	**±2.01**	**0.98**	**0.00**
Aug	**27**	**8.25**	**±0.13**	**14.66**	**±1.08**	**0.99**	**0.00**
Sep	**22**	**7.80**	**±0.24**	**12.45**	**±2.43**	**0.98**	**0.00**
Oct	**23**	**7.79**	**±0.13**	**11.91**	**±1.75**	**0.99**	**0.00**
Nov	**25**	**8.23**	**±0.16**	**17.92**	**±2.19**	**0.99**	**0.00**
Dec	**13**	**7.82**	**±0.39**	**13.78**	**±6.94**	**0.97**	**0.00**
Win	**58**	**7.78**	**±0.16**	**11.25**	**±3.04**	**0.98**	**0.00**
Spr	**76**	**7.91**	**±0.10**	**11.41**	**±1.18**	**0.99**	**0.00**
Sum	**76**	**7.94**	**±0.14**	**11.21**	**±1.08**	**0.98**	**0.00**
Aut	**70**	**7.91**	**±0.10**	**13.54**	**±1.20**	**0.99**	**0.00**
$\delta^{18}O$ vs. PDt							
Group	***n***	***Slope***		***y-Int***		***r^2***	***p-value***
Jan	**24**	**0.81**	**±0.16**	**-12.75**	**±1.33**	**0.53**	**0.00**
Feb	**21**	**0.62**	**±0.22**	**-13.51**	**±1.75**	**0.29**	**0.01**
Mar	**25**	**0.71**	**±0.12**	**-12.88**	**±0.64**	**0.61**	**0.00**
Apr	**23**	**0.61**	**±0.14**	**-13.08**	**±0.96**	**0.49**	**0.00**
May	**28**	**0.47**	**±0.14**	**-13.44**	**±1.79**	**0.31**	**0.00**
Jun	**27**	**0.29**	**±0.11**	**-11.43**	**±1.75**	**0.23**	**0.01**
Jul	**22**	**0.61**	**±0.10**	**-18.89**	**±1.98**	**0.64**	**0.00**
Aug	**27**	**0.40**	**±0.18**	**-15.47**	**±3.51**	**0.16**	**0.04**
Sep	**22**	**0.71**	**±0.13**	**-19.92**	**±2.09**	**0.58**	**0.00**
Oct	**23**	**0.43**	**±0.21**	**-16.14**	**±1.90**	**0.17**	**0.05**
Nov	**25**	**0.53**	**±0.13**	**-15.10**	**±0.69**	**0.41**	**0.00**
Dec	**13**	**0.54**	**±0.20**	**-15.42**	**±1.36**	**0.41**	**0.02**
Win	**58**	**0.62**	**±0.10**	**-14.11**	**±0.80**	**0.39**	**0.00**
Spr	**76**	**0.52**	**±0.05**	**-13.34**	**±0.42**	**0.63**	**0.00**

Sum	**76**	**0.29**	**±0.07**	**-12.49**	**±1.33**	**0.18**	**0.00**
Aut	**70**	**0.44**	**±0.06**	**-15.58**	**±0.62**	**0.45**	**0.00**
δ^{18}O vs. PDa							
Group	***n***	***Slope***		***y-Int***		***r^2***	***p-value***
Jan	**24**	**5.56**	**±1.51**	**-32.57**	**±3.96**	**0.38**	**0.00**
Feb	*21*	*1.65*	*±1.90*	*-21.47*	*±4.67*	*0.04*	*0.40*
Mar	*25*	*0.40*	*±1.28*	*-15.31*	*±3.53*	*0.00*	*0.76*
Apr	*23*	*0.74*	*±1.07*	*-11.99*	*±3.24*	*0.02*	*0.50*
May	*28*	*0.20*	*±0.79*	*-8.14*	*±2.16*	*0.00*	*0.81*
Jun	*27*	*0.61*	*±0.64*	*-8.41*	*±1.70*	*0.03*	*0.35*
Jul	*22*	*0.05*	*±0.63*	*-7.41*	*±1.78*	*0.00*	*0.94*
Aug	*27*	*1.08*	*±0.65*	*-10.94*	*±1.97*	*0.10*	*0.11*
Sep	*22*	*0.63*	*±0.92*	*-11.09*	*±2.77*	*0.02*	*0.50*
Oct	**23**	**-3.41**	**±1.30**	**-2.35**	**±3.94**	**0.25**	**0.02**
Nov	*25*	*-0.71*	*±0.92*	*-11.10*	*±2.88*	*0.03*	*0.45*
Dec	*13*	*-0.59*	*±2.66*	*-15.39*	*±7.31*	*0.00*	*0.83*
Win	**58**	**2.50**	**±1.10**	**-24.06**	**±2.87**	**0.08**	**0.03**
Spr	*76*	*0.43*	*±0.70*	*-11.65*	*±2.00*	*0.01*	*0.54*
Sum	*76*	*0.46*	*±0.36*	*-8.54*	*±1.02*	*0.02*	*0.21*
Aut	*70*	*-0.67*	*±0.63*	*-9.78*	*±1.94*	*0.02*	*0.29*

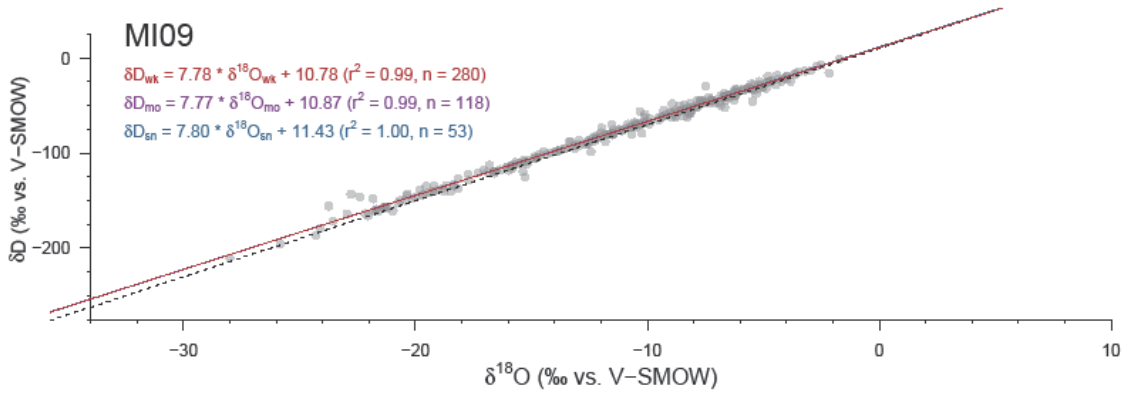

Figure A5.J1. Local meteoric water line for MI09. Gray circles represent values at their original weekly resolution while linear trends are plotted for weekly (red), aggregated monthly (violet), and aggregated seasonal (blue) resolutions. The dashed black line represents the global meteoric water line.

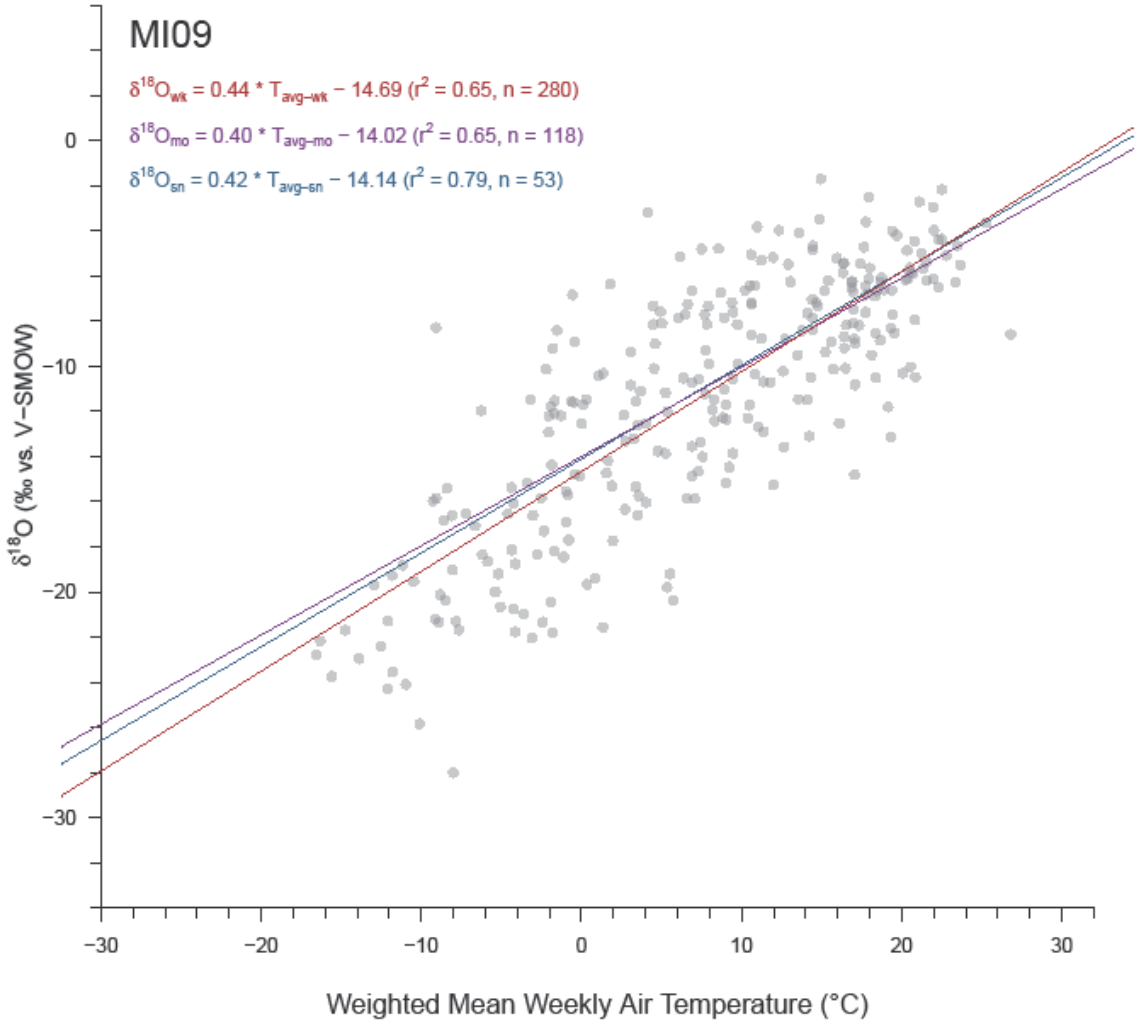

Figure A5.J2. Relationship between precipitation $\delta^{18}O$ and mean PDt at site MI09. Gray circles represent values at their original weekly resolution while linear trends are plotted for weekly (red), aggregated monthly (violet), and aggregated seasonal (blue) resolutions.

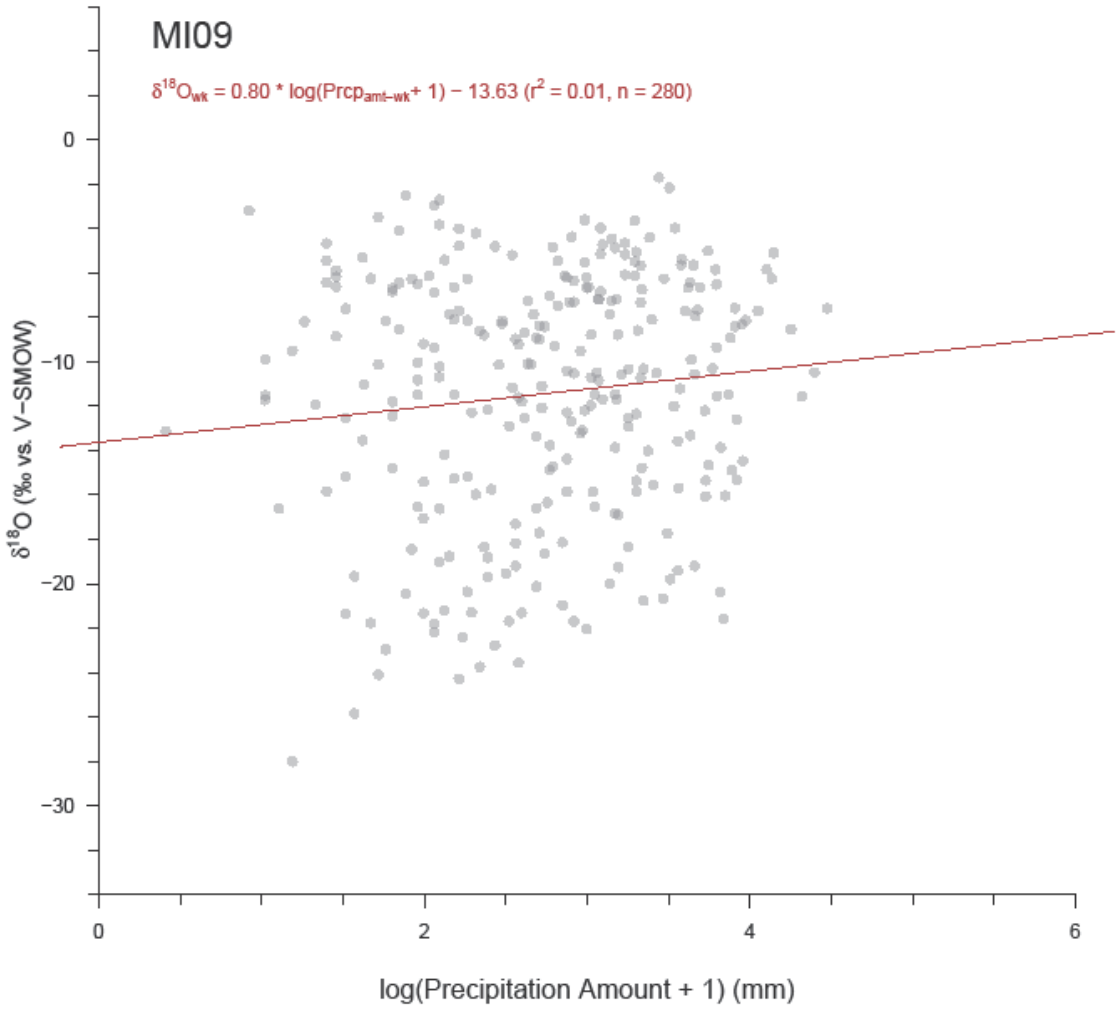

Figure A5.J3. Relationship between precipitation $\delta^{18}O$ and PDa at site MI09. Actual precipitation amounts were normalized by a log transformation. Gray circles represent values at their original weekly resolution with the weekly linear trend plotted in red. Precipitation amount data cannot be weight-averaged for aggregation, and thus regression was only performed at weekly resolution.

MN27

Table A5.K1. Regression results for MN27 at weekly, monthly, and seasonal resolutions. Significant results ($p \leq 0.05$) are bolded, while insignificant results are italicized. Actual precipitation amounts were normalized by a log transformation. Precipitation amount data cannot be weight-averaged for aggregation, and thus regression was only performed at weekly resolution.

LMWL (δD vs. $\delta^{18}O$)							
Resolution	***n***	***Slope***		***y-Int***		***r^2***	***p-value***
Weekly	**286**	**7.78**	**±0.07**	**7.84**	**±0.66**	**0.98**	**0.00**
Monthly	**124**	**7.88**	**±0.08**	**9.27**	**±0.84**	**0.99**	**0.00**
Seasonal	**54**	**7.89**	**±0.09**	**9.50**	**±0.96**	**0.99**	**0.00**
$\delta^{18}O$ vs. PDt							
Resolution	***n***	***Slope***		***y-Int***		***r^2***	***p-value***
Weekly	**286**	**0.39**	**±0.02**	**-13.59**	**±0.30**	**0.61**	**0.00**
Monthly	**124**	**0.40**	**±0.02**	**-13.65**	**±0.35**	**0.69**	**0.00**
Seasonal	**54**	**0.41**	**±0.03**	**-14.13**	**±0.41**	**0.80**	**0.00**
$\delta^{18}O$ vs. PDa							
Resolution	***n***	***Slope***		***y-Int***		***r^2***	***p-value***
Weekly	**286**	**1.12**	**±0.30**	**-11.62**	**±0.87**	**0.05**	**0.00**

Table A5.K2. Percent change in MN27 regression values (Table A5.K1) due to aggregation.

LMWL (δD vs. $\delta^{18}O$)					
Aggregation	***Slope***	***Slope Error***	***y-Int***	***y-Int Error***	***r^2***
Weekly-Monthly	1%	16%	18%	27%	1%
Weekly-Seasonal	1%	27%	18%	36%	1%
Monthly-Seasonal	0%	12%	2%	13%	1%
$\delta^{18}O$ vs. PDt					
Aggregation	***Slope***	***Slope Error***	***y-Int***	***y-Int Error***	***r^2***
Weekly-Monthly	2%	32%	0%	19%	12%
Weekly-Seasonal	6%	43%	4%	32%	27%
Monthly-Seasonal	3%	16%	3%	14%	14%

Table A5.K3. MN27 temperature estimates and standard errors for three $\delta^{18}O$ values (vs. V-SMOW) at weekly, monthly, and seasonal resolutions. The three $\delta^{18}O$ values span much of the natural range of precipitation $\delta^{18}O$ in the study region, and -6‰ is close to the mean $\delta^{18}O$ value of all sites.

	Temperature Estimate (°C) when Precipitation $\delta^{18}O$ =		
Aggregation	***-20‰***	***-6‰***	***0‰***
Weekly	-5.0 ±11.8	17.0 ±11.7	26.5 ±11.7
Monthly	-7.7 ±11.5	16.5 ±11.3	26.8 ±11.5
Seasonal	-9.2 ±9.4	17.8 ±9.0	29.4 ±9.4

Table A5.K4. Weight-averaged weekly values of $\delta^{18}O$ and average surface temperature for MN27 grouped by month and season. Blue (red) cells show low (high) values of note.

Group	***n***	***$\delta^{18}O_{wt}$***	***PDt***
Jan	5	-18.27 ±2.68	-10.8 ±2.6
Feb	8	-18.55 ±1.17	-4.6 ±2.0
Mar	22	-9.08 ±1.00	3.9 ±1.2
Apr	28	-9.10 ±0.66	6.3 ±0.9
May	39	-7.50 ±0.58	13.8 ±0.9
Jun	43	-5.93 ±0.45	19.6 ±0.5
Jul	36	-5.53 ±0.43	22.8 ±0.4
Aug	35	-5.75 ±0.34	20.1 ±0.5
Sep	29	-7.32 ±0.66	17.2 ±0.8
Oct	20	-10.77 ±0.83	10.0 ±1.1
Nov	15	-14.86 ±0.84	-0.5 ±1.2
Dec	6	-15.49 ±1.32	-1.9 ±0.6
Win	19	-17.27 ±0.96	-5.6 ±1.3
Spr	89	-8.44 ±0.42	10.4 ±0.7
Sum	114	-5.98 ±0.24	19.8 ±0.3
Aut	64	-9.83 ±0.56	12.4 ±1.1

Table A5.K5. Regression results for MN27 when weekly data is grouped by month and by season. Significant results ($p \leq 0.05$) are bolded, while insignificant results are italicized. Actual precipitation amounts were normalized by a log transformation. Blue (red) cells show low (high) values of note.

LMWL (δD vs. $\delta^{18}O$)							
Group	***n***	***Slope***		***y-Int***		***r^2***	***p-value***
Jan	**5**	**8.21**	**±0.16**	**12.22**	**±2.99**	**1.00**	**0.00**
Feb	**8**	**7.96**	**±0.48**	**9.63**	**±9.20**	**0.98**	**0.00**
Mar	**22**	**8.48**	**±0.25**	**16.28**	**±2.80**	**0.98**	**0.00**
Apr	**28**	**7.81**	**±0.41**	**8.48**	**±4.05**	**0.93**	**0.00**
May	**39**	**7.91**	**±0.16**	**9.23**	**±1.37**	**0.99**	**0.00**
Jun	**43**	**7.55**	**±0.26**	**6.24**	**±1.78**	**0.95**	**0.00**
Jul	**36**	**7.04**	**±0.34**	**2.33**	**±2.01**	**0.93**	**0.00**
Aug	**35**	**6.69**	**±0.44**	**1.45**	**±2.60**	**0.88**	**0.00**
Sep	**29**	**7.92**	**±0.30**	**8.59**	**±2.46**	**0.96**	**0.00**
Oct	**20**	**8.25**	**±0.31**	**14.33**	**±3.76**	**0.98**	**0.00**
Nov	**15**	**7.93**	**±0.49**	**12.33**	**±7.03**	**0.95**	**0.00**
Dec	**6**	**8.76**	**±0.51**	**25.49**	**±8.02**	**0.99**	**0.00**
Win	**19**	**8.37**	**±0.22**	**17.47**	**±3.91**	**0.99**	**0.00**
Spr	**89**	**8.05**	**±0.15**	**10.76**	**±1.43**	**0.97**	**0.00**
Sum	**114**	**7.22**	**±0.19**	**3.98**	**±1.17**	**0.93**	**0.00**
Aut	**64**	**7.79**	**±0.16**	**8.66**	**±1.76**	**0.98**	**0.00**
$\delta^{18}O$ vs. PDt							
Group	***n***	***Slope***		***y-Int***		***r^2***	***p-value***
Jan	*5*	*0.63*	*±0.48*	*-11.49*	*±5.73*	*0.36*	*0.28*
Feb	**8**	**0.43**	**±0.16**	**-16.96**	**±1.08**	**0.55**	**0.04**
Mar	**22**	**0.52**	**±0.14**	**-12.02**	**±0.90**	**0.40**	**0.00**
Apr	**28**	**0.43**	**±0.13**	**-12.01**	**±0.99**	**0.31**	**0.00**
May	**39**	**0.41**	**±0.08**	**-13.43**	**±1.17**	**0.42**	**0.00**
Jun	**43**	**0.33**	**±0.12**	**-12.65**	**±2.41**	**0.15**	**0.01**
Jul	**36**	**0.50**	**±0.15**	**-16.37**	**±3.31**	**0.25**	**0.00**
Aug	**35**	**0.28**	**±0.11**	**-11.34**	**±2.22**	**0.17**	**0.01**
Sep	**29**	**0.52**	**±0.12**	**-16.47**	**±2.15**	**0.41**	**0.00**
Oct	**20**	**0.49**	**±0.13**	**-15.96**	**±1.28**	**0.45**	**0.00**
Nov	*15*	*0.19*	*±0.18*	*-13.94*	*±0.83*	*0.08*	*0.30*
Dec	*6*	*1.58*	*±0.75*	*-12.33*	*±1.82*	*0.52*	*0.10*
Win	**19**	**0.41**	**±0.14**	**-15.42**	**±1.10**	**0.33**	**0.01**
Spr	**89**	**0.36**	**±0.05**	**-12.04**	**±0.53**	**0.40**	**0.00**

Sum	**114**	**0.35**	**±0.07**	**-12.98**	**±1.43**	**0.19**	**0.00**
Aut	**64**	**0.40**	**±0.04**	**-14.49**	**±0.59**	**0.58**	**0.00**
δ^{18}O vs. PDa							
Group	***n***	***Slope***		***y-Int***		***r^2***	***p-value***
Jan	*5*	*3.63*	*±2.02*	*-26.18*	*±4.89*	*0.52*	*0.17*
Feb	*8*	*1.57*	*±6.38*	*-22.40*	*±14.84*	*0.01*	*0.81*
Mar	*22*	*0.76*	*±1.09*	*-12.13*	*±2.64*	*0.02*	*0.50*
Apr	*28*	*-0.11*	*±0.81*	*-8.92*	*±2.22*	*0.00*	*0.90*
May	*39*	*-0.14*	*±0.71*	*-7.34*	*±2.20*	*0.00*	*0.84*
Jun	*43*	*0.40*	*±0.45*	*-7.40*	*±1.42*	*0.02*	*0.37*
Jul	**36**	**-1.38**	**±0.50**	**-1.39**	**±1.52**	**0.18**	**0.01**
Aug	*35*	*-0.54*	*±0.40*	*-3.96*	*±1.26*	*0.05*	*0.19*
Sep	*29*	*-0.09*	*±0.76*	*-7.16*	*±2.21*	*0.00*	*0.91*
Oct	*20*	*1.35*	*±0.83*	*-15.09*	*±2.26*	*0.13*	*0.12*
Nov	*15*	*-1.98*	*±1.07*	*-9.33*	*±2.62*	*0.21*	*0.09*
Dec	*6*	*-2.14*	*±7.11*	*-11.66*	*±12.82*	*0.02*	*0.78*
Win	*19*	*1.99*	*±1.53*	*-21.80*	*±3.36*	*0.09*	*0.21*
Spr	*89*	*0.52*	*±0.46*	*-10.27*	*±1.32*	*0.01*	*0.27*
Sum	*114*	*-0.29*	*±0.27*	*-4.90*	*±0.84*	*0.01*	*0.29*
Aut	*64*	*0.72*	*±0.62*	*-12.13*	*±1.71*	*0.02*	*0.26*

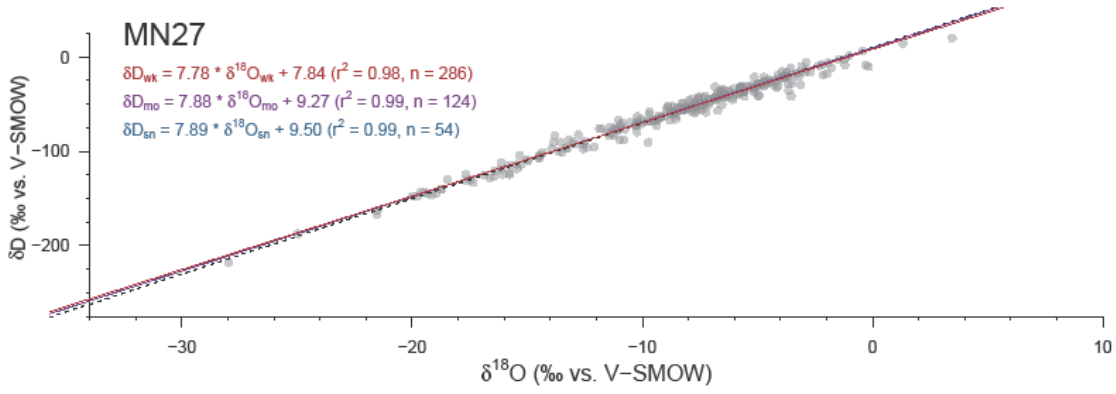

Figure A5.K1. Local meteoric water line for MN27. Gray circles represent values at their original weekly resolution while linear trends are plotted for weekly (red), aggregated monthly (violet), and aggregated seasonal (blue) resolutions. The dashed black line represents the global meteoric water line.

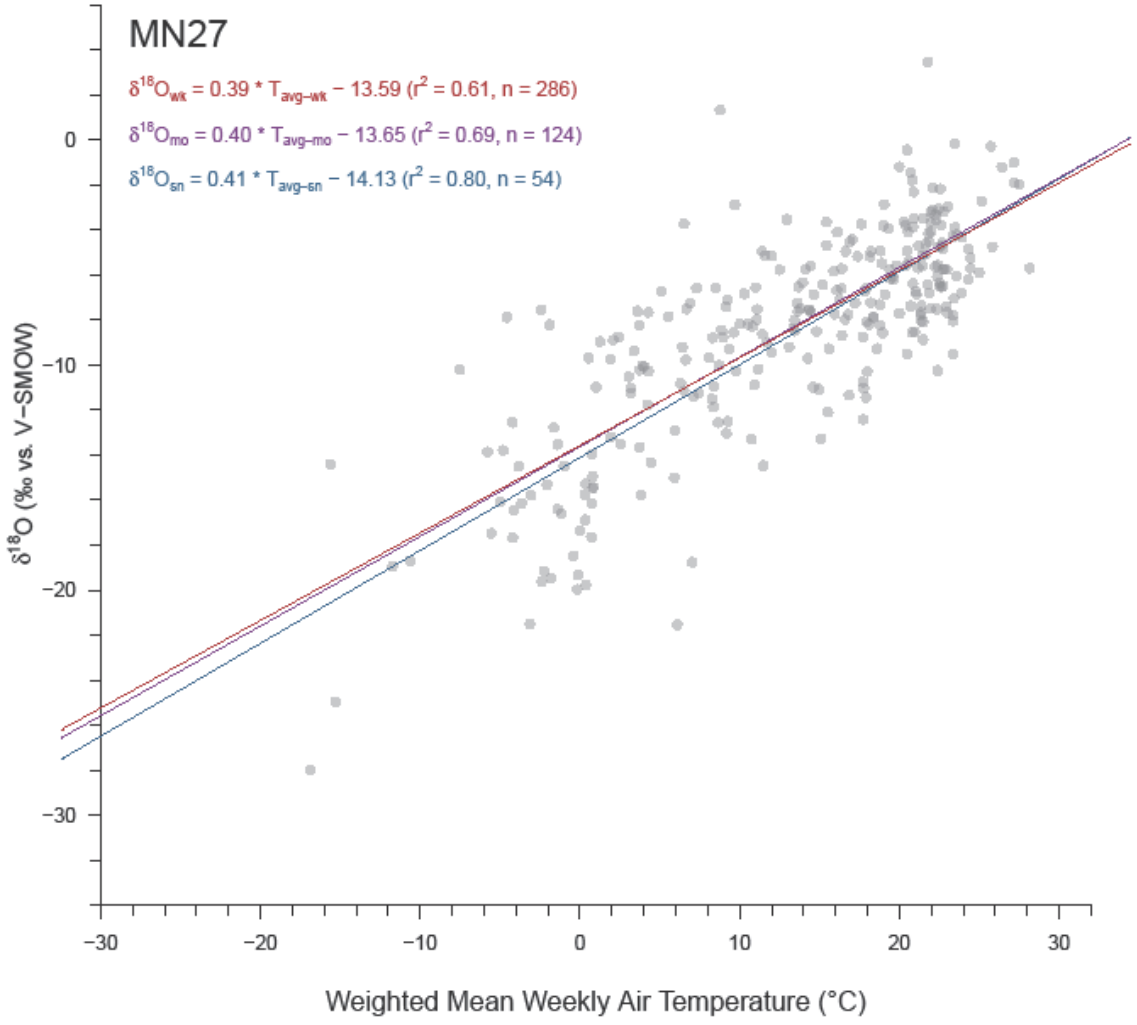

Figure A5.K2. Relationship between precipitation $\delta^{18}O$ and mean PDt at site MN27. Gray circles represent values at their original weekly resolution while linear trends are plotted for weekly (red), aggregated monthly (violet), and aggregated seasonal (blue) resolutions.

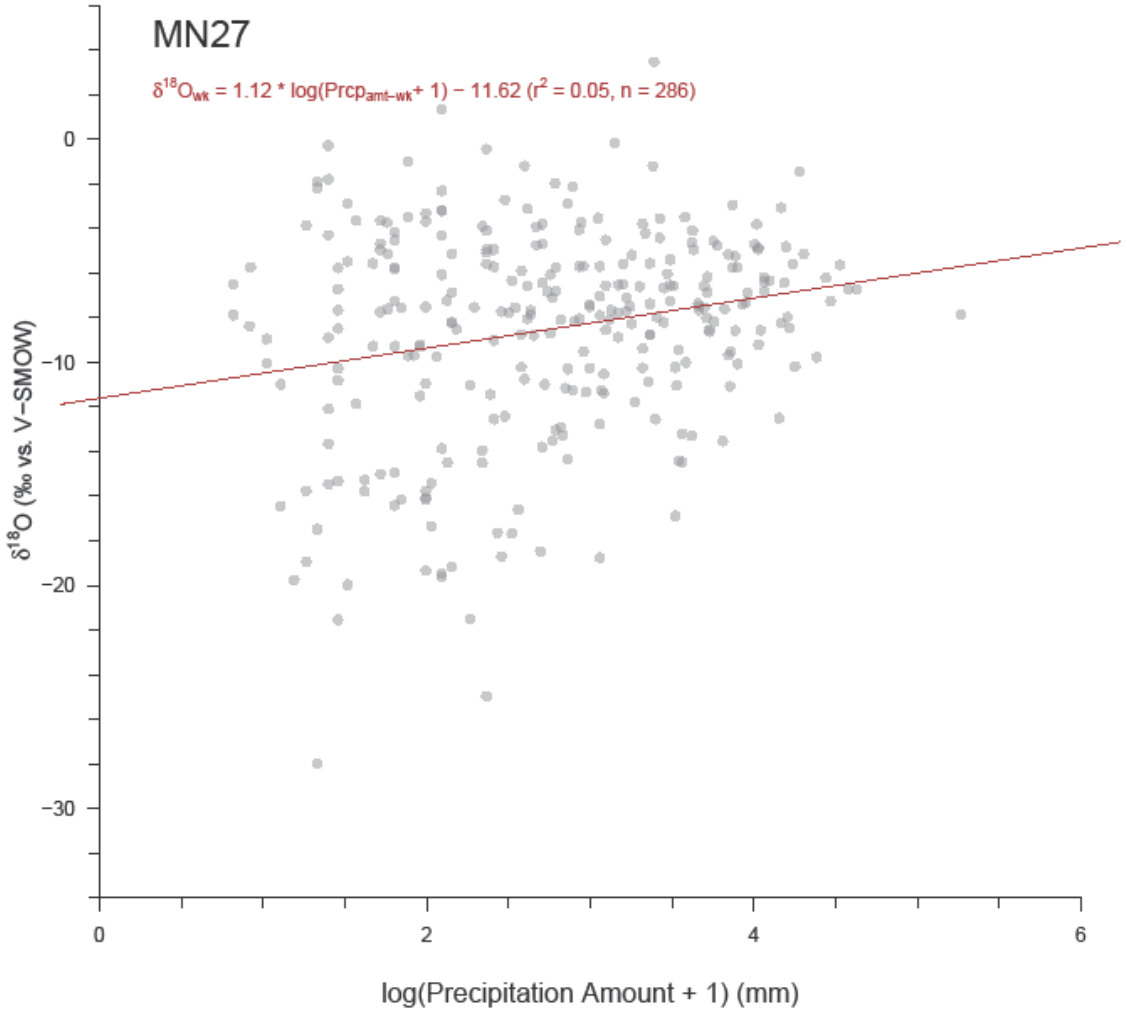

Figure A5.K3. Relationship between precipitation $\delta^{18}O$ and PDa at site MN27. Actual precipitation amounts were normalized by a log transformation. Gray circles represent values at their original weekly resolution with the weekly linear trend plotted in red. Precipitation amount data cannot be weight-averaged for aggregation, and thus regression was only performed at weekly resolution.

MS30

Table A5.L1. Regression results for MS30 at weekly, monthly, and seasonal resolutions. Significant results ($p \leq 0.05$) are bolded, while insignificant results are italicized. Actual precipitation amounts were normalized by a log transformation. Precipitation amount data cannot be weight-averaged for aggregation, and thus regression was only performed at weekly resolution.

LMWL (δD vs. $\delta^{18}O$)							
Resolution	***n***	***Slope***		***y-Int***		***r^2***	***p-value***
Weekly	**279**	**7.85**	**±0.13**	**10.90**	**±0.73**	**0.93**	**0.00**
Monthly	**135**	**7.65**	**±0.19**	**9.90**	**±1.05**	**0.92**	**0.00**
Seasonal	**55**	**7.82**	**±0.34**	**10.80**	**±1.85**	**0.91**	**0.00**
$\delta^{18}O$ vs. PDt							
Resolution	***n***	***Slope***		***y-Int***		***r^2***	***p-value***
Weekly	**279**	**0.21**	**±0.02**	**-8.49**	**±0.38**	**0.26**	**0.00**
Monthly	**135**	**0.18**	**±0.02**	**-8.24**	**±0.45**	**0.30**	**0.00**
Seasonal	**55**	**0.16**	**±0.03**	**-7.93**	**±0.62**	**0.29**	**0.00**
$\delta^{18}O$ vs. PDa							
Resolution	***n***	***Slope***		***y-Int***		***r^2***	***p-value***
Weekly	**279**	**-0.61**	**±0.17**	**-3.02**	**±0.59**	**0.04**	**0.00**

Table A5.L2. Percent change in MS30 regression values (Table A5.L1) due to aggregation.

LMWL (δD vs. $\delta^{18}O$)					
Aggregation	***Slope***	***Slope Error***	***y-Int***	***y-Int Error***	***r^2***
Weekly-Monthly	-3%	51%	-9%	44%	-1%
Weekly-Seasonal	0%	112%	-1%	107%	-3%
Monthly-Seasonal	2%	44%	8%	43%	-2%
$\delta^{18}O$ vs. PDt					
Aggregation	***Slope***	***Slope Error***	***y-Int***	***y-Int Error***	***r^2***
Weekly-Monthly	-11%	15%	-3%	19%	15%
Weekly-Seasonal	-27%	52%	-7%	53%	11%
Monthly-Seasonal	-17%	28%	-4%	27%	-3%

Table A5.L3. MS30 temperature estimates and standard errors for three $\delta^{18}O$ values (vs. V-SMOW) at weekly, monthly, and seasonal resolutions. The three $\delta^{18}O$ values span much of the natural range of precipitation $\delta^{18}O$ in the study region, and -6‰ is close to the mean $\delta^{18}O$ value of all sites.

	Temperature Estimate (°C) when Precipitation $\delta^{18}O$ =					
Aggregation	***-20‰***		***-6‰***		***0‰***	
Weekly	-2.1	±12.3	15.7	±11.7	23.3	±11.8
Monthly	-7.1	±12.5	16.1	±10.7	26.0	±10.9
Seasonal	-10.2	±15.3	16.2	±9.6	27.5	±10.5

Table A5.L4. Weight-averaged weekly values of $\delta^{18}O$ and average surface temperature for MS30 grouped by month and season. Blue (red) cells show low (high) values of note.

Group	***n***	***$\delta^{18}O_{wt}$***		***PDt***	
Jan	31	-6.73	±0.52	9.3	±0.7
Feb	25	-7.12	±0.65	10.8	±0.9
Mar	29	-4.64	±0.50	12.1	±0.8
Apr	22	-4.95	±0.48	16.9	±0.6
May	19	-3.79	±0.53	20.9	±0.5
Jun	29	-4.40	±0.34	23.9	±0.3
Jul	21	-3.40	±0.40	25.3	±0.3
Aug	15	-2.28	±0.33	25.9	±0.5
Sep	21	-4.91	±0.48	23.7	±0.8
Oct	23	-5.74	±0.52	19.3	±0.6
Nov	22	-5.71	±0.47	15.2	±0.8
Dec	22	-5.59	±0.71	10.8	±0.9
Win	78	-6.38	±0.36	10.6	±0.5
Spr	70	-4.54	±0.29	16.7	±0.6
Sum	65	-4.03	±0.23	24.5	±0.2
Aut	66	-5.65	±0.29	19.2	±0.6

Table A5.L5. Regression results for MS30 when weekly data is grouped by month and by season. Significant results ($p \leq 0.05$) are bolded, while insignificant results are italicized. Actual precipitation amounts were normalized by a log transformation. Blue (red) cells show low (high) values of note.

LMWL (δD vs. $\delta^{18}O$)							
Group	***n***	***Slope***		***y-Int***		***r^2***	***p-value***
Jan	**31**	**8.28**	**±0.58**	**14.66**	**±4.02**	**0.88**	**0.00**
Feb	**25**	**8.31**	**±0.34**	**14.73**	**±2.77**	**0.96**	**0.00**
Mar	**29**	**8.10**	**±0.35**	**12.95**	**±1.95**	**0.95**	**0.00**
Apr	**22**	**7.67**	**±0.39**	**11.19**	**±1.89**	**0.95**	**0.00**
May	**19**	**8.39**	**±0.37**	**12.19**	**±1.68**	**0.97**	**0.00**
Jun	**29**	**7.67**	**±0.51**	**8.24**	**±2.26**	**0.89**	**0.00**
Jul	**21**	**8.16**	**±0.50**	**9.72**	**±1.90**	**0.93**	**0.00**
Aug	**15**	**6.28**	**±1.06**	**6.81**	**±2.78**	**0.73**	**0.00**
Sep	**21**	**7.09**	**±0.46**	**3.98**	**±2.32**	**0.93**	**0.00**
Oct	**23**	**8.12**	**±0.42**	**12.41**	**±2.49**	**0.95**	**0.00**
Nov	**22**	**8.10**	**±0.67**	**13.10**	**±4.00**	**0.88**	**0.00**
Dec	**22**	**8.30**	**±0.41**	**17.69**	**±2.96**	**0.95**	**0.00**
Win	**78**	**8.32**	**±0.27**	**15.71**	**±1.97**	**0.93**	**0.00**
Spr	**70**	**8.02**	**±0.22**	**12.10**	**±1.09**	**0.95**	**0.00**
Sum	**65**	**7.81**	**±0.32**	**9.10**	**±1.25**	**0.90**	**0.00**
Aut	**66**	**7.68**	**±0.31**	**9.23**	**±1.74**	**0.91**	**0.00**
$\delta^{18}O$ vs. PDt							
Group	***n***	***Slope***		***y-Int***		***r^2***	***p-value***
Jan	**31**	**0.27**	**±0.12**	**-8.66**	**±1.15**	**0.15**	**0.03**
Feb	**25**	**0.51**	**±0.11**	**-12.68**	**±1.30**	**0.46**	**0.00**
Mar	*29*	*0.23*	*±0.12*	*-7.72*	*±1.54*	*0.13*	*0.06*
Apr	*22*	*0.25*	*±0.17*	*-8.57*	*±2.92*	*0.10*	*0.16*
May	*19*	*-0.05*	*±0.24*	*-2.90*	*±5.07*	*0.00*	*0.83*
Jun	*29*	*0.21*	*±0.21*	*-9.07*	*±5.08*	*0.03*	*0.33*
Jul	**21**	**0.79**	**±0.27**	**-23.24**	**±6.73**	**0.32**	**0.01**
Aug	*15*	*0.31*	*±0.18*	*-10.45*	*±4.66*	*0.19*	*0.10*
Sep	**21**	**0.41**	**±0.11**	**-14.16**	**±2.70**	**0.40**	**0.00**
Oct	**23**	**-0.38**	**±0.16**	**1.87**	**±3.12**	**0.21**	**0.03**
Nov	**22**	**0.37**	**±0.11**	**-11.06**	**±1.72**	**0.35**	**0.00**
Dec	**22**	**0.40**	**±0.16**	**-10.12**	**±1.61**	**0.24**	**0.02**
Win	**78**	**0.35**	**±0.08**	**-10.02**	**±0.78**	**0.22**	**0.00**
Spr	**70**	**0.15**	**±0.06**	**-6.84**	**±1.01**	**0.08**	**0.02**

Sum	**65**	**0.46**	**±0.11**	**-14.93**	**±2.80**	**0.21**	**0.00**
Aut	**66**	**0.14**	**±0.06**	**-7.82**	**±1.14**	**0.08**	**0.02**
δ^{18}O vs. PDa							
Group	***n***	***Slope***		***y-Int***		***r^2***	***p-value***
Jan	*31*	*-1.08*	*±0.62*	*-2.93*	*±1.99*	*0.10*	*0.09*
Feb	*25*	*0.54*	*±0.76*	*-9.26*	*±2.72*	*0.02*	*0.49*
Mar	*29*	*-0.07*	*±0.57*	*-4.60*	*±1.88*	*0.00*	*0.91*
Apr	**22**	**-1.20**	**±0.49**	**0.04**	**±1.86**	**0.23**	**0.02**
May	*19*	*-0.51*	*±0.49*	*-2.30*	*±1.72*	*0.06*	*0.32*
Jun	**29**	**-1.13**	**±0.30**	**-0.17**	**±1.07**	**0.35**	**0.00**
Jul	**21**	**-0.94**	**±0.34**	**-0.36**	**±1.14**	**0.29**	**0.01**
Aug	*15*	*-0.17*	*±0.39*	*-1.83*	*±1.18*	*0.01*	*0.67*
Sep	*21*	*-0.88*	*±0.61*	*-2.05*	*±1.83*	*0.10*	*0.17*
Oct	**23**	**-1.43**	**±0.43**	**-0.49**	**±1.53**	**0.35**	**0.00**
Nov	*22*	*-0.32*	*±0.49*	*-4.50*	*±1.65*	*0.02*	*0.52*
Dec	*22*	*1.08*	*±0.84*	*-9.99*	*±2.90*	*0.08*	*0.22*
Win	*78*	*-0.02*	*±0.42*	*-6.61*	*±1.43*	*0.00*	*0.96*
Spr	*70*	*-0.48*	*±0.30*	*-2.83*	*±1.06*	*0.04*	*0.12*
Sum	**65**	**-0.98**	**±0.20**	**-0.26**	**±0.68**	**0.28**	**0.00**
Aut	**66**	**-0.93**	**±0.28**	**-2.21**	**±0.93**	**0.15**	**0.00**

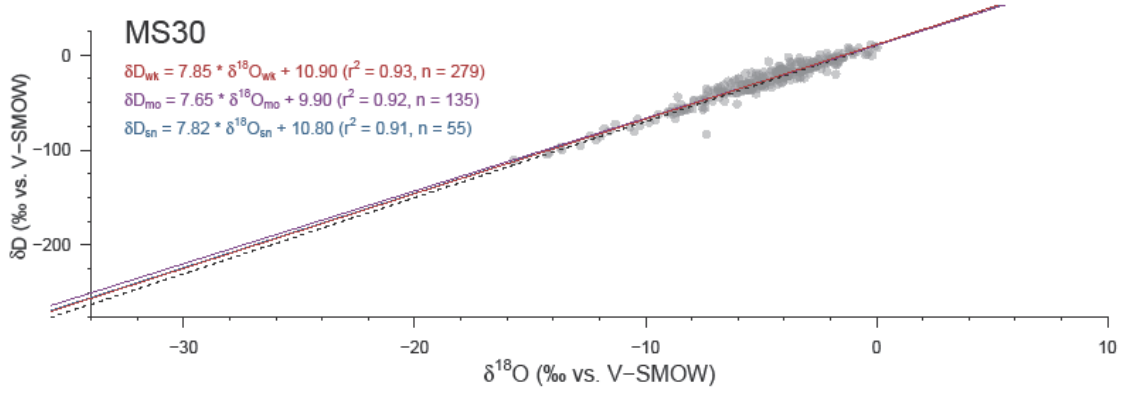

Figure A5.L1. Local meteoric water line for MS30. Gray circles represent values at their original weekly resolution while linear trends are plotted for weekly (red), aggregated monthly (violet), and aggregated seasonal (blue) resolutions. The dashed black line represents the global meteoric water line.

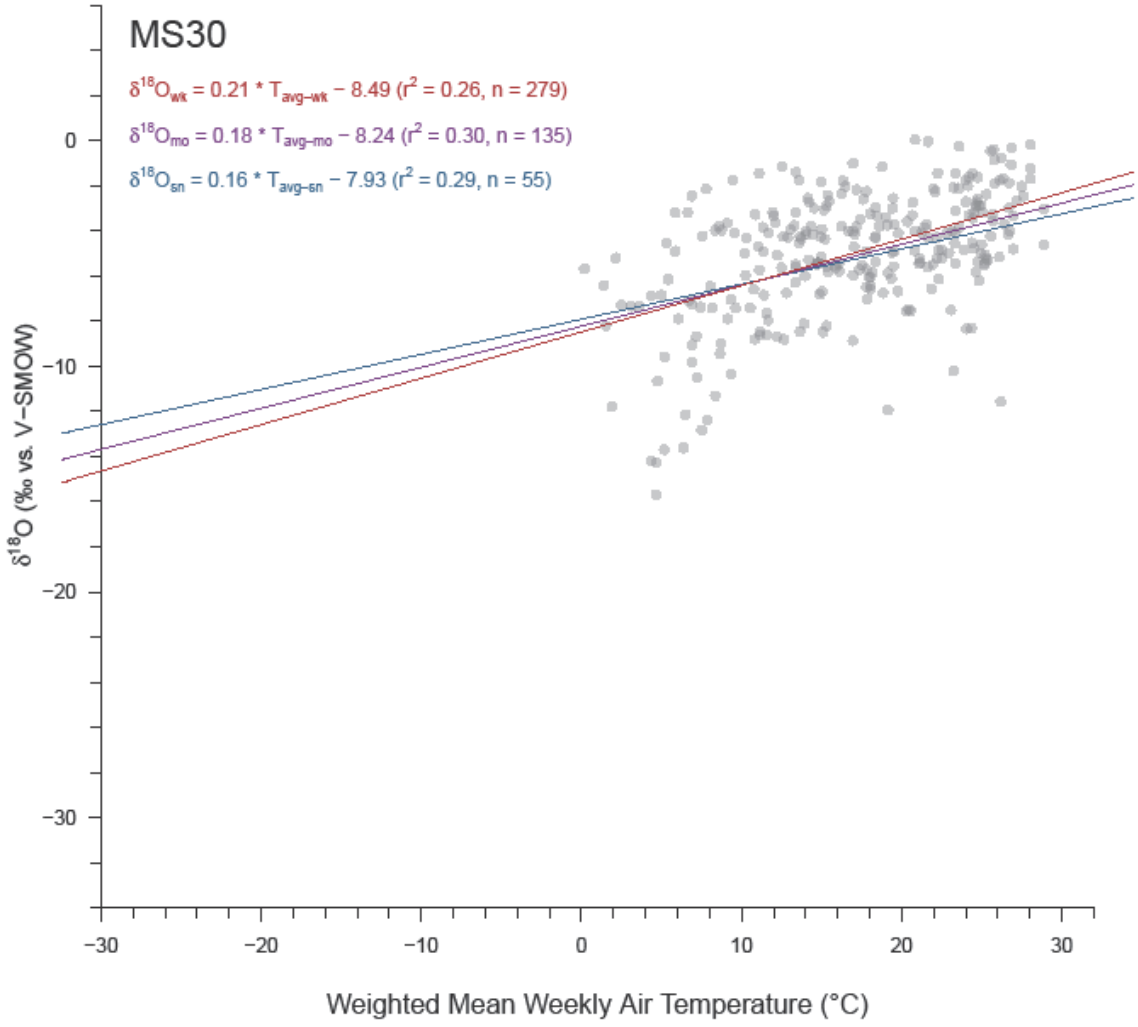

Figure A5.L2. Relationship between precipitation $\delta^{18}O$ and mean PDt at site MS30. Gray circles represent values at their original weekly resolution while linear trends are plotted for weekly (red), aggregated monthly (violet), and aggregated seasonal (blue) resolutions.

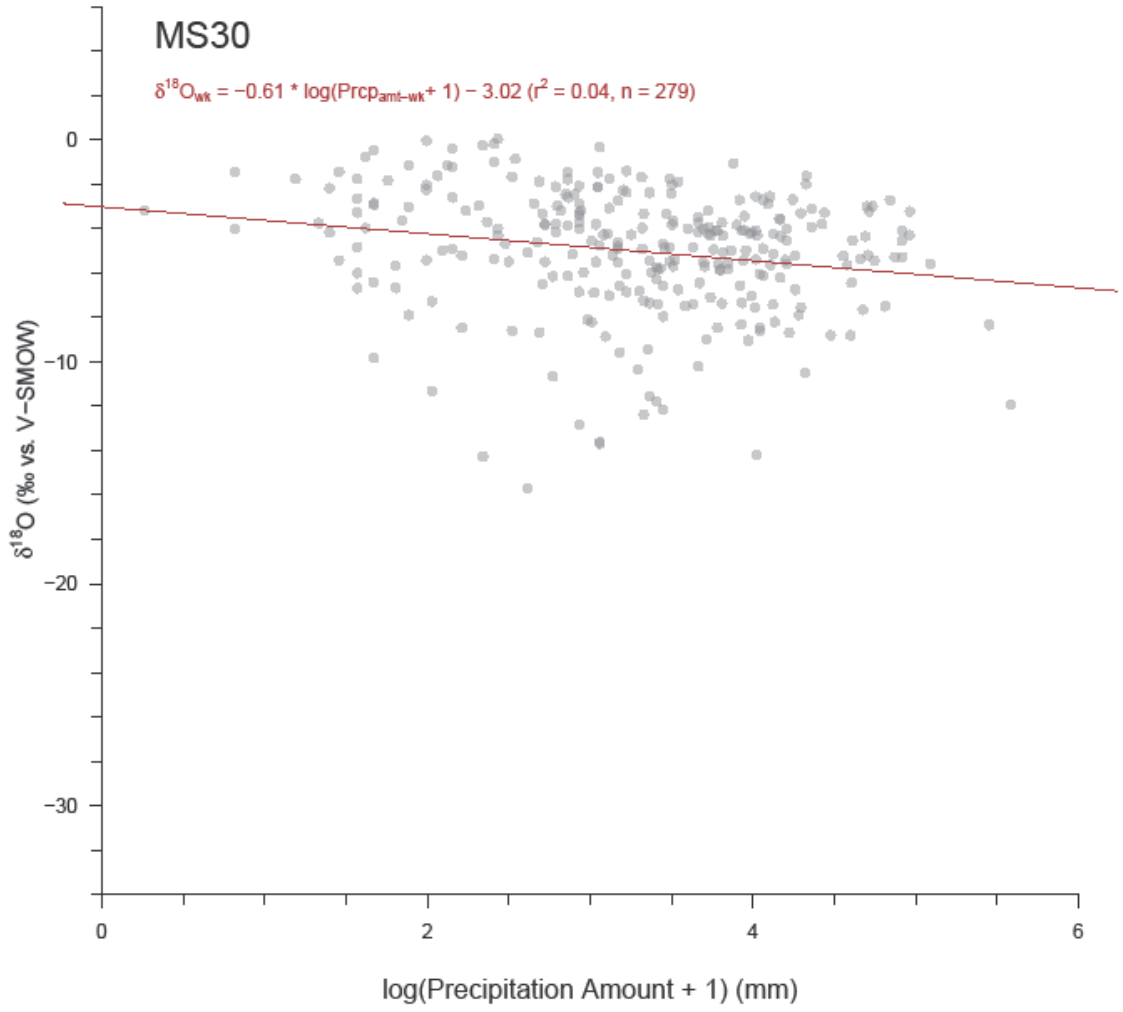

Figure A5.L3. Relationship between precipitation $\delta^{18}O$ and PDa at site MS30. Actual precipitation amounts were normalized by a log transformation. Gray circles represent values at their original weekly resolution with the weekly linear trend plotted in red. Precipitation amount data cannot be weight-averaged for aggregation, and thus regression was only performed at weekly resolution.

NC35

Table A5.M1. Regression results for NC35 at weekly, monthly, and seasonal resolutions. Significant results ($p \leq 0.05$) are bolded, while insignificant results are italicized. Actual precipitation amounts were normalized by a log transformation. Precipitation amount data cannot be weight-averaged for aggregation, and thus regression was only performed at weekly resolution.

LMWL (δD vs. $\delta^{18}O$)							
Resolution	***n***	***Slope***		***y-Int***		***r^2***	***p-value***
Weekly	**222**	**7.73**	**±0.13**	**11.77**	**±0.70**	**0.94**	**0.00**
Monthly	**98**	**8.00**	**±0.19**	**13.29**	**±0.96**	**0.95**	**0.00**
Seasonal	**45**	**7.87**	**±0.32**	**13.34**	**±1.63**	**0.93**	**0.00**
$\delta^{18}O$ vs. PDt							
Resolution	***n***	***Slope***		***y-Int***		***r^2***	***p-value***
Weekly	**222**	**0.14**	**±0.02**	**-7.08**	**±0.39**	**0.19**	**0.00**
Monthly	**98**	**0.10**	**±0.03**	**-6.56**	**±0.48**	**0.15**	**0.00**
Seasonal	**45**	**0.07**	**±0.03**	**-6.07**	**±0.61**	**0.11**	**0.03**
$\delta^{18}O$ vs. PDa							
Resolution	***n***	***Slope***		***y-Int***		***r^2***	***p-value***
Weekly	**222**	**-0.58**	**±0.20**	**-2.79**	**±0.62**	**0.04**	**0.00**

Table A5.M2. Percent change in NC35 regression values (Table A5.M1) due to aggregation.

LMWL (δD vs. $\delta^{18}O$)					
Aggregation	***Slope***	***Slope Error***	***y-Int***	***y-Int Error***	***r^2***
Weekly-Monthly	3%	42%	13%	38%	1%
Weekly-Seasonal	2%	101%	12%	96%	-1%
Monthly-Seasonal	-2%	42%	0%	41%	-2%
$\delta^{18}O$ vs. PDt					
Aggregation	***Slope***	***Slope Error***	***y-Int***	***y-Int Error***	***r^2***
Weekly-Monthly	-28%	25%	-7%	24%	-19%
Weekly-Seasonal	-67%	49%	-16%	46%	-53%
Monthly-Seasonal	-41%	22%	-8%	21%	-41%

Table A5.M3. NC35 temperature estimates and standard errors for three $\delta^{18}O$ values (vs. V-SMOW) at weekly, monthly, and seasonal resolutions. The three $\delta^{18}O$ values span much of the natural range of precipitation $\delta^{18}O$ in the study region, and -6‰ is close to the mean $\delta^{18}O$ value of all sites.

	Temperature Estimate (°C) when Precipitation $\delta^{18}O$ =		
Aggregation	***-20‰***	***-6‰***	***0‰***
Weekly	-2.6 ±15.4	15.7 ±14.4	23.5 ±14.5
Monthly	-4.6 ±17.8	15.7 ±14.2	24.5 ±14.6
Seasonal	-4.7 ±24.4	15.7 ±14.6	24.4 ±15.7

Table A5.M4. Weight-averaged weekly values of $\delta^{18}O$ and average surface temperature for NC35 grouped by month and season. Blue (red) cells show low (high) values of note.

Group	***n***	***$\delta^{18}O_{wt}$***	***PDt***
Jan	20	-5.96 ±0.66	8.4 ±1.1
Feb	18	-5.49 ±0.76	7.3 ±1.1
Mar	22	-4.71 ±0.62	12.4 ±1.1
Apr	15	-3.81 ±0.79	16.1 ±1.3
May	8	-3.13 ±0.77	20.0 ±1.5
Jun	25	-4.22 ±0.30	24.9 ±0.5
Jul	20	-3.89 ±0.44	26.4 ±0.4
Aug	22	-4.69 ±0.33	25.2 ±0.4
Sep	21	-5.18 ±0.55	22.8 ±0.5
Oct	19	-5.03 ±0.57	19.4 ±0.8
Nov	17	-5.83 ±0.42	13.0 ±1.1
Dec	15	-5.15 ±1.14	8.9 ±1.7
Win	53	-5.68 ±0.48	8.0 ±0.7
Spr	45	-4.07 ±0.43	15.6 ±0.9
Sum	67	-4.47 ±0.20	25.4 ±0.3
Aut	57	-5.07 ±0.30	18.5 ±0.7

Table A5.M5. Regression results for NC35 when weekly data is grouped by month and by season. Significant results ($p \leq 0.05$) are bolded, while insignificant results are italicized. Actual precipitation amounts were normalized by a log transformation. Blue (red) cells show low (high) values of note.

LMWL (δD vs. $\delta^{18}O$)							
Group	***n***	***Slope***		***y-Int***		***r^2***	***p-value***
Jan	**20**	**8.47**	**±0.51**	**17.89**	**±3.32**	**0.94**	**0.00**
Feb	**18**	**5.81**	**±0.71**	**1.74**	**±3.92**	**0.81**	**0.00**
Mar	**22**	**7.90**	**±0.26**	**13.44**	**±1.46**	**0.98**	**0.00**
Apr	**15**	**8.04**	**±0.28**	**13.93**	**±1.35**	**0.98**	**0.00**
May	**8**	**7.67**	**±0.55**	**11.91**	**±1.90**	**0.97**	**0.00**
Jun	**25**	**7.43**	**±0.86**	**8.41**	**±3.70**	**0.76**	**0.00**
Jul	**20**	**8.99**	**±0.51**	**15.02**	**±1.96**	**0.95**	**0.00**
Aug	**22**	**8.50**	**±0.24**	**14.61**	**±1.02**	**0.98**	**0.00**
Sep	**21**	**8.35**	**±0.15**	**14.07**	**±0.81**	**0.99**	**0.00**
Oct	**19**	**7.94**	**±0.27**	**13.34**	**±1.41**	**0.98**	**0.00**
Nov	**17**	**7.22**	**±0.75**	**10.58**	**±4.34**	**0.86**	**0.00**
Dec	**15**	**8.03**	**±0.25**	**13.59**	**±1.81**	**0.99**	**0.00**
Win	**53**	**7.46**	**±0.31**	**10.58**	**±2.03**	**0.92**	**0.00**
Spr	**45**	**7.90**	**±0.17**	**13.27**	**±0.84**	**0.98**	**0.00**
Sum	**67**	**8.37**	**±0.35**	**13.05**	**±1.44**	**0.90**	**0.00**
Aut	**57**	**7.94**	**±0.21**	**13.24**	**±1.13**	**0.96**	**0.00**
$\delta^{18}O$ vs. PDt							
Group	***n***	***Slope***		***y-Int***		***r^2***	***p-value***
Jan	*20*	*0.26*	*±0.13*	*-8.08*	*±1.27*	*0.18*	*0.06*
Feb	*18*	*0.19*	*±0.16*	*-6.14*	*±1.49*	*0.08*	*0.25*
Mar	**22**	**0.29**	**±0.10**	**-8.30**	**±1.34**	**0.28**	**0.01**
Apr	**15**	**0.44**	**±0.11**	**-10.89**	**±1.85**	**0.55**	**0.00**
May	*8*	*0.31*	*±0.16*	*-9.16*	*±3.41*	*0.38*	*0.11*
Jun	*25*	*-0.03*	*±0.13*	*-3.38*	*±3.22*	*0.00*	*0.84*
Jul	**20**	**0.71**	**±0.24**	**-22.52**	**±6.49**	**0.33**	**0.01**
Aug	*22*	*0.29*	*±0.16*	*-11.31*	*±4.06*	*0.14*	*0.09*
Sep	**21**	**0.50**	**±0.20**	**-16.40**	**±4.66**	**0.25**	**0.02**
Oct	*19*	*0.26*	*±0.15*	*-9.47*	*±2.85*	*0.15*	*0.10*
Nov	*17*	*0.16*	*±0.09*	*-7.78*	*±1.30*	*0.17*	*0.10*
Dec	**15**	**0.46**	**±0.13**	**-9.81**	**±1.36**	**0.50**	**0.00**
Win	**53**	**0.33**	**±0.08**	**-8.17**	**±0.78**	**0.25**	**0.00**
Spr	**45**	**0.31**	**±0.06**	**-8.79**	**±0.90**	**0.41**	**0.00**

Sum	**67**	**0.23**	**±0.09**	**-9.64**	**±2.28**	**0.09**	**0.01**
Aut	**57**	**0.16**	**±0.05**	**-7.92**	**±1.06**	**0.13**	**0.01**
δ^{18}O vs. PDa							
Group	***n***	***Slope***		***y-Int***		***r^2***	***p-value***
Jan	*20*	*-1.06*	*±0.79*	*-2.69*	*±2.48*	*0.09*	*0.20*
Feb	**18**	**-1.77**	**±0.86**	**-0.21**	**±2.23**	**0.21**	**0.05**
Mar	*22*	*-0.11*	*±0.75*	*-4.57*	*±2.21*	*0.00*	*0.89*
Apr	*15*	*0.03*	*±1.02*	*-3.99*	*±3.19*	*0.00*	*0.98*
May	*8*	*-1.52*	*±0.75*	*1.72*	*±2.31*	*0.41*	*0.09*
Jun	*25*	*-0.71*	*±0.47*	*-1.58*	*±1.67*	*0.09*	*0.15*
Jul	*20*	*-0.73*	*±0.46*	*-1.05*	*±1.49*	*0.12*	*0.13*
Aug	**22**	**-1.19**	**±0.26**	**-0.07**	**±0.90**	**0.51**	**0.00**
Sep	*21*	*-0.78*	*±0.53*	*-2.03*	*±1.94*	*0.10*	*0.16*
Oct	**19**	**-1.42**	**±0.48**	**-0.61**	**±1.45**	**0.33**	**0.01**
Nov	*17*	*-0.97*	*±0.60*	*-2.47*	*±1.99*	*0.15*	*0.13*
Dec	*15*	*1.49*	*±1.47*	*-9.76*	*±3.94*	*0.07*	*0.33*
Win	*53*	*-0.72*	*±0.57*	*-3.50*	*±1.61*	*0.03*	*0.21*
Spr	*45*	*-0.26*	*±0.52*	*-3.42*	*±1.57*	*0.01*	*0.62*
Sum	**67**	**-0.94**	**±0.22**	**-0.69**	**±0.75**	**0.22**	**0.00**
Aut	**57**	**-1.00**	**±0.29**	**-1.77**	**±0.97**	**0.17**	**0.00**

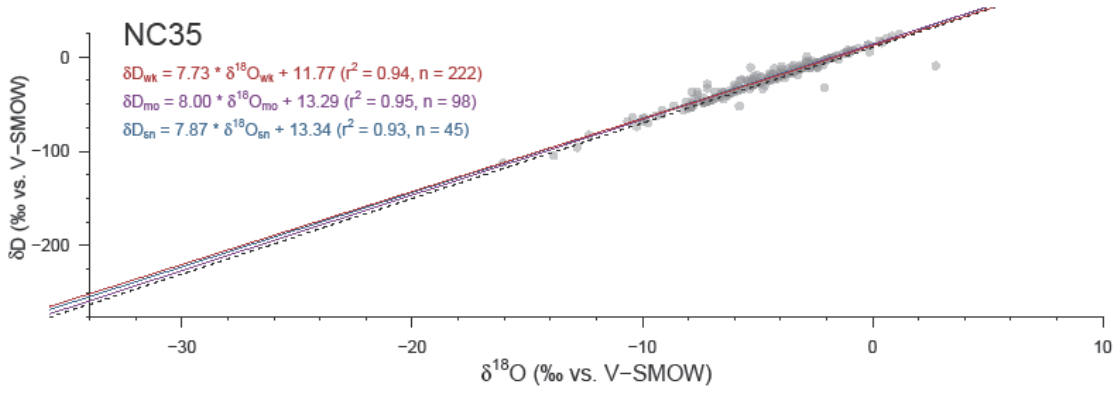

Figure A5.M1. Local meteoric water line for NC35. Gray circles represent values at their original weekly resolution while linear trends are plotted for weekly (red), aggregated monthly (violet), and aggregated seasonal (blue) resolutions. The dashed black line represents the global meteoric water line.

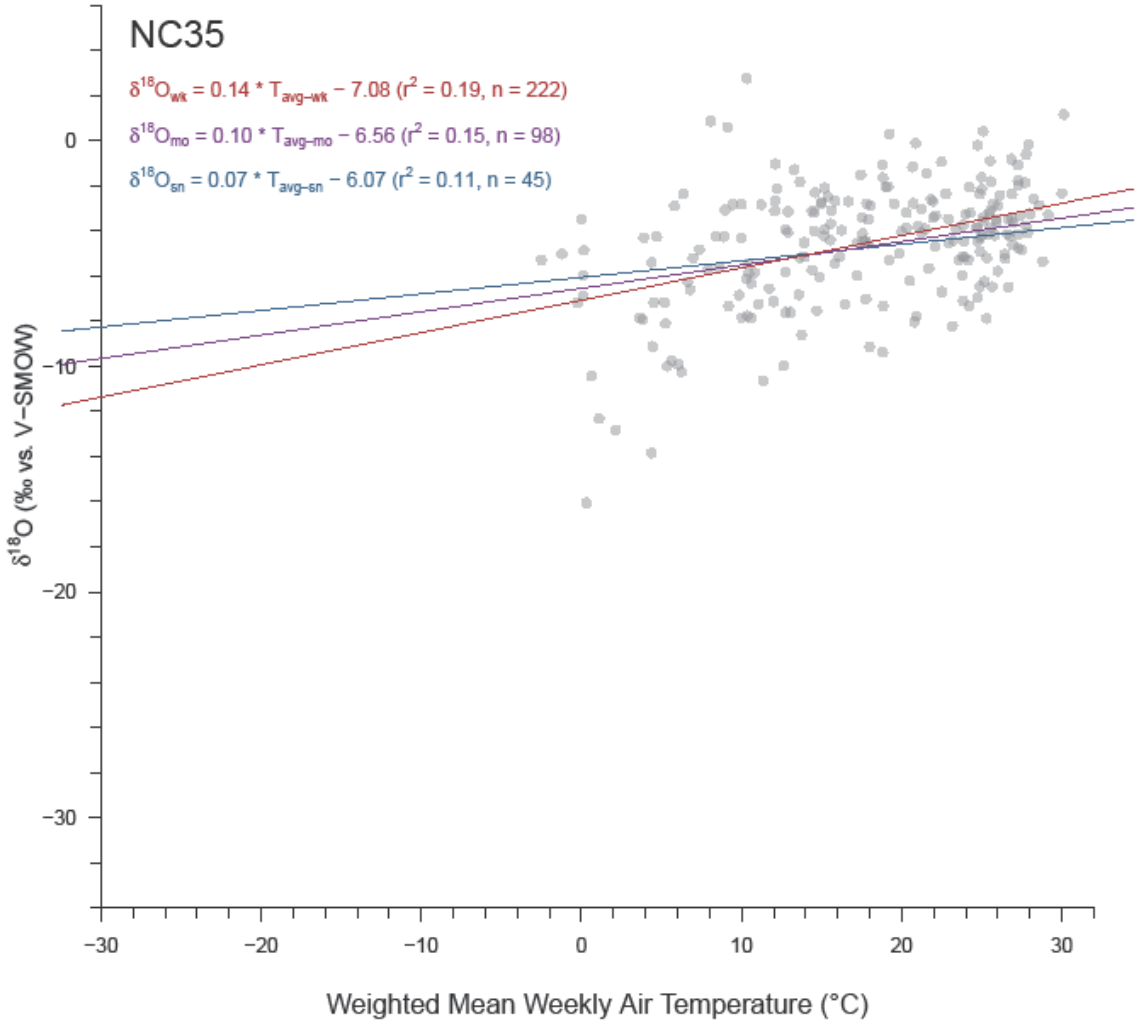

Figure A5.M2. Relationship between precipitation $\delta^{18}O$ and mean PDt at site NC35. Gray circles represent values at their original weekly resolution while linear trends are plotted for weekly (red), aggregated monthly (violet), and aggregated seasonal (blue) resolutions.

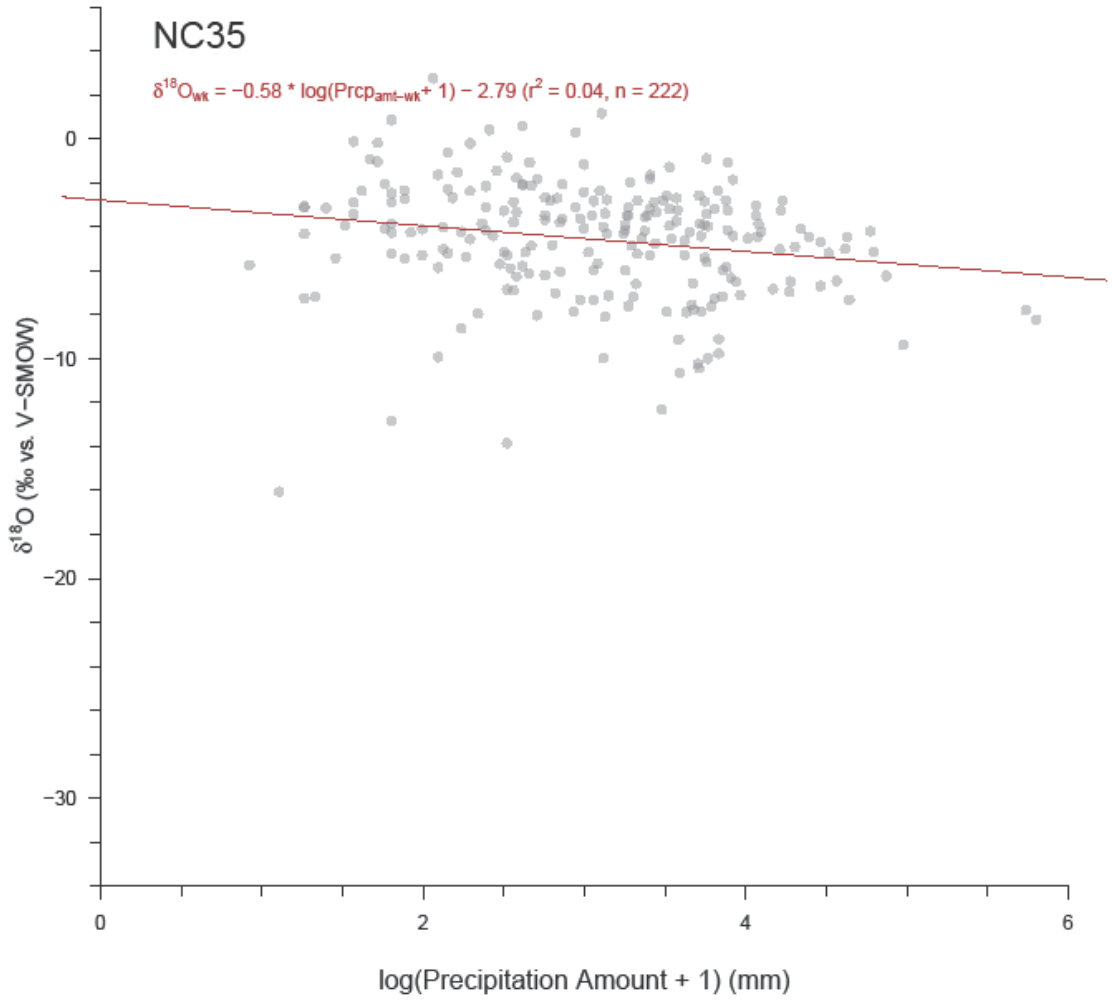

Figure A5.M3. Relationship between precipitation $\delta^{18}O$ and PDa at site NC35. Actual precipitation amounts were normalized by a log transformation. Gray circles represent values at their original weekly resolution with the weekly linear trend plotted in red. Precipitation amount data cannot be weight-averaged for aggregation, and thus regression was only performed at weekly resolution.

ND08

Table A5.N1. Regression results for ND08 at weekly, monthly, and seasonal resolutions. Significant results ($p \leq 0.05$) are bolded, while insignificant results are italicized. Actual precipitation amounts were normalized by a log transformation. Precipitation amount data cannot be weight-averaged for aggregation, and thus regression was only performed at weekly resolution.

LMWL (δD vs. $\delta^{18}O$)							
Resolution	***n***	***Slope***		***y-Int***		***r^2***	***p-value***
Weekly	**233**	**7.85**	**±0.07**	**3.28**	**±0.92**	**0.98**	**0.00**
Monthly	**114**	**7.88**	**±0.09**	**4.17**	**±1.30**	**0.98**	**0.00**
Seasonal	**53**	**7.94**	**±0.16**	**5.18**	**±2.30**	**0.98**	**0.00**
$\delta^{18}O$ vs. PDt							
Resolution	***n***	***Slope***		***y-Int***		***r^2***	***p-value***
Weekly	**233**	**0.41**	**±0.02**	**-15.69**	**±0.32**	**0.59**	**0.00**
Monthly	**114**	**0.42**	**±0.03**	**-15.78**	**±0.37**	**0.67**	**0.00**
Seasonal	**53**	**0.40**	**±0.03**	**-15.68**	**±0.43**	**0.73**	**0.00**
$\delta^{18}O$ vs. PDa							
Resolution	***n***	***Slope***		***y-Int***		***r^2***	***p-value***
Weekly	**233**	**1.57**	**±0.45**	**-15.88**	**±1.19**	**0.05**	**0.00**

Table A5.N2. Percent change in ND08 regression values (Table A5.N1) due to aggregation.

LMWL (δD vs. $\delta^{18}O$)					
Aggregation	***Slope***	***Slope Error***	***y-Int***	***y-Int Error***	***r^2***
Weekly-Monthly	0%	33%	27%	42%	0%
Weekly-Seasonal	1%	102%	46%	106%	0%
Monthly-Seasonal	1%	43%	20%	43%	-1%
$\delta^{18}O$ vs. PDt					
Aggregation	***Slope***	***Slope Error***	***y-Int***	***y-Int Error***	***r^2***
Weekly-Monthly	1%	23%	1%	16%	13%
Weekly-Seasonal	-3%	39%	0%	30%	21%
Monthly-Seasonal	-5%	17%	-1%	14%	9%

Table A5.N3. ND08 temperature estimates and standard errors for three $\delta^{18}O$ values (vs. V-SMOW) at weekly, monthly, and seasonal resolutions. The three $\delta^{18}O$ values span much of the natural range of precipitation $\delta^{18}O$ in the study region, and -6‰ is close to the mean $\delta^{18}O$ value of all sites.

	Temperature Estimate (°C) when Precipitation $\delta^{18}O$ =					
Aggregation	***-20‰***		***-6‰***		***0‰***	
Weekly	-2.4	±13.7	17.6	±13.7	26.2	±13.8
Monthly	-4.4	±13.2	17.9	±13.2	27.5	±13.4
Seasonal	-6.2	±12.1	19.5	±12.1	30.6	±12.6

Table A5.N4. Weight-averaged weekly values of $\delta^{18}O$ and average surface temperature for ND08 grouped by month and season. Blue (red) cells show low (high) values of note.

Group	***n***	***$\delta^{18}O_{wt}$***		***PDt***	
Jan	8	-21.80	±1.48	-16.9	±2.7
Feb	8	-22.61	±1.81	-11.1	±2.9
Mar	12	-14.66	±1.37	-3.1	±1.9
Apr	20	-12.75	±1.06	3.7	±1.2
May	30	-9.60	±0.60	11.1	±1.0
Jun	34	-8.83	±0.47	16.9	±0.6
Jul	23	-8.69	±0.67	18.3	±0.7
Aug	30	-8.39	±0.52	19.1	±0.7
Sep	24	-10.33	±0.82	14.1	±0.8
Oct	19	-15.75	±1.48	5.1	±1.2
Nov	16	-16.54	±1.41	-0.9	±1.3
Dec	9	-19.47	±1.53	-7.2	±1.3
Win	25	-20.33	±0.93	-10.5	±1.4
Spr	62	-11.48	±0.59	6.6	±1.0
Sum	87	-8.81	±0.31	17.4	±0.4
Aut	59	-13.50	±0.77	9.3	±1.0

Table A5.N5. Regression results for ND08 when weekly data is grouped by month and by season. Significant results ($p \leq 0.05$) are bolded, while insignificant results are italicized. Actual precipitation amounts were normalized by a log transformation. Blue (red) cells show low (high) values of note.

LMWL (δD vs. $\delta^{18}O$)							
Group	***n***	***Slope***		***y-Int***		***r^2***	***p-value***
Jan	**8**	**8.12**	**±0.40**	**12.39**	**±8.42**	**0.99**	**0.00**
Feb	**8**	**7.58**	**±0.45**	**-6.11**	**±10.59**	**0.98**	**0.00**
Mar	**12**	**7.90**	**±0.42**	**4.06**	**±6.75**	**0.97**	**0.00**
Apr	**20**	**8.35**	**±0.34**	**10.89**	**±4.45**	**0.97**	**0.00**
May	**30**	**7.72**	**±0.40**	**1.57**	**±3.98**	**0.93**	**0.00**
Jun	**34**	**7.88**	**±0.42**	**5.08**	**±3.96**	**0.92**	**0.00**
Jul	**23**	**7.69**	**±0.26**	**-0.03**	**±2.44**	**0.98**	**0.00**
Aug	**30**	**8.18**	**±0.40**	**5.10**	**±3.46**	**0.94**	**0.00**
Sep	**24**	**8.28**	**±0.33**	**7.27**	**±3.63**	**0.97**	**0.00**
Oct	**19**	**7.64**	**±0.15**	**0.28**	**±2.30**	**0.99**	**0.00**
Nov	**16**	**7.64**	**±0.25**	**-0.59**	**±4.32**	**0.99**	**0.00**
Dec	**9**	**8.86**	**±0.42**	**25.69**	**±8.48**	**0.98**	**0.00**
Win	**25**	**8.31**	**±0.27**	**13.95**	**±5.75**	**0.98**	**0.00**
Spr	**62**	**7.94**	**±0.19**	**4.60**	**±2.37**	**0.97**	**0.00**
Sum	**87**	**7.87**	**±0.22**	**3.19**	**±2.01**	**0.94**	**0.00**
Aut	**59**	**7.79**	**±0.12**	**2.33**	**±1.76**	**0.99**	**0.00**
$\delta^{18}O$ vs. PDt							
Group	***n***	***Slope***		***y-Int***		***r^2***	***p-value***
Jan	*8*	*0.29*	*±0.18*	*-17.13*	*±2.68*	*0.30*	*0.16*
Feb	**8**	**0.45**	**±0.18**	**-17.70**	**±2.51**	**0.51**	**0.05**
Mar	**12**	**0.63**	**±0.11**	**-13.52**	**±0.74**	**0.78**	**0.00**
Apr	**20**	**0.45**	**±0.18**	**-14.27**	**±1.23**	**0.25**	**0.02**
May	**30**	**0.30**	**±0.10**	**-12.76**	**±1.18**	**0.27**	**0.00**
Jun	*34*	*0.16*	*±0.15*	*-11.76*	*±2.48*	*0.03*	*0.29*
Jul	**23**	**0.60**	**±0.18**	**-20.00**	**±3.40**	**0.35**	**0.00**
Aug	**30**	**0.32**	**±0.14**	**-14.26**	**±2.65**	**0.16**	**0.03**
Sep	**24**	**0.44**	**±0.21**	**-16.44**	**±3.04**	**0.17**	**0.04**
Oct	*19*	*0.43*	*±0.28*	*-16.92*	*±2.26*	*0.12*	*0.14*
Nov	**16**	**0.54**	**±0.25**	**-15.66**	**±1.34**	**0.25**	**0.05**
Dec	*9*	*0.48*	*±0.42*	*-16.49*	*±3.27*	*0.15*	*0.30*
Win	**25**	**0.38**	**±0.11**	**-17.24**	**±1.41**	**0.32**	**0.00**
Spr	**62**	**0.43**	**±0.05**	**-14.14**	**±0.53**	**0.52**	**0.00**

Sum	**87**	**0.33**	**±0.08**	**-14.62**	**±1.52**	**0.16**	**0.00**
Aut	**59**	**0.43**	**±0.08**	**-16.38**	**±0.85**	**0.34**	**0.00**
δ^{18}O vs. PDa							
Group	***n***	***Slope***		***y-Int***		***r^2***	***p-value***
Jan	**8**	**-5.53**	**±1.84**	**-9.10**	**±4.03**	**0.60**	**0.02**
Feb	*8*	*6.90*	*±3.53*	*-35.06*	*±6.41*	*0.39*	*0.10*
Mar	**12**	**2.62**	**±1.21**	**-21.84**	**±3.19**	**0.32**	**0.05**
Apr	*20*	*-1.07*	*±1.54*	*-9.62*	*±4.01*	*0.03*	*0.50*
May	*30*	*0.14*	*±0.82*	*-9.75*	*±2.31*	*0.00*	*0.87*
Jun	*34*	*-0.03*	*±0.54*	*-9.06*	*±1.62*	*0.00*	*0.95*
Jul	*23*	*-0.49*	*±0.90*	*-7.50*	*±2.34*	*0.01*	*0.59*
Aug	*30*	*-0.62*	*±0.61*	*-6.47*	*±1.75*	*0.04*	*0.32*
Sep	*24*	*0.45*	*±1.08*	*-11.40*	*±3.16*	*0.01*	*0.68*
Oct	*19*	*-3.81*	*±1.88*	*-6.16*	*±4.22*	*0.19*	*0.06*
Nov	*16*	*0.18*	*±2.41*	*-17.04*	*±5.12*	*0.00*	*0.94*
Dec	*9*	*6.53*	*±3.08*	*-33.07*	*±6.39*	*0.39*	*0.07*
Win	*25*	*1.88*	*±1.89*	*-24.84*	*±3.85*	*0.04*	*0.33*
Spr	*62*	*0.99*	*±0.74*	*-14.04*	*±2.01*	*0.03*	*0.19*
Sum	*87*	*-0.35*	*±0.37*	*-7.74*	*±1.04*	*0.01*	*0.34*
Aut	*59*	*0.66*	*±0.97*	*-14.80*	*±2.44*	*0.01*	*0.50*

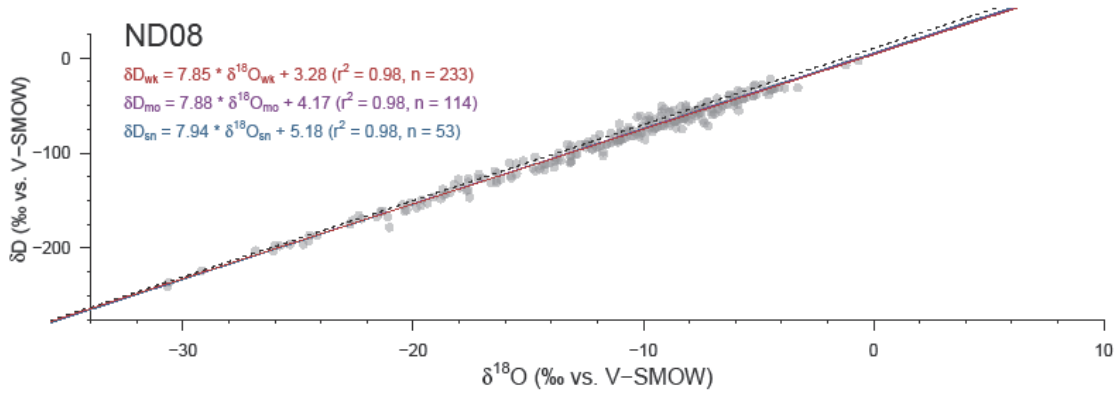

Figure A5.N1. Local meteoric water line for ND08. Gray circles represent values at their original weekly resolution while linear trends are plotted for weekly (red), aggregated monthly (violet), and aggregated seasonal (blue) resolutions. The dashed black line represents the global meteoric water line.

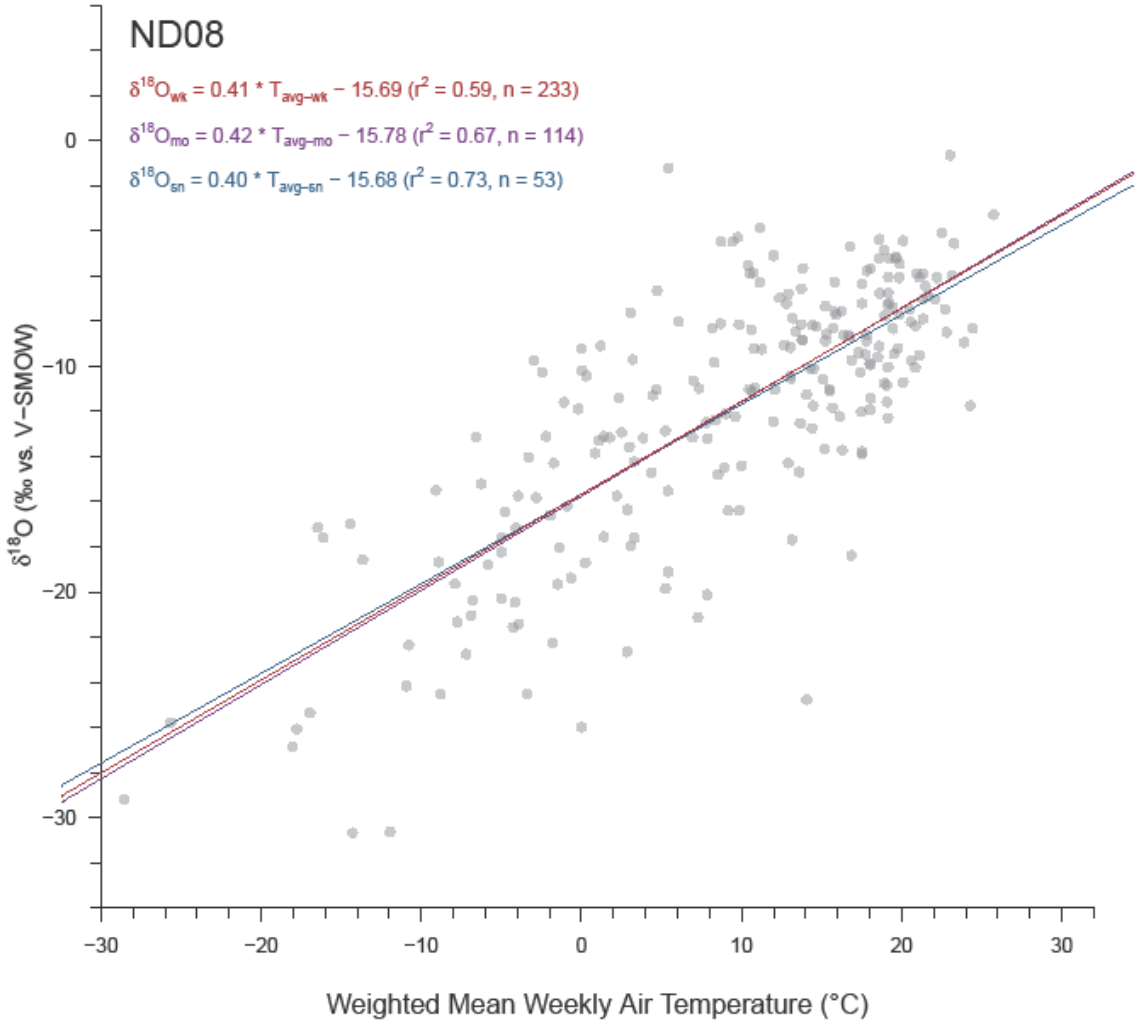

Figure A5.N2. Relationship between precipitation $\delta^{18}O$ and mean PDt at site ND08. Gray circles represent values at their original weekly resolution while linear trends are plotted for weekly (red), aggregated monthly (violet), and aggregated seasonal (blue) resolutions.

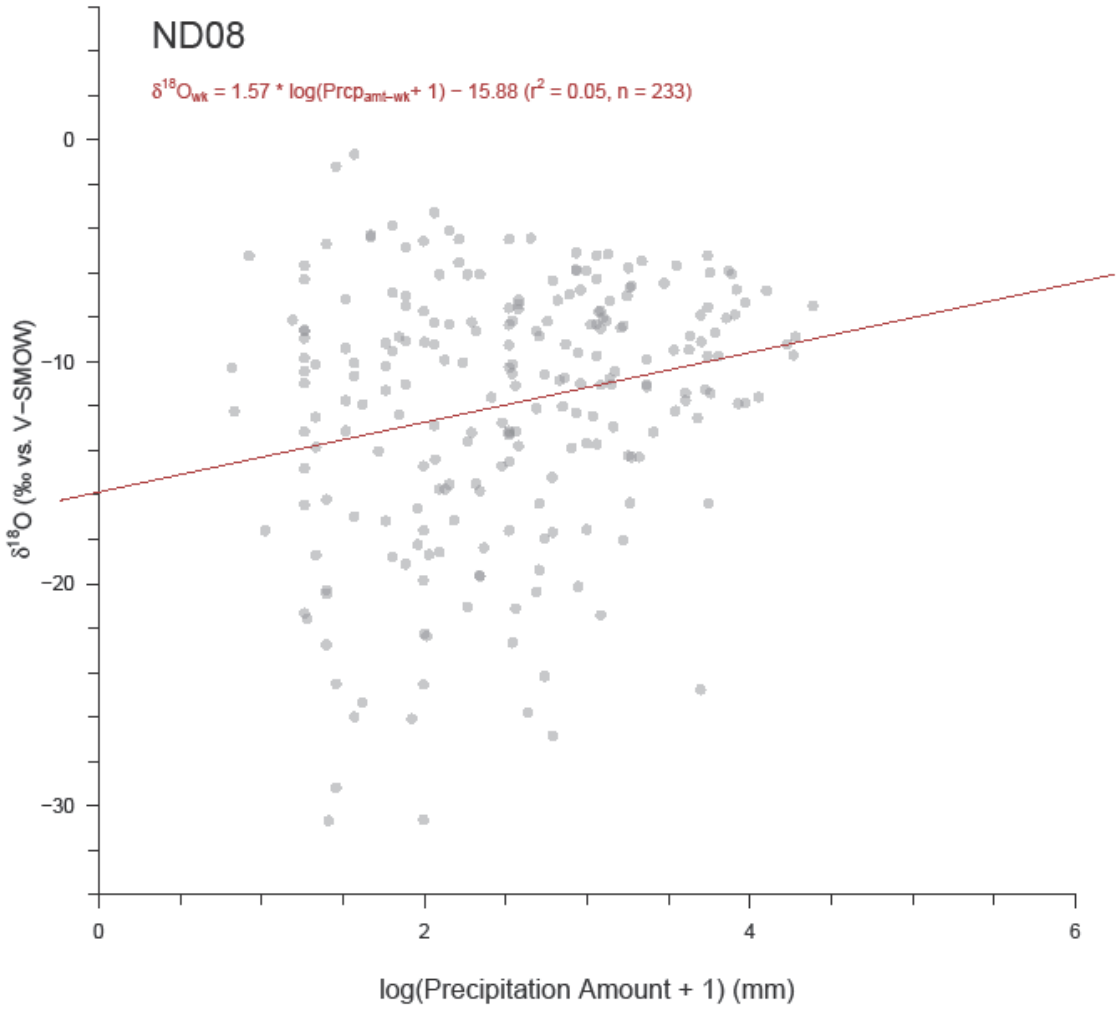

Figure A5.N3. Relationship between precipitation $\delta^{18}O$ and PDa at site ND08. Actual precipitation amounts were normalized by a log transformation. Gray circles represent values at their original weekly resolution with the weekly linear trend plotted in red. Precipitation amount data cannot be weight-averaged for aggregation, and thus regression was only performed at weekly resolution.

NE99

Table A5.O1. Regression results for NE99 at weekly, monthly, and seasonal resolutions. Significant results ($p \leq 0.05$) are bolded, while insignificant results are italicized. Actual precipitation amounts were normalized by a log transformation. Precipitation amount data cannot be weight-averaged for aggregation, and thus regression was only performed at weekly resolution.

LMWL (δD vs. $\delta^{18}O$)							
Resolution	***n***	***Slope***		***y-Int***		***r^2***	***p-value***
Weekly	**213**	**7.71**	**±0.09**	**6.10**	**±0.83**	**0.97**	**0.00**
Monthly	**94**	**7.76**	**±0.12**	**6.96**	**±1.20**	**0.98**	**0.00**
Seasonal	**42**	**7.95**	**±0.13**	**8.93**	**±1.39**	**0.99**	**0.00**
$\delta^{18}O$ vs. PDt							
Resolution	***n***	***Slope***		***y-Int***		***r^2***	***p-value***
Weekly	**213**	**0.34**	**±0.02**	**-13.45**	**±0.38**	**0.52**	**0.00**
Monthly	**94**	**0.34**	**±0.03**	**-13.50**	**±0.42**	**0.61**	**0.00**
Seasonal	**42**	**0.36**	**±0.05**	**-13.90**	**±0.66**	**0.58**	**0.00**
$\delta^{18}O$ vs. PDa							
Resolution	***n***	***Slope***		***y-Int***		***r^2***	***p-value***
Weekly	*213*	*-0.01*	*±0.37*	*-8.63*	*±1.01*	*0.00*	*0.98*

Table A5.O2. Percent change in NE99 regression values (Table A5.O1) due to aggregation.

LMWL (δD vs. $\delta^{18}O$)					
Aggregation	***Slope***	***Slope Error***	***y-Int***	***y-Int Error***	***r^2***
Weekly-Monthly	1%	35%	14%	45%	1%
Weekly-Seasonal	3%	39%	41%	47%	2%
Monthly-Seasonal	2%	11%	22%	14%	1%
$\delta^{18}O$ vs. PDt					
Aggregation	***Slope***	***Slope Error***	***y-Int***	***y-Int Error***	***r^2***
Weekly-Monthly	-2%	23%	0%	11%	18%
Weekly-Seasonal	4%	89%	3%	67%	10%
Monthly-Seasonal	6%	41%	3%	36%	-5%

Table A5.O3. NE99 temperature estimates and standard errors for three $\delta^{18}O$ values (vs. V-SMOW) at weekly, monthly, and seasonal resolutions. The three $\delta^{18}O$ values span much of the natural range of precipitation $\delta^{18}O$ in the study region, and -6‰ is close to the mean $\delta^{18}O$ value of all sites.

Temperature Estimate (°C) when Precipitation $\delta^{18}O$ =

Aggregation	*-20‰*	*-6‰*	*0‰*
Weekly	-3.1 ±12.4	17.9 ±12.2	26.9 ±12.3
Monthly	-7.1 ±12.1	18.2 ±11.8	29.0 ±12.1
Seasonal	-5.2 ±11.9	17.5 ±11.1	27.2 ±11.8

Table A5.O4. Weight-averaged weekly values of $\delta^{18}O$ and average surface temperature for NE99 grouped by month and season. Blue (red) cells show low (high) values of note.

Group	*n*	*$\delta^{18}O_{wt}$*		*PDt*	
Jan	1	-20.88	-	-5.3	-
Feb	6	-15.51	±2.02	-4.5	±2.7
Mar	16	-11.66	±1.01	1.7	±1.3
Apr	19	-9.78	±0.78	6.7	±1.0
May	27	-7.35	±0.47	13.9	±0.8
Jun	36	-8.05	±0.48	19.0	±0.6
Jul	28	-6.01	±0.45	22.3	±0.6
Aug	31	-6.11	±0.45	22.4	±0.6
Sep	21	-9.33	±0.71	16.0	±1.1
Oct	16	-10.11	±1.23	8.9	±1.2
Nov	8	-14.03	±0.73	-0.5	±1.6
Dec	4	-16.99	±2.29	1.2	±1.6
Win	11	-16.37	±1.37	-1.8	±1.7
Spr	62	-8.72	±0.45	8.5	±0.8
Sum	95	-6.82	±0.28	21.0	±0.4
Aut	45	-11.05	±0.63	10.3	±1.2

Table A5.O5. Regression results for NE99 when weekly data is grouped by month and by season. Significant results ($p \leq 0.05$) are bolded, while insignificant results are italicized. Actual precipitation amounts were normalized by a log transformation. Blue (red) cells show low (high) values of note.

LMWL (δD vs. $\delta^{18}O$)							
Group	***n***	***Slope***		***y-Int***		***r^2***	***p-value***
Jan	*1*	-	-	-	-	-	-
Feb	**6**	**8.15**	**±0.29**	**12.26**	**±4.86**	**0.99**	**0.00**
Mar	**16**	**8.05**	**±0.35**	**8.46**	**±4.02**	**0.97**	**0.00**
Apr	**19**	**7.94**	**±0.43**	**9.59**	**±4.53**	**0.95**	**0.00**
May	**27**	**7.29**	**±0.46**	**3.29**	**±3.42**	**0.91**	**0.00**
Jun	**36**	**7.63**	**±0.24**	**5.02**	**±2.03**	**0.97**	**0.00**
Jul	**28**	**7.80**	**±0.43**	**4.53**	**±2.86**	**0.93**	**0.00**
Aug	**31**	**7.20**	**±0.34**	**3.21**	**±2.13**	**0.94**	**0.00**
Sep	**21**	**7.89**	**±0.39**	**9.04**	**±3.63**	**0.96**	**0.00**
Oct	**16**	**7.88**	**±0.29**	**9.45**	**±3.47**	**0.98**	**0.00**
Nov	**8**	**8.62**	**±1.13**	**22.90**	**±16.32**	**0.91**	**0.00**
Dec	**4**	**8.66**	**±0.73**	**20.13**	**±13.26**	**0.99**	**0.01**
Win	**11**	**8.31**	**±0.26**	**14.61**	**±4.58**	**0.99**	**0.00**
Spr	**62**	**7.82**	**±0.21**	**7.14**	**±1.99**	**0.96**	**0.00**
Sum	**95**	**7.55**	**±0.18**	**4.24**	**±1.28**	**0.95**	**0.00**
Aut	**45**	**7.77**	**±0.20**	**8.62**	**±2.26**	**0.97**	**0.00**
$\delta^{18}O$ vs. PDt							
Group	***n***	***Slope***		***y-Int***		***r^2***	***p-value***
Jan	*1*	-	-	-	-	-	-
Feb	*6*	*0.30*	*±0.35*	*-14.73*	*±2.64*	*0.15*	*0.44*
Mar	**16**	**0.49**	**±0.16**	**-11.86**	**±0.89**	**0.41**	**0.01**
Apr	**19**	**0.38**	**±0.17**	**-12.66**	**±1.40**	**0.22**	**0.04**
May	*27*	*0.21*	*±0.11*	*-9.85*	*±1.58*	*0.12*	*0.07*
Jun	**36**	**0.40**	**±0.12**	**-15.28**	**±2.23**	**0.26**	**0.00**
Jul	**28**	**0.27**	**±0.14**	**-12.19**	**±3.01**	**0.13**	**0.05**
Aug	**31**	**0.51**	**±0.10**	**-17.21**	**±2.28**	**0.47**	**0.00**
Sep	**21**	**0.43**	**±0.11**	**-15.82**	**±1.88**	**0.45**	**0.00**
Oct	**16**	**0.62**	**±0.22**	**-16.44**	**±2.23**	**0.37**	**0.01**
Nov	*8*	*0.09*	*±0.19*	*-14.23*	*±0.78*	*0.04*	*0.65*
Dec	*4*	*0.50*	*±0.97*	*-18.30*	*±2.76*	*0.12*	*0.65*
Win	*11*	*0.20*	*±0.26*	*-16.63*	*±1.56*	*0.06*	*0.45*
Spr	**62**	**0.35**	**±0.06**	**-11.92**	**±0.60**	**0.40**	**0.00**

Sum	**95**	**0.43**	**±0.06**	**-15.54**	**±1.29**	**0.35**	**0.00**
Aut	**45**	**0.37**	**±0.06**	**-14.45**	**±0.80**	**0.47**	**0.00**
δ^{18}O vs. PDa							
Group	***n***	***Slope***		***y-Int***		***r^2***	***p-value***
Jan	*1*	-	-	-	-	-	-
Feb	*6*	*1.50*	*±3.29*	*-19.87*	*±8.49*	*0.05*	*0.67*
Mar	*16*	*-2.73*	*±1.65*	*-4.64*	*±3.78*	*0.16*	*0.12*
Apr	*19*	*0.63*	*±0.95*	*-11.62*	*±2.53*	*0.03*	*0.51*
May	**27**	**-1.67**	**±0.63**	**-2.76**	**±1.67**	**0.22**	**0.01**
Jun	**36**	**-1.29**	**±0.59**	**-3.82**	**±1.87**	**0.12**	**0.04**
Jul	*28*	*-0.55*	*±0.60*	*-4.73*	*±1.64*	*0.03*	*0.36*
Aug	*31*	*-1.04*	*±0.56*	*-2.87*	*±1.65*	*0.11*	*0.07*
Sep	*21*	*-1.48*	*±0.82*	*-5.39*	*±1.98*	*0.15*	*0.09*
Oct	*16*	*1.22*	*±1.70*	*-13.93*	*±4.57*	*0.04*	*0.48*
Nov	*8*	*1.26*	*±1.60*	*-17.53*	*±4.22*	*0.09*	*0.46*
Dec	*4*	*-10.96*	*±2.85*	*2.92*	*±5.49*	*0.88*	*0.06*
Win	*11*	*0.59*	*±2.37*	*-18.51*	*±5.49*	*0.01*	*0.81*
Spr	*62*	*-0.50*	*±0.63*	*-7.65*	*±1.62*	*0.01*	*0.43*
Sum	**95**	**-1.16**	**±0.34**	**-3.36**	**±1.00**	**0.11**	**0.00**
Aut	*45*	*-0.75*	*±0.83*	*-8.61*	*±2.13*	*0.02*	*0.37*

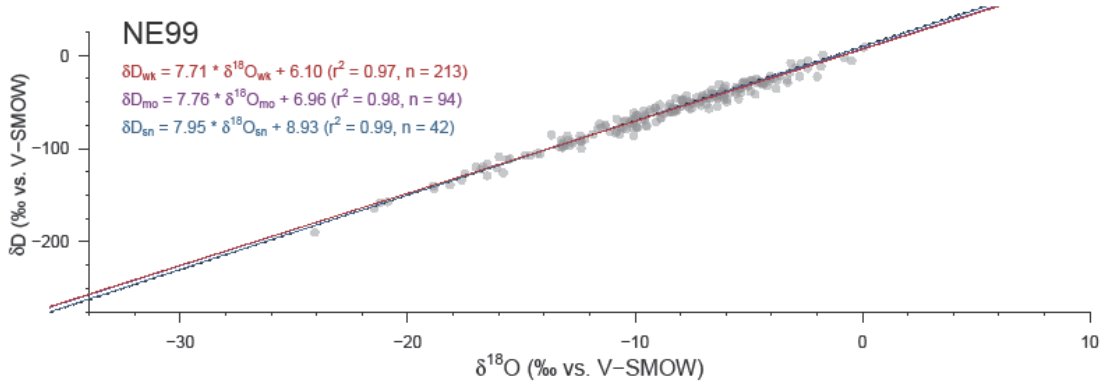

Figure A5.O1. Local meteoric water line for NE99. Gray circles represent values at their original weekly resolution while linear trends are plotted for weekly (red), aggregated monthly (violet), and aggregated seasonal (blue) resolutions. The dashed black line represents the global meteoric water line.

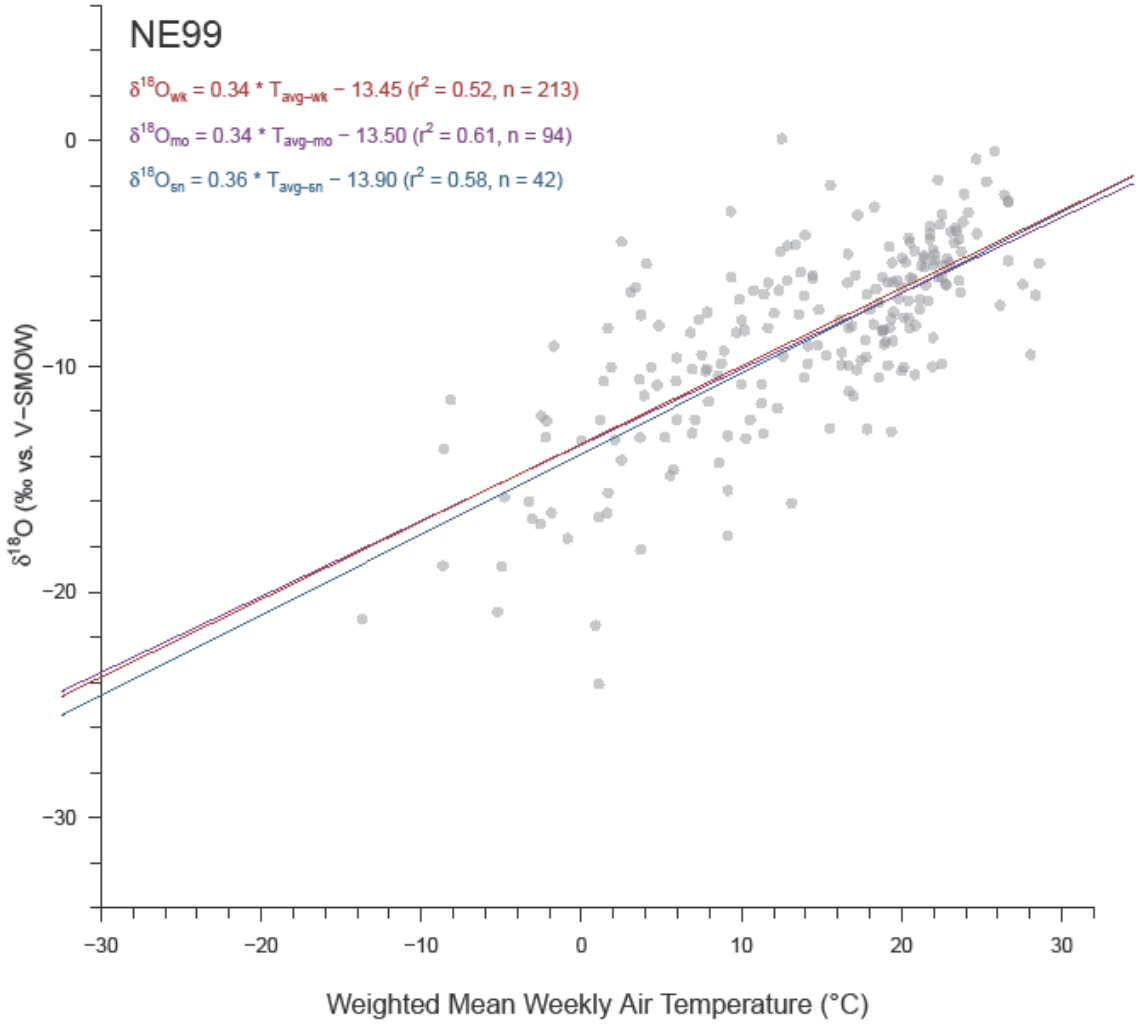

Figure A5.O2. Relationship between precipitation $\delta^{18}O$ and mean PDt at site NE99. Gray circles represent values at their original weekly resolution while linear trends are plotted for weekly (red), aggregated monthly (violet), and aggregated seasonal (blue) resolutions.

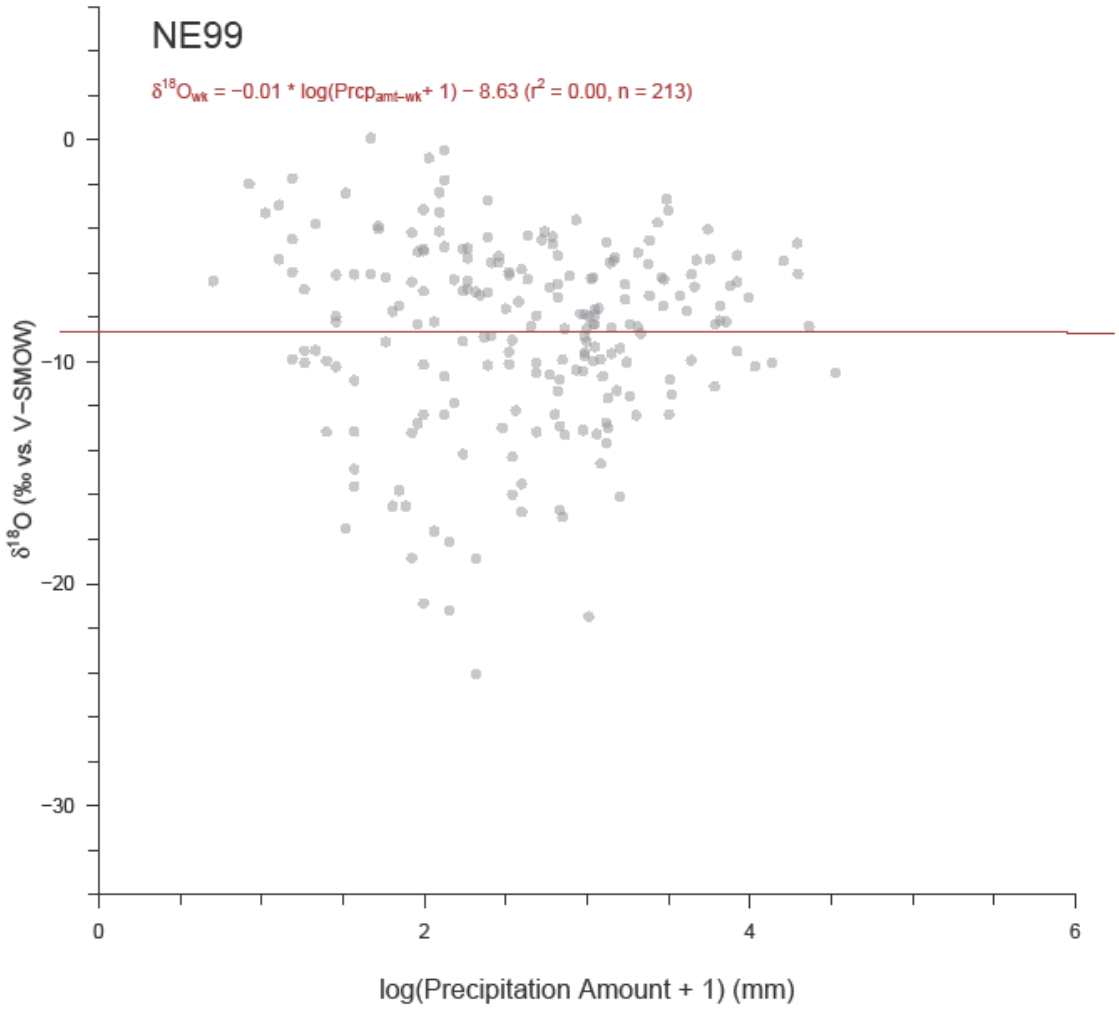

Figure A5.O3. Relationship between precipitation $\delta^{18}O$ and PDa at site NE99. Actual precipitation amounts were normalized by a log transformation. Gray circles represent values at their original weekly resolution with the weekly linear trend plotted in red. Precipitation amount data cannot be weight-averaged for aggregation, and thus regression was only performed at weekly resolution.

NM01

Table A5.P1. Regression results for NM01 at weekly, monthly, and seasonal resolutions. Significant results ($p \leq 0.05$) are bolded, while insignificant results are italicized. Actual precipitation amounts were normalized by a log transformation. Precipitation amount data cannot be weight-averaged for aggregation, and thus regression was only performed at weekly resolution.

LMWL (δD vs. $\delta^{18}O$)								
Resolution	***n***	***Slope***		***y-Int***		***r^2***	***p-value***
Weekly	**175**	**7.36**	**±0.10**	**2.87**	**±0.91**	**0.97**	**0.00**
Monthly	**97**	**7.51**	**±0.14**	**4.43**	**±1.43**	**0.97**	**0.00**
Seasonal	**45**	**7.54**	**±0.14**	**4.93**	**±1.40**	**0.98**	**0.00**
$\delta^{18}O$ vs. PDt							
Resolution	***n***	***Slope***		***y-Int***		***r^2***	***p-value***
Weekly	**175**	**0.47**	**±0.04**	**-13.89**	**±0.63**	**0.43**	**0.00**
Monthly	**97**	**0.43**	**±0.05**	**-13.95**	**±0.78**	**0.40**	**0.00**
Seasonal	**45**	**0.46**	**±0.06**	**-14.71**	**±0.83**	**0.59**	**0.00**
$\delta^{18}O$ vs. PDa							
Resolution	***n***	***Slope***		***y-Int***		***r^2***	***p-value***
Weekly	**175**	**-1.06**	**±0.49**	**-5.04**	**±1.29**	**0.03**	**0.03**

Table A5.P2. Percent change in NM01 regression values (Table A5.P1) due to aggregation.

LMWL (δD vs. $\delta^{18}O$)					
Aggregation	***Slope***	***Slope Error***	***y-Int***	***y-Int Error***	***r^2***
Weekly-Monthly	2%	46%	54%	57%	0%
Weekly-Seasonal	2%	31%	47%	35%	2%
Monthly-Seasonal	0%	-1%	10%	-2%	2%
$\delta^{18}O$ vs. PDt					
Aggregation	***Slope***	***Slope Error***	***y-Int***	***y-Int Error***	***r^2***
Weekly-Monthly	-7%	33%	0%	25%	-6%
Weekly-Seasonal	-2%	32%	6%	26%	41%
Monthly-Seasonal	6%	7%	5%	6%	32%

Table A5.P3. NM01 temperature estimates and standard errors for three $\delta^{18}O$ values (vs. V-SMOW) at weekly, monthly, and seasonal resolutions. The three $\delta^{18}O$ values span much of the natural range of precipitation $\delta^{18}O$ in the study region, and -6‰ is close to the mean $\delta^{18}O$ value of all sites.

	Temperature Estimate (°C) when Precipitation $\delta^{18}O$ =		
Aggregation	***-20‰***	***-6‰***	***0‰***
Weekly	2.1 ±11.1	14.9 ±11.0	20.4 ±11.0
Monthly	1.8 ±11.6	14.7 ±11.4	20.2 ±11.5
Seasonal	-1.6 ±9.8	16.3 ±9.1	24.0 ±9.6

Table A5.P4. Weight-averaged weekly values of $\delta^{18}O$ and average surface temperature for NM01 grouped by month and season. Blue (red) cells show low (high) values of note.

Group	***n***	***$\delta^{18}O_{wt}$***	***PDt***
Jan	8	-12.65 ±2.11	2.9 ±0.9
Feb	15	-12.11 ±1.42	4.1 ±0.8
Mar	14	-9.05 ±1.09	5.9 ±0.5
Apr	10	-10.58 ±1.05	8.6 ±1.2
May	8	-7.10 ±0.98	15.5 ±1.0
Jun	7	-3.45 ±1.10	18.2 ±1.2
Jul	17	-4.38 ±0.76	22.0 ±0.3
Aug	35	-4.77 ±0.56	20.2 ±0.2
Sep	22	-5.93 ±0.66	18.7 ±0.5
Oct	17	-10.40 ±1.03	13.4 ±0.6
Nov	10	-11.43 ±0.96	8.5 ±1.2
Dec	12	-13.51 ±1.73	3.0 ±0.8
Win	35	-13.86 ±0.95	3.6 ±0.5
Spr	32	-9.46 ±0.63	8.8 ±0.8
Sum	59	-4.81 ±0.41	20.3 ±0.3
Aut	49	-8.74 ±0.60	15.3 ±0.7

Table A5.P5. Regression results for NM01 when weekly data is grouped by month and by season. Significant results ($p \leq 0.05$) are bolded, while insignificant results are italicized. Actual precipitation amounts were normalized by a log transformation. Blue (red) cells show low (high) values of note.

LMWL (δD vs. $\delta^{18}O$)							
Group	***n***	***Slope***		***y-Int***		***r^2***	***p-value***
Jan	**8**	**7.80**	**±0.15**	**5.77**	**±2.03**	**1.00**	**0.00**
Feb	**15**	**7.74**	**±0.17**	**4.35**	**±2.25**	**0.99**	**0.00**
Mar	**14**	**7.62**	**±0.31**	**8.85**	**±3.02**	**0.98**	**0.00**
Apr	**10**	**7.27**	**±0.88**	**-1.34**	**±9.19**	**0.90**	**0.00**
May	**8**	**8.06**	**±0.48**	**7.12**	**±3.74**	**0.98**	**0.00**
Jun	**7**	**7.22**	**±0.49**	**0.04**	**±2.47**	**0.98**	**0.00**
Jul	**17**	**7.00**	**±0.30**	**-0.86**	**±1.33**	**0.97**	**0.00**
Aug	**35**	**6.24**	**±0.31**	**-2.97**	**±1.57**	**0.93**	**0.00**
Sep	**22**	**7.78**	**±0.22**	**6.96**	**±1.40**	**0.98**	**0.00**
Oct	**17**	**7.53**	**±0.73**	**9.88**	**±7.61**	**0.88**	**0.00**
Nov	**10**	**8.14**	**±0.55**	**14.14**	**±6.20**	**0.97**	**0.00**
Dec	**12**	**7.99**	**±0.30**	**12.05**	**±4.22**	**0.99**	**0.00**
Win	**35**	**7.83**	**±0.14**	**7.19**	**±1.93**	**0.99**	**0.00**
Spr	**32**	**7.64**	**±0.32**	**5.64**	**±3.07**	**0.95**	**0.00**
Sum	**59**	**6.53**	**±0.21**	**-2.10**	**±1.05**	**0.94**	**0.00**
Aut	**49**	**7.45**	**±0.27**	**6.80**	**±2.48**	**0.94**	**0.00**
$\delta^{18}O$ vs. PDt							
Group	***n***	***Slope***		***y-Int***		***r^2***	***p-value***
Jan	*8*	*-1.06*	*±0.83*	*-9.76*	*±3.10*	*0.21*	*0.25*
Feb	*15*	*0.51*	*±0.47*	*-14.50*	*±2.43*	*0.08*	*0.30*
Mar	*14*	*0.19*	*±0.61*	*-9.91*	*±3.65*	*0.01*	*0.77*
Apr	*10*	*0.40*	*±0.28*	*-13.50*	*±2.66*	*0.20*	*0.19*
May	**8**	**0.67**	**±0.28**	**-17.32**	**±4.27**	**0.49**	**0.05**
Jun	*7*	*0.27*	*±0.39*	*-8.97*	*±6.95*	*0.09*	*0.53*
Jul	**17**	**1.38**	**±0.44**	**-33.55**	**±9.62**	**0.40**	**0.01**
Aug	**35**	**0.94**	**±0.45**	**-23.05**	**±9.22**	**0.12**	**0.05**
Sep	*22*	*0.34*	*±0.32*	*-11.88*	*±5.92*	*0.05*	*0.30*
Oct	*17*	*0.49*	*±0.43*	*-16.00*	*±5.77*	*0.08*	*0.28*
Nov	*10*	*0.21*	*±0.27*	*-12.73*	*±2.51*	*0.07*	*0.47*
Dec	*12*	*-0.29*	*±0.65*	*-11.94*	*±2.91*	*0.02*	*0.67*
Win	*35*	*-0.02*	*±0.34*	*-12.58*	*±1.57*	*0.00*	*0.95*
Spr	*32*	*0.26*	*±0.13*	*-11.15*	*±1.34*	*0.11*	*0.06*

Sum	**59**	**0.54**	**±0.19**	**-14.86**	**±3.90**	**0.12**	**0.01**
Aut	**49**	**0.50**	**±0.11**	**-15.39**	**±1.64**	**0.32**	**0.00**
δ^{18}O vs. PDa							
Group	***n***	***Slope***		***y-Int***		***r^2***	***p-value***
Jan	*8*	*-2.90*	*±3.16*	*-5.90*	*±7.74*	*0.12*	*0.39*
Feb	*15*	*-2.88*	*±1.70*	*-6.33*	*±3.82*	*0.18*	*0.11*
Mar	*14*	*-1.30*	*±2.16*	*-6.03*	*±4.82*	*0.03*	*0.56*
Apr	*10*	*-1.84*	*±1.23*	*-5.60*	*±3.09*	*0.22*	*0.17*
May	**8**	**-4.33**	**±1.71**	**1.00**	**±3.36**	**0.52**	**0.04**
Jun	*7*	*2.16*	*±1.98*	*-8.57*	*±4.07*	*0.19*	*0.33*
Jul	**17**	**-2.83**	**±0.62**	**4.27**	**±1.71**	**0.58**	**0.00**
Aug	**35**	**-2.82**	**±0.71**	**3.68**	**±1.98**	**0.33**	**0.00**
Sep	*22*	*-0.66*	*±0.77*	*-3.84*	*±2.15*	*0.04*	*0.40*
Oct	*17*	*-0.31*	*±1.34*	*-8.74*	*±3.81*	*0.00*	*0.82*
Nov	*10*	*-1.25*	*±1.12*	*-7.47*	*±3.26*	*0.14*	*0.29*
Dec	*12*	*-3.09*	*±2.01*	*-5.53*	*±5.09*	*0.19*	*0.16*
Win	**35**	**-2.93**	**±1.12**	**-6.04**	**±2.68**	**0.17**	**0.01**
Spr	**32**	**-2.27**	**±0.94**	**-3.89**	**±2.13**	**0.16**	**0.02**
Sum	**59**	**-2.16**	**±0.49**	**1.84**	**±1.33**	**0.25**	**0.00**
Aut	*49*	*-0.86*	*±0.70*	*-5.74*	*±2.00*	*0.03*	*0.23*

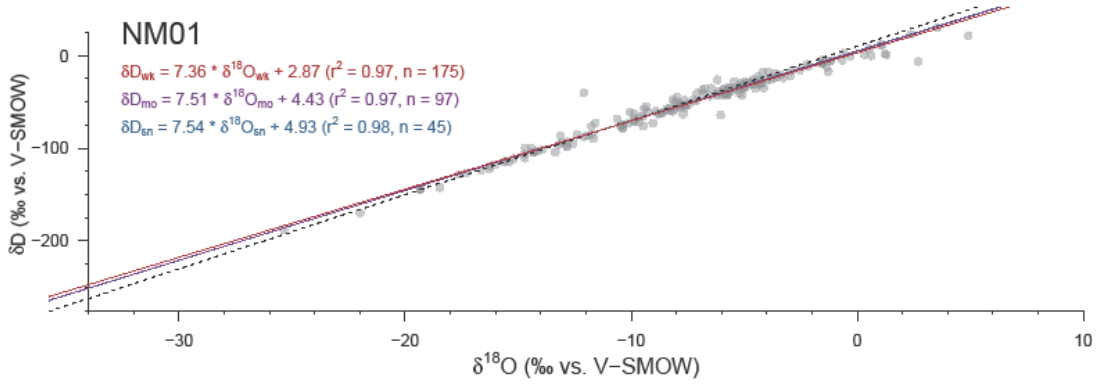

Figure A5.P1. Local meteoric water line for NM01. Gray circles represent values at their original weekly resolution while linear trends are plotted for weekly (red), aggregated monthly (violet), and aggregated seasonal (blue) resolutions. The dashed black line represents the global meteoric water line.

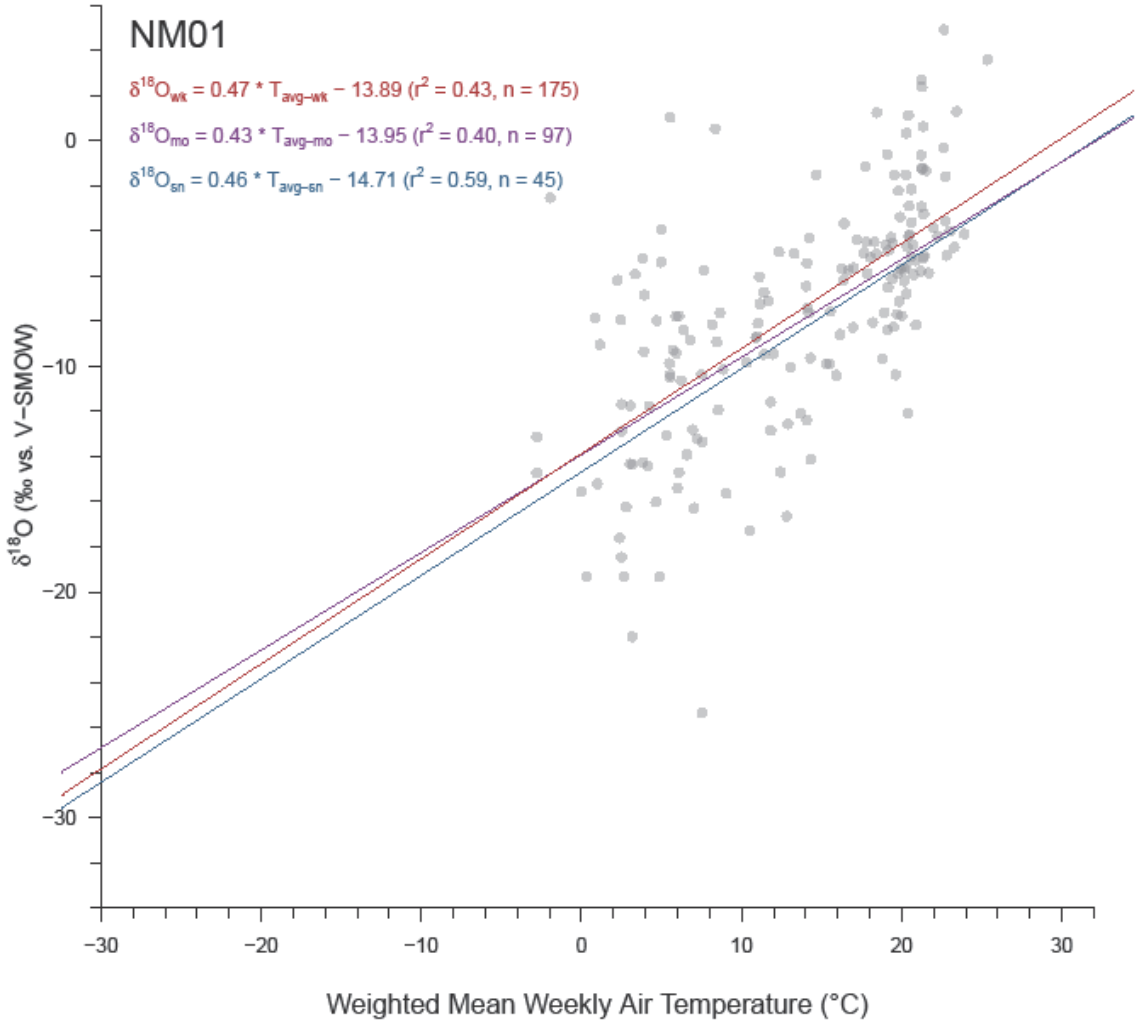

Figure A5.P2. Relationship between precipitation $\delta^{18}O$ and mean PDt at site NM01. Gray circles represent values at their original weekly resolution while linear trends are plotted for weekly (red), aggregated monthly (violet), and aggregated seasonal (blue) resolutions.

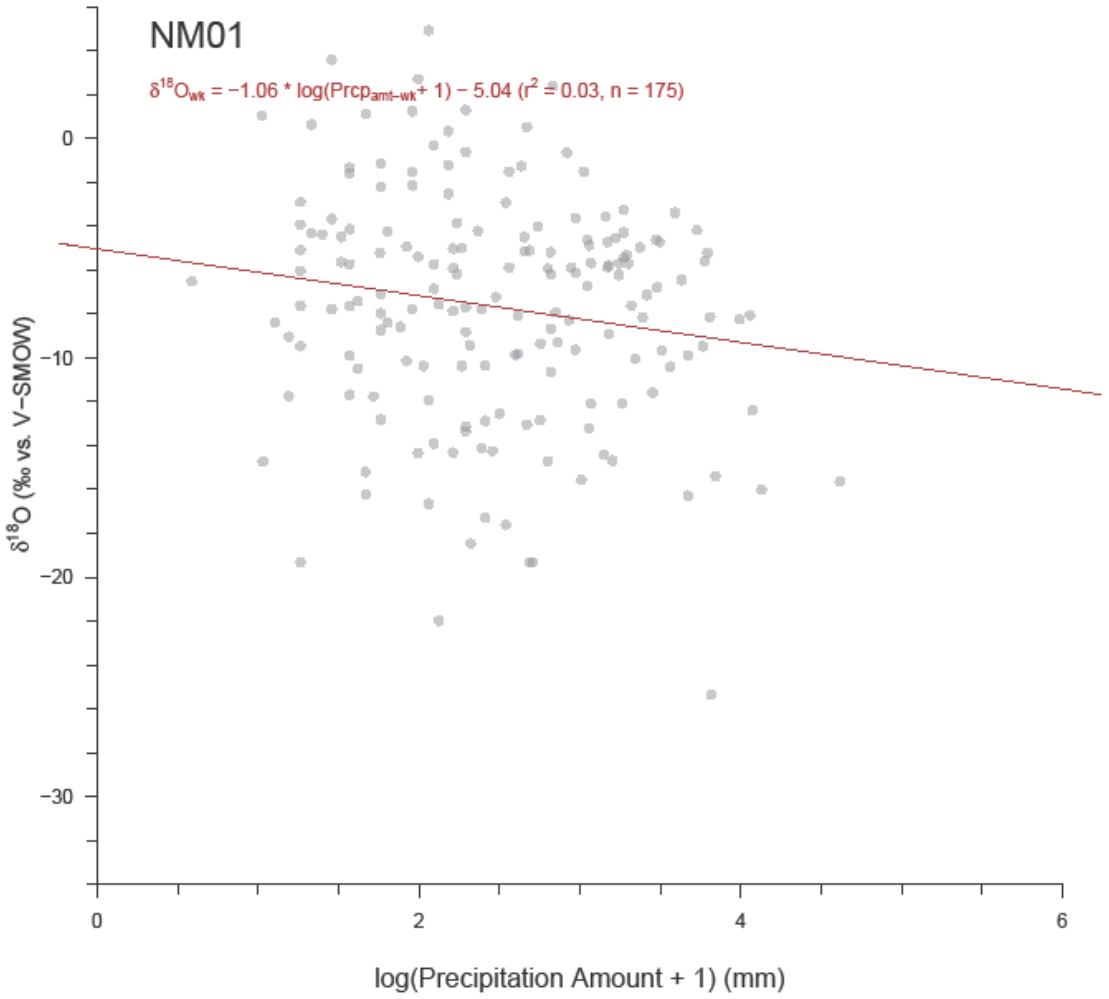

Figure A5.P3. Relationship between precipitation $\delta^{18}O$ and PDa at site NM01. Actual precipitation amounts were normalized by a log transformation. Gray circles represent values at their original weekly resolution with the weekly linear trend plotted in red. Precipitation amount data cannot be weight-averaged for aggregation, and thus regression was only performed at weekly resolution.

NM08

Table A5.Q1. Regression results for NM08 at weekly, monthly, and seasonal resolutions. Significant results ($p \leq 0.05$) are bolded, while insignificant results are italicized. Actual precipitation amounts were normalized by a log transformation. Precipitation amount data cannot be weight-averaged for aggregation, and thus regression was only performed at weekly resolution.

LMWL (δD vs. δ^{18}O)							
Resolution	***n***	***Slope***		***y-Int***		***r^2***	***p-value***
Weekly	**173**	**8.19**	**±0.09**	**13.96**	**±0.83**	**0.98**	**0.00**
Monthly	**101**	**8.26**	**±0.12**	**14.66**	**±1.20**	**0.98**	**0.00**
Seasonal	**46**	**8.44**	**±0.14**	**16.45**	**±1.43**	**0.99**	**0.00**
δ^{18}O vs. PDt							
Resolution	***n***	***Slope***		***y-Int***		***r^2***	***p-value***
Weekly	**173**	**0.40**	**±0.03**	**-13.52**	**±0.47**	**0.49**	**0.00**
Monthly	**101**	**0.39**	**±0.04**	**-13.50**	**±0.51**	**0.54**	**0.00**
Seasonal	**46**	**0.48**	**±0.05**	**-14.73**	**±0.64**	**0.70**	**0.00**
δ^{18}O vs. PDa							
Resolution	***n***	***Slope***		***y-Int***		***r^2***	***p-value***
Weekly	*173*	*0.36*	*±0.37*	*-9.33*	*±1.06*	*0.01*	*0.33*

Table A5.Q2. Percent change in NM08 regression values (Table A5.Q1) due to aggregation.

LMWL (δD vs. δ^{18}O)					
Aggregation	***Slope***	***Slope Error***	***y-Int***	***y-Int Error***	***r^2***
Weekly-Monthly	1%	38%	5%	45%	0%
Weekly-Seasonal	3%	41%	17%	50%	1%
Monthly-Seasonal	2%	12%	11%	16%	1%
δ^{18}O vs. PDt					
Aggregation	***Slope***	***Slope Error***	***y-Int***	***y-Int Error***	***r^2***
Weekly-Monthly	-2%	17%	0%	9%	9%
Weekly-Seasonal	21%	45%	9%	32%	39%
Monthly-Seasonal	19%	23%	8%	19%	23%

Table A5.Q3. NM08 temperature estimates and standard errors for three $\delta^{18}O$ values (vs. V-SMOW) at weekly, monthly, and seasonal resolutions. The three $\delta^{18}O$ values span much of the natural range of precipitation $\delta^{18}O$ in the study region, and -6‰ is close to the mean $\delta^{18}O$ value of all sites.

	Temperature Estimate (°C) when Precipitation $\delta^{18}O$ =		
Aggregation	***-20‰***	***-6‰***	***0‰***
Weekly	-1.3 ±11.2	15.8 ±11.0	23.1 ±11.1
Monthly	-3.5 ±11.3	15.7 ±11.0	23.9 ±11.2
Seasonal	-4.4 ±9.2	15.9 ±8.8	24.6 ±9.2

Table A5.Q4. Weight-averaged weekly values of $\delta^{18}O$ and average surface temperature for NM08 grouped by month and season. Blue (red) cells show low (high) values of note.

Group	***n***	***$\delta^{18}O_{wt}$***	***PDt***
Jan	6	-12.62 ±1.90	2.5 ±1.6
Feb	14	-15.24 ±1.30	2.9 ±0.9
Mar	11	-9.81 ±0.95	3.9 ±1.2
Apr	7	-10.36 ±0.94	7.1 ±1.6
May	10	-5.77 ±0.66	14.4 ±1.0
Jun	14	-5.84 ±1.13	18.7 ±0.6
Jul	25	-6.82 ±0.63	20.6 ±0.4
Aug	33	-5.46 ±0.38	18.7 ±0.3
Sep	19	-7.02 ±0.69	17.3 ±0.6
Oct	15	-9.41 ±0.70	12.2 ±0.7
Nov	11	-10.39 ±0.68	3.6 ±1.4
Dec	8	-14.81 ±1.07	-1.4 ±1.8
Win	28	-15.83 ±0.82	0.4 ±0.8
Spr	28	-8.04 ±0.61	9.9 ±1.1
Sum	72	-6.04 ±0.35	19.2 ±0.2
Aut	45	-8.32 ±0.46	12.9 ±0.9

Table A5.Q5. Regression results for NM08 when weekly data is grouped by month and by season. Significant results ($p \leq 0.05$) are bolded, while insignificant results are italicized. Actual precipitation amounts were normalized by a log transformation. Blue (red) cells show low (high) values of note.

LMWL (δD vs. $\delta^{18}O$)							
Group	***n***	***Slope***		***y-Int***		***r^2***	***p-value***
Jan	**6**	**8.31**	**±0.48**	**12.38**	**±6.42**	**0.99**	**0.00**
Feb	**14**	**8.53**	**±0.23**	**17.52**	**±3.61**	**0.99**	**0.00**
Mar	**11**	**8.77**	**±0.36**	**21.24**	**±3.59**	**0.99**	**0.00**
Apr	**7**	**7.70**	**±0.86**	**9.59**	**±8.99**	**0.94**	**0.00**
May	**10**	**6.75**	**±0.60**	**6.30**	**±3.70**	**0.94**	**0.00**
Jun	**14**	**8.04**	**±0.39**	**12.00**	**±2.87**	**0.97**	**0.00**
Jul	**25**	**8.05**	**±0.40**	**11.19**	**±2.80**	**0.95**	**0.00**
Aug	**33**	**7.67**	**±0.35**	**11.73**	**±1.92**	**0.94**	**0.00**
Sep	**19**	**7.95**	**±0.23**	**11.34**	**±1.79**	**0.99**	**0.00**
Oct	**15**	**8.42**	**±0.48**	**18.87**	**±4.61**	**0.96**	**0.00**
Nov	**11**	**6.92**	**±0.41**	**2.63**	**±4.57**	**0.97**	**0.00**
Dec	**8**	**10.59**	**±0.85**	**49.33**	**±12.64**	**0.96**	**0.00**
Win	**28**	**8.68**	**±0.26**	**19.72**	**±3.90**	**0.98**	**0.00**
Spr	**28**	**8.10**	**±0.26**	**14.26**	**±2.35**	**0.97**	**0.00**
Sum	**72**	**8.02**	**±0.21**	**12.35**	**±1.35**	**0.95**	**0.00**
Aut	**45**	**7.74**	**±0.19**	**11.20**	**±1.80**	**0.97**	**0.00**
$\delta^{18}O$ vs. PDt							
Group	***n***	***Slope***		***y-Int***		***r^2***	***p-value***
Jan	*6*	*0.61*	*±0.51*	*-14.12*	*±2.22*	*0.26*	*0.30*
Feb	*14*	*0.43*	*±0.38*	*-16.59*	*±1.88*	*0.10*	*0.28*
Mar	*11*	*0.37*	*±0.24*	*-11.13*	*±1.36*	*0.21*	*0.16*
Apr	**7**	**0.52**	**±0.13**	**-14.01**	**±1.08**	**0.76**	**0.01**
May	*10*	*0.38*	*±0.19*	*-11.14*	*±2.70*	*0.33*	*0.08*
Jun	*14*	*0.72*	*±0.52*	*-19.11*	*±9.55*	*0.14*	*0.19*
Jul	*25*	*0.46*	*±0.35*	*-15.78*	*±7.20*	*0.07*	*0.20*
Aug	*33*	*0.26*	*±0.23*	*-10.03*	*±4.43*	*0.04*	*0.27*
Sep	**19**	**0.94**	**±0.18**	**-23.15**	**±3.11**	**0.62**	**0.00**
Oct	*15*	*0.31*	*±0.28*	*-12.98*	*±3.48*	*0.08*	*0.30*
Nov	*11*	*-0.04*	*±0.16*	*-10.74*	*±0.91*	*0.01*	*0.81*
Dec	*8*	*-0.03*	*±0.24*	*-14.69*	*±1.19*	*0.00*	*0.91*
Win	*28*	*0.20*	*±0.19*	*-14.81*	*±0.90*	*0.04*	*0.29*
Spr	**28**	**0.41**	**±0.08**	**-11.89**	**±0.79**	**0.52**	**0.00**

Sum	*72*	*0.30*	*±0.17*	*-11.60*	*±3.42*	*0.04*	*0.09*
Aut	**45**	**0.28**	**±0.06**	**-12.19**	**±0.85**	**0.32**	**0.00**
δ^{18}O vs. PDa							
Group	***n***	***Slope***		***y-Int***		***r^2***	***p-value***
Jan	*6*	*-2.38*	*±4.32*	*-6.74*	*±10.87*	*0.07*	*0.61*
Feb	*14*	*-0.87*	*±1.90*	*-13.15*	*±4.34*	*0.02*	*0.65*
Mar	*11*	*-2.42*	*±2.26*	*-4.86*	*±4.52*	*0.11*	*0.31*
Apr	*7*	*0.50*	*±0.94*	*-11.46*	*±2.65*	*0.05*	*0.62*
May	*10*	*1.13*	*±1.57*	*-8.76*	*±4.09*	*0.06*	*0.49*
Jun	*14*	*-0.82*	*±1.27*	*-4.00*	*±3.40*	*0.03*	*0.53*
Jul	*25*	*-0.90*	*±0.74*	*-3.82*	*±2.08*	*0.06*	*0.24*
Aug	**33**	**-1.36**	**±0.34**	**-0.43**	**±1.20**	**0.35**	**0.00**
Sep	*19*	*-1.22*	*±0.96*	*-3.47*	*±2.94*	*0.09*	*0.22*
Oct	*15*	*0.29*	*±1.10*	*-10.07*	*±3.01*	*0.01*	*0.80*
Nov	*11*	*-0.05*	*±0.73*	*-10.74*	*±1.90*	*0.00*	*0.94*
Dec	*8*	*-1.88*	*±0.89*	*-9.54*	*±2.56*	*0.43*	*0.08*
Win	*28*	*-1.23*	*±1.02*	*-11.48*	*±2.58*	*0.05*	*0.24*
Spr	*28*	*0.61*	*±0.85*	*-9.82*	*±2.08*	*0.02*	*0.48*
Sum	**72**	**-0.70**	**±0.35**	**-3.59**	**±1.11**	**0.05**	**0.05**
Aut	*45*	*0.19*	*±0.58*	*-9.27*	*±1.66*	*0.00*	*0.75*

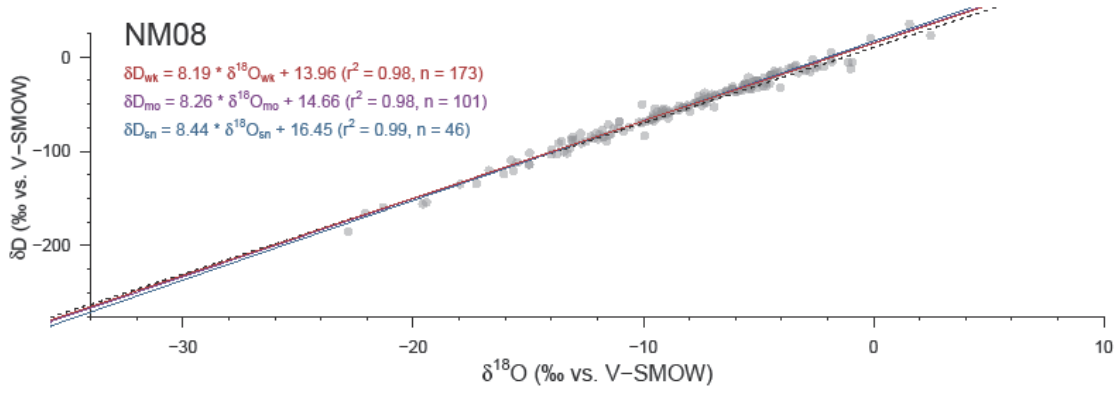

Figure A5.Q1. Local meteoric water line for NM08. Gray circles represent values at their original weekly resolution while linear trends are plotted for weekly (red), aggregated monthly (violet), and aggregated seasonal (blue) resolutions. The dashed black line represents the global meteoric water line.

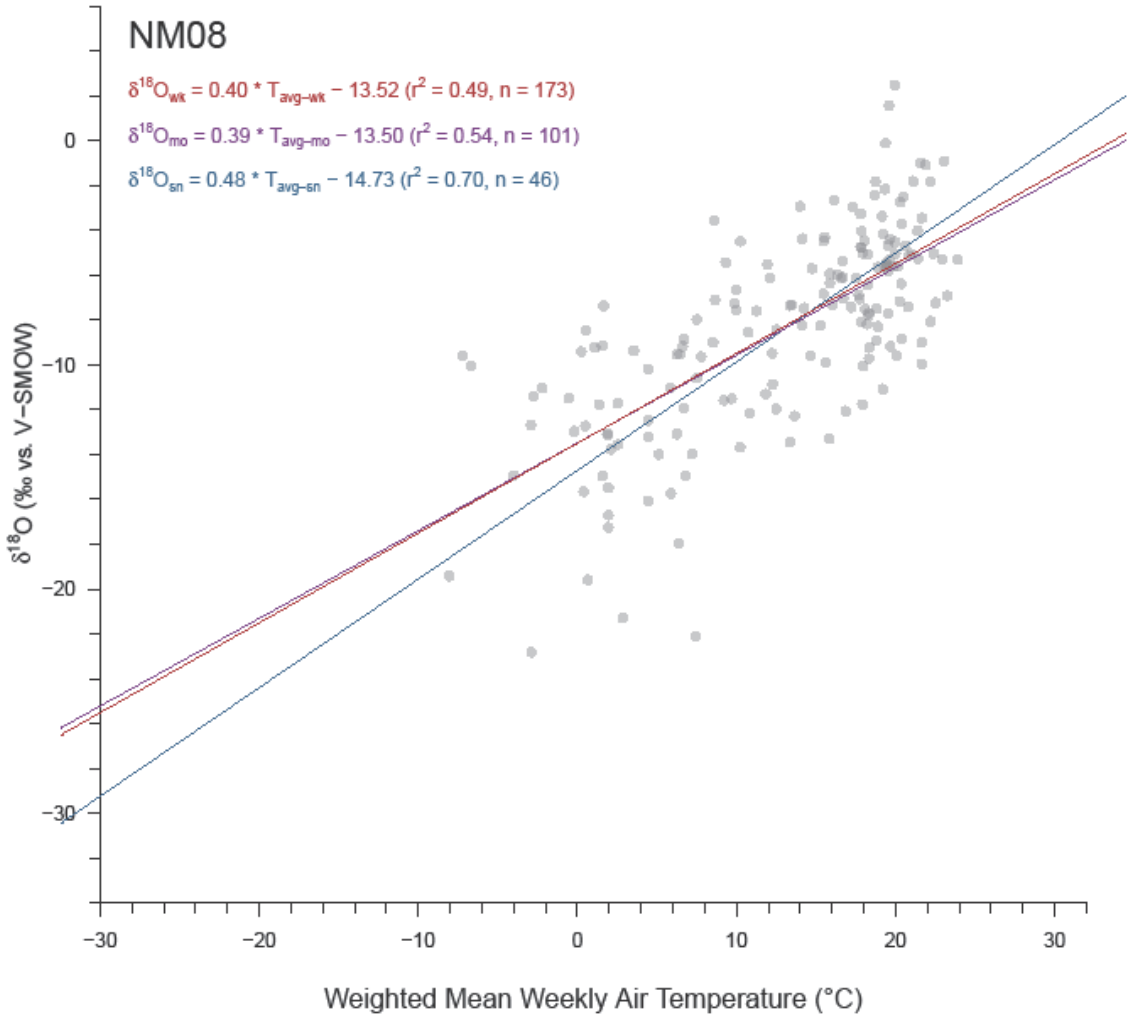

Figure A5.Q2. Relationship between precipitation $\delta^{18}O$ and mean PDt at site NM08. Gray circles represent values at their original weekly resolution while linear trends are plotted for weekly (red), aggregated monthly (violet), and aggregated seasonal (blue) resolutions.

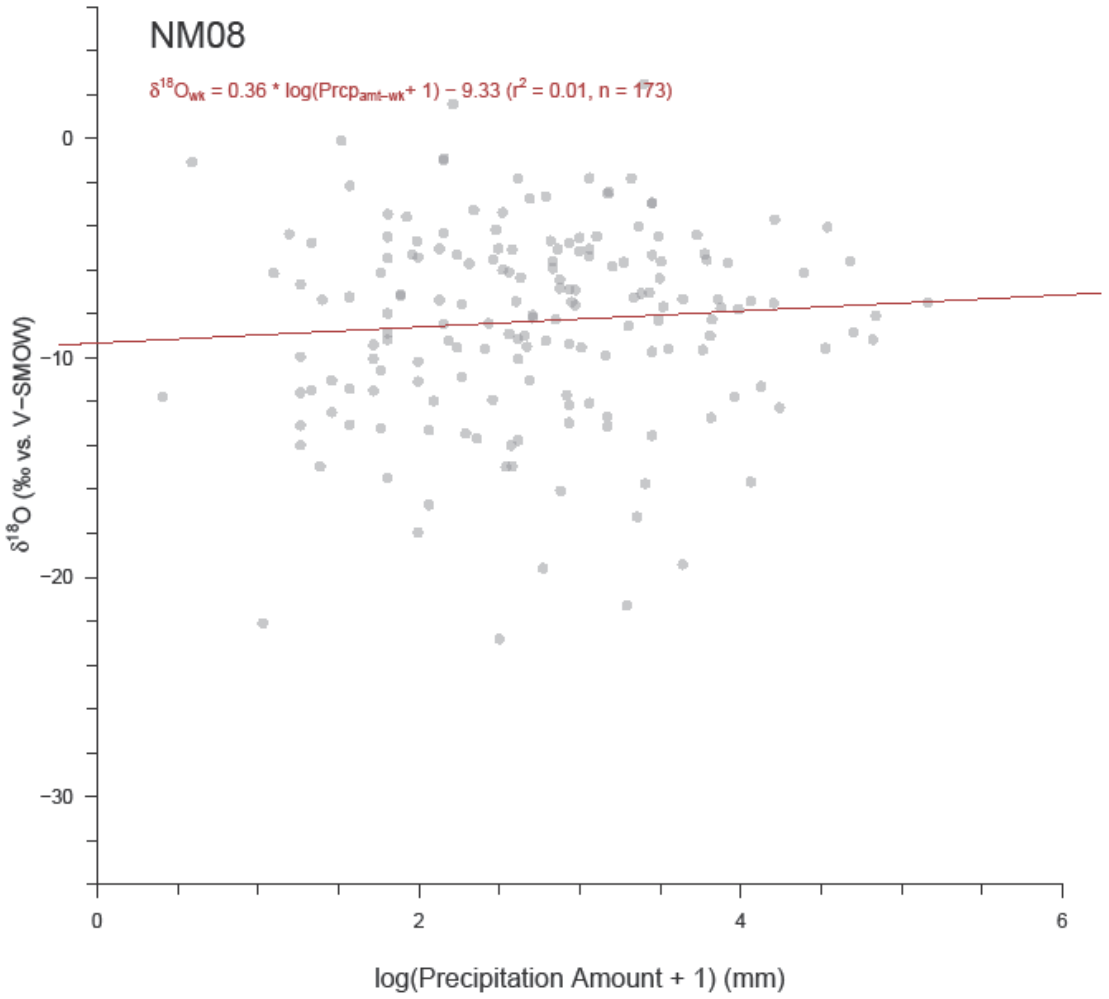

Figure A5.Q3. Relationship between precipitation $\delta^{18}O$ and PDa at site NM08. Actual precipitation amounts were normalized by a log transformation. Gray circles represent values at their original weekly resolution with the weekly linear trend plotted in red. Precipitation amount data cannot be weight-averaged for aggregation, and thus regression was only performed at weekly resolution.

NM12

Table A5.R1. Regression results for NM12 at weekly, monthly, and seasonal resolutions. Significant results ($p \leq 0.05$) are bolded, while insignificant results are italicized. Actual precipitation amounts were normalized by a log transformation. Precipitation amount data cannot be weight-averaged for aggregation, and thus regression was only performed at weekly resolution.

LMWL (δD vs. δ^{18}O)							
Resolution	***n***	***Slope***		***y-Int***		***r^2***	***p-value***
Weekly	**170**	**7.43**	**±0.07**	**5.24**	**±0.74**	**0.99**	**0.00**
Monthly	**94**	**7.47**	**±0.07**	**5.75**	**±0.88**	**0.99**	**0.00**
Seasonal	**46**	**7.53**	**±0.09**	**6.46**	**±1.12**	**0.99**	**0.00**
δ^{18}O vs. PDt							
Resolution	***n***	***Slope***		***y-Int***		***r^2***	***p-value***
Weekly	**170**	**0.51**	**±0.03**	**-15.99**	**±0.49**	**0.60**	**0.00**
Monthly	**94**	**0.52**	**±0.04**	**-16.20**	**±0.53**	**0.67**	**0.00**
Seasonal	**46**	**0.51**	**±0.06**	**-16.15**	**±0.77**	**0.63**	**0.00**
δ^{18}O vs. PDa							
Resolution	***n***	***Slope***		***y-Int***		***r^2***	***p-value***
Weekly	*170*	*0.36*	*±0.49*	*-10.34*	*±1.39*	*0.00*	*0.46*

Table A5.R2. Percent change in NM12 regression values (Table A5.R1) due to aggregation.

LMWL (δD vs. δ^{18}O)					
Aggregation	***Slope***	***Slope Error***	***y-Int***	***y-Int Error***	***r^2***
Weekly-Monthly	1%	8%	10%	18%	1%
Weekly-Seasonal	1%	34%	21%	43%	1%
Monthly-Seasonal	1%	21%	11%	22%	0%
δ^{18}O vs. PDt					
Aggregation	***Slope***	***Slope Error***	***y-Int***	***y-Int Error***	***r^2***
Weekly-Monthly	1%	18%	1%	9%	11%
Weekly-Seasonal	0%	71%	1%	55%	5%
Monthly-Seasonal	-1%	36%	0%	32%	-6%

Table A5.R3. NM12 temperature estimates and standard errors for three $\delta^{18}O$ values (vs. V-SMOW) at weekly, monthly, and seasonal resolutions. The three $\delta^{18}O$ values span much of the natural range of precipitation $\delta^{18}O$ in the study region, and -6‰ is close to the mean $\delta^{18}O$ value of all sites.

	Temperature Estimate (°C) when Precipitation $\delta^{18}O$ =		
Aggregation	***-20‰***	***-6‰***	***0‰***
Weekly	0.4 ±10.1	17.0 ±9.9	24.1 ±10.0
Monthly	-1.3 ±9.9	16.9 ±9.8	24.7 ±10.0
Seasonal	-0.9 ±10.3	16.5 ±10.0	23.9 ±10.4

Table A5.R4. Weight-averaged weekly values of $\delta^{18}O$ and average surface temperature for NM12 grouped by month and season. Blue (red) cells show low (high) values of note.

Group	***n***	***$\delta^{18}O_{wt}$***	***PDt***
Jan	5	-15.83 ±1.49	-3.3 ±1.7
Feb	3	-18.70 ±2.58	0.4 ±1.5
Mar	10	-15.37 ±1.49	1.3 ±1.4
Apr	13	-13.56 ±0.92	5.8 ±0.8
May	18	-10.62 ±0.97	11.8 ±1.0
Jun	22	-8.12 ±0.73	15.9 ±0.6
Jul	24	-6.30 ±0.68	20.4 ±0.4
Aug	31	-5.69 ±0.47	19.6 ±0.2
Sep	21	-6.36 ±0.87	17.2 ±0.7
Oct	9	-10.32 ±1.32	11.0 ±1.4
Nov	12	-15.37 ±1.32	0.0 ±0.7
Dec	2	-20.46 ±3.70	0.4 ±0.1
Win	10	-17.27 ±1.29	-1.1 ±1.1
Spr	41	-13.10 ±0.71	7.2 ±0.9
Sum	77	-6.32 ±0.36	19.2 ±0.3
Aut	42	-9.70 ±0.85	10.9 ±1.2

Table A5.R5. Regression results for NM12 when weekly data is grouped by month and by season. Significant results ($p \leq 0.05$) are bolded, while insignificant results are italicized. Actual precipitation amounts were normalized by a log transformation. Blue (red) cells show low (high) values of note.

LMWL (δD vs. $\delta^{18}O$)							
Group	***n***	***Slope***		***y-Int***		***r^2***	***p-value***
Jan	**5**	**7.27**	**±0.44**	**1.32**	**±6.99**	**0.99**	**0.00**
Feb	**3**	**7.85**	**±0.64**	**11.83**	**±12.17**	**0.99**	**0.05**
Mar	**10**	**8.07**	**±0.30**	**15.94**	**±4.81**	**0.99**	**0.00**
Apr	**13**	**8.24**	**±0.17**	**16.83**	**±2.33**	**1.00**	**0.00**
May	**18**	**7.45**	**±0.18**	**4.01**	**±1.98**	**0.99**	**0.00**
Jun	**22**	**6.73**	**±0.31**	**-1.10**	**±2.52**	**0.96**	**0.00**
Jul	**24**	**7.07**	**±0.21**	**2.57**	**±1.66**	**0.98**	**0.00**
Aug	**31**	**6.61**	**±0.35**	**0.44**	**±2.15**	**0.93**	**0.00**
Sep	**21**	**7.26**	**±0.28**	**6.14**	**±2.07**	**0.97**	**0.00**
Oct	**9**	**7.40**	**±0.59**	**8.07**	**±5.98**	**0.96**	**0.00**
Nov	**12**	**7.81**	**±0.36**	**9.02**	**±5.61**	**0.98**	**0.00**
Dec	*2*	*-*	*-*	*-*	*-*	*-*	*-*
Win	**10**	**7.37**	**±0.22**	**3.23**	**±4.02**	**0.99**	**0.00**
Spr	**41**	**7.60**	**±0.13**	**7.26**	**±1.69**	**0.99**	**0.00**
Sum	**77**	**6.88**	**±0.16**	**1.19**	**±1.20**	**0.96**	**0.00**
Aut	**42**	**7.67**	**±0.15**	**8.60**	**±1.70**	**0.98**	**0.00**
$\delta^{18}O$ vs. PDt							
Group	***n***	***Slope***		***y-Int***		***r^2***	***p-value***
Jan	*5*	*-0.29*	*±0.47*	*-16.47*	*±2.09*	*0.12*	*0.57*
Feb	*3*	*0.72*	*±1.54*	*-18.96*	*±3.35*	*0.18*	*0.72*
Mar	*10*	*0.62*	*±0.32*	*-16.50*	*±1.39*	*0.32*	*0.09*
Apr	*13*	*0.40*	*±0.32*	*-15.46*	*±2.11*	*0.12*	*0.25*
May	**18**	**0.62**	**±0.19**	**-17.19**	**±2.38**	**0.39**	**0.01**
Jun	**22**	**0.59**	**±0.23**	**-17.20**	**±3.86**	**0.25**	**0.02**
Jul	*24*	*0.57*	*±0.31*	*-18.68*	*±6.40*	*0.13*	*0.08*
Aug	*31*	*0.14*	*±0.35*	*-8.38*	*±6.90*	*0.01*	*0.70*
Sep	**21**	**0.70**	**±0.26**	**-18.31**	**±4.38**	**0.29**	**0.01**
Oct	**9**	**0.78**	**±0.18**	**-18.44**	**±2.22**	**0.72**	**0.00**
Nov	*12*	*0.90*	*±0.50*	*-15.29*	*±1.20*	*0.25*	*0.10*
Dec	*2*	*-*	*-*	*-*	*-*	*-*	*-*
Win	*10*	*-0.39*	*±0.41*	*-18.00*	*±1.40*	*0.10*	*0.37*
Spr	**41**	**0.56**	**±0.09**	**-16.47**	**±0.86**	**0.48**	**0.00**

Sum	**77**	**0.41**	**±0.13**	**-14.39**	**±2.48**	**0.12**	**0.00**
Aut	**42**	**0.56**	**±0.07**	**-15.69**	**±0.90**	**0.64**	**0.00**
δ^{18}O vs. PDa							
Group	***n***	***Slope***		***y-Int***		***r^2***	***p-value***
Jan	*5*	*2.42*	*±2.09*	*-20.70*	*±4.58*	*0.31*	*0.33*
Feb	**3**	**-8.70**	**±0.08**	**0.93**	**±0.19**	**1.00**	**0.01**
Mar	*10*	*0.65*	*±3.00*	*-17.26*	*±7.97*	*0.01*	*0.83*
Apr	*13*	*-1.38*	*±1.50*	*-9.85*	*±3.69*	*0.07*	*0.38*
May	*18*	*-0.75*	*±1.27*	*-8.13*	*±3.33*	*0.02*	*0.56*
Jun	*22*	*-1.63*	*±0.95*	*-2.47*	*±2.94*	*0.13*	*0.10*
Jul	*24*	*-0.64*	*±0.63*	*-5.28*	*±1.88*	*0.04*	*0.32*
Aug	*31*	*-0.98*	*±0.72*	*-2.64*	*±2.27*	*0.06*	*0.18*
Sep	*21*	*-2.13*	*±1.06*	*-0.77*	*±2.92*	*0.17*	*0.06*
Oct	*9*	*-1.50*	*±1.62*	*-6.30*	*±3.68*	*0.11*	*0.39*
Nov	*12*	*1.98*	*±2.18*	*-20.23*	*±5.78*	*0.08*	*0.39*
Dec	*2*	-	-	-	-	-	-
Win	*10*	*-0.39*	*±2.44*	*-16.65*	*±5.59*	*0.00*	*0.88*
Spr	*41*	*-0.83*	*±1.05*	*-10.28*	*±2.71*	*0.02*	*0.43*
Sum	**77**	**-0.84**	**±0.42**	**-4.10**	**±1.30**	**0.05**	**0.05**
Aut	*42*	*-0.89*	*±1.12*	*-7.31*	*±2.94*	*0.02*	*0.43*

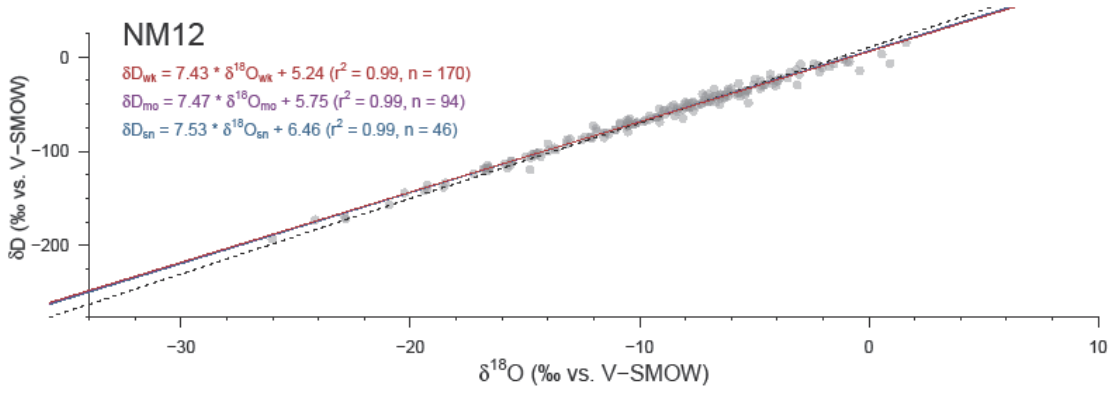

Figure A5.R1. Local meteoric water line for NM12. Gray circles represent values at their original weekly resolution while linear trends are plotted for weekly (red), aggregated monthly (violet), and aggregated seasonal (blue) resolutions. The dashed black line represents the global meteoric water line.

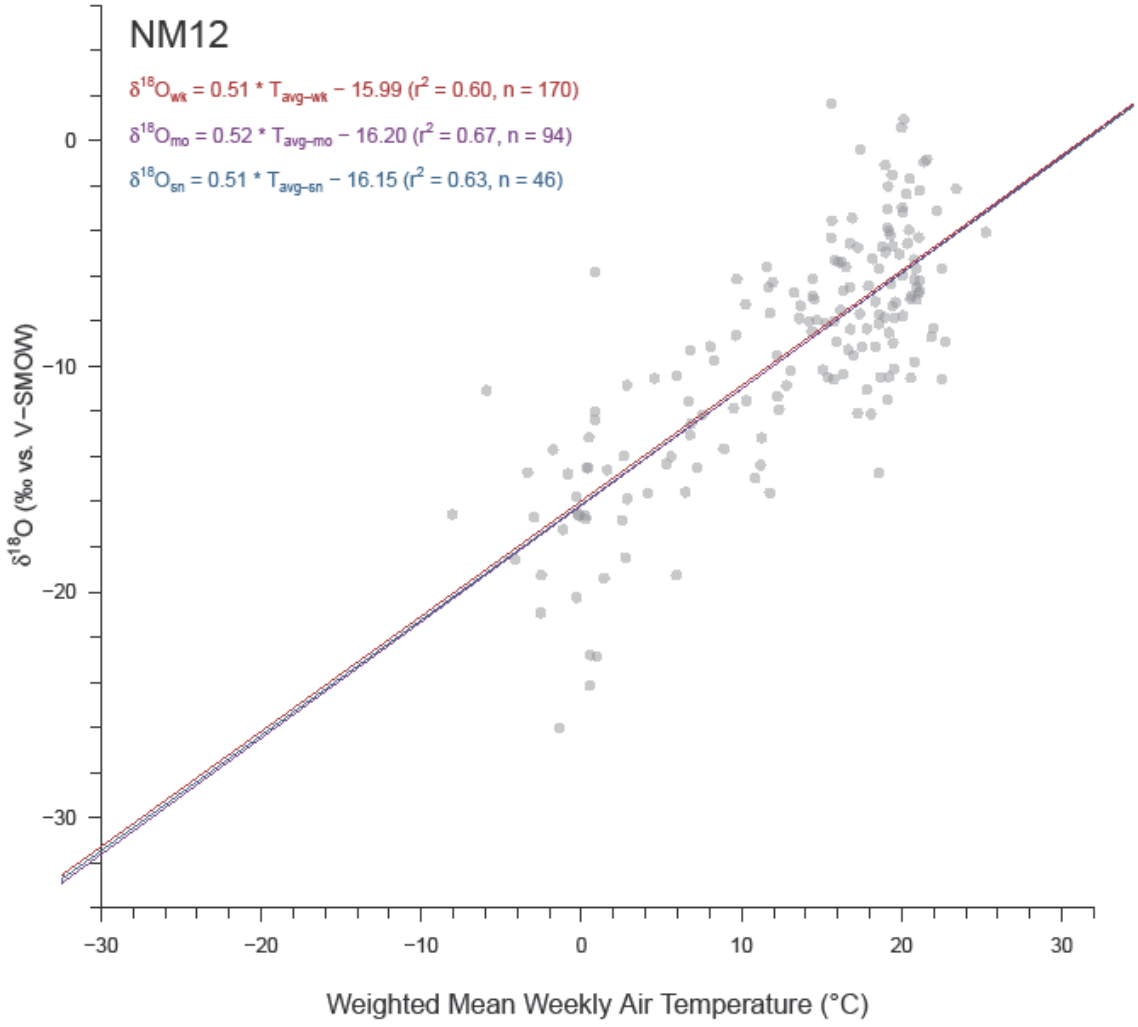

Figure A5.R2. Relationship between precipitation $\delta^{18}O$ and mean PDt at site NM12. Gray circles represent values at their original weekly resolution while linear trends are plotted for weekly (red), aggregated monthly (violet), and aggregated seasonal (blue) resolutions.

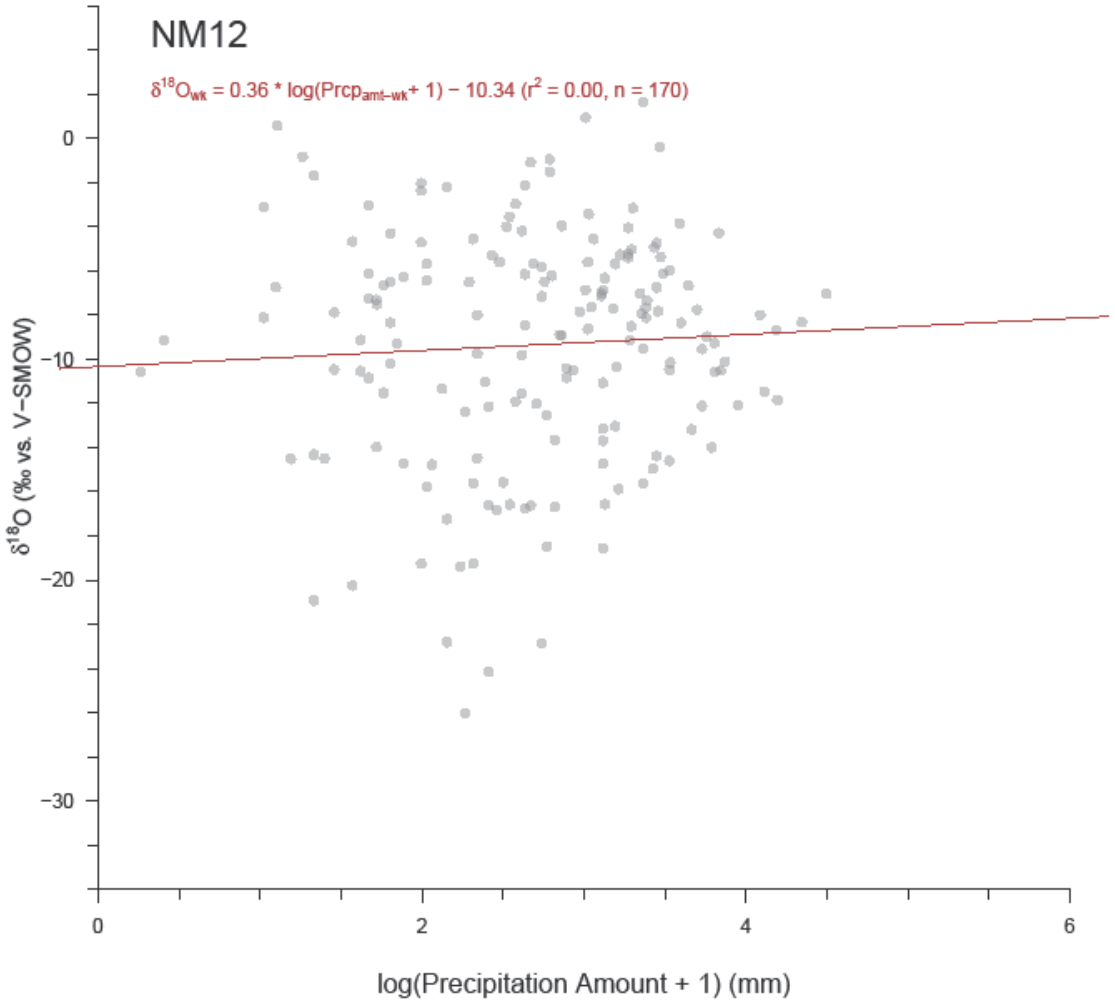

Figure A5.R3. Relationship between precipitation $\delta^{18}O$ and PDa at site NM12. Actual precipitation amounts were normalized by a log transformation. Gray circles represent values at their original weekly resolution with the weekly linear trend plotted in red. Precipitation amount data cannot be weight-averaged for aggregation, and thus regression was only performed at weekly resolution.

NY10

Table A5.S1. Regression results for NY10 at weekly, monthly, and seasonal resolutions. Significant results ($p \leq 0.05$) are bolded, while insignificant results are italicized. Actual precipitation amounts were normalized by a log transformation. Precipitation amount data cannot be weight-averaged for aggregation, and thus regression was only performed at weekly resolution.

LMWL (δD vs. δ^{18}O)							
Resolution	***n***	***Slope***		***y-Int***		***r^2***	***p-value***
Weekly	**296**	**7.40**	**±0.06**	**8.17**	**±0.70**	**0.98**	**0.00**
Monthly	**128**	**7.23**	**±0.11**	**5.88**	**±1.24**	**0.97**	**0.00**
Seasonal	**56**	**7.23**	**±0.16**	**6.07**	**±1.71**	**0.97**	**0.00**
δ^{18}O vs. PDt							
Resolution	***n***	***Slope***		***y-Int***		***r^2***	***p-value***
Weekly	**296**	**0.37**	**±0.02**	**-13.00**	**±0.25**	**0.54**	**0.00**
Monthly	**128**	**0.34**	**±0.03**	**-12.97**	**±0.35**	**0.54**	**0.00**
Seasonal	**56**	**0.34**	**±0.04**	**-13.04**	**±0.47**	**0.59**	**0.00**
δ^{18}O vs. PDa							
Resolution	***n***	***Slope***		***y-Int***		***r^2***	***p-value***
Weekly	*296*	*0.22*	*±0.35*	*-10.53*	*±1.08*	*0.00*	*0.53*

Table A5.S2. Percent change in NY10 regression values (Table A5.S1) due to aggregation.

LMWL (δD vs. δ^{18}O)					
Aggregation	***Slope***	***Slope Error***	***y-Int***	***y-Int Error***	***r^2***
Weekly-Monthly	-2%	79%	-28%	78%	-1%
Weekly-Seasonal	-2%	84%	-36%	81%	0%
Monthly-Seasonal	0%	29%	3%	27%	0%
δ^{18}O vs. PDt					
Aggregation	***Slope***	***Slope Error***	***y-Int***	***y-Int Error***	***r^2***
Weekly-Monthly	-9%	42%	0%	41%	-1%
Weekly-Seasonal	-10%	66%	0%	64%	8%
Monthly-Seasonal	-1%	27%	1%	26%	9%

Table A5.S3. NY10 temperature estimates and standard errors for three $\delta^{18}O$ values (vs. V-SMOW) at weekly, monthly, and seasonal resolutions. The three $\delta^{18}O$ values span much of the natural range of precipitation $\delta^{18}O$ in the study region, and -6‰ is close to the mean $\delta^{18}O$ value of all sites.

	Temperature Estimate (°C) when Precipitation $\delta^{18}O$ =					
Aggregation	***-20‰***		***-6‰***		***0‰***	
Weekly	-6.4	±12.4	14.1	±12.3	22.9	±12.4
Monthly	-7.1	±12.4	15.0	±12.2	24.5	±12.4
Seasonal	-8.4	±11.5	16.0	±10.9	26.5	±11.5

Table A5.S4. Weight-averaged weekly values of $\delta^{18}O$ and average surface temperature for NY10 grouped by month and season. Blue (red) cells show low (high) values of note.

Group	***n***	***$\delta^{18}O_{wt}$***		***PDt***	
Jan	28	-13.70	±0.92	-2.3	±1.1
Feb	25	-13.45	±0.90	-2.0	±1.2
Mar	28	-11.25	±0.84	0.6	±0.9
Apr	29	-8.95	±0.67	7.6	±0.6
May	23	-5.91	±0.68	13.6	±0.9
Jun	33	-6.94	±0.38	17.3	±0.6
Jul	19	-6.33	±0.50	21.1	±0.6
Aug	21	-8.24	±0.59	19.4	±0.6
Sep	19	-8.64	±0.63	16.8	±0.8
Oct	24	-10.95	±0.67	10.3	±0.8
Nov	27	-10.86	±0.70	5.9	±0.8
Dec	20	-15.17	±0.94	-1.6	±1.1
Win	73	-13.82	±0.54	-1.6	±0.7
Spr	80	-8.60	±0.49	7.7	±0.7
Sum	73	-7.15	±0.28	19.1	±0.4
Aut	70	-10.76	±0.41	10.9	±0.7

Table A5.S5. Regression results for NY10 when weekly data is grouped by month and by season. Significant results ($p \leq 0.05$) are bolded, while insignificant results are italicized. Actual precipitation amounts were normalized by a log transformation. Blue (red) cells show low (high) values of note.

LMWL (δD vs. $\delta^{18}O$)							
Group	***n***	***Slope***		***y-Int***		***r^2***	***p-value***
Jan	**28**	**7.51**	**±0.18**	**9.89**	**±2.72**	**0.99**	**0.00**
Feb	**25**	**8.08**	**±0.19**	**16.39**	**±2.60**	**0.99**	**0.00**
Mar	**28**	**7.38**	**±0.20**	**6.58**	**±2.42**	**0.98**	**0.00**
Apr	**29**	**6.54**	**±0.43**	**-1.69**	**±4.09**	**0.90**	**0.00**
May	**23**	**7.38**	**±0.44**	**6.07**	**±3.09**	**0.93**	**0.00**
Jun	**33**	**7.79**	**±0.24**	**10.78**	**±1.74**	**0.97**	**0.00**
Jul	**19**	**7.30**	**±0.29**	**7.11**	**±1.77**	**0.97**	**0.00**
Aug	**21**	**7.57**	**±0.27**	**9.75**	**±2.03**	**0.98**	**0.00**
Sep	**19**	**7.55**	**±0.21**	**10.52**	**±1.80**	**0.99**	**0.00**
Oct	**24**	**7.73**	**±0.32**	**11.86**	**±3.45**	**0.96**	**0.00**
Nov	**27**	**7.84**	**±0.17**	**15.40**	**±1.83**	**0.99**	**0.00**
Dec	**20**	**7.66**	**±0.29**	**15.35**	**±4.51**	**0.98**	**0.00**
Win	**73**	**7.67**	**±0.13**	**12.62**	**±1.90**	**0.98**	**0.00**
Spr	**80**	**7.15**	**±0.17**	**4.03**	**±1.73**	**0.96**	**0.00**
Sum	**73**	**7.56**	**±0.15**	**9.19**	**±1.04**	**0.97**	**0.00**
Aut	**70**	**7.70**	**±0.13**	**12.56**	**±1.39**	**0.98**	**0.00**
$\delta^{18}O$ vs. PDt							
Group	***n***	***Slope***		***y-Int***		***r^2***	***p-value***
Jan	**28**	**0.68**	**±0.11**	**-12.05**	**±0.67**	**0.61**	**0.00**
Feb	**25**	**0.62**	**±0.09**	**-12.34**	**±0.55**	**0.65**	**0.00**
Mar	**28**	**0.52**	**±0.14**	**-12.08**	**±0.71**	**0.34**	**0.00**
Apr	**29**	**0.56**	**±0.19**	**-13.11**	**±1.53**	**0.25**	**0.01**
May	*23*	*0.22*	*±0.15*	*-9.13*	*±2.08*	*0.10*	*0.15*
Jun	**33**	**0.25**	**±0.10**	**-11.20**	**±1.79**	**0.17**	**0.02**
Jul	*19*	*0.25*	*±0.19*	*-11.04*	*±3.94*	*0.10*	*0.20*
Aug	**21**	**0.70**	**±0.16**	**-21.04**	**±3.26**	**0.49**	**0.00**
Sep	*19*	*0.34*	*±0.17*	*-13.75*	*±2.87*	*0.19*	*0.06*
Oct	*24*	*0.18*	*±0.18*	*-12.16*	*±1.88*	*0.04*	*0.34*
Nov	**27**	**0.55**	**±0.15**	**-13.73**	**±1.09**	**0.35**	**0.00**
Dec	**20**	**0.49**	**±0.16**	**-14.58**	**±0.80**	**0.35**	**0.01**
Win	**73**	**0.59**	**±0.07**	**-12.92**	**±0.39**	**0.53**	**0.00**
Spr	**80**	**0.44**	**±0.06**	**-12.05**	**±0.54**	**0.42**	**0.00**

Sum	**73**	**0.31**	**±0.07**	**-12.62**	**±1.40**	**0.21**	**0.00**
Aut	**70**	**0.29**	**±0.06**	**-12.72**	**±0.75**	**0.23**	**0.00**
δ^{18}O vs. PDa							
Group	***n***	***Slope***		***y-Int***		***r^2***	***p-value***
Jan	*28*	*1.65*	*±1.55*	*-18.72*	*±4.35*	*0.04*	*0.30*
Feb	*25*	*0.76*	*±1.75*	*-15.16*	*±4.91*	*0.01*	*0.67*
Mar	*28*	*-1.47*	*±1.19*	*-7.35*	*±3.54*	*0.05*	*0.23*
Apr	*29*	*-0.22*	*±0.91*	*-8.16*	*±3.10*	*0.00*	*0.81*
May	*23*	*0.16*	*±0.66*	*-6.67*	*±2.17*	*0.00*	*0.81*
Jun	*33*	*0.48*	*±0.52*	*-8.27*	*±1.62*	*0.03*	*0.37*
Jul	**19**	**-1.53**	**±0.62**	**-0.73**	**±2.10**	**0.26**	**0.02**
Aug	*21*	*-0.94*	*±0.68*	*-4.44*	*±2.08*	*0.09*	*0.18*
Sep	*19*	*-1.04*	*±0.58*	*-4.95*	*±1.83*	*0.16*	*0.09*
Oct	*24*	*-1.92*	*±0.85*	*-4.72*	*±2.62*	*0.19*	*0.03*
Nov	**27**	**-3.77**	**±1.26**	**1.74**	**±4.07**	**0.27**	**0.01**
Dec	*20*	*0.49*	*±1.30*	*-16.47*	*±3.69*	*0.01*	*0.71*
Win	*73*	*0.98*	*±0.87*	*-16.75*	*±2.45*	*0.02*	*0.27*
Spr	*80*	*-0.06*	*±0.58*	*-8.86*	*±1.86*	*0.00*	*0.92*
Sum	*73*	*-0.33*	*±0.36*	*-5.66*	*±1.14*	*0.01*	*0.37*
Aut	**70**	**-1.80**	**±0.50**	**-4.22**	**±1.57**	**0.16**	**0.00**

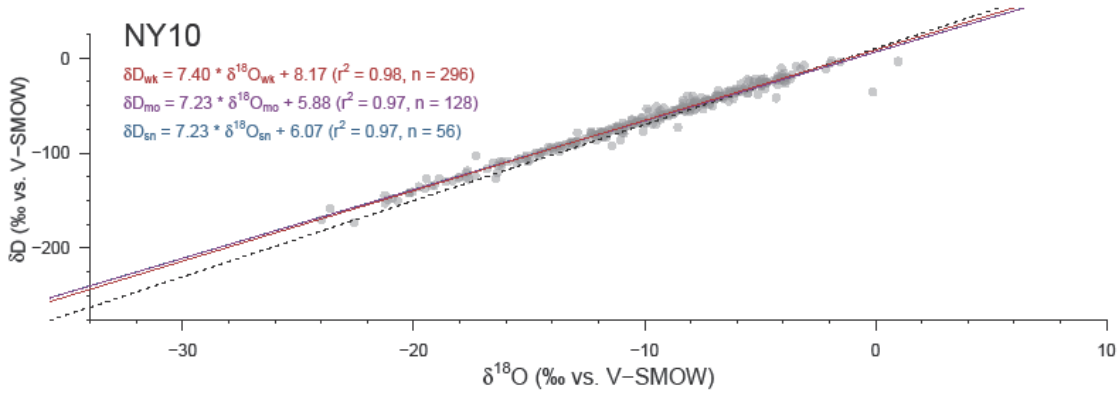

Figure A5.S1. Local meteoric water line for NY10. Gray circles represent values at their original weekly resolution while linear trends are plotted for weekly (red), aggregated monthly (violet), and aggregated seasonal (blue) resolutions. The dashed black line represents the global meteoric water line.

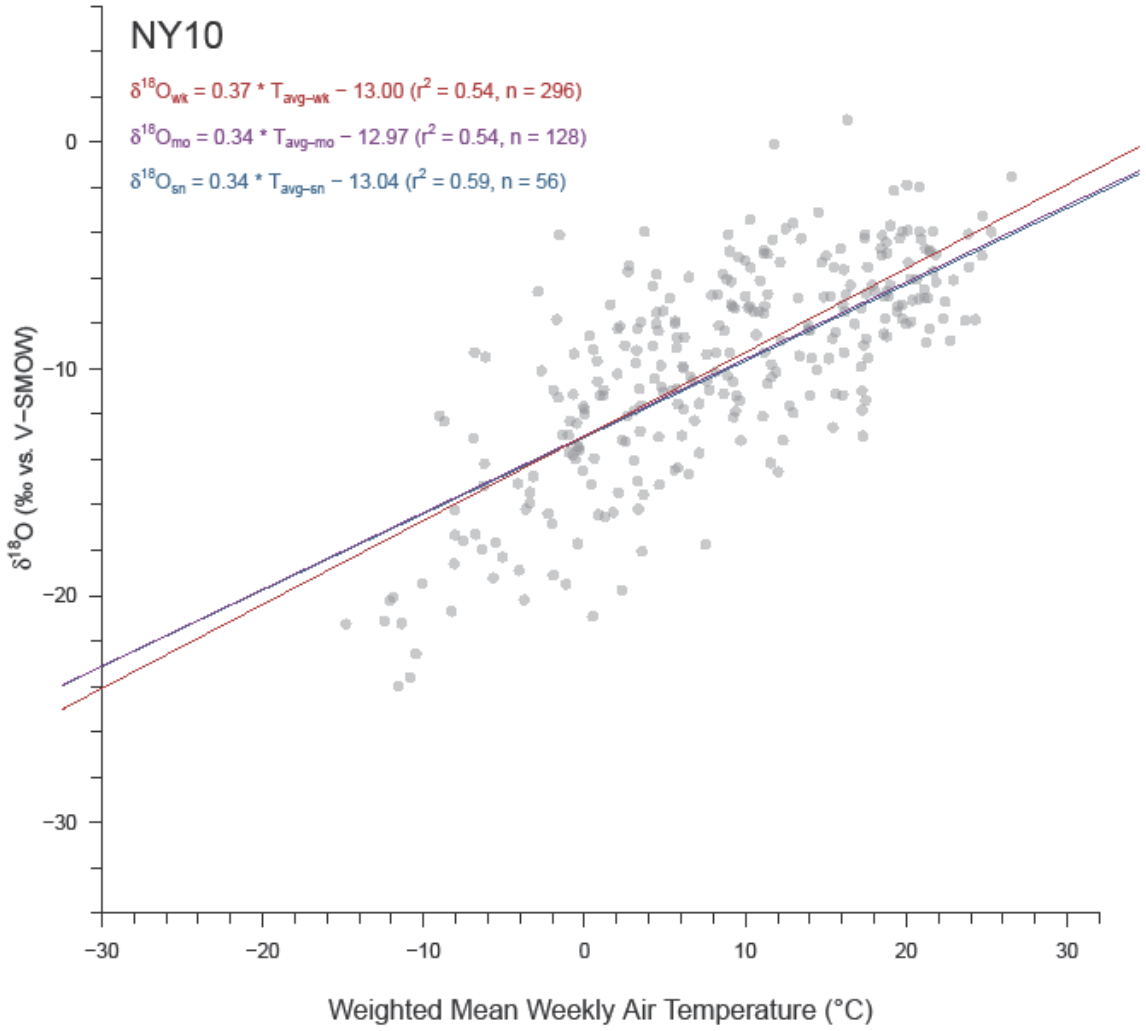

Figure A5.S2. Relationship between precipitation $\delta^{18}O$ and mean PDt at site NY10. Gray circles represent values at their original weekly resolution while linear trends are plotted for weekly (red), aggregated monthly (violet), and aggregated seasonal (blue) resolutions.

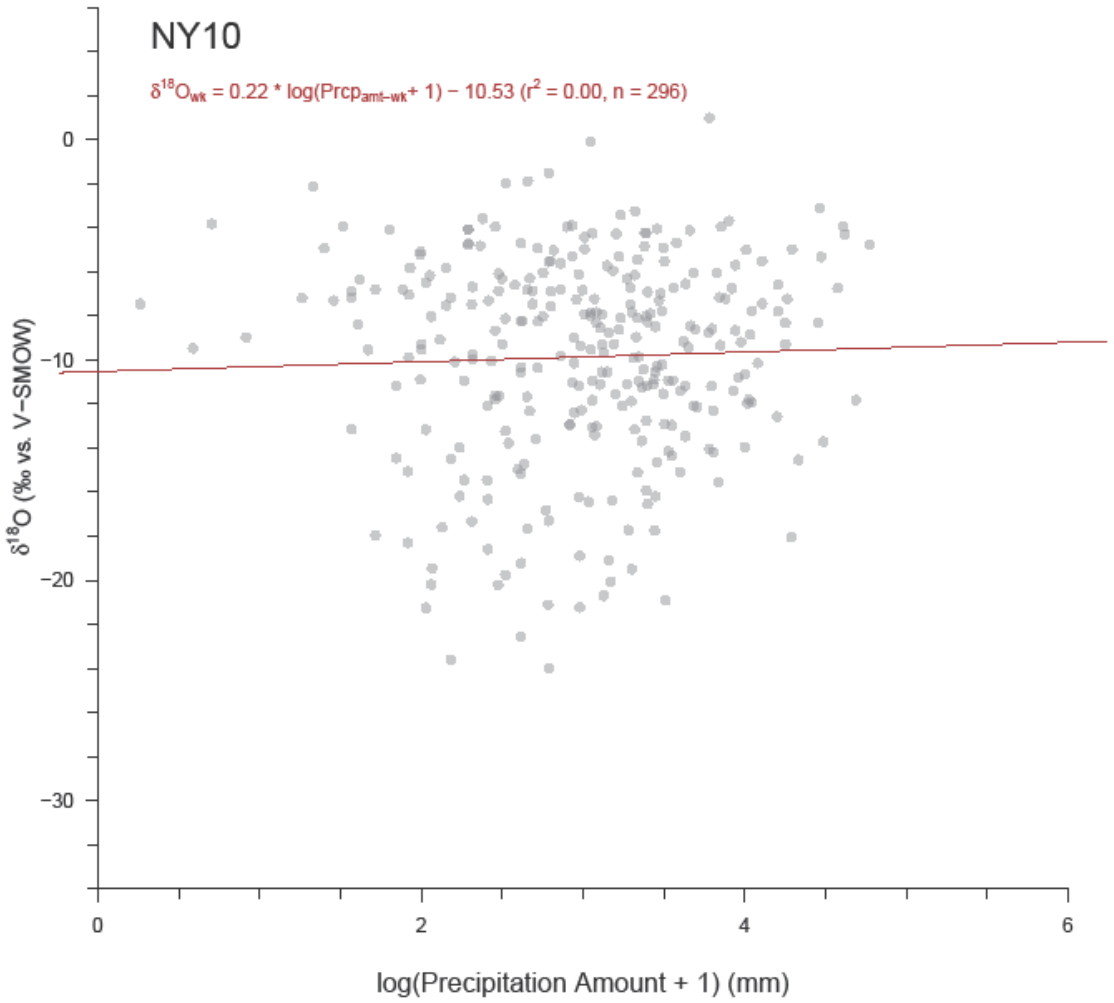

Figure A5.S3. Relationship between precipitation $\delta^{18}O$ and PDa at site NY10. Actual precipitation amounts were normalized by a log transformation. Gray circles represent values at their original weekly resolution with the weekly linear trend plotted in red. Precipitation amount data cannot be weight-averaged for aggregation, and thus regression was only performed at weekly resolution.

OH49

Table A5.T1. Regression results for OH49 at weekly, monthly, and seasonal resolutions. Significant results ($p \leq 0.05$) are bolded, while insignificant results are italicized. Actual precipitation amounts were normalized by a log transformation. Precipitation amount data cannot be weight-averaged for aggregation, and thus regression was only performed at weekly resolution.

LMWL (δD vs. δ^{18}O)							
Resolution	***n***	***Slope***		***y-Int***		***r^2***	***p-value***
Weekly	**249**	**7.93**	**±0.05**	**12.76**	**±0.46**	**0.99**	**0.00**
Monthly	**119**	**7.94**	**±0.06**	**12.74**	**±0.57**	**0.99**	**0.00**
Seasonal	**56**	**7.95**	**±0.09**	**13.13**	**±0.86**	**0.99**	**0.00**
δ^{18}O vs. PDt							
Resolution	***n***	***Slope***		***y-Int***		***r^2***	***p-value***
Weekly	**249**	**0.36**	**±0.03**	**-12.45**	**±0.38**	**0.45**	**0.00**
Monthly	**119**	**0.34**	**±0.03**	**-12.34**	**±0.50**	**0.47**	**0.00**
Seasonal	**56**	**0.33**	**±0.05**	**-12.45**	**±0.78**	**0.42**	**0.00**
δ^{18}O vs. PDa							
Resolution	***n***	***Slope***		***y-Int***		***r^2***	***p-value***
Weekly	*249*	*-0.18*	*±0.36*	*-7.45*	*±1.12*	*0.00*	*0.62*

Table A5.T2. Percent change in OH49 regression values (Table A5.T1) due to aggregation.

LMWL (δD vs. δ^{18}O)					
Aggregation	***Slope***	***Slope Error***	***y-Int***	***y-Int Error***	***r^2***
Weekly-Monthly	0%	26%	0%	25%	0%
Weekly-Seasonal	0%	70%	3%	72%	0%
Monthly-Seasonal	0%	33%	3%	34%	0%
δ^{18}O vs. PDt					
Aggregation	***Slope***	***Slope Error***	***y-Int***	***y-Int Error***	***r^2***
Weekly-Monthly	-6%	32%	-1%	32%	4%
Weekly-Seasonal	-7%	84%	0%	80%	-6%
Monthly-Seasonal	-1%	37%	1%	36%	-11%

Table A5.T3. OH49 temperature estimates and standard errors for three $\delta^{18}O$ values (vs. V-SMOW) at weekly, monthly, and seasonal resolutions. The three $\delta^{18}O$ values span much of the natural range of precipitation $\delta^{18}O$ in the study region, and -6‰ is close to the mean $\delta^{18}O$ value of all sites.

	Temperature Estimate (°C) when Precipitation $\delta^{18}O$ =		
Aggregation	***-20‰***	***-6‰***	***0‰***
Weekly	-2.7 ±12.5	15.0 ±12.4	22.6 ±12.4
Monthly	-3.9 ±12.5	15.5 ±12.1	23.8 ±12.3
Seasonal	-2.3 ±13.0	15.4 ±12.2	23.0 ±12.6

Table A5.T4. Weight-averaged weekly values of $\delta^{18}O$ and average surface temperature for OH49 grouped by month and season. Blue (red) cells show low (high) values of note.

Group	***n***	***$\delta^{18}O_{wt}$***	***PDt***
Jan	27	-11.25 ±1.13	2.5 ±0.9
Feb	19	-11.28 ±1.11	3.0 ±0.8
Mar	23	-9.68 ±0.91	7.6 ±1.0
Apr	20	-6.71 ±0.71	11.5 ±0.9
May	16	-7.14 ±1.06	17.1 ±0.7
Jun	27	-5.28 ±0.50	20.6 ±0.6
Jul	21	-4.21 ±0.29	24.4 ±0.4
Aug	15	-5.16 ±0.61	21.6 ±0.7
Sep	18	-6.33 ±0.64	19.7 ±0.8
Oct	24	-8.39 ±0.60	13.7 ±0.8
Nov	23	-8.73 ±0.64	9.4 ±0.7
Dec	16	-11.76 ±0.96	3.7 ±1.6
Win	62	-11.29 ±0.64	3.1 ±0.6
Spr	59	-8.60 ±0.56	11.4 ±0.8
Sum	63	-4.90 ±0.28	22.5 ±0.4
Aut	65	-8.16 ±0.39	13.9 ±0.7

Table A5.T5. Regression results for OH49 when weekly data is grouped by month and by season. Significant results ($p \leq 0.05$) are bolded, while insignificant results are italicized. Actual precipitation amounts were normalized by a log transformation. Blue (red) cells show low (high) values of note.

LMWL (δD vs. $\delta^{18}O$)							
Group	***n***	***Slope***		***y-Int***		***r^2***	***p-value***
Jan	**27**	**8.00**	**±0.08**	**13.41**	**±1.09**	**1.00**	**0.00**
Feb	**19**	**8.22**	**±0.29**	**14.96**	**±3.35**	**0.98**	**0.00**
Mar	**23**	**8.04**	**±0.16**	**13.67**	**±1.78**	**0.99**	**0.00**
Apr	**20**	**7.88**	**±0.25**	**12.29**	**±1.74**	**0.98**	**0.00**
May	**16**	**7.93**	**±0.12**	**12.87**	**±0.91**	**1.00**	**0.00**
Jun	**27**	**7.84**	**±0.19**	**11.31**	**±1.17**	**0.99**	**0.00**
Jul	**21**	**7.50**	**±0.46**	**10.36**	**±2.11**	**0.93**	**0.00**
Aug	**15**	**7.84**	**±0.26**	**11.77**	**±1.40**	**0.99**	**0.00**
Sep	**18**	**7.44**	**±0.31**	**8.40**	**±1.94**	**0.97**	**0.00**
Oct	**24**	**8.07**	**±0.30**	**14.77**	**±2.66**	**0.97**	**0.00**
Nov	**23**	**7.90**	**±0.26**	**14.61**	**±2.31**	**0.98**	**0.00**
Dec	**16**	**8.52**	**±0.23**	**21.38**	**±2.95**	**0.99**	**0.00**
Win	**62**	**8.11**	**±0.10**	**14.90**	**±1.32**	**0.99**	**0.00**
Spr	**59**	**7.97**	**±0.09**	**12.99**	**±0.80**	**0.99**	**0.00**
Sum	**63**	**7.83**	**±0.14**	**11.55**	**±0.78**	**0.98**	**0.00**
Aut	**65**	**7.68**	**±0.16**	**11.48**	**±1.32**	**0.97**	**0.00**
$\delta^{18}O$ vs. PDt							
Group	***n***	***Slope***		***y-Int***		***r^2***	***p-value***
Jan	**27**	**0.65**	**±0.21**	**-13.29**	**±1.05**	**0.29**	**0.00**
Feb	**19**	**0.62**	**±0.29**	**-12.94**	**±1.48**	**0.21**	**0.05**
Mar	**23**	**0.64**	**±0.13**	**-14.29**	**±1.10**	**0.53**	**0.00**
Apr	**20**	**0.40**	**±0.16**	**-11.15**	**±2.08**	**0.25**	**0.02**
May	*16*	*0.41*	*±0.37*	*-12.80*	*±6.35*	*0.08*	*0.29*
Jun	*27*	*-0.01*	*±0.17*	*-5.38*	*±3.52*	*0.00*	*0.95*
Jul	*21*	*0.26*	*±0.17*	*-10.62*	*±4.20*	*0.10*	*0.15*
Aug	**15**	**0.68**	**±0.18**	**-19.83**	**±3.86**	**0.54**	**0.00**
Sep	*18*	*0.18*	*±0.20*	*-9.07*	*±3.94*	*0.05*	*0.39*
Oct	*24*	*0.08*	*±0.16*	*-9.43*	*±2.29*	*0.01*	*0.63*
Nov	**23**	**0.46**	**±0.18**	**-12.56**	**±1.71**	**0.23**	**0.02**
Dec	**16**	**0.39**	**±0.12**	**-13.49**	**±0.86**	**0.43**	**0.01**
Win	**62**	**0.54**	**±0.11**	**-13.17**	**±0.64**	**0.28**	**0.00**
Spr	**59**	**0.48**	**±0.08**	**-13.09**	**±0.96**	**0.41**	**0.00**

Sum	**63**	**0.22**	**±0.09**	**-9.97**	**±2.00**	**0.09**	**0.02**
Aut	**65**	**0.25**	**±0.07**	**-10.99**	**±0.97**	**0.18**	**0.00**
δ^{18}O vs. PDa							
Group	***n***	***Slope***		***y-Int***		***r^2***	***p-value***
Jan	*27*	*2.44*	*±1.36*	*-19.27*	*±4.18*	*0.11*	*0.09*
Feb	*19*	*-2.91*	*±1.43*	*-1.78*	*±4.47*	*0.20*	*0.06*
Mar	*23*	*-0.84*	*±1.09*	*-7.56*	*±3.26*	*0.03*	*0.45*
Apr	*20*	*0.55*	*±0.81*	*-7.82*	*±2.39*	*0.02*	*0.51*
May	*16*	*-2.01*	*±1.54*	*0.31*	*±4.93*	*0.11*	*0.21*
Jun	*27*	*-1.08*	*±0.57*	*-2.11*	*±1.90*	*0.13*	*0.07*
Jul	*21*	*-0.66*	*±0.32*	*-2.26*	*±1.08*	*0.18*	*0.06*
Aug	*15*	*-0.61*	*±0.85*	*-2.95*	*±2.72*	*0.04*	*0.48*
Sep	**18**	**-1.83**	**±0.78**	**-0.55**	**±2.24**	**0.25**	**0.03**
Oct	*24*	*-1.65*	*±0.79*	*-3.47*	*±2.40*	*0.17*	*0.05*
Nov	*23*	*-0.57*	*±0.88*	*-6.90*	*±2.61*	*0.02*	*0.52*
Dec	*16*	*2.21*	*±1.44*	*-18.53*	*±4.26*	*0.14*	*0.15*
Win	*62*	*0.90*	*±0.87*	*-14.32*	*±2.67*	*0.02*	*0.31*
Spr	*59*	*-0.37*	*±0.69*	*-6.57*	*±2.09*	*0.01*	*0.60*
Sum	**63**	**-0.84**	**±0.33**	**-2.34**	**±1.10**	**0.09**	**0.01**
Aut	**65**	**-1.45**	**±0.51**	**-3.49**	**±1.51**	**0.11**	**0.01**

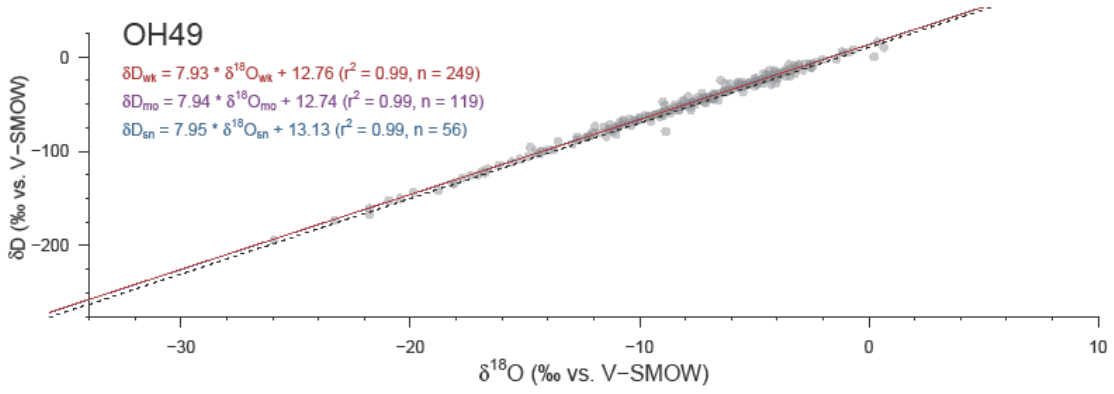

Figure A5.T1. Local meteoric water line for OH49. Gray circles represent values at their original weekly resolution while linear trends are plotted for weekly (red), aggregated monthly (violet), and aggregated seasonal (blue) resolutions. The dashed black line represents the global meteoric water line.

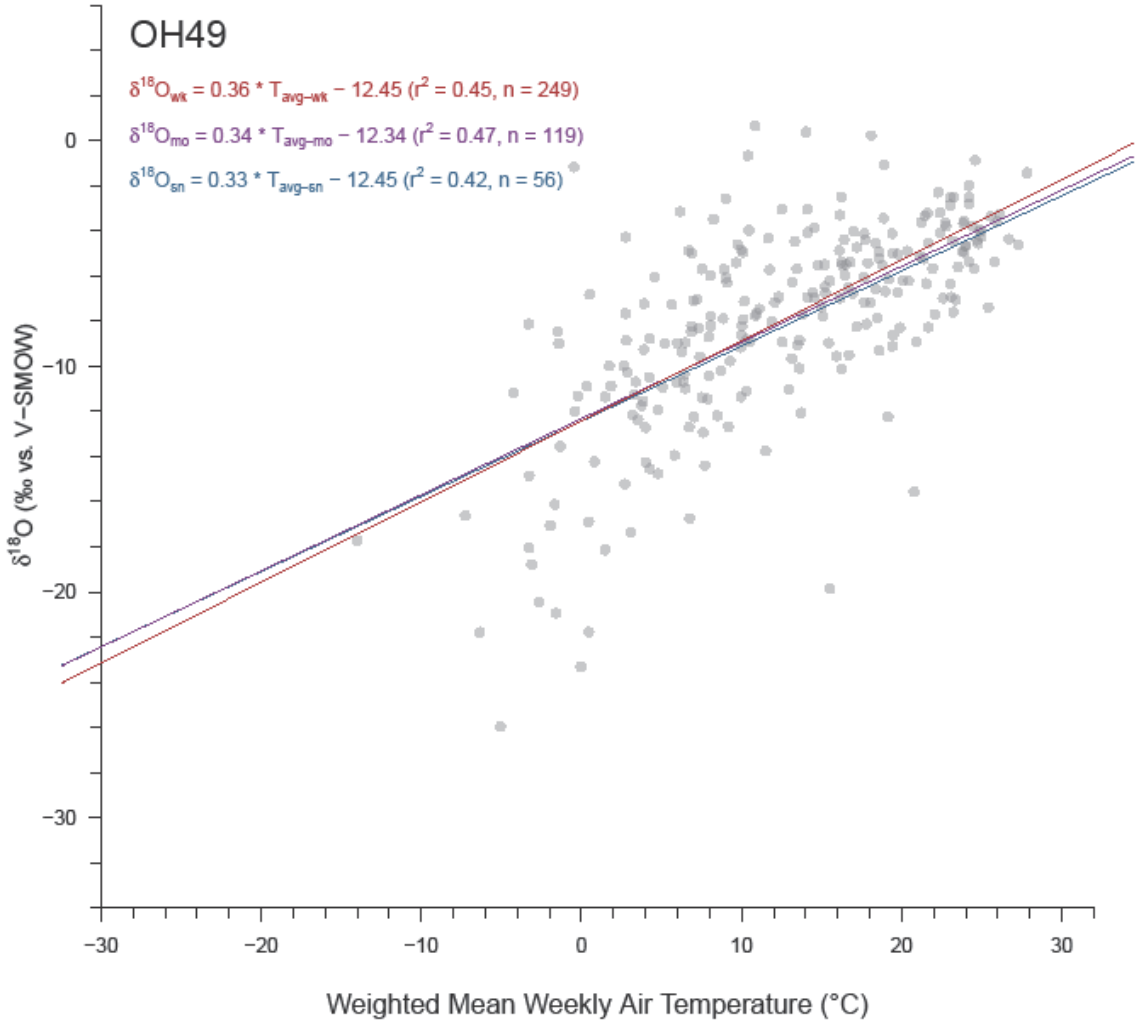

Figure A5.T2. Relationship between precipitation $\delta^{18}O$ and mean PDt at site OH49. Gray circles represent values at their original weekly resolution while linear trends are plotted for weekly (red), aggregated monthly (violet), and aggregated seasonal (blue) resolutions.

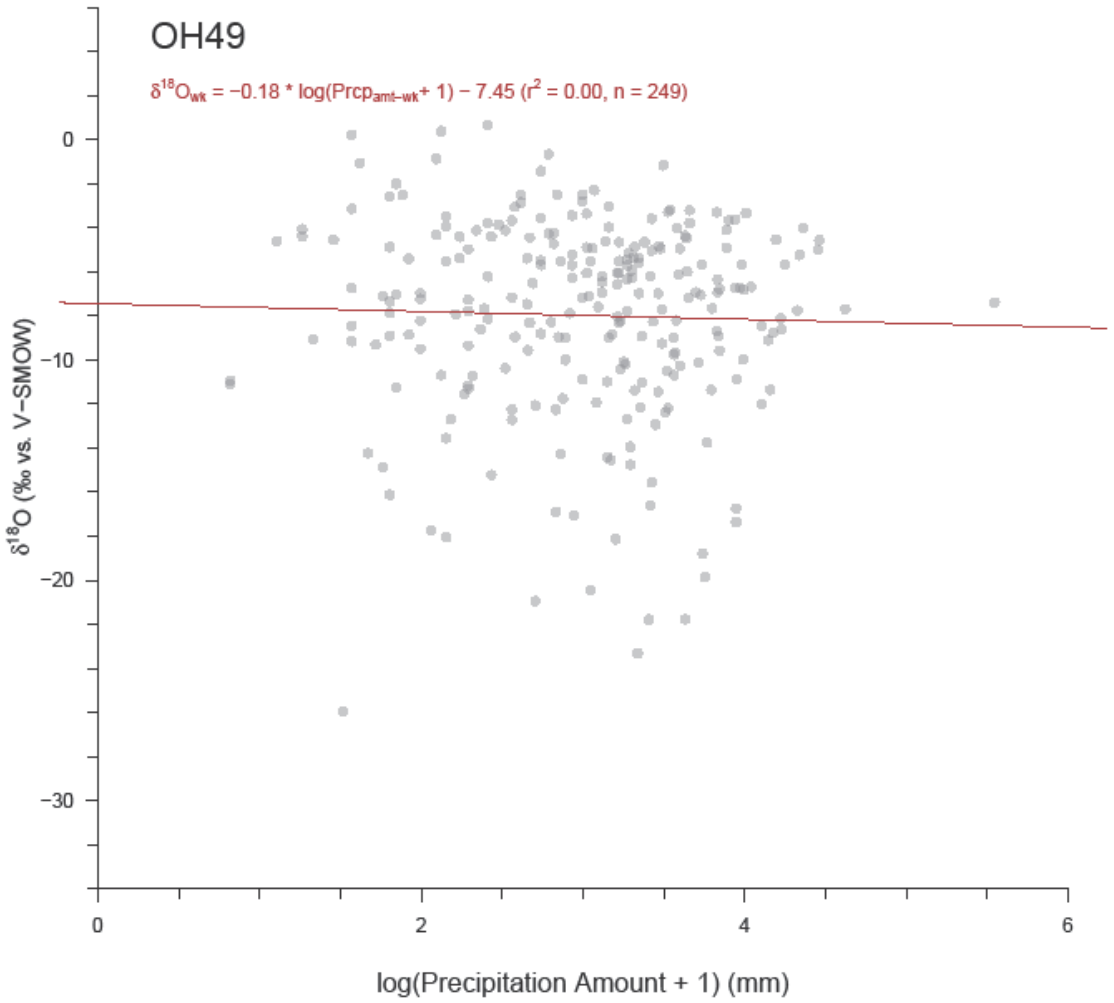

Figure A5.T3. Relationship between precipitation $\delta^{18}O$ and PDa at site OH49. Actual precipitation amounts were normalized by a log transformation. Gray circles represent values at their original weekly resolution with the weekly linear trend plotted in red. Precipitation amount data cannot be weight-averaged for aggregation, and thus regression was only performed at weekly resolution.

PA15

Table A5.U1. Regression results for PA15 at weekly, monthly, and seasonal resolutions. Significant results ($p \leq 0.05$) are bolded, while insignificant results are italicized. Actual precipitation amounts were normalized by a log transformation. Precipitation amount data cannot be weight-averaged for aggregation, and thus regression was only performed at weekly resolution.

LMWL (δD vs. δ^{18}O)							
Resolution	***n***	***Slope***		***y-Int***		***r^2***	***p-value***
Weekly	**50**	**7.86**	**±0.16**	**13.52**	**±1.44**	**0.98**	**0.00**
Monthly	**27**	**7.78**	**±0.24**	**12.56**	**±2.16**	**0.98**	**0.00**
Seasonal	**13**	**7.50**	**±0.28**	**10.41**	**±2.60**	**0.98**	**0.00**
δ^{18}O vs. PDt							
Resolution	***n***	***Slope***		***y-Int***		***r^2***	***p-value***
Weekly	**50**	**0.32**	**±0.06**	**-12.03**	**±0.86**	**0.37**	**0.00**
Monthly	**27**	**0.22**	**±0.06**	**-10.88**	**±0.89**	**0.32**	**0.00**
Seasonal	**13**	**0.27**	**±0.07**	**-11.81**	**±1.01**	**0.55**	**0.00**
δ^{18}O vs. PDa							
Resolution	***n***	***Slope***		***y-Int***		***r^2***	***p-value***
Weekly	*50*	*0.53*	*±0.73*	*-9.78*	*±2.18*	*0.01*	*0.47*

Table A5.U2. Percent change in PA15 regression values (Table A5.U1) due to aggregation.

LMWL (δD vs. δ^{18}O)					
Aggregation	***Slope***	***Slope Error***	***y-Int***	***y-Int Error***	***r^2***
Weekly-Monthly	-1%	57%	-7%	50%	-1%
Weekly-Seasonal	-5%	53%	-25%	54%	0%
Monthly-Seasonal	-4%	14%	-21%	17%	1%
δ^{18}O vs. PDt					
Aggregation	***Slope***	***Slope Error***	***y-Int***	***y-Int Error***	***r^2***
Weekly-Monthly	-33%	4%	-10%	4%	-14%
Weekly-Seasonal	-24%	20%	-2%	17%	57%
Monthly-Seasonal	20%	14%	8%	11%	42%

Table A5.U3. PA15 temperature estimates and standard errors for three $\delta^{18}O$ values (vs. V-SMOW) at weekly, monthly, and seasonal resolutions. The three $\delta^{18}O$ values span much of the natural range of precipitation $\delta^{18}O$ in the study region, and -6‰ is close to the mean $\delta^{18}O$ value of all sites.

	Temperature Estimate (°C) when Precipitation $\delta^{18}O$ =					
Aggregation	***-20‰***		***-6‰***		***0‰***	
Weekly	-1.7	±13.8	14.2	±12.9	21.1	±13.4
Monthly	-5.3	±17.1	15.2	±13.8	24.0	±15.5
Seasonal	-11.6	±18.7	16.9	±13.1	29.1	±16.6

Table A5.U4. Weight-averaged weekly values of $\delta^{18}O$ and average surface temperature for PA15 grouped by month and season. Blue (red) cells show low (high) values of note.

Group	***n***	***$\delta^{18}O_{wt}$***		***PDt***	
Jan	3	-9.26	±5.99	6.6	±3.2
Feb	5	-10.92	±2.23	2.1	±1.9
Mar	2	-8.64	±0.70	7.1	±1.8
Apr	4	-8.35	±1.68	11.7	±2.3
May	4	-5.54	±1.12	14.1	±1.4
Jun	5	-6.65	±1.09	21.6	±0.8
Jul	2	-6.67	±1.63	22.6	±1.0
Aug	4	-4.91	±1.12	24.1	±1.8
Sep	3	-7.41	±2.11	20.2	±1.8
Oct	4	-6.51	±1.53	12.9	±1.7
Nov	7	-9.61	±1.38	8.3	±1.2
Dec	7	-10.67	±0.88	3.9	±0.4
Win	15	-11.04	±1.31	3.5	±0.9
Spr	10	-7.16	±0.97	11.9	±1.3
Sum	11	-6.15	±0.69	22.4	±0.8
Aut	14	-8.54	±1.03	12.9	±1.5

Table A5.U5. Regression results for PA15 when weekly data is grouped by month and by season. Significant results ($p \leq 0.05$) are bolded, while insignificant results are italicized. Actual precipitation amounts were normalized by a log transformation. Blue (red) cells show low (high) values of note.

LMWL (δD vs. $\delta^{18}O$)							
Group	***n***	***Slope***		***y-Int***		***r^2***	***p-value***
Jan	**3**	**8.06**	**±0.08**	**14.44**	**±1.15**	**1.00**	**0.01**
Feb	**5**	**8.37**	**±0.26**	**17.90**	**±3.10**	**1.00**	**0.00**
Mar	*2*	-	-	-	-	-	-
Apr	**4**	**9.01**	**±1.31**	**20.85**	**±11.95**	**0.96**	**0.02**
May	**4**	**7.61**	**±0.44**	**10.04**	**±2.29**	**0.99**	**0.00**
Jun	**5**	**7.84**	**±0.50**	**10.52**	**±3.15**	**0.99**	**0.00**
Jul	*2*	-	-	-	-	-	-
Aug	**4**	**7.15**	**±0.89**	**9.95**	**±4.36**	**0.97**	**0.02**
Sep	**3**	**9.07**	**±0.23**	**20.03**	**±1.48**	**1.00**	**0.02**
Oct	**4**	**7.32**	**±1.36**	**10.44**	**±10.47**	**0.94**	**0.03**
Nov	**7**	**7.84**	**±0.44**	**18.30**	**±4.91**	**0.98**	**0.00**
Dec	**7**	**8.04**	**±0.89**	**18.13**	**±9.04**	**0.94**	**0.00**
Win	**15**	**8.21**	**±0.21**	**17.84**	**±2.49**	**0.99**	**0.00**
Spr	**10**	**8.38**	**±0.47**	**14.55**	**±3.65**	**0.98**	**0.00**
Sum	**11**	**7.76**	**±0.37**	**11.41**	**±2.23**	**0.98**	**0.00**
Aut	**14**	**7.58**	**±0.36**	**13.73**	**±3.38**	**0.97**	**0.00**
$\delta^{18}O$ vs. PDt							
Group	***n***	***Slope***		***y-Int***		***r^2***	***p-value***
Jan	*3*	*1.84*	*±0.48*	*-22.33*	*±3.37*	*0.94*	*0.16*
Feb	*5*	*0.60*	*±0.57*	*-12.07*	*±2.49*	*0.27*	*0.37*
Mar	*2*	-	-	-	-	-	-
Apr	*4*	*-0.34*	*±0.46*	*-4.92*	*±5.46*	*0.21*	*0.54*
May	*4*	*0.34*	*±0.54*	*-9.72*	*±7.66*	*0.17*	*0.59*
Jun	*5*	*-0.63*	*±0.70*	*7.60*	*±14.94*	*0.22*	*0.43*
Jul	*2*	-	-	-	-	-	-
Aug	*4*	*0.51*	*±0.27*	*-16.87*	*±6.45*	*0.65*	*0.19*
Sep	*3*	*0.67*	*±0.95*	*-19.36*	*±19.36*	*0.33*	*0.61*
Oct	*4*	*0.29*	*±0.61*	*-10.49*	*±7.18*	*0.10*	*0.69*
Nov	**7**	**0.93**	**±0.31**	**-18.12**	**±2.64**	**0.65**	**0.03**
Dec	*7*	*-0.63*	*±0.91*	*-7.22*	*±3.94*	*0.09*	*0.52*
Win	**15**	**0.88**	**±0.33**	**-13.97**	**±1.64**	**0.36**	**0.02**
Spr	*10*	*0.14*	*±0.25*	*-8.77*	*±3.09*	*0.04*	*0.59*

Sum	*11*	*0.23*	*±0.28*	*-10.77*	*±6.38*	*0.07*	*0.43*
Aut	**14**	**0.47**	**±0.14**	**-14.02**	**±1.81**	**0.48**	**0.01**
δ^{18}O vs. PDa							
Group	***n***	***Slope***		***y-Int***		***r^2***	***p-value***
Jan	*3*	*12.73*	*±9.94*	*-37.04*	*±20.01*	*0.62*	*0.42*
Feb	*5*	*2.43*	*±2.61*	*-17.15*	*±7.15*	*0.22*	*0.42*
Mar	*2*	*-*	*-*	*-*	*-*	*-*	*-*
Apr	*4*	*0.65*	*±5.33*	*-10.83*	*±17.82*	*0.01*	*0.91*
May	*4*	*-0.54*	*±1.16*	*-3.46*	*±3.33*	*0.10*	*0.69*
Jun	*5*	*-1.40*	*±1.20*	*-1.62*	*±3.85*	*0.31*	*0.33*
Jul	*2*	*-*	*-*	*-*	*-*	*-*	*-*
Aug	*4*	*-2.15*	*±2.72*	*2.33*	*±8.75*	*0.24*	*0.51*
Sep	*3*	*-0.78*	*±2.89*	*-3.71*	*±8.44*	*0.07*	*0.83*
Oct	*4*	*2.45*	*±2.19*	*-13.69*	*±5.97*	*0.38*	*0.38*
Nov	*7*	*-1.43*	*±2.16*	*-6.34*	*±6.52*	*0.08*	*0.54*
Dec	*7*	*-1.13*	*±1.17*	*-6.55*	*±3.59*	*0.16*	*0.38*
Win	*15*	*1.89*	*±1.51*	*-15.66*	*±4.19*	*0.11*	*0.23*
Spr	*10*	*-0.92*	*±1.14*	*-4.48*	*±3.43*	*0.08*	*0.44*
Sum	*11*	*-1.67*	*±0.93*	*-0.23*	*±3.02*	*0.26*	*0.11*
Aut	*14*	*-0.71*	*±1.38*	*-6.61*	*±4.04*	*0.02*	*0.62*

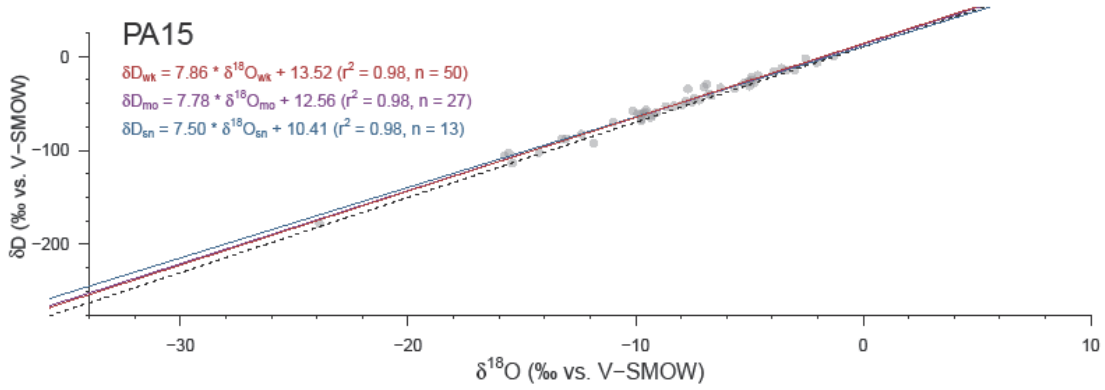

Figure A5.U1. Local meteoric water line for PA15. Gray circles represent values at their original weekly resolution while linear trends are plotted for weekly (red), aggregated monthly (violet), and aggregated seasonal (blue) resolutions. The dashed black line represents the global meteoric water line.

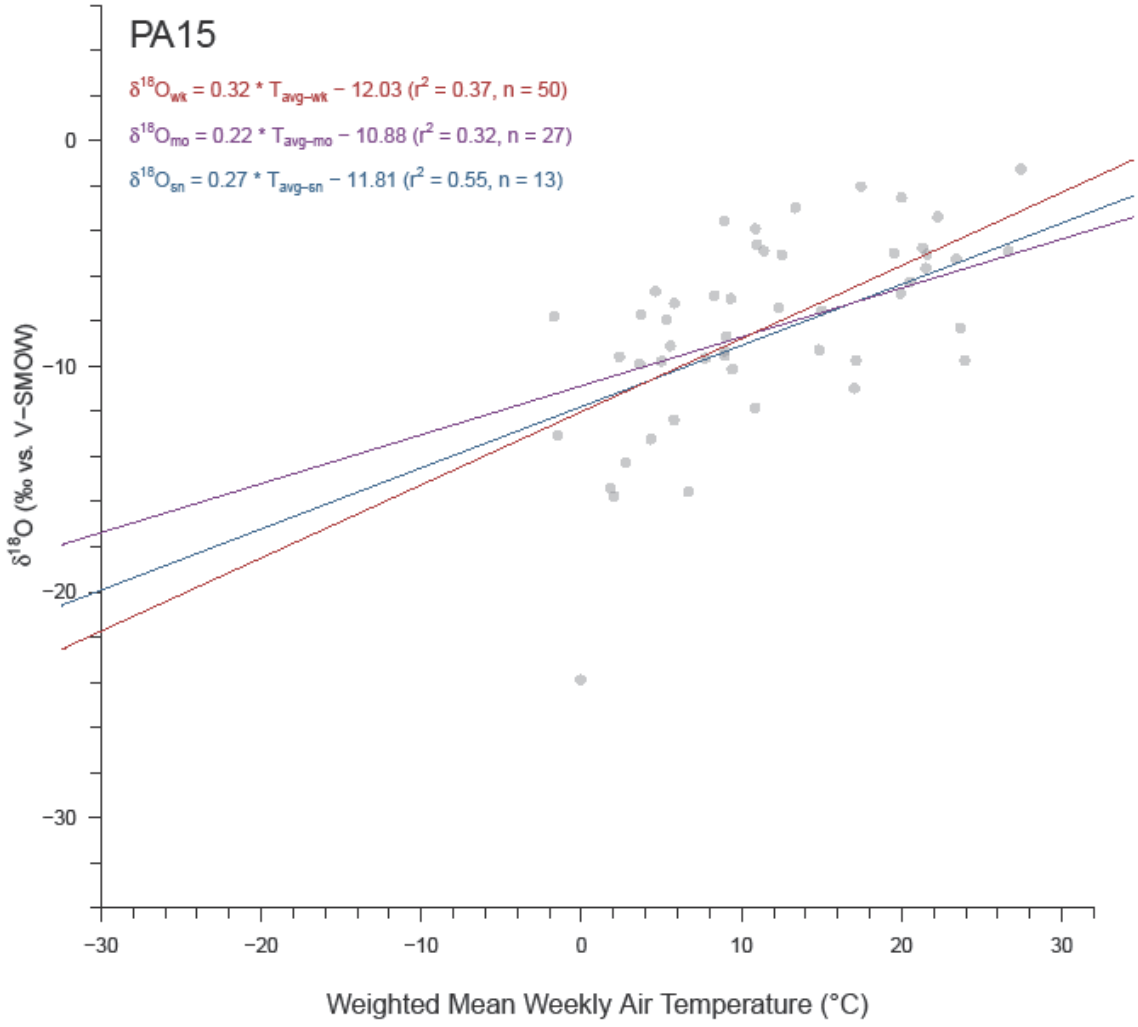

Figure A5.U2. Relationship between precipitation $\delta^{18}O$ and mean PDt at site PA15. Gray circles represent values at their original weekly resolution while linear trends are plotted for weekly (red), aggregated monthly (violet), and aggregated seasonal (blue) resolutions.

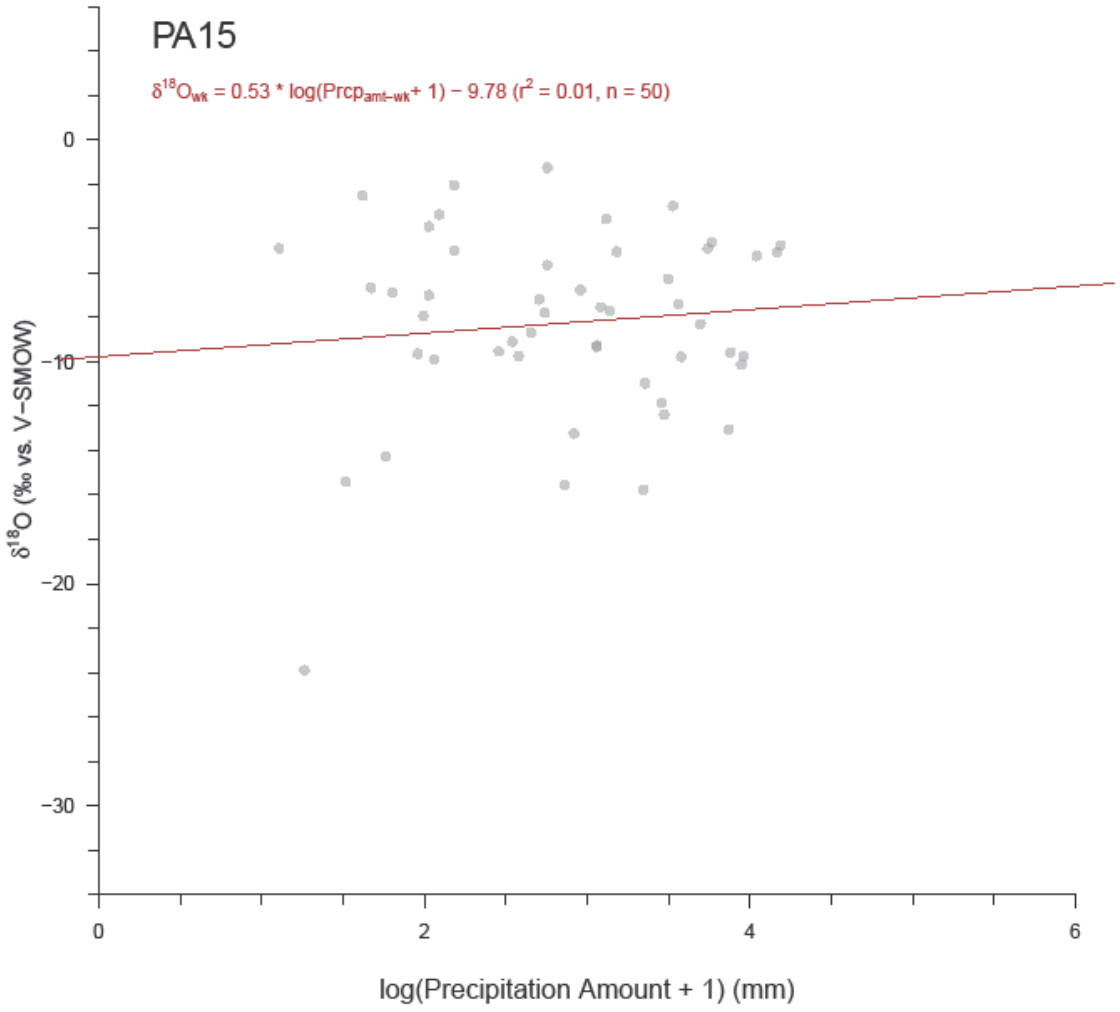

Figure A5.U3. Relationship between precipitation $\delta^{18}O$ and PDa at site PA15. Actual precipitation amounts were normalized by a log transformation. Gray circles represent values at their original weekly resolution with the weekly linear trend plotted in red. Precipitation amount data cannot be weight-averaged for aggregation, and thus regression was only performed at weekly resolution.

TN00

Table A5.V1. Regression results for TN00 at weekly, monthly, and seasonal resolutions. Significant results ($p \leq 0.05$) are bolded, while insignificant results are italicized. Actual precipitation amounts were normalized by a log transformation. Precipitation amount data cannot be weight-averaged for aggregation, and thus regression was only performed at weekly resolution.

LMWL (δD vs. δ^{18}O)							
Resolution	***n***	***Slope***		***y-Int***		***r^2***	***p-value***
Weekly	**213**	**8.27**	**±0.14**	**14.39**	**±0.94**	**0.95**	**0.00**
Monthly	**101**	**8.27**	**±0.18**	**14.63**	**±1.15**	**0.96**	**0.00**
Seasonal	**45**	**8.27**	**±0.30**	**15.03**	**±1.93**	**0.95**	**0.00**
δ^{18}O vs. PDt							
Resolution	***n***	***Slope***		***y-Int***		***r^2***	***p-value***
Weekly	**213**	**0.25**	**±0.02**	**-10.09**	**±0.42**	**0.34**	**0.00**
Monthly	**101**	**0.18**	**±0.03**	**-8.99**	**±0.53**	**0.27**	**0.00**
Seasonal	**45**	**0.17**	**±0.04**	**-8.84**	**±0.76**	**0.26**	**0.00**
δ^{18}O vs. PDa							
Resolution	***n***	***Slope***		***y-Int***		***r^2***	***p-value***
Weekly	*213*	*-0.46*	*±0.25*	*-4.65*	*±0.84*	*0.02*	*0.07*

Table A5.V2. Percent change in TN00 regression values (Table A5.V1) due to aggregation.

LMWL (δD vs. δ^{18}O)					
Aggregation	***Slope***	***Slope Error***	***y-Int***	***y-Int Error***	***r^2***
Weekly-Monthly	0%	31%	2%	23%	1%
Weekly-Seasonal	0%	93%	4%	87%	0%
Monthly-Seasonal	0%	41%	3%	41%	-1%
δ^{18}O vs. PDt					
Aggregation	***Slope***	***Slope Error***	***y-Int***	***y-Int Error***	***r^2***
Weekly-Monthly	-28%	23%	-11%	26%	-19%
Weekly-Seasonal	-41%	69%	-14%	64%	-27%
Monthly-Seasonal	-3%	33%	-2%	30%	-3%

Table A5.V3. TN00 temperature estimates and standard errors for three $\delta^{18}O$ values (vs. V-SMOW) at weekly, monthly, and seasonal resolutions. The three $\delta^{18}O$ values span much of the natural range of precipitation $\delta^{18}O$ in the study region, and -6‰ is close to the mean $\delta^{18}O$ value of all sites.

	Temperature Estimate (°C) when Precipitation $\delta^{18}O$ =		
Aggregation	***-20‰***	***-6‰***	***0‰***
Weekly	-2.9 ±12.4	16.2 ±11.9	24.4 ±12.0
Monthly	-4.6 ±13.9	16.7 ±12.0	25.9 ±12.3
Seasonal	-5.2 ±15.7	16.1 ±11.2	25.3 ±12.2

Table A5.V4. Weight-averaged weekly values of $\delta^{18}O$ and average surface temperature for TN00 grouped by month and season. Blue (red) cells show low (high) values of note.

Group	***n***	***$\delta^{18}O_{wt}$***	***PDt***
Jan	18	-8.40 ±0.78	6.3 ±1.0
Feb	17	-7.54 ±0.82	8.5 ±1.0
Mar	25	-6.66 ±0.54	12.4 ±0.9
Apr	20	-5.64 ±0.82	15.1 ±0.9
May	14	-6.53 ±0.77	18.6 ±0.8
Jun	21	-4.51 ±0.36	23.3 ±0.5
Jul	20	-3.88 ±0.30	25.5 ±0.3
Aug	14	-4.38 ±0.52	25.1 ±0.5
Sep	11	-7.08 ±0.67	21.6 ±0.9
Oct	18	-6.37 ±0.54	18.1 ±0.7
Nov	21	-7.06 ±0.75	12.8 ±0.7
Dec	14	-6.14 ±0.97	7.8 ±1.1
Win	49	-7.22 ±0.49	7.4 ±0.6
Spr	59	-5.98 ±0.41	14.5 ±0.7
Sum	55	-4.31 ±0.22	23.9 ±0.3
Aut	50	-7.14 ±0.39	17.1 ±0.7

Table A5.V5. Regression results for TN00 when weekly data is grouped by month and by season. Significant results ($p \leq 0.05$) are bolded, while insignificant results are italicized. Actual precipitation amounts were normalized by a log transformation. Blue (red) cells show low (high) values of note.

LMWL (δD vs. $\delta^{18}O$)							
Group	***n***	***Slope***		***y-Int***		***r^2***	***p-value***
Jan	**18**	**7.53**	**±0.41**	**9.62**	**±3.86**	**0.95**	**0.00**
Feb	**17**	**8.25**	**±0.22**	**15.93**	**±2.01**	**0.99**	**0.00**
Mar	**25**	**9.79**	**±0.50**	**22.68**	**±3.63**	**0.94**	**0.00**
Apr	**20**	**7.42**	**±0.55**	**9.81**	**±3.51**	**0.91**	**0.00**
May	**14**	**8.83**	**±0.35**	**15.84**	**±2.19**	**0.98**	**0.00**
Jun	**21**	**8.36**	**±0.40**	**14.07**	**±1.97**	**0.96**	**0.00**
Jul	**20**	**7.82**	**±0.70**	**13.48**	**±2.77**	**0.87**	**0.00**
Aug	**14**	**8.05**	**±0.61**	**11.52**	**±2.83**	**0.93**	**0.00**
Sep	**11**	**10.38**	**±0.45**	**25.70**	**±2.91**	**0.98**	**0.00**
Oct	**18**	**9.07**	**±0.49**	**17.95**	**±3.24**	**0.96**	**0.00**
Nov	**21**	**7.49**	**±0.34**	**13.37**	**±2.55**	**0.96**	**0.00**
Dec	**14**	**9.89**	**±0.65**	**26.64**	**±5.19**	**0.95**	**0.00**
Win	**49**	**8.48**	**±0.28**	**17.50**	**±2.47**	**0.95**	**0.00**
Spr	**59**	**8.51**	**±0.31**	**14.50**	**±2.12**	**0.93**	**0.00**
Sum	**55**	**8.22**	**±0.31**	**13.69**	**±1.41**	**0.93**	**0.00**
Aut	**50**	**8.16**	**±0.31**	**14.62**	**±2.17**	**0.93**	**0.00**
$\delta^{18}O$ vs. PDt							
Group	***n***	***Slope***		***y-Int***		***r^2***	***p-value***
Jan	**18**	**0.41**	**±0.16**	**-11.71**	**±1.32**	**0.29**	**0.02**
Feb	*17*	*0.34*	*±0.20*	*-11.15*	*±1.76*	*0.16*	*0.11*
Mar	**25**	**0.31**	**±0.10**	**-10.25**	**±1.25**	**0.28**	**0.01**
Apr	**20**	**0.60**	**±0.16**	**-14.26**	**±2.52**	**0.43**	**0.00**
May	*14*	*0.21*	*±0.27*	*-9.62*	*±5.05*	*0.05*	*0.44*
Jun	*21*	*0.07*	*±0.16*	*-6.35*	*±3.70*	*0.01*	*0.66*
Jul	**20**	**0.64**	**±0.14**	**-20.18**	**±3.68**	**0.53**	**0.00**
Aug	**14**	**0.84**	**±0.22**	**-25.38**	**±5.66**	**0.54**	**0.00**
Sep	*11*	*0.41*	*±0.20*	*-15.34*	*±4.70*	*0.30*	*0.08*
Oct	*18*	*0.17*	*±0.18*	*-9.29*	*±3.13*	*0.06*	*0.34*
Nov	**21**	**0.57**	**±0.19**	**-14.36**	**±2.70**	**0.31**	**0.01**
Dec	*14*	*0.30*	*±0.24*	*-9.50*	*±2.02*	*0.12*	*0.23*
Win	**49**	**0.36**	**±0.11**	**-10.91**	**±0.94**	**0.18**	**0.00**
Spr	**59**	**0.32**	**±0.07**	**-10.51**	**±1.07**	**0.26**	**0.00**

Sum	**55**	**0.35**	**±0.09**	**-12.93**	**±2.27**	**0.22**	**0.00**
Aut	**50**	**0.21**	**±0.08**	**-9.98**	**±1.37**	**0.13**	**0.01**
δ^{18}O vs. PDa							
Group	***n***	***Slope***		***y-Int***		***r^2***	***p-value***
Jan	*18*	*0.27*	*±1.30*	*-9.70*	*±4.34*	*0.00*	*0.84*
Feb	*17*	*1.56*	*±0.99*	*-13.76*	*±3.46*	*0.14*	*0.14*
Mar	*25*	*0.02*	*±0.61*	*-6.88*	*±2.05*	*0.00*	*0.97*
Apr	*20*	*-1.15*	*±0.82*	*-1.47*	*±2.78*	*0.10*	*0.18*
May	*14*	*-1.09*	*±1.76*	*-2.19*	*±5.63*	*0.03*	*0.55*
Jun	**21**	**-1.03**	**±0.27**	**-1.00**	**±1.00**	**0.44**	**0.00**
Jul	*20*	*-0.54*	*±0.28*	*-2.06*	*±0.91*	*0.18*	*0.07*
Aug	*14*	*-1.62*	*±0.74*	*0.95*	*±2.41*	*0.28*	*0.05*
Sep	*11*	*-0.68*	*±0.83*	*-3.57*	*±3.13*	*0.07*	*0.43*
Oct	**18**	**-1.29**	**±0.55**	**-2.40**	**±1.73**	**0.25**	**0.03**
Nov	*21*	*-0.22*	*±0.92*	*-5.94*	*±3.11*	*0.00*	*0.81*
Dec	*14*	*0.84*	*±1.34*	*-9.87*	*±4.28*	*0.03*	*0.54*
Win	*49*	*0.86*	*±0.67*	*-11.06*	*±2.24*	*0.03*	*0.20*
Spr	*59*	*-0.59*	*±0.48*	*-4.08*	*±1.60*	*0.03*	*0.22*
Sum	**55**	**-0.94**	**±0.20**	**-1.13**	**±0.68**	**0.30**	**0.00**
Aut	*50*	*-0.65*	*±0.44*	*-4.27*	*±1.49*	*0.04*	*0.15*

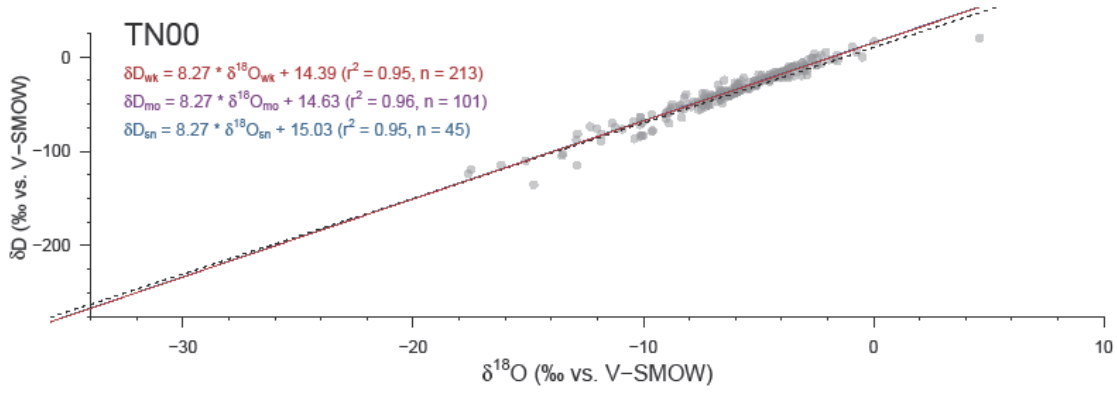

Figure A5.V1. Local meteoric water line for TN00. Gray circles represent values at their original weekly resolution while linear trends are plotted for weekly (red), aggregated monthly (violet), and aggregated seasonal (blue) resolutions. The dashed black line represents the global meteoric water line.

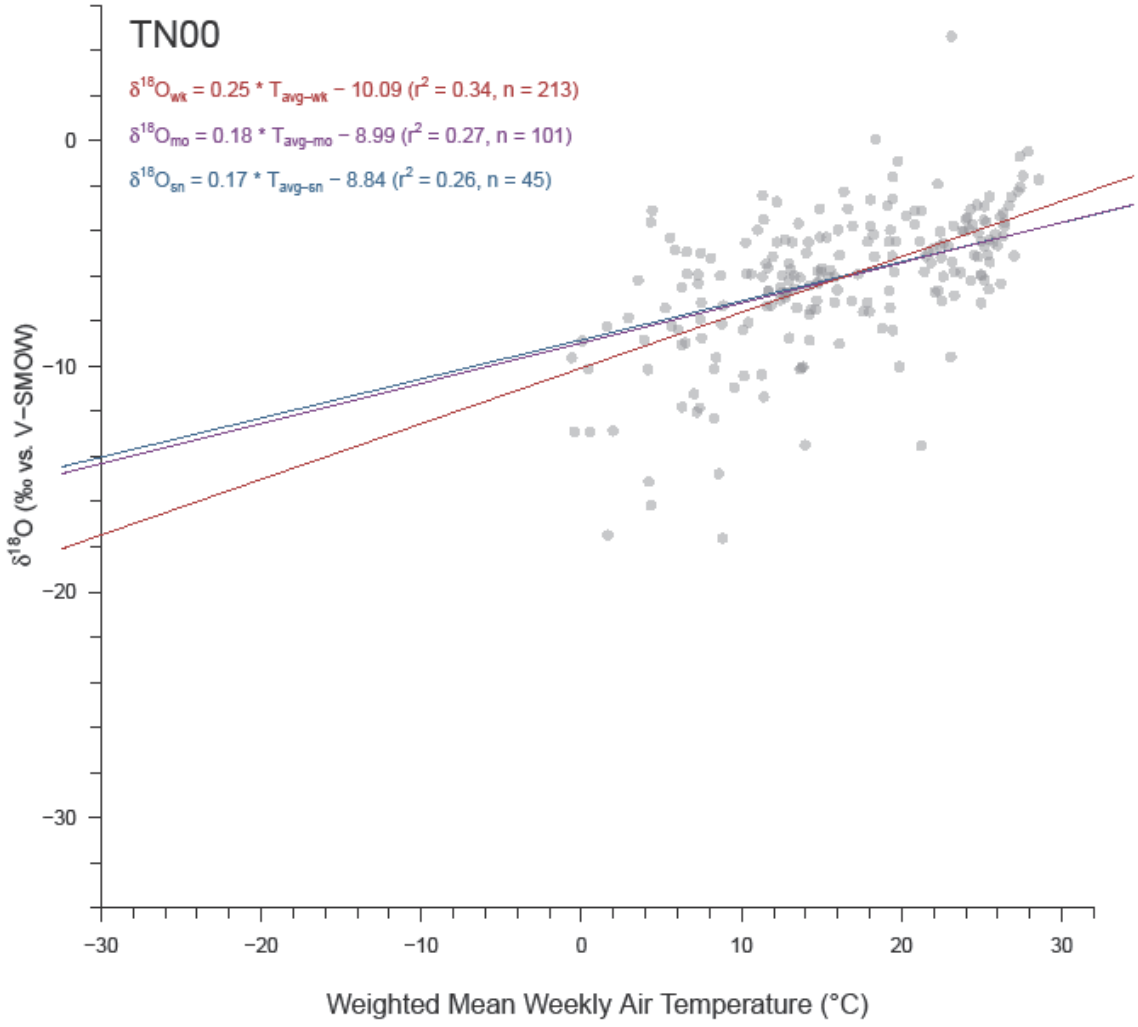

Figure A5.V2. Relationship between precipitation $\delta^{18}O$ and mean PDt at site TN00. Gray circles represent values at their original weekly resolution while linear trends are plotted for weekly (red), aggregated monthly (violet), and aggregated seasonal (blue) resolutions.

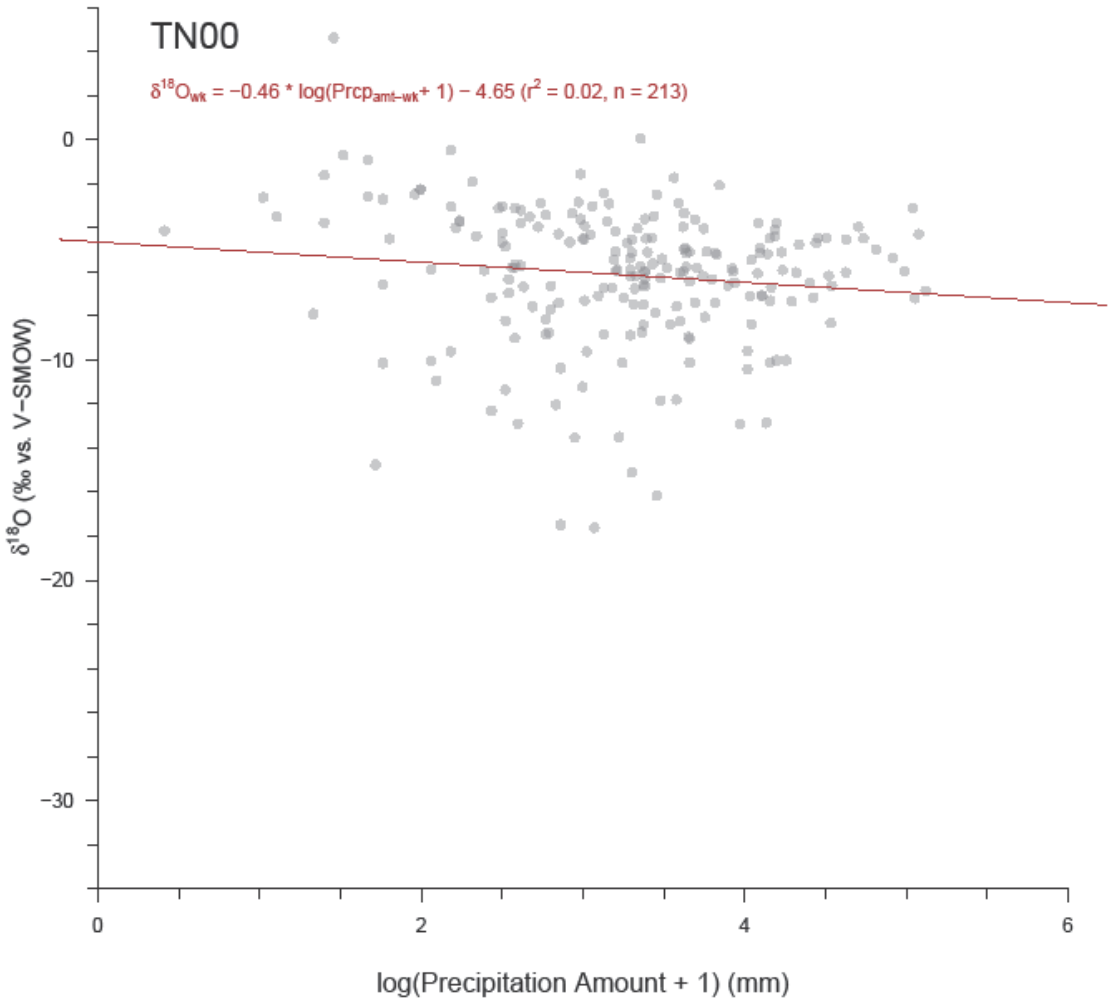

Figure A5.V3. Relationship between precipitation $\delta^{18}O$ and PDa at site TN00. Actual precipitation amounts were normalized by a log transformation. Gray circles represent values at their original weekly resolution with the weekly linear trend plotted in red. Precipitation amount data cannot be weight-averaged for aggregation, and thus regression was only performed at weekly resolution.

VT99

Table A5.W1. Regression results for VT99 at weekly, monthly, and seasonal resolutions. Significant results ($p \leq 0.05$) are bolded, while insignificant results are italicized. Actual precipitation amounts were normalized by a log transformation. Precipitation amount data cannot be weight-averaged for aggregation, and thus regression was only performed at weekly resolution.

LMWL (δD vs. $\delta^{18}O$)							
Resolution	***n***	***Slope***		***y-Int***		***r^2***	***p-value***
Weekly	**399**	**7.90**	**±0.04**	**10.33**	**±0.52**	**0.99**	**0.00**
Monthly	**164**	**7.91**	**±0.05**	**10.27**	**±0.63**	**0.99**	**0.00**
Seasonal	**60**	**7.93**	**±0.11**	**10.27**	**±1.20**	**0.99**	**0.00**
$\delta^{18}O$ vs. PDt							
Resolution	***n***	***Slope***		***y-Int***		***r^2***	***p-value***
Weekly	**399**	**0.34**	**±0.02**	**-14.01**	**±0.24**	**0.45**	**0.00**
Monthly	**164**	**0.32**	**±0.03**	**-13.97**	**±0.34**	**0.48**	**0.00**
Seasonal	**60**	**0.30**	**±0.03**	**-13.90**	**±0.38**	**0.63**	**0.00**
$\delta^{18}O$ vs. PDa							
Resolution	***n***	***Slope***		***y-Int***		***r^2***	***p-value***
Weekly	**399**	**0.90**	**±0.32**	**-13.72**	**±1.01**	**0.02**	**0.01**

Table A5.W2. Percent change in VT99 regression values (Table A5.W1) due to aggregation.

LMWL (δD vs. $\delta^{18}O$)					
Aggregation	***Slope***	***Slope Error***	***y-Int***	***y-Int Error***	***r^2***
Weekly-Monthly	0%	23%	-1%	20%	0%
Weekly-Seasonal	0%	114%	-1%	108%	0%
Monthly-Seasonal	0%	49%	0%	48%	0%
$\delta^{18}O$ vs. PDt					
Aggregation	***Slope***	***Slope Error***	***y-Int***	***y-Int Error***	***r^2***
Weekly-Monthly	-6%	38%	0%	38%	7%
Weekly-Seasonal	-12%	45%	-1%	42%	37%
Monthly-Seasonal	-6%	15%	-1%	13%	23%

Table A5.W3. VT99 temperature estimates and standard errors for three $\delta^{18}O$ values (vs. V-SMOW) at weekly, monthly, and seasonal resolutions. The three $\delta^{18}O$ values span much of the natural range of precipitation $\delta^{18}O$ in the study region, and -6‰ is close to the mean $\delta^{18}O$ value of all sites.

	Temperature Estimate (°C) when Precipitation $\delta^{18}O$ =		
Aggregation	***-20‰***	***-6‰***	***0‰***
Weekly	-3.1 ±13.8	15.5 ±13.8	23.5 ±13.8
Monthly	-4.2 ±12.8	17.0 ±12.7	26.1 ±12.9
Seasonal	-9.2 ±10.9	20.0 ±10.4	32.6 ±11.2

Table A5.W4. Weight-averaged weekly values of $\delta^{18}O$ and average surface temperature for VT99 grouped by month and season. Blue (red) cells show low (high) values of note.

Group	***n***	***$\delta^{18}O_{wt}$***	***PDt***
Jan	32	-15.67 ±1.08	-1.9 ±1.1
Feb	31	-15.37 ±0.81	-3.5 ±1.0
Mar	30	-11.74 ±0.84	2.7 ±0.7
Apr	29	-10.96 ±0.73	8.1 ±0.8
May	32	-9.20 ±0.62	13.9 ±0.5
Jun	34	-8.02 ±0.56	18.0 ±0.6
Jul	29	-7.78 ±0.37	20.4 ±0.5
Aug	31	-7.95 ±0.44	21.4 ±0.4
Sep	33	-8.63 ±0.41	16.4 ±0.5
Oct	43	-10.93 ±0.54	10.7 ±0.5
Nov	41	-12.82 ±0.64	5.8 ±0.6
Dec	34	-12.71 ±0.70	0.6 ±0.9
Win	97	-14.34 ±0.52	-1.8 ±0.6
Spr	91	-10.60 ±0.45	9.0 ±0.6
Sum	94	-7.97 ±0.27	20.0 ±0.3
Aut	117	-11.04 ±0.35	11.4 ±0.5

Table A5.W5. Regression results for VT99 when weekly data is grouped by month and by season. Significant results ($p \leq 0.05$) are bolded, while insignificant results are italicized. Actual precipitation amounts were normalized by a log transformation. Blue (red) cells show low (high) values of note.

LMWL (δD vs. $\delta^{18}O$)							
Group	***n***	***Slope***		***y-Int***		***r^2***	***p-value***
Jan	**32**	**7.74**	**±0.15**	**7.05**	**±2.67**	**0.99**	**0.00**
Feb	**31**	**7.87**	**±0.11**	**9.12**	**±1.77**	**0.99**	**0.00**
Mar	**30**	**7.78**	**±0.15**	**9.43**	**±2.09**	**0.99**	**0.00**
Apr	**29**	**8.06**	**±0.15**	**10.73**	**±1.66**	**0.99**	**0.00**
May	**32**	**7.91**	**±0.12**	**9.88**	**±1.17**	**0.99**	**0.00**
Jun	**34**	**8.08**	**±0.17**	**10.75**	**±1.48**	**0.99**	**0.00**
Jul	**29**	**8.12**	**±0.16**	**11.58**	**±1.26**	**0.99**	**0.00**
Aug	**31**	**7.66**	**±0.26**	**6.87**	**±2.14**	**0.97**	**0.00**
Sep	**33**	**7.83**	**±0.30**	**10.57**	**±2.47**	**0.96**	**0.00**
Oct	**43**	**7.93**	**±0.19**	**12.91**	**±2.11**	**0.98**	**0.00**
Nov	**41**	**7.78**	**±0.25**	**10.61**	**±3.10**	**0.96**	**0.00**
Dec	**34**	**8.45**	**±0.19**	**16.95**	**±2.60**	**0.98**	**0.00**
Win	**97**	**7.94**	**±0.09**	**10.32**	**±1.38**	**0.99**	**0.00**
Spr	**91**	**7.85**	**±0.08**	**9.42**	**±0.91**	**0.99**	**0.00**
Sum	**94**	**7.97**	**±0.12**	**9.84**	**±0.97**	**0.98**	**0.00**
Aut	**117**	**7.81**	**±0.12**	**11.03**	**±1.34**	**0.97**	**0.00**
$\delta^{18}O$ vs. PDt							
Group	***n***	***Slope***		***y-Int***		***r^2***	***p-value***
Jan	**32**	**0.39**	**±0.17**	**-15.27**	**±1.19**	**0.15**	**0.03**
Feb	**31**	**0.40**	**±0.14**	**-13.75**	**±0.90**	**0.22**	**0.01**
Mar	**30**	**0.63**	**±0.18**	**-14.43**	**±0.83**	**0.31**	**0.00**
Apr	*29*	*-0.01*	*±0.18*	*-10.56*	*±1.48*	*0.00*	*0.96*
May	*32*	*0.15*	*±0.24*	*-11.14*	*±3.22*	*0.01*	*0.54*
Jun	**34**	**0.60**	**±0.12**	**-18.66**	**±2.19**	**0.44**	**0.00**
Jul	**29**	**0.36**	**±0.13**	**-15.16**	**±2.74**	**0.22**	**0.01**
Aug	*31*	*0.14*	*±0.23*	*-10.69*	*±4.87*	*0.01*	*0.55*
Sep	**33**	**0.45**	**±0.12**	**-15.55**	**±2.06**	**0.31**	**0.00**
Oct	**43**	**0.52**	**±0.14**	**-16.24**	**±1.59**	**0.25**	**0.00**
Nov	**41**	**0.44**	**±0.15**	**-14.45**	**±1.04**	**0.18**	**0.01**
Dec	**34**	**0.45**	**±0.11**	**-12.70**	**±0.58**	**0.35**	**0.00**
Win	**97**	**0.45**	**±0.08**	**-13.76**	**±0.51**	**0.25**	**0.00**
Spr	**91**	**0.32**	**±0.07**	**-13.32**	**±0.68**	**0.18**	**0.00**

Sum	**94**	**0.38**	**±0.08**	**-15.36**	**±1.55**	**0.21**	**0.00**
Aut	**117**	**0.40**	**±0.05**	**-14.63**	**±0.61**	**0.35**	**0.00**
δ^{18}O vs. PDa							
Group	***n***	***Slope***		***y-Int***		***r^2***	***p-value***
Jan	*32*	*2.09*	*±1.68*	*-22.37*	*±4.67*	*0.05*	*0.22*
Feb	*31*	*0.62*	*±1.48*	*-16.90*	*±4.00*	*0.01*	*0.68*
Mar	*30*	*0.60*	*±1.15*	*-14.52*	*±3.13*	*0.01*	*0.61*
Apr	*29*	*-0.59*	*±0.92*	*-8.85*	*±2.85*	*0.02*	*0.52*
May	*32*	*0.16*	*±1.01*	*-9.68*	*±3.23*	*0.00*	*0.87*
Jun	*34*	*-0.37*	*±0.99*	*-6.75*	*±3.23*	*0.00*	*0.71*
Jul	*29*	*-0.66*	*±0.51*	*-5.40*	*±1.78*	*0.06*	*0.21*
Aug	**31**	**-1.56**	**±0.56**	**-2.50**	**±1.93**	**0.21**	**0.01**
Sep	**33**	**-1.10**	**±0.50**	**-4.18**	**±1.73**	**0.14**	**0.03**
Oct	*43*	*-0.52*	*±0.75*	*-9.01*	*±2.38*	*0.01*	*0.50*
Nov	**41**	**-3.54**	**±0.77**	**-1.06**	**±2.45**	**0.35**	**0.00**
Dec	*34*	*1.84*	*±0.96*	*-18.59*	*±2.95*	*0.10*	*0.06*
Win	**97**	**1.99**	**±0.78**	**-20.51**	**±2.22**	**0.06**	**0.01**
Spr	*91*	*0.61*	*±0.59*	*-12.67*	*±1.79*	*0.01*	*0.31*
Sum	**94**	**-0.89**	**±0.40**	**-4.83**	**±1.34**	**0.05**	**0.03**
Aut	**117**	**-1.17**	**±0.47**	**-6.63**	**±1.52**	**0.05**	**0.01**

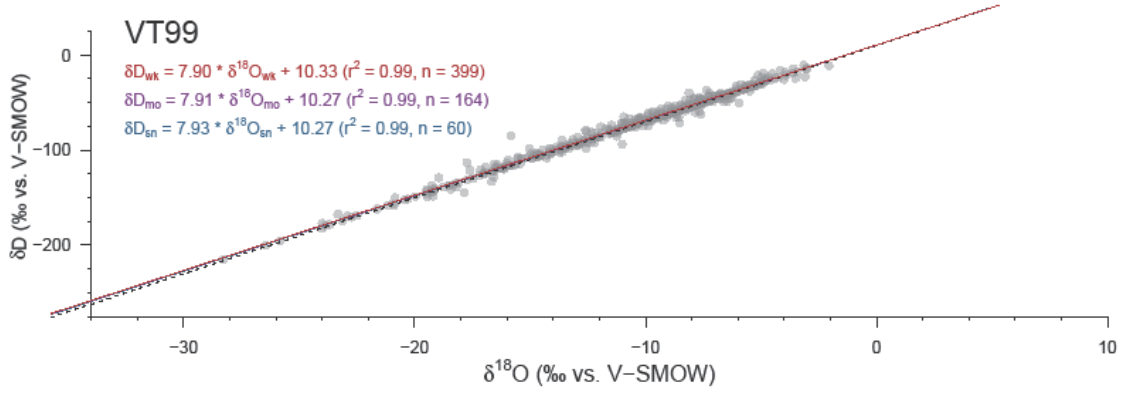

Figure A5.W1. Local meteoric water line for VT99. Gray circles represent values at their original weekly resolution while linear trends are plotted for weekly (red), aggregated monthly (violet), and aggregated seasonal (blue) resolutions. The dashed black line represents the global meteoric water line.

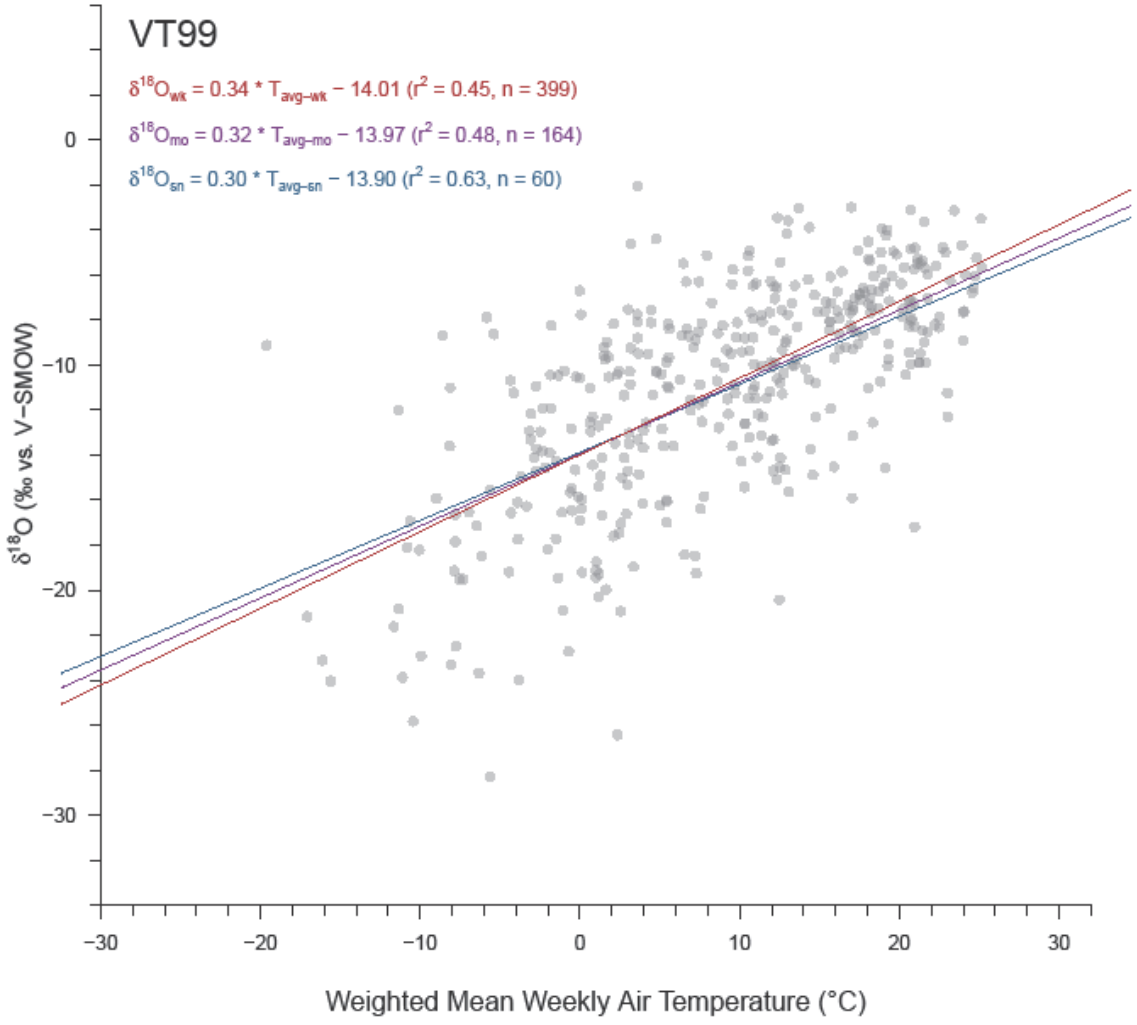

Figure A5.W2. Relationship between precipitation $\delta^{18}O$ and mean PDt at site VT99. Gray circles represent values at their original weekly resolution while linear trends are plotted for weekly (red), aggregated monthly (violet), and aggregated seasonal (blue) resolutions.

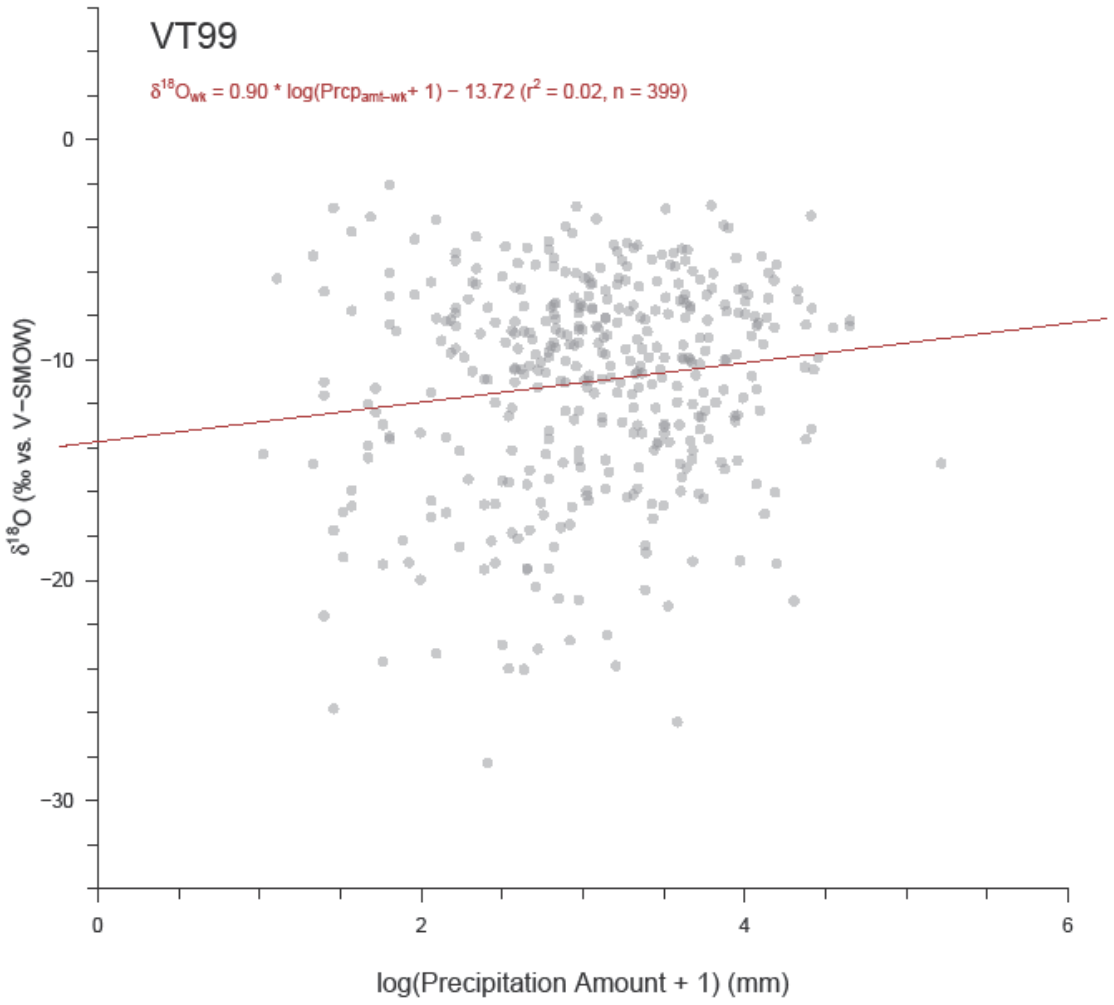

Figure A5.W3. Relationship between precipitation $\delta^{18}O$ and PDa at site VT99. Actual precipitation amounts were normalized by a log transformation. Gray circles represent values at their original weekly resolution with the weekly linear trend plotted in red. Precipitation amount data cannot be weight-averaged for aggregation, and thus regression was only performed at weekly resolution.

WI36

Table A5.X1. Regression results for WI36 at weekly, monthly, and seasonal resolutions. Significant results ($p \leq 0.05$) are bolded, while insignificant results are italicized. Actual precipitation amounts were normalized by a log transformation. Precipitation amount data cannot be weight-averaged for aggregation, and thus regression was only performed at weekly resolution.

LMWL (δD vs. δ^{18}O)							
Resolution	***n***	***Slope***		***y-Int***		***r^2***	***p-value***
Weekly	**411**	**7.78**	**±0.06**	**6.91**	**±0.80**	**0.97**	**0.00**
Monthly	**162**	**7.83**	**±0.08**	**7.76**	**±1.05**	**0.98**	**0.00**
Seasonal	**66**	**7.73**	**±0.13**	**6.62**	**±1.64**	**0.98**	**0.00**
δ^{18}O vs. PDt							
Resolution	***n***	***Slope***		***y-Int***		***r^2***	***p-value***
Weekly	**411**	**0.40**	**±0.02**	**-14.44**	**±0.22**	**0.56**	**0.00**
Monthly	**162**	**0.40**	**±0.03**	**-14.34**	**±0.32**	**0.59**	**0.00**
Seasonal	**66**	**0.39**	**±0.04**	**-14.21**	**±0.44**	**0.63**	**0.00**
δ^{18}O vs. PDa							
Resolution	***n***	***Slope***		***y-Int***		***r^2***	***p-value***
Weekly	**411**	**1.44**	**±0.34**	**-15.42**	**±0.96**	**0.04**	**0.00**

Table A5.X2. Percent change in WI36 regression values (Table A5.X1) due to aggregation.

LMWL (δD vs. δ^{18}O)					
Aggregation	***Slope***	***Slope Error***	***y-Int***	***y-Int Error***	***r^2***
Weekly-Monthly	1%	29%	12%	31%	1%
Weekly-Seasonal	-1%	82%	-4%	80%	1%
Monthly-Seasonal	-1%	37%	-17%	36%	0%
δ^{18}O vs. PDt					
Aggregation	***Slope***	***Slope Error***	***y-Int***	***y-Int Error***	***r^2***
Weekly-Monthly	-1%	50%	-1%	43%	5%
Weekly-Seasonal	-2%	77%	-2%	68%	12%
Monthly-Seasonal	-1%	30%	-1%	28%	7%

Table A5.X3. WI36 temperature estimates and standard errors for three $\delta^{18}O$ values (vs. V-SMOW) at weekly, monthly, and seasonal resolutions. The three $\delta^{18}O$ values span much of the natural range of precipitation $\delta^{18}O$ in the study region, and -6‰ is close to the mean $\delta^{18}O$ value of all sites.

	Temperature Estimate (°C) when Precipitation $\delta^{18}O$ =		
Aggregation	***-20‰***	***-6‰***	***0‰***
Weekly	-4.5 ±13.2	15.0 ±13.2	23.3 ±13.3
Monthly	-5.7 ±13.0	15.0 ±12.9	23.8 ±13.1
Seasonal	-6.8 ±12.1	15.5 ±12.0	25.1 ±12.4

Table A5.X4. Weight-averaged weekly values of $\delta^{18}O$ and average surface temperature for WI36 grouped by month and season. Blue (red) cells show low (high) values of note.

Group	***n***	***$\delta^{18}O_{wt}$***	***PDt***
Jan	26	-18.38 ±1.02	-8.7 ±1.0
Feb	18	-18.53 ±1.44	-6.7 ±0.9
Mar	28	-14.95 ±1.08	-1.7 ±0.8
Apr	43	-10.84 ±0.64	3.2 ±0.8
May	41	-8.43 ±0.47	12.2 ±0.8
Jun	39	-8.46 ±0.41	15.6 ±0.5
Jul	47	-7.50 ±0.39	18.7 ±0.4
Aug	36	-7.70 ±0.40	18.5 ±0.4
Sep	41	-8.33 ±0.55	15.2 ±0.6
Oct	41	-12.39 ±0.63	6.4 ±0.7
Nov	30	-12.40 ±0.89	1.1 ±0.7
Dec	21	-16.89 ±1.22	-5.2 ±1.3
Win	65	-17.60 ±0.68	-7.7 ±0.7
Spr	112	-10.44 ±0.47	6.5 ±0.7
Sum	122	-7.95 ±0.23	17.1 ±0.3
Aut	112	-10.90 ±0.43	9.3 ±0.6

Table A5.X5. Regression results for WI36 when weekly data is grouped by month and by season. Significant results ($p \leq 0.05$) are bolded, while insignificant results are italicized. Actual precipitation amounts were normalized by a log transformation. Blue (red) cells show low (high) values of note.

LMWL (δD vs. $\delta^{18}O$)							
Group	***n***	***Slope***		***y-Int***		***r^2***	***p-value***
Jan	**26**	**7.32**	**±0.17**	**-3.35**	**±3.15**	**0.99**	**0.00**
Feb	**18**	**7.18**	**±0.21**	**-6.74**	**±3.96**	**0.99**	**0.00**
Mar	**28**	**8.19**	**±0.24**	**13.60**	**±3.98**	**0.98**	**0.00**
Apr	**43**	**7.55**	**±0.26**	**4.76**	**±3.19**	**0.95**	**0.00**
May	**41**	**8.48**	**±0.23**	**14.44**	**±2.21**	**0.97**	**0.00**
Jun	**39**	**8.26**	**±0.41**	**11.50**	**±3.63**	**0.92**	**0.00**
Jul	**47**	**6.78**	**±0.52**	**-2.65**	**±4.25**	**0.79**	**0.00**
Aug	**36**	**7.66**	**±0.59**	**6.21**	**±4.81**	**0.83**	**0.00**
Sep	**41**	**7.80**	**±0.31**	**8.02**	**±2.87**	**0.94**	**0.00**
Oct	**41**	**7.82**	**±0.30**	**7.46**	**±3.97**	**0.95**	**0.00**
Nov	**30**	**7.64**	**±0.16**	**6.04**	**±2.24**	**0.99**	**0.00**
Dec	**21**	**7.87**	**±0.19**	**8.89**	**±3.52**	**0.99**	**0.00**
Win	**65**	**7.46**	**±0.11**	**-0.06**	**±2.16**	**0.99**	**0.00**
Spr	**112**	**7.98**	**±0.12**	**9.98**	**±1.53**	**0.97**	**0.00**
Sum	**122**	**7.44**	**±0.30**	**3.69**	**±2.49**	**0.84**	**0.00**
Aut	**112**	**7.77**	**±0.14**	**7.42**	**±1.66**	**0.97**	**0.00**
$\delta^{18}O$ vs. PDt							
Group	***n***	***Slope***		***y-Int***		***r^2***	***p-value***
Jan	**26**	**0.49**	**±0.19**	**-13.99**	**±1.93**	**0.22**	**0.02**
Feb	*18*	*0.39*	*±0.38*	*-15.38*	*±3.19*	*0.06*	*0.32*
Mar	**28**	**0.68**	**±0.23**	**-14.28**	**±1.05**	**0.25**	**0.01**
Apr	**43**	**0.38**	**±0.11**	**-12.37**	**±0.63**	**0.24**	**0.00**
May	**41**	**0.41**	**±0.07**	**-13.67**	**±0.82**	**0.51**	**0.00**
Jun	**39**	**0.29**	**±0.12**	**-12.99**	**±1.94**	**0.13**	**0.02**
Jul	**47**	**0.26**	**±0.13**	**-12.57**	**±2.47**	**0.08**	**0.05**
Aug	*36*	*0.27*	*±0.15*	*-12.74*	*±2.75*	*0.09*	*0.08*
Sep	**41**	**0.65**	**±0.10**	**-18.03**	**±1.47**	**0.52**	**0.00**
Oct	**41**	**0.53**	**±0.13**	**-15.89**	**±0.96**	**0.31**	**0.00**
Nov	**30**	**0.67**	**±0.19**	**-13.85**	**±0.77**	**0.31**	**0.00**
Dec	**21**	**0.47**	**±0.18**	**-14.82**	**±1.48**	**0.27**	**0.02**
Win	**65**	**0.45**	**±0.12**	**-14.69**	**±1.10**	**0.18**	**0.00**
Spr	**112**	**0.44**	**±0.05**	**-13.64**	**±0.42**	**0.44**	**0.00**

Sum	**122**	**0.28**	**±0.07**	**-12.84**	**±1.23**	**0.12**	**0.00**
Aut	**112**	**0.45**	**±0.05**	**-14.82**	**±0.49**	**0.44**	**0.00**
δ^{18}O vs. PDa							
Group	***n***	***Slope***		***y-Int***		***r^2***	***p-value***
Jan	*26*	*0.64*	*±1.93*	*-19.82*	*±4.50*	*0.00*	*0.74*
Feb	*18*	*2.78*	*±2.68*	*-25.01*	*±6.62*	*0.06*	*0.31*
Mar	*28*	*2.80*	*±1.47*	*-22.77*	*±3.90*	*0.12*	*0.07*
Apr	*43*	*-0.14*	*±0.74*	*-10.97*	*±2.14*	*0.00*	*0.85*
May	*41*	*0.59*	*±0.62*	*-10.74*	*±1.96*	*0.02*	*0.35*
Jun	*39*	*-0.48*	*±0.49*	*-7.08*	*±1.54*	*0.03*	*0.33*
Jul	*47*	*-0.54*	*±0.48*	*-6.21*	*±1.37*	*0.03*	*0.27*
Aug	*36*	*0.37*	*±0.55*	*-8.93*	*±1.66*	*0.01*	*0.50*
Sep	*41*	*0.51*	*±0.75*	*-10.19*	*±2.25*	*0.01*	*0.50*
Oct	*41*	*-0.18*	*±0.87*	*-12.07*	*±2.37*	*0.00*	*0.84*
Nov	*30*	*-0.19*	*±1.21*	*-12.77*	*±3.37*	*0.00*	*0.88*
Dec	*21*	*2.08*	*±2.44*	*-22.56*	*±6.03*	*0.04*	*0.40*
Win	*65*	*1.71*	*±1.28*	*-22.12*	*±3.09*	*0.03*	*0.18*
Spr	**112**	**1.37**	**±0.56**	**-15.40**	**±1.65**	**0.05**	**0.02**
Sum	*122*	*-0.34*	*±0.29*	*-7.03*	*±0.86*	*0.01*	*0.24*
Aut	*112*	*0.46*	*±0.57*	*-12.60*	*±1.63*	*0.01*	*0.42*

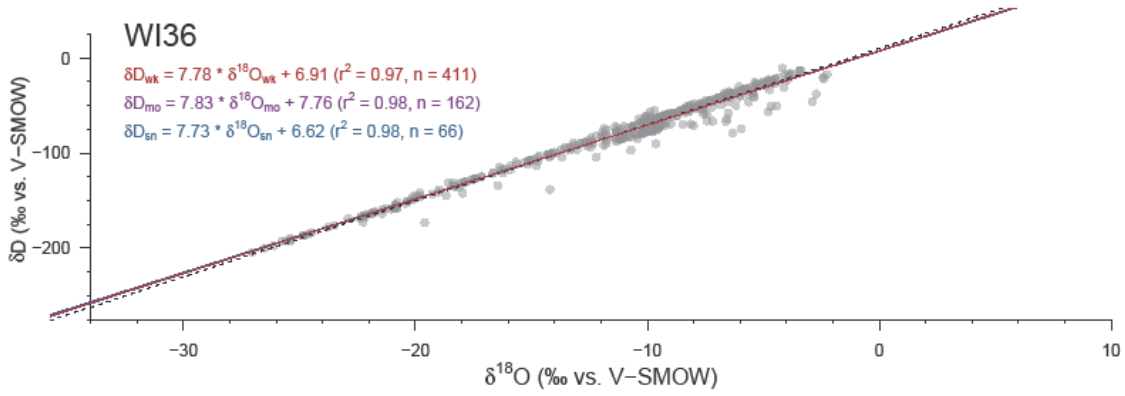

Figure A5.X1. Local meteoric water line for WI36. Gray circles represent values at their original weekly resolution while linear trends are plotted for weekly (red), aggregated monthly (violet), and aggregated seasonal (blue) resolutions. The dashed black line represents the global meteoric water line.

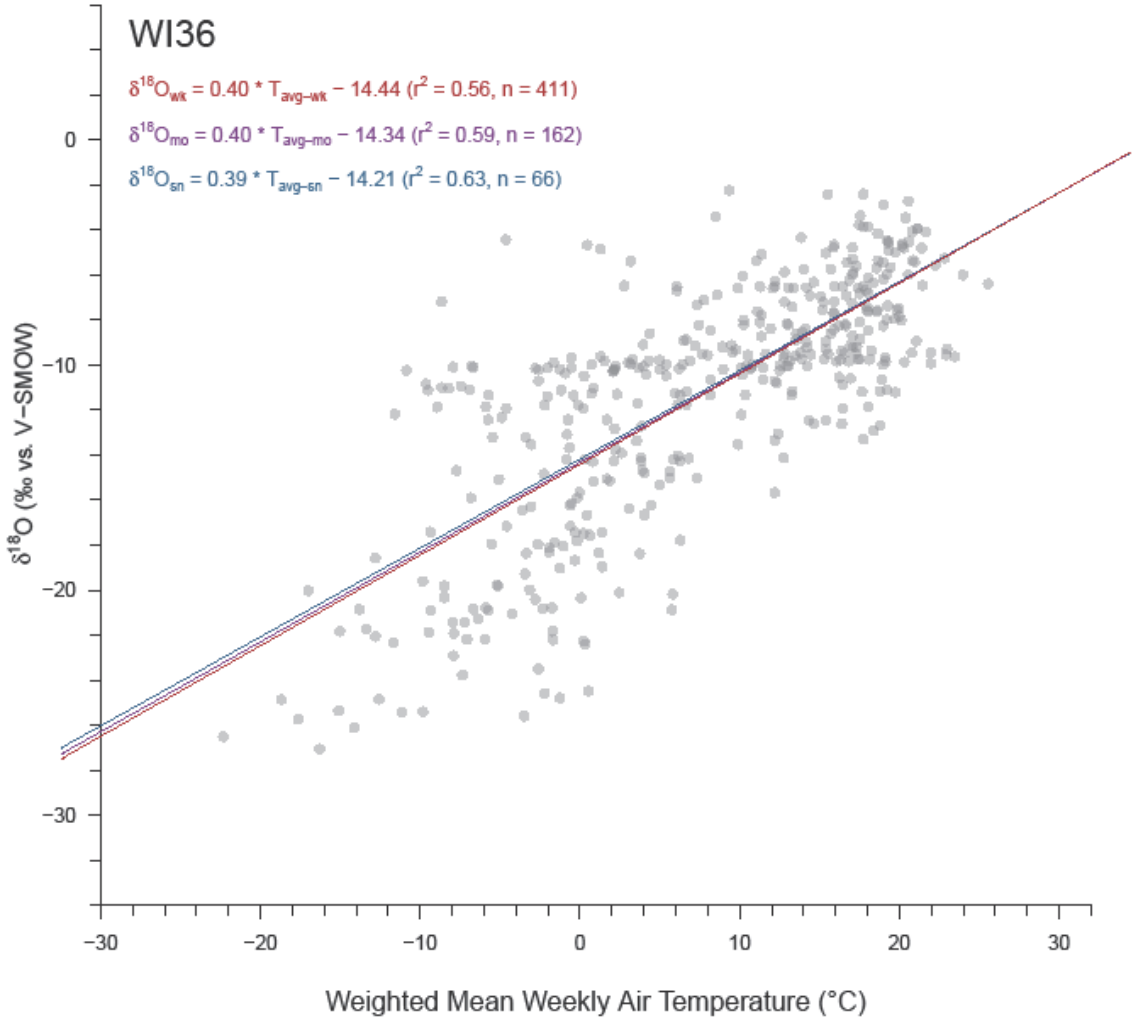

Figure A5.X2. Relationship between precipitation $\delta^{18}O$ and mean PDt at site WI36. Gray circles represent values at their original weekly resolution while linear trends are plotted for weekly (red), aggregated monthly (violet), and aggregated seasonal (blue) resolutions.

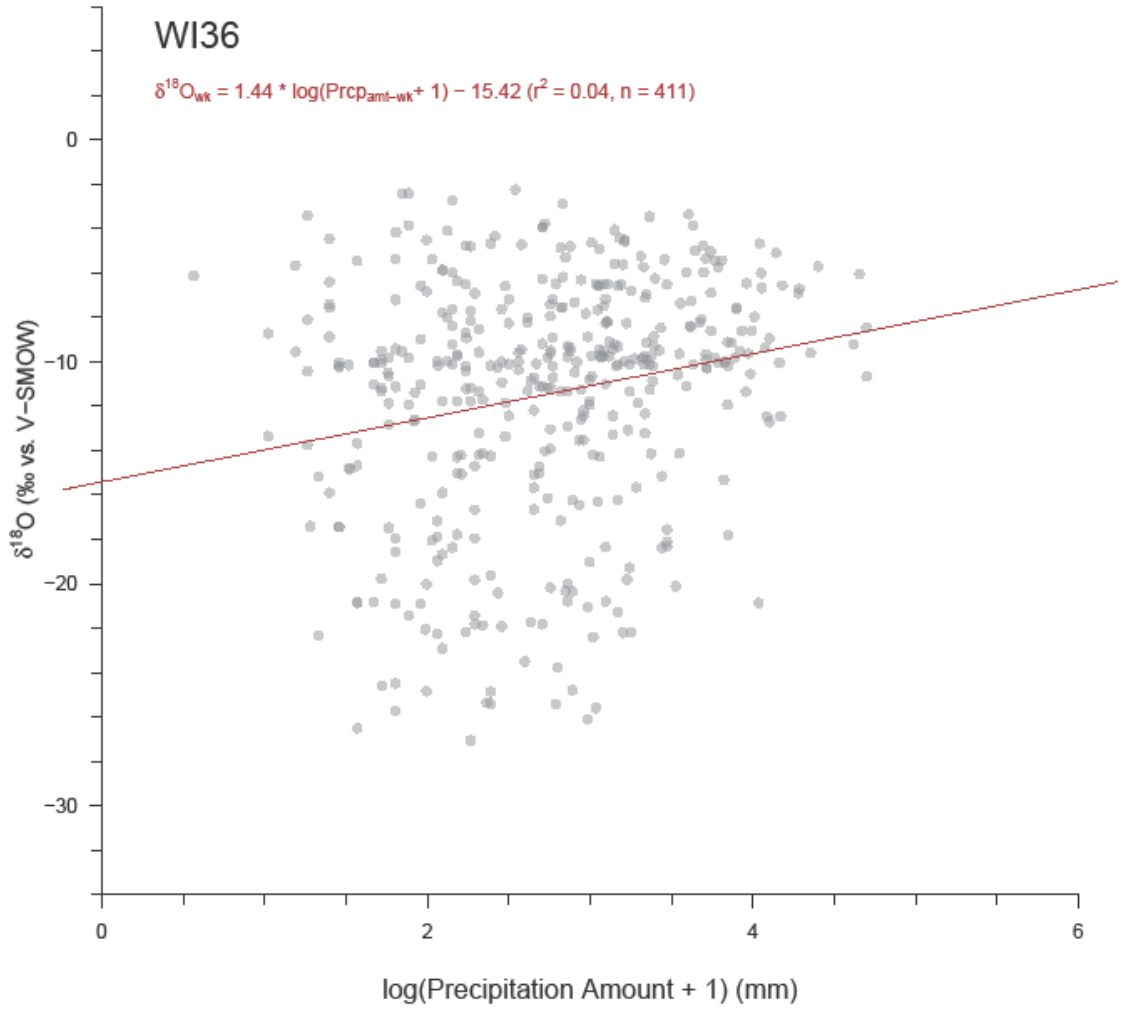

Figure A5.X3. Relationship between precipitation $\delta^{18}O$ and PDa at site WI36. Actual precipitation amounts were normalized by a log transformation. Gray circles represent values at their original weekly resolution with the weekly linear trend plotted in red. Precipitation amount data cannot be weight-averaged for aggregation, and thus regression was only performed at weekly resolution.

WI99

Table A5.Y1. Regression results for WI99 at weekly, monthly, and seasonal resolutions. Significant results ($p \leq 0.05$) are bolded, while insignificant results are italicized. Actual precipitation amounts were normalized by a log transformation. Precipitation amount data cannot be weight-averaged for aggregation, and thus regression was only performed at weekly resolution.

LMWL (δD vs. δ^{18}O)							
Resolution	***n***	***Slope***		***y-Int***		***r^2***	***p-value***
Weekly	**373**	**7.90**	**±0.06**	**9.03**	**±0.58**	**0.98**	**0.00**
Monthly	**146**	**7.90**	**±0.08**	**9.34**	**±0.82**	**0.98**	**0.00**
Seasonal	**59**	**7.79**	**±0.15**	**8.58**	**±1.39**	**0.98**	**0.00**
δ^{18}O vs. PDt							
Resolution	***n***	***Slope***		***y-Int***		***r^2***	***p-value***
Weekly	**373**	**0.38**	**±0.02**	**-12.62**	**±0.26**	**0.52**	**0.00**
Monthly	**146**	**0.36**	**±0.03**	**-12.41**	**±0.35**	**0.56**	**0.00**
Seasonal	**59**	**0.36**	**±0.03**	**-12.48**	**±0.45**	**0.65**	**0.00**
δ^{18}O vs. PDa							
Resolution	***n***	***Slope***		***y-Int***		***r^2***	***p-value***
Weekly	**373**	**0.75**	**±0.28**	**-10.84**	**±0.81**	**0.02**	**0.01**

Table A5.Y2. Percent change in WI99 regression values (Table A5.Y1) due to aggregation.

LMWL (δD vs. δ^{18}O)					
Aggregation	***Slope***	***Slope Error***	***y-Int***	***y-Int Error***	***r^2***
Weekly-Monthly	0%	45%	3%	43%	0%
Weekly-Seasonal	-1%	106%	-5%	100%	0%
Monthly-Seasonal	-1%	43%	-9%	41%	0%
δ^{18}O vs. PDt					
Aggregation	***Slope***	***Slope Error***	***y-Int***	***y-Int Error***	***r^2***
Weekly-Monthly	-4%	42%	-2%	39%	8%
Weekly-Seasonal	-4%	62%	-1%	54%	23%
Monthly-Seasonal	0%	24%	1%	21%	13%

Table A5.Y3. WI99 temperature estimates and standard errors for three $\delta^{18}O$ values (vs. V-SMOW) at weekly, monthly, and seasonal resolutions. The three $\delta^{18}O$ values span much of the natural range of precipitation $\delta^{18}O$ in the study region, and -6‰ is close to the mean $\delta^{18}O$ value of all sites.

	Temperature Estimate (°C) when Precipitation $\delta^{18}O$ =		
Aggregation	***-20‰***	***-6‰***	***0‰***
Weekly	-5.4 ±12.5	14.1 ±12.4	22.5 ±12.4
Monthly	-7.5 ±12.0	14.4 ±11.8	23.8 ±11.9
Seasonal	-10.0 ±10.2	15.3 ±9.5	26.1 ±9.9

Table A5.Y4. Weight-averaged weekly values of $\delta^{18}O$ and average surface temperature for WI99 grouped by month and season. Blue (red) cells show low (high) values of note.

Group	***n***	***$\delta^{18}O_{wt}$***	***PDt***
Jan	29	-15.28 ±0.95	-3.0 ±0.8
Feb	22	-11.40 ±1.10	-1.3 ±0.8
Mar	33	-9.64 ±0.76	3.4 ±1.0
Apr	34	-9.01 ±0.74	6.5 ±0.7
May	36	-5.95 ±0.52	14.5 ±0.7
Jun	38	-5.96 ±0.38	18.9 ±0.6
Jul	31	-5.01 ±0.29	21.7 ±0.5
Aug	35	-5.33 ±0.40	20.9 ±0.5
Sep	29	-6.97 ±0.45	17.3 ±0.7
Oct	35	-9.19 ±0.60	10.4 ±0.7
Nov	32	-10.39 ±0.57	4.6 ±0.7
Dec	19	-13.78 ±1.28	0.9 ±0.7
Win	70	-13.05 ±0.64	-0.5 ±0.5
Spr	103	-7.82 ±0.42	9.7 ±0.6
Sum	104	-5.49 ±0.22	19.7 ±0.4
Aut	96	-9.33 ±0.35	11.2 ±0.6

Table A5.Y5. Regression results for WI99 when weekly data is grouped by month and by season. Significant results ($p \leq 0.05$) are bolded, while insignificant results are italicized. Actual precipitation amounts were normalized by a log transformation. Blue (red) cells show low (high) values of note.

LMWL (δD vs. $\delta^{18}O$)							
Group	***n***	***Slope***		***y-Int***		***r^2***	***p-value***
Jan	**29**	**8.12**	**±0.17**	**12.58**	**±2.78**	**0.99**	**0.00**
Feb	**22**	**8.11**	**±0.22**	**11.76**	**±3.06**	**0.99**	**0.00**
Mar	**33**	**7.99**	**±0.22**	**11.41**	**±2.50**	**0.98**	**0.00**
Apr	**34**	**8.23**	**±0.20**	**12.20**	**±1.95**	**0.98**	**0.00**
May	**36**	**8.34**	**±0.22**	**12.08**	**±1.55**	**0.98**	**0.00**
Jun	**38**	**7.45**	**±0.54**	**4.09**	**±3.71**	**0.84**	**0.00**
Jul	**31**	**7.27**	**±0.50**	**4.16**	**±2.54**	**0.88**	**0.00**
Aug	**35**	**8.54**	**±0.21**	**10.92**	**±1.19**	**0.98**	**0.00**
Sep	**29**	**7.92**	**±0.38**	**9.46**	**±2.76**	**0.94**	**0.00**
Oct	**35**	**7.81**	**±0.25**	**9.59**	**±2.46**	**0.97**	**0.00**
Nov	**32**	**7.86**	**±0.31**	**9.58**	**±3.36**	**0.96**	**0.00**
Dec	**19**	**8.23**	**±0.23**	**13.65**	**±3.20**	**0.99**	**0.00**
Win	**70**	**8.14**	**±0.11**	**12.51**	**±1.66**	**0.99**	**0.00**
Spr	**103**	**8.08**	**±0.11**	**11.18**	**±1.07**	**0.98**	**0.00**
Sum	**104**	**7.88**	**±0.24**	**7.17**	**±1.46**	**0.91**	**0.00**
Aut	**96**	**7.82**	**±0.15**	**9.18**	**±1.47**	**0.97**	**0.00**
$\delta^{18}O$ vs. PDt							
Group	***n***	***Slope***		***y-Int***		***r^2***	***p-value***
Jan	**29**	**0.52**	**±0.22**	**-13.64**	**±1.11**	**0.17**	**0.02**
Feb	*22*	*0.52*	*±0.30*	*-12.40*	*±1.09*	*0.13*	*0.10*
Mar	**33**	**0.65**	**±0.08**	**-12.15**	**±0.49**	**0.68**	**0.00**
Apr	*34*	*0.31*	*±0.18*	*-10.88*	*±1.47*	*0.09*	*0.09*
May	**36**	**0.42**	**±0.11**	**-11.97**	**±1.59**	**0.29**	**0.00**
Jun	**38**	**0.24**	**±0.09**	**-10.94**	**±1.71**	**0.17**	**0.01**
Jul	**31**	**0.37**	**±0.08**	**-12.83**	**±1.80**	**0.41**	**0.00**
Aug	*35*	*0.17*	*±0.14*	*-8.91*	*±2.98*	*0.04*	*0.22*
Sep	**29**	**0.35**	**±0.10**	**-12.91**	**±1.83**	**0.29**	**0.00**
Oct	**35**	**0.41**	**±0.13**	**-13.44**	**±1.42**	**0.23**	**0.00**
Nov	**32**	**0.56**	**±0.12**	**-12.91**	**±0.73**	**0.40**	**0.00**
Dec	**19**	**1.41**	**±0.28**	**-14.10**	**±0.88**	**0.60**	**0.00**
Win	**70**	**0.68**	**±0.14**	**-12.91**	**±0.58**	**0.27**	**0.00**
Spr	**103**	**0.44**	**±0.05**	**-11.90**	**±0.51**	**0.43**	**0.00**

Sum	**104**	**0.29**	**±0.06**	**-11.42**	**±1.14**	**0.21**	**0.00**
Aut	**96**	**0.33**	**±0.04**	**-12.42**	**±0.53**	**0.38**	**0.00**
δ^{18}O vs. PDa							
Group	***n***	***Slope***		***y-Int***		***r^2***	***p-value***
Jan	**29**	**2.93**	**±1.43**	**-22.10**	**±3.46**	**0.13**	**0.05**
Feb	*22*	*0.69*	*±2.14*	*-14.64*	*±5.46*	*0.01*	*0.75*
Mar	*33*	*0.50*	*±0.92*	*-11.68*	*±2.57*	*0.01*	*0.59*
Apr	*34*	*-0.70*	*±0.87*	*-6.62*	*±2.64*	*0.02*	*0.43*
May	*36*	*-0.60*	*±0.67*	*-4.40*	*±2.21*	*0.02*	*0.37*
Jun	*38*	*-0.19*	*±0.46*	*-5.84*	*±1.56*	*0.00*	*0.68*
Jul	*31*	*-0.25*	*±0.28*	*-4.24*	*±0.79*	*0.03*	*0.40*
Aug	*35*	*0.11*	*±0.41*	*-5.55*	*±1.17*	*0.00*	*0.79*
Sep	*29*	*0.12*	*±0.52*	*-7.28*	*±1.59*	*0.00*	*0.81*
Oct	*35*	*-0.69*	*±0.73*	*-7.48*	*±2.06*	*0.03*	*0.35*
Nov	*32*	*0.80*	*±0.77*	*-12.40*	*±2.06*	*0.03*	*0.31*
Dec	*19*	*0.78*	*±2.02*	*-14.71*	*±5.52*	*0.01*	*0.70*
Win	**70**	**2.05**	**±1.00**	**-18.88**	**±2.56**	**0.06**	**0.05**
Spr	*103*	*0.27*	*±0.49*	*-9.19*	*±1.51*	*0.00*	*0.58*
Sum	*104*	*-0.30*	*±0.22*	*-4.73*	*±0.67*	*0.02*	*0.18*
Aut	*96*	*0.31*	*±0.42*	*-9.80*	*±1.20*	*0.01*	*0.46*

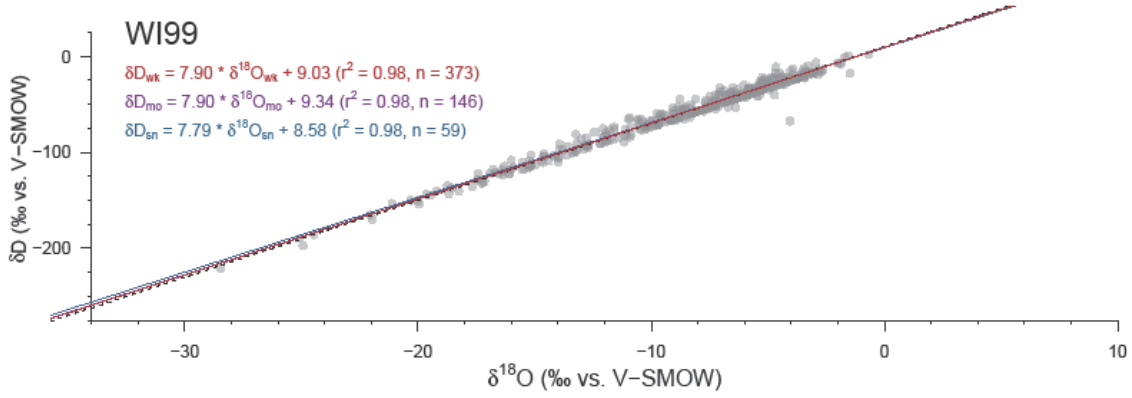

Figure A5.Y1. Local meteoric water line for WI99. Gray circles represent values at their original weekly resolution while linear trends are plotted for weekly (red), aggregated monthly (violet), and aggregated seasonal (blue) resolutions. The dashed black line represents the global meteoric water line.

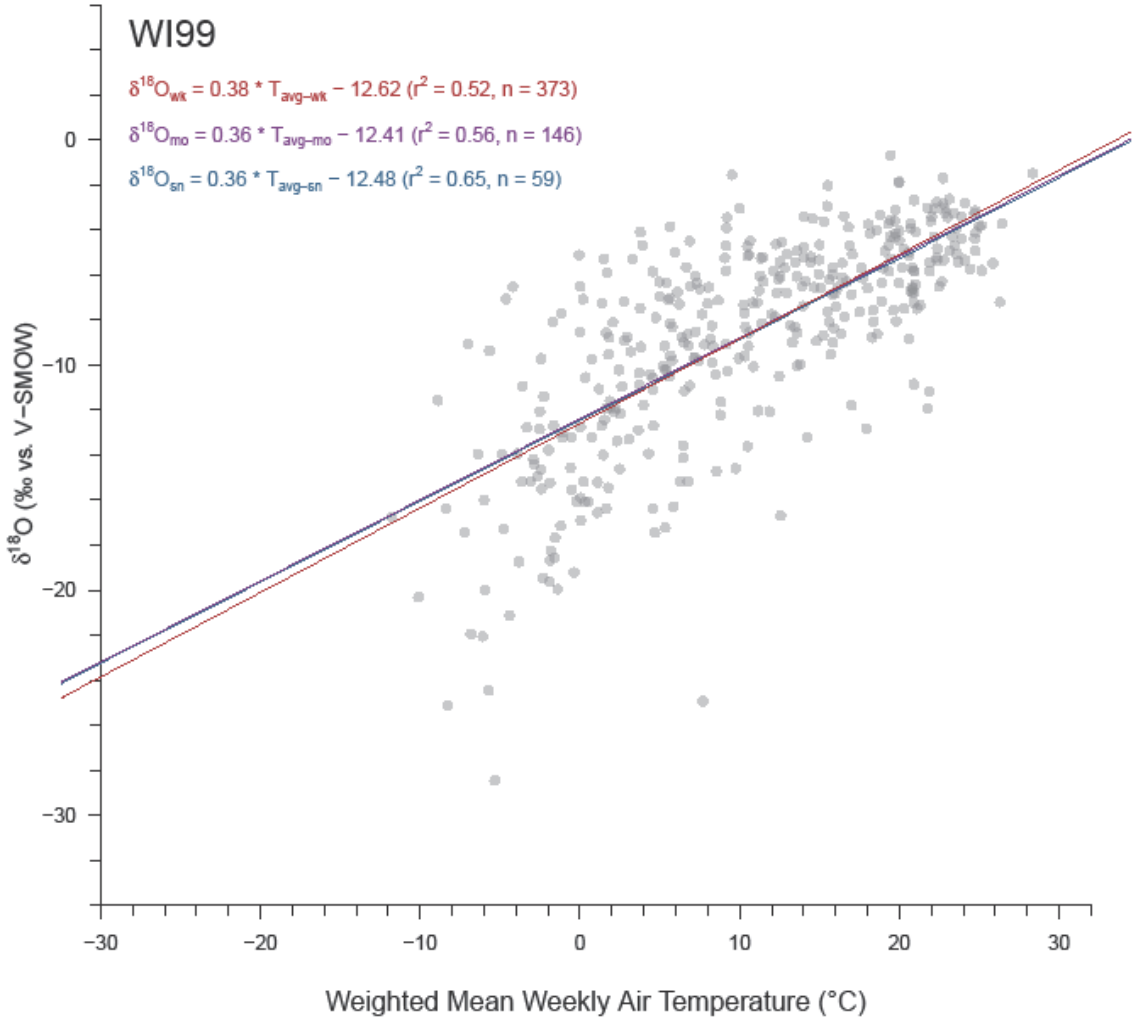

Figure A5.Y2. Relationship between precipitation $\delta^{18}O$ and mean PDt at site WI99. Gray circles represent values at their original weekly resolution while linear trends are plotted for weekly (red), aggregated monthly (violet), and aggregated seasonal (blue) resolutions.

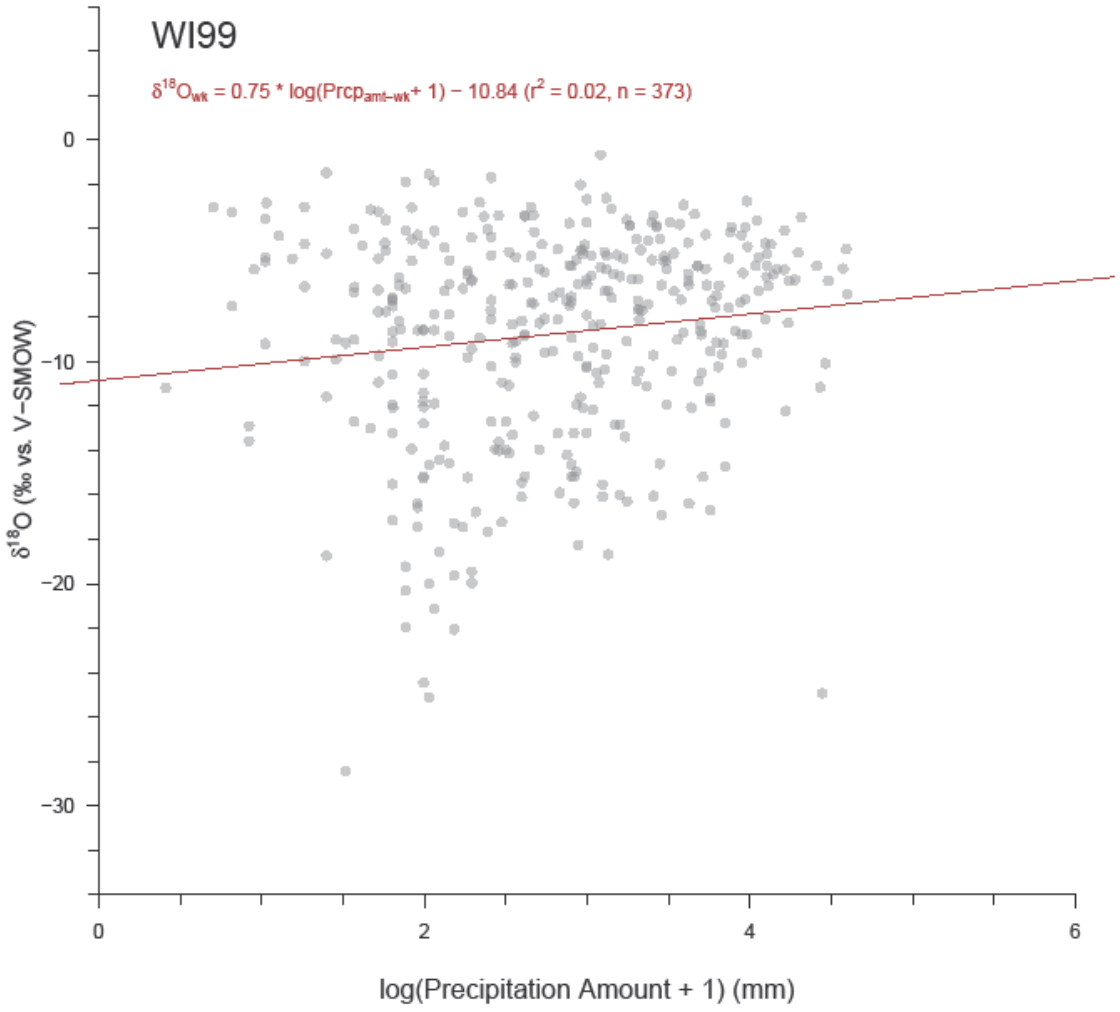

Figure A5.Y3. Relationship between precipitation $\delta^{18}O$ and PDa at site WI99. Actual precipitation amounts were normalized by a log transformation. Gray circles represent values at their original weekly resolution with the weekly linear trend plotted in red. Precipitation amount data cannot be weight-averaged for aggregation, and thus regression was only performed at weekly resolution.

APPENDIX SIX:

R CODE SCRIPT FOR DISSERTATION DATA ANALYSIS AND FIGURE CONSTRUCTION

This appendix contains code written in R programming language to import raw data, perform analysis, and plot figures for this dissertation research.

```
#=============================================================================================================
#=======================================USNIP Data Analysis=====================================================
#=============================================================================================================

#USNIP Looping All Sites Aggregation and Correlation Script
#Aggregating GCHN data for all sites and calculating correlations and stats
#Written by Pete D Akers 2014, Edited into looped form 2015


#---------------------Column Standard Deviations Function----------------
#This function calculates standard deviations for all columns
#NOTE: Columns must be numeric
#Shamelessly stolen from StackOverflow user sgibb at
        #http://stackoverflow.com/questions/17549762/is-there-such-colsd-in-r

colSD <- function(x, na.rm=TRUE) {
 if (na.rm) {
 n <- colSums(!is.na(x)) # thanks @flodel
 } else {
 n <- nrow(x)
 }
 colVar <- colMeans(x*x, na.rm=na.rm) - (colMeans(x, na.rm=na.rm))^2
 return(sqrt(colVar * n/(n-1)))
}

#---------------------Weighted Standard Deviation Function----------------
#This function calculates standard deviations for a weighted dataset
#NOTE: Columns must be numeric
#NOTE: Dataset should be matrix with columns, weight should be vector
#Written by Pete D Akers, 2015

sd.wt <- function(dataset, weight) {
        mu <- colSums(weight * dataset)
        if(length(dataset) > 1) {
```

```
                return(sqrt(colSums(weight * t((t(dataset) - mu)^2))))
                }
        else {
                return(sqrt(colSums(weight * (dataset - mu)^2)))
                }
        }

#Quick function from StackOverflow to print out exact digits for plots
specify.decimal <- function(x, k) format(round(x, k), nsmall=k)

#-------------------------------------------------------------------------------------------------
#-----------------------------------------All Sites-----------------------------------------------
allsites.all <- read.table(file="usnip-gchn_weekly_summary.csv", sep=",", header=TRUE)
allsites <- allsites.all[allsites.all$gchn.prcp != 0, ]
allsites <- allsites[complete.cases(allsites$d2H), ]
allsites$usnip.date <- as.character(allsites$usnip.date)
allsites$usnip.date <- as.Date(allsites$usnip.date, "%Y%m%d")
allsites$gchn.date <- as.character(allsites$gchn.date)
allsites$gchn.date <- as.Date(allsites$gchn.date, "%Y%m%d")
allsites$site <- tolower(as.character(allsites$site))

#Adding month, year, and season columns
mo <- strftime(allsites$usnip.date, "%m")
yr <- strftime(allsites$usnip.date, "%Y")
allsites$mo <- mo
allsites$yr<- yr
allsites$season[allsites$mo == "12" | allsites$mo == "01" | allsites$mo == "02"] <- "win"
allsites$season[allsites$mo == "03" | allsites$mo == "04" | allsites$mo == "05"] <- "spr"
allsites$season[allsites$mo == "06" | allsites$mo == "07" | allsites$mo == "08"] <- "sum"
allsites$season[allsites$mo == "09" | allsites$mo == "10" | allsites$mo == "11"] <- "aut"

#This script incorporates the climate of Thibodaux, LA as a proxy for Gulf of Mexico climate
gulf.climate <- read.table("gulf_climate.csv", header=TRUE, sep=",")
gulf.climate$date <- as.character(gulf.climate$date)
```

```
gulf.climate$date <- as.Date(gulf.climate$date, "%Y%m%d")

#This loop calculates a mean gulf temperature for each week with USNIP data
gulf.match.index <- NA
gulf.week.tavg <- NA
for (i in 1:length(allsites$usnip.date)) {
        gulf.match.index <- which(gulf.climate$date == allsites$usnip.date[i])
        gulf.week.data <- gulf.climate[c((gulf.match.index-6):gulf.match.index), ]
        gulf.week.tavg[i] <- round(mean(gulf.week.data$tavg), 1)
        }

#Subsetting data to only have numeric and time columns
allsites.data <- allsites[c(3,4,5,7,8,9,10,11,12,13)]
usnip.dates <- allsites$usnip.date

gulf.site.diff <- gulf.week.tavg - round(allsites$tavg, 1) #Tavg difference between gulf and site
allsites.data$tdif <- gulf.site.diff

totalsites.data <- list(NA)
totalsites.dates <- list(NA)
total.mo.aggr.wt <- list(NA)
total.mo.aggr.wt.sd <- list(NA)
total.mo.indv.wt <- list(NA)
total.season.aggr.wt <- list(NA)
total.season.aggr.wt.sd <- list(NA)
total.season.indv.wt <- list(NA)
total.water.yr.wt <- list(NA)
total.water.yr.indv <- list(NA)
total.week.d18O.corr <- list(NA)
total.mo.usnip.prcp.sum <- list(NA)
total.season.usnip.prcp.sum <- list(NA)
#total.water.yr.usnip.prcp.sum <- list(NA) #Not used currently
totalsites.lmwl <- list(NA)
```

```
site.index <- sort(unique(allsites$site))

for (h in 1:length(site.index)) {

        siteloop.data <- allsites.data[allsites$site == site.index[h], ]
        siteloop.dates <- usnip.dates[allsites$site == site.index[h]]

        siteloop.lmwl <- lm(siteloop.data$d2H~siteloop.data$d18O) #calculating the local mean water line
        totalsites.lmwl[[h]] <- siteloop.lmwl
        #summary(siteloop.lmwl)
        d.excess <- siteloop.data$d2H - 8*siteloop.data$d18O
        #The d.excess calculation below is wrong, but preserved because it may be in old data
        #d.excess <- siteloop.data$d2H - siteloop.lmwl$coefficients[2]*siteloop.data$d18O
        siteloop.data$d.ex <- d.excess

        #Putting d.ex near other iso data
        siteloop.data <- siteloop.data[ , c(1,2,3,12,4,5,6,7,8,9,10,11)]

        #Filling in USNIP amount = -9 with GCHN data
        siteloop.data$usnip.prcp[siteloop.data$usnip.prcp == -9] <- siteloop.data$gchn.prcp[siteloop.data$usnip.prcp == -9]

        #Deleting USNIP data where no precip was found in GCHN
        siteloop.data <- siteloop.data[siteloop.data$gchn.prcp != 0, ]
        siteloop.dates <- siteloop.dates[siteloop.data$gchn.prcp != 0]

        #Eliminating outlying data where GCHN and USNIP precip amounts greatly differ (> 10x)
        if (length(which(abs(log(siteloop.data$usnip.prcp+1)- log(siteloop.data$gchn.prcp+1)) > 1) >= 1)) {
                delete.if <- c(which(abs(log(siteloop.data$usnip.prcp+1)-
                        log(siteloop.data$gchn.prcp+1)) > 1))
                siteloop.data <- siteloop.data[-delete.if, ]
                siteloop.dates <- siteloop.dates[-delete.if]
                        }

        #Plotting USNIP vs. GCHN precipitation amounts
```

```
#dev.new()
#plot(log(siteloop.data$usnip.prcp+1), log(siteloop.data$gchn.prcp+1), pch=20)

#dev.new()
#stripchart((log(siteloop.data$usnip.prcp+1)-log(siteloop.data$gchn.prcp+1)))



#-------------------------Weekly Data-----------------------------------------------------
#-------------------------Correlations Between Iso Signatures & Weather------------------

cor.index <- c(1,3,4,6,7,8,12)
week.d18O.cor <- data.frame(matrix(nrow=length(cor.index), ncol=4))
for (i in 1:7) {
        week.d18O.cor[i,1] <- cor.test(siteloop.data$d18O, siteloop.data[ , cor.index[i]])$estimate
        week.d18O.cor[i,2] <- cor.test(siteloop.data$d18O, siteloop.data[ , cor.index[i]])$p.value
        week.d18O.cor[i,3] <- cor.test(siteloop.data$d18O, siteloop.data[ , cor.index[i]],
                method="spearman")$estimate
        week.d18O.cor[i,4] <- cor.test(siteloop.data$d18O, siteloop.data[ , cor.index[i]],
                method="spearman")$p.value
        }
rownames(week.d18O.cor) <- c("usnip.prcp", "d2H", "d.ex", "tmin", "tmax", "tavg", "tdif")
colnames(week.d18O.cor) <- c("R", "R pval", "Rho", "Rho pval")
siteloop.week.d18O.corr <- week.d18O.cor
siteloop.week.d18O.corr <- cbind(round(siteloop.week.d18O.corr[1], 3),
        round(siteloop.week.d18O.corr[2], 4), round(siteloop.week.d18O.corr[3], 3),
        round(siteloop.week.d18O.corr[4], 4))
total.week.d18O.corr[[h]] <- siteloop.week.d18O.corr

#-------------------------------------Monthly Data-----------------------------------------
#Creating monthly datasets
tmp.mo <- NULL
mo.aggr <-data.frame(matrix(nrow=12, ncol=9))
mo.id <- c("01", "02", "03", "04", "05", "06", "07", "08", "09",
```

```
          "10", "11", "12")
season.id <- c("win", "spr", "sum", "aut")

#Loop to determine average monthly values
for (i in 1:12) {
          tmp.mo <- siteloop.data[siteloop.data$mo == mo.id[i], ]
          mo.aggr[i, ] <- t(colMeans(tmp.mo[ ,-c(9:11)]))
          }
rownames(mo.aggr) <- c("Jan", "Feb", "Mar", "Apr", "May", "Jun", "Jul",
          "Aug", "Sep", "Oct", "Nov", "Dec")
colnames(mo.aggr) <- c("usnip.prcp", "d18O", "d2H", "d.ex", "gchn.prcp", "tmin",
          "tmax", "tavg", "tdif")

#Loop to determine weighted average monthly values
mo.aggr.wt <- data.frame(matrix(nrow=12, ncol=9))
mo.aggr.wt.sd <- data.frame(matrix(nrow=12, ncol=9))
mo.indv.wt <- data.frame(matrix(nrow=0, ncol=9))
mo.indv.index <- data.frame(matrix(nrow=0, ncol=2))
mo.usnip.prcp.sum <- NULL
k.yr <- c(1989:2006) #To link k index value to correct year
for (i in 1:12) { #Month by month loop
          tmp.mo <- siteloop.data[siteloop.data$mo == mo.id[i], ]
          wt.sum <- data.frame(matrix(nrow=18, ncol=(length(tmp.mo)-3)))
          indv.index <- data.frame(matrix(nrow=18, ncol=2))
          usnip.prcp.sum.tmp <- NULL
          for (k in 1:length(k.yr)) { #Group by year loop
                    tmp.yr <- tmp.mo[tmp.mo$yr == k.yr[k], ]
                    frac.mo <- NULL
                    weighted <- data.frame(matrix(nrow=length(tmp.yr$yr), ncol=(length(tmp.yr)-3)))
                    for (j in 1:length(tmp.yr$usnip.prcp)) { #Weighted average for a single month
                              frac.mo[j] <- tmp.yr$usnip.prcp[j]/sum(tmp.yr$usnip.prcp)
                              weighted[j, ] <- (tmp.yr[j,-c(9:11)] * frac.mo[j])
                              }
                    wt.sum[k, ] <- t(colSums(weighted)) #All weekly weighted values for a single month
```

```
                indv.index[k,1] <- mo.id[i]
                indv.index[k,2] <- k.yr[k]
                usnip.prcp.sum.tmp[k] <- sum(tmp.yr$usnip.prcp) #Summing all prcp for month
                }
        mo.aggr.wt[i, ] <- t(colMeans(wt.sum, na.rm=TRUE)) #Weighted mean of all weekly values for a single month
        mo.aggr.wt.sd[i, ] <- t(colSD(wt.sum, na.rm=TRUE)) #Standard deviation of all weekly values for a single month
        mo.indv.wt <- rbind(mo.indv.wt, wt.sum)
        mo.indv.index <- rbind(mo.indv.index, indv.index)
        mo.usnip.prcp.sum <- c(mo.usnip.prcp.sum, usnip.prcp.sum.tmp)
        }
rownames(mo.aggr.wt) <- c("Jan", "Feb", "Mar", "Apr", "May", "Jun", "Jul",
         "Aug", "Sep", "Oct", "Nov", "Dec")
colnames(mo.aggr.wt) <- c("usnip.prcp", "d18O", "d2H", "d.ex", "gchn.prcp", "tmin",
        "tmax", "tavg", "tdif")
rownames(mo.aggr.wt.sd) <- c("Jan", "Feb", "Mar", "Apr", "May", "Jun", "Jul",
         "Aug", "Sep", "Oct", "Nov", "Dec")
colnames(mo.aggr.wt.sd) <- c("usnip.prcp", "d18O", "d2H", "d.ex", "gchn.prcp", "tmin",
        "tmax", "tavg", "tdif")

#Variable containing individual month/yr data
mo.indv.wt <- data.frame(mo.indv.wt, mo.indv.index)
colnames(mo.indv.wt) <- c("usnip.prcp", "d18O", "d2H", "d.ex", "gchn.prcp", "tmin",
        "tmax", "tavg", "tdif", "mo", "yr")
mo.indv.wt <- na.omit(mo.indv.wt)

mo.usnip.prcp.sum <- data.frame(mo.usnip.prcp.sum, mo.indv.index)
colnames(mo.usnip.prcp.sum) <- c("prcp.sum", "mo", "yr")
mo.usnip.prcp.sum <- mo.usnip.prcp.sum[mo.usnip.prcp.sum$prcp.sum > 0, ]


#Deleting precip columns because they don't mean anything in reality (because not complete aggregates)
mo.aggr.wt <- mo.aggr.wt[-c(1,5)]
mo.aggr.wt.sd <- mo.aggr.wt.sd[-c(1,5)]
mo.indv.wt <- mo.indv.wt[-c(1,5)]
```

```
siteloop.mo.aggr.wt <- mo.aggr.wt
siteloop.mo.aggr.wt.sd <- mo.aggr.wt.sd
siteloop.mo.indv.wt <- mo.indv.wt
siteloop.mo.usnip.prcp.sum <- mo.usnip.prcp.sum
siteloop.mo.aggr.wt$site <- site.index[h]
siteloop.mo.aggr.wt.sd$site <- site.index[h]
siteloop.mo.indv.wt$site <- site.index[h]
siteloop.mo.usnip.prcp.sum$site <- site.index[h]

total.mo.aggr.wt[[h]] <- siteloop.mo.aggr.wt
total.mo.aggr.wt.sd[[h]] <- siteloop.mo.aggr.wt.sd
total.mo.indv.wt[[h]] <- siteloop.mo.indv.wt
total.mo.usnip.prcp.sum[[h]] <- siteloop.mo.usnip.prcp.sum

#---------------------------------------Seasonal Data----------------------------------------
#Calculating seasonal data

#Loop to determine weighted average seasonal values
season.aggr.wt <-data.frame(matrix(nrow=4, ncol=9))
season.aggr.wt.sd <-data.frame(matrix(nrow=4, ncol=9))
season.indv.wt <- data.frame(matrix(nrow=0, ncol=9))
season.indv.index <- data.frame(matrix(nrow=0, ncol=2))
season.usnip.prcp.sum <- NULL
k.yr <- c(1989:2006) #To link k index value to correct year
for (i in 1:4) { #Season by season loop
        tmp.season <- siteloop.data[siteloop.data$season == season.id[i], ]
        wt.sum <- data.frame(matrix(nrow=4, ncol=(length(tmp.season)-3)))
        indv.index <- data.frame(matrix(nrow=4, ncol=2))
        usnip.prcp.sum.tmp <- NULL
        for (k in 1:length(k.yr)) { #Group by year loop
                tmp.yr <- tmp.season[tmp.season$yr == k.yr[k], ]
                frac.season <- NULL
```

```
                weighted <- data.frame(matrix(nrow=length(tmp.yr$yr), ncol=(length(tmp.yr)-3)))
                for (j in 1:length(tmp.yr$usnip.prcp)) { #Weighted average for a single season
                        frac.season[j] <- tmp.yr$usnip.prcp[j]/sum(tmp.yr$usnip.prcp)
                        weighted[j, ] <- (tmp.yr[j,-c(9:11)] * frac.season[j])
                        }
                wt.sum[k, ] <- t(colSums(weighted)) #All yearly weighted values for a single season
                indv.index[k,1] <- season.id[i]
                indv.index[k,2] <- k.yr[k]
                usnip.prcp.sum.tmp[k] <- sum(tmp.yr$usnip.prcp) #Summing all prcp for season
                }
        season.aggr.wt[i, ] <- t(colMeans(wt.sum, na.rm=TRUE)) #Weighted mean of all weekly values for a single season
        season.aggr.wt.sd[i, ] <- t(colSD(wt.sum, na.rm=TRUE)) #Standard deviation of all weekly values for a single season
        season.indv.wt <- rbind(season.indv.wt, wt.sum)
        season.indv.index <- rbind(season.indv.index, indv.index)
        season.usnip.prcp.sum <- c(season.usnip.prcp.sum, usnip.prcp.sum.tmp)
        }
rownames(season.aggr.wt) <- c("win", "spr", "sum", "aut")
colnames(season.aggr.wt) <- c("usnip.prcp", "d18O", "d2H", "d.ex", "gchn.prcp", "tmin",
        "tmax", "tavg", "tdif")
rownames(season.aggr.wt.sd) <- c("win", "spr", "sum", "aut")
colnames(season.aggr.wt.sd) <- c("usnip.prcp", "d18O", "d2H", "d.ex", "gchn.prcp", "tmin",
        "tmax", "tavg", "tdif")

#Variable containing individual season/yr data
season.indv.wt <- data.frame(season.indv.wt, season.indv.index)
colnames(season.indv.wt) <- c("usnip.prcp", "d18O", "d2H", "d.ex", "gchn.prcp", "tmin",
        "tmax", "tavg", "tdif", "season", "yr")
season.indv.wt <- na.omit(season.indv.wt)

season.usnip.prcp.sum <- data.frame(season.usnip.prcp.sum, season.indv.index)
colnames(season.usnip.prcp.sum) <- c("prcp.sum", "season", "yr")
season.usnip.prcp.sum <- season.usnip.prcp.sum[season.usnip.prcp.sum$prcp.sum > 0, ]

#Deleting precip columns because they don't mean anything in reality
```

```
season.aggr.wt <- season.aggr.wt[-c(1,5)]
season.aggr.wt.sd <- season.aggr.wt.sd[-c(1,5)]
season.indv.wt <- season.indv.wt[-c(1,5)]

siteloop.season.aggr.wt <- season.aggr.wt
siteloop.season.aggr.wt.sd <- season.aggr.wt.sd
siteloop.season.indv.wt <- season.indv.wt
siteloop.season.usnip.prcp.sum <- season.usnip.prcp.sum
siteloop.season.aggr.wt$site <- site.index[h]
siteloop.season.aggr.wt.sd$site <- site.index[h]
siteloop.season.indv.wt$site <- site.index[h]
siteloop.season.usnip.prcp.sum$site <- site.index[h]

total.season.aggr.wt[[h]] <- siteloop.season.aggr.wt
total.season.aggr.wt.sd[[h]] <- siteloop.season.aggr.wt.sd
total.season.indv.wt[[h]] <- siteloop.season.indv.wt
total.season.usnip.prcp.sum[[h]] <- siteloop.season.usnip.prcp.sum

#---------------------------------------Water Yearly Data-----------------------------------------
#Calculating water-yearly datasets
#Note: Data from Jan-Sep 1989 and Oct-Dec 2004 not included due to lack of full
#water year data.

water.yr.id <- c("01", "02", "03", "04", "05", "06", "07", "08", "09",
        "10", "11", "12")
k.yr <- c(1989:2006) #To link k index value to correct year
water.yr.wt <- data.frame(matrix(nrow=15, ncol=(length(tmp.mo)-3)))
water.yr.indv <- data.frame(matrix(nrow=0, ncol=9))
water.yr.indv.index <- NULL
for (i in 1:15) {
        water.yr.a <- siteloop.data[(siteloop.data$mo == water.yr.id[10] | siteloop.data$mo == water.yr.id[11] |
                siteloop.data$mo == water.yr.id[12]) & siteloop.data$yr == k.yr[i], ] #Oct-Dec portion
        water.yr.b <- siteloop.data[(siteloop.data$mo == water.yr.id[1] | siteloop.data$mo == water.yr.id[2] |
                siteloop.data$mo == water.yr.id[3] | siteloop.data$mo == water.yr.id[4] |
```

```
                siteloop.data$mo == water.yr.id[5] | siteloop.data$mo == water.yr.id[6] |
                siteloop.data$mo == water.yr.id[7] | siteloop.data$mo == water.yr.id[8] |
                siteloop.data$mo == water.yr.id[9]) & siteloop.data$yr == k.yr[i+1], ] #Jan-Sep portion
        tmp.water.yr <- rbind(water.yr.a, water.yr.b)
        frac.water.yr <- NULL
        weighted <- data.frame(matrix(nrow=length(tmp.water.yr$yr), ncol=(length(tmp.yr)-3)))
        if (length(tmp.water.yr$usnip.prcp != 0)) {
                for (j in 1:length(tmp.water.yr$usnip.prcp)) { #Weighted average for a single water yr
                        frac.water.yr[j] <- tmp.water.yr$usnip.prcp[j]/sum(tmp.water.yr$usnip.prcp)
                        weighted[j, ] <- (tmp.water.yr[j,-c(9:11)] * frac.water.yr[j])
                        water.yr.indv.index <- c(water.yr.indv.index, k.yr[i+1])
                        }
                }
        water.yr.wt[i, ] <- t(colSums(weighted)) #All yearly weighted values for a single water yr
        #Individual data not weighted because already at weekly scale
        water.yr.indv <- rbind(water.yr.indv, tmp.water.yr[ , -c(9:11)])
        }
rownames(water.yr.wt) <- c(1990:2004)
colnames(water.yr.wt) <- c("usnip.prcp", "d18O", "d2H", "d.ex", "gchn.prcp", "tmin",
        "tmax", "tavg", "tdif")

#Variable containing individual month/yr data
water.yr.indv <- data.frame(water.yr.indv, water.yr.indv.index)
colnames(water.yr.indv) <- c("usnip.prcp", "d18O", "d2H", "d.ex", "gchn.prcp", "tmin",
        "tmax", "tavg", "tdif", "water.yr")
water.yr.indv <- na.omit(water.yr.indv)

siteloop.water.yr.wt <- water.yr.wt
siteloop.water.yr.indv <- water.yr.indv
siteloop.water.yr.wt$site <- site.index[h]
siteloop.water.yr.indv$site <- site.index[h]

total.water.yr.wt[[h]] <- siteloop.water.yr.wt
total.water.yr.indv[[h]] <- siteloop.water.yr.indv
```

```
        siteloop.data$site <- site.index[h]
        totalsites.data[[h]] <- siteloop.data
        totalsites.dates[[h]] <- siteloop.dates
        }

names(totalsites.data) <- site.index
names(totalsites.dates) <- site.index
names(totalsites.lmwl) <- site.index
names(total.week.d18O.corr) <- site.index
names(total.mo.aggr.wt) <- site.index
names(total.mo.aggr.wt.sd) <- site.index
names(total.mo.indv.wt) <- site.index
names(total.season.aggr.wt) <- site.index
names(total.season.aggr.wt.sd) <- site.index
names(total.season.indv.wt) <- site.index
names(total.water.yr.wt) <- site.index
names(total.water.yr.indv) <- site.index
names(total.mo.usnip.prcp.sum) <- site.index
names(total.season.usnip.prcp.sum) <- site.index
```

```
#=============================================================================================================
#-------------------------------------------------------------------------------------------------------------
#This script loops through every site and sorts out the data by groups and aggregations and calculates
        #a correlation and linear model for data.
#Written by Pete D. Akers 2015
#----------------------------------Week Relationships-----------------------------------------
```

```
week.lmcor <- data.frame(matrix(ncol=25, nrow=length(site.index)))#List of sites, each with list of aggr
        #monthly correlations and linear models

for (i in 1:length(site.index)) { #Looping through each site
        #---Average Temperature----
        tavg.d18O.lm <- (lm(totalsites.data[[i]]$d18O ~ totalsites.data[[i]]$tavg))
        week.lmcor[i,1] <- length(totalsites.data[[i]]$tavg)
        week.lmcor[i,2] <- tavg.d18O.lm$coefficients[2]
        week.lmcor[i,3] <- tavg.d18O.lm$coefficients[1]
        week.lmcor[i,4] <- summary(tavg.d18O.lm)$coefficients[4]
        week.lmcor[i,5] <- summary(tavg.d18O.lm)$coefficients[3]
        if(length(totalsites.data[[i]]$tavg) > 2) {
                week.lmcor[i,6] <- (cor(totalsites.data[[i]]$tavg, totalsites.data[[i]]$d18O))^2
                week.lmcor[i,7] <- cor.test(totalsites.data[[i]]$tavg, totalsites.data[[i]]$d18O)$p.value
                }
        #---Temperature Difference----
        tdif.d18O.lm <- (lm(totalsites.data[[i]]$d18O ~ totalsites.data[[i]]$tdif))
        week.lmcor[i,8] <- tdif.d18O.lm$coefficients[2]
        week.lmcor[i,9] <- tdif.d18O.lm$coefficients[1]
        week.lmcor[i,10] <- summary(tdif.d18O.lm)$coefficients[4]
        week.lmcor[i,11] <- summary(tdif.d18O.lm)$coefficients[3]
        if(length(totalsites.data[[i]]$tdif) > 2) {
                week.lmcor[i,12] <- (cor(totalsites.data[[i]]$tdif, totalsites.data[[i]]$d18O))^2
                week.lmcor[i,13] <- cor.test(totalsites.data[[i]]$tdif, totalsites.data[[i]]$d18O)$p.value
                }
        #---Precipitation Amount----
        prcp.d18O.lm <- (lm(totalsites.data[[i]]$d18O ~ log(totalsites.data[[i]]$usnip.prcp + 1)))
        week.lmcor[i,14] <- prcp.d18O.lm$coefficients[2]
        week.lmcor[i,15] <- prcp.d18O.lm$coefficients[1]
        week.lmcor[i,16] <- summary(prcp.d18O.lm)$coefficients[4]
        week.lmcor[i,17] <- summary(prcp.d18O.lm)$coefficients[3]
        if(length(totalsites.data[[i]]$usnip.prcp) > 2) {
                week.lmcor[i,18] <- (cor(log(totalsites.data[[i]]$usnip.prcp + 1), totalsites.data[[i]]$d18O))^2
                week.lmcor[i,19] <- cor.test(log(totalsites.data[[i]]$usnip.prcp + 1),
```

```
                totalsites.data[[i]]$d18O)$p.value
        }
    #---LMWL-------------------
    d18O.d2H.lm <- (lm(totalsites.data[[i]]$d2H ~ totalsites.data[[i]]$d18O))
    week.lmcor[i,20] <- d18O.d2H.lm$coefficients[2]
    week.lmcor[i,21] <- d18O.d2H.lm$coefficients[1]
    week.lmcor[i,22] <- summary(d18O.d2H.lm)$coefficients[4]
    week.lmcor[i,23] <- summary(d18O.d2H.lm)$coefficients[3]
    if(length(totalsites.data[[i]]$d2H) > 2) {
        week.lmcor[i,24] <- (cor(totalsites.data[[i]]$d18O, totalsites.data[[i]]$d2H))^2
        week.lmcor[i,25] <- cor.test(totalsites.data[[i]]$d18O, totalsites.data[[i]]$d2H)$p.value
        }
    }
rownames(week.lmcor) <- site.index
colnames(week.lmcor) <- c("n.wk", "tavg.slope", "tavg.yint", "tavg.slope.err", "tavg.yint.err", "tavg.r2",
    "tavg.pval", "tdif.slope", "tdif.yint", "tdif.slope.err", "tdif.yint.err", "tdif.r2",
    "tdif.pval", "prcp.slope", "prcp.yint", "prcp.slope.err", "prcp.yint.err", "prcp.r2", "prcp.pval",
    "lmwl.slope", "lmwl.yint", "lmwl.slope.err", "lmwl.yint.err", "lmwl.r2", "lmwl.pval")
week.lmcor <- round(week.lmcor, 4)
#write.table(week.lmcor, "usnip_slope_week.csv", sep=",", row.names=TRUE, col.names=NA)

#-----------------------------------Week R2----------------------------------------
#This produces results similar to the aggregated r2
week.r2 <- data.frame(matrix(ncol=8, nrow=25))#List of sites, each with list of aggr season correlations and linear models

for (i in 1:length(site.index)) { #Looping through each site
    #---Calculating r2 with d18O
        week.r2[i,1] <- length(totalsites.data[[i]]$d18O)
    if(length(totalsites.data[[i]]$d18O) > 2) {
        week.r2[i,2] <- (cor(totalsites.data[[i]]$d2H, totalsites.data[[i]]$d18O))^2
        week.r2[i,3] <- (cor(totalsites.data[[i]]$d.ex, totalsites.data[[i]]$d18O))^2
        week.r2[i,4] <- (cor(totalsites.data[[i]]$tmax, totalsites.data[[i]]$d18O))^2
        week.r2[i,5] <- (cor(totalsites.data[[i]]$tmin, totalsites.data[[i]]$d18O))^2
        week.r2[i,6] <- (cor(totalsites.data[[i]]$tavg, totalsites.data[[i]]$d18O))^2
```

```
                week.r2[i,7]      <- (cor(totalsites.data[[i]]$tdif, totalsites.data[[i]]$d18O))^2
                week.r2[i,8]      <- (cor(log(totalsites.data[[i]]$usnip.prcp + 1), totalsites.data[[i]]$d18O))^2
                }
        }
rownames(week.r2) <- site.index
colnames(week.r2) <- c("n.week", "d2H.r2.week", "dex.r2.week", "tmax.r2.week", "tmin.r2.week",
        "tavg.r2.week", "tdif.r2.week", "prcp.r2.week")
week.r2 <- round(week.r2, 4)
#write.table(week.r2, "usnip_r2_week.csv", sep=",", row.names=TRUE, col.names=NA)

#-----------------------------------Aggregate Month Relationships-----------------------------------------
aggr.month <- list(NULL) #Splits mo.indv.wt into subsets for later loop to use
mo.aggr.lmcor <- data.frame(matrix(ncol=19, nrow=length(site.index)))#List of sites, each with list of aggr monthly correlations and linear
models

for (i in 1:length(site.index)) { #Looping through each site
        aggr.month[[i]] <- total.mo.indv.wt[[i]]
        #-----Average Temperature-------
        tavg.d18O.lm <- (lm(aggr.month[[i]]$d18O ~ aggr.month[[i]]$tavg))
        mo.aggr.lmcor[i,1] <- length(aggr.month[[i]]$tavg)
        mo.aggr.lmcor[i,2] <- tavg.d18O.lm$coefficients[2]
        mo.aggr.lmcor[i,3] <- tavg.d18O.lm$coefficients[1]
        mo.aggr.lmcor[i,4] <- summary(tavg.d18O.lm)$coefficients[4]
        mo.aggr.lmcor[i,5] <- summary(tavg.d18O.lm)$coefficients[3]
        if(length(aggr.month[[i]]$tavg) > 2) {
                mo.aggr.lmcor[i,6] <- (cor(aggr.month[[i]]$tavg, aggr.month[[i]]$d18O))^2
                mo.aggr.lmcor[i,7]        <- cor.test(aggr.month[[i]]$tavg, aggr.month[[i]]$d18O)$p.value
                }
        #-----Temperature Diff----------
        tdif.d18O.lm <- (lm(aggr.month[[i]]$d18O ~ aggr.month[[i]]$tdif))
        mo.aggr.lmcor[i,8] <- tdif.d18O.lm$coefficients[2]
        mo.aggr.lmcor[i,9] <- tdif.d18O.lm$coefficients[1]
        mo.aggr.lmcor[i,10] <- summary(tdif.d18O.lm)$coefficients[4]
        mo.aggr.lmcor[i,11] <- summary(tdif.d18O.lm)$coefficients[3]
```

```
	if(length(aggr.month[[i]]$tdif) > 2) {
		mo.aggr.lmcor[i,12] <- (cor(aggr.month[[i]]$tdif, aggr.month[[i]]$d18O))^2
		mo.aggr.lmcor[i,13]	<- cor.test(aggr.month[[i]]$tdif, aggr.month[[i]]$d18O)$p.value
		}
	#-----LMWL----------
	d18O.d2H.lm <- (lm(aggr.month[[i]]$d2H ~ aggr.month[[i]]$d18O))
	mo.aggr.lmcor[i,14] <- d18O.d2H.lm$coefficients[2]
	mo.aggr.lmcor[i,15] <- d18O.d2H.lm$coefficients[1]
	mo.aggr.lmcor[i,16] <- summary(d18O.d2H.lm)$coefficients[4]
	mo.aggr.lmcor[i,17] <- summary(d18O.d2H.lm)$coefficients[3]
	if(length(aggr.month[[i]]$d2H) > 2) {
		mo.aggr.lmcor[i,18] <- (cor(aggr.month[[i]]$d18O, aggr.month[[i]]$d2H))^2
		mo.aggr.lmcor[i,19]	<- cor.test(aggr.month[[i]]$d18O, aggr.month[[i]]$d2H)$p.value
		}
	}
rownames(mo.aggr.lmcor) <- site.index
colnames(mo.aggr.lmcor) <- c("n.mo", "slope.tavg.mo", "yint.tavg.mo", "slope.err.tavg.mo.",
	"yint.err.tavg.mo", "r2.tavg.mo", "pval.tavg.mo", "slope.tdif.mo", "yint.tdif.mo",
	"slope.err.tdif.mo", "yint.err.tdif.mo", "r2.tdif.mo", "pval.tdif.mo", "slope.lmwl.mo",
	"yint.lmwl.mo", "slope.err.lmwl.mo", "yint.err.lmwl.mo", "r2.lmwl.mo", "pval.lmwl.mo")
mo.aggr.lmcor <- round(mo.aggr.lmcor, 4)
#write.table(mo.aggr.lmcor, "usnip_slope_mo_aggr.csv", sep=",", row.names=TRUE, col.names=NA)

#-------------------------------------Aggregate Season Relationships-----------------------------------------------------
aggr.season <- list(NULL) #Splits season.indv.wt into subsets for later loop to use
season.index <- c("01", "02", "03", "04", "05", "06", "07", "08",
		"09", "10", "11", "12")
season.aggr.lmcor <- data.frame(matrix(ncol=19, nrow=length(site.index)))#List of sites, each with list of aggr monthly correlations and linear
models


for (i in 1:length(site.index)) { #Looping through each site
	aggr.season[[i]] <- total.season.indv.wt[[i]]
	#-----Average Temperature-------
```

```
        tavg.d18O.lm <- (lm(aggr.season[[i]]$d18O ~ aggr.season[[i]]$tavg))
        season.aggr.lmcor[i,1] <- length(aggr.season[[i]]$tavg)
        season.aggr.lmcor[i,2] <- tavg.d18O.lm$coefficients[2]
        season.aggr.lmcor[i,3] <- tavg.d18O.lm$coefficients[1]
        season.aggr.lmcor[i,4] <- summary(tavg.d18O.lm)$coefficients[4]
        season.aggr.lmcor[i,5] <- summary(tavg.d18O.lm)$coefficients[3]
        if(length(aggr.season[[i]]$tavg) > 2) {
                season.aggr.lmcor[i,6] <- (cor(aggr.season[[i]]$tavg, aggr.season[[i]]$d18O))^2
                season.aggr.lmcor[i,7]    <- cor.test(aggr.season[[i]]$tavg, aggr.season[[i]]$d18O)$p.value
                }
        #-----Temperature Diff----------
        tdif.d18O.lm <- (lm(aggr.season[[i]]$d18O ~ aggr.season[[i]]$tdif))
        season.aggr.lmcor[i,8] <- tdif.d18O.lm$coefficients[2]
        season.aggr.lmcor[i,9] <- tdif.d18O.lm$coefficients[1]
        season.aggr.lmcor[i,10] <- summary(tdif.d18O.lm)$coefficients[4]
        season.aggr.lmcor[i,11] <- summary(tdif.d18O.lm)$coefficients[3]
        if(length(aggr.season[[i]]$tdif) > 2) {
                season.aggr.lmcor[i,12] <- (cor(aggr.season[[i]]$tdif, aggr.season[[i]]$d18O))^2
                season.aggr.lmcor[i,13] <- cor.test(aggr.season[[i]]$tdif, aggr.season[[i]]$d18O)$p.value
                }
        #-----LMWL----------
        d18O.d2H.lm <- (lm(aggr.season[[i]]$d2H ~ aggr.season[[i]]$d18O))
        season.aggr.lmcor[i,14] <- d18O.d2H.lm$coefficients[2]
        season.aggr.lmcor[i,15] <- d18O.d2H.lm$coefficients[1]
        season.aggr.lmcor[i,16] <- summary(d18O.d2H.lm)$coefficients[4]
        season.aggr.lmcor[i,17] <- summary(d18O.d2H.lm)$coefficients[3]
        if(length(aggr.season[[i]]$d2H) > 2) {
                season.aggr.lmcor[i,18] <- (cor(aggr.season[[i]]$d18O, aggr.season[[i]]$d2H))^2
                season.aggr.lmcor[i,19] <- cor.test(aggr.season[[i]]$d18O, aggr.season[[i]]$d2H)$p.value
                }
        }
rownames(season.aggr.lmcor) <- site.index
colnames(season.aggr.lmcor) <- c("n.season", "slope.tavg.season", "yint.tavg.season", "slope.err.tavg.season.",
        "yint.err.tavg.season", "r2.tavg.season", "pval.tavg.season", "slope.tdif.season", "yint.tdif.season",
```

```
        "slope.err.tdif.season", "yint.err.tdif.season", "r2.tdif.season", "pval.tdif.season", "slope.lmwl.season",
        "yint.lmwl.season", "slope.err.lmwl.season", "yint.err.lmwl.season", "r2.lmwl.season", "pval.lmwl.season")
season.aggr.lmcor <- round(season.aggr.lmcor, 4)
#write.table(season.aggr.lmcor, "usnip_slope_season_aggr.csv", sep=",", row.names=TRUE, col.names=NA)

#-----------------------------------Aggregate Month R2----------------------------------------
aggr.month <- list(NULL) #List of sites, each with list of monthly aggregate data
mo.aggr.r2 <- data.frame(matrix(ncol=7, nrow=length(site.index)))#List of sites, each with list of aggr monthly correlations and linear models

for (i in 1:length(site.index)) { #Looping through each site
        aggr.month[[i]] <- total.mo.indv.wt[[i]]
        #---Calculating r2 with d18O
        mo.aggr.r2[i,1] <- length(aggr.month[[i]]$d18O)
        if(length(aggr.month[[i]]$d18O) > 2) {
                mo.aggr.r2[i,2] <- (cor(aggr.month[[i]]$d2H, aggr.month[[i]]$d18O))^2
                mo.aggr.r2[i,3] <- (cor(aggr.month[[i]]$d.ex, aggr.month[[i]]$d18O))^2
                mo.aggr.r2[i,4] <- (cor(aggr.month[[i]]$tmax, aggr.month[[i]]$d18O))^2
                mo.aggr.r2[i,5] <- (cor(aggr.month[[i]]$tmin, aggr.month[[i]]$d18O))^2
                mo.aggr.r2[i,6] <- (cor(aggr.month[[i]]$tavg, aggr.month[[i]]$d18O))^2
                mo.aggr.r2[i,7]  <- (cor(aggr.month[[i]]$tdif, aggr.month[[i]]$d18O))^2
                }
        }
rownames(mo.aggr.r2) <- site.index
colnames(mo.aggr.r2) <- c("n.mo", "d2H.r2.mo", "dex.r2.mo", "tmax.r2.mo", "tmin.r2.mo",
        "tavg.r2.mo", "tdif.r2.mo")
mo.aggr.r2 <- round(mo.aggr.r2, 4)
#write.table(mo.aggr.r2, "usnip_r2_mo_aggr.csv", sep=",", row.names=TRUE, col.names=NA)


#-----------------------------------Aggregate Season R2----------------------------------------
aggr.season <- list(NULL) #List of sites, each with list of season aggregate data
season.aggr.r2 <- data.frame(matrix(ncol=7, nrow=length(site.index)))#List of sites, each with list of aggr season correlations and linear models

for (i in 1:length(site.index)) { #Looping through each site
```

```
		aggr.season[[i]] <- total.season.indv.wt[[i]]
		#---Calculating r2 with d18O
		season.aggr.r2[i,1] <- length(aggr.season[[i]]$d18O)
		if(length(aggr.season[[i]]$d18O) > 2) {
			season.aggr.r2[i,2] <- (cor(aggr.season[[i]]$d2H, aggr.season[[i]]$d18O))^2
			season.aggr.r2[i,3] <- (cor(aggr.season[[i]]$d.ex, aggr.season[[i]]$d18O))^2
			season.aggr.r2[i,4] <- (cor(aggr.season[[i]]$tmax, aggr.season[[i]]$d18O))^2
			season.aggr.r2[i,5] <- (cor(aggr.season[[i]]$tmin, aggr.season[[i]]$d18O))^2
			season.aggr.r2[i,6] <- (cor(aggr.season[[i]]$tavg, aggr.season[[i]]$d18O))^2
			season.aggr.r2[i,7]	<- (cor(aggr.season[[i]]$tdif, aggr.season[[i]]$d18O))^2
			}
		}
rownames(season.aggr.r2) <- site.index
colnames(season.aggr.r2) <- c("n.season", "d2H.r2.season", "dex.r2.season", "tmax.r2.season", "tmin.r2.season",
		"tavg.r2.season", "tdif.r2.season")
season.aggr.r2 <- round(season.aggr.r2, 4)
#write.table(season.aggr.r2, "usnip_r2_season_aggr.csv", sep=",", row.names=TRUE, col.names=NA)


#----------------------------------------Grouped Monthly Relationships----------------------------
by.mo <- list(NULL) #Splits total weekly into monthly subsets for later loop to use
wt.mo <- list(NULL) #Splits aggregated weighted monthly values into subset for later loop to use
mo.data <- list(NULL) #List of sites, each with list of monthly data
mo.index <- c("01", "02", "03", "04", "05", "06", "07", "08",
			"09", "10", "11", "12")
mo.lmcor <- list(NULL) #List of sites, each with list of monthly correlations and linear models


for (j in 1:length(site.index)) { #Looping through each site
		by.mo[[j]] <- totalsites.data[[j]]
		wt.mo[[j]] <- total.mo.aggr.wt[[j]]
		mo.data.tmp <- list(NULL)
		mo.lmcor.tmp <- data.frame(matrix(nrow=12, ncol=31))
		for (i in 1:length(unique(by.mo[[j]]$mo))) { #Looping through each mo
```

```
mo.data.tmp[[i]] <- by.mo[[j]][by.mo[[j]]$mo == mo.index[i], c(1:4, 8, 12)]
colnames(mo.lmcor.tmp) <- c("n.wk", "tavg.slope", "tavg.yint", "tavg.slope.err", "tavg.yint.err",
"tavg.r2", "tavg.pval", "tdif.slope", "tdif.yint", "tdif.slope.err", "tdif.yint.err", "tdif.r2",
"tdif.pval", "prcp.slope", "prcp.yint", "prcp.slope.err", "prcp.yint.err", "prcp.r2",
"prcp.pval", "lmwl.slope", "lmwl.yint", "lmwl.slope.err", "lmwl.yint.err", "lmwl.r2",
"lmwl.pval", "d18O.wt", "d18O.wt.err", "tavg.wt", "tavg.wt.err", "tdif.wt", "tdif.wt.err")
rownames(mo.lmcor.tmp) <- c("jan", "feb", "mar", "apr", "may", "jun", "jul", "aug",
                    "sep", "oct", "nov", "dec")
#---Average Temperature----
tavg.d18O.lm.tmp <- (lm(mo.data.tmp[[i]]$d18O ~ mo.data.tmp[[i]]$tavg))
mo.lmcor.tmp[i,1] <- length(mo.data.tmp[[i]]$tavg)
mo.lmcor.tmp[i,2] <- tavg.d18O.lm.tmp$coefficients[2]
mo.lmcor.tmp[i,3] <- tavg.d18O.lm.tmp$coefficients[1]
mo.lmcor.tmp[i,4] <- summary(tavg.d18O.lm.tmp)$coefficients[4]
mo.lmcor.tmp[i,5] <- summary(tavg.d18O.lm.tmp)$coefficients[3]
if(length(mo.data.tmp[[i]]$tavg) > 2) {
        mo.lmcor.tmp[i,6] <- (cor(mo.data.tmp[[i]]$tavg, mo.data.tmp[[i]]$d18O))^2
        mo.lmcor.tmp[i,7]       <- cor.test(mo.data.tmp[[i]]$tavg, mo.data.tmp[[i]]$d18O)$p.value
        }
#---Temperature Difference----
tdif.d18O.lm.tmp <- (lm(mo.data.tmp[[i]]$d18O ~ mo.data.tmp[[i]]$tdif))
mo.lmcor.tmp[i,8] <- tdif.d18O.lm.tmp$coefficients[2]
mo.lmcor.tmp[i,9] <- tdif.d18O.lm.tmp$coefficients[1]
mo.lmcor.tmp[i,10] <- summary(tdif.d18O.lm.tmp)$coefficients[4]
mo.lmcor.tmp[i,11] <- summary(tdif.d18O.lm.tmp)$coefficients[3]
if(length(mo.data.tmp[[i]]$tdif) > 2) {
        mo.lmcor.tmp[i,12] <- (cor(mo.data.tmp[[i]]$tdif, mo.data.tmp[[i]]$d18O))^2
        mo.lmcor.tmp[i,13]      <- cor.test(mo.data.tmp[[i]]$tdif, mo.data.tmp[[i]]$d18O)$p.value
        }
#---USNIP Precipitation Amount----
prcp.d18O.lm.tmp <- (lm(mo.data.tmp[[i]]$d18O ~ log(mo.data.tmp[[i]]$usnip.prcp +1)))
mo.lmcor.tmp[i,14] <- prcp.d18O.lm.tmp$coefficients[2]
mo.lmcor.tmp[i,15] <- prcp.d18O.lm.tmp$coefficients[1]
mo.lmcor.tmp[i,16] <- summary(prcp.d18O.lm.tmp)$coefficients[4]
```

```
                mo.lmcor.tmp[i,17] <- summary(prcp.d18O.lm.tmp)$coefficients[3]
                if(length(mo.data.tmp[[i]]$usnip.prcp) > 2) {
                        mo.lmcor.tmp[i,18] <- (cor(log(mo.data.tmp[[i]]$usnip.prcp +1),
                                mo.data.tmp[[i]]$d18O))^2
                        mo.lmcor.tmp[i,19]      <- cor.test(log(mo.data.tmp[[i]]$usnip.prcp +1),
                                mo.data.tmp[[i]]$d18O)$p.value
                        }
                #---LMWL----
                d18O.d2H.lm.tmp <- (lm(mo.data.tmp[[i]]$d2H ~ mo.data.tmp[[i]]$d18O))
                mo.lmcor.tmp[i,20] <- d18O.d2H.lm.tmp$coefficients[2]
                mo.lmcor.tmp[i,21] <- d18O.d2H.lm.tmp$coefficients[1]
                mo.lmcor.tmp[i,22] <- summary(d18O.d2H.lm.tmp)$coefficients[4]
                mo.lmcor.tmp[i,23] <- summary(d18O.d2H.lm.tmp)$coefficients[3]
                if(length(mo.data.tmp[[i]]$d2H) > 2) {
                        mo.lmcor.tmp[i,24] <- (cor(mo.data.tmp[[i]]$d18O, mo.data.tmp[[i]]$d2H))^2
                        mo.lmcor.tmp[i,25]      <- cor.test(mo.data.tmp[[i]]$d18O, mo.data.tmp[[i]]$d2H)$p.value
                        }
                mo.lmcor.tmp[i,26] <- wt.mo[[j]]$d18O[i]
                mo.lmcor.tmp[i,27] <- sd(mo.data.tmp[[i]]$d18O)/sqrt(length(mo.data.tmp[[i]]$d18O))
                mo.lmcor.tmp[i,28] <- wt.mo[[j]]$tavg[i]
                mo.lmcor.tmp[i,29] <- sd(mo.data.tmp[[i]]$tavg)/sqrt(length(mo.data.tmp[[i]]$tavg))
                mo.lmcor.tmp[i,30] <- wt.mo[[j]]$tdif[i]
                mo.lmcor.tmp[i,31] <- sd(mo.data.tmp[[i]]$tdif)/sqrt(length(mo.data.tmp[[i]]$tdif))
                }
        mo.lmcor.tmp <- round(mo.lmcor.tmp, 4)
        mo.data[[j]] <- mo.data.tmp
        names(mo.data[[j]]) <- c("jan", "feb", "mar", "apr", "may", "jun", "jul", "aug",
                                "sep", "oct", "nov", "dec")
        mo.lmcor[[j]] <- mo.lmcor.tmp
        }
names(mo.data) <- site.index
names(mo.lmcor) <- site.index
#write.table(mo.lmcor, "usnip_slope_mo.csv", sep=",", row.names=TRUE, col.names=NA)
```

```
#---------------------------------------Grouped Season Relationships----------------------------
by.season <- list(NULL) #Splits total weekly into monthly subsets for later loop to use
wt.season <- list(NULL) #Splits aggregated weighted monthly values into subset for later loop to use
season.data <- list(NULL) #List of sites, each with list of monthly data
season.index <- c("win", "spr", "sum", "aut")
season.lmcor <- list(NULL) #List of sites, each with list of monthly correlations and linear models


for (j in 1:length(site.index)) { #Looping through each site
        by.season[[j]] <- totalsites.data[[j]]
        wt.season[[j]] <- total.season.aggr.wt[[j]]
        season.data.tmp <- list(NULL)
        season.lmcor.tmp <- data.frame(matrix(nrow=4, ncol=31))
        for (i in 1:length(unique(by.season[[j]]$season))) { #Looping through each season
                season.data.tmp[[i]] <- by.season[[j]][by.season[[j]]$season == season.index[i], c(1:4, 8, 12)]
                colnames(season.lmcor.tmp) <- c("n.wk", "tavg.slope", "tavg.yint", "tavg.slope.err", "tavg.yint.err",
                "tavg.r2", "tavg.pval", "tdif.slope", "tdif.yint", "tdif.slope.err", "tdif.yint.err", "tdif.r2",
                "tdif.pval", "prcp.slope", "prcp.yint", "prcp.slope.err", "prcp.yint.err", "prcp.r2",
                "prcp.pval", "lmwl.slope", "lmwl.yint", "lmwl.slope.err", "lmwl.yint.err", "lmwl.r2",
                "lmwl.pval", "d18O.wt", "d18O.wt.err", "tavg.wt", "tavg.wt.err", "tdif.wt", "dif.wt.err")
                rownames(season.lmcor.tmp) <- c("win", "spr", "sum", "aut")
                #---Average Temperature----
                tavg.d18O.lm.tmp <- (lm(season.data.tmp[[i]]$d18O ~ season.data.tmp[[i]]$tavg))
                season.lmcor.tmp[i,1] <- length(season.data.tmp[[i]]$tavg)
                season.lmcor.tmp[i,2] <- tavg.d18O.lm.tmp$coefficients[2]
                season.lmcor.tmp[i,3] <- tavg.d18O.lm.tmp$coefficients[1]
                season.lmcor.tmp[i,4] <- summary(tavg.d18O.lm.tmp)$coefficients[4]
                season.lmcor.tmp[i,5] <- summary(tavg.d18O.lm.tmp)$coefficients[3]
                if(length(season.data.tmp[[i]]$tavg) > 2) {
                        season.lmcor.tmp[i,6] <- (cor(season.data.tmp[[i]]$tavg, season.data.tmp[[i]]$d18O))^2
                        season.lmcor.tmp[i,7]    <- cor.test(season.data.tmp[[i]]$tavg, season.data.tmp[[i]]$d18O)$p.value
                        }
                #---Temperature Difference----
```

```
tdif.d18O.lm.tmp <- (lm(season.data.tmp[[i]]$d18O ~ season.data.tmp[[i]]$tdif))
season.lmcor.tmp[i,8] <- tdif.d18O.lm.tmp$coefficients[2]
season.lmcor.tmp[i,9] <- tdif.d18O.lm.tmp$coefficients[1]
season.lmcor.tmp[i,10] <- summary(tdif.d18O.lm.tmp)$coefficients[4]
season.lmcor.tmp[i,11] <- summary(tdif.d18O.lm.tmp)$coefficients[3]
if(length(season.data.tmp[[i]]$tdif) > 2) {
        season.lmcor.tmp[i,12] <- (cor(season.data.tmp[[i]]$tdif, season.data.tmp[[i]]$d18O))^2
        season.lmcor.tmp[i,13]  <- cor.test(season.data.tmp[[i]]$tdif, season.data.tmp[[i]]$d18O)$p.value
        }
#---USNIP Precipitation Amount----
prcp.d18O.lm.tmp <- (lm(season.data.tmp[[i]]$d18O ~ log(season.data.tmp[[i]]$usnip.prcp +1)))
season.lmcor.tmp[i,14] <- prcp.d18O.lm.tmp$coefficients[2]
season.lmcor.tmp[i,15] <- prcp.d18O.lm.tmp$coefficients[1]
season.lmcor.tmp[i,16] <- summary(prcp.d18O.lm.tmp)$coefficients[4]
season.lmcor.tmp[i,17] <- summary(prcp.d18O.lm.tmp)$coefficients[3]
if(length(season.data.tmp[[i]]$usnip.prcp) > 2) {
        season.lmcor.tmp[i,18] <- (cor(log(season.data.tmp[[i]]$usnip.prcp +1),
                season.data.tmp[[i]]$d18O))^2
        season.lmcor.tmp[i,19]  <- cor.test(log(season.data.tmp[[i]]$usnip.prcp +1),
                season.data.tmp[[i]]$d18O)$p.value
        }
#---LMWL----
d18O.d2H.lm.tmp <- (lm(season.data.tmp[[i]]$d2H ~ season.data.tmp[[i]]$d18O))
season.lmcor.tmp[i,20] <- d18O.d2H.lm.tmp$coefficients[2]
season.lmcor.tmp[i,21] <- d18O.d2H.lm.tmp$coefficients[1]
season.lmcor.tmp[i,22] <- summary(d18O.d2H.lm.tmp)$coefficients[4]
season.lmcor.tmp[i,23] <- summary(d18O.d2H.lm.tmp)$coefficients[3]
if(length(season.data.tmp[[i]]$d2H) > 2) {
        season.lmcor.tmp[i,24] <- (cor(season.data.tmp[[i]]$d18O, season.data.tmp[[i]]$d2H))^2
        season.lmcor.tmp[i,25]  <- cor.test(season.data.tmp[[i]]$d18O, season.data.tmp[[i]]$d2H)$p.value
        }
season.lmcor.tmp[i,26] <- wt.season[[j]]$d18O[i]
season.lmcor.tmp[i,27] <- sd(season.data.tmp[[i]]$d18O)/sqrt(length(season.data.tmp[[i]]$d18O))
season.lmcor.tmp[i,28] <- wt.season[[j]]$tavg[i]
```

```
                season.lmcor.tmp[i,29] <- sd(season.data.tmp[[i]]$tavg)/sqrt(length(season.data.tmp[[i]]$tavg))
                season.lmcor.tmp[i,30] <- wt.season[[j]]$tdif[i]
                season.lmcor.tmp[i,31] <- sd(season.data.tmp[[i]]$tdif)/sqrt(length(season.data.tmp[[i]]$tdif))
                }
        season.lmcor.tmp <- round(season.lmcor.tmp, 4)
        season.data[[j]] <- season.data.tmp
        names(season.data[[j]]) <- c("win", "spr", "sum", "aut")
        season.lmcor[[j]] <- season.lmcor.tmp
        }
names(season.data) <- site.index
names(season.lmcor) <- site.index
#write.table(season.lmcor, "usnip_slope_season.csv", sep=",", row.names=TRUE, col.names=NA)

#This section splits up the seasonally grouped data correlations by season for easier mapping
#and comparison
lmcor.win <- data.frame(matrix(nrow=0, ncol=length(season.lmcor[[1]])))
for(i in 1:length(site.index)) {
        lmcor.win <- rbind(lmcor.win, season.lmcor[[i]][1, ])
        }
rownames(lmcor.win) <- site.index
#write.table(lmcor.win, "usnip_lmcor_win.csv", sep=",", row.names=TRUE, col.names=NA)

lmcor.spr <- data.frame(matrix(nrow=0, ncol=length(season.lmcor[[1]])))
for(i in 1:length(site.index)) {
        lmcor.spr <- rbind(lmcor.spr, season.lmcor[[i]][1, ])
        }
rownames(lmcor.spr) <- site.index
#write.table(lmcor.spr, "usnip_lmcor_spr.csv", sep=",", row.names=TRUE, col.names=NA)

lmcor.sum <- data.frame(matrix(nrow=0, ncol=length(season.lmcor[[1]])))
for(i in 1:length(site.index)) {
        lmcor.sum <- rbind(lmcor.sum, season.lmcor[[i]][1, ])
        }
rownames(lmcor.sum) <- site.index
```

```
#write.table(lmcor.sum, "usnip_lmcor_sum.csv", sep=",", row.names=TRUE, col.names=NA)

lmcor.aut <- data.frame(matrix(nrow=0, ncol=length(season.lmcor[[1]])))
for(i in 1:length(site.index)) {
        lmcor.aut <- rbind(lmcor.aut, season.lmcor[[i]][1, ])
        }
rownames(lmcor.aut) <- site.index
#write.table(lmcor.aut, "usnip_lmcor_aut.csv", sep=",", row.names=TRUE, col.names=NA)


#------------------------------Grouped Monthly R2 and d18O SD-----------------------------
mo.index <- c("01", "02", "03", "04", "05", "06", "07", "08",
              "09", "10", "11", "12")
by.mo <- list(NULL) #Splits total weekly into monthly subsets for later loop to use
mo.data <- list(NULL) #List of sites, each with list of monthly data
mo.r2 <- list(NULL) #List of sites, each with list of monthly correlations with d18O

for (j in 1:length(site.index)) { #Looping through each site
        by.mo[[j]] <- totalsites.data[[j]]
        mo.data.tmp <- list(NULL)
        mo.r2.tmp <- data.frame(matrix(nrow=12, ncol=5))
        for (i in 1:length(unique(by.mo[[j]]$mo))) { #Looping through each mo
                mo.data.tmp[[i]] <- by.mo[[j]][by.mo[[j]]$mo == mo.index[i], c(1:4,8,12)]
                colnames(mo.r2.tmp) <- c("d2H.r2", "dex.r2", "tavg.r2", "tdif.r2", "prcp.r2")
                rownames(mo.r2.tmp) <- c("jan", "feb", "mar", "apr", "may", "jun", "jul", "aug",
                                         "sep", "oct", "nov", "dec")
                #---R2 with d18O----
                tavg.d18O.lm.tmp <- (lm(mo.data.tmp[[i]]$d18O ~ mo.data.tmp[[i]]$tavg))
                if(length(mo.data.tmp[[i]]$d18O) > 2) {
                        mo.r2.tmp[i,1] <- (cor(mo.data.tmp[[i]]$d2H, mo.data.tmp[[i]]$d18O))^2
                        mo.r2.tmp[i,2] <- (cor(mo.data.tmp[[i]]$d.ex, mo.data.tmp[[i]]$d18O))^2
                        mo.r2.tmp[i,3] <- (cor(mo.data.tmp[[i]]$tavg, mo.data.tmp[[i]]$d18O))^2
                        mo.r2.tmp[i,4] <- (cor(mo.data.tmp[[i]]$tdif, mo.data.tmp[[i]]$d18O))^2
                        mo.r2.tmp[i,5] <- (cor(log(mo.data.tmp[[i]]$usnip.prcp +1),
```

```
                                mo.data.tmp[[i]]$d18O))^2

                        }
                }
        mo.data[[j]] <- mo.data.tmp
        names(mo.data[[j]]) <- c("jan", "feb", "mar", "apr", "may", "jun", "jul", "aug",
                                "sep", "oct", "nov", "dec")
        mo.r2.tmp <- round(mo.r2.tmp, 4)
        mo.r2[[j]] <- mo.r2.tmp
        }

names(mo.data) <- site.index #A list of sites each with a list of months with individual weekly data
names(mo.r2) <- site.index #A list of sites with correlations between d18O and other variables
#write.table(mo.r2, "usnip_r2_mo.csv", sep=",", row.names=TRUE, col.names=NA)

#Calculating monthly changes in standard deviation of d18O
mo.index <- c("01", "02", "03", "04", "05", "06", "07", "08",
                "09", "10", "11", "12")
by.mo <- NA
mo.sd.d18O <- data.frame(matrix(nrow=length(site.index), ncol=12))

for (j in 1:length(site.index)) { #Looping through each site
        by.mo <- totalsites.data[[j]]
        sd.per.site <- NA
        for (i in 1:12) { #Looping through each mo
                mo.sd.d18O.tmp <- by.mo[by.mo$mo == mo.index[i], ]
                if (length(mo.sd.d18O.tmp$d18O) >=10) { #Only months with more than 10 entries
                        sd.iter <- sd(mo.sd.d18O.tmp$d18O)
                        } else {
                        sd.iter <- NA
                        }
                sd.per.site[i] <- sd.iter
                }
        mo.sd.d18O[j, ] <- sd.per.site
```

```
	}
colnames(mo.sd.d18O) <- c("jan", "feb", "mar", "apr", "may", "jun", "jul", "aug",
                          "sep", "oct", "nov", "dec")
mo.sd.d18O$site <- site.index
#write.table(mo.sd.d18O, "usnip_sd_d18O_mo.csv", sep=",", row.names=TRUE, col.names=NA)

#----------------------------------Grouped Seasonal R2 and d18O SD-----------------------------
season.index <- c("win", "spr", "sum", "aut")
by.season <- list(NULL) #Splits total weekly into seasonal subsets for later loop to use
season.data <- list(NULL) #List of sites, each with list of seasonal data
season.r2 <- list(NULL) #List of sites, each with list of seasonal correlations with d18O

for (j in 1:length(site.index)) { #Looping through each site
	by.season[[j]] <- totalsites.data[[j]]
	season.data.tmp <- list(NULL)
	season.r2.tmp <- data.frame(matrix(nrow=4, ncol=5))
	for (i in 1:length(unique(by.season[[j]]$season))) { #Looping through each season
		season.data.tmp[[i]] <- by.season[[j]][by.season[[j]]$season == season.index[i], c(1:4,8,12)]
		colnames(season.r2.tmp) <- c("d2H.r2", "dex.r2", "tavg.r2", "tdif.r2", "prcp.r2")
		rownames(season.r2.tmp) <- c("win", "spr", "sum", "aut")
		#---R2 with d18O----
		tavg.d18O.lm.tmp <- (lm(season.data.tmp[[i]]$d18O ~ season.data.tmp[[i]]$tavg))
		if(length(season.data.tmp[[i]]$d18O) > 2) {
			season.r2.tmp[i,1] <- (cor(season.data.tmp[[i]]$d2H, season.data.tmp[[i]]$d18O))^2
			season.r2.tmp[i,2] <- (cor(season.data.tmp[[i]]$d.ex, season.data.tmp[[i]]$d18O))^2
			season.r2.tmp[i,3] <- (cor(season.data.tmp[[i]]$tavg, season.data.tmp[[i]]$d18O))^2
			season.r2.tmp[i,4] <- (cor(season.data.tmp[[i]]$tdif, season.data.tmp[[i]]$d18O))^2
			season.r2.tmp[i,5] <- (cor(log(season.data.tmp[[i]]$usnip.prcp +1),
				season.data.tmp[[i]]$d18O))^2

			}
		}
	season.data[[j]] <- season.data.tmp
	names(season.data[[j]]) <- c("win", "spr", "sum", "aut")
```

```
        season.r2.tmp <- round(season.r2.tmp, 4)
        season.r2[[j]] <- season.r2.tmp
        }

names(season.data) <- site.index #A list of sites each with a list of seasons with individual weekly data
names(season.r2) <- site.index #A list of sites with correlations between d18O and other variables
#write.table(season.r2, "usnip_r2_season.csv", sep=",", row.names=TRUE, col.names=NA)

#Calculating seasonal changes in standard deviation of d18O
season.index <- c("win", "spr", "sum", "aut")
by.season <- NA
season.sd.d18O <- data.frame(matrix(nrow=length(site.index), ncol=4))

for (j in 1:length(site.index)) { #Looping through each site
        by.season <- totalsites.data[[j]]
        sd.per.site <- NA
        for (i in 1:length(unique(by.season$season))) { #Looping through each season
                season.sd.d18O.tmp <- by.season[by.season$season == season.index[i], ]
                sd.iter <- sd(season.sd.d18O.tmp$d18O)
                sd.per.site[i] <- sd.iter
                }
        season.sd.d18O[j, ] <- sd.per.site
        }

colnames(season.sd.d18O) <- c("win", "spr", "sum", "aut")
season.sd.d18O$site <- site.index
#write.table(season.sd.d18O, "usnip_sd_d18O_season.csv", sep=",", row.names=TRUE, col.names=NA)

#==================================Calculating Correlation Values================================
#This section calculates correlations (r) as opposed to fit (r2)
        #---------------------------------Week Correlation (r)----------------------------------------
        #This produces results similar to the aggregated crlt
        week.crlt <- data.frame(matrix(ncol=8, nrow=25))#List of sites, each with list of aggr season correlations and linear models
```

```
	for (i in 1:length(site.index)) { #Looping through each site
		#---Calculating crlt with d18O
			week.crlt[i,1] <- length(totalsites.data[[i]]$d18O)
		if(length(totalsites.data[[i]]$d18O) > 2) {
			week.crlt[i,2] <- (cor(totalsites.data[[i]]$d2H, totalsites.data[[i]]$d18O))
			week.crlt[i,3] <- (cor(totalsites.data[[i]]$d.ex, totalsites.data[[i]]$d18O))
			week.crlt[i,4] <- (cor(totalsites.data[[i]]$tmax, totalsites.data[[i]]$d18O))
			week.crlt[i,5] <- (cor(totalsites.data[[i]]$tmin, totalsites.data[[i]]$d18O))
			week.crlt[i,6] <- (cor(totalsites.data[[i]]$tavg, totalsites.data[[i]]$d18O))
			week.crlt[i,7]	<- (cor(totalsites.data[[i]]$tdif, totalsites.data[[i]]$d18O))
			week.crlt[i,8]	<- (cor(log(totalsites.data[[i]]$usnip.prcp + 1), totalsites.data[[i]]$d18O))
			}
		}
	rownames(week.crlt) <- site.index
	colnames(week.crlt) <- c("n.week", "d2H.crlt.week", "dex.crlt.week", "tmax.crlt.week", "tmin.crlt.week",
		"tavg.crlt.week", "tdif.crlt.week", "prcp.crlt.week")
	week.crlt <- round(week.crlt, 4)
	#write.table(week.crlt, "usnip_crlt_week.csv", sep=",", row.names=TRUE, col.names=NA)

	#-----------------------------------Aggregate Month Correlation (r)----------------------------------------
	aggr.month <- list(NULL) #List of sites, each with list of monthly aggregate data
	mo.aggr.crlt <- data.frame(matrix(ncol=7, nrow=length(site.index)))#List of sites, each with list of aggr monthly correlations and linear
models

	for (i in 1:length(site.index)) { #Looping through each site
		aggr.month[[i]] <- total.mo.indv.wt[[i]]
		#---Calculating crlt with d18O
		mo.aggr.crlt[i,1] <- length(aggr.month[[i]]$d18O)
		if(length(aggr.month[[i]]$d18O) > 2) {
			mo.aggr.crlt[i,2] <- (cor(aggr.month[[i]]$d2H, aggr.month[[i]]$d18O))
			mo.aggr.crlt[i,3] <- (cor(aggr.month[[i]]$d.ex, aggr.month[[i]]$d18O))
			mo.aggr.crlt[i,4] <- (cor(aggr.month[[i]]$tmax, aggr.month[[i]]$d18O))
			mo.aggr.crlt[i,5] <- (cor(aggr.month[[i]]$tmin, aggr.month[[i]]$d18O))
			mo.aggr.crlt[i,6] <- (cor(aggr.month[[i]]$tavg, aggr.month[[i]]$d18O))
```

```
                mo.aggr.crlt[i,7]<- (cor(aggr.month[[i]]$tdif, aggr.month[[i]]$d18O))
                }
        }
    rownames(mo.aggr.crlt) <- site.index
    colnames(mo.aggr.crlt) <- c("n.mo", "d2H.crlt.mo", "dex.crlt.mo", "tmax.crlt.mo", "tmin.crlt.mo",
        "tavg.crlt.mo", "tdif.crlt.mo")
    mo.aggr.crlt <- round(mo.aggr.crlt, 4)
    #write.table(mo.aggr.crlt, "usnip_crlt_mo_aggr.csv", sep=",", row.names=TRUE, col.names=NA)


    #-----------------------------------Aggregate Season Correlation (r)----------------------------------------
    aggr.season <- list(NULL) #List of sites, each with list of season aggregate data
    season.aggr.crlt <- data.frame(matrix(ncol=7, nrow=length(site.index)))#List of sites, each with list of aggr season correlations and linear
models

    for (i in 1:length(site.index)) { #Looping through each site
        aggr.season[[i]] <- total.season.indv.wt[[i]]
        #---Calculating crlt with d18O
        season.aggr.crlt[i,1] <- length(aggr.season[[i]]$d18O)
        if(length(aggr.season[[i]]$d18O) > 2) {
            season.aggr.crlt[i,2] <- (cor(aggr.season[[i]]$d2H, aggr.season[[i]]$d18O))
            season.aggr.crlt[i,3] <- (cor(aggr.season[[i]]$d.ex, aggr.season[[i]]$d18O))
            season.aggr.crlt[i,4] <- (cor(aggr.season[[i]]$tmax, aggr.season[[i]]$d18O))
            season.aggr.crlt[i,5] <- (cor(aggr.season[[i]]$tmin, aggr.season[[i]]$d18O))
            season.aggr.crlt[i,6] <- (cor(aggr.season[[i]]$tavg, aggr.season[[i]]$d18O))
            season.aggr.crlt[i,7]       <- (cor(aggr.season[[i]]$tdif, aggr.season[[i]]$d18O))
            }
        }
    rownames(season.aggr.crlt) <- site.index
    colnames(season.aggr.crlt) <- c("n.season", "d2H.crlt.season", "dex.crlt.season", "tmax.crlt.season", "tmin.crlt.season",
        "tavg.crlt.season", "tdif.crlt.season")
    season.aggr.crlt <- round(season.aggr.crlt, 4)
    #write.table(season.aggr.crlt, "usnip_crlt_season_aggr.csv", sep=",", row.names=TRUE, col.names=NA)
```

```
#------------------------------Grouped Monthly Correlation (r)--------------------------
mo.index <- c("01", "02", "03", "04", "05", "06", "07", "08",
                    "09", "10", "11", "12")
by.mo <- list(NULL) #Splits total weekly into monthly subsets for later loop to use
mo.data <- list(NULL) #List of sites, each with list of monthly data
mo.crlt <- list(NULL) #List of sites, each with list of monthly correlations with d18O

for (j in 1:length(site.index)) { #Looping through each site
        by.mo[[j]] <- totalsites.data[[j]]
        mo.data.tmp <- list(NULL)
        mo.crlt.tmp <- data.frame(matrix(nrow=12, ncol=5))
        for (i in 1:length(unique(by.mo[[j]]$mo))) { #Looping through each mo
                mo.data.tmp[[i]] <- by.mo[[j]][by.mo[[j]]$mo == mo.index[i], c(1:4,8,12)]
                colnames(mo.crlt.tmp) <- c("d2H.crlt", "dex.crlt", "tavg.crlt", "tdif.crlt", "prcp.crlt")
                rownames(mo.crlt.tmp) <- c("jan", "feb", "mar", "apr", "may", "jun", "jul", "aug",
                                "sep", "oct", "nov", "dec")
                #---crlt with d18O----
                tavg.d18O.lm.tmp <- (lm(mo.data.tmp[[i]]$d18O ~ mo.data.tmp[[i]]$tavg))
                if(length(mo.data.tmp[[i]]$d18O) > 2) {
                        mo.crlt.tmp[i,1] <- (cor(mo.data.tmp[[i]]$d2H, mo.data.tmp[[i]]$d18O))
                        mo.crlt.tmp[i,2] <- (cor(mo.data.tmp[[i]]$d.ex, mo.data.tmp[[i]]$d18O))
                        mo.crlt.tmp[i,3] <- (cor(mo.data.tmp[[i]]$tavg, mo.data.tmp[[i]]$d18O))
                        mo.crlt.tmp[i,4] <- (cor(mo.data.tmp[[i]]$tdif, mo.data.tmp[[i]]$d18O))
                        mo.crlt.tmp[i,5] <- (cor(log(mo.data.tmp[[i]]$usnip.prcp +1),
                                mo.data.tmp[[i]]$d18O))

                        }
```

```
		}
	mo.data[[j]] <- mo.data.tmp
	names(mo.data[[j]]) <- c("jan", "feb", "mar", "apr", "may", "jun", "jul", "aug",
				"sep", "oct", "nov", "dec")
	mo.crlt.tmp <- round(mo.crlt.tmp, 4)
	mo.crlt[[j]] <- mo.crlt.tmp
	}

names(mo.data) <- site.index #A list of sites each with a list of months with individual weekly data
names(mo.crlt) <- site.index #A list of sites with correlations between d18O and other variables
#write.table(mo.crlt, "usnip_crlt_mo.csv", sep=",", row.names=TRUE, col.names=NA)

#----------------------------------Grouped Seasonal Correlation (r)----------------------------
season.index <- c("win", "spr", "sum", "aut")
by.season <- list(NULL) #Splits total weekly into seasonal subsets for later loop to use
season.data <- list(NULL) #List of sites, each with list of seasonal data
season.crlt <- list(NULL) #List of sites, each with list of seasonal correlations with d18O

for (j in 1:length(site.index)) { #Looping through each site
	by.season[[j]] <- totalsites.data[[j]]
	season.data.tmp <- list(NULL)
	season.crlt.tmp <- data.frame(matrix(nrow=4, ncol=5))
	for (i in 1:length(unique(by.season[[j]]$season))) { #Looping through each season
		season.data.tmp[[i]] <- by.season[[j]][by.season[[j]]$season == season.index[i], c(1:4,8,12)]
		colnames(season.crlt.tmp) <- c("d2H.crlt", "dex.crlt", "tavg.crlt", "tdif.crlt", "prcp.crlt")
		rownames(season.crlt.tmp) <- c("win", "spr", "sum", "aut")
		#---crlt with d18O----
		tavg.d18O.lm.tmp <- (lm(season.data.tmp[[i]]$d18O ~ season.data.tmp[[i]]$tavg))
		if(length(season.data.tmp[[i]]$d18O) > 2) {
			season.crlt.tmp[i,1] <- (cor(season.data.tmp[[i]]$d2H, season.data.tmp[[i]]$d18O))
			season.crlt.tmp[i,2] <- (cor(season.data.tmp[[i]]$d.ex, season.data.tmp[[i]]$d18O))
			season.crlt.tmp[i,3] <- (cor(season.data.tmp[[i]]$tavg, season.data.tmp[[i]]$d18O))
			season.crlt.tmp[i,4] <- (cor(season.data.tmp[[i]]$tdif, season.data.tmp[[i]]$d18O))
			season.crlt.tmp[i,5] <- (cor(log(season.data.tmp[[i]]$usnip.prcp +1),
```

```
                                        season.data.tmp[[i]]$d18O))

                                }
                        }
                season.data[[j]] <- season.data.tmp
                names(season.data[[j]]) <- c("win", "spr", "sum", "aut")
                season.crlt.tmp <- round(season.crlt.tmp, 4)
                season.crlt[[j]] <- season.crlt.tmp
                }

        names(season.data) <- site.index #A list of sites each with a list of seasons with individual weekly data
        names(season.crlt) <- site.index #A list of sites with correlations between d18O and other variables
        #write.table(season.crlt, "usnip_crlt_season.csv", sep=",", row.names=TRUE, col.names=NA)


#-------------------------Weighted Means and SD for Aggregates---------------------------------
#NOTE: Weekly, Monthly, and Seasonal Means are the same. Since they are all based off the same
        #initial weighted data, aggregating does not change the mean values

weekly.wt.mean <- data.frame(matrix(ncol=7, nrow=length(site.index)))
weekly.wt.sd <- data.frame(matrix(ncol=7, nrow=length(site.index)))
monthly.wt.mean <- data.frame(matrix(ncol=7, nrow=length(site.index)))
monthly.wt.sd <- data.frame(matrix(ncol=7, nrow=length(site.index)))
seasonal.wt.mean <- data.frame(matrix(ncol=7, nrow=length(site.index)))
seasonal.wt.sd <- data.frame(matrix(ncol=7, nrow=length(site.index)))

for (i in 1:length(site.index)) { #Looping through each site
        #Weekly (Raw) data
        prcp.frac.tmp <- totalsites.data[[i]]$usnip.prcp / sum(totalsites.data[[i]]$usnip.prcp)
        weekly.wt.mean.tmp <- round(colSums(prcp.frac.tmp * totalsites.data[[i]][c(2,3,4,6,7,8,12)]),2)
        weekly.wt.mean[i, 1:7] <- weekly.wt.mean.tmp
        weekly.wt.sd.tmp <- round(sd.wt(totalsites.data[[i]][c(2,3,4,6,7,8,12)],prcp.frac.tmp),2)
        weekly.wt.sd[i, 1:7] <- weekly.wt.sd.tmp
```

```
        #Monthly aggregated data
        totalsites.data.monthly <- data.frame(total.mo.indv.wt[[i]], total.mo.usnip.prcp.sum[[i]]$prcp.sum)
        names(totalsites.data.monthly)[11] <- "prcp.sum"
        prcp.frac.tmp <- totalsites.data.monthly$prcp.sum / sum(totalsites.data.monthly$prcp.sum)
        monthly.wt.mean.tmp <- round(colSums(prcp.frac.tmp * totalsites.data.monthly[c(1:7)]),2)
        monthly.wt.mean[i, 1:7] <- monthly.wt.mean.tmp
        monthly.wt.sd.tmp <- round(sd.wt(totalsites.data.monthly[c(1:7)],prcp.frac.tmp),2)
        monthly.wt.sd[i, 1:7] <- monthly.wt.sd.tmp

        #Seasonally aggregated data
        totalsites.data.seasonal <- data.frame(total.season.indv.wt[[i]],
                total.season.usnip.prcp.sum[[i]]$prcp.sum)
        names(totalsites.data.seasonal)[11] <- "prcp.sum"
        prcp.frac.tmp <- totalsites.data.seasonal$prcp.sum / sum(totalsites.data.seasonal$prcp.sum)
        seasonal.wt.mean.tmp <- round(colSums(prcp.frac.tmp * totalsites.data.seasonal[c(1:7)]),2)
        seasonal.wt.mean[i, 1:7] <- seasonal.wt.mean.tmp
        seasonal.wt.sd.tmp <- round(sd.wt(totalsites.data.seasonal[c(1:7)],prcp.frac.tmp),2)
        seasonal.wt.sd[i, 1:7] <- seasonal.wt.sd.tmp
        }

colnames(weekly.wt.mean) <- c("d18O", "d2H", "d.ex", "tmin", "tmax", "tavg", "tdif")
colnames(weekly.wt.sd) <- c("d18O", "d2H", "d.ex", "tmin", "tmax", "tavg", "tdif")
colnames(monthly.wt.mean) <- c("d18O", "d2H", "d.ex", "tmin", "tmax", "tavg", "tdif")
colnames(monthly.wt.sd) <- c("d18O", "d2H", "d.ex", "tmin", "tmax", "tavg", "tdif")
colnames(seasonal.wt.mean) <- c("d18O", "d2H", "d.ex", "tmin", "tmax", "tavg", "tdif")
colnames(seasonal.wt.sd) <- c("d18O", "d2H", "d.ex", "tmin", "tmax", "tavg", "tdif")

rownames(weekly.wt.mean) <- site.index
rownames(weekly.wt.sd) <- site.index
rownames(monthly.wt.mean) <- site.index
rownames(monthly.wt.sd) <- site.index
rownames(seasonal.wt.mean) <- site.index
rownames(seasonal.wt.sd) <- site.index
```

```
#write.table(weekly.wt.mean, "usnip_means_weekly_wt.csv", sep=",", row.names=TRUE, col.names=NA)
#write.table(weekly.wt.sd, "usnip_sd_weekly_wt.csv", sep=",", row.names=TRUE, col.names=NA)
#write.table(monthly.wt.sd, "usnip_sd_monthly_wt.csv", sep=",", row.names=TRUE, col.names=NA)
#write.table(seasonal.wt.sd, "usnip_sd_seasonal_wt.csv", sep=",", row.names=TRUE, col.names=NA)



#-------------------------d18O Characteristics by 10C Temperature Increments---------------------------------
#Calculating weekly changes in d18O character at different 10C increments
sd.tavg.incr.wk <- data.frame(matrix(nrow = length(site.index), ncol=6))
d18O.tavg.incr.wk <- data.frame(matrix(nrow = length(site.index), ncol=6))
count.tavg.incr.wk <- data.frame(matrix(nrow = length(site.index), ncol=6))

for (i in 1:length(site.index)) {
        loop.data <- totalsites.data[[i]]
        sd.per.site <- NULL
        count.per.site <- NULL
        d18O.per.site <- NULL
        for (j in 1:6) { #Getting a stdev, count, and d18O wt mean for each 10C increment
                count.iter <- length(loop.data$d18O[loop.data$tavg >= (j*10-30) & loop.data$tavg < (j*10-20)])
                count.per.site[j] <- count.iter
                if (count.iter >=10) {
                        sd.iter <- sd(loop.data$d18O[loop.data$tavg >= (j*10-30) & loop.data$tavg < (j*10-20)])
                        d18O.iter <- sum(((loop.data$d18O[loop.data$tavg >= (j*10-30) & loop.data$tavg < (j*10-20)]) *
                                (loop.data$usnip.prcp[loop.data$tavg >= (j*10-30) & loop.data$tavg < (j*10-20)])) /
                                sum(loop.data$usnip.prcp[loop.data$tavg >= (j*10-30) & loop.data$tavg < (j*10-20)]))
                        } else {
                        sd.iter <- NA
                        d18O.iter <- NA
                        }
                sd.per.site[j] <- sd.iter
                d18O.per.site[j] <- d18O.iter
                }
        sd.tavg.incr.wk[i,] <- sd.per.site
```

```
        d18O.tavg.incr.wk[i,] <- d18O.per.site
        count.tavg.incr.wk[i,] <- count.per.site
        }
colnames(sd.tavg.incr.wk) <- c("-20:-10", "-10:0", "0:10", "10:20", "20:30", "30:40")
sd.tavg.incr.wk$site <- site.index
colnames(d18O.tavg.incr.wk) <- c("-20:-10", "-10:0", "0:10", "10:20", "20:30", "30:40")
d18O.tavg.incr.wk$site <- site.index
colnames(count.tavg.incr.wk) <- c("-20:-10", "-10:0", "0:10", "10:20", "20:30", "30:40")
count.tavg.incr.wk$site <- site.index

#write.table(sd.tavg.incr.wk, "usnip_temp_increments_sd_wk.csv", sep=",", row.names=TRUE, col.names=NA)
#write.table(d18O.tavg.incr.wk, "usnip_temp_increments_d18O_wk.csv", sep=",", row.names=TRUE, col.names=NA)
#write.table(count.tavg.incr.wk, "usnip_temp_increments_count_wk.csv", sep=",", row.names=TRUE, col.names=NA)

#Calculating monthly changes in d18O character at different 10C increments
sd.tavg.incr.mo <- data.frame(matrix(nrow = length(site.index), ncol=6))
d18O.tavg.incr.mo <- data.frame(matrix(nrow = length(site.index), ncol=6))
count.tavg.incr.mo <- data.frame(matrix(nrow = length(site.index), ncol=6))

for (i in 1:length(site.index)) {
        loop.data <- total.mo.indv.wt[[i]]
        sd.per.site <- NULL
        count.per.site <- NULL
        d18O.per.site <- NULL
        for (j in 1:6) { #Getting a stdev, count, and d18O wt mean for each 10C increment
                count.iter <- length(loop.data$d18O[loop.data$tavg >= (j*10-30) & loop.data$tavg < (j*10-20)])
                count.per.site[j] <- count.iter
                if (count.iter >=10) {
                        sd.iter <- sd(loop.data$d18O[loop.data$tavg >= (j*10-30) & loop.data$tavg < (j*10-20)])
                        d18O.iter <- mean(loop.data$d18O[loop.data$tavg >= (j*10-30) & loop.data$tavg < (j*10-20)])
                        } else {
                        sd.iter <- NA
                        d18O.iter <- NA
                        }
```

```
                sd.per.site[j] <- sd.iter
                d18O.per.site[j] <- d18O.iter
                }
        sd.tavg.incr.mo[i,] <- sd.per.site
        d18O.tavg.incr.mo[i,] <- d18O.per.site
        count.tavg.incr.mo[i,] <- count.per.site
        }
colnames(sd.tavg.incr.mo) <- c("-20:-10", "-10:0", "0:10", "10:20", "20:30", "30:40")
sd.tavg.incr.mo$site <- site.index
colnames(d18O.tavg.incr.mo) <- c("-20:-10", "-10:0", "0:10", "10:20", "20:30", "30:40")
d18O.tavg.incr.mo$site <- site.index
colnames(count.tavg.incr.mo) <- c("-20:-10", "-10:0", "0:10", "10:20", "20:30", "30:40")
count.tavg.incr.mo$site <- site.index

#write.table(sd.tavg.incr.mo, "usnip_temp_increments_sd_mo.csv", sep=",", row.names=TRUE, col.names=NA)
#write.table(d18O.tavg.incr.mo, "usnip_temp_increments_d18O_mo.csv", sep=",", row.names=TRUE, col.names=NA)
#write.table(count.tavg.incr.mo, "usnip_temp_increments_count_mo.csv", sep=",", row.names=TRUE, col.names=NA)

#Calculating seasonal changes in d18O character at different 10C increments
sd.tavg.incr.sn <- data.frame(matrix(nrow = length(site.index), ncol=6))
d18O.tavg.incr.sn <- data.frame(matrix(nrow = length(site.index), ncol=6))
count.tavg.incr.sn <- data.frame(matrix(nrow = length(site.index), ncol=6))

for (i in 1:length(site.index)) {
        loop.data <- total.season.indv.wt[[i]]
        sd.per.site <- NULL
        count.per.site <- NULL
        d18O.per.site <- NULL
        for (j in 1:6) { #Getting a stdev, count, and d18O mean for each 10C increment
                count.iter <- length(loop.data$d18O[loop.data$tavg >= (j*10-30) & loop.data$tavg < (j*10-20)])
                count.per.site[j] <- count.iter
                if (count.iter >=10) {
                        sd.iter <- sd(loop.data$d18O[loop.data$tavg >= (j*10-30) & loop.data$tavg < (j*10-20)])
                        d18O.iter <- mean(loop.data$d18O[loop.data$tavg >= (j*10-30) & loop.data$tavg < (j*10-20)])
```

```
                        } else {
                        sd.iter <- NA
                        d18O.iter <- NA
                        }
                sd.per.site[j] <- sd.iter
                d18O.per.site[j] <- d18O.iter
                }
        sd.tavg.incr.sn[i,] <- sd.per.site
        d18O.tavg.incr.sn[i,] <- d18O.per.site
        count.tavg.incr.sn[i,] <- count.per.site
        }
colnames(sd.tavg.incr.sn) <- c("-20:-10", "-10:0", "0:10", "10:20", "20:30", "30:40")
sd.tavg.incr.sn$site <- site.index
colnames(d18O.tavg.incr.sn) <- c("-20:-10", "-10:0", "0:10", "10:20", "20:30", "30:40")
d18O.tavg.incr.sn$site <- site.index
colnames(count.tavg.incr.sn) <- c("-20:-10", "-10:0", "0:10", "10:20", "20:30", "30:40")
count.tavg.incr.sn$site <- site.index

#write.table(sd.tavg.incr.sn, "usnip_temp_increments_sd_sn.csv", sep=",", row.names=TRUE, col.names=NA)
#write.table(d18O.tavg.incr.sn, "usnip_temp_increments_d18O_sn.csv", sep=",", row.names=TRUE, col.names=NA)
#write.table(count.tavg.incr.sn, "usnip_temp_increments_count_sn.csv", sep=",", row.names=TRUE, col.names=NA)

#Mean SD values per aggregation
colMeans(sd.tavg.incr.wk[1:5], na.rm=TRUE)
colMeans(sd.tavg.incr.mo[1:5], na.rm=TRUE)
colMeans(sd.tavg.incr.sn[1:5], na.rm=TRUE)

#=============================================================================================================
#=============================================================================================================
#=============================================================================================================
#----------USNIP Tavg Prediction from d18O at Different Aggregates Function---------
#This function uses the linear model of tavg and d18O from the USNIP-GHCN dataset
#and predicts a tavg from a given d18O with 95% confidence limits. Data is
#reported for weekly, monthly, and seasonal aggregates
```

```
#WARNING: Looping All Sites Script must be run prior to this function


usnip.predict.tavg <- function(site.entry, d18O.input) { #temperature is in C, site.entry lowercase in quotes
        site.num <- which(site.index == site.entry)
        site.data.wk <- totalsites.data[[site.num]]
        tavg <- site.data.wk$tavg
        d18O <- site.data.wk$d18O
        wk.lm <- lm(tavg~d18O)

        site.data.mo <- total.mo.indv.wt[[site.num]]
        tavg <- site.data.mo$tavg
        d18O <- site.data.mo$d18O
        mo.lm <- lm(tavg~d18O)

        site.data.sn <- total.season.indv.wt[[site.num]]
        tavg <- site.data.sn$tavg
        d18O <- site.data.sn$d18O
        sn.lm <- lm(tavg~d18O)


        d18O.entry <- data.frame(d18O = d18O.input)
        wk.predict <- data.frame(predict(wk.lm, newdata = d18O.entry, interval="predict"))
        mo.predict <- data.frame(predict(mo.lm, newdata = d18O.entry, interval="predict"))
        sn.predict <- data.frame(predict(sn.lm, newdata = d18O.entry, interval="predict"))
        wk.predict$aggr <- "wk"
        mo.predict$aggr <- "mo"
        sn.predict$aggr <- "sn"
        aggregation.prediction <- rbind (wk.predict, mo.predict, sn.predict)
        aggregation.prediction <- data.frame(d18O.input, aggregation.prediction)
        colnames(aggregation.prediction) <- c("d18O", "fit", "lwr", "upr", "aggr")
        return(aggregation.prediction)
        }
```

```
#----------USNIP Tavg Prediction from d18O for all 12 months and 4 seasons Function---------
#This function uses the linear model of tavg and d18O from the USNIP-GHCN dataset
#and predicts a tavg from a given d18O with 95% confidence limits. Data is
#reported for each month and season

#WARNING: Looping All Sites Script must be run prior to this function


usnip.predict.tavg.bygroup <- function(site.entry, d18O.input) { #temperature is in C, site.entry lowercase in quotes

	month.predictions <- data.frame(matrix(nrow=12, ncol=5))
	season.predictions <- data.frame(matrix(nrow=4, ncol=5))
	month.index <- c("01", "02", "03", "04", "05", "06", "07", "08", "09",
		"10", "11", "12")
	season.index <- c("win", "spr", "sum", "aut")

	for (i in 1:length(month.index)) {
		site.num <- which(site.index == site.entry)
		site.data.tmp <- totalsites.data[[site.num]][totalsites.data[[site.num]]$mo == month.index[i], ]
		tavg <- site.data.tmp$tavg
		d18O <- site.data.tmp$d18O
		tmp.lm <- lm(tavg~d18O)

		d18O.entry <- data.frame(d18O = d18O.input)
		aggregation.prediction <- data.frame(predict(tmp.lm, newdata = d18O.entry, interval="predict"))
		aggregation.prediction <- data.frame(d18O.input, aggregation.prediction)
		month.predictions[i, ] <- aggregation.prediction
		colnames(month.predictions) <- c("d18O", "fit", "lwr", "upr", "range")
		rownames(month.predictions) <- c("jan", "feb", "mar", "apr", "may", "jun", "jul", "aug",
				"sep", "oct", "nov", "dec")
		}

	for (i in 1:length(season.index)) {
```

```
                site.num <- which(site.index == site.entry)
                site.data.tmp <- totalsites.data[[site.num]][totalsites.data[[site.num]]$season == season.index[i], ]
                tavg <- site.data.tmp$tavg
                d18O <- site.data.tmp$d18O
                tmp.lm <- lm(tavg~d18O)

                d18O.entry <- data.frame(d18O = d18O.input)
                aggregation.prediction <- data.frame(predict(tmp.lm, newdata = d18O.entry, interval="predict"))
                aggregation.prediction <- data.frame(d18O.input, aggregation.prediction)
                season.predictions[i, ] <- aggregation.prediction
                colnames(season.predictions) <- c("d18O", "fit", "lwr", "upr", "range")
                rownames(season.predictions) <- c("win", "spr", "sum", "aut")
                }

        all.predictions <- rbind(month.predictions, season.predictions)
        all.predictions$range <- all.predictions$upr - all.predictions$lwr
        return(all.predictions)
        }

        #Examples
        #usnip.predict.tavg.bygroup("in22", -6)
        #usnip.predict.tavg.bygroup("mn27", -6)


#This script calculates tavg predictions for input d18O
#Written Pete D Akers Aug 2015
#NOTE: Function usnip.predict.tavg must be loaded prior to running this script

tavg.0.tmp <- data.frame(matrix(nrow=0, ncol=4))
tavg.06.tmp <- data.frame(matrix(nrow=0, ncol=4))
tavg.20.tmp <- data.frame(matrix(nrow=0, ncol=4))

for (i in 1:length(site.index)) {
        iter.0 <-NA
```

```
        iter.0 <- data.frame(usnip.predict.tavg(site.index[i], 0))
        iter.0$site <- site.index[i]
        tavg.0.tmp <- rbind(tavg.0.tmp, iter.0)

        iter.06 <-NA
        iter.06 <- data.frame(usnip.predict.tavg(site.index[i], -6))
        iter.06$site <- site.index[i]
        tavg.06.tmp <- rbind(tavg.06.tmp, iter.06)

        iter.20 <-NA
        iter.20 <- data.frame(usnip.predict.tavg(site.index[i], -20))
        iter.20$site <- site.index[i]
        tavg.20.tmp <- rbind(tavg.20.tmp, iter.20)
        }

tavg.0.err <- tavg.0.tmp$fit-tavg.0.tmp$lwr
tavg.0.aggr <- c("wk", "mo", "sn")
tavg.0 <- data.frame(tavg.0.aggr, round(tavg.0.tmp$fit, 1), round(tavg.0.err, 1), tavg.0.tmp$site)
colnames(tavg.0) <- c("Aggregation", "Fit", "Error", "Site")

tavg.06.err <- tavg.06.tmp$fit-tavg.06.tmp$lwr
tavg.06.aggr <- c("wk", "mo", "sn")
tavg.06 <- data.frame(tavg.06.aggr, round(tavg.06.tmp$fit, 1), round(tavg.06.err, 1), tavg.06.tmp$site)
colnames(tavg.06) <- c("Aggregation", "Fit", "Error", "Site")

tavg.20.err <- tavg.20.tmp$fit-tavg.20.tmp$lwr
tavg.20.aggr <- c("wk", "mo", "sn")
tavg.20 <- data.frame(tavg.20.aggr, round(tavg.20.tmp$fit, 1), round(tavg.20.err, 1), tavg.20.tmp$site)
colnames(tavg.20) <- c("Aggregation", "Fit", "Error", "Site")

tavg.predictions <- list(tavg.0, tavg.06, tavg.20)
names(tavg.predictions) <- c("0", "-6", "-20")
#write.table(tavg.predictions, "usnip_tavg_predictions.csv", sep=",", row.names=TRUE, col.names=NA)
```

```
tavg.06.wk <- tavg.06[tavg.06$Aggregation == "wk", ]
tavg.06.mo <- tavg.06[tavg.06$Aggregation == "mo", ]
tavg.06.sn <- tavg.06[tavg.06$Aggregation == "sn", ]
mean(tavg.06.wk$Error)
mean(tavg.06.mo$Error)
mean(tavg.06.sn$Error)


tavg.0.wk <- tavg.0[tavg.0$Aggregation == "wk", ]
tavg.0.mo <- tavg.0[tavg.0$Aggregation == "mo", ]
tavg.0.sn <- tavg.0[tavg.0$Aggregation == "sn", ]
mean(tavg.0.wk$Error)
mean(tavg.0.mo$Error)
mean(tavg.0.sn$Error)


tavg.20.wk <- tavg.20[tavg.20$Aggregation == "wk", ]
tavg.20.mo <- tavg.20[tavg.20$Aggregation == "mo", ]
tavg.20.sn <- tavg.20[tavg.20$Aggregation == "sn", ]
mean(tavg.20.wk$Error)
mean(tavg.20.mo$Error)
mean(tavg.20.sn$Error)

#=============================================================================================================
#====================================Moisture Source Analysis=================================================
#=============================================================================================================
#This script matches moisture source inputs to climate data and plots the necessary analysis
#Written by Pete D Akers 2015
ms.index <- c("in22", "il78", "mn27", "nc35", "ne99", "pa15", "wi36")
gchn.fullweek <- read.table("usnip-ghcn_fullweek_frac.csv", sep=",", header=TRUE)
site.gchn <- c("GHCND:USC00030220","GHCND:USC00096335","GHCND:USC00136316","GHCND:USC00112353",
        "GHCND:USC00115768","GHCND:USC00129113","GHCND:USC00144972","GHCND:USC00152040","GHCND:USC00187806",
        "GHCND:USW00014841","GHCND:USC00214546","GHCND:USC00223645","GHCND:USC00311881","GHCND:USC00321435",
        "GHCND:USC00256075","GHCND:USC00293530","GHCND:USC00292865","GHCND:USC00293706","GHCND:USC00304207",
```

```
        "GHCND:USC00331197","GHCND:USC00368449","GHCND:USC00405158","GHCND:USC00432769","GHCND:USC00475516",
        "GHCND:USC00471205")
gchn.fullweek$site <- site.index[match(as.character(gchn.fullweek$station), site.gchn)]

#Breaking weekly data up by site
allsites.weekly <- list(NA)
for (i in 1:length(site.index)) {
        allsites.weekly[[i]] <- allsites.all[allsites.all$site == toupper(site.index[i]), ]
        (allsites.weekly[[i]]$usnip.prcp[allsites.weekly[[i]]$usnip.prcp == -9]
                <- allsites.weekly[[i]]$gchn.prcp[allsites.weekly[[i]]$usnip.prcp == -9])
        }
names(allsites.weekly) <- site.index


#Breaking daily data up by site
allsites.fullweek <- list(NA)
for (i in 1:length(site.index)) {
        allsites.fullweek[[i]] <- gchn.fullweek[gchn.fullweek$site == site.index[i], ]
        }
names(allsites.fullweek) <- site.index

#Uploading source files
allsites.ms <- read.table("allsites_hysplit_data.csv", header=TRUE, sep=",")
allsites.ms$date <- as.Date(as.character(allsites.ms$date), "%Y%m%d")
ms.data <- list(NA)
for (i in 1:length(ms.index)) {
        ms.data[[i]] <- allsites.ms[allsites.ms$site == ms.index[i], ]
        }
names(ms.data) <- ms.index

#Getting d18O-tavg regression data for moisture source sites
ms.lmdata <- list(NA)
for (k in 1:length(ms.index)) {
        ms.lmdata[[k]] <- summary(lm(totalsites.data[[match(ms.index[k], site.index)]]$d18O ~
```

```
                totalsites.data[[match(ms.index[k], site.index)]]$tavg))
        }
names(ms.lmdata) <- ms.index

#-------------------------------------------------------------

ms.weekly.data <- list(NA)
for (k in 1:length(ms.index)) {
        loop.source <- ms.data[[ms.index[k]]]
        loop.daily <- allsites.fullweek[[match(ms.index[k], site.index)]]
        loop.daily$date <- as.Date(as.character(loop.daily$date), "%Y%m%d")
        loop.weekly <- allsites.weekly[[match(ms.index[k], site.index)]]
        loop.weekly$date <- as.Date(as.character(loop.weekly$usnip.date), "%Y%m%d")
        loop.weekly$dex <- loop.weekly$d2H - 8 * loop.weekly$d18O
        loop.daily$src1 <- character(length=length(loop.daily$date))
        loop.daily$src2 <- character(length=length(loop.daily$date))

        daily.index <- match(loop.source$date, loop.daily$date)
        for (i in 1:length(daily.index)) {
                loop.daily$src1[daily.index[i]] <- as.character(loop.source$src1[i])
                loop.daily$src2[daily.index[i]] <- as.character(loop.source$src2[i])
                }

        tot.frac <- data.frame(matrix(nrow=length(loop.weekly$date), ncol=13))
        colnames(tot.frac) <- c("p", "matl", "g", "cs", "cw", "cmw", "ce", "cn", "cma", "csw", "arc",
                "pyuk", "pgc")
        num.week <- length(loop.weekly$date)
        for (i in 1:num.week) {
                frac.p <- 0
                frac.matl <- 0
                frac.g <- 0
                frac.cs <- 0
                frac.cw <- 0
                frac.cmw <- 0
```

```
frac.ce <- 0
frac.cn <- 0
frac.cma <- 0
frac.csw <- 0
frac.arc <- 0
frac.pyuk <- 0
frac.pgc <- 0
for (j in 1:7) {
        if (loop.daily$src1[(i-1)*7 +j] == "p") {
                frac.p <- frac.p + loop.daily$frac[(i-1)*7 +j]
                }
        if (loop.daily$src1[(i-1)*7 +j] == "matl") {
                frac.matl <- frac.matl + loop.daily$frac[(i-1)*7 +j]
                }
        if (loop.daily$src1[(i-1)*7 +j] == "g") {
                frac.g <- frac.g + loop.daily$frac[(i-1)*7 +j]
                }
        if (loop.daily$src1[(i-1)*7 +j] == "cs") {
                frac.cs <- frac.cs + loop.daily$frac[(i-1)*7 +j]
                }
        if (loop.daily$src1[(i-1)*7 +j] == "cw") {
                frac.cw <- frac.cw + loop.daily$frac[(i-1)*7 +j]
                }
        if (loop.daily$src1[(i-1)*7 +j] == "cmw") {
                frac.cmw <- frac.cmw + loop.daily$frac[(i-1)*7 +j]
                }
        if (loop.daily$src1[(i-1)*7 +j] == "ce") {
                frac.ce <- frac.ce + loop.daily$frac[(i-1)*7 +j]
                }
        if (loop.daily$src1[(i-1)*7 +j] == "cn") {
                frac.cn <- frac.cn + loop.daily$frac[(i-1)*7 +j]
                }
        if (loop.daily$src1[(i-1)*7 +j] == "cma") {
                frac.cma <- frac.cma + loop.daily$frac[(i-1)*7 +j]
```

```
                }
        if (loop.daily$src1[(i-1)*7 +j] == "csw") {
                frac.csw <- frac.csw + loop.daily$frac[(i-1)*7 +j]
                }
        if (loop.daily$src1[(i-1)*7 +j] == "arc") {
                frac.arc <- frac.arc + loop.daily$frac[(i-1)*7 +j]
                }
        if (loop.daily$src1[(i-1)*7 +j] == "pyuk") {
                frac.pyuk <- frac.pyuk + loop.daily$frac[(i-1)*7 +j]
                }
        if (loop.daily$src1[(i-1)*7 +j] == "pgc") {
                frac.pgc <- frac.pgc + loop.daily$frac[(i-1)*7 +j]
                }
    tot.frac$p[i] <- as.numeric(specify.decimal(frac.p, 2))
    tot.frac$matl[i] <- as.numeric(specify.decimal(frac.matl, 2))
    tot.frac$g[i] <- as.numeric(specify.decimal(frac.g, 2))
    tot.frac$cs[i] <- as.numeric(specify.decimal(frac.cs, 2))
    tot.frac$cw[i] <- as.numeric(specify.decimal(frac.cw, 2))
    tot.frac$cmw[i] <- as.numeric(specify.decimal(frac.cmw, 2))
    tot.frac$ce[i] <- as.numeric(specify.decimal(frac.ce, 2))
    tot.frac$cn[i] <- as.numeric(specify.decimal(frac.cn, 2))
    tot.frac$cma[i] <- as.numeric(specify.decimal(frac.cma, 2))
    tot.frac$csw[i] <- as.numeric(specify.decimal(frac.csw, 2))
    tot.frac$arc[i] <- as.numeric(specify.decimal(frac.arc, 2))
    tot.frac$pyuk[i] <- as.numeric(specify.decimal(frac.pyuk, 2))
    tot.frac$pgc[i] <- as.numeric(specify.decimal(frac.pgc, 2))
        }
}

loop.weekly.source <- data.frame(loop.weekly, tot.frac)
loop.ms.weekly <- loop.weekly.source[rowSums(loop.weekly.source[ ,c(13:24)]) != 0, ]#Removing weeks that aren't covered in ms
ms.weekly.data[[k]] <- loop.ms.weekly
ms.weekly.data[[k]]$site <- ms.index[[k]]
}
```

```
names(ms.weekly.data) <- ms.index

#write.table(ms.weekly.data, file="allsites_weekly_ms.csv", sep=",", row.names=FALSE)

#Making composite moisture sources
for (k in 1:length(ms.index)) {
        ms.weekly.data[[k]]$all.p <- ms.weekly.data[[k]]$p + ms.weekly.data[[k]]$pyuk
                + ms.weekly.data[[k]]$pgc
        ms.weekly.data[[k]]$main.c <- ms.weekly.data[[k]]$cw + ms.weekly.data[[k]]$cmw +
                ms.weekly.data[[k]]$ce + ms.weekly.data[[k]]$csw
        ms.weekly.data[[k]]$all.c <- ms.weekly.data[[k]]$cw + ms.weekly.data[[k]]$cmw +
                ms.weekly.data[[k]]$ce + ms.weekly.data[[k]]$csw + ms.weekly.data[[k]]$cs +
                ms.weekly.data[[k]]$cma
        ms.weekly.data[[k]]$g.cs <- ms.weekly.data[[k]]$cs + ms.weekly.data[[k]]$g
        ms.weekly.data[[k]]$matl.cma <- ms.weekly.data[[k]]$cma + ms.weekly.data[[k]]$matl
        }

#---------------------------------------NO PYUK, CE, OR CMA-----------------------------------------------
#-----------------------------------80% Threshold (Is Better)-----------------------------------------
for (k in 1:length(ms.index)) {
        ms.weekly.data[[k]]$isotemp.residual <- round(ms.weekly.data[[k]]$d18O -
                (ms.lmdata[[k]]$coef[2]*ms.weekly.data[[k]]$tavg + ms.lmdata[[k]]$coef[1]), 2)
        }

source.index <- c("g", "p", "arc", "matl", "cs", "csw", "cw", "cmw", "cn",
                "g.cs", "main.c", "all.c")

#Creating a list of sites each with a list of data specific to the moisture source
#Also rearranging source order to make more geographic sense
allsource.data.80 <- list(NA)
source.data <- list(NA)
for (k in 1:length(ms.index)) {
        col.index <- c(1,3,4,5,10,11,12,31)
        source.data[[1]] <- ms.weekly.data[[k]][ms.weekly.data[[k]]$g > 0.8, col.index]
```

```
        source.data[[2]] <- ms.weekly.data[[k]][ms.weekly.data[[k]]$p > 0.8, col.index]
        source.data[[3]] <- ms.weekly.data[[k]][ms.weekly.data[[k]]$arc > 0.8, col.index]
        source.data[[4]] <- ms.weekly.data[[k]][ms.weekly.data[[k]]$matl > 0.8, col.index]
        source.data[[5]] <- ms.weekly.data[[k]][ms.weekly.data[[k]]$cs > 0.8, col.index]
        source.data[[6]] <- ms.weekly.data[[k]][ms.weekly.data[[k]]$csw > 0.8, col.index]
        source.data[[7]] <- ms.weekly.data[[k]][ms.weekly.data[[k]]$cw > 0.8, col.index]
        source.data[[8]] <- ms.weekly.data[[k]][ms.weekly.data[[k]]$cmw > 0.8, col.index]
        source.data[[9]] <- ms.weekly.data[[k]][ms.weekly.data[[k]]$cn > 0.8, col.index]
        source.data[[10]] <- ms.weekly.data[[k]][ms.weekly.data[[k]]$g.cs > 0.8, col.index]
        source.data[[11]] <- ms.weekly.data[[k]][ms.weekly.data[[k]]$main.c > 0.8, col.index]
        source.data[[12]] <- ms.weekly.data[[k]][ms.weekly.data[[k]]$all.c > 0.8, col.index]
        names(source.data) <- source.index
        allsource.data.80[[k]] <- source.data
        }
names(allsource.data.80) <- ms.index


mean.sources <- data.frame(matrix(nrow=length(source.index), ncol=7))
sd.sources <- data.frame(matrix(nrow=length(source.index), ncol=7))
median.sources <- data.frame(matrix(nrow=length(source.index), ncol=7))
mad.sources <- data.frame(matrix(nrow=length(source.index), ncol=7))
ms.mean.80 <- list(NA)
ms.sd.80 <- list(NA)
ms.sem.80 <- list(NA)
ms.median.80 <- list(NA)
ms.mad.80 <- list(NA)

#Moisture source stats
for (k in 1:length(ms.index)) {
        for (j in 1:length(source.index)) {
                mean.sources[j,1] <- length(allsource.data.80[[k]][[j]]$d18O)
                mean.sources[j, c(2:7)] <- round(t(colMeans(allsource.data.80[[k]][[j]][c(2,3,4,5,7,8)])), 2)
                colnames(mean.sources) <- c("n", "usnip.prcp", "d18O", "d2H", "tavg",
                        "dex", "isotemp.residual")
```

```
                rownames(mean.sources) <- source.index

                sd.sources[j,1] <- length(allsource.data.80[[k]][[j]]$d18O)
                sd.sources[j, c(2:7)] <- round(t(apply(allsource.data.80[[k]][[j]][c(2,3,4,5,7,8)], 2, sd)), 2)
                colnames(sd.sources) <- c("n", "usnip.prcp", "d18O", "d2H", "tavg",
                                "dex", "isotemp.residual")
                rownames(sd.sources) <- source.index

                median.sources[j,1] <- length(allsource.data.80[[k]][[j]]$d18O)
                median.sources[j, c(2:7)] <- round(t(apply(allsource.data.80[[k]][[j]][c(2,3,4,5,7,8)], 2, median)), 2)
                colnames(median.sources) <- c("n", "usnip.prcp", "d18O", "d2H", "tavg",
                                "dex", "isotemp.residual")
                rownames(median.sources) <- source.index

                mad.sources[j,1] <- length(allsource.data.80[[k]][[j]]$d18O)
                mad.sources[j, c(2:7)] <- round(t(apply(allsource.data.80[[k]][[j]][c(2,3,4,5,7,8)], 2, mad)), 2)
                colnames(mad.sources) <- c("n", "usnip.prcp", "d18O", "d2H", "tavg",
                                "dex", "isotemp.residual")
                rownames(mad.sources) <- source.index
                }
        ms.mean.80[[k]] <- mean.sources
        ms.sd.80[[k]] <- sd.sources
        ms.sem.80[[k]] <- specify.decimal((sd.sources)/sqrt(sd.sources$n), 2)
        ms.sem.80[[k]]$n <- sd.sources$n
        ms.median.80[[k]] <- median.sources
        ms.mad.80[[k]] <- mad.sources
        }
names(ms.mean.80) <- ms.index
names(ms.sd.80) <- ms.index
names(ms.sem.80) <- ms.index
names(ms.median.80) <- ms.index
names(ms.mad.80) <- ms.index

#write.table(ms.mean.80, "ms_mean_80.csv", sep=",", row.names=TRUE, col.names=NA)
```

```
#write.table(ms.sd.80, "ms_sd_80.csv", sep=",", row.names=TRUE, col.names=NA)
#write.table(ms.sem.80, "ms_sem_80.csv", sep=",", row.names=TRUE, col.names=NA)
#write.table(ms.median.80, "ms_median_80.csv", sep=",", row.names=TRUE, col.names=NA)
#write.table(ms.mad.80, "ms_mad_80.csv", sep=",", row.names=TRUE, col.names=NA)

#Weird plot that's not useful
#dev.new(height=8, width=8)
#plot(allsource.data.80[[1]][[1]]$d18O, allsource.data.80[[1]]$isotemp.residual, type="n")
#points(allsource.data.80[[1]][[13]]$d18O, pch=16, cex=0.7, col="steelblue4") #all.p
#points(allsource.data.80[[1]][[1]]$d18O, pch=16, cex=0.7, col="red") #gulf
#points(allsource.data.80[[1]][[14]]$d18O, pch=16, cex=0.7, col="green") #main.c
#points(allsource.data.80[[1]][[1]]$d18O, pch=16, cex=0.7, col="black")
#points(allsource.data.80[[1]][[1]]$d18O, pch=16, cex=0.7, col="green")

#Adding a moisture source column
for (k in 1:length(ms.index)) {
        for (j in 1:length(source.index)) {
                if(length(allsource.data.80[[k]][[j]]$d18O > 0)) {
                        allsource.data.80[[k]][[j]]$ms <- source.index[j]
                        }
                }
        }

#Making a list of sites with all moisture source weeks in one matrix so plotting by ms works
ms.plot.data.80 <- list(NA)
site.ttest.p <- list(NA)
for (k in 1:length(ms.index)) {
        ms.plot.data.tmp <- data.frame(matrix(nrow=0, ncol=9))
        for (j in 1:length(source.index)) {
                ms.plot.data.tmp <- rbind(ms.plot.data.tmp, allsource.data.80[[k]][[j]])
                }
        ms.plot.data.80[[k]] <- ms.plot.data.tmp
        }
```

```
#Calculating t-test p.values for each site's moisture source isotemp residual
#Sample sizes are too small for t-test p values to really mean much more than tell sample size
for (k in 1:length(ms.index)) {
	site.ttest.p.tmp <- NA
	for (i in 1:length(source.index)) {
		if(length(ms.plot.data.80[[k]]$isotemp.residual[ms.plot.data.80[[k]]$ms
			== source.index[i]]) > 2) {
			site.ttest.p.tmp[i] <- t.test(ms.plot.data.80[[k]]$isotemp.residual
				[ms.plot.data.80[[k]]$ms == source.index[i]])$p.value
			}
		else {
			site.ttest.p.tmp[i] <- NA
			}
		}
	site.ttest.p[[k]] <- site.ttest.p.tmp
names(site.ttest.p[[k]]) <- source.index
	}
names(site.ttest.p) <- ms.index

#write.table(site.ttest.p, "ms_site_ttest.csv", sep=",", row.names=TRUE, col.names=NA)

#Making a single matrix with all moisture source weeks and sites
ms.all.80 <- data.frame(matrix(nrow=0, ncol=9))
for (k in 1:length(ms.index)) {
	ms.all.80 <- rbind(ms.all.80, ms.plot.data.80[[k]])
	}

#Calculating median and mad of all sites combined per source
ms.all.80.median <- aggregate(ms.all.80[ , c(2,3,4,5,7,8)], list(ms.all.80$ms), median)
ms.all.80.median <- ms.all.80.median[c(8,12,2,11,5,6,7,3,4,9,10,1),]
ms.all.80.mad <- aggregate(ms.all.80[ , c(2,3,4,5,7,8)], list(ms.all.80$ms), mad)
ms.all.80.mad <- ms.all.80.mad[c(8,12,2,11,5,6,7,3,4,9,10,1),]

#Calculating t-test p.values for combined sites' moisture source isotemp residual
```

```
#Sample sizes are too small for t-test p values to really mean much more than tell sample size
all.ttest.p <- NA
for (i in 1:length(source.index)) {
	all.ttest.p[i] <- t.test(ms.all.80$isotemp.residual[ms.all.80$ms == source.index[i]])$p.value
	}
names(all.ttest.p) <- source.index

mo <- strftime(ms.all.80$date, "%m")
yr <- strftime(ms.all.80$date, "%Y")
ms.all.80$mo <- mo
ms.all.80$yr<- yr
ms.all.80$sn[ms.all.80$mo == "12" | ms.all.80$mo == "01" | ms.all.80$mo == "02"] <- "win"
ms.all.80$sn[ms.all.80$mo == "03" | ms.all.80$mo == "04" | ms.all.80$mo == "05"] <- "spr"
ms.all.80$sn[ms.all.80$mo == "06" | ms.all.80$mo == "07" | ms.all.80$mo == "08"] <- "sum"
ms.all.80$sn[ms.all.80$mo == "09" | ms.all.80$mo == "10" | ms.all.80$mo == "11"] <- "aut"

ms.win.80 <- ms.all.80[ms.all.80$sn == "win", ]
ms.spr.80 <- ms.all.80[ms.all.80$sn == "spr", ]
ms.sum.80 <- ms.all.80[ms.all.80$sn == "sum", ]
ms.aut.80 <- ms.all.80[ms.all.80$sn == "aut", ]

#Checking seasonal changes: There aren't much
specify.decimal(table(ms.win.80$ms)/sum(table(ms.win.80$ms)), 3)
specify.decimal(table(ms.spr.80$ms)/sum(table(ms.spr.80$ms)), 3)
specify.decimal(table(ms.sum.80$ms)/sum(table(ms.sum.80$ms)), 3)
specify.decimal(table(ms.aut.80$ms)/sum(table(ms.aut.80$ms)), 3)

source.color.index <- c("firebrick", "darkorange", "dodgerblue3", "mediumorchid4", "darkgreen",
	"gold4", "yellow3", "lawngreen", "darkcyan", "firebrick", "lawngreen", "darkgreen")

for (k in 1:length(ms.index)) {
	#isotemp.residual
	dev.new(height=6, width=10)
	stripchart(ms.plot.data.80[[k]]$isotemp.residual~factor(ms.plot.data.80[[k]]$ms, levels=source.index),
```

```
            col=adjustcolor(source.color.index, alpha=0.5), pch=15, ylab="", yaxt="n", xaxt="n",
            vertical=TRUE, ylim=c(-12,10))
        axis(2, at=seq(-10, 10, 5), las=1)
        axis(2, at=seq(-12, 10, 1),labels=FALSE, tck=-0.01)
        axis(1, at=(1:12), labels=source.index)
        text(y=-12, x=1, pos=4, toupper(ms.index[k]), cex=1.5)
        mtext(side=2, expression(paste({delta}^18*O, " Residual (‰)")),
            line=2.5, cex=1.2)
        points(c(1:12), ms.median.80[[k]]$isotemp.residual, pch=23, cex=2, col="black", lwd=2.5,
            bg=source.color.index)
        points(c(1:12), ms.median.80[[k]]$isotemp.residual+ms.mad.80[[k]]$isotemp.residual, pch="-", cex=2, col="black", lwd=2.5,)
        points(c(1:12), ms.median.80[[k]]$isotemp.residual-ms.mad.80[[k]]$isotemp.residual, pch="-", cex=2, col="black", lwd=2.5,)
        }

for (k in 1:length(ms.index)) {
        #dex
        dev.new(height=6, width=10)
        stripchart(ms.plot.data.80[[k]]$dex~factor(ms.plot.data.80[[k]]$ms, levels=source.index),
            col=adjustcolor(source.color.index, alpha=0.5), pch=15, ylab="", yaxt="n", xaxt="n",
            vertical=TRUE, ylim=c(-10,35))
        axis(2, at=seq(-10, 30, 10), las=1)
        axis(2, at=seq(-10, 35, 5),labels=FALSE, tck=-0.01)
        axis(1, at=(1:12), labels=source.index)
        text(y=-10, x=1, pos=4, paste(toupper(ms.index[k])), cex=1.5)
        mtext(side=2, "Deuterium Excess (‰)", line=2.5, cex=1.2)
        points(c(1:12), ms.median.80[[k]]$dex, pch=23, cex=2, col="black", lwd=2.5,
            bg=source.color.index)
        points(c(1:12), ms.median.80[[k]]$dex+ms.mad.80[[k]]$dex, pch="-", cex=2, col="black", lwd=2.5,)
        points(c(1:12), ms.median.80[[k]]$dex-ms.mad.80[[k]]$dex, pch="-", cex=2, col="black", lwd=2.5,)
        }

for (k in 1:length(ms.index)) {
        #log(prcp amt) for all data
        dev.new(height=6, width=10)
```

```
        stripchart(log(ms.plot.data.80[[k]]$usnip.prcp+1)~factor(ms.plot.data.80[[k]]$ms, levels=source.index),
                col=adjustcolor(source.color.index, alpha=0.5), pch=15, ylab="", yaxt="n", xaxt="n",
                vertical=TRUE, ylim=c(0,6))
        axis(2, at=seq(0, 6, 2), las=1)
        axis(2, at=seq(0, 6, 1),labels=FALSE, tck=-0.01)
        axis(1, at=(1:12), labels=source.index)
        text(y=0, x=1, pos=4, paste(toupper(ms.index[k])), cex=1.5)
        mtext(side=2, "ln(Precipitation Amount +1) (mm)", line=2.5, cex=1.2)
        points(c(1:12), log(ms.median.80[[k]]$usnip.prcp+1), pch=23, cex=2, col="black", lwd=2.5,
                bg=source.color.index)
        points(c(1:12), log(ms.median.80[[k]]$usnip.prcp+ms.mad.80[[k]]$usnip.prcp+1), pch="-", cex=2, col="black", lwd=2.5,)
        points(c(1:12), log(ms.median.80[[k]]$usnip.prcp-ms.mad.80[[k]]$usnip.prcp+1), pch="-", cex=2, col="black", lwd=2.5,)
        }


for (k in 1:length(ms.index)) {
        #tavg
        dev.new(height=6, width=10)
        stripchart(ms.plot.data.80[[k]]$tavg~factor(ms.plot.data.80[[k]]$ms, levels=source.index),
                col=adjustcolor(source.color.index, alpha=0.5), pch=15, ylab="", yaxt="n", xaxt="n",
                vertical=TRUE, ylim=c(-15,30))
        axis(2, at=seq(-10, 30, 10), las=1)
        axis(2, at=seq(-15, 30, 2),labels=FALSE, tck=-0.01)
        axis(1, at=(1:12), labels=source.index)
        text(y=0, x=1, pos=4, paste(toupper(ms.index[k])), cex=1.5)
        mtext(side=2, "Surface Temperature (°C)", line=2.5, cex=1.2)
        points(c(1:12), ms.median.80[[k]]$tavg, pch=23, cex=2, col="black", lwd=2.5,
                bg=source.color.index)
        points(c(1:12), ms.median.80[[k]]$tavg+ms.mad.80[[k]]$tavg, pch="-", cex=2, col="black", lwd=2.5,)
        points(c(1:12), ms.median.80[[k]]$tavg-ms.mad.80[[k]]$tavg, pch="-", cex=2, col="black", lwd=2.5,)
        }


for (k in 1:length(ms.index)) {
```

```
        #d18O
        dev.new(height=6, width=10)
        stripchart(ms.plot.data.80[[k]]$d18O~factor(ms.plot.data.80[[k]]$ms, levels=source.index),
                col=adjustcolor(source.color.index, alpha=0.5), pch=15, ylab="", yaxt="n", xaxt="n",
                vertical=TRUE, ylim=c(-26,2))
        axis(2, at=seq(-20, 0, 10), las=1)
        axis(2, at=seq(-25, 0, 5),labels=FALSE, tck=-0.01)
        axis(1, at=(1:12), labels=source.index)
        text(y=-25, x=1, pos=4, paste(toupper(ms.index[k])), cex=1.5)
        mtext(side=2, expression(paste({delta}^18*O, "(‰ vs. V-SMOW)")),
                line=2.5, cex=1.2)
        points(c(1:12), ms.median.80[[k]]$d18O, pch=23, cex=2, col="black", lwd=2.5,
                bg=source.color.index)
        points(c(1:12), ms.median.80[[k]]$d18O+ms.mad.80[[k]]$d18O, pch="-", cex=2, col="black", lwd=2.5,)
        points(c(1:12), ms.median.80[[k]]$d18O-ms.mad.80[[k]]$d18O, pch="-", cex=2, col="black", lwd=2.5,)
        }


#isotemp.residual for all data
dev.new(height=6, width=10)
stripchart(ms.all.80$isotemp.residual~factor(ms.all.80$ms, levels=source.index),
        col=adjustcolor(source.color.index, alpha=0.5), pch=15, ylab="", yaxt="n", xaxt="n",
        vertical=TRUE, ylim=c(-12,10))
axis(2, at=seq(-10, 10, 5), las=1)
axis(2, at=seq(-12, 10, 1),labels=FALSE, tck=-0.01)
axis(1, at=(1:12), labels=source.index)
text(y=-12, x=1, pos=4, "All Sites", cex=1.5)
mtext(side=2, expression(paste({delta}^18*O, " Residual (‰)")),
        line=2.5, cex=1.2)
points(c(1:12), ms.all.80.median$isotemp.residual, pch=23, cex=2, col="black", lwd=2.5,
        bg=source.color.index)
points(c(1:12), ms.all.80.median$isotemp.residual+ms.all.80.mad$isotemp.residual, pch="-", cex=2, col="black", lwd=2.5,)
points(c(1:12), ms.all.80.median$isotemp.residual-ms.all.80.mad$isotemp.residual, pch="-", cex=2, col="black", lwd=2.5,)
```

```
#prcp amt for all data
dev.new(height=6, width=10)
stripchart(ms.all.80$usnip.prcp~factor(ms.all.80$ms, levels=source.index),
        col=adjustcolor(source.color.index, alpha=0.5), pch=15, ylab="", yaxt="n", xaxt="n",
        vertical=TRUE, ylim=c(0,175))
axis(2, at=seq(0, 150, 50), las=1)
axis(2, at=seq(0, 175, 25),labels=FALSE, tck=-0.01)
axis(1, at=(1:12), labels=source.index)
text(y=-12, x=1, pos=4, "All Sites", cex=1.5)
mtext(side=2, "Precipitation Amount (mm)", line=2.5, cex=1.2)
points(c(1:12), ms.all.80.median$usnip.prcp, pch=23, cex=2, col="black", lwd=2.5,
        bg=source.color.index)
points(c(1:12), ms.all.80.median$usnip.prcp+ms.all.80.mad$usnip.prcp, pch="-", cex=2, col="black", lwd=2.5,)
points(c(1:12), ms.all.80.median$usnip.prcp-ms.all.80.mad$usnip.prcp, pch="-", cex=2, col="black", lwd=2.5,)

#log(prcp amt) for all data
dev.new(height=6, width=10)
stripchart(log(ms.all.80$usnip.prcp+1)~factor(ms.all.80$ms, levels=source.index),
        col=adjustcolor(source.color.index, alpha=0.5), pch=15, ylab="", yaxt="n", xaxt="n",
        vertical=TRUE, ylim=c(0,6))
axis(2, at=seq(0, 6, 2), las=1)
axis(2, at=seq(0, 6, 1),labels=FALSE, tck=-0.01)
axis(1, at=(1:12), labels=source.index)
text(y=-12, x=1, pos=4, "All Sites", cex=1.5)
mtext(side=2, "log(Precipitation Amount +1) (mm)", line=2.5, cex=1.2)
points(c(1:12), log(ms.all.80.median$usnip.prcp+1), pch=23, cex=2, col="black", lwd=2.5,
        bg=source.color.index)
points(c(1:12), log(ms.all.80.median$usnip.prcp+ms.all.80.mad$usnip.prcp+1), pch="-", cex=2, col="black", lwd=2.5,)
points(c(1:12), log(ms.all.80.median$usnip.prcp-ms.all.80.mad$usnip.prcp+1), pch="-", cex=2, col="black", lwd=2.5,)

#tavg for all data
dev.new(height=6, width=10)
stripchart(ms.all.80$tavg~factor(ms.all.80$ms, levels=source.index),
```

```
        col=adjustcolor(source.color.index, alpha=0.5), pch=15, ylab="", yaxt="n", xaxt="n",
        vertical=TRUE, ylim=c(-15,30))
axis(2, at=seq(-10, 30, 10), las=1)
axis(2, at=seq(-15, 30, 5),labels=FALSE, tck=-0.01)
axis(1, at=(1:12), labels=source.index)
text(y=-12, x=1, pos=4, "All Sites", cex=1.5)
mtext(side=2, "Surface Temperature (°C)", line=2.5, cex=1.2)
points(c(1:12), ms.all.80.median$tavg, pch=23, cex=2, col="black", lwd=2.5,
        bg=source.color.index)
points(c(1:12), ms.all.80.median$tavg+ms.all.80.mad$tavg, pch="-", cex=2, col="black", lwd=2.5,)
points(c(1:12), ms.all.80.median$tavg-ms.all.80.mad$tavg, pch="-", cex=2, col="black", lwd=2.5,)

#d18O for all data
dev.new(height=6, width=10)
stripchart(ms.all.80$d18O~factor(ms.all.80$ms, levels=source.index),
        col=adjustcolor(source.color.index, alpha=0.5), pch=15, ylab="", yaxt="n", xaxt="n",
        vertical=TRUE, ylim=c(-26,2))
axis(2, at=seq(-20, 0, 10), las=1)
axis(2, at=seq(-25, 0, 5),labels=FALSE, tck=-0.01)
axis(1, at=(1:12), labels=source.index)
text(y=-25, x=1, pos=4, "All Sites", cex=1.5)
        mtext(side=2, expression(paste({delta}^18*O, " (‰ vs. V-SMOW)")),
                line=2.5, cex=1.2)
points(c(1:12), ms.all.80.median$d18O, pch=23, cex=2, col="black", lwd=2.5,
        bg=source.color.index)
points(c(1:12), ms.all.80.median$d18O+ms.all.80.mad$d18O, pch="-", cex=2, col="black", lwd=2.5,)
points(c(1:12), ms.all.80.median$d18O-ms.all.80.mad$d18O, pch="-", cex=2, col="black", lwd=2.5,)


#Calculating t-test p.values for combined sites' moisture source isotemp residual
#Sample sizes are too small for t-test p values to really mean much more than tell sample size
all.ttest.p <- NA
for (i in 1:length(source.index)) {
        all.ttest.p[i] <- t.test(ms.all.80$isotemp.residual[ms.all.80$ms == source.index[i]])$p.value
```

```
        }
names(all.ttest.p) <- source.index

#=============================================================================================================
#=====================================SSA Model and Verification==============================================
#=============================================================================================================
#--------------------Seasonal Fraction Function-----------------------------
#This function calculates the proportion of precipitation likely to be winter and summer
#for a given site and d18O value

#WARNING: season.lmcor must be calculated beforehand
#WARNING: Will return negative and >1 fractions if d18O input is less/greater than seasonal signal

#NOTE: Sites with a low seasonal tavg-d18O r^2 are likely not appropriate for this function


seasonal.fraction <- function(signal, site) { #signal is d18O in VSMOW, site must be in quotes
        win.frac <- (signal - season.lmcor[[site]]["sum","d18O.wt"]) /
                (season.lmcor[[site]]["win","d18O.wt"] - season.lmcor[[site]]["sum","d18O.wt"])
        seas.frac <- data.frame(signal, win.frac, (1-win.frac))
        colnames(seas.frac) <- c("d18O", "winter.fraction", "summer.fraction")
        return(seas.frac)
        }

#This script creates fake years of precipitation data for IN22 by randomly selecting defined fractions
#of winter and summer weekly data. These fake years are used to see how well the SSA metric can
#predict seasonality based on real data
#-----------------------------90 points Replace=TRUE-----------------------------------------------------
#Rougly equal to 3 years
sum.frac <- seq(.15, .85, .1)
win.frac <- 1 - sum.frac
n.wk.entry <- 90
```

```
#Indiana generally sees 120 days of precipitation per year
#1992, 1993, and 2004 had 32, 28, and 38 weeks with precipitation at IN22

all.win <- totalsites.data[[6]][totalsites.data[[6]]$season == "win", ]
all.spr <- totalsites.data[[6]][totalsites.data[[6]]$season == "spr", ]
all.sum <- totalsites.data[[6]][totalsites.data[[6]]$season == "sum", ]
all.aut <- totalsites.data[[6]][totalsites.data[[6]]$season == "aut", ]

sum.sample.n <- ceiling(sum.frac * n.wk.entry)
win.sample.n <- ceiling(win.frac * n.wk.entry)
n.wk <- sum.sample.n + win.sample.n


n.iter <- 100
all.fake.yr <- list(NA)
all.fake.yr.wtmean <- list(NA)
all.fake.yr.ssa <- data.frame(matrix(nrow=n.iter, ncol=length(sum.frac)))
predict.fake.yr <- data.frame(matrix(nrow=n.iter, ncol=length(sum.frac)))
predict.fake.yr.ssa <- data.frame(matrix(nrow=n.iter, ncol=length(sum.frac)))
predict.stats <- data.frame(matrix(nrow=length(sum.frac), ncol=4))
for (k in 1:length(sum.frac)) {
        fake.yr <- list(NA)
        fake.yr.wtmean <- data.frame(matrix(nrow = n.iter, ncol = 3))
        fake.yr.ssa <- NA
        for (i in 1:n.iter) {
                sum.sample <- all.sum[sample(nrow(all.sum), sum.sample.n[k], replace=TRUE), ]
                win.sample <- all.win[sample(nrow(all.win), win.sample.n[k], replace=TRUE), ]
                fake.yr[[i]] <- rbind(sum.sample, win.sample)
                fake.yr.ssa[i] <- (sum(sum.sample$usnip.prcp) / (sum(sum.sample$usnip.prcp) +
                        sum(win.sample$usnip.prcp))) - 0.65
                fake.yr.wkfrac <- fake.yr[[i]]$usnip.prcp/sum(fake.yr[[i]]$usnip.prcp)
                fake.yr.wtmean[i,] <- c(colSums(fake.yr[[i]][c(2,8)] * fake.yr.wkfrac),
                        sum(fake.yr[[i]][1]))
                }
```

```
colnames(fake.yr.wtmean) <- c("d18O", "tavg", "usnip.prcp")
all.fake.yr[[k]] <- fake.yr
all.fake.yr.wtmean[[k]] <- fake.yr.wtmean
all.fake.yr.ssa[k] <- fake.yr.ssa


#Testing
predict.fake.yr[k] <- seasonal.fraction(all.fake.yr.wtmean[[k]][1], "in22")$summer.fraction
predict.fake.yr.ssa[k] <- seasonal.fraction(all.fake.yr.wtmean[[k]][1], "in22")$summer.fraction - 0.65

predict.stats[k,1] <- mean(predict.fake.yr.ssa[,k])
predict.stats[k,2] <-       sd(predict.fake.yr.ssa[,k])/sqrt(length(predict.fake.yr.ssa[,k]))
predict.stats[k,c(3,4)] <-              c(mean(predict.fake.yr.ssa[,k])+2*sd(predict.fake.yr.ssa[,k]),
          mean(predict.fake.yr.ssa[,k])-2*sd(predict.fake.yr.ssa[,k]))
colnames(predict.stats) <- c("mean", "error", "ci+", "ci-")

#Plots of SSA prediction distributions
dev.new(height=10, width=10)
plot(density(predict.fake.yr.ssa[,k]), xlim=c(-1, 1.1), ylim=c(0,6), bty = "n",
          main="", bty="n", type="n", xlab="", xaxt="n",
          ylab="", yaxt="n", cex.main=1.8)
points(density(predict.fake.yr.ssa[,k]), type="l", lwd=1.5)
mtext(side=2, text="Estimate Kernel Density", line=2.0, cex=2)
mtext(side=1, text="Estimated SSA", line=2.0, cex=2)
axis(1, at=(seq(-1,1,0.2)), las=1, pos=0, cex.axis=1.5)
axis(1, at=(seq(-1,1,0.1)), pos=0, labels=FALSE, tck=-0.01)
axis(2, at=(seq(0,6,1)), las=1, pos=-1, cex.axis=1.5)
axis(2, at=(seq(0,6,0.5)), pos=-1, labels=FALSE, tck=-0.01)
abline(v=predict.stats[k,1], col="firebrick", lwd=2)
abline(v=(mean(all.fake.yr.ssa[[k]])), col="dodgerblue", lty=2, lwd=2)
abline(v=predict.stats[k,3], col="gray60", lty=3, lwd=1.2)
abline(v=predict.stats[k,4], col="gray60", lty=3, lwd=1.2)
legend(legend=c(paste("Actual SSA = ", specify.decimal(mean(all.fake.yr.ssa[[k]]),2)),
          paste("SSA Estimate Mean = ", specify.decimal(predict.stats[k,1],2)),
```

```
            paste("SSA Estimate 2σ = ±", specify.decimal(2*sd(predict.fake.yr[,k]),2))), y.intersp = 1.5,
            x=0.25, y=6.2, lty=c(2, 1, 3), col=c("dodgerblue", "firebrick", "gray60"), bty="n", cex=1.3, lwd=2)

        #Plots of SSA prediction distributions both actual and estimated distributions
        dev.new(height=10, width=10)
        plot(density(predict.fake.yr.ssa[,k]), xlim=c(-1, 1.1), ylim=c(0,20), bty = "n",
            main="", bty="n", type="n", xlab="", xaxt="n",
            ylab="", yaxt="n", cex.main=1.8)
        points(density(predict.fake.yr.ssa[,k]+0.06), type="l", lwd=1.5, col="firebrick")
        points(density(all.fake.yr.ssa[[k]]), type="l", lwd=1.5, col="dodgerblue")
        mtext(side=2, text="Kernel Density", line=2.0, cex=2)
        mtext(side=1, text="SSA", line=2.0, cex=2)
        axis(1, at=(seq(-1,1,0.2)), las=1, pos=0, cex.axis=1.5)
        axis(1, at=(seq(-1,1,0.1)), pos=0, labels=FALSE, tck=-0.01)
        axis(2, at=(seq(0,20,5)), las=1, pos=-1, cex.axis=1.5)
        axis(2, at=(seq(0,20,1)), pos=-1, labels=FALSE, tck=-0.01)
        abline(v=predict.stats[k,1]+0.06, col="firebrick", lwd=2)
        abline(v=(mean(all.fake.yr.ssa[[k]])), col="dodgerblue", lty=2, lwd=2)
        abline(v=predict.stats[k,3]+0.06, col="gray60", lty=3, lwd=1.2)
        abline(v=predict.stats[k,4]+0.06, col="gray60", lty=3, lwd=1.2)
        legend(legend=c(paste("SSA Actual Mean = ", specify.decimal(mean(all.fake.yr.ssa[[k]]),2)),
            paste("SSA Actual 2σ = ±", specify.decimal(2*sd(all.fake.yr.ssa[[k]]),2)),
            paste("SSA Estimate Mean = ", specify.decimal(predict.stats[k,1]+0.06,2)),
            paste("SSA Estimate 2σ = ±", specify.decimal(2*sd(predict.fake.yr[,k]),2))), y.intersp = 1.5,
            x=0.25, y=6.2, lty=c(2, NA, 1, 3), col=c("dodgerblue", NA, "firebrick", "gray60"), bty="n", cex=1.3, lwd=2)
        }

#Combining data from all iteration sets
actual.ssa <- vector()
est.ssa <- vector()
for (k in 1:length(sum.frac)) {
        actual.ssa <- c(actual.ssa, all.fake.yr.ssa[,k])
        est.ssa <- c(est.ssa, predict.fake.yr.ssa[,k])
        }
```

```
cor(est.ssa, actual.ssa)
ssa.verify.lm <- summary(lm(est.ssa ~ actual.ssa))

#Plotting estimated SSA vs Actual SSA
dev.new(height=10, width=10)
plot(all.fake.yr.ssa[,k], predict.fake.yr.ssa[,k], xlim=c(-0.8, 0.4), ylim=c(-0.8,0.4),
        main="", bty="n", type="n", xlab="", xaxt="n",
        ylab="", yaxt="n", cex.main=1.8)
        abline(a=0, b=1, col="black", lwd=2)
        points(actual.ssa, est.ssa, pch=16, cex=1.3, col=adjustcolor("gray45", alpha=0.8))
        mtext(side=2, text="Estimated SSA", line=2.0, cex=2)
        mtext(side=1, text="Actual SSA", line=2.0, cex=2)
        axis(1, at=(seq(-0.8,0.4,0.2)), las=1, pos=-0.8, cex.axis=1.5)
        axis(1, at=(seq(-0.8,0.4,0.1)), pos=-0.8, labels=FALSE, tck=-0.01)
        axis(2, at=(seq(-0.8,0.4,0.2)), las=1, pos=-0.8, cex.axis=1.5)
        axis(2, at=(seq(-0.8,0.4,0.1)), pos=-0.8, labels=FALSE, tck=-0.01)
        abline(a=ssa.verify.lm$coefficients[1], b=ssa.verify.lm$coefficients[2], col="firebrick", lwd=2)
        legend(legend=c(paste("y = ", specify.decimal(ssa.verify.lm$coefficients[2],2), "x + ",
                specify.decimal(ssa.verify.lm$coefficients[1],2)),
                paste("r² = ", specify.decimal(ssa.verify.lm$r.squared,2))),
                y.intersp = 1.5, x=-0.75, y=0.38, lty=c(1, 1), col=c("firebrick", NA), bty="n", cex=1.8, lwd=2)

ttest <- list()
for (k in 1:length(sum.frac)) {
        ttest[[k]] <- t.test(predict.fake.yr.ssa[,k], mu=sum.frac[k]-0.65)
        }

#=============================================================================================================
#=====================================Interannual d18O controls================================================
#=============================================================================================================
#This script examines GNIP and USNIP data to determine climate correlations with interannual d18O
#values, sometimes through bootstrapping and other fun statistical tools
#Written by Pete D. Akers, September 2015, and continuously edited through 2016
```

```
#NOTE: Requires Allsites Looping Script run first

#Loading this function here rather than separately
seasonal.fraction <- function(signal, site) { #signal is d18O in VSMOW, site must be in quotes
        win.frac <- (signal - season.lmcor[[site]]["sum","d18O.wt"]) /
                (season.lmcor[[site]]["win","d18O.wt"] - season.lmcor[[site]]["sum","d18O.wt"])
        seas.frac <- data.frame(signal, win.frac, (1-win.frac))
        colnames(seas.frac) <- c("d18O", "winter.fraction", "summer.fraction")
        return(seas.frac)
        }

pdo <- read.table("pdo_monthly.csv", header=TRUE, sep=",")
mei <- read.table("mei_monthly.csv", header=TRUE, sep=",")
nao <- read.table("nao_noaa_monthly.csv", header=TRUE, sep=",")
amo <- read.table("amo_monthly.csv", header=TRUE, sep=",")
pna <- read.table("pna_monthly.csv", header=TRUE, sep=",")
bhi <- read.table("bhi_monthly.csv", header=TRUE, sep=",")

pdo <- pdo[pdo$year >= 1950 & pdo$year <= 2013, ]
mei <- mei[mei$year >= 1950 & mei$year <= 2013, ]
nao <- nao[nao$year >= 1950 & nao$year <= 2013, ]
amo <- amo[amo$year >= 1950 & amo$year <= 2013, ]
pna <- pna[pna$year >= 1950 & pna$year <= 2013, ]
bhi <- bhi[bhi$year >= 1950 & bhi$year <= 2013, ]

osc.index <- c("pdo", "mei", "nao", "amo", "pna", "bhi")
osc <- list(pdo, mei, nao, amo, pna, bhi)
names(osc) <- osc.index


#Loading airport data to make constructed years with USNIP data
indy <- read.table(file="airport_indy_climate.csv", sep=",", header=TRUE)
indy$date <- as.character(indy$date)
```

```
indy$date <- as.Date(indy$date, "%Y%m%d")

lvlle <- read.table(file="airport_louisville_climate.csv", sep=",", header=TRUE)
lvlle$date <- as.character(lvlle$date)
lvlle$date <- as.Date(lvlle$date, "%Y%m%d")

moln <- read.table(file="airport_moline_climate.csv", sep=",", header=TRUE)
moln$date <- as.character(moln$date)
moln$date <- as.Date(moln$date, "%Y%m%d")

#O'Hare removed due to short record, replaced with Midway
#ohare <- read.table(file="airport_ohare_climate.csv", sep=",", header=TRUE)
#ohare$date <- as.character(ohare$date)
#ohare$date <- as.Date(ohare$date, "%Y%m%d")

mdwy <- read.table(file="airport_midway_climate.csv", sep=",", header=TRUE)
mdwy$date <- as.character(mdwy$date)
mdwy$date <- as.Date(mdwy$date, "%Y%m%d")

chst <- read.table(file="airport_charleston_climate.csv", sep=",", header=TRUE)
chst$date <- as.character(chst$date)
chst$date <- as.Date(chst$date, "%Y%m%d")

arpt <- list(indy, lvlle, moln, mdwy, chst)
arpt.index <- c("indy", "lvlle", "moln", "mdwy", "chst")
arpt.usnip <- c("in22", "in22", "il78", "wi99", "oh49")
arpt.name <- c("Indianapolis", "Louisville", "Moline", "Midway", "Charleston")

#Loading Chicago GNIP Data
chi.gnip.raw.all <- read.table("gnip_chicago.csv", header=TRUE, sep=",")
chi.gnip.raw <- na.omit(chi.gnip.raw.all)
chi.gnip.lmdata <- lm(chi.gnip.raw$d18O ~ chi.gnip.raw$tavg)
chi.gnip.raw$isotemp.residual <- round(chi.gnip.raw$d18O -
        (chi.gnip.lmdata$coef[2]*chi.gnip.raw$tavg + chi.gnip.lmdata$coef[1]), 2)
```

```
mo.index <- c("01", "02", "03", "04", "05", "06", "07", "08", "09", "10", "11", "12")

#Loading USNIP weekly data for sites to perform bootstrapping and extract the fullest years
chosen.usnip.wk.index <- c("il78", "in22", "ky03", "oh49", "wi99")
chosen.usnip.wk.data <-list()
for (k in 1:length(chosen.usnip.wk.index)) {
	site.iter.data <- totalsites.data[[chosen.usnip.wk.index[k]]]
	names(site.iter.data)[names(site.iter.data) == "usnip.prcp"] <- "prcp"
	osc.usnip.wk.match.siteiter <- data.frame(matrix(ncol=length(osc.index), nrow=length(site.iter.data$yr)))
	for (j in 1:length(osc.index)){
		yr.match <- osc[[j]][match(site.iter.data$yr, osc[[j]]$year), ] #extracting the year of oscillation data
		for (m in 1:length(yr.match$year)) {
			osc.usnip.wk.match.siteiter[m,j] <- yr.match[m,(match(site.iter.data$mo, mo.index)+1)[m]] #picking the right month out
of the selected year
			}
		}
	colnames(osc.usnip.wk.match.siteiter) <- osc.index
	chosen.usnip.wk.data[[k]] <- data.frame(site.iter.data, osc.usnip.wk.match.siteiter)
	chosen.usnip.wk.data[[k]]$mo <- match(chosen.usnip.wk.data[[k]]$mo, mo.index)
	chosen.usnip.wk.lmdata <- lm(chosen.usnip.wk.data[[k]]$d18O ~ chosen.usnip.wk.data[[k]]$tavg)
	chosen.usnip.wk.data[[k]]$isotemp.residual <- round(chosen.usnip.wk.data[[k]]$d18O -
		(chosen.usnip.wk.lmdata$coef[2]*chosen.usnip.wk.data[[k]]$tavg + chosen.usnip.wk.lmdata$coef[1]), 2)
	}
names(chosen.usnip.wk.data) <- chosen.usnip.wk.index

#Loading USNIP monthly data for sites to perform bootstrapping and extract the fullest years
chosen.usnip.mo.index <- c("il78", "in22", "ky03", "oh49", "wi99")
chosen.usnip.mo.data <-list()
for (k in 1:length(chosen.usnip.mo.index)) {
	site.iter.data <- total.mo.indv.wt[[chosen.usnip.mo.index[k]]]
	site.iter.data$prcp <- total.mo.usnip.prcp.sum[[chosen.usnip.mo.index[k]]]$prcp.sum
	osc.usnip.mo.match.siteiter <- data.frame(matrix(ncol=length(osc.index), nrow=length(site.iter.data$yr)))
	for (j in 1:length(osc.index)){
```

```
                yr.match <- osc[[j]][match(site.iter.data$yr, osc[[j]]$year), ] #extracting the year of oscillation data
                for (m in 1:length(yr.match$year)) {
                        osc.usnip.mo.match.siteiter[m,j] <- yr.match[m,(match(site.iter.data$mo, mo.index)+1)[m]] #picking the right month out
of the selected year
                        }
                }
        colnames(osc.usnip.mo.match.siteiter) <- osc.index
        chosen.usnip.mo.data[[k]] <- data.frame(site.iter.data, osc.usnip.mo.match.siteiter)
        chosen.usnip.mo.data[[k]]$mo <- match(chosen.usnip.mo.data[[k]]$mo, mo.index)
        chosen.usnip.mo.lmdata <- lm(chosen.usnip.mo.data[[k]]$d18O ~ chosen.usnip.mo.data[[k]]$tavg)
        chosen.usnip.mo.data[[k]]$isotemp.residual <- round(chosen.usnip.mo.data[[k]]$d18O -
                (chosen.usnip.mo.lmdata$coef[2]*chosen.usnip.mo.data[[k]]$tavg + chosen.usnip.mo.lmdata$coef[1]), 2)
        }
names(chosen.usnip.mo.data) <- chosen.usnip.mo.index


#Counting how many samples per month in database
btsp.count <- list()
for (k in 1:length(chosen.usnip.mo.index)) {
        btsp.count[[k]] <- count(chosen.usnip.mo.data[[k]], 'mo')
        }
names(btsp.count) <- chosen.usnip.mo.index
btsp.count$chi.gnip <- count(chi.gnip.raw, 'mo')
#write.table(btsp.count, "btsp_data_mo_count.csv", sep=",", row.names=TRUE, col.names=NA)


#-------------------------------------------------------------------------------------
#-------------Actual year correlations-----------------------------------------------

#Chicago GNIP
chi.gnip <- list()
yr.index <- seq(1962,1979)
for (i in 1:(length(yr.index)-1)) { #Making years with December of previous year
        yearly.tmp <- chi.gnip.raw[chi.gnip.raw$yr == yr.index[i+1], ]
```

```
        yearly.tmp <- yearly.tmp[yearly.tmp$mo < 12, ]
        year.prior <- chi.gnip.raw[chi.gnip.raw$yr == yr.index[i], ]
        dec.prior <- year.prior[year.prior$mo == 12, ]
        chi.gnip[[i]] <- rbind(dec.prior, yearly.tmp)
        }

chi.gnip.yr <- data.frame(matrix(nrow=(length(yr.index)-1), ncol=14))

for (i in 1:(length(yr.index)-1)) {
        if(length(chi.gnip[[i]]$yr) == 12) {
                prcp.yr <- sum(chi.gnip[[i]]$prcp)
                win.data <- chi.gnip[[i]][(chi.gnip[[i]]$mo == 1 | chi.gnip[[i]]$mo == 2 | chi.gnip[[i]]$mo == 12), ]
                spr.data <- chi.gnip[[i]][(chi.gnip[[i]]$mo == 3 | chi.gnip[[i]]$mo == 4 | chi.gnip[[i]]$mo == 5), ]
                sum.data <- chi.gnip[[i]][(chi.gnip[[i]]$mo == 6 | chi.gnip[[i]]$mo == 7 | chi.gnip[[i]]$mo == 8), ]
                aut.data <- chi.gnip[[i]][(chi.gnip[[i]]$mo == 9 | chi.gnip[[i]]$mo == 10 | chi.gnip[[i]]$mo == 11), ]
                win.frac <- sum(win.data$prcp)/prcp.yr
                spr.frac <- sum(spr.data$prcp)/prcp.yr
                sum.frac <- sum(sum.data$prcp)/prcp.yr
                aut.frac <- sum(aut.data$prcp)/prcp.yr

                chi.gnip.yr[i,1] <- sum(chi.gnip[[i]]$d18O*(chi.gnip[[i]]$prcp/prcp.yr))
                chi.gnip.yr[i,2] <- prcp.yr
                chi.gnip.yr[i,3] <- sum(chi.gnip[[i]]$tavg*(chi.gnip[[i]]$prcp/prcp.yr))
                chi.gnip.yr[i,4] <- mean(chi.gnip[[i]]$pdo)
                chi.gnip.yr[i,5] <- mean(chi.gnip[[i]]$mei)
                chi.gnip.yr[i,6] <- mean(chi.gnip[[i]]$nao)
                chi.gnip.yr[i,7] <- mean(chi.gnip[[i]]$amo)
                chi.gnip.yr[i,8] <- mean(chi.gnip[[i]]$pna)
                chi.gnip.yr[i,9] <- mean(chi.gnip[[i]]$bhi)
                chi.gnip.yr[i,10] <- sum(chi.gnip[[i]]$isotemp.residual*(chi.gnip[[i]]$prcp/prcp.yr))
                chi.gnip.yr[i,11] <- win.frac
                chi.gnip.yr[i,12] <- spr.frac
                chi.gnip.yr[i,13] <- sum.frac
                chi.gnip.yr[i,14] <- aut.frac
```

```
		}
	else {
		chi.gnip.yr[i, ] <- NA
		}
	}
colnames(chi.gnip.yr) <- c("d18O", "prcp", "tavg", "pdo", "mei", "nao", "amo", "pna", "bhi",
	"isotemp.residual", "win.frac", "spr.frac", "sum.frac", "aut.frac")
chi.gnip.yr$yr <- yr.index[-1]

#Removing years without 12 months of data
chi.yr.na <- na.omit(chi.gnip.yr)

chi.yearly.d18O <-
	(chi.yr.na$win.frac * season.lmcor[["wi99"]]["win","d18O.wt"] +
	chi.yr.na$spr.frac * season.lmcor[["wi99"]]["spr","d18O.wt"] +
	chi.yr.na$sum.frac * season.lmcor[["wi99"]]["sum","d18O.wt"] +
	chi.yr.na$aut.frac * season.lmcor[["wi99"]]["aut","d18O.wt"])

chi.seasonal.fraction <- seasonal.fraction(chi.yearly.d18O, "wi99") #Load seasonal fraction function
median(chi.seasonal.fraction$summer.fraction)
max(chi.seasonal.fraction$summer.fraction)
min(chi.seasonal.fraction$summer.fraction)
chi.ssa <- chi.seasonal.fraction$summer.fraction - mean(chi.seasonal.fraction$summer.fraction)

#Subsetting the oscillation database to only have years matching Chicago GNIP full years
osc.yr.chi <- list()
for (i in 1:length(osc.index)) {
	osc.yr.chi[[i]] <- osc[[i]][(osc[[i]]$year %in% chi.yr.na$yr), ]
}
names(osc.yr.chi) <- osc.index

#Making a list of a list of seasonal oscillation correlations with Chicago d18O
osc.iter <- list()
chi.osc.cor.table <- data.frame(matrix(nrow=0, ncol=2))
```

```
for (j in 1:length(osc.index)) {
	osc.iter[[1]] <- cor.test(chi.yr.na$d18O, osc.yr.chi[[j]]$year.mean)
	osc.iter[[2]] <- cor.test(chi.yr.na$d18O, osc.yr.chi[[j]]$win.mean)
	osc.iter[[3]] <- cor.test(chi.yr.na$d18O, osc.yr.chi[[j]]$spr.mean)
	osc.iter[[4]] <- cor.test(chi.yr.na$d18O, osc.yr.chi[[j]]$sum.mean)
	osc.iter[[5]] <- cor.test(chi.yr.na$d18O, osc.yr.chi[[j]]$aut.mean)

	osc.cor.table.iter <- data.frame(matrix(nrow=5, ncol=2))
	for (i in 1:5) { # Looping to construct a table of correlations
		osc.cor.table.iter[i,1] <- round(osc.iter[[i]]$estimate, 3)
		osc.cor.table.iter[i,2] <- round(osc.iter[[i]]$p.value, 3)
		}
	colnames(osc.cor.table.iter) <- c("r", "pval")
	rownames(osc.cor.table.iter) <- c(paste(osc.index[j], ".yr", sep=""), paste(osc.index[j], ".win", sep=""),
		paste(osc.index[j], ".spr", sep=""), paste(osc.index[j], ".sum", sep=""),
		paste(osc.index[j], ".aut", sep=""))

	chi.osc.cor.table <- rbind(chi.osc.cor.table, osc.cor.table.iter)
	}
#write.table(chi.osc.cor.table, "chi_gnip_osc_cor_fullyear.csv", sep=",", row.names=TRUE, col.names=NA)


#Calculating correlations with tavg and ssa
d18O.cor <- list()
d18O.cor[[1]] <- cor.test(chi.yr.na$d18O, chi.yr.na$tavg)
d18O.cor[[2]] <- cor.test(chi.yr.na$d18O, chi.ssa)

chi.wx.cor.table <- data.frame(matrix(nrow=2, ncol=2))
	for (i in 1:2) {
		chi.wx.cor.table[i,1] <- round(d18O.cor[[i]]$estimate, 3)
		chi.wx.cor.table[i,2] <- round(d18O.cor[[i]]$p.value, 3)
		}
colnames(chi.wx.cor.table) <- c("r", "pval")
rownames(chi.wx.cor.table) <- c("tavg", "ssa")
```

```
#Combining oscillation index and weather correlations into single table, sorting by r value
chi.cor.table.realyr <- rbind(chi.wx.cor.table, chi.osc.cor.table)
chi.cor.table.realyr <- chi.cor.table.realyr[order(-abs(chi.cor.table.realyr$r)),]



#-------------------------------------------------------------------------------------------
#-------------------------------------12 Mo Running Average---------------------------------
chi.gnip.raw.all$isotemp.residual <- round(chi.gnip.raw.all$d18O -
        (chi.gnip.lmdata$coef[2]*chi.gnip.raw.all$tavg + chi.gnip.lmdata$coef[1]), 2)
chi.gnip.12mo <- list()
for (i in 1:(length(chi.gnip.raw.all$pna)-12)) {
        chi.gnip.12mo[[i]] <- chi.gnip.raw.all[i:(i+11), ]
        chi.gnip.12mo[[i]] <- na.omit(chi.gnip.12mo[[i]])
        }

chi.gnip.12mo.yr <- data.frame(matrix(nrow=length(yr.index), ncol=14))
osc.yr.chi.12mo <- list()
osc.yr.chi.12mo[[1]] <- data.frame(matrix(nrow=length(chi.gnip.12mo), ncol=5))
osc.yr.chi.12mo[[2]] <- data.frame(matrix(nrow=length(chi.gnip.12mo), ncol=5))
osc.yr.chi.12mo[[3]] <- data.frame(matrix(nrow=length(chi.gnip.12mo), ncol=5))
osc.yr.chi.12mo[[4]] <- data.frame(matrix(nrow=length(chi.gnip.12mo), ncol=5))
osc.yr.chi.12mo[[5]] <- data.frame(matrix(nrow=length(chi.gnip.12mo), ncol=5))
osc.yr.chi.12mo[[6]] <- data.frame(matrix(nrow=length(chi.gnip.12mo), ncol=5))
colnames(osc.yr.chi.12mo[[1]]) <- c("year.mean", "spr.mean", "sum.mean", "aut.mean", "win.mean")
colnames(osc.yr.chi.12mo[[2]]) <- c("year.mean", "spr.mean", "sum.mean", "aut.mean", "win.mean")
colnames(osc.yr.chi.12mo[[3]]) <- c("year.mean", "spr.mean", "sum.mean", "aut.mean", "win.mean")
colnames(osc.yr.chi.12mo[[4]]) <- c("year.mean", "spr.mean", "sum.mean", "aut.mean", "win.mean")
colnames(osc.yr.chi.12mo[[5]]) <- c("year.mean", "spr.mean", "sum.mean", "aut.mean", "win.mean")
colnames(osc.yr.chi.12mo[[6]]) <- c("year.mean", "spr.mean", "sum.mean", "aut.mean", "win.mean")


for (i in 1:length(chi.gnip.12mo)) {
```

```
if(length(chi.gnip.12mo[[i]]$yr) == 12) {
        prcp.yr <- sum(chi.gnip.12mo[[i]]$prcp)
        win.data <- chi.gnip.12mo[[i]][(chi.gnip.12mo[[i]]$mo == 1 | chi.gnip.12mo[[i]]$mo == 2 | chi.gnip.12mo[[i]]$mo == 12), ]
        spr.data <- chi.gnip.12mo[[i]][(chi.gnip.12mo[[i]]$mo == 3 | chi.gnip.12mo[[i]]$mo == 4 | chi.gnip.12mo[[i]]$mo == 5), ]
        sum.data <- chi.gnip.12mo[[i]][(chi.gnip.12mo[[i]]$mo == 6 | chi.gnip.12mo[[i]]$mo == 7 | chi.gnip.12mo[[i]]$mo == 8), ]
        aut.data <- chi.gnip.12mo[[i]][(chi.gnip.12mo[[i]]$mo == 9 | chi.gnip.12mo[[i]]$mo == 10 | chi.gnip.12mo[[i]]$mo == 11), ]
        win.frac <- sum(win.data$prcp)/prcp.yr
        spr.frac <- sum(spr.data$prcp)/prcp.yr
        sum.frac <- sum(sum.data$prcp)/prcp.yr
        aut.frac <- sum(aut.data$prcp)/prcp.yr

        osc.yr.chi.12mo[[1]][i,c(1:5)] <- c(mean(chi.gnip.12mo[[i]]$pdo), mean(spr.data$pdo),
                mean(sum.data$pdo), mean(aut.data$pdo), mean(win.data$pdo))
        osc.yr.chi.12mo[[2]][i,c(1:5)] <- c(mean(chi.gnip.12mo[[i]]$mei), mean(spr.data$mei),
                mean(sum.data$mei), mean(aut.data$mei), mean(win.data$mei))
        osc.yr.chi.12mo[[3]][i,c(1:5)] <- c(mean(chi.gnip.12mo[[i]]$nao), mean(spr.data$nao),
                mean(sum.data$nao), mean(aut.data$nao), mean(win.data$nao))
        osc.yr.chi.12mo[[4]][i,c(1:5)] <- c(mean(chi.gnip.12mo[[i]]$amo), mean(spr.data$amo),
                mean(sum.data$amo), mean(aut.data$amo), mean(win.data$amo))
        osc.yr.chi.12mo[[5]][i,c(1:5)] <- c(mean(chi.gnip.12mo[[i]]$pna), mean(spr.data$pna),
                mean(sum.data$pna), mean(aut.data$pna), mean(win.data$pna))
        osc.yr.chi.12mo[[6]][i,c(1:5)] <- c(mean(chi.gnip.12mo[[i]]$bhi), mean(spr.data$bhi),
                mean(sum.data$bhi), mean(aut.data$bhi), mean(win.data$bhi))

        chi.gnip.12mo.yr[i,1] <- sum(chi.gnip.12mo[[i]]$prcp/prcp.yr * chi.gnip.12mo[[i]]$d18O)
        chi.gnip.12mo.yr[i,2] <- prcp.yr
        chi.gnip.12mo.yr[i,3] <- sum(chi.gnip.12mo[[i]]$prcp/prcp.yr * chi.gnip.12mo[[i]]$tavg)
        chi.gnip.12mo.yr[i,4] <- sum(chi.gnip.12mo[[i]]$prcp/prcp.yr * chi.gnip.12mo[[i]]$pdo)
        chi.gnip.12mo.yr[i,5] <- sum(chi.gnip.12mo[[i]]$prcp/prcp.yr * chi.gnip.12mo[[i]]$mei)
        chi.gnip.12mo.yr[i,6] <- sum(chi.gnip.12mo[[i]]$prcp/prcp.yr * chi.gnip.12mo[[i]]$nao)
        chi.gnip.12mo.yr[i,7] <- sum(chi.gnip.12mo[[i]]$prcp/prcp.yr * chi.gnip.12mo[[i]]$amo)
        chi.gnip.12mo.yr[i,8] <- sum(chi.gnip.12mo[[i]]$prcp/prcp.yr * chi.gnip.12mo[[i]]$pna)
        chi.gnip.12mo.yr[i,9] <- sum(chi.gnip.12mo[[i]]$prcp/prcp.yr * chi.gnip.12mo[[i]]$bhi)
        chi.gnip.12mo.yr[i,10] <- sum(chi.gnip.12mo[[i]]$prcp/prcp.yr * chi.gnip.12mo[[i]]$isotemp.residual)
```

```
                chi.gnip.12mo.yr[i,11] <- win.frac
                chi.gnip.12mo.yr[i,12] <- spr.frac
                chi.gnip.12mo.yr[i,13] <- sum.frac
                chi.gnip.12mo.yr[i,14] <- aut.frac
                }
        else {
                chi.gnip.12mo.yr[i, ] <- NA
                }
        }
colnames(chi.gnip.12mo.yr) <- c("d18O", "prcp", "tavg", "pdo", "mei", "nao", "amo", "pna", "bhi",
        "isotemp.residual", "win.frac", "spr.frac", "sum.frac", "aut.frac")
names(osc.yr.chi.12mo) <- osc.index

#Removing running 12 months lacking data
chi.12mo.yr.na <- na.omit(chi.gnip.12mo.yr)

osc.yr.chi.12mo.na <- list()
for (i in 1:6) {
        osc.yr.chi.12mo.na[[i]] <- na.omit(osc.yr.chi.12mo[[i]])
        }

chi.12mo.d18O <-
        (chi.12mo.yr.na$win.frac * season.lmcor[["wi99"]]["win","d18O.wt"] +
        chi.12mo.yr.na$spr.frac * season.lmcor[["wi99"]]["spr","d18O.wt"] +
        chi.12mo.yr.na$sum.frac * season.lmcor[["wi99"]]["sum","d18O.wt"] +
        chi.12mo.yr.na$aut.frac * season.lmcor[["wi99"]]["aut","d18O.wt"])

chi.12mo.seasonal.fraction <- seasonal.fraction(chi.12mo.d18O, "wi99") #Load seasonal fraction function
median(chi.12mo.seasonal.fraction$summer.fraction)
max(chi.12mo.seasonal.fraction$summer.fraction)
min(chi.12mo.seasonal.fraction$summer.fraction)
chi.12mo.ssa <- chi.12mo.seasonal.fraction$summer.fraction -
        mean(chi.12mo.seasonal.fraction$summer.fraction)
```

```
#Making a list of a list of seasonal oscillation correlations with Chicago d18O
osc.12mo.iter <- list()
chi.osc.cor.table.12mo <- data.frame(matrix(nrow=0, ncol=2))
for (j in 1:length(osc.index)) {
	osc.12mo.iter[[1]] <- cor.test(chi.12mo.yr.na$d18O, osc.yr.chi.12mo.na[[j]]$year.mean)
	osc.12mo.iter[[2]] <- cor.test(chi.12mo.yr.na$d18O, osc.yr.chi.12mo.na[[j]]$win.mean)
	osc.12mo.iter[[3]] <- cor.test(chi.12mo.yr.na$d18O, osc.yr.chi.12mo.na[[j]]$spr.mean)
	osc.12mo.iter[[4]] <- cor.test(chi.12mo.yr.na$d18O, osc.yr.chi.12mo.na[[j]]$sum.mean)
	osc.12mo.iter[[5]] <- cor.test(chi.12mo.yr.na$d18O, osc.yr.chi.12mo.na[[j]]$aut.mean)

	osc.cor.table.12mo.iter <- data.frame(matrix(nrow=5, ncol=2))
	for (i in 1:5) { # Looping to construct a table of correlations
		osc.cor.table.12mo.iter[i,1] <- round(osc.12mo.iter[[i]]$estimate, 3)
		osc.cor.table.12mo.iter[i,2] <- round(osc.12mo.iter[[i]]$p.value, 3)
		}
	colnames(osc.cor.table.12mo.iter) <- c("r", "pval")
	rownames(osc.cor.table.12mo.iter) <- c(paste(osc.index[j], ".yr", sep=""), paste(osc.index[j], ".win", sep=""),
		paste(osc.index[j], ".spr", sep=""), paste(osc.index[j], ".sum", sep=""),
		paste(osc.index[j], ".aut", sep=""))

	chi.osc.cor.table.12mo <- rbind(chi.osc.cor.table.12mo, osc.cor.table.12mo.iter)
	}
#write.table(chi.osc.cor.table.12mo, "chi_gnip_osc_cor_12mo.csv", sep=",", row.names=TRUE, col.names=NA)


#Calculating correlations with tavg and ssa
d18O.cor.12mo <- list()
d18O.cor.12mo[[1]] <- cor.test(chi.12mo.yr.na$d18O, chi.12mo.yr.na$tavg)
d18O.cor.12mo[[2]] <- cor.test(chi.12mo.yr.na$d18O, chi.12mo.ssa)

chi.wx.cor.table.12mo <- data.frame(matrix(nrow=2, ncol=2))
	for (i in 1:2) {
		chi.wx.cor.table.12mo[i,1] <- round(d18O.cor.12mo[[i]]$estimate, 3)
```

```
                chi.wx.cor.table.12mo[i,2] <- round(d18O.cor.12mo[[i]]$p.value, 3)
                }
colnames(chi.wx.cor.table.12mo) <- c("r", "pval")
rownames(chi.wx.cor.table.12mo) <- c("tavg", "ssa")

#Combining oscillation index and weather correlations into single table, sorting by r value
chi.cor.table.12mo <- rbind(chi.wx.cor.table.12mo, chi.osc.cor.table.12mo)
chi.cor.table.12mo.nosort <- chi.cor.table.12mo
chi.cor.table.12mo <- chi.cor.table.12mo[order(-abs(chi.cor.table.12mo$r)),]

chi.cor.table.12mo

#This data makes fake yearly data by bootstrapping GNIP and USNIP data. This set picks one of each month
#Running 30 iterations to check for variance in bootstrapping (make sure to run 12 mo first!)
interannual.cor <- list()
for (m in 1:30) {
        #-------------------------------------------------------------------------------------------
        #----------------------------------------Bootstrapping--------------------------------------
        #Chicago GNIP
        chi.gnip.btsp <- data.frame(matrix(nrow=1000, ncol=14))
        chi.gnip.btsp.ssn.osc <- list()
        fake.yr <- data.frame(matrix(nrow=12, ncol=12))
        for (i in 1:1000) {
                jan.iter <- chi.gnip.raw[chi.gnip.raw$mo == 1, ]
                fake.yr[1, ] <- jan.iter[sample(nrow(jan.iter), 1, replace=TRUE), ]
                feb.iter <- chi.gnip.raw[chi.gnip.raw$mo == 2, ]
                fake.yr[2, ] <- feb.iter[sample(nrow(feb.iter), 1, replace=TRUE), ]
                mar.iter <- chi.gnip.raw[chi.gnip.raw$mo == 3, ]
                fake.yr[3, ] <- mar.iter[sample(nrow(mar.iter), 1, replace=TRUE), ]
                apr.iter <- chi.gnip.raw[chi.gnip.raw$mo == 4, ]
                fake.yr[4, ] <- apr.iter[sample(nrow(apr.iter), 1, replace=TRUE), ]
                may.iter <- chi.gnip.raw[chi.gnip.raw$mo == 5, ]
                fake.yr[5, ] <- may.iter[sample(nrow(may.iter), 1, replace=TRUE), ]
                jun.iter <- chi.gnip.raw[chi.gnip.raw$mo == 6, ]
```

```
fake.yr[6, ] <- jun.iter[sample(nrow(jun.iter), 1, replace=TRUE), ]
jul.iter <- chi.gnip.raw[chi.gnip.raw$mo == 7, ]
fake.yr[7, ] <- jul.iter[sample(nrow(jul.iter), 1, replace=TRUE), ]
aug.iter <- chi.gnip.raw[chi.gnip.raw$mo == 8, ]
fake.yr[8, ] <- aug.iter[sample(nrow(aug.iter), 1, replace=TRUE), ]
sep.iter <- chi.gnip.raw[chi.gnip.raw$mo == 9, ]
fake.yr[9, ] <- sep.iter[sample(nrow(sep.iter), 1, replace=TRUE), ]
oct.iter <- chi.gnip.raw[chi.gnip.raw$mo == 10, ]
fake.yr[10, ] <- oct.iter[sample(nrow(oct.iter), 1, replace=TRUE), ]
nov.iter <- chi.gnip.raw[chi.gnip.raw$mo == 11, ]
fake.yr[11, ] <- nov.iter[sample(nrow(nov.iter), 1, replace=TRUE), ]
dec.iter <- chi.gnip.raw[chi.gnip.raw$mo == 12, ]
fake.yr[12, ] <- dec.iter[sample(nrow(dec.iter), 1, replace=TRUE), ]
colnames(fake.yr) <- colnames(jan.iter)
win.data <- fake.yr[(fake.yr$mo == 1 | fake.yr$mo == 2 | fake.yr$mo == 12), ]
spr.data <- fake.yr[(fake.yr$mo == 3 | fake.yr$mo == 4 | fake.yr$mo == 5), ]
sum.data <- fake.yr[(fake.yr$mo == 6 | fake.yr$mo == 7 | fake.yr$mo == 8), ]
aut.data <- fake.yr[(fake.yr$mo == 9 | fake.yr$mo == 10 | fake.yr$mo == 11), ]
win.frac <- sum(win.data$prcp)/sum(fake.yr$prcp)
spr.frac <- sum(spr.data$prcp)/sum(fake.yr$prcp)
sum.frac <- sum(sum.data$prcp)/sum(fake.yr$prcp)
aut.frac <- sum(aut.data$prcp)/sum(fake.yr$prcp)

chi.gnip.btsp[i,1] <- sum(fake.yr$prcp/sum(fake.yr$prcp) * fake.yr$d18O)
chi.gnip.btsp[i,2] <- sum(fake.yr$prcp)
chi.gnip.btsp[i,3] <- sum(fake.yr$prcp/sum(fake.yr$prcp) * fake.yr$tavg)
chi.gnip.btsp[i,4] <- sum(fake.yr$prcp/sum(fake.yr$prcp) * fake.yr$pdo)
chi.gnip.btsp[i,5] <- sum(fake.yr$prcp/sum(fake.yr$prcp) * fake.yr$mei)
chi.gnip.btsp[i,6] <- sum(fake.yr$prcp/sum(fake.yr$prcp) * fake.yr$nao)
chi.gnip.btsp[i,7] <- sum(fake.yr$prcp/sum(fake.yr$prcp) * fake.yr$amo)
chi.gnip.btsp[i,8] <- sum(fake.yr$prcp/sum(fake.yr$prcp) * fake.yr$pna)
chi.gnip.btsp[i,9] <- sum(fake.yr$prcp/sum(fake.yr$prcp) * fake.yr$bhi)
chi.gnip.btsp[i,10] <- sum(fake.yr$prcp/sum(fake.yr$prcp) * fake.yr$isotemp.residual)
chi.gnip.btsp[i,11] <- win.frac
```

```
chi.gnip.btsp[i,12] <- spr.frac
chi.gnip.btsp[i,13] <- sum.frac
chi.gnip.btsp[i,14] <- aut.frac

#Calculating seasonal oscillation weighted means
win.fake.iter <- fake.yr[fake.yr$mo == 12 | fake.yr$mo == 1 | fake.yr$mo == 2, ]
spr.fake.iter <- fake.yr[fake.yr$mo == 3 | fake.yr$mo == 4 | fake.yr$mo == 5, ]
sum.fake.iter <- fake.yr[fake.yr$mo == 6 | fake.yr$mo == 7 | fake.yr$mo == 8, ]
aut.fake.iter <- fake.yr[fake.yr$mo == 9 | fake.yr$mo == 10 | fake.yr$mo == 11, ]
fake.yr.ssn.osc <- data.frame(matrix(nrow=5, ncol=length(osc.index)))

for (j in 1:length(osc.index)) {
        fake.yr.ssn.osc[1,j] <- sum(fake.yr[osc.index[j]] * fake.yr$prcp / sum(fake.yr$prcp))
        if(length(win.fake.iter$yr) > 0) {
                fake.yr.ssn.osc[2,j] <- sum(win.fake.iter$prcp/sum(win.fake.iter$prcp) * win.fake.iter[osc.index[j]])
                } else {
                fake.yr.ssn.osc[2,j] <- NA
                }
        if(length(spr.fake.iter$yr) > 0) {
                fake.yr.ssn.osc[3,j] <- sum(spr.fake.iter$prcp/sum(spr.fake.iter$prcp) * spr.fake.iter[osc.index[j]])
                } else {
                fake.yr.ssn.osc[3,j] <- NA
                }
        if(length(sum.fake.iter$yr) > 0) {
                fake.yr.ssn.osc[4,j] <- sum(sum.fake.iter$prcp/sum(sum.fake.iter$prcp) * sum.fake.iter[osc.index[j]])
                } else {
                fake.yr.ssn.osc[4,j] <- NA
                }
        if(length(aut.fake.iter$yr) > 0) {
                fake.yr.ssn.osc[5,j] <- sum(aut.fake.iter$prcp/sum(aut.fake.iter$prcp) * aut.fake.iter[osc.index[j]])
                } else {
                fake.yr.ssn.osc[5,j] <- NA
                }
        }
```

```
        colnames(fake.yr.ssn.osc) <- osc.index
        rownames(fake.yr.ssn.osc) <- c("year", season.index)

        chi.gnip.btsp.ssn.osc[[i]] <- fake.yr.ssn.osc
        }

colnames(chi.gnip.btsp) <- c("d18O", "prcp", "tavg", "pdo", "mei", "nao", "amo", "pna", "bhi",
        "isotemp.residual", "win.frac", "spr.frac", "sum.frac", "aut.frac")


chi.gnip.btsp.sumsig <- seasonal.fraction(
        (chi.gnip.btsp$win.frac * season.lmcor[["wi99"]]["win","d18O.wt"] +
        chi.gnip.btsp$spr.frac * season.lmcor[["wi99"]]["spr","d18O.wt"] +
        chi.gnip.btsp$sum.frac * season.lmcor[["wi99"]]["sum","d18O.wt"] +
        chi.gnip.btsp$aut.frac * season.lmcor[["wi99"]]["aut","d18O.wt"]), "wi99")$summer.fraction

chi.gnip.btsp.ssa <- chi.gnip.btsp.sumsig - mean(chi.gnip.btsp.sumsig)


#Calculating correlations for bootstrapped d18O and other variables
osc.iter <- list()
chi.btsp.osc.cor.table <- data.frame(matrix(nrow=0, ncol=2))
for (j in 1:length(osc.index)) {
        osc.iter[[1]] <- cor.test(chi.gnip.btsp$d18O, sapply(chi.gnip.btsp.ssn.osc, "[[", osc.index[j])[1,])
        osc.iter[[2]] <- cor.test(chi.gnip.btsp$d18O, sapply(chi.gnip.btsp.ssn.osc, "[[", osc.index[j])[2,])
        osc.iter[[3]] <- cor.test(chi.gnip.btsp$d18O, sapply(chi.gnip.btsp.ssn.osc, "[[", osc.index[j])[3,])
        osc.iter[[4]] <- cor.test(chi.gnip.btsp$d18O, sapply(chi.gnip.btsp.ssn.osc, "[[", osc.index[j])[4,])
        osc.iter[[5]] <- cor.test(chi.gnip.btsp$d18O, sapply(chi.gnip.btsp.ssn.osc, "[[", osc.index[j])[5,])

        osc.cor.table.iter <- data.frame(matrix(nrow=5, ncol=2))
        for (i in 1:5) { # Looping to construct a table of correlations
                osc.cor.table.iter[i,1] <- round(osc.iter[[i]]$estimate, 3)
                osc.cor.table.iter[i,2] <- round(osc.iter[[i]]$p.value, 3)
                }
```

```
        colnames(osc.cor.table.iter) <- c("r", "pval")
        rownames(osc.cor.table.iter) <- c(paste(osc.index[j], ".yr", sep=""), paste(osc.index[j], ".win", sep=""),
                paste(osc.index[j], ".spr", sep=""), paste(osc.index[j], ".sum", sep=""),
                paste(osc.index[j], ".aut", sep=""))

        chi.btsp.osc.cor.table <- rbind(chi.btsp.osc.cor.table, osc.cor.table.iter)
        }

#Calculating correlations with tavg and ssa
d18O.btsp.cor <- list()
d18O.btsp.cor[[1]] <- cor.test(chi.gnip.btsp$d18O, chi.gnip.btsp$tavg)
d18O.btsp.cor[[2]] <- cor.test(chi.gnip.btsp$d18O, chi.gnip.btsp.ssa)

chi.btsp.wx.cor.table <- data.frame(matrix(nrow=2, ncol=2))
        for (i in 1:2) {
                chi.btsp.wx.cor.table[i,1] <- round(d18O.btsp.cor[[i]]$estimate, 3)
                chi.btsp.wx.cor.table[i,2] <- round(d18O.btsp.cor[[i]]$p.value, 3)
                }
colnames(chi.btsp.wx.cor.table) <- c("r", "pval")
rownames(chi.btsp.wx.cor.table) <- c("tavg", "ssa")

#Combining oscillation index and weather correlations into single table, sorting by r value
chi.cor.table.btsp <- rbind(chi.btsp.wx.cor.table, chi.btsp.osc.cor.table)
chi.cor.table.btsp.nosort <- chi.cor.table.btsp
chi.cor.table.btsp <- chi.cor.table.btsp[order(-abs(chi.cor.table.btsp$r)),]

chi.cor.table.btsp

#--------------------------------------
#Monthly chosen USNIP data bootstrapping BUT PICKING ONE FROM EACH MONTH
usnip.cor.table.btsp.mo.nosort <- list()
usnip.cor.table.btsp.mo <- list()
for (k in 1:length(chosen.usnip.mo.index)) {
        usnip.btsp.siteiter <- data.frame(matrix(nrow=1000, ncol=14))
```

```
usnip.btsp.siteiter.ssn.osc <- list()
fake.yr <- data.frame(matrix(nrow=12, ncol=18))
for (i in 1:1000) {
        jan.iter <- chosen.usnip.mo.data[[k]][chosen.usnip.mo.data[[k]]$mo == 1, ]
        fake.yr[1, ] <- jan.iter[sample(nrow(jan.iter), 1, replace=TRUE), ]
        feb.iter <- chosen.usnip.mo.data[[k]][chosen.usnip.mo.data[[k]]$mo == 2, ]
        fake.yr[2, ] <- feb.iter[sample(nrow(feb.iter), 1, replace=TRUE), ]
        mar.iter <- chosen.usnip.mo.data[[k]][chosen.usnip.mo.data[[k]]$mo == 3, ]
        fake.yr[3, ] <- mar.iter[sample(nrow(mar.iter), 1, replace=TRUE), ]
        apr.iter <- chosen.usnip.mo.data[[k]][chosen.usnip.mo.data[[k]]$mo == 4, ]
        fake.yr[4, ] <- apr.iter[sample(nrow(apr.iter), 1, replace=TRUE), ]
        may.iter <- chosen.usnip.mo.data[[k]][chosen.usnip.mo.data[[k]]$mo == 5, ]
        fake.yr[5, ] <- may.iter[sample(nrow(may.iter), 1, replace=TRUE), ]
        jun.iter <- chosen.usnip.mo.data[[k]][chosen.usnip.mo.data[[k]]$mo == 6, ]
        fake.yr[6, ] <- jun.iter[sample(nrow(jun.iter), 1, replace=TRUE), ]
        jul.iter <- chosen.usnip.mo.data[[k]][chosen.usnip.mo.data[[k]]$mo == 7, ]
        fake.yr[7, ] <- jul.iter[sample(nrow(jul.iter), 1, replace=TRUE), ]
        aug.iter <- chosen.usnip.mo.data[[k]][chosen.usnip.mo.data[[k]]$mo == 8, ]
        fake.yr[8, ] <- aug.iter[sample(nrow(aug.iter), 1, replace=TRUE), ]
        sep.iter <- chosen.usnip.mo.data[[k]][chosen.usnip.mo.data[[k]]$mo == 9, ]
        fake.yr[9, ] <- sep.iter[sample(nrow(sep.iter), 1, replace=TRUE), ]
        oct.iter <- chosen.usnip.mo.data[[k]][chosen.usnip.mo.data[[k]]$mo == 10, ]
        fake.yr[10, ] <- oct.iter[sample(nrow(oct.iter), 1, replace=TRUE), ]
        nov.iter <- chosen.usnip.mo.data[[k]][chosen.usnip.mo.data[[k]]$mo == 11, ]
        fake.yr[11, ] <- nov.iter[sample(nrow(nov.iter), 1, replace=TRUE), ]
        dec.iter <- chosen.usnip.mo.data[[k]][chosen.usnip.mo.data[[k]]$mo == 12, ]
        fake.yr[12, ] <- dec.iter[sample(nrow(dec.iter), 1, replace=TRUE), ]
        colnames(fake.yr) <- colnames(jan.iter)
        win.data <- fake.yr[(fake.yr$mo == 1 | fake.yr$mo == 2 | fake.yr$mo == 12), ]
        spr.data <- fake.yr[(fake.yr$mo == 3 | fake.yr$mo == 4 | fake.yr$mo == 5), ]
        sum.data <- fake.yr[(fake.yr$mo == 6 | fake.yr$mo == 7 | fake.yr$mo == 8), ]
        aut.data <- fake.yr[(fake.yr$mo == 9 | fake.yr$mo == 10 | fake.yr$mo == 11), ]
        win.frac <- sum(win.data$prcp)/sum(fake.yr$prcp)
        spr.frac <- sum(spr.data$prcp)/sum(fake.yr$prcp)
```

```
sum.frac <- sum(sum.data$prcp)/sum(fake.yr$prcp)
aut.frac <- sum(aut.data$prcp)/sum(fake.yr$prcp)

usnip.btsp.siteiter[i,1] <- sum(fake.yr$prcp/sum(fake.yr$prcp) * fake.yr$d18O)
usnip.btsp.siteiter[i,2] <- sum(fake.yr$prcp)
usnip.btsp.siteiter[i,3] <- sum(fake.yr$prcp/sum(fake.yr$prcp) * fake.yr$tavg)
usnip.btsp.siteiter[i,4] <- sum(fake.yr$prcp/sum(fake.yr$prcp) * fake.yr$pdo)
usnip.btsp.siteiter[i,5] <- sum(fake.yr$prcp/sum(fake.yr$prcp) * fake.yr$mei)
usnip.btsp.siteiter[i,6] <- sum(fake.yr$prcp/sum(fake.yr$prcp) * fake.yr$nao)
usnip.btsp.siteiter[i,7] <- sum(fake.yr$prcp/sum(fake.yr$prcp) * fake.yr$amo)
usnip.btsp.siteiter[i,8] <- sum(fake.yr$prcp/sum(fake.yr$prcp) * fake.yr$pna)
usnip.btsp.siteiter[i,9] <- sum(fake.yr$prcp/sum(fake.yr$prcp) * fake.yr$bhi)
usnip.btsp.siteiter[i,10] <- sum(fake.yr$prcp/sum(fake.yr$prcp) * fake.yr$isotemp.residual)
usnip.btsp.siteiter[i,11] <- win.frac
usnip.btsp.siteiter[i,12] <- spr.frac
usnip.btsp.siteiter[i,13] <- sum.frac
usnip.btsp.siteiter[i,14] <- aut.frac

#Calculating seasonal oscillation weighted means
win.fake.iter <- fake.yr[fake.yr$mo == 12 | fake.yr$mo == 1 | fake.yr$mo == 2, ]
spr.fake.iter <- fake.yr[fake.yr$mo == 3 | fake.yr$mo == 4 | fake.yr$mo == 5, ]
sum.fake.iter <- fake.yr[fake.yr$mo == 6 | fake.yr$mo == 7 | fake.yr$mo == 8, ]
aut.fake.iter <- fake.yr[fake.yr$mo == 9 | fake.yr$mo == 10 | fake.yr$mo == 11, ]
fake.yr.ssn.osc <- data.frame(matrix(nrow=5, ncol=length(osc.index)))

for (j in 1:length(osc.index)) {
        fake.yr.ssn.osc[1,j] <- sum(fake.yr[osc.index[j]] * fake.yr$prcp / sum(fake.yr$prcp))
        if(length(win.fake.iter$yr) > 0) {
                fake.yr.ssn.osc[2,j] <- sum(win.fake.iter$prcp/sum(win.fake.iter$prcp) * win.fake.iter[osc.index[j]])
                } else {
                fake.yr.ssn.osc[2,j] <- NA
                }
        if(length(spr.fake.iter$yr) > 0) {
                fake.yr.ssn.osc[3,j] <- sum(spr.fake.iter$prcp/sum(spr.fake.iter$prcp) * spr.fake.iter[osc.index[j]])
```

```
                                        } else {
                                        fake.yr.ssn.osc[3,j] <- NA
                                        }
                                if(length(sum.fake.iter$yr) > 0) {
                                        fake.yr.ssn.osc[4,j] <- sum(sum.fake.iter$prcp/sum(sum.fake.iter$prcp) * sum.fake.iter[osc.index[j]])
                                        } else {
                                        fake.yr.ssn.osc[4,j] <- NA
                                        }
                                if(length(aut.fake.iter$yr) > 0) {
                                        fake.yr.ssn.osc[5,j] <- sum(aut.fake.iter$prcp/sum(aut.fake.iter$prcp) * aut.fake.iter[osc.index[j]])
                                        } else {
                                        fake.yr.ssn.osc[5,j] <- NA
                                        }
                                }
                        colnames(fake.yr.ssn.osc) <- osc.index
                        rownames(fake.yr.ssn.osc) <- c("year", season.index)

                        usnip.btsp.siteiter.ssn.osc[[i]] <- fake.yr.ssn.osc
                        }

                colnames(usnip.btsp.siteiter) <- c("d18O", "prcp", "tavg", "pdo", "mei", "nao", "amo", "pna", "bhi",
                        "isotemp.residual", "win.frac", "spr.frac", "sum.frac", "aut.frac")


                usnip.btsp.siteiter.sumsig <- seasonal.fraction(
                        (usnip.btsp.siteiter$win.frac * season.lmcor[[arpt.usnip[k]]]["win","d18O.wt"] +
                        usnip.btsp.siteiter$spr.frac * season.lmcor[[arpt.usnip[k]]]["spr","d18O.wt"] +
                        usnip.btsp.siteiter$sum.frac * season.lmcor[[arpt.usnip[k]]]["sum","d18O.wt"] +
                        usnip.btsp.siteiter$aut.frac * season.lmcor[[arpt.usnip[k]]]["aut","d18O.wt"]),
chosen.usnip.mo.index[k])$summer.fraction

                usnip.btsp.siteiter.ssa <- usnip.btsp.siteiter.sumsig - mean(usnip.btsp.siteiter.sumsig)
```

```
#Calculating correlations for bootstrapped d18O and other variables
osc.iter <- list()
usnip.btsp.siteiter.osc.cor.table <- data.frame(matrix(nrow=0, ncol=2))
for (j in 1:length(osc.index)) {
	osc.iter[[1]] <- cor.test(usnip.btsp.siteiter$d18O,
		sapply(usnip.btsp.siteiter.ssn.osc, "[[", osc.index[j])[1,])
	osc.iter[[2]] <- cor.test(usnip.btsp.siteiter$d18O,
		sapply(usnip.btsp.siteiter.ssn.osc, "[[", osc.index[j])[2,])
	osc.iter[[3]] <- cor.test(usnip.btsp.siteiter$d18O,
		sapply(usnip.btsp.siteiter.ssn.osc, "[[", osc.index[j])[3,])
	osc.iter[[4]] <- cor.test(usnip.btsp.siteiter$d18O,
		sapply(usnip.btsp.siteiter.ssn.osc, "[[", osc.index[j])[4,])
	osc.iter[[5]] <- cor.test(usnip.btsp.siteiter$d18O,
		sapply(usnip.btsp.siteiter.ssn.osc, "[[", osc.index[j])[5,])

	osc.cor.table.iter <- data.frame(matrix(nrow=5, ncol=2))
	for (i in 1:5) { # Looping to construct a table of correlations
		osc.cor.table.iter[i,1] <- round(osc.iter[[i]]$estimate, 3)
		osc.cor.table.iter[i,2] <- round(osc.iter[[i]]$p.value, 3)
		}
	colnames(osc.cor.table.iter) <- c("r", "pval")
	rownames(osc.cor.table.iter) <- c(paste(osc.index[j], ".yr", sep=""), paste(osc.index[j], ".win", sep=""),
		paste(osc.index[j], ".spr", sep=""), paste(osc.index[j], ".sum", sep=""),
		paste(osc.index[j], ".aut", sep=""))

	usnip.btsp.siteiter.osc.cor.table <- rbind(usnip.btsp.siteiter.osc.cor.table, osc.cor.table.iter)
	}

#Calculating correlations with tavg and ssa
d18O.btsp.siteiter.cor <- list()
d18O.btsp.siteiter.cor[[1]] <- cor.test(usnip.btsp.siteiter$d18O, usnip.btsp.siteiter$tavg)
d18O.btsp.siteiter.cor[[2]] <- cor.test(usnip.btsp.siteiter$d18O, usnip.btsp.siteiter.ssa)

usnip.btsp.siteiter.wx.cor.table <- data.frame(matrix(nrow=2, ncol=2))
```

```
                for (i in 1:2) {
                        usnip.btsp.siteiter.wx.cor.table[i,1] <- round(d18O.btsp.siteiter.cor[[i]]$estimate, 3)
                        usnip.btsp.siteiter.wx.cor.table[i,2] <- round(d18O.btsp.siteiter.cor[[i]]$p.value, 3)
                        }
            colnames(usnip.btsp.siteiter.wx.cor.table) <- c("r", "pval")
            rownames(usnip.btsp.siteiter.wx.cor.table) <- c("tavg", "ssa")

            #Combining oscillation index and weather correlations into single table, sorting by r value
            usnip.cor.table.btsp.siteiter <- rbind(usnip.btsp.siteiter.wx.cor.table, usnip.btsp.siteiter.osc.cor.table)
            usnip.cor.table.btsp.siteiter.nosort <- usnip.cor.table.btsp.siteiter
            usnip.cor.table.btsp.siteiter <- usnip.cor.table.btsp.siteiter[order(-abs(usnip.cor.table.btsp.siteiter$r)),]

            usnip.cor.table.btsp.mo.nosort[[k]] <- usnip.cor.table.btsp.siteiter.nosort
            usnip.cor.table.btsp.mo[[k]] <- usnip.cor.table.btsp.siteiter
            }
        names(usnip.cor.table.btsp.mo.nosort) <- chosen.usnip.mo.index
        names(usnip.cor.table.btsp.mo) <- chosen.usnip.mo.index

        interannual.cor.iter <- data.frame(chi.cor.table.12mo.nosort$r, chi.cor.table.btsp.nosort$r, usnip.cor.table.btsp.mo.nosort[[1]]$r,
            usnip.cor.table.btsp.mo.nosort[[2]]$r, usnip.cor.table.btsp.mo.nosort[[3]]$r, usnip.cor.table.btsp.mo.nosort[[4]]$r,
            usnip.cor.table.btsp.mo.nosort[[5]]$r)
        colnames(interannual.cor.iter) <- c("chi.12mo", "chi.btsp", "il78", "in22", "ky03", "oh49", "wi99")
        rownames(interannual.cor.iter) <- rownames(usnip.cor.table.btsp.mo.nosort[[k]])
        interannual.cor[[m]] <- interannual.cor.iter
        }


#Putting all 30 iteration correlations into single table
chi.12mo.iterated <- data.frame(matrix(nrow=32, ncol=30))
chi.btsp.iterated <- data.frame(matrix(nrow=32, ncol=30))
il78.iterated <- data.frame(matrix(nrow=32, ncol=30))
in22.iterated <- data.frame(matrix(nrow=32, ncol=30))
ky03.iterated <- data.frame(matrix(nrow=32, ncol=30))
oh49.iterated <- data.frame(matrix(nrow=32, ncol=30))
```

```
wi99.iterated <- data.frame(matrix(nrow=32, ncol=30))
for (m in 1:30) {
        chi.12mo.iterated[ ,m] <- interannual.cor[[m]]$chi.12mo
        chi.btsp.iterated[ ,m] <- interannual.cor[[m]]$chi.btsp
        il78.iterated[ ,m] <- interannual.cor[[m]]$il78
        in22.iterated[ ,m] <- interannual.cor[[m]]$in22
        ky03.iterated[ ,m] <- interannual.cor[[m]]$ky03
        oh49.iterated[ ,m] <- interannual.cor[[m]]$oh49
        wi99.iterated[ ,m] <- interannual.cor[[m]]$wi99
        }
rownames(chi.12mo.iterated) <- rownames(usnip.cor.table.btsp.mo.nosort[[k]])
rownames(chi.btsp.iterated) <- rownames(usnip.cor.table.btsp.mo.nosort[[k]])
rownames(il78.iterated) <- rownames(usnip.cor.table.btsp.mo.nosort[[k]])
rownames(in22.iterated) <- rownames(usnip.cor.table.btsp.mo.nosort[[k]])
rownames(ky03.iterated) <- rownames(usnip.cor.table.btsp.mo.nosort[[k]])
rownames(oh49.iterated) <- rownames(usnip.cor.table.btsp.mo.nosort[[k]])
rownames(wi99.iterated) <- rownames(usnip.cor.table.btsp.mo.nosort[[k]])

#Making tables of iteration means and SD
interannual.cor.iterated.mean <- specify.decimal(data.frame(rowMeans(chi.12mo.iterated), rowMeans(chi.btsp.iterated),
                rowMeans(il78.iterated), rowMeans(in22.iterated), rowMeans(ky03.iterated),
                rowMeans(oh49.iterated), rowMeans(wi99.iterated)), 3)
colnames(interannual.cor.iterated.mean) <- c("chi.12mo", "chi.btsp", "il78", "in22", "ky03", "oh49", "wi99")

interannual.cor.iterated.sd <- specify.decimal(data.frame(apply(chi.12mo.iterated, 1, sd), apply(chi.btsp.iterated, 1, sd),
                apply(il78.iterated, 1, sd), apply(in22.iterated, 1, sd), apply(ky03.iterated, 1, sd),
                apply(oh49.iterated, 1, sd), apply(wi99.iterated, 1, sd)), 3)
colnames(interannual.cor.iterated.sd) <- c("chi.12mo", "chi.btsp", "il78", "in22", "ky03", "oh49", "wi99")

#write.table(interannual.cor.iterated.mean, "interannual_cor_d18O_mean_eachmo.csv", sep=",", row.names=TRUE, col.names=NA)
#write.table(interannual.cor.iterated.sd, "interannual_cor_d18O_sd_eachmo.csv", sep=",", row.names=TRUE, col.names=NA)

#This script only runs one iteration of 1000 years in order to calculate means and sds of the USNIP
#bootstrapped data for comparison with modern data
```

```
usnip.btsp.annual.data <- list()
usnip.btsp.mean <- data.frame(matrix(nrow=15, ncol=length(chosen.usnip.mo.index)))
usnip.btsp.sd <- data.frame(matrix(nrow=15, ncol=length(chosen.usnip.mo.index)))
for (k in 1:length(chosen.usnip.mo.index)) {
        usnip.btsp.siteiter <- data.frame(matrix(nrow=1000, ncol=14))
        usnip.btsp.siteiter.ssn.osc <- list()

        for (i in 1:1000) {
                jan.iter <- chosen.usnip.mo.data[[k]][chosen.usnip.mo.data[[k]]$mo == 1, ]
                fake.yr[1, ] <- jan.iter[sample(nrow(jan.iter), 1, replace=TRUE), ]
                feb.iter <- chosen.usnip.mo.data[[k]][chosen.usnip.mo.data[[k]]$mo == 2, ]
                fake.yr[2, ] <- feb.iter[sample(nrow(feb.iter), 1, replace=TRUE), ]
                mar.iter <- chosen.usnip.mo.data[[k]][chosen.usnip.mo.data[[k]]$mo == 3, ]
                fake.yr[3, ] <- mar.iter[sample(nrow(mar.iter), 1, replace=TRUE), ]
                apr.iter <- chosen.usnip.mo.data[[k]][chosen.usnip.mo.data[[k]]$mo == 4, ]
                fake.yr[4, ] <- apr.iter[sample(nrow(apr.iter), 1, replace=TRUE), ]
                may.iter <- chosen.usnip.mo.data[[k]][chosen.usnip.mo.data[[k]]$mo == 5, ]
                fake.yr[5, ] <- may.iter[sample(nrow(may.iter), 1, replace=TRUE), ]
                jun.iter <- chosen.usnip.mo.data[[k]][chosen.usnip.mo.data[[k]]$mo == 6, ]
                fake.yr[6, ] <- jun.iter[sample(nrow(jun.iter), 1, replace=TRUE), ]
                jul.iter <- chosen.usnip.mo.data[[k]][chosen.usnip.mo.data[[k]]$mo == 7, ]
                fake.yr[7, ] <- jul.iter[sample(nrow(jul.iter), 1, replace=TRUE), ]
                aug.iter <- chosen.usnip.mo.data[[k]][chosen.usnip.mo.data[[k]]$mo == 8, ]
                fake.yr[8, ] <- aug.iter[sample(nrow(aug.iter), 1, replace=TRUE), ]
                sep.iter <- chosen.usnip.mo.data[[k]][chosen.usnip.mo.data[[k]]$mo == 9, ]
                fake.yr[9, ] <- sep.iter[sample(nrow(sep.iter), 1, replace=TRUE), ]
                oct.iter <- chosen.usnip.mo.data[[k]][chosen.usnip.mo.data[[k]]$mo == 10, ]
                fake.yr[10, ] <- oct.iter[sample(nrow(oct.iter), 1, replace=TRUE), ]
                nov.iter <- chosen.usnip.mo.data[[k]][chosen.usnip.mo.data[[k]]$mo == 11, ]
                fake.yr[11, ] <- nov.iter[sample(nrow(nov.iter), 1, replace=TRUE), ]
                dec.iter <- chosen.usnip.mo.data[[k]][chosen.usnip.mo.data[[k]]$mo == 12, ]
                fake.yr[12, ] <- dec.iter[sample(nrow(dec.iter), 1, replace=TRUE), ]
                win.data <- fake.yr[(fake.yr$mo == 1 | fake.yr$mo == 2 | fake.yr$mo == 12), ]
                spr.data <- fake.yr[(fake.yr$mo == 3 | fake.yr$mo == 4 | fake.yr$mo == 5), ]
```

```
sum.data <- fake.yr[(fake.yr$mo == 6 | fake.yr$mo == 7 | fake.yr$mo == 8), ]
aut.data <- fake.yr[(fake.yr$mo == 9 | fake.yr$mo == 10 | fake.yr$mo == 11), ]
win.frac <- sum(win.data$prcp)/sum(fake.yr$prcp)
spr.frac <- sum(spr.data$prcp)/sum(fake.yr$prcp)
sum.frac <- sum(sum.data$prcp)/sum(fake.yr$prcp)
aut.frac <- sum(aut.data$prcp)/sum(fake.yr$prcp)

usnip.btsp.siteiter[i,1] <- sum(fake.yr$prcp/sum(fake.yr$prcp) * fake.yr$d18O)
usnip.btsp.siteiter[i,2] <- sum(fake.yr$prcp)
usnip.btsp.siteiter[i,3] <- sum(fake.yr$prcp/sum(fake.yr$prcp) * fake.yr$tavg)
usnip.btsp.siteiter[i,4] <- sum(fake.yr$prcp/sum(fake.yr$prcp) * fake.yr$pdo)
usnip.btsp.siteiter[i,5] <- sum(fake.yr$prcp/sum(fake.yr$prcp) * fake.yr$mei)
usnip.btsp.siteiter[i,6] <- sum(fake.yr$prcp/sum(fake.yr$prcp) * fake.yr$nao)
usnip.btsp.siteiter[i,7] <- sum(fake.yr$prcp/sum(fake.yr$prcp) * fake.yr$amo)
usnip.btsp.siteiter[i,8] <- sum(fake.yr$prcp/sum(fake.yr$prcp) * fake.yr$pna)
usnip.btsp.siteiter[i,9] <- sum(fake.yr$prcp/sum(fake.yr$prcp) * fake.yr$bhi)
usnip.btsp.siteiter[i,10] <- sum(fake.yr$prcp/sum(fake.yr$prcp) * fake.yr$isotemp.residual)
usnip.btsp.siteiter[i,11] <- win.frac
usnip.btsp.siteiter[i,12] <- spr.frac
usnip.btsp.siteiter[i,13] <- sum.frac
usnip.btsp.siteiter[i,14] <- aut.frac

#Calculating seasonal oscillation weighted means
win.fake.iter <- fake.yr[fake.yr$mo == 12 | fake.yr$mo == 1 | fake.yr$mo == 2, ]
spr.fake.iter <- fake.yr[fake.yr$mo == 3 | fake.yr$mo == 4 | fake.yr$mo == 5, ]
sum.fake.iter <- fake.yr[fake.yr$mo == 6 | fake.yr$mo == 7 | fake.yr$mo == 8, ]
aut.fake.iter <- fake.yr[fake.yr$mo == 9 | fake.yr$mo == 10 | fake.yr$mo == 11, ]
fake.yr.ssn.osc <- data.frame(matrix(nrow=5, ncol=length(osc.index)))

for (j in 1:length(osc.index)) {
        fake.yr.ssn.osc[1,j] <- sum(fake.yr[osc.index[j]] * fake.yr$prcp / sum(fake.yr$prcp))
        if(length(win.fake.iter$yr) > 0) {
                fake.yr.ssn.osc[2,j] <- sum(win.fake.iter$prcp/sum(win.fake.iter$prcp) * win.fake.iter[osc.index[j]])
                } else {
```

```
                fake.yr.ssn.osc[2,j] <- NA
                }
        if(length(spr.fake.iter$yr) > 0) {
                fake.yr.ssn.osc[3,j] <- sum(spr.fake.iter$prcp/sum(spr.fake.iter$prcp) * spr.fake.iter[osc.index[j]])
                } else {
                fake.yr.ssn.osc[3,j] <- NA
                }
        if(length(sum.fake.iter$yr) > 0) {
                fake.yr.ssn.osc[4,j] <- sum(sum.fake.iter$prcp/sum(sum.fake.iter$prcp) * sum.fake.iter[osc.index[j]])
                } else {
                fake.yr.ssn.osc[4,j] <- NA
                }
        if(length(aut.fake.iter$yr) > 0) {
                fake.yr.ssn.osc[5,j] <- sum(aut.fake.iter$prcp/sum(aut.fake.iter$prcp) * aut.fake.iter[osc.index[j]])
                } else {
                fake.yr.ssn.osc[5,j] <- NA
                }
        }
    colnames(fake.yr.ssn.osc) <- osc.index
    rownames(fake.yr.ssn.osc) <- c("year", season.index)

    usnip.btsp.siteiter.ssn.osc[[i]] <- fake.yr.ssn.osc
    }

colnames(usnip.btsp.siteiter) <- c("d18O", "prcp", "tavg", "pdo", "mei", "nao", "amo", "pna", "bhi",
    "isotemp.residual", "win.frac", "spr.frac", "sum.frac", "aut.frac")


usnip.btsp.siteiter.sumsig <- seasonal.fraction(
    (usnip.btsp.siteiter$win.frac * season.lmcor[[arpt.usnip[k]]]["win","d18O.wt"] +
    usnip.btsp.siteiter$spr.frac * season.lmcor[[arpt.usnip[k]]]["spr","d18O.wt"] +
    usnip.btsp.siteiter$sum.frac * season.lmcor[[arpt.usnip[k]]]["sum","d18O.wt"] +
    usnip.btsp.siteiter$aut.frac * season.lmcor[[arpt.usnip[k]]]["aut","d18O.wt"]), chosen.usnip.mo.index[k])$summer.fraction
```

```
        usnip.btsp.siteiter.ssa <- usnip.btsp.siteiter.sumsig - mean(usnip.btsp.siteiter.sumsig)
        usnip.btsp.siteiter$ssa <- usnip.btsp.siteiter.ssa
        usnip.btsp.annual.data[[k]] <- usnip.btsp.siteiter

        usnip.btsp.mean[,k] <- as.numeric(specify.decimal(apply(usnip.btsp.siteiter, 2, mean), 3))
        usnip.btsp.sd[,k] <- as.numeric(specify.decimal(apply(usnip.btsp.siteiter, 2, sd), 3))
        }
rownames(usnip.btsp.mean) <- c("d18O", "prcp", "tavg", "pdo", "mei", "nao", "amo", "pna", "bhi",
        "isotemp.residual", "win.frac", "spr.frac", "sum.frac", "aut.frac", "ssa")
rownames(usnip.btsp.sd) <- c("d18O", "prcp", "tavg", "pdo", "mei", "nao", "amo", "pna", "bhi",
        "isotemp.residual", "win.frac", "spr.frac", "sum.frac", "aut.frac", "ssa")
colnames(usnip.btsp.mean) <- chosen.usnip.mo.index
colnames(usnip.btsp.sd) <- chosen.usnip.mo.index

#write.table(usnip.btsp.mean, "usnip_btsp_means_eachmo.csv", sep=",", row.names=TRUE, col.names=NA)
#write.table(usnip.btsp.sd, "usnip_btsp_sd_eachmo.csv", sep=",", row.names=TRUE, col.names=NA)
chi.btsp.mean <- as.numeric(specify.decimal(apply(chi.gnip.btsp, 2, mean), 2))
chi.btsp.sd <- as.numeric(specify.decimal(apply(chi.gnip.btsp, 2, sd), 2))
mean(chi.gnip.btsp.ssa)
sd(chi.gnip.btsp.ssa)


#-------------------------------------------------------------------------------------------------
#----------------------------------------Modern Airport Data--------------------------------------
#----------------------------------------USNIP Seasonal Signals-----------------------------------
#This loop takes the list of airport data and sorts it into yearly values and calculates SSA based
#on USNIP seasonal signals for the nearest USNIP site
yearly.frac <- list()
modern.d18O <- list()
modern.ssa <- list()
modern.tavg <- list()
modern.tavg.unwt <- list()
modern.prcp <- list()
arpt.data <- list()
```

```
arpt.tavg <- data.frame(matrix(nrow=2, ncol=length(arpt.index)))
arpt.tavg.unwt <- data.frame(matrix(nrow=2, ncol=length(arpt.index)))
arpt.prcp <- data.frame(matrix(nrow=2, ncol=length(arpt.index)))
arpt.ssa <- data.frame(matrix(nrow=2, ncol=length(arpt.index)))
for (k in 1:length(arpt.index)) {
        #Adding month, year, and season columns
        mo <- strftime(arpt[[k]]$date, "%m")
        yr <- strftime(arpt[[k]]$date, "%Y")
        arpt[[k]]$mo <- mo
        arpt[[k]]$yr<- yr
        arpt[[k]]$season[arpt[[k]]$mo == "12" | arpt[[k]]$mo == "01" | arpt[[k]]$mo == "02"] <- "win"
        arpt[[k]]$season[arpt[[k]]$mo == "03" | arpt[[k]]$mo == "04" | arpt[[k]]$mo == "05"] <- "spr"
        arpt[[k]]$season[arpt[[k]]$mo == "06" | arpt[[k]]$mo == "07" | arpt[[k]]$mo == "08"] <- "sum"
        arpt[[k]]$season[arpt[[k]]$mo == "09" | arpt[[k]]$mo == "10" | arpt[[k]]$mo == "11"] <- "aut"

        arpt[[k]]$snow[arpt[[k]]$snow == -9999] <- NA
        arpt[[k]]$prcp[arpt[[k]]$prcp == -999.9] <- NA
        arpt[[k]]$snow.depth[arpt[[k]]$snow.depth == -9999] <- NA
        arpt[[k]]$wind.speed[arpt[[k]]$wind.speed == -9999] <- NA
        arpt[[k]]$wind.speed[arpt[[k]]$wind.speed == -999.9] <- NA
        arpt[[k]]$wind.dir[arpt[[k]]$wind.dir == -9999] <- NA


        #Subsetting data to only have numeric and time columns
        arpt.data.iter <- arpt[[k]][seq(7,17)]


        #Calculating monthly datasets
        temp.mo <- NULL
        mo.aggr <-data.frame(matrix(nrow=12, ncol=8))
        mo.id <- c("01", "02", "03", "04", "05", "06", "07", "08", "09",
                "10", "11", "12")
        season.id <- c("win", "spr", "sum", "aut")
```

```
#Loop to determine average monthly values
for (i in 1:12) {
        temp.mo <- arpt.data.iter[arpt.data.iter$mo == mo.id[i], ]
        mo.aggr[i, ] <- t(colMeans(temp.mo[ ,-c(9:11)], na.rm=TRUE))
        }
rownames(mo.aggr) <- c("Jan", "Feb", "Mar", "Apr", "May", "Jun", "Jul",
         "Aug", "Sep", "Oct", "Nov", "Dec")
colnames(mo.aggr) <- c("prcp", "snow", "snow.depth", "tmax", "tmin", "tavg",
        "wind.speed", "wind.dir")

arpt.mo.aggr.iter <- mo.aggr

#----------------------------------Calculating SSA Values-------------------------------------
#This loop calculates all season precip fractions for each airport site
#NOTE: This is the calculation used in the dissertation
arpt.data.iter <- arpt.data.iter[arpt.data.iter$yr < 2015 & arpt.data.iter$yr >= 1949, ]
year.index <- as.numeric(sort(unique(arpt.data.iter$yr)))
yearly.frac.iter <- data.frame(matrix(nrow=(length(year.index)-1), ncol=5))
modern.tavg.iter <- NA
modern.tavg.iter.unwt <- NA
modern.prcp.iter <- NA
for (i in 1:(length(year.index)-1)) { #cut out a year because of Dec previous for winter
        year.iter <- NULL
        win.tot <- NULL
        spr.tot <- NULL
        sum.tot <- NULL
        aut.tot <- NULL
        win.frac <- NULL
        spr.frac <- NULL
        sum.frac <- NULL
        aut.frac <- NULL
        year.iter <- arpt.data.iter[arpt.data.iter$yr == year.index[i+1], ] #this iteration's data
        last.year.iter <- arpt.data.iter[arpt.data.iter$yr == year.index[i], ] #this iteration's data for December
        win.tot <- sum(c(year.iter$prcp[year.iter$mo == "01" | year.iter$mo == "02"]),
```

```
                last.year.iter$prcp[last.year.iter$mo == "12"])
        spr.tot <- sum(year.iter$prcp[year.iter$season == "spr"])
        sum.tot <- sum(year.iter$prcp[year.iter$season == "sum"])
        aut.tot <- sum(year.iter$prcp[year.iter$season == "aut"])
        win.frac <- win.tot / (win.tot + spr.tot + sum.tot + aut.tot)
        spr.frac <- spr.tot / (win.tot + spr.tot + sum.tot + aut.tot)
        sum.frac <- sum.tot / (win.tot + spr.tot + sum.tot + aut.tot)
        aut.frac <- aut.tot / (win.tot + spr.tot + sum.tot + aut.tot)
        yearly.frac.iter[i,1] <- year.index[i+1]
        yearly.frac.iter[i,2] <- win.frac
        yearly.frac.iter[i,3] <- spr.frac
        yearly.frac.iter[i,4] <- sum.frac
        yearly.frac.iter[i,5] <- aut.frac

        #Yearly tavg wt mean
        tavg.yr.data <- rbind(last.year.iter[last.year.iter$mo == "12", ],
                year.iter[year.iter$mo != "12", ])
        modern.tavg.iter[i] <- sum(tavg.yr.data$tavg*tavg.yr.data$prcp/sum(tavg.yr.data$prcp))

        #Yearly tavg not weighted mean
        tavg.yr.data <- rbind(last.year.iter[last.year.iter$mo == "12", ],
                year.iter[year.iter$mo != "12", ])
        modern.tavg.iter.unwt[i] <- mean(tavg.yr.data$tavg)

        #Yearly prcp
        prcp.yr.data <- rbind(last.year.iter[last.year.iter$mo == "12", ],
                year.iter[year.iter$mo != "12", ])
        modern.prcp.iter[i] <- sum(prcp.yr.data$prcp)

        }
colnames(yearly.frac.iter) <- c("yr", "win.frac", "spr.frac", "sum.frac", "aut.frac")


#This part is taking seasonal precip fractions per year, converting them into d18O
```

```
#values based on USNIP seasonal signals, summing them to make a yearly d18O signal,
#and then converting that yearly signal into a summer signal using the same seaonal USNIP signals
modern.d18O.iter <-
        (yearly.frac.iter$win.frac * season.lmcor[[arpt.usnip[k]]]["win","d18O.wt"] +
        yearly.frac.iter$spr.frac * season.lmcor[[arpt.usnip[k]]]["spr","d18O.wt"] +
        yearly.frac.iter$sum.frac * season.lmcor[[arpt.usnip[k]]]["sum","d18O.wt"] +
        yearly.frac.iter$aut.frac * season.lmcor[[arpt.usnip[k]]]["aut","d18O.wt"])

seasonal.fraction.iter <- seasonal.fraction(modern.d18O.iter, arpt.usnip[k]) #Load seasonal fraction function
sumsigfrac.iter <- mean(seasonal.fraction.iter$summer.fraction) #average summer signal fraction
sumsigfrac.iter.err <- sd(seasonal.fraction.iter$summer.fraction) /
        sqrt(length(seasonal.fraction.iter$summer.fraction)) #standard error of the summer signal fraction


#Calculating modern day annual summer signal anomalies for each site
modern.ssa.iter <- seasonal.fraction.iter$summer.fraction - mean(seasonal.fraction.iter$summer.fraction)
modern.ssa.iter <- data.frame(seq(1950,2014), modern.ssa.iter)
colnames(modern.ssa.iter) <- c("year", "ssa")

#Three-year modern SSA average
ssa.iter.3yr <- data.frame(matrix(ncol=2, nrow=(length(modern.ssa.iter$ssa) - 3)))
for (i in 1:(length(modern.ssa.iter$ssa) - 3)) {
        ssa.iter.3yr[i,1] <- modern.ssa.iter$year[i+1]
        ssa.iter.3yr[i,2] <- mean(modern.ssa.iter$ssa[i:(i+2)])
        }
colnames(ssa.iter.3yr) <- c("year", "ssa.3yr.avg")

#Plot of modern SSA with modern 3 yr mean 2SD Box
dev.new(height=5,width=12)
plot(modern.ssa.iter$year, modern.ssa.iter$ssa, type="n", bty="n", xaxt="n", yaxt="n",
        xlab="", ylab="", xlim=c(1949,2014), ylim=c(-0.16, 0.16))
rect(1949, -2*sd(ssa.iter.3yr$ssa.3yr.avg), 2014, #2-sigma range of modern anomalies
        2*sd(ssa.iter.3yr$ssa.3yr.avg), col="gray90", border=NA)
abline(h=0.0, col="firebrick", lwd=1.5) #modern summer signal anomaly for indianapolis
```

```
        rect(1998, 0.13, 2000, 0.15, col="gray90", border=NA)
        points(modern.ssa.iter$year, modern.ssa.iter$ssa, type="l", col="black", lwd=1.5)
        text(x=2000, y=0.14, "2σ Range of 3-Yr Average", col="gray50", pos=4) #sigma shows as 's'
        text(x=1949, y=0.14, arpt.name[k], col="black", pos=4, cex=1.4) #sigma shows as 's'
        axis(2, at=seq(-0.15, 0.15, 0.05), pos=1949, las=1, col="black",
             col.axis="black", labels=c("-0.15", "-0.10", "-0.05", "0.00", "0.05", "0.10", "0.15"))
        axis(2, at=seq(-0.16, 0.16, 0.01), pos=1949, las=1, col="black",
             col.axis="black", labels=FALSE, tck=-0.01)
        axis(1, at=seq(1950,2010,10), pos=-0.16)
        axis(1, at=seq(1950,2014,2), pos=-0.16, labels=FALSE, tck=-0.01)
        axis(1, at=seq(1949,1950,1), pos=-0.16, labels=FALSE, tck=-0.01)
        mtext(side=1, "Year (AD)", line=2, cex=1.3)
        mtext(side=2, "Summer Signal Anomaly", line=1.3, cex=1.2, col="black")

        yearly.frac[[k]] <- yearly.frac.iter
        modern.d18O[[k]] <- modern.d18O.iter
        modern.ssa[[k]] <- modern.ssa.iter$ssa
        modern.tavg[[k]] <- modern.tavg.iter
        modern.tavg.unwt[[k]] <- modern.tavg.iter.unwt
        modern.prcp[[k]] <- modern.prcp.iter
        arpt.tavg[1,k] <- mean(modern.tavg.iter)
        arpt.tavg[2,k] <- sd(modern.tavg.iter)
        arpt.tavg.unwt[1,k] <- mean(modern.tavg.iter.unwt)
        arpt.tavg.unwt[2,k] <- sd(modern.tavg.iter.unwt)
        arpt.ssa[1,k] <- mean(modern.ssa.iter$ssa)
        arpt.ssa[2,k] <- sd(modern.ssa.iter$ssa)
        arpt.data[[k]] <- arpt.data.iter
        }
names(yearly.frac) <- arpt.index
names(modern.d18O) <- arpt.index
names(modern.ssa) <- arpt.index
names(modern.tavg) <- arpt.index
names(modern.tavg.unwt) <- arpt.index
names(modern.prcp) <- arpt.index
```

```
names(arpt.data) <- arpt.index
rownames(arpt.tavg) <- c("mean", "sd")
colnames(arpt.tavg) <- arpt.index
rownames(arpt.tavg.unwt) <- c("mean", "sd")
colnames(arpt.tavg.unwt) <- arpt.index
rownames(arpt.ssa) <- c("mean", "sd")
colnames(arpt.ssa) <- arpt.index

#Making a list of a list of airport seasonal oscillation correlations with USNIP d18O
usnip.cor.table <- list()
usnip.cor.table.nosort <- list()
for (k in 1:length(arpt.index)) {
	osc.usnip.iter <- list()
	usnip.osc.cor.table.siteiter <- data.frame(matrix(nrow=0, ncol=2))
	for (j in 1:length(osc.index)) {
		d18O.cor.iter <- modern.d18O[[k]][-65] #removing 2014
		osc.usnip.iter[[1]] <- cor.test(d18O.cor.iter, osc[[j]]$year.mean)
		osc.usnip.iter[[2]] <- cor.test(d18O.cor.iter, osc[[j]]$win.mean)
		osc.usnip.iter[[3]] <- cor.test(d18O.cor.iter, osc[[j]]$spr.mean)
		osc.usnip.iter[[4]] <- cor.test(d18O.cor.iter, osc[[j]]$sum.mean)
		osc.usnip.iter[[5]] <- cor.test(d18O.cor.iter, osc[[j]]$aut.mean)

		osc.cor.table.usnip.iter <- data.frame(matrix(nrow=5, ncol=2))
		for (i in 1:5) { # Looping to construct a table of correlations
			osc.cor.table.usnip.iter[i,1] <- round(osc.usnip.iter[[i]]$estimate, 3)
			osc.cor.table.usnip.iter[i,2] <- round(osc.usnip.iter[[i]]$p.value, 3)
			}
		colnames(osc.cor.table.usnip.iter) <- c("r", "pval")
		rownames(osc.cor.table.usnip.iter) <- c(paste(osc.index[j], ".yr", sep=""), paste(osc.index[j], ".win", sep=""),
			paste(osc.index[j], ".spr", sep=""), paste(osc.index[j], ".sum", sep=""),
			paste(osc.index[j], ".aut", sep=""))

		usnip.osc.cor.table.siteiter <- rbind(usnip.osc.cor.table.siteiter, osc.cor.table.usnip.iter)
		}
```

```
        #Calculating correlations with tavg and ssa
        usnip.wx.cor <- list()
        modern.ssa.cor.iter <- modern.ssa[[k]][-65] #removing 2014
        modern.tavg.cor.iter <- modern.tavg[[k]][-65] #removing 2014
        usnip.wx.cor[[1]] <- cor.test(d18O.cor.iter, modern.tavg.cor.iter)
        usnip.wx.cor[[2]] <- cor.test(d18O.cor.iter, modern.ssa.cor.iter)
        usnip.wx.cor.table.siteiter <- data.frame(matrix(nrow=0, ncol=2))
                for (i in 1:2) {
                        usnip.wx.cor.table.siteiter[i,1] <- round(usnip.wx.cor[[i]]$estimate, 3)
                        usnip.wx.cor.table.siteiter[i,2] <- round(usnip.wx.cor[[i]]$p.value, 3)
                        }
        colnames(usnip.wx.cor.table.siteiter) <- c("r", "pval")
        rownames(usnip.wx.cor.table.siteiter) <- c("tavg", "ssa")

        #Combining oscillation index and weather correlations into single table, sorting by r value
        usnip.cor.table.siteiter <- rbind(usnip.wx.cor.table.siteiter, usnip.osc.cor.table.siteiter)
        usnip.cor.table.nosort[[k]] <- usnip.cor.table.siteiter
        usnip.cor.table.siteiter <- usnip.cor.table.siteiter[order(-abs(usnip.cor.table.siteiter$r)),]
        usnip.cor.table[[k]] <- usnip.cor.table.siteiter
        }
names(usnip.cor.table) <- arpt.index
names(usnip.cor.table.nosort) <- arpt.index

#=============================================================================================
#This section makes plots of d18O vs tavg and ssa to compare the Chicago GNIP 12mo vs bootstrap

chi.12mo.yr.na$ssa <- chi.12mo.ssa

#12mo d18O vs tavg
dev.new(height=8, width=8)
plot(chi.12mo.yr.na$tavg, chi.12mo.yr.na$d18O, xlim=c(7,17), ylim=c(-10, -2), type="n",
        bty="n", xaxt="n", yaxt="n", xlab="", ylab="")
points(chi.12mo.yr.na$tavg, chi.12mo.yr.na$d18O, pch=16)
```

```
axis(2, at=seq(-10, -2, 2), pos=7, las=1, col="black", col.axis="black", cex.axis=1.4)
axis(2, at=seq(-10, -2, 1), pos=7, las=1, col="black", col.axis="black", labels=FALSE, tck=-0.01)
axis(1, at=seq(8,16,2), pos=-10, cex.axis=1.4)
axis(1, at=seq(7,17,1), pos=-10, labels=FALSE, tck=-0.01)
mtext(side=1, "Mean Annual Temperature", line=2, cex=1.5)
mtext(side=2, expression(paste("Annual Precipitation ",{delta}^18*O, " (‰ vs. V-SMOW)")),
      line=2, cex=1.5, col="black")
text(x=7.3, y=-2.5, pos=4, "Consecutive 12-Month", cex=1.8)

#Bootstrapped d18O vs tavg
dev.new(height=8, width=8)
plot(chi.gnip.btsp$tavg, chi.gnip.btsp$d18O, xlim=c(7,17), ylim=c(-10, -2), type="n",
      bty="n", xaxt="n", yaxt="n", xlab="", ylab="")
points(chi.gnip.btsp$tavg, chi.gnip.btsp$d18O, pch=16)
axis(2, at=seq(-10, -2, 2), pos=7, las=1, col="black", col.axis="black", cex.axis=1.4)
axis(2, at=seq(-10, -2, 1), pos=7, las=1, col="black", col.axis="black", labels=FALSE, tck=-0.01)
axis(1, at=seq(8,16,2), pos=-10, cex.axis=1.4)
axis(1, at=seq(7,17,1), pos=-10, labels=FALSE, tck=-0.01)
mtext(side=1, "Mean Annual Temperature", line=2, cex=1.5)
mtext(side=2, expression(paste("Annual Precipitation ",{delta}^18*O, " (‰ vs. V-SMOW)")),
      line=2, cex=1.5, col="black")
text(x=7.3, y=-2.5, pos=4, "Bootstrapped", cex=1.8)



#12mo d18O vs SSA
dev.new(height=8, width=8)
plot(chi.12mo.yr.na$ssa, chi.12mo.yr.na$d18O, xlim=c(-0.2,0.2), ylim=c(-10, -2), type="n",
      bty="n", xaxt="n", yaxt="n", xlab="", ylab="")
points(chi.12mo.yr.na$ssa, chi.12mo.yr.na$d18O, pch=16)
axis(2, at=seq(-10, -2, 2), pos=-0.2, las=1, col="black", col.axis="black", cex.axis=1.4)
axis(2, at=seq(-10, -2, 1), pos=-0.2, las=1, col="black", col.axis="black", labels=FALSE, tck=-0.01)
axis(1, at=seq(-0.2,0.2,0.1), pos=-10, cex.axis=1.4)
axis(1, at=seq(-0.2,0.2,0.05), pos=-10, labels=FALSE, tck=-0.01)
```

```
mtext(side=1, "Summer Seasonal Anomaly", line=2, cex=1.5)
mtext(side=2, expression(paste("Annual Precipitation ",{delta}^18*O, " (‰ vs. V-SMOW)")),
	line=2, cex=1.5, col="black")
text(x=-0.18, y=-2.5, pos=4, "Consecutive 12-Month", cex=1.8)

#Bootstrapped d18O vs SSA
dev.new(height=8, width=8)
plot(chi.gnip.btsp.ssa, chi.gnip.btsp$d18O, xlim=c(-0.2,0.2), ylim=c(-10, -2), type="n",
	bty="n", xaxt="n", yaxt="n", xlab="", ylab="")
points(chi.gnip.btsp.ssa, chi.gnip.btsp$d18O, pch=16)
axis(2, at=seq(-10, -2, 2), pos=-0.2, las=1, col="black", col.axis="black", cex.axis=1.4)
axis(2, at=seq(-10, -2, 1), pos=-0.2, las=1, col="black", col.axis="black", labels=FALSE, tck=-0.01)
axis(1, at=seq(-0.2,0.2,0.1), pos=-10, cex.axis=1.4)
axis(1, at=seq(-0.2,0.2,0.05), pos=-10, labels=FALSE, tck=-0.01)
mtext(side=1, "Summer Seasonal Anomaly", line=2, cex=1.5)
mtext(side=2, expression(paste("Annual Precipitation ",{delta}^18*O, " (‰ vs. V-SMOW)")),
	line=2, cex=1.5, col="black")
text(x=-0.18, y=-2.5, pos=4, "Bootstrapped", cex=1.8)



#=============================================================================================
#This is the same bootstrapping as before, but it picks 12 random months, NOT one of each month
#Running 30 iterations to check for variance in bootstrapping (make sure to run 12 mo first!)
interannual.cor <- list()
for (m in 1:30) {
	#-------------------------------------------------------------------------------------------
	#----------------------------------------Bootstrapping--------------------------------------
	#Chicago GNIP
	chi.gnip.btsp <- data.frame(matrix(nrow=1000, ncol=14))
	chi.gnip.btsp.ssn.osc <- list()

	for (i in 1:1000) {
		fake.yr <- chi.gnip.raw[sample(nrow(chi.gnip.raw), 12, replace=TRUE), ]
```

```
win.data <- fake.yr[(fake.yr$mo == 1 | fake.yr$mo == 2 | fake.yr$mo == 12), ]
spr.data <- fake.yr[(fake.yr$mo == 3 | fake.yr$mo == 4 | fake.yr$mo == 5), ]
sum.data <- fake.yr[(fake.yr$mo == 6 | fake.yr$mo == 7 | fake.yr$mo == 8), ]
aut.data <- fake.yr[(fake.yr$mo == 9 | fake.yr$mo == 10 | fake.yr$mo == 11), ]
win.frac <- sum(win.data$prcp)/sum(fake.yr$prcp)
spr.frac <- sum(spr.data$prcp)/sum(fake.yr$prcp)
sum.frac <- sum(sum.data$prcp)/sum(fake.yr$prcp)
aut.frac <- sum(aut.data$prcp)/sum(fake.yr$prcp)

chi.gnip.btsp[i,1] <- sum(fake.yr$prcp/sum(fake.yr$prcp) * fake.yr$d18O)
chi.gnip.btsp[i,2] <- sum(fake.yr$prcp)
chi.gnip.btsp[i,3] <- sum(fake.yr$prcp/sum(fake.yr$prcp) * fake.yr$tavg)
chi.gnip.btsp[i,4] <- sum(fake.yr$prcp/sum(fake.yr$prcp) * fake.yr$pdo)
chi.gnip.btsp[i,5] <- sum(fake.yr$prcp/sum(fake.yr$prcp) * fake.yr$mei)
chi.gnip.btsp[i,6] <- sum(fake.yr$prcp/sum(fake.yr$prcp) * fake.yr$nao)
chi.gnip.btsp[i,7] <- sum(fake.yr$prcp/sum(fake.yr$prcp) * fake.yr$amo)
chi.gnip.btsp[i,8] <- sum(fake.yr$prcp/sum(fake.yr$prcp) * fake.yr$pna)
chi.gnip.btsp[i,9] <- sum(fake.yr$prcp/sum(fake.yr$prcp) * fake.yr$bhi)
chi.gnip.btsp[i,10] <- sum(fake.yr$prcp/sum(fake.yr$prcp) * fake.yr$isotemp.residual)
chi.gnip.btsp[i,11] <- win.frac
chi.gnip.btsp[i,12] <- spr.frac
chi.gnip.btsp[i,13] <- sum.frac
chi.gnip.btsp[i,14] <- aut.frac

#Calculating seasonal oscillation weighted means
win.fake.iter <- fake.yr[fake.yr$mo == 12 | fake.yr$mo == 1 | fake.yr$mo == 2, ]
spr.fake.iter <- fake.yr[fake.yr$mo == 3 | fake.yr$mo == 4 | fake.yr$mo == 5, ]
sum.fake.iter <- fake.yr[fake.yr$mo == 6 | fake.yr$mo == 7 | fake.yr$mo == 8, ]
aut.fake.iter <- fake.yr[fake.yr$mo == 9 | fake.yr$mo == 10 | fake.yr$mo == 11, ]
fake.yr.ssn.osc <- data.frame(matrix(nrow=5, ncol=length(osc.index)))

for (j in 1:length(osc.index)) {
        fake.yr.ssn.osc[1,j] <- sum(fake.yr[osc.index[j]] * fake.yr$prcp / sum(fake.yr$prcp))
        if(length(win.fake.iter$yr) > 0) {
```

```
                fake.yr.ssn.osc[2,j] <- sum(win.fake.iter$prcp/sum(win.fake.iter$prcp) * win.fake.iter[osc.index[j]])
                } else {
                fake.yr.ssn.osc[2,j] <- NA
                }
        if(length(spr.fake.iter$yr) > 0) {
                fake.yr.ssn.osc[3,j] <- sum(spr.fake.iter$prcp/sum(spr.fake.iter$prcp) * spr.fake.iter[osc.index[j]])
                } else {
                fake.yr.ssn.osc[3,j] <- NA
                }
        if(length(sum.fake.iter$yr) > 0) {
                fake.yr.ssn.osc[4,j] <- sum(sum.fake.iter$prcp/sum(sum.fake.iter$prcp) * sum.fake.iter[osc.index[j]])
                } else {
                fake.yr.ssn.osc[4,j] <- NA
                }
        if(length(aut.fake.iter$yr) > 0) {
                fake.yr.ssn.osc[5,j] <- sum(aut.fake.iter$prcp/sum(aut.fake.iter$prcp) * aut.fake.iter[osc.index[j]])
                } else {
                fake.yr.ssn.osc[5,j] <- NA
                }
        }
    colnames(fake.yr.ssn.osc) <- osc.index
    rownames(fake.yr.ssn.osc) <- c("year", season.index)

    chi.gnip.btsp.ssn.osc[[i]] <- fake.yr.ssn.osc
    }

colnames(chi.gnip.btsp) <- c("d18O", "prcp", "tavg", "pdo", "mei", "nao", "amo", "pna", "bhi",
    "isotemp.residual", "win.frac", "spr.frac", "sum.frac", "aut.frac")


chi.gnip.btsp.sumsig <- seasonal.fraction(
    (chi.gnip.btsp$win.frac * season.lmcor[["wi99"]]["win","d18O.wt"] +
    chi.gnip.btsp$spr.frac * season.lmcor[["wi99"]]["spr","d18O.wt"] +
    chi.gnip.btsp$sum.frac * season.lmcor[["wi99"]]["sum","d18O.wt"] +
```

```
        chi.gnip.btsp$aut.frac * season.lmcor[["wi99"]]["aut","d18O.wt"]), "wi99")$summer.fraction

chi.gnip.btsp.ssa <- chi.gnip.btsp.sumsig - mean(chi.gnip.btsp.sumsig)


#Calculating correlations for bootstrapped d18O and other variables
osc.iter <- list()
chi.btsp.osc.cor.table <- data.frame(matrix(nrow=0, ncol=2))
for (j in 1:length(osc.index)) {
        osc.iter[[1]] <- cor.test(chi.gnip.btsp$d18O, sapply(chi.gnip.btsp.ssn.osc, "[[", osc.index[j])[1,])
        osc.iter[[2]] <- cor.test(chi.gnip.btsp$d18O, sapply(chi.gnip.btsp.ssn.osc, "[[", osc.index[j])[2,])
        osc.iter[[3]] <- cor.test(chi.gnip.btsp$d18O, sapply(chi.gnip.btsp.ssn.osc, "[[", osc.index[j])[3,])
        osc.iter[[4]] <- cor.test(chi.gnip.btsp$d18O, sapply(chi.gnip.btsp.ssn.osc, "[[", osc.index[j])[4,])
        osc.iter[[5]] <- cor.test(chi.gnip.btsp$d18O, sapply(chi.gnip.btsp.ssn.osc, "[[", osc.index[j])[5,])

        osc.cor.table.iter <- data.frame(matrix(nrow=5, ncol=2))
        for (i in 1:5) { # Looping to construct a table of correlations
                osc.cor.table.iter[i,1] <- round(osc.iter[[i]]$estimate, 3)
                osc.cor.table.iter[i,2] <- round(osc.iter[[i]]$p.value, 3)
                }
        colnames(osc.cor.table.iter) <- c("r", "pval")
        rownames(osc.cor.table.iter) <- c(paste(osc.index[j], ".yr", sep=""), paste(osc.index[j], ".win", sep=""),
                paste(osc.index[j], ".spr", sep=""), paste(osc.index[j], ".sum", sep=""),
                paste(osc.index[j], ".aut", sep=""))

        chi.btsp.osc.cor.table <- rbind(chi.btsp.osc.cor.table, osc.cor.table.iter)
        }

#Calculating correlations with tavg and ssa
d18O.btsp.cor <- list()
d18O.btsp.cor[[1]] <- cor.test(chi.gnip.btsp$d18O, chi.gnip.btsp$tavg)
d18O.btsp.cor[[2]] <- cor.test(chi.gnip.btsp$d18O, chi.gnip.btsp.ssa)

chi.btsp.wx.cor.table <- data.frame(matrix(nrow=2, ncol=2))
```

```
        for (i in 1:2) {
                chi.btsp.wx.cor.table[i,1] <- round(d18O.btsp.cor[[i]]$estimate, 3)
                chi.btsp.wx.cor.table[i,2] <- round(d18O.btsp.cor[[i]]$p.value, 3)
                }
colnames(chi.btsp.wx.cor.table) <- c("r", "pval")
rownames(chi.btsp.wx.cor.table) <- c("tavg", "ssa")

#Combining oscillation index and weather correlations into single table, sorting by r value
chi.cor.table.btsp <- rbind(chi.btsp.wx.cor.table, chi.btsp.osc.cor.table)
chi.cor.table.btsp.nosort <- chi.cor.table.btsp
chi.cor.table.btsp <- chi.cor.table.btsp[order(-abs(chi.cor.table.btsp$r)),]

chi.cor.table.btsp

#-------------------------------------
#Monthly chosen USNIP data bootstrapping
usnip.cor.table.btsp.mo.nosort <- list()
usnip.cor.table.btsp.mo <- list()
for (k in 1:length(chosen.usnip.mo.index)) {
        usnip.btsp.siteiter <- data.frame(matrix(nrow=1000, ncol=14))
        usnip.btsp.siteiter.ssn.osc <- list()

        for (i in 1:1000) {
                fake.yr <- chosen.usnip.mo.data[[k]][sample(nrow(chosen.usnip.mo.data[[k]]), 12, replace=TRUE), ]
                win.data <- fake.yr[(fake.yr$mo == 1 | fake.yr$mo == 2 | fake.yr$mo == 12), ]
                spr.data <- fake.yr[(fake.yr$mo == 3 | fake.yr$mo == 4 | fake.yr$mo == 5), ]
                sum.data <- fake.yr[(fake.yr$mo == 6 | fake.yr$mo == 7 | fake.yr$mo == 8), ]
                aut.data <- fake.yr[(fake.yr$mo == 9 | fake.yr$mo == 10 | fake.yr$mo == 11), ]
                win.frac <- sum(win.data$prcp)/sum(fake.yr$prcp)
                spr.frac <- sum(spr.data$prcp)/sum(fake.yr$prcp)
                sum.frac <- sum(sum.data$prcp)/sum(fake.yr$prcp)
                aut.frac <- sum(aut.data$prcp)/sum(fake.yr$prcp)

                usnip.btsp.siteiter[i,1] <- sum(fake.yr$prcp/sum(fake.yr$prcp) * fake.yr$d18O)
```

```
usnip.btsp.siteiter[i,2] <- sum(fake.yr$prcp)
usnip.btsp.siteiter[i,3] <- sum(fake.yr$prcp/sum(fake.yr$prcp) * fake.yr$tavg)
usnip.btsp.siteiter[i,4] <- sum(fake.yr$prcp/sum(fake.yr$prcp) * fake.yr$pdo)
usnip.btsp.siteiter[i,5] <- sum(fake.yr$prcp/sum(fake.yr$prcp) * fake.yr$mei)
usnip.btsp.siteiter[i,6] <- sum(fake.yr$prcp/sum(fake.yr$prcp) * fake.yr$nao)
usnip.btsp.siteiter[i,7] <- sum(fake.yr$prcp/sum(fake.yr$prcp) * fake.yr$amo)
usnip.btsp.siteiter[i,8] <- sum(fake.yr$prcp/sum(fake.yr$prcp) * fake.yr$pna)
usnip.btsp.siteiter[i,9] <- sum(fake.yr$prcp/sum(fake.yr$prcp) * fake.yr$bhi)
usnip.btsp.siteiter[i,10] <- sum(fake.yr$prcp/sum(fake.yr$prcp) * fake.yr$isotemp.residual)
usnip.btsp.siteiter[i,11] <- win.frac
usnip.btsp.siteiter[i,12] <- spr.frac
usnip.btsp.siteiter[i,13] <- sum.frac
usnip.btsp.siteiter[i,14] <- aut.frac

#Calculating seasonal oscillation weighted means
win.fake.iter <- fake.yr[fake.yr$mo == 12 | fake.yr$mo == 1 | fake.yr$mo == 2, ]
spr.fake.iter <- fake.yr[fake.yr$mo == 3 | fake.yr$mo == 4 | fake.yr$mo == 5, ]
sum.fake.iter <- fake.yr[fake.yr$mo == 6 | fake.yr$mo == 7 | fake.yr$mo == 8, ]
aut.fake.iter <- fake.yr[fake.yr$mo == 9 | fake.yr$mo == 10 | fake.yr$mo == 11, ]
fake.yr.ssn.osc <- data.frame(matrix(nrow=5, ncol=length(osc.index)))

for (j in 1:length(osc.index)) {
        fake.yr.ssn.osc[1,j] <- sum(fake.yr[osc.index[j]] * fake.yr$prcp / sum(fake.yr$prcp))
        if(length(win.fake.iter$yr) > 0) {
                fake.yr.ssn.osc[2,j] <- sum(win.fake.iter$prcp/sum(win.fake.iter$prcp) * win.fake.iter[osc.index[j]])
                } else {
                fake.yr.ssn.osc[2,j] <- NA
                }
        if(length(spr.fake.iter$yr) > 0) {
                fake.yr.ssn.osc[3,j] <- sum(spr.fake.iter$prcp/sum(spr.fake.iter$prcp) * spr.fake.iter[osc.index[j]])
                } else {
                fake.yr.ssn.osc[3,j] <- NA
                }
        if(length(sum.fake.iter$yr) > 0) {
```

```
                                        fake.yr.ssn.osc[4,j] <- sum(sum.fake.iter$prcp/sum(sum.fake.iter$prcp) * sum.fake.iter[osc.index[j]])
                                        } else {
                                        fake.yr.ssn.osc[4,j] <- NA
                                        }
                                if(length(aut.fake.iter$yr) > 0) {
                                        fake.yr.ssn.osc[5,j] <- sum(aut.fake.iter$prcp/sum(aut.fake.iter$prcp) * aut.fake.iter[osc.index[j]])
                                        } else {
                                        fake.yr.ssn.osc[5,j] <- NA
                                        }
                                }
                        colnames(fake.yr.ssn.osc) <- osc.index
                        rownames(fake.yr.ssn.osc) <- c("year", season.index)

                        usnip.btsp.siteiter.ssn.osc[[i]] <- fake.yr.ssn.osc
                        }

                colnames(usnip.btsp.siteiter) <- c("d18O", "prcp", "tavg", "pdo", "mei", "nao", "amo", "pna", "bhi",
                        "isotemp.residual", "win.frac", "spr.frac", "sum.frac", "aut.frac")


                usnip.btsp.siteiter.sumsig <- seasonal.fraction(
                        (usnip.btsp.siteiter$win.frac * season.lmcor[[arpt.usnip[k]]]["win","d18O.wt"] +
                        usnip.btsp.siteiter$spr.frac * season.lmcor[[arpt.usnip[k]]]["spr","d18O.wt"] +
                        usnip.btsp.siteiter$sum.frac * season.lmcor[[arpt.usnip[k]]]["sum","d18O.wt"] +
                        usnip.btsp.siteiter$aut.frac * season.lmcor[[arpt.usnip[k]]]["aut","d18O.wt"]),
chosen.usnip.mo.index[k])$summer.fraction

                usnip.btsp.siteiter.ssa <- usnip.btsp.siteiter.sumsig - mean(usnip.btsp.siteiter.sumsig)


                #Calculating correlations for bootstrapped d18O and other variables
                osc.iter <- list()
                usnip.btsp.siteiter.osc.cor.table <- data.frame(matrix(nrow=0, ncol=2))
                for (j in 1:length(osc.index)) {
```

```
        osc.iter[[1]] <- cor.test(usnip.btsp.siteiter$d18O,
                sapply(usnip.btsp.siteiter.ssn.osc, "[[", osc.index[j])[1,])
        osc.iter[[2]] <- cor.test(usnip.btsp.siteiter$d18O,
                sapply(usnip.btsp.siteiter.ssn.osc, "[[", osc.index[j])[2,])
        osc.iter[[3]] <- cor.test(usnip.btsp.siteiter$d18O,
                sapply(usnip.btsp.siteiter.ssn.osc, "[[", osc.index[j])[3,])
        osc.iter[[4]] <- cor.test(usnip.btsp.siteiter$d18O,
                sapply(usnip.btsp.siteiter.ssn.osc, "[[", osc.index[j])[4,])
        osc.iter[[5]] <- cor.test(usnip.btsp.siteiter$d18O,
                sapply(usnip.btsp.siteiter.ssn.osc, "[[", osc.index[j])[5,])

        osc.cor.table.iter <- data.frame(matrix(nrow=5, ncol=2))
        for (i in 1:5) { # Looping to construct a table of correlations
                osc.cor.table.iter[i,1] <- round(osc.iter[[i]]$estimate, 3)
                osc.cor.table.iter[i,2] <- round(osc.iter[[i]]$p.value, 3)
                }
        colnames(osc.cor.table.iter) <- c("r", "pval")
        rownames(osc.cor.table.iter) <- c(paste(osc.index[j], ".yr", sep=""), paste(osc.index[j], ".win", sep=""),
                paste(osc.index[j], ".spr", sep=""), paste(osc.index[j], ".sum", sep=""),
                paste(osc.index[j], ".aut", sep=""))

        usnip.btsp.siteiter.osc.cor.table <- rbind(usnip.btsp.siteiter.osc.cor.table, osc.cor.table.iter)
        }

#Calculating correlations with tavg and ssa
d18O.btsp.siteiter.cor <- list()
d18O.btsp.siteiter.cor[[1]] <- cor.test(usnip.btsp.siteiter$d18O, usnip.btsp.siteiter$tavg)
d18O.btsp.siteiter.cor[[2]] <- cor.test(usnip.btsp.siteiter$d18O, usnip.btsp.siteiter.ssa)

usnip.btsp.siteiter.wx.cor.table <- data.frame(matrix(nrow=2, ncol=2))
        for (i in 1:2) {
                usnip.btsp.siteiter.wx.cor.table[i,1] <- round(d18O.btsp.siteiter.cor[[i]]$estimate, 3)
                usnip.btsp.siteiter.wx.cor.table[i,2] <- round(d18O.btsp.siteiter.cor[[i]]$p.value, 3)
                }
```

```
            colnames(usnip.btsp.siteiter.wx.cor.table) <- c("r", "pval")
            rownames(usnip.btsp.siteiter.wx.cor.table) <- c("tavg", "ssa")

            #Combining oscillation index and weather correlations into single table, sorting by r value
            usnip.cor.table.btsp.siteiter <- rbind(usnip.btsp.siteiter.wx.cor.table, usnip.btsp.siteiter.osc.cor.table)
            usnip.cor.table.btsp.siteiter.nosort <- usnip.cor.table.btsp.siteiter
            usnip.cor.table.btsp.siteiter <- usnip.cor.table.btsp.siteiter[order(-abs(usnip.cor.table.btsp.siteiter$r)),]

            usnip.cor.table.btsp.mo.nosort[[k]] <- usnip.cor.table.btsp.siteiter.nosort
            usnip.cor.table.btsp.mo[[k]] <- usnip.cor.table.btsp.siteiter
            }
        names(usnip.cor.table.btsp.mo.nosort) <- chosen.usnip.mo.index
        names(usnip.cor.table.btsp.mo) <- chosen.usnip.mo.index

        interannual.cor.iter <- data.frame(chi.cor.table.12mo.nosort$r, chi.cor.table.btsp.nosort$r, usnip.cor.table.btsp.mo.nosort[[1]]$r,
            usnip.cor.table.btsp.mo.nosort[[2]]$r, usnip.cor.table.btsp.mo.nosort[[3]]$r, usnip.cor.table.btsp.mo.nosort[[4]]$r,
            usnip.cor.table.btsp.mo.nosort[[5]]$r)
        colnames(interannual.cor.iter) <- c("chi.12mo", "chi.btsp", "il78", "in22", "ky03", "oh49", "wi99")
        rownames(interannual.cor.iter) <- rownames(usnip.cor.table.btsp.mo.nosort[[k]])
        #write.table(interannual.cor, paste("interannual_cor_d18O_", m, ".csv"), sep=",", row.names=TRUE, col.names=NA)
        interannual.cor[[m]] <- interannual.cor.iter
        }


#Putting all 30 iteration correlations into single table
chi.12mo.iterated <- data.frame(matrix(nrow=32, ncol=30))
chi.btsp.iterated <- data.frame(matrix(nrow=32, ncol=30))
il78.iterated <- data.frame(matrix(nrow=32, ncol=30))
in22.iterated <- data.frame(matrix(nrow=32, ncol=30))
ky03.iterated <- data.frame(matrix(nrow=32, ncol=30))
oh49.iterated <- data.frame(matrix(nrow=32, ncol=30))
wi99.iterated <- data.frame(matrix(nrow=32, ncol=30))
for (m in 1:30) {
        chi.12mo.iterated[ ,m] <- interannual.cor[[m]]$chi.12mo
```

```
        chi.btsp.iterated[ ,m] <- interannual.cor[[m]]$chi.btsp
        il78.iterated[ ,m] <- interannual.cor[[m]]$il78
        in22.iterated[ ,m] <- interannual.cor[[m]]$in22
        ky03.iterated[ ,m] <- interannual.cor[[m]]$ky03
        oh49.iterated[ ,m] <- interannual.cor[[m]]$oh49
        wi99.iterated[ ,m] <- interannual.cor[[m]]$wi99
        }
rownames(chi.12mo.iterated) <- rownames(usnip.cor.table.btsp.mo.nosort[[k]])
rownames(chi.btsp.iterated) <- rownames(usnip.cor.table.btsp.mo.nosort[[k]])
rownames(il78.iterated) <- rownames(usnip.cor.table.btsp.mo.nosort[[k]])
rownames(in22.iterated) <- rownames(usnip.cor.table.btsp.mo.nosort[[k]])
rownames(ky03.iterated) <- rownames(usnip.cor.table.btsp.mo.nosort[[k]])
rownames(oh49.iterated) <- rownames(usnip.cor.table.btsp.mo.nosort[[k]])
rownames(wi99.iterated) <- rownames(usnip.cor.table.btsp.mo.nosort[[k]])

#Making tables of iteration means and SD
interannual.cor.iterated.mean <- specify.decimal(data.frame(rowMeans(chi.12mo.iterated), rowMeans(chi.btsp.iterated),
                rowMeans(il78.iterated), rowMeans(in22.iterated), rowMeans(ky03.iterated),
                rowMeans(oh49.iterated), rowMeans(wi99.iterated)), 3)
colnames(interannual.cor.iterated.mean) <- c("chi.12mo", "chi.btsp", "il78", "in22", "ky03", "oh49", "wi99")

interannual.cor.iterated.sd <- specify.decimal(data.frame(apply(chi.12mo.iterated, 1, sd), apply(chi.btsp.iterated, 1, sd),
                apply(il78.iterated, 1, sd), apply(in22.iterated, 1, sd), apply(ky03.iterated, 1, sd),
                apply(oh49.iterated, 1, sd), apply(wi99.iterated, 1, sd)), 3)
colnames(interannual.cor.iterated.sd) <- c("chi.12mo", "chi.btsp", "il78", "in22", "ky03", "oh49", "wi99")

#write.table(interannual.cor.iterated.mean, "interannual_cor_d18O_mean_allmo.csv", sep=",", row.names=TRUE, col.names=NA)
#write.table(interannual.cor.iterated.sd, "interannual_cor_d18O_sd_allmo.csv", sep=",", row.names=TRUE, col.names=NA)




#====================================Bootstrapped Stats=======================================
#This script only runs one iteration of 1000 years in order to calculate means and sds of the USNIP
```

```
#bootstrapped data for comparison with modern data
usnip.btsp.annual.data <- list()
usnip.btsp.mean <- data.frame(matrix(nrow=15, ncol=length(chosen.usnip.mo.index)))
usnip.btsp.sd <- data.frame(matrix(nrow=15, ncol=length(chosen.usnip.mo.index)))
for (k in 1:length(chosen.usnip.mo.index)) {
	usnip.btsp.siteiter <- data.frame(matrix(nrow=1000, ncol=14))
	usnip.btsp.siteiter.ssn.osc <- list()

	for (i in 1:1000) {
		fake.yr <- chosen.usnip.mo.data[[k]][sample(nrow(chosen.usnip.mo.data[[k]]), 12, replace=TRUE), ]
		win.data <- fake.yr[(fake.yr$mo == 1 | fake.yr$mo == 2 | fake.yr$mo == 12), ]
		spr.data <- fake.yr[(fake.yr$mo == 3 | fake.yr$mo == 4 | fake.yr$mo == 5), ]
		sum.data <- fake.yr[(fake.yr$mo == 6 | fake.yr$mo == 7 | fake.yr$mo == 8), ]
		aut.data <- fake.yr[(fake.yr$mo == 9 | fake.yr$mo == 10 | fake.yr$mo == 11), ]
		win.frac <- sum(win.data$prcp)/sum(fake.yr$prcp)
		spr.frac <- sum(spr.data$prcp)/sum(fake.yr$prcp)
		sum.frac <- sum(sum.data$prcp)/sum(fake.yr$prcp)
		aut.frac <- sum(aut.data$prcp)/sum(fake.yr$prcp)

		usnip.btsp.siteiter[i,1] <- sum(fake.yr$prcp/sum(fake.yr$prcp) * fake.yr$d18O)
		usnip.btsp.siteiter[i,2] <- sum(fake.yr$prcp)
		usnip.btsp.siteiter[i,3] <- sum(fake.yr$prcp/sum(fake.yr$prcp) * fake.yr$tavg)
		usnip.btsp.siteiter[i,4] <- sum(fake.yr$prcp/sum(fake.yr$prcp) * fake.yr$pdo)
		usnip.btsp.siteiter[i,5] <- sum(fake.yr$prcp/sum(fake.yr$prcp) * fake.yr$mei)
		usnip.btsp.siteiter[i,6] <- sum(fake.yr$prcp/sum(fake.yr$prcp) * fake.yr$nao)
		usnip.btsp.siteiter[i,7] <- sum(fake.yr$prcp/sum(fake.yr$prcp) * fake.yr$amo)
		usnip.btsp.siteiter[i,8] <- sum(fake.yr$prcp/sum(fake.yr$prcp) * fake.yr$pna)
		usnip.btsp.siteiter[i,9] <- sum(fake.yr$prcp/sum(fake.yr$prcp) * fake.yr$bhi)
		usnip.btsp.siteiter[i,10] <- sum(fake.yr$prcp/sum(fake.yr$prcp) * fake.yr$isotemp.residual)
		usnip.btsp.siteiter[i,11] <- win.frac
		usnip.btsp.siteiter[i,12] <- spr.frac
		usnip.btsp.siteiter[i,13] <- sum.frac
		usnip.btsp.siteiter[i,14] <- aut.frac
```

```
#Calculating seasonal oscillation weighted means
win.fake.iter <- fake.yr[fake.yr$mo == 12 | fake.yr$mo == 1 | fake.yr$mo == 2, ]
spr.fake.iter <- fake.yr[fake.yr$mo == 3 | fake.yr$mo == 4 | fake.yr$mo == 5, ]
sum.fake.iter <- fake.yr[fake.yr$mo == 6 | fake.yr$mo == 7 | fake.yr$mo == 8, ]
aut.fake.iter <- fake.yr[fake.yr$mo == 9 | fake.yr$mo == 10 | fake.yr$mo == 11, ]
fake.yr.ssn.osc <- data.frame(matrix(nrow=5, ncol=length(osc.index)))

for (j in 1:length(osc.index)) {
        fake.yr.ssn.osc[1,j] <- sum(fake.yr[osc.index[j]] * fake.yr$prcp / sum(fake.yr$prcp))
        if(length(win.fake.iter$yr) > 0) {
                fake.yr.ssn.osc[2,j] <- sum(win.fake.iter$prcp/sum(win.fake.iter$prcp) * win.fake.iter[osc.index[j]])
                } else {
                fake.yr.ssn.osc[2,j] <- NA
                }
        if(length(spr.fake.iter$yr) > 0) {
                fake.yr.ssn.osc[3,j] <- sum(spr.fake.iter$prcp/sum(spr.fake.iter$prcp) * spr.fake.iter[osc.index[j]])
                } else {
                fake.yr.ssn.osc[3,j] <- NA
                }
        if(length(sum.fake.iter$yr) > 0) {
                fake.yr.ssn.osc[4,j] <- sum(sum.fake.iter$prcp/sum(sum.fake.iter$prcp) * sum.fake.iter[osc.index[j]])
                } else {
                fake.yr.ssn.osc[4,j] <- NA
                }
        if(length(aut.fake.iter$yr) > 0) {
                fake.yr.ssn.osc[5,j] <- sum(aut.fake.iter$prcp/sum(aut.fake.iter$prcp) * aut.fake.iter[osc.index[j]])
                } else {
                fake.yr.ssn.osc[5,j] <- NA
                }
        }
colnames(fake.yr.ssn.osc) <- osc.index
rownames(fake.yr.ssn.osc) <- c("year", season.index)

usnip.btsp.siteiter.ssn.osc[[i]] <- fake.yr.ssn.osc
```

```
		}

	colnames(usnip.btsp.siteiter) <- c("d18O", "prcp", "tavg", "pdo", "mei", "nao", "amo", "pna", "bhi",
		"isotemp.residual", "win.frac", "spr.frac", "sum.frac", "aut.frac")


	usnip.btsp.siteiter.sumsig <- seasonal.fraction(
		(usnip.btsp.siteiter$win.frac * season.lmcor[[arpt.usnip[k]]]["win","d18O.wt"] +
		usnip.btsp.siteiter$spr.frac * season.lmcor[[arpt.usnip[k]]]["spr","d18O.wt"] +
		usnip.btsp.siteiter$sum.frac * season.lmcor[[arpt.usnip[k]]]["sum","d18O.wt"] +
		usnip.btsp.siteiter$aut.frac * season.lmcor[[arpt.usnip[k]]]["aut","d18O.wt"]), chosen.usnip.mo.index[k])$summer.fraction

	usnip.btsp.siteiter.ssa <- usnip.btsp.siteiter.sumsig - mean(usnip.btsp.siteiter.sumsig)
	usnip.btsp.siteiter$ssa <- usnip.btsp.siteiter.ssa
	usnip.btsp.annual.data[[k]] <- usnip.btsp.siteiter

	usnip.btsp.mean[,k] <- as.numeric(specify.decimal(apply(usnip.btsp.siteiter, 2, mean), 3))
	usnip.btsp.sd[,k] <- as.numeric(specify.decimal(apply(usnip.btsp.siteiter, 2, sd), 3))
	}
rownames(usnip.btsp.mean) <- c("d18O", "prcp", "tavg", "pdo", "mei", "nao", "amo", "pna", "bhi",
	"isotemp.residual", "win.frac", "spr.frac", "sum.frac", "aut.frac", "ssa")
rownames(usnip.btsp.sd) <- c("d18O", "prcp", "tavg", "pdo", "mei", "nao", "amo", "pna", "bhi",
	"isotemp.residual", "win.frac", "spr.frac", "sum.frac", "aut.frac", "ssa")
colnames(usnip.btsp.mean) <- chosen.usnip.mo.index
colnames(usnip.btsp.sd) <- chosen.usnip.mo.index

#write.table(usnip.btsp.mean, "usnip_btsp_means.csv", sep=",", row.names=TRUE, col.names=NA)
#write.table(usnip.btsp.sd, "usnip_btsp_sd.csv", sep=",", row.names=TRUE, col.names=NA)

#=========================================================================
#Weekly chosen USNIP data bootstrapping
#Not used in official analysis, but preserved here for later possible use
usnip.cor.table.btsp.wk <- list()
for (k in 1:length(chosen.usnip.wk.index)) {
```

```
usnip.btsp.siteiter <- data.frame(matrix(nrow=1000, ncol=14))
usnip.btsp.siteiter.ssn.osc <- list()

for (i in 1:1000) {
        fake.yr <- chosen.usnip.wk.data[[k]][sample(nrow(chosen.usnip.wk.data[[k]]), 30, replace=TRUE), ]
        win.data <- fake.yr[(fake.yr$mo == 1 | fake.yr$mo == 2 | fake.yr$mo == 12), ]
        spr.data <- fake.yr[(fake.yr$mo == 3 | fake.yr$mo == 4 | fake.yr$mo == 5), ]
        sum.data <- fake.yr[(fake.yr$mo == 6 | fake.yr$mo == 7 | fake.yr$mo == 8), ]
        aut.data <- fake.yr[(fake.yr$mo == 9 | fake.yr$mo == 10 | fake.yr$mo == 11), ]
        win.frac <- sum(win.data$prcp)/sum(fake.yr$prcp)
        spr.frac <- sum(spr.data$prcp)/sum(fake.yr$prcp)
        sum.frac <- sum(sum.data$prcp)/sum(fake.yr$prcp)
        aut.frac <- sum(aut.data$prcp)/sum(fake.yr$prcp)

        usnip.btsp.siteiter[i,1] <- sum(fake.yr$prcp/sum(fake.yr$prcp) * fake.yr$d18O)
        usnip.btsp.siteiter[i,2] <- sum(fake.yr$prcp)
        usnip.btsp.siteiter[i,3] <- sum(fake.yr$prcp/sum(fake.yr$prcp) * fake.yr$tavg)
        usnip.btsp.siteiter[i,4] <- sum(fake.yr$prcp/sum(fake.yr$prcp) * fake.yr$pdo)
        usnip.btsp.siteiter[i,5] <- sum(fake.yr$prcp/sum(fake.yr$prcp) * fake.yr$mei)
        usnip.btsp.siteiter[i,6] <- sum(fake.yr$prcp/sum(fake.yr$prcp) * fake.yr$nao)
        usnip.btsp.siteiter[i,7] <- sum(fake.yr$prcp/sum(fake.yr$prcp) * fake.yr$awk)
        usnip.btsp.siteiter[i,8] <- sum(fake.yr$prcp/sum(fake.yr$prcp) * fake.yr$pna)
        usnip.btsp.siteiter[i,9] <- sum(fake.yr$prcp/sum(fake.yr$prcp) * fake.yr$bhi)
        usnip.btsp.siteiter[i,10] <- sum(fake.yr$prcp/sum(fake.yr$prcp) * fake.yr$isotemp.residual)
        usnip.btsp.siteiter[i,11] <- win.frac
        usnip.btsp.siteiter[i,12] <- spr.frac
        usnip.btsp.siteiter[i,13] <- sum.frac
        usnip.btsp.siteiter[i,14] <- aut.frac

        #Calculating seasonal oscillation weighted means
        win.fake.iter <- fake.yr[fake.yr$mo == 12 | fake.yr$mo == 1 | fake.yr$mo == 2, ]
        spr.fake.iter <- fake.yr[fake.yr$mo == 3 | fake.yr$mo == 4 | fake.yr$mo == 5, ]
        sum.fake.iter <- fake.yr[fake.yr$mo == 6 | fake.yr$mo == 7 | fake.yr$mo == 8, ]
        aut.fake.iter <- fake.yr[fake.yr$mo == 9 | fake.yr$mo == 10 | fake.yr$mo == 11, ]
```

```
        fake.yr.ssn.osc <- data.frame(matrix(nrow=5, ncol=length(osc.index)))

        for (j in 1:length(osc.index)) {
                fake.yr.ssn.osc[1,j] <- sum(fake.yr[osc.index[j]] * fake.yr$prcp / sum(fake.yr$prcp))
                if(length(win.fake.iter$yr) > 0) {
                        fake.yr.ssn.osc[2,j] <- sum(win.fake.iter$prcp/sum(win.fake.iter$prcp) * win.fake.iter[osc.index[j]])
                        } else {
                        fake.yr.ssn.osc[2,j] <- NA
                        }
                if(length(spr.fake.iter$yr) > 0) {
                        fake.yr.ssn.osc[3,j] <- sum(spr.fake.iter$prcp/sum(spr.fake.iter$prcp) * spr.fake.iter[osc.index[j]])
                        } else {
                        fake.yr.ssn.osc[3,j] <- NA
                        }
                if(length(sum.fake.iter$yr) > 0) {
                        fake.yr.ssn.osc[4,j] <- sum(sum.fake.iter$prcp/sum(sum.fake.iter$prcp) * sum.fake.iter[osc.index[j]])
                        } else {
                        fake.yr.ssn.osc[4,j] <- NA
                        }
                if(length(aut.fake.iter$yr) > 0) {
                        fake.yr.ssn.osc[5,j] <- sum(aut.fake.iter$prcp/sum(aut.fake.iter$prcp) * aut.fake.iter[osc.index[j]])
                        } else {
                        fake.yr.ssn.osc[5,j] <- NA
                        }
                }
        colnames(fake.yr.ssn.osc) <- osc.index
        rownames(fake.yr.ssn.osc) <- c("year", season.index)

        usnip.btsp.siteiter.ssn.osc[[i]] <- fake.yr.ssn.osc
        }

colnames(usnip.btsp.siteiter) <- c("d18O", "prcp", "tavg", "pdo", "mei", "nao", "awk", "pna", "bhi",
        "isotemp.residual", "win.frac", "spr.frac", "sum.frac", "aut.frac")
```

```
usnip.btsp.siteiter.sumsig <- seasonal.fraction(
	(usnip.btsp.siteiter$win.frac * season.lmcor[[arpt.usnip[k]]]["win","d18O.wt"] +
	usnip.btsp.siteiter$spr.frac * season.lmcor[[arpt.usnip[k]]]["spr","d18O.wt"] +
	usnip.btsp.siteiter$sum.frac * season.lmcor[[arpt.usnip[k]]]["sum","d18O.wt"] +
	usnip.btsp.siteiter$aut.frac * season.lmcor[[arpt.usnip[k]]]["aut","d18O.wt"]), chosen.usnip.mo.index[k])$summer.fraction

usnip.btsp.siteiter.ssa <- usnip.btsp.siteiter.sumsig - mean(usnip.btsp.siteiter.sumsig)


#Calculating correlations for bootstrapped d18O and other variables
osc.iter <- list()
usnip.btsp.siteiter.osc.cor.table <- data.frame(matrix(nrow=0, ncol=2))
for (j in 1:length(osc.index)) {
	osc.iter[[1]] <- cor.test(usnip.btsp.siteiter$d18O,
		sapply(usnip.btsp.siteiter.ssn.osc, "[[", osc.index[j])[1,])
	osc.iter[[2]] <- cor.test(usnip.btsp.siteiter$d18O,
		sapply(usnip.btsp.siteiter.ssn.osc, "[[", osc.index[j])[2,])
	osc.iter[[3]] <- cor.test(usnip.btsp.siteiter$d18O,
		sapply(usnip.btsp.siteiter.ssn.osc, "[[", osc.index[j])[3,])
	osc.iter[[4]] <- cor.test(usnip.btsp.siteiter$d18O,
		sapply(usnip.btsp.siteiter.ssn.osc, "[[", osc.index[j])[4,])
	osc.iter[[5]] <- cor.test(usnip.btsp.siteiter$d18O,
		sapply(usnip.btsp.siteiter.ssn.osc, "[[", osc.index[j])[5,])

	osc.cor.table.iter <- data.frame(matrix(nrow=5, ncol=2))
	for (i in 1:5) { # Looping to construct a table of correlations
		osc.cor.table.iter[i,1] <- round(osc.iter[[i]]$estimate, 3)
		osc.cor.table.iter[i,2] <- round(osc.iter[[i]]$p.value, 3)
		}
	colnames(osc.cor.table.iter) <- c("r", "pval")
	rownames(osc.cor.table.iter) <- c(paste(osc.index[j], ".yr", sep=""), paste(osc.index[j], ".win", sep=""),
		paste(osc.index[j], ".spr", sep=""), paste(osc.index[j], ".sum", sep=""),
		paste(osc.index[j], ".aut", sep=""))
```

```
                usnip.btsp.siteiter.osc.cor.table <- rbind(usnip.btsp.siteiter.osc.cor.table, osc.cor.table.iter)
                }

        #Calculating correlations with tavg and ssa
        d18O.btsp.siteiter.cor <- list()
        d18O.btsp.siteiter.cor[[1]] <- cor.test(usnip.btsp.siteiter$d18O, usnip.btsp.siteiter$tavg)
        d18O.btsp.siteiter.cor[[2]] <- cor.test(usnip.btsp.siteiter$d18O, usnip.btsp.siteiter.ssa)

        usnip.btsp.siteiter.wx.cor.table <- data.frame(matrix(nrow=2, ncol=2))
                for (i in 1:2) {
                        usnip.btsp.siteiter.wx.cor.table[i,1] <- round(d18O.btsp.siteiter.cor[[i]]$estimate, 3)
                        usnip.btsp.siteiter.wx.cor.table[i,2] <- round(d18O.btsp.siteiter.cor[[i]]$p.value, 3)
                        }
        colnames(usnip.btsp.siteiter.wx.cor.table) <- c("r", "pval")
        rownames(usnip.btsp.siteiter.wx.cor.table) <- c("tavg", "ssa")

        #Combining oscillation index and weather correlations into single table, sorting by r value
        usnip.cor.table.btsp.siteiter <- rbind(usnip.btsp.siteiter.wx.cor.table, usnip.btsp.siteiter.osc.cor.table)
        usnip.cor.table.btsp.siteiter <- usnip.cor.table.btsp.siteiter[order(-abs(usnip.cor.table.btsp.siteiter$r)),]

        usnip.cor.table.btsp.wk[[k]] <- usnip.cor.table.btsp.siteiter
        }
names(usnip.cor.table.btsp.wk) <- chosen.usnip.wk.index

#=============================================================================================================================
#--------------------Calcite d18O Estimate-----------------------------
#This function calculates the d18O of calcite from a known temperature
#and initial water d18O based on Kim & O'Neil 1997. The output is
#d18O vs. VPDB
#WARNING: The temperature must be in Kelvin
#WARNING: d18O.H20 is entered as VSMOW
#NOTE: Modern Indiana Caverns temperature = 13.4 C (286.55 K)
#NOTE: Modern Indianapolis temperature = 11.7 C (284.85 K)
```

```
calculate.calcite.d18O <- function(temp, d18O.H2O) {
        d18O.calc <- (-1000 + (1000 + d18O.H2O) * exp(((18.03 * 10^3 / temp)
                - 32.42) / 1000)) * 0.97002 - 29.98
        return(d18O.calc)
        }

#=============================================================================================================
#=========================================Stalagmite Analysis=================================================
#=============================================================================================================
#StalAge Scripts for Upper Porter stalagmites
#NOTE: NEEDS STALAGE SCRIPT RAN PREVIOUSLY
Daten_orig <- read.table("up3_ages.csv", header=TRUE, sep=",")
Daten_orig <- Daten_orig[-5,] #Removing age that doesn't fit linear trend
attach(Daten_orig)
depths.uvl <- read.table("up3_uvldepths.csv", header=TRUE, sep=",")
attach(depths.uvl) #make sure depth header is different from Daten_orig header
depths.refl <- read.table("up3_refldepths.csv", header=TRUE, sep=",")
attach(depths.refl) #make sure depth header is different from Daten_orig header
depths.iso <- read.table("up3_isodepths.csv", header=TRUE, sep=",")
attach(depths.iso) #make sure depth header is different from Daten_orig header
Daten <- scan(depth, age, error)
Daten <-scan_fine(Daten)
fit <- age_model(Daten, d.uvl)
write.table(fit, file="up3_uvl.csv", sep=",")
fit <- age_model(Daten, d.refl)
write.table(fit, file="up3_refl.csv", sep=",")
fit <- age_model(Daten, d.iso)
write.table(fit, file="up3_iso.csv", sep=",")

plot(fit$y, depths$lum, type="l")


#Plotting image for UP4 linear hiatus model
```

```
up4.ages <- read.table("up4_ages.csv", header=TRUE, sep=",")

dev.new(height=8, width=8)
plot(up4.ages$depth, up4.ages$age, xlim=c(0,320), ylim=c(1800, 9000), type="n",
        bty="n", xaxt="n", yaxt="n", xlab="", ylab="")
points(up4.ages$depth, up4.ages$age, pch=16)
axis(2, at=seq(2000, 9000, 1000), pos=0, las=1, col="black", col.axis="black", cex.axis=1.4)
#axis(2, at=seq(1800, 9000, 200), pos=0, las=1, col="black", col.axis="black", labels=FALSE, tck=-0.01)
axis(1, at=seq(0, 300, 50), pos=1800, cex.axis=1.4)
#axis(1, at=seq(0, 300, 10), pos=1800, labels=FALSE, tck=-0.01)
mtext(side=1, "Depth (mm)", line=2, cex=1.5)
mtext(side=2, "Age (cal yr BP)", line=3, cex=1.5, col="black")
#text(x=-0.18, y=-2.5, pos=4, "Consecutive 12-Month", cex=1.8)

abline(v=105.5)
abline(v=145.5)
abline(v=211.5)
abline(v=231)
abline(a=2282.4, b=3.8322)
abline(a=2561, b=3.4356)
abline(a=2196.1, b=9.4772)
abline(a=2688.8, b=9.4772)
abline(a=4923.9, b=11.36)

#UP4 Plotting Script
#Written by Pete D. Akers, September 2015
#Worked again March 2016
up4.iso <- read.table("up4_iso.csv", header=TRUE, sep=",")
up4.iso <- up4.iso[-c(787,791),] #Removing two missing data
up4.uvl <- read.table("up4_uvl.csv", header=TRUE, sep=",")
up4.refl <- read.table("up4_refl.csv", header=TRUE, sep=",")

up3.iso <- read.table("up3_iso.csv", header=TRUE, sep=",")
up3.uvl <- read.table("up3_uvl.csv", header=TRUE, sep=",")
```

```
up3.refl <- read.table("up3_refl.csv", header=TRUE, sep=",")

#Making moving average datasets
moving.avg <- function(time.series, points) {
        filter(time.series, rep(1/points,points), sides=2)
        }

#UP4-----------------------------
#Per 5
up4.iso.5pt <- data.frame(moving.avg(up4.iso$d13C,5), moving.avg(up4.iso$d18O,5))
colnames(up4.iso.5pt) <- c("d13C", "d18O")
up4.uvl.5pt <- data.frame(moving.avg(up4.uvl$uvl,5))
colnames(up4.uvl.5pt) <- c("uvl")
up4.refl.5pt <- data.frame(moving.avg(up4.refl$refl,5))
colnames(up4.refl.5pt) <- c("refl")
#Per 10
up4.iso.10pt <- data.frame(moving.avg(up4.iso$d13C,10), moving.avg(up4.iso$d18O,10))
colnames(up4.iso.10pt) <- c("d13C", "d18O")
up4.uvl.10pt <- data.frame(moving.avg(up4.uvl$uvl,10))
colnames(up4.uvl.10pt) <- c("uvl")
up4.refl.10pt <- data.frame(moving.avg(up4.refl$refl,10))
colnames(up4.refl.10pt) <- c("refl")
#Per 30
up4.iso.30pt <- data.frame(moving.avg(up4.iso$d13C,30), moving.avg(up4.iso$d18O,30))
colnames(up4.iso.30pt) <- c("d13C", "d18O")
up4.uvl.30pt <- data.frame(moving.avg(up4.uvl$uvl,30))
colnames(up4.uvl.30pt) <- c("uvl")
up4.refl.30pt <- data.frame(moving.avg(up4.refl$refl,30))
colnames(up4.refl.30pt) <- c("refl")
#Per 40
up4.iso.40pt <- data.frame(moving.avg(up4.iso$d13C,40), moving.avg(up4.iso$d18O,40))
colnames(up4.iso.40pt) <- c("d13C", "d18O")
up4.uvl.40pt <- data.frame(moving.avg(up4.uvl$uvl,40))
colnames(up4.uvl.40pt) <- c("uvl")
```

```
up4.refl.40pt <- data.frame(moving.avg(up4.refl$refl,40))
colnames(up4.refl.40pt) <- c("refl")
#Per 60
up4.refl.60pt <- data.frame(moving.avg(up4.refl$refl,60))
colnames(up4.refl.60pt) <- c("refl")
#Per 100
up4.refl.100pt <- data.frame(moving.avg(up4.refl$refl,100))
colnames(up4.refl.100pt) <- c("refl")


#UP3------------------------------
#Per 5
up3.iso.5pt <- data.frame(moving.avg(up3.iso$d13C,5), moving.avg(up3.iso$d18O,5))
colnames(up3.iso.5pt) <- c("d13C", "d18O")
up3.uvl.5pt <- data.frame(moving.avg(up3.uvl$uvl,5))
colnames(up3.uvl.5pt) <- c("uvl")
up3.refl.5pt <- data.frame(moving.avg(up3.refl$refl,5))
colnames(up3.refl.5pt) <- c("refl")
#Per 10
up3.iso.10pt <- data.frame(moving.avg(up3.iso$d13C,10), moving.avg(up3.iso$d18O,10))
colnames(up3.iso.10pt) <- c("d13C", "d18O")
up3.uvl.10pt <- data.frame(moving.avg(up3.uvl$uvl,10))
colnames(up3.uvl.10pt) <- c("uvl")
up3.refl.10pt <- data.frame(moving.avg(up3.refl$refl,10))
colnames(up3.refl.10pt) <- c("refl")
#Per 30
up3.iso.30pt <- data.frame(moving.avg(up3.iso$d13C,30), moving.avg(up3.iso$d18O,30))
colnames(up3.iso.30pt) <- c("d13C", "d18O")
up3.uvl.30pt <- data.frame(moving.avg(up3.uvl$uvl,30))
colnames(up3.uvl.30pt) <- c("uvl")
up3.refl.30pt <- data.frame(moving.avg(up3.refl$refl,30))
colnames(up3.refl.30pt) <- c("refl")
#Per 40
up3.iso.40pt <- data.frame(moving.avg(up3.iso$d13C,40), moving.avg(up3.iso$d18O,40))
```

```
colnames(up3.iso.40pt) <- c("d13C", "d18O")
up3.uvl.40pt <- data.frame(moving.avg(up3.uvl$uvl,40))
colnames(up3.uvl.40pt) <- c("uvl")
up3.refl.40pt <- data.frame(moving.avg(up3.refl$refl,40))
colnames(up3.refl.40pt) <- c("refl")
#Per 60
up3.refl.60pt <- data.frame(moving.avg(up3.refl$refl,60))
colnames(up3.refl.60pt) <- c("refl")
#Per 100
up3.refl.100pt <- data.frame(moving.avg(up3.refl$refl,100))
colnames(up3.refl.100pt) <- c("refl")


#=============================================================================================================
#=============================================UP4============================================================
#d18O time series
dev.new(height=5,width=12)
plot(up4.iso$age, up4.iso$d18O, type="n", bty="n", xaxt="n", yaxt="n",
     xlab="", ylab="", xlim=c(2000,9000), ylim=c(-6.6, -3.8))
points(up4.iso$age, up4.iso$d18O, type="l", col=adjustcolor("steelblue4", alpha=0.4), lwd=1.0)
#points(up4.iso$age, up4.iso.5pt$d18O, type="l", col="steelblue4", lwd=2)
points(up4.iso$age, up4.iso.10pt$d18O, type="l", col="steelblue4", lwd=1.75)
#points(up4.iso$age, up4.iso.30pt$d18O, type="l", col="steelblue4", lwd=1.75)
axis(2, at=seq(-6, -4, 1), pos=2000, las=1, col="steelblue4",
     col.axis="steelblue4", cex.axis=1.4)
axis(2, at=seq(-6.6, -3.8, 0.2), pos=2000, las=1, col="steelblue4",
     col.axis="steelblue4", labels=FALSE, tck=-0.01)
axis(1, at=seq(2000,9000,1000), pos=-6.6, cex.axis=1.4)
axis(1, at=seq(2000,9000,500), pos=-6.6, labels=FALSE, tck=-0.01)
mtext(side=1, "Age (cal yr BP)", line=2, cex=1.8)
mtext(side=2, expression(paste({delta}^18*O, " (‰ vs. V-PDB)")),
     line=.3, cex=1.6, col="steelblue4")

#d13C time series
```

```
dev.new(height=5,width=12)
plot(up4.iso$age, up4.iso$d13C, type="n", bty="n", xaxt="n", yaxt="n",
        xlab="", ylab="", xlim=c(2000,9000), ylim=c(-11, -5))
points(up4.iso$age, up4.iso$d13C, type="l", col=adjustcolor("firebrick", alpha=0.4), lwd=1.0)
points(up4.iso$age, up4.iso.10pt$d13C, type="l", col="firebrick", lwd=1.75)
axis(4, at=seq(-11, -5, 2), pos=9000, las=1, col="firebrick",
        col.axis="firebrick", cex.axis=1.4)
axis(4, at=seq(-11, -5, 1), pos=9000, las=1, col="firebrick",
        col.axis="firebrick", labels=FALSE, tck=-0.01)
mtext(side=4, expression(paste({delta}^13*C, " (‰ vs. V-PDB)")),
        line=.8, cex=1.6, col="firebrick")

#uvl time series
dev.new(height=5,width=12)
plot(up4.uvl$age, up4.uvl$uvl, type="n", bty="n", xaxt="n", yaxt="n",
        xlab="", ylab="", xlim=c(2000,9000), ylim=c(255, 0))
points(up4.uvl$age, up4.uvl$uvl, type="l", col=adjustcolor("olivedrab", alpha=0.4), lwd=1.0)
points(up4.uvl$age, up4.uvl.30pt$uvl, type="l", col="olivedrab", lwd=1.75)
axis(2, at=seq(250, 0, -100), pos=2000, las=1, col="olivedrab",
        col.axis="olivedrab", cex.axis=1.4)
axis(2, at=seq(250, 0, -25), pos=2000, las=1, col="olivedrab",
        col.axis="olivedrab", labels=FALSE, tck=-0.01)
mtext(side=2, text="Luminescence Pixel Intensity", line=1, cex=1.6,
        col="olivedrab", at=125)

#refl time series
dev.new(height=5,width=12)
plot(up4.refl$age, up4.refl$refl, type="n", bty="n", xaxt="n", yaxt="n",
        xlab="", ylab="", xlim=c(2000,9000), ylim=c(255, 0))
points(up4.refl$age, up4.refl$refl, type="l", col=adjustcolor("mediumorchid4", alpha=0.4), lwd=1.0)
points(up4.refl$age, up4.refl.100pt$refl, type="l", col="mediumorchid4", lwd=1.75)
axis(4, at=seq(250, 0, -100), pos=9000, las=1, col="mediumorchid4",
        col.axis="mediumorchid4", cex.axis=1.4)
axis(4, at=seq(250, 0, -25), pos=9000, las=1, col="mediumorchid4",
```

```
        col.axis="mediumorchid4", labels=FALSE, tck=-0.01)
mtext(side=4, text="Reflectance Pixel Intensity", line=1, cex=1.6,
        col="mediumorchid4", at=125)



#----------------------UP4 Correlations
up4.iso.nogap <- na.omit(up4.iso)
num.iso <- length(up4.iso.nogap$age)
up4.uvl.nogap <- na.omit(up4.uvl)
up4.refl.nogap <- na.omit(up4.refl)

#Averaging UV-Luminescence data to match isotope sampling interval
up4.uvl.cndn <- NULL #cndn = condensed
for (i in 1:num.iso) {
up4.uvl.cndn[i] <- mean(up4.uvl.nogap[up4.uvl.nogap$age < up4.iso.nogap$age[i] &
        up4.uvl.nogap$age >= up4.iso.nogap$age[i+1], 3])
}

#Averaging reflectance data to match isotope sampling interval
up4.refl.cndn <- NULL
for (i in 1:num.iso) {
up4.refl.cndn[i] <- mean(up4.refl.nogap[up4.refl.nogap$age < up4.iso.nogap$age[i] &
        up4.refl.nogap$age >= up4.iso.nogap$age[i+1], 3])
}


#Spearman Correlation Tests
cor.d18O.d13C <- cor.test(up4.iso.nogap$d18O, up4.iso.nogap$d13C, method="spearman")
cor.uvl.d18O <- cor.test(up4.uvl.cndn, up4.iso.nogap$d18O, method="spearman")
cor.uvl.d13C <- cor.test(up4.uvl.cndn, up4.iso.nogap$d13C, method="spearman")
cor.refl.d18O <- cor.test(up4.refl.cndn, up4.iso.nogap$d18O, method="spearman")
cor.refl.d13C <- cor.test(up4.refl.cndn, up4.iso.nogap$d13C, method="spearman")
cor.refl.uvl <- cor.test(up4.refl.cndn, up4.uvl.cndn, method="spearman")
```

```
#=================================================================================================
#=============================================UP3=================================================
#UP3 d18O time series
dev.new(height=5,width=12)
plot(up3.iso$age, up3.iso$d18O, type="n", bty="n", xaxt="n", yaxt="n",
     xlab="", ylab="", xlim=c(7300,8600), ylim=c(-6.6, -3.8))
points(up3.iso$age, up3.iso$d18O, type="l", col="steelblue4", lwd=1.75)
#points(up3.iso$age, up3.iso.5pt$d18O, type="l", col="steelblue4", lwd=2)
#points(up3.iso$age, up3.iso.10pt$d18O, type="l", col="steelblue4", lwd=1.75)
#points(up3.iso$age, up3.iso.30pt$d18O, type="l", col="steelblue4", lwd=1.75)
axis(2, at=seq(-6, -3.8, 1), pos=7300, las=1, col="steelblue4",
     col.axis="steelblue4", cex.axis=1.4)
axis(2, at=seq(-6.6, -3.8, 0.2), pos=7300, las=1, col="steelblue4",
     col.axis="steelblue4", labels=FALSE, tck=-0.01)
axis(1, at=seq(7400,8600,200), pos=-6.6, cex.axis=1.4)
axis(1, at=seq(7300,8600,100), pos=-6.6, labels=FALSE, tck=-0.01)
mtext(side=1, "Age (cal yr BP)", line=2.5, cex=1.8)
mtext(side=2, expression(paste({delta}^18*O, " (‰ vs. V-PDB)")),
     line=0.6, cex=1.6, col="steelblue4")

#UP3 d13C time series
dev.new(height=5,width=12)
plot(up3.iso$age, up3.iso$d13C, type="n", bty="n", xaxt="n", yaxt="n",
     xlab="", ylab="", xlim=c(7300,8600), ylim=c(-11, -5))
points(up3.iso$age, up3.iso$d13C, type="l", col="firebrick", lwd=1.75)
axis(4, at=seq(-11, -5, 2), pos=8600, las=1, col="firebrick",
     col.axis="firebrick", cex.axis=1.4)
axis(4, at=seq(-11, -5, 1), pos=8600, las=1, col="firebrick",
     col.axis="firebrick", labels=FALSE, tck=-0.01)
mtext(side=4, expression(paste({delta}^13*C, " (‰ vs. V-PDB)")),
     line=.8, cex=1.6, col="firebrick")

#UP3 uvl time series
```

```
dev.new(height=5,width=12)
plot(up3.uvl$age, up3.uvl$uvl, type="n", bty="n", xaxt="n", yaxt="n",
        xlab="", ylab="", xlim=c(7300,8600), ylim=c(255, 0))
points(up3.uvl$age, up3.uvl$uvl, type="l", col=adjustcolor("olivedrab", alpha=0.4), lwd=1.0)
points(up3.uvl$age, up3.uvl.30pt$uvl, type="l", col="olivedrab", lwd=1.75)
axis(2, at=seq(250, 0, -100), pos=7300, las=1, col="olivedrab",
        col.axis="olivedrab", cex.axis=1.4)
axis(2, at=seq(250, 0, -25), pos=7300, las=1, col="olivedrab",
        col.axis="olivedrab", labels=FALSE, tck=-0.01)
mtext(side=2, text="Luminescence Pixel Intensity", line=1, cex=1.6,
        col="olivedrab", at=125)
abline(v=7321)
abline(v=7407)
abline(v=7522)
abline(v=7629)
abline(v=7884)
abline(v=8104)

#UP3 refl time series
dev.new(height=5,width=12)
plot(up3.refl$age, up3.refl$refl, type="n", bty="n", xaxt="n", yaxt="n",
        xlab="", ylab="", xlim=c(7300,8600), ylim=c(255, 0))
points(up3.refl$age, up3.refl$refl, type="l", col=adjustcolor("mediumorchid4", alpha=0.4), lwd=1.0)
points(up3.refl$age, up3.refl.100pt$refl, type="l", col="mediumorchid4", lwd=1.75)
axis(4, at=seq(250, 0, -100), pos=8600, las=1, col="mediumorchid4",
        col.axis="mediumorchid4", cex.axis=1.4)
axis(4, at=seq(250, 0, -25), pos=8600, las=1, col="mediumorchid4",
        col.axis="mediumorchid4", labels=FALSE, tck=-0.01)
mtext(side=4, text="Reflectance Pixel Intensity", line=1, cex=1.6,
        col="mediumorchid4", at=125)
abline(v=7321)
abline(v=7407)
abline(v=7522)
abline(v=7629)
```

```
abline(v=7884)
abline(v=8104)

#UP4 LENGTH series-----------------------------
#UP3 d18O time series UP4 LENGTH
dev.new(height=5,width=12)
plot(up3.iso$age, up3.iso$d18O, type="n", bty="n", xaxt="n", yaxt="n",
        xlab="", ylab="", xlim=c(2000,9000), ylim=c(-6.6, -3.8))
points(up3.iso$age, up3.iso$d18O, type="l", col="steelblue4", lwd=1.75)
axis(2, at=seq(-6, -4, 1), pos=2000, las=1, col="steelblue4",
        col.axis="steelblue4", cex.axis=1.4)
axis(2, at=seq(-6.6, -3.8, 0.2), pos=2000, las=1, col="steelblue4",
        col.axis="steelblue4", labels=FALSE, tck=-0.01)
axis(1, at=seq(2000,9000,1000), pos=-6.6, cex.axis=1.4)
axis(1, at=seq(2000,9000,500), pos=-6.6, labels=FALSE, tck=-0.01)
mtext(side=1, "Age (cal yr BP)", line=2, cex=1.6)
mtext(side=2, expression(paste({delta}^18*O, " (‰ vs. V-PDB)")),
        line=.3, cex=1.6, col="steelblue4")

#UP3 d13C time series UP4 LENGTH
dev.new(height=5,width=12)
plot(up3.iso$age, up3.iso$d13C, type="n", bty="n", xaxt="n", yaxt="n",
        xlab="", ylab="", xlim=c(2000,9000), ylim=c(-11, -5))
points(up3.iso$age, up3.iso$d13C, type="l", col="firebrick", lwd=1.75)
axis(4, at=seq(-11, -5, 2), pos=9000, las=1, col="firebrick",
        col.axis="firebrick", cex.axis=1.4)
axis(4, at=seq(-11, -5, 1), pos=9000, las=1, col="firebrick",
        col.axis="firebrick", labels=FALSE, tck=-0.01)
mtext(side=4, expression(paste({delta}^13*C, " (‰ vs. V-PDB)")),
        line=.8, cex=1.6, col="firebrick")



#UP3 uvl time series UP4 LENGTH
```

```
dev.new(height=5,width=12)
plot(up3.uvl$age, up3.uvl$uvl, type="n", bty="n", xaxt="n", yaxt="n",
        xlab="", ylab="", xlim=c(2000,9000), ylim=c(255, 0))
points(up3.uvl$age, up3.uvl$uvl, type="l", col=adjustcolor("olivedrab", alpha=0.4), lwd=1.0)
points(up3.uvl$age, up3.uvl.30pt$uvl, type="l", col="olivedrab", lwd=1.75)
axis(2, at=seq(250, 0, -100), pos=2000, las=1, col="olivedrab",
        col.axis="olivedrab", cex.axis=1.4)
axis(2, at=seq(250, 0, -25), pos=2000, las=1, col="olivedrab",
        col.axis="olivedrab", labels=FALSE, tck=-0.01)
mtext(side=2, text="Luminescence Pixel Intensity", line=1, cex=1.6,
        col="olivedrab", at=125)

#UP3 refl time series UP4 LENGTH
dev.new(height=5,width=12)
plot(up3.refl$age, up3.refl$refl, type="n", bty="n", xaxt="n", yaxt="n",
        xlab="", ylab="", xlim=c(2000,9000), ylim=c(255, 0))
points(up3.refl$age, up3.refl$refl, type="l", col=adjustcolor("mediumorchid4", alpha=0.4), lwd=1.0)
points(up3.refl$age, up3.refl.100pt$refl, type="l", col="mediumorchid4", lwd=1.75)
axis(4, at=seq(250, 0, -100), pos=9000, las=1, col="mediumorchid4",
        col.axis="mediumorchid4", cex.axis=1.4)
axis(4, at=seq(250, 0, -25), pos=9000, las=1, col="mediumorchid4",
        col.axis="mediumorchid4", labels=FALSE, tck=-0.01)
mtext(side=4, text="Reflectance Pixel Intensity", line=1, cex=1.6,
        col="mediumorchid4", at=125)



#----------------------UP3 Correlations
up3.iso.nogap <- na.omit(up3.iso)
num.iso <- length(up3.iso.nogap$age)
up3.uvl.nogap <- na.omit(up3.uvl)
up3.refl.nogap <- na.omit(up3.refl)

#Averaging UV-Luminescence data to match isotope sampling interval
```

```
up3.uvl.cndn <- NULL #cndn = condensed
for (i in 1:num.iso) {
up3.uvl.cndn[i] <- mean(up3.uvl.nogap[up3.uvl.nogap$age < up3.iso.nogap$age[i] &
        up3.uvl.nogap$age >= up3.iso.nogap$age[i+1], 5])
}

#Averaging reflectance data to match isotope sampling interval
up3.refl.cndn <- NULL
for (i in 1:num.iso) {
up3.refl.cndn[i] <- mean(up3.refl.nogap[up3.refl.nogap$age < up3.iso.nogap$age[i] &
        up3.refl.nogap$age >= up3.iso.nogap$age[i+1], 5])
}


#Spearman Correlation Tests
cor.d18O.d13C <- cor.test(up3.iso.nogap$d18O, up3.iso.nogap$d13C, method="spearman")
cor.uvl.d18O <- cor.test(up3.uvl.cndn, up3.iso.nogap$d18O, method="spearman")
cor.uvl.d13C <- cor.test(up3.uvl.cndn, up3.iso.nogap$d13C, method="spearman")
cor.refl.d18O <- cor.test(up3.refl.cndn, up3.iso.nogap$d18O, method="spearman")
cor.refl.d13C <- cor.test(up3.refl.cndn, up3.iso.nogap$d13C, method="spearman")
cor.refl.uvl <- cor.test(up3.refl.cndn, up3.uvl.cndn, method="spearman")


#------------------------------UP4 Tone and Clarity Isotope Relationships------------------
up4.petro.alldata <- read.table("up4_iso.csv", sep=",", header=TRUE)
up4.petro.alldata <- na.omit(up4.petro.alldata)
tone.index <- c("vd", "d-vd", "d", "m-d", "m", "m-l", "l", "l-vl", "vl")
tone.d13C.color.index <- c("darkred", "firebrick4", "firebrick", "firebrick3", "firebrick2", "firebrick1",
        "brown1", "indianred1", "palevioletred1")
tone.d18O.color.index <- c("midnightblue", "navy", "royalblue4", "steelblue4", "steelblue", "steelblue3",
        "steelblue2", "steelblue1", "skyblue")
clarity.index <- c("o", "o-pt", "pt", "t-pt", "t")
clarity.d13C.color.index <- c("firebrick4", "firebrick", "firebrick3", "firebrick2", "firebrick1")
clarity.d18O.color.index <- c("steelblue4", "steelblue", "steelblue3", "steelblue2", "steelblue1")
```

```
clarity.color.index <- ("steelblue4")
up4.index <- c("all", "8ka", "5ka", "4ka", "3ka", "2ka")

up4.petro <- up4.petro.alldata[up4.petro.alldata$tone != 'dlvd', ]
up4.petro <- up4.petro[up4.petro$tone != 'ld', ]
up4.petro <- up4.petro[up4.petro$tone != 'vdl', ]
up4.petro <- up4.petro[up4.petro$tone != 'dvl', ]
up4.petro$tone[up4.petro$tone == "mvd"] <- "md"
up4.petro$tone[up4.petro$tone == "mvl"] <- "ml"
up4.petro$tone[up4.petro$tone == "lm"] <- "ml"
up4.petro$clarity[up4.petro$clarity == "ot"] <- "tpt"

#Splitting UP4 by growth period
up4.petro.8ka <- up4.petro[up4.petro$age < 8600 & up4.petro$age > 7400, ]
up4.petro.5ka <- up4.petro[up4.petro$age < 5000 & up4.petro$age > 4600, ]
up4.petro.4ka <- up4.petro[up4.petro$age < 4300 & up4.petro$age > 3500, ]
up4.petro.3ka <- up4.petro[up4.petro$age < 3200 & up4.petro$age > 2800, ]
up4.petro.2ka <- up4.petro[up4.petro$age < 2800 & up4.petro$age > 2200, ]

#A list of all the various parts of UP4
up4.petro.list <- list(up4.petro, up4.petro.8ka, up4.petro.5ka, up4.petro.4ka,
        up4.petro.3ka, up4.petro.2ka)
names(up4.petro.list) <- up4.index

#Calculating means and sd for stable isotopes per growth period
tone.petro.list <- list()
clarity.petro.list <- list()
for(i in 1:length(up4.index)) {
        tone.length.iter <- aggregate(up4.petro.list[[i]][ , 4:5], list(up4.petro.list[[i]]$tone), length)
        tone.mean.iter <- aggregate(up4.petro.list[[i]][ , 4:5], list(up4.petro.list[[i]]$tone), mean)
        tone.sd.iter <- aggregate(up4.petro.list[[i]][ , 4:5], list(up4.petro.list[[i]]$tone), sd)
        tone.petro.list[[i]] <- data.frame(tone.length.iter[,c(1,3)], tone.mean.iter[,2:3], tone.sd.iter[,2:3])
        tone.petro.list[[i]][, 3:6] <- round(tone.petro.list[[i]][, 3:6], 2)
        colnames(tone.petro.list[[i]]) <- c("tone", "n", "d13C.mean", "d18O.mean", "d13C.sd", "d18O.sd")
```

```
        clarity.length.iter <- aggregate(up4.petro.list[[i]][ , 4:5], list(up4.petro.list[[i]]$clarity), length)
        clarity.mean.iter <- aggregate(up4.petro.list[[i]][ , 4:5], list(up4.petro.list[[i]]$clarity), mean)
        clarity.sd.iter <- aggregate(up4.petro.list[[i]][ , 4:5], list(up4.petro.list[[i]]$clarity), sd)
        clarity.petro.list[[i]] <- data.frame(clarity.length.iter[,c(1,3)], clarity.mean.iter[,2:3], clarity.sd.iter[,2:3])
        clarity.petro.list[[i]][, 3:6] <- round(clarity.petro.list[[i]][, 3:6], 2)
        colnames(clarity.petro.list[[i]]) <- c("clarity", "n", "d13C.mean", "d18O.mean", "d13C.sd", "d18O.sd")
        }
names(tone.petro.list) <- up4.index
names(clarity.petro.list) <- up4.index

#write.table(rbind(tone.petro.list[[1]], tone.petro.list[[2]], tone.petro.list[[3]],
        tone.petro.list[[4]], tone.petro.list[[5]], tone.petro.list[[6]]), "up4_tone_iso.csv",
        sep=",", row.names=TRUE, col.names=NA)
#write.table(rbind(clarity.petro.list[[1]], clarity.petro.list[[2]], clarity.petro.list[[3]],
        clarity.petro.list[[4]], clarity.petro.list[[5]], clarity.petro.list[[6]]), "up4_clarity_iso.csv",
        sep=",", row.names=TRUE, col.names=NA)

for(i in 1:length(up4.index)) {
        #d13C tone
        dev.new(height=6, width=10)
        stripchart(up4.petro.list[[i]]$d13C~factor(up4.petro.list[[i]]$tone, levels=tone.index),
                col=adjustcolor(tone.d13C.color.index, alpha=0.5), pch=15, ylab="", axes=FALSE,
                vertical=TRUE, ylim=c(-12,-5), cex=1.8)
        points(factor(tone.petro.list[[i]]$tone, levels=tone.index), tone.petro.list[[i]]$d13C.mean,
                pch=23, cex=3.5, col="black", lwd=2.5, bg=adjustcolor("yellow", alpha=0.6))
        axis(2, at=seq(-12, -5, 3), las=1, cex.axis=1.5)
        axis(2, at=seq(-12, -5, 1),labels=FALSE, tck=-0.01)
        axis(1, at=(1:length(tone.index)), labels=toupper(tone.index), cex.axis=1.5)
        mtext(side=2, expression(paste({delta}^13*C, " (‰ vs. V-PDB)")),
                line=2, cex=1.8)
        mtext(side=1, "Tone", line=3, cex=1.8)
        text(x=1, y=-5.5, labels=up4.index[i], cex=1.8, pos=4)
```

```
#d18O tone
dev.new(height=6, width=10)
stripchart(up4.petro.list[[i]]$d18O~factor(up4.petro.list[[i]]$tone, levels=tone.index),
        col=adjustcolor(tone.d18O.color.index, alpha=0.5), pch=15, ylab="", axes=FALSE,
        vertical=TRUE, ylim=c(-6.5,-4), cex=1.8,)
points(factor(tone.petro.list[[i]]$tone, levels=tone.index), tone.petro.list[[i]]$d18O.mean,
        pch=23, cex=3.5, col="black", lwd=2.5, bg=adjustcolor("yellow", alpha=0.6))
axis(2, at=seq(-6, -4, 1), las=1, cex.axis=1.5)
axis(2, at=seq(-6.5, -4, 0.5),labels=FALSE, tck=-0.01)
axis(1, at=(1:length(tone.index)), labels=toupper(tone.index), cex.axis=1.5)
mtext(side=2, expression(paste({delta}^18*O, " (‰ vs. V-PDB)")),
        line=2, cex=1.8)
mtext(side=1, "Tone", line=3, cex=1.8)
text(x=1, y=-4.2, labels=up4.index[i], cex=1.8, pos=4)

#d13C clarity
dev.new(height=6, width=6)
stripchart(up4.petro.list[[i]]$d13C~factor(up4.petro.list[[i]]$clarity, levels=clarity.index),
        col=adjustcolor(clarity.d13C.color.index, alpha=0.5), pch=15, ylab="", axes=FALSE,
        vertical=TRUE, ylim=c(-12,-5), cex=1.8)
points(factor(clarity.petro.list[[i]]$clarity, levels=clarity.index), clarity.petro.list[[i]]$d13C.mean,
        pch=23, cex=3.5, col="black", lwd=2.5, bg=adjustcolor("yellow", alpha=0.6))
axis(2, at=seq(-12, -5, 3), las=1, cex.axis=1.5)
axis(2, at=seq(-12, -5, 1),labels=FALSE, tck=-0.01)
axis(1, at=(1:length(clarity.index)), labels=toupper(clarity.index), cex.axis=1.5)
mtext(side=2, expression(paste({delta}^13*C, " (‰ vs. V-PDB)")),
        line=2, cex=1.8)
mtext(side=1, "Clarity", line=3, cex=1.8)
text(x=1, y=-5.5, labels=up4.index[i], cex=1.8, pos=4)

#d18O clarity
dev.new(height=6, width=6)
stripchart(up4.petro.list[[i]]$d18O~factor(up4.petro.list[[i]]$clarity, levels=clarity.index),
        col=adjustcolor(clarity.d18O.color.index, alpha=0.5), pch=15, ylab="", axes=FALSE,
```

```
            vertical=TRUE, ylim=c(-6.5,-4), cex=1.8,)
        points(factor(clarity.petro.list[[i]]$clarity, levels=clarity.index), clarity.petro.list[[i]]$d18O.mean,
            pch=23, cex=3.5, col="black", lwd=2.5, bg=adjustcolor("yellow", alpha=0.6))
        axis(2, at=seq(-6, -4, 1), las=1, cex.axis=1.5)
        axis(2, at=seq(-6.5, -4, 0.5),labels=FALSE, tck=-0.01)
        axis(1, at=(1:length(clarity.index)), labels=toupper(clarity.index), cex.axis=1.5)
        mtext(side=2, expression(paste({delta}^18*O, " (‰ vs. V-PDB)")),
            line=2, cex=1.8)
        mtext(side=1, "Clarity", line=3, cex=1.8)
        text(x=1, y=-4.2, labels=up4.index[i], cex=1.8, pos=4)
        }



#--------------------UP4 Correlations for early Holocene only
up4.petro.8ka.nogap <- na.omit(up4.petro.8ka)
num.iso <- length(up4.petro.8ka.nogap$age)
up4.uvl.nogap <- na.omit(up4.uvl)
up4.refl.nogap <- na.omit(up4.refl)

#Averaging UV-Luminescence data to match isotope sampling interval
up4.uvl.cndn <- NULL #cndn = condensed
for (i in 1:num.iso) {
up4.uvl.cndn[i] <- mean(up4.uvl.nogap[up4.uvl.nogap$age < up4.petro.8ka.nogap$age[i] &
        up4.uvl.nogap$age >= up4.petro.8ka.nogap$age[i+1], 3])
}

#Averaging reflectance data to match isotope sampling interval
up4.refl.cndn <- NULL
for (i in 1:num.iso) {
up4.refl.cndn[i] <- mean(up4.refl.nogap[up4.refl.nogap$age < up4.petro.8ka.nogap$age[i] &
        up4.refl.nogap$age >= up4.petro.8ka.nogap$age[i+1], 3])
}
```

```
#Spearman Correlation Tests
cor.d18O.d13C <- cor.test(up4.petro.8ka.nogap$d18O, up4.petro.8ka.nogap$d13C, method="spearman")
cor.uvl.d18O <- cor.test(up4.uvl.cndn, up4.petro.8ka.nogap$d18O, method="spearman")
cor.uvl.d13C <- cor.test(up4.uvl.cndn, up4.petro.8ka.nogap$d13C, method="spearman")
cor.refl.d18O <- cor.test(up4.refl.cndn, up4.petro.8ka.nogap$d18O, method="spearman")
cor.refl.d13C <- cor.test(up4.refl.cndn, up4.petro.8ka.nogap$d13C, method="spearman")
cor.refl.uvl <- cor.test(up4.refl.cndn, up4.uvl.cndn, method="spearman")

#----------Calculating means per section--------------
up4.d18O.means <- NA
up4.d13C.means <- NA
for(i in 1:length(up4.index)) {
        up4.d18O.means[i] <- mean(up4.petro.list[[i]]$d18O)
        up4.d13C.means[i] <- mean(up4.petro.list[[i]]$d13C)
        }
up4.d18O.means
up4.d13C.means
mean(up3.iso$d18O)
mean(up3.iso$d13C)




#-------------------------------UP3 Tone and Clarity Isotope Relationships-------------------
up3.petro.alldata <- read.table("up3_iso.csv", sep=",", header=TRUE)
up3.petro.alldata <- na.omit(up3.petro.alldata)
tone.index <- c("vd", "d-vd", "d", "m-d", "m", "m-l", "l", "l-vl", "vl")
tone.d13C.color.index <- c("darkred", "firebrick4", "firebrick", "firebrick3", "firebrick2", "firebrick1",
        "brown1", "indianred1", "palevioletred1")
tone.d18O.color.index <- c("midnightblue", "navy", "royalblue4", "steelblue4", "steelblue", "steelblue3",
        "steelblue2", "steelblue1", "skyblue")
clarity.index <- c("o", "o-pt", "pt", "t-pt", "t")
```

```
clarity.d13C.color.index <- c("firebrick4", "firebrick", "firebrick3", "firebrick2", "firebrick1")
clarity.d18O.color.index <- c("steelblue4", "steelblue", "steelblue3", "steelblue2", "steelblue1")
clarity.color.index <- ("steelblue4")
up3.index <- c("all", "8ka", "5ka", "4ka", "3ka", "2ka")

up3.petro <- up3.petro.alldata[up3.petro.alldata$tone != 'dlvd', ]
up3.petro <- up3.petro[up3.petro$tone != 'ld', ]
up3.petro <- up3.petro[up3.petro$tone != 'vdl', ]
up3.petro <- up3.petro[up3.petro$tone != 'dvl', ]
up3.petro$tone[up3.petro$tone == "mvd"] <- "md"
up3.petro$tone[up3.petro$tone == "mvl"] <- "ml"
up3.petro$tone[up3.petro$tone == "lm"] <- "ml"
up3.petro$clarity[up3.petro$clarity == "ot"] <- "tpt"

tone.length <- aggregate(up3.petro[ , 4:5], list(up3.petro$tone), length)
tone.mean <- aggregate(up3.petro[ , 4:5], list(up3.petro$tone), mean)
tone.sd <- aggregate(up3.petro[ , 4:5], list(up3.petro$tone), sd)
tone.petro <- data.frame(tone.length[,c(1,3)], tone.mean[,2:3], tone.sd[,2:3])
tone.petro[, 3:6] <- round(tone.petro[, 3:6], 2)
colnames(tone.petro) <- c("tone", "n", "d13C.mean", "d18O.mean", "d13C.sd", "d18O.sd")

clarity.length <- aggregate(up3.petro[ , 4:5], list(up3.petro$clarity), length)
clarity.mean <- aggregate(up3.petro[ , 4:5], list(up3.petro$clarity), mean)
clarity.sd <- aggregate(up3.petro[ , 4:5], list(up3.petro$clarity), sd)
clarity.petro <- data.frame(clarity.length[,c(1,3)], clarity.mean[,2:3], clarity.sd[,2:3])
clarity.petro[, 3:6] <- round(clarity.petro[, 3:6], 2)
colnames(clarity.petro) <- c("clarity", "n", "d13C.mean", "d18O.mean", "d13C.sd", "d18O.sd")

#d13C tone
dev.new(height=6, width=10)
stripchart(up3.petro$d13C~factor(up3.petro$tone, levels=tone.index),
        col=adjustcolor(tone.d13C.color.index, alpha=0.5), pch=15, ylab="", axes=FALSE,
        vertical=TRUE, ylim=c(-12,-5), cex=1.8)
points(factor(tone.petro$tone, levels=tone.index), tone.petro$d13C.mean,
```

```
        pch=23, cex=3.5, col="black", lwd=2.5, bg=adjustcolor("yellow", alpha=0.6))
axis(2, at=seq(-12, -5, 3), las=1, cex.axis=1.5)
axis(2, at=seq(-12, -5, 1),labels=FALSE, tck=-0.01)
axis(1, at=(1:length(tone.index)), labels=toupper(tone.index), cex.axis=1.5)
mtext(side=2, expression(paste({delta}^13*C, " (‰ vs. V-PDB)")),
        line=2, cex=1.8)
mtext(side=1, "Tone", line=3, cex=1.8)

#d18O tone
dev.new(height=6, width=10)
stripchart(up3.petro$d18O~factor(up3.petro$tone, levels=tone.index),
        col=adjustcolor(tone.d18O.color.index, alpha=0.5), pch=15, ylab="", axes=FALSE,
        vertical=TRUE, ylim=c(-6.5,-4), cex=1.8,)
points(factor(tone.petro$tone, levels=tone.index), tone.petro$d18O.mean,
        pch=23, cex=3.5, col="black", lwd=2.5, bg=adjustcolor("yellow", alpha=0.6))
axis(2, at=seq(-6, -4, 1), las=1, cex.axis=1.5)
axis(2, at=seq(-6.5, -4, 0.5),labels=FALSE, tck=-0.01)
axis(1, at=(1:length(tone.index)), labels=toupper(tone.index), cex.axis=1.5)
mtext(side=2, expression(paste({delta}^18*O, " (‰ vs. V-PDB)")),
        line=2, cex=1.8)
mtext(side=1, "Tone", line=3, cex=1.8)

#d13C clarity
dev.new(height=6, width=6)
stripchart(up3.petro$d13C~factor(up3.petro$clarity, levels=clarity.index),
        col=adjustcolor(clarity.d13C.color.index, alpha=0.5), pch=15, ylab="", axes=FALSE,
        vertical=TRUE, ylim=c(-12,-5), cex=1.8)
points(factor(clarity.petro$clarity, levels=clarity.index), clarity.petro$d13C.mean,
        pch=23, cex=3.5, col="black", lwd=2.5, bg=adjustcolor("yellow", alpha=0.6))
axis(2, at=seq(-12, -5, 3), las=1, cex.axis=1.5)
axis(2, at=seq(-12, -5, 1),labels=FALSE, tck=-0.01)
axis(1, at=(1:length(clarity.index)), labels=toupper(clarity.index), cex.axis=1.5)
mtext(side=2, expression(paste({delta}^13*C, " (‰ vs. V-PDB)")),
        line=2, cex=1.8)
```

```
mtext(side=1, "Clarity", line=3, cex=1.8)

#d18O clarity
dev.new(height=6, width=6)
stripchart(up3.petro$d18O~factor(up3.petro$clarity, levels=clarity.index),
        col=adjustcolor(clarity.d18O.color.index, alpha=0.5), pch=15, ylab="", axes=FALSE,
        vertical=TRUE, ylim=c(-6.5,-4), cex=1.8,)
points(factor(clarity.petro$clarity, levels=clarity.index), clarity.petro$d18O.mean,
        pch=23, cex=3.5, col="black", lwd=2.5, bg=adjustcolor("yellow", alpha=0.6))
axis(2, at=seq(-6, -4, 1), las=1, cex.axis=1.5)
axis(2, at=seq(-6.5, -4, 0.5),labels=FALSE, tck=-0.01)
axis(1, at=(1:length(clarity.index)), labels=toupper(clarity.index), cex.axis=1.5)
mtext(side=2, expression(paste({delta}^18*O, " (‰ vs. V-PDB)")),
        line=2, cex=1.8)
mtext(side=1, "Clarity", line=3, cex=1.8)

#=============================================================================================================
#=========================================All Stalagmites Combined Code=======================================
#=============================================================================================================

#---------------------------Indiana Stalagmite Ages Horizontal Error Bar Plot Condensed-----------------------------------------
#This script plots the U-Th Ages collected from Indiana stals so far. The ages have had the unreliable
#ages culled out in the imported data. This is a condensed script eliminating the trial plotting of the
#previous stalagmite age plotting script
#Written by Pete D. Akers, September 2015, condensed March 2016

in.ages <- read.table("in_stal_ages_culled.csv", sep=",", header=TRUE)
ycons <- numeric(length(in.ages$age)) #set of zeros as long as the number of ages
ycons.minus <- ycons - 0.03
ycons.plus <- ycons + 0.03
error.minus <- in.ages$age - in.ages$error
error.plus <- in.ages$age + in.ages$error

#Making a stal index
```

```
stal.index <- unique(in.ages$stal)
stal.list <- list()
for (i in 1:length(stal.index)) {
        stal.list[[i]] <- in.ages[in.ages$stal == stal.index[i], ]
        stal.list[[i]]$y.val <- i
        stal.list[[i]]$y.val.minus <- stal.list[[i]]$y.val - 0.1
        stal.list[[i]]$y.val.plus <- stal.list[[i]]$y.val + 0.1
        stal.list[[i]]$error.minus <- stal.list[[i]]$age - stal.list[[i]]$error
        stal.list[[i]]$error.plus <- stal.list[[i]]$age + stal.list[[i]]$error
        }
names(stal.list) <- stal.index

#Bars for Stal Span
min.age <- vector()
max.age <- vector()
for (i in 1:length(stal.index)) {
        min.age[i] <- min(stal.list[[i]]$error.minus)
        max.age[i] <- max(stal.list[[i]]$error.plus)
        }


#Making the ORDERED stal list
stal.list.order <- list(stal.list[[9]], stal.list[[8]], stal.list[[4]], stal.list[[1]], stal.list[[7]],
        stal.list[[3]], stal.list[[13]], stal.list[[10]], stal.list[[2]], stal.list[[11]], stal.list[[12]],
        stal.list[[6]], stal.list[[14]], stal.list[[5]])
min.age.order <- vector()
max.age.order <- vector()
stal.index.order <- stal.index[c(9,8,4,1,7,3,13,10,2,11,12,6,14,5)]
for (i in 1:length(stal.index)) {
        min.age.order[i] <- min(stal.list.order[[i]]$error.minus)
        max.age.order[i] <- max(stal.list.order[[i]]$error.plus)
        }
```

```
#Plot with Stal Age Bars and Age Dots ORDERED
dev.new(height=6,width=12)
plot(min.age, seq(1,length(min.age)), bty="n", yaxt="n", xaxt="n", ylab="", xlab="",
	ylim=c(0, max(length(stal.index.order))), type="n", xlim=c(0,100000))
	for (i in 1:length(stal.index.order)) {
		stal.list.order[[i]]$y.val <- i #values for a single stalagmite
		stal.list.order[[i]]$y.val.minus <- i-0.1
		stal.list.order[[i]]$y.val.plus <- i+0.1
		y.val.iter <- stal.list.order[[i]]$y.val #values for a single stalagmite
		y.val.minus.iter <- stal.list.order[[i]]$y.val.minus
		y.val.plus.iter <- stal.list.order[[i]]$y.val.plus
		error.minus.iter <- stal.list.order[[i]]$error.minus
		error.plus.iter <- stal.list.order[[i]]$error.plus
		rect(min.age.order[i], i+0.3, max.age.order[i], i-0.3, col='gray75', border=NA)
		segments(error.minus.iter[1:length(y.val.iter)],y.val.iter[1:length(y.val.iter)], error.plus.iter[1:length(y.val.iter)],
			y.val.iter[1:length(y.val.iter)], col='gray25', lwd=0.5)
		points(stal.list.order[[i]]$age, y.val.iter, pch=20, col="firebrick")
		segments(error.minus.iter[1:length(y.val.iter)], y.val.minus.iter[1:length(y.val.iter)], error.minus.iter[1:length(y.val.iter)],
			y.val.plus.iter[1:length(y.val.iter)], col='gray25', lwd=0.5)
		segments(error.plus.iter[1:length(y.val.iter)], y.val.minus.iter[1:length(y.val.iter)], error.plus.iter[1:length(y.val.iter)],
			y.val.plus.iter[1:length(y.val.iter)], col='gray25', lwd=0.5)
		}
	axis(1, at=seq(0,100000,20000), pos=0.5, labels=format(seq(0,100000,20000),
		scientific=FALSE), cex.axis=1.4)
	axis(1, at=seq(0,100000,5000), pos=0.5, labels=FALSE, tck=-0.01)
	mtext(side=1, "Age (cal yr BP)", line=1.7, cex=1.7)
	axis(2, at=seq(1,length(stal.index.order)), pos=0, labels=toupper(stal.index.order), tck=-0.01,
		las=1, cex.axis=1.2)
	mtext(side=2, "Stalagmite", line=2.5, cex=1.7)



#=============================================================================================
```

```
#-------------------------------------Related Paleo Data---------------------------------------

#NGRIP
ngrip <- read.table("ngrip.csv", sep=",", header=TRUE)
dev.new(height=5,width=12)
plot(ngrip$age, ngrip$d18O, bty="n", yaxt="n", xaxt="n", ylab="", xlab="", ylim=c(-48,-32),
        type="n", xlim=c(0,100000))
points(ngrip$age, ngrip$d18O, type="l", lwd=1.3, col="lightblue4")
axis(4, at=seq(-48,-32,4), pos=100000, las=1, col="lightblue4", col.axis="lightblue4", cex.axis=1.4)
axis(4, at=seq(-48,-32,1), pos=100000, labels=FALSE, tck=-0.01, col="lightblue4")
axis(1, at=seq(0,100000,20000), pos=-48, labels=format(seq(0,100000,20000), scientific=FALSE),
        cex.axis=1.4)
#axis(1, at=seq(0,100000,5000), pos=-48, labels=FALSE, tck=-0.01)
mtext(side=4, expression(paste({delta}^18*O, " (‰ vs. V-SMOW)")),
        line=0.8, cex=1.6, col="lightblue4")

#EPICA Temp
epica <- read.table("epica_temp.csv", sep=",", header=TRUE)
dev.new(height=5,width=12)
plot(epica$age, epica$temp, bty="n", yaxt="n", xaxt="n", ylab="", xlab="", ylim=c(-11,6),
        type="n", xlim=c(0,100000))
points(epica$age, epica$temp, type="l", lwd=1.3, col="lightgoldenrod4")
axis(2, at=seq(-10,5,5), pos=0, las=1, col="lightgoldenrod4", col.axis="lightgoldenrod4", cex.axis=1.4)
axis(2, at=seq(-11,6,1), pos=0, labels=FALSE, tck=-0.01, col="lightgoldenrod4")
axis(1, at=seq(0,100000,20000), pos=-11, labels=format(seq(0,100000,20000), scientific=FALSE),
        cex.axis=1.4)
#axis(1, at=seq(0,100000,10000), pos=-11, labels=FALSE, tck=-0.01)
mtext(side=2, "Temperature Deviation (°C)", line=1, cex=1.6, col="lightgoldenrod4")


#Insol June
insol.jun <- read.table("insol_jun.csv", sep=",", header=TRUE)
dev.new(height=5,width=12)
plot(insol.jun$age, insol.jun$N60, bty="n", yaxt="n", xaxt="n", ylab="", xlab="", ylim=c(430,560),
```

```
        type="n", xlim=c(0,100000))
#points(insol.jun$age, insol.jun$N60, type="l", lwd=1.3, col="steelblue4")
points(insol.jun$age, insol.jun$N30, type="l", lwd=2, col="mediumorchid4")
axis(2, at=seq(450,550,50), pos=0, cex.axis=1.4, las=1, col="mediumorchid4", col.axis="mediumorchid4")
axis(2, at=seq(430,560,10), pos=0, labels=FALSE, tck=-0.01, col="mediumorchid4")
axis(1, at=seq(0,100000,20000), pos=430, labels=format(seq(0,100000,20000), scientific=FALSE),
        cex.axis=1.4)
axis(1, at=seq(0,100000,5000), pos=430, labels=FALSE, tck=-0.01)
mtext(side=1, "Age (cal yr BP)", line=2.5, cex=1.7)
mtext(side=2, "Solar Radiation (W / m²)", line=2.5, cex=1.6, col="mediumorchid4",)
text("30°N June Radiation", cex=1.7, x=1000, y=540, pos=4, col="mediumorchid4")

#-----------------------All Stal Iso Plotting Script----------------------
#This script makes isotope plots for all Indiana stalagmites
#Written by Pete D. Akers, March 2016

in.iso <- read.table("in_stal_iso.csv", header=TRUE, sep=",")
in.stal.index <- unique(in.iso$stal)

#Separating out the stals from the combined data
in.stal.list <- list(NA)
for(i in 1:length(in.stal.index)) {
        in.stal.list[[i]] <- in.iso[in.iso$stal == in.stal.index[i], ]
        }
names(in.stal.list) <- in.stal.index

#Eliminating DC20 samples with bad ages due to hiatuses
in.stal.list$dc20 <- in.stal.list[["dc20"]][in.stal.list[["dc20"]]$age >= 46500, ]

in.color.index <- c("firebrick", "red", "mediumorchid4", "orange2", "steelblue4", "cyan3",
        "orangered", "seagreen", "green4", "olivedrab", "royalblue", "dodgerblue")
in.legend <- toupper(in.stal.index)

#d18O time series
```

```
dev.new(height=5,width=12)
plot(in.iso$age, in.iso$d18O, type="n", bty="n", xaxt="n", yaxt="n",
        xlab="", ylab="", xlim=c(0,90000), ylim=c(-6.6, -3.0))
for(i in 1:length(in.stal.index)) {
        points(in.stal.list[[i]]$age, in.stal.list[[i]]$d18O, pch=16,
                col=adjustcolor(in.color.index[[i]], alpha=0.4), cex=1.2)
        }
axis(2, at=seq(-6, -3, 1), pos=0, las=1, col="steelblue4",
        col.axis="steelblue4", cex.axis=1.4)
axis(2, at=seq(-6.5, -3, 0.25), pos=0, las=1, col="steelblue4",
        col.axis="steelblue4", labels=FALSE, tck=-0.01)
axis(1, at=seq(0,90000,10000), pos=-6.5, cex.axis=1.4)
axis(1, at=seq(0,90000,2000), pos=-6.5, labels=FALSE, tck=-0.01)
mtext(side=1, "Age (cal yr BP)", line=2.8, cex=1.8)
mtext(side=2, expression(paste({delta}^18*O, " (‰ vs. V-PDB)")),
        line=.3, cex=1.6, col="steelblue4")
legend(legend=in.legend, text.col=in.color.index, x=20000, y=-3, pch=16,
        col=adjustcolor(in.color.index, alpha=0.7), bty="n", cex=1.2)

#d13C time series
dev.new(height=5,width=12)
plot(in.iso$age, in.iso$d13C, type="n", bty="n", xaxt="n", yaxt="n",
        xlab="", ylab="", xlim=c(0,90000), ylim=c(-12, 3))
for(i in 1:length(in.stal.index)) {
        points(in.stal.list[[i]]$age, in.stal.list[[i]]$d13C, pch=16,
                col=adjustcolor(in.color.index[[i]], alpha=0.4), cex=1.2)
        }
axis(4, at=seq(-12, 3, 3), pos=90000, las=1, col="firebrick",
        col.axis="firebrick", cex.axis=1.4)
axis(4, at=seq(-12, 3, 1), pos=90000, las=1, col="firebrick",
        col.axis="firebrick", labels=FALSE, tck=-0.01)
mtext(side=4, expression(paste({delta}^13*C, " (‰ vs. V-PDB)")),
        line=.8, cex=1.6, col="firebrick")
legend(legend=in.legend, text.col=in.color.index, x=20000, y=3, pch=16,
```

```
        col=adjustcolor(in.color.index, alpha=0.7), bty="n", cex=1.2)

#d13C vs d18O time series
dev.new(height=10,width=10)
plot(in.iso$d18O, in.iso$d13C, type="n", bty="n", xaxt="n", yaxt="n",
        xlab="", ylab="", xlim=c(-6.6, -3.0), ylim=c(-12, 3))
for(i in 1:length(in.stal.index)) {
        points(in.stal.list[[i]]$d18O, in.stal.list[[i]]$d13C, pch=16,
                col=adjustcolor(in.color.index[[i]], alpha=0.4), cex=1.2)
        }
axis(2, at=seq(-12, 3, 3), pos=-6.5, las=1, col="firebrick",
        col.axis="firebrick", cex.axis=1.4)
axis(2, at=seq(-12, 3, 1), pos=-6.5, las=1, col="firebrick",
        col.axis="firebrick", labels=FALSE, tck=-0.01)
axis(1, at=seq(-6, -3, 1), pos=-12, las=1, col="steelblue4",
        col.axis="steelblue4", cex.axis=1.4)
axis(1, at=seq(-6.5, -3, 0.25), pos=-12, las=1, col="steelblue4",
        col.axis="steelblue4", labels=FALSE, tck=-0.01)
mtext(side=2, expression(paste({delta}^13*C, " (‰ vs. V-PDB)")),
        line=.8, cex=1.6, col="firebrick")
mtext(side=1, expression(paste({delta}^18*O, " (‰ vs. V-PDB)")),
        line=2, cex=1.6, col="steelblue4")
legend(legend=in.legend, text.col=in.color.index, x=-6.5, y=3, pch=16,
        col=adjustcolor(in.color.index, alpha=0.7), bty="n", cex=1.2)



#------------------Correction factors application---------------------------------------------
#Correction factors were found by comparing stalagmite stable isotope values at 8360 cal yr BP

in.stal.list.crct <- in.stal.list
in.stal.list.crct[["ic5"]]$d18O <- in.stal.list[["ic5"]]$d18O - 0.56
in.stal.list.crct[["ic5"]]$d13C <- in.stal.list[["ic5"]]$d13C - 8.76
in.stal.list.crct[["ic6"]]$d18O <- in.stal.list[["ic6"]]$d18O - 0.56
```

```
in.stal.list.crct[["ic6"]]$d13C <- in.stal.list[["ic6"]]$d13C - 8.76
in.stal.list.crct[["ic14"]]$d18O <- in.stal.list[["ic14"]]$d18O - 0.56
in.stal.list.crct[["ic14"]]$d13C <- in.stal.list[["ic14"]]$d13C - 8.76
in.stal.list.crct[["ic15"]]$d18O <- in.stal.list[["ic15"]]$d18O - 0.56
in.stal.list.crct[["ic15"]]$d13C <- in.stal.list[["ic15"]]$d13C - 8.76

in.stal.list.crct[["rc11"]]$d18O <- in.stal.list[["rc11"]]$d18O - 1.08
in.stal.list.crct[["rc11"]]$d13C <- in.stal.list[["rc11"]]$d13C + 0.71
in.stal.list.crct[["rc12"]]$d18O <- in.stal.list[["rc12"]]$d18O - 1.08
in.stal.list.crct[["rc12"]]$d13C <- in.stal.list[["rc12"]]$d13C + 0.71
in.stal.list.crct[["rc13"]]$d18O <- in.stal.list[["rc13"]]$d18O - 1.08
in.stal.list.crct[["rc13"]]$d13C <- in.stal.list[["rc13"]]$d13C + 0.71
in.stal.list.crct[["dc20"]]$d18O <- in.stal.list[["dc20"]]$d18O - 1.08
in.stal.list.crct[["dc20"]]$d13C <- in.stal.list[["dc20"]]$d13C + 0.71

#d18O corrected time series
dev.new(height=5,width=12)
plot(in.iso$age, in.iso$d18O, type="n", bty="n", xaxt="n", yaxt="n",
        xlab="", ylab="", xlim=c(0,90000), ylim=c(-6.5, -3.0))
for(i in 1:length(in.stal.index)) {
        points(in.stal.list.crct[[i]]$age, in.stal.list.crct[[i]]$d18O, pch=16,
                col=adjustcolor(in.color.index[[i]], alpha=0.4), cex=1.2)
        }
axis(2, at=seq(-6, -3, 1), pos=0, las=1, col="steelblue4",
        col.axis="steelblue4", cex.axis=1.4)
axis(2, at=seq(-6.5, -3, 0.25), pos=0, las=1, col="steelblue4",
        col.axis="steelblue4", labels=FALSE, tck=-0.01)
axis(1, at=seq(0,90000,10000), pos=-6.5, cex.axis=1.4)
axis(1, at=seq(0,90000,2000), pos=-6.5, labels=FALSE, tck=-0.01)
mtext(side=1, "Age (cal yr BP)", line=2.8, cex=1.8)
mtext(side=2, expression(paste({delta}^18*O, " (‰ vs. V-PDB)")),
        line=.3, cex=1.6, col="steelblue4")

#d13C corrected time series
```

```
dev.new(height=5,width=12)
plot(in.iso$age, in.iso$d13C, type="n", bty="n", xaxt="n", yaxt="n",
        xlab="", ylab="", xlim=c(0,90000), ylim=c(-15, 0))
for(i in 1:length(in.stal.index)) {
        points(in.stal.list.crct[[i]]$age, in.stal.list.crct[[i]]$d13C, pch=16,
                col=adjustcolor(in.color.index[[i]], alpha=0.4), cex=1.2)
        }
axis(2, at=seq(-15, 0, 3), pos=0, las=1, col="firebrick",
        col.axis="firebrick", cex.axis=1.4)
axis(2, at=seq(-15, 0, 1), pos=0, las=1, col="firebrick",
        col.axis="firebrick", labels=FALSE, tck=-0.01)
mtext(side=2, expression(paste({delta}^13*C, " (‰ vs. V-PDB)")),
        line=.8, cex=1.6, col="firebrick")
```